INDIAN AGRICULTURAL
RESEARCH INSTITUTE NEW DELHI

I. A. R. I. 6.
MGIPC—S4—10 AR—21 6 49—1 000

PROCEEDINGS

OF THE

ROYAL SOCIETY OF LONDON

SERIES A MATHEMATICAL AND PHYSICAL SCIENCES

VOL 172

LONDON
Printed and published for the Royal Society
By the Cambridge University Press
Bentley House N W 1

4 September 1939

PRINTED IN GREAT BRITAIN BY
WALTER LEWIS, M.A.
AT THE CAMBRIDGE UNIVERSITY PRESS

CONTENTS

SERIES A VOL 172

No. 948. 19 July 1939

PAGE

A study of sensitized explosions. IV. The carbon monoxide-oxygen reaction catalysed by nitrogen peroxide. By E. J. Buckler and R. G. W. Norrish, F.R.S. 1

The mobility of alkali ions in gases. I. The attachment of water molecules to alkali ions in gases. By R. J. Munson and A. M. Tyndall, F.R.S. . 28

The mobility of alkali ions in gases. II. The attachment of inert gas atoms to alkali ions. By R. J. Munson and K. Hoselitz . . . 43

The mobility of alkali ions in gases. III. The mobility of alkali ions in water vapour. By R. J. Munson 51

Natural convection in liquids. By O. A. Saunders 55

The excitation of γ-radiation in processes of proton capture. By S. C. Curran and J. E. Strothers 72

Fine structure of the Raman lines of carbon tetrachloride. By A. C. Menzies 89

Theory of electrical breakdown in ionic crystals. II. By H. Fröhlich . 94

The formation of HeH^+ molecules. By M. B. M'Ewen and F. L. Arnot . 107

Diffraction of X-rays by crystals at elevated temperatures. By G. D. Preston 116

Resonance phenomena in the scattering of α-particles by some light nuclei. By S. Devons 127

Thermal diffusion in mixtures of the inert gases. By B. E. Atkins, R. E. Bastick and T. L. Ibbs 142

No. 949. 3 August 1939

Vacuum wave-length measurements in the iron spectrum by means of the reflection echelon grating. By W. E. Williams and A. Middleton . 159

The infra-red absorption spectrum of tetra-deuteroethylene. By G. K. T. Conn and G. B. B. M. Sutherland 172

Some observations on cosmic rays using a large randomly operated cloud chamber. By E. J. Williams 194

PAGE

The two-dimensional hydrodynamical theory of moving aerofoils. III. By R. M. Morris 213

The lower limiting crystallite size and internal strains in some cold-worked metals. By W. A. Wood 231

Calculated wave functions and energy values for X-ray terms of potassium. By W. A. Thatcher 242

The friction of clean metals and the influence of adsorbed gases. The temperature coefficient of friction. By F. P. Bowden and T. P. Hughes 263

The mechanism of sliding on ice and snow. By F. P. Bowden and T. P. Hughes 280

No. 950. 23 August 1939

The action of ultra-violet radiation on barium and strontium azides. By W. E. Garner, F.R.S. and J. Maggs 299

The thermal decomposition of crystals of barium axide. By A. Wischin . 314

On the decomposition of metallic azides. By N. F. Mott, F.R.S. . . 325

A crystallographic investigation of glacier structure and the mechanism of glacier flow. By M. F. Perutz and G. Seligman 335

A theory of electric polarization, electro-optical Kerr effect and electric saturation in liquids and solutions. By A. Piekara 360

Classical theory of mesons. By H. J. Bhabha 384

Distribution of charge and potential in an electrolyte bounded by two plane infinite parallel plates. By A. J. Corkill and L. Rosenhead . 410

The absorption spectrum of nitrosyl chloride. By C. F. Goodeve and S. Katz 432

No. 951. 4 September 1939

The photosynthesis of carbohydrates from hydrated carbon dioxide. By E. C. C. Baly, F.R.S. 445

On fluctuations in electromagnetic radiation. By M. Born, F.R.S. and K. Fuchs 465

ABSTRACTS

OF PAPERS COMMUNICATED TO THE ROYAL SOCIETY OF LONDON

In accordance with a resolution of Council, summaries or abstracts of papers are to be published as soon as practicable. The publication of such abstracts in no way indicates that the papers have been accepted for publication in any fuller form. These abstracts are issued for convenience with the "Proceedings of the Royal Society of London" but do not form a part of the "Proceedings".

19 JULY 1939

Defect lattices in some ternary alloys. By H. LIPSON and A. TAYLOR. (*Communicated by A. J. Bradley, F.R.S. -Received* 9 *June* 1939.)

In the Ni-Al system, the solution of Al in the β-Ni-Al (body-centred cubic) structure has been shown to be accompanied by an omission of Ni atoms from some of the lattice points. A study of the Cu-Ni-Al system shows that the omission of atoms begins at a line of constant ratio of valency electrons to atoms, and this is supported by evidence from the systems Fe-Cu-Al and Fe-Ni-Al.

These results may be explained by the accommodation of electrons in the Brillouin zone. If the electrons fill the zone to a given energy level (which, in this case, is very near to the inscribed sphere of the zone), then the number of electrons per unit cell should be constant. It is shown that this is so for the Ni-Al system, but it is not true for the Cu-Ni-Al system, the number of electrons in the zone increasing as Cu is added. It is presumed that the energy relationships are affected by the atomic size factor, Cu being a larger atom than Ni.

The magnetic susceptibility of nickel chloride. By H. R. NETTLETON and S. SUGDEN, F.R.S. (*Received* 10 *June* 1939.)

A solution of nickel chloride appears to be very suitable as a standard for magnetic measurements since the nickel content can be accurately determined by standard analytical methods and the molar susceptibility is independent of dilution. A new determination of the molar susceptibility has been made using null methods to determine the field in the gap of a specially designed magnet followed by measurements of the susceptibility of carefully analysed nickel chloride solutions by the Gouy method.

The mean value found $10^6\chi_{20^\circ} = 4436$ is in good agreement with that of earlier workers, viz. 4448 (Weiss and Bruins 1915), 4423 (Brant 1921). These earlier determinations were made by different physical methods so that the susceptibility of nickel chloride is now known with considerable accuracy.

A brief discussion is appended on the use of solutions of nickel chloride to calibrate vessels for measuring magnetic susceptibilities.

Shower production by penetrating cosmic rays. By A. C. B. LOVELL. (*Communicated by P. M. S. Blackett, F.R.S.—Received* 12 *June* 1939.)

A counter-controlled cloud chamber has been used to investigate cosmic ray showers under thick layers of lead. 5800 photographs, containing 463 electronic showers of not less than five particles, have been taken in a magnetic field of 750 gauss.

An analysis of the evidence and probabilities for various possible processes of shower production is carried out, and it is shown that the showers observed can be accounted for as cascade showers, produced by an electron which has been knocked on in a direct collision with a mesotron. It is unnecessary to assume the occurrence of other processes of appreciable cross-section.

Due to the influence of the incident energy spectrum of mesotrons, the majority of large showers are produced as fluctuations, and in general, the lowest mesotron energy which is able to produce a shower of N particles is only slightly lower than the most probable energy for the production of such a shower.

A search has been made to find showers, or single secondary particles, produced by neutral particles in cosmic radiation, with negative results.

The lamellar structure of potash-soda felspars. By S. H. CHAO and W. H. TAYLOR. (*Communicated by W. L. Bragg, F.R.S.—Received* 13 *June* 1939.)

A previous general survey of orthoclase-microperthites suggested the existence of different types of lamellar structure according as the proportion of soda felspar is less than or greater than 30 % approximately. A new and more detailed examination confirms this, and suggests that the low-soda structure comprises monoclinic potash felspar with triclinic soda felspar lamellae in the mutual orientation characteristic of pericline twins, while the high-soda structure comprises monoclinic potash felspar with triclinic soda felspar lamellae oriented in accordance with the albite twin-law. The constitution of the soda felspar and the bearing of the new data on the general theory of microperthitic structures are discussed.

An examination of a Korean moonstone, apparently identical with material in which Ito claims to have established the existence of *monoclinic* soda felspar, reveals a lamellar structure of the low-soda type described above. Ito's results are discussed.

Self-consistent field with exchange for carbon. By A. JUCYS. (*Communicated by D. R. Hartree, F.R.S.—Received* 14 *June* 1939.)

Solutions of Fock's equations for the self-consistent field with exchange have been carried out for the normal states of C^{+4} and C^{++}, and for all three configurations (^3P, ^1D and ^1S) arising from the normal configuration of neutral C.

For neutral C, the energies of the $(2s)$ $(2p)$ have been calculated both without and with the inclusion of the term arising from the superposition of the $(2p)^4$ configuration on the normal $(2s)^2$ $(2p)^2$ configuration.

Tables of wave functions and energies are given.

On the intensities of electron diffraction rings. By M. BLACKMAN. (*Communicated by G. P. Thomson, F.R.S.—Received* 14 *June* 1939.)

The reflexion of electrons by a thin film is examined from the point of view of the dynamical theory in the Laue case. The formulae are used to obtain a criterion which determines when the scattering is sufficiently small to allow the kinematical theory to be applied; it is found that this theory is not in general applicable to the thin films used in work with fast electrons. The total intensity scattered from a film when it is turned through its range of reflexion is also found and the result is used to obtain an approximate intensity function showing how the intensities of the diffraction rings from a polycrystalline film will vary when the scattering is sufficiently large for the kinematical theory to be inapplicable. This intensity function is tested by comparing it with the experimental intensity function found for copper and silver. It is found possible to obtain a good fit with very reasonable assumptions as to the average crystal size.

A mathematical analysis of the distribution in maize of *Heliothis armigera* (Huebner) [= *obsoleta* F.]. By MARJORY G. WALKER, PH.D. (*Communicated by W. R. Thompson, F.R.S.—Received* 22 *June* 1939.)

The distribution among maize plants of the eggs of the American boll-worm, *Heliothis armigera* (Huebner), is discussed and analysed.

The problem is considered in relation to what is known of the connexion between the state of development of maize plants and their attractiveness to ovipositing boll-worm moths. The actual frequency distribution of the eggs suggests a random, as opposed to a uniform, distribution, but it is shown that the conditions required for a pure mathematical random distribution cannot be satisfied. Because the maize plants differ from one another in absolute degree of attractiveness at any one time, and in relative degree of attractiveness with the passing of time, it is not true that every plant has the same chance of receiving any particular egg.

It is demonstrated that a mathematical theory, which is essentially one of random distribution, but which incorporates a modification to allow for the varying degrees of attractiveness of the plants, gives a fairly good representation of the egg distribution found in the field.

It is pointed out that the method of mathematical analysis employed is only a rough approximation to what it is really intended to express, and that it cannot deal adequately with the essential difficulty of the problem—the fact of the continuous change in nature.

For the further study of problems of animal distribution it is desirable that the mathematical theories should be improved.

A note on the mechanism of boundary lubrication suggested by the static friction of esters.

By A. Fogg. (*Communicated by C. G. Darwin, F.R.S.—Received* 22 *June* 1939.)

The note gives the results of static friction measurements of steel surfaces lubricated with series of methyl and ethyl esters. The series of ethyl esters was chosen to obtain a relation between coefficient of friction and molecular weight, and an unexpected feature of the relation obtained is a maximum value of coefficient of friction at a molecular weight of about 120.

A suggested explanation of this phenomenon is given by making certain assumptions regarding the structure and method of attachment of the molecules to the surface.

On the basis of these assumptions, the behaviour of a series of methyl esters was predicted before making tests and the results of the tests subsequently carried out agree with the forecast.

The microscopic analysis of intermediate phases in some age-hardening alloys.

By M. L. V. Gayler. (*Communicated by C. H. Desch, F.R.S.—Received* 22 *June* 1939.)

A microscopic analysis has been carried out at high ageing temperatures on high-purity aluminium alloys containing 4 % copper and 4 % copper + 0·5 % magnesium and also on an alloy of the duralumin type, but without manganese, containing 4 % copper, 0·5% magnesium, 0·3% silicon and 0·1% iron.

In the 4 % copper alloy, plates of the intermediate phase, α-$CuAl_2$, have been observed on (100) planes partly or completely changed to β-$CuAl_2$. It is deduced, therefore, that α-$CuAl_2$ is a polymorphic form of β-$CuAl_2$ and is metastable at temperatures of ageing below the quenching temperature.

A second intermediate phase has been identified, during ageing, together with α-$CuAl_2$ on (100) planes in the alloy containing 4 % copper and 0·5 % magnesium. This new intermediate phase also differs from another phase observed when the alloy of the duralumin type is aged.

ABSTRACTS

OF PAPERS COMMUNICATED TO THE ROYAL SOCIETY OF LONDON

In accordance with a resolution of Council, summaries or abstracts of papers are to be published as soon as practicable. The publication of such abstracts in no way indicates that the papers have been accepted for publication in any fuller form. These abstracts are issued for convenience with the "Proceedings of the Royal Society of London" but do not form a part of the "Proceedings".

---

3 August 1939

The particle aspect of meson theory. By N. Kemmer. (*Communicated by S. Chapman, F.R.S.—Received* 22 *June* 1939.)

It is shown that a reformulation of the meson equations is helpful in the interpretation of the meson as a localized particle. Instead of using the usual tensor form, the wave equations are stated as

$$\frac{\partial}{\partial x_\mu}\beta_\mu\psi+\frac{mc}{\hbar}\psi=0,$$

where the β_μ are operators completely defined by a set of commutation rules first given by Duffin (1938). The theory can be developed in strikingly close correspondence to Dirac's electron theory, practically all the definitions of which find their exact counterpart, e.g. spin, magnetic moment, etc. The algebraic properties of the β_μ are studied in detail, a comparison with other similar formulations is given and the limiting non-relativistic theory is developed. The formalism proves simple to handle and is expected to be useful in all calculations primarily concerned with the particle aspect of the meson.

Stress systems in aeolotropic plates. I. By A. E. Green, and G. I. Taylor, F.R.S. (*Received* 22 *June* 1939.)

Equations which can be used for a system of generalized plane stress in a plate whose material has any kind of aeolotropy have been obtained recently by Huber. When the material has two directions of symmetry at right angles in the plane of the plate the equation for the stress function takes a comparatively simple form. In the present paper solutions in polar co-ordinates of this equation are obtained which give single-valued expressions for the displacements, and these solutions are applied to the problem of an isolated force acting at an internal point of an infinite aeolotropic plate. The stress distributions due to such a force acting at a point of certain highly aeolotropic materials such as oak and spruce are represented by polar diagrams.

Stress systems in aeolotropic plates. II. By A. E. Green. (*Communicated by G. I. Taylor, F.R.S.—Received* 22 *June* 1939.)

In a previous paper by G. I. Taylor and the present writer, generalized plane stress systems were examined for infinite aeolotropic plates. In the present paper formulae are obtained for generalized plane stress systems in an infinite aeolotropic strip and also in a semi-infinite plate. In particular, a solution is given for the general problem of any force acting at any point either within or on the boundary of such plates. The stresses due to any distribution of force may be deduced by integration.

When a force acts on the boundary of a semi-infinite plate the stresses may be deduced from our general results, but this case is dealt with independently by solving the problem of an isolated force at the vertex of a wedge. The method used here differs from that used by Michell who was the first to solve this problem.

The stress distributions due to forces either within or on the boundary of a semi-infinite plate are illustrated numerically for a specimen of spruce wood which is highly aeolotropic.

The equilibrium and stability of thin aeolotropic plates. By A. E. Green. (*Communicated by G. I. Taylor, F.R.S.—Received* 22 *June* 1939.)

An equation is established governing the equilibrium of any thin aeolotropic plane plate which is bent by transverse forces and also an equation for the stability of any thin aeolotropic plane plate under forces in its plane. The results are obtained by an elementary approximate method which is equivalent to that used by Huber who was the first to give the equation for the equilibrium of any thin aeolotropic plane plate which is bent by transverse forces. Some of the more elementary problems of equilibrium and stability are solved. Numerical results are given for the stability of thin rectangular sheets of oak and spruce woods when they are acted on by edge thrusts, and also for the stability of a rectangular sheet of spruce under shearing forces.

Behaviour of the crystalline structure of brass under slow and rapid cyclic stresses. By P. L. Thorpe, *Engineering Department*, and W. A. Wood, *Physics Department, National Physical Laboratory, Teddington, Middlesex.* (*Communicated by G. W. C. Kaye, F.R.S.—Received* 1 *July* 1939.)

The stress-extension relationships for an annealed brass have been measured for static tensile stress and for a symmetrical alternating tension-compression applied at a frequency of 2200 cyc./min., and the mechanical properties indicated by the curves have been studied in relation to the changes in crystalline structure of the grains as shown by the X-ray diffraction method. It is shown that the dispersal of the grains into widely oriented crystallites, which constitutes the physical characteristic of the change at the yield point under ordinary static or slow cyclic stress, is entirely suppressed under the same regions of cyclic stress when applied at the high frequency, and that, after the cyclic stressing has ceased, this suppression persists up to a static load equal to the maximum of the prior stress cycle employed; the mechanical measurements indicate a corresponding inhibition of the primitive yield point. A further result is obtained by a precise comparison of the dimensions of the atomic lattice of specimens subjected to cycles of an unsafe range of stress; these show that an appreciable internal strain of the nature of a volume expansion is built up in the lattice during the rapid cyclic stressing, and it is considered that it is this distortion which is associated with the inhibition of the dispersed crystallite formation and rise in primitive static yield point.

A quantitative study of pleochroic haloes. IV. New types of haloes. By G. H. Henderson and F. W. Sparks. (*Communicated by J. Chadwick, F.R.S.—Received* 3 *July* 1939.)

Four types of haloes, provisionally designated as *A*, *B*, *C* and *D* are described, three of them for the first time. These haloes have one, two, three and one rings respectively. Measurements of ring radii are given. The mode of occurrence of the haloes is described. It is shown that they are probably due to α particles from certain later members of the uranium family, whose lives are exceedingly short on a geological time scale.

A quantitative study of pleochroic haloes. V. The genesis of haloes. By G. H. Henderson. (*Communicated by J. Chadwick, F.R.S.—Received* 3 *July* 1939.)

Six types of pleochroic haloes are discussed in this and the preceding paper, divided into two classes "active" and "extinct". To the former class belong uranium and thorium haloes; to the latter class types designated tentatively *A*, *B*, *C* and *D*.

To account for extinct types of haloes a hypothesis is advanced that they originate from hydrothermal solutions. Such solutions diffused through conduits or clefts in the biotite crystal and particular radioactive elements of the uranium family were deposited from them at certain centres of precipitation. By a continuous process there was thus incorporated in a halo nucleus a quantity of a short-lived element sufficient to produce a halo. In this way all four extinct types can be explained. In active haloes this method of halo formation also occurred but the possibility is also open that the halo nucleus was formed prior to the crystallization of the biotite. All halo rings can be accounted for by known types of α particles and no evidence is found for unknown elements which may once have existed in the earth and have now disappeared.

The actions of iodine and hypoiodous acid on pepsin. By J. St L. Philpot and P. A. Small. (*Communicated by R. A. Peters, F.R.S.—Received 3 July* 1939.)

When iodine acts on pepsin the initial ratio of fall in Folin blue value to fall in peptic activity decreases with increasing pH and temperature, reaching a very low figure at pH 6 and 38° C. The same occurs with "diazopepsin", in which the reactive tyrosine groups have previously been attacked by nitrous acid.

When pepsin is treated with small amounts of hypoiodous acid the initial ratio of fall in Folin blue value to amount of hypoiodous acid is much lower than for tyrosine, being practically nil at pH 5·4. The hypoiodous acid required to produce a just perceptible fall in Folin blue value is sufficient to destroy most of the peptic activity.

It is concluded that some groups other than tyrosine are concerned and reasons are given for excluding other amino-acids.

Thermal ionization of barium. By B. N. Srivastava, M.Sc. (*Communicated by M. N. Saha, F.R.S.—Received 3 July* 1939.)

In this paper a new method has been described for experimentally studying the thermal ionization of gases. The apparatus used has already been described in detail by Saha and Tandon elsewhere. Thermal ionization of barium vapour has been investigated at various temperatures and the equilibrium constant and the effective energy of ionization have been calculated. The results obtained agree, within the limits of experimental error, with the theory of thermal ionization. The results also support the usual interpretation of the well-known barium anomaly in the solar spectrum, and yield for the effective ionization energy at 1500° C a value of 114·1 kcal. though the ionization potential of barium is 5·19 V corresponding to 119·5 kcal. The theoretical value for this quantity at 1500° C is 114·4 kcal. The agreement is therefore quite satisfactory.

The influence of diabetogenic anterior pituitary extracts on the islets of Langerhans in dogs. By K. C. Richardson. (*Communicated by Sir Henry Dale, F.R.S.—Received 4 July* 1939.)

The experimental investigation of the aetiology of diabetes mellitus in intact animals has been made possible by the discovery that the daily injection into dogs, of large amounts of a crude anterior pituitary extract results in a clearly defined diabetic condition which may continue after the injections cease and become permanently established.

The histological condition of the pancreas, in a series of dogs so treated, has been examined to determine the influence of the diabetogenic anterior pituitary extract, particularly on the beta cells of the islets of Langerhans. Partial or complete degranulation of the majority of the beta cells, accompanied by hydropic degeneration in individual beta cells, was found in the material taken during the period of injections with pituitary extract, when the dogs were exhibiting temporary symptoms of diabetes. A characteristic vacuolation of the intralobular duct epithelium was also observed.

Vacuolation of the duct epithelium and slight loss of cytoplasmic granules in beta cells, occurred in the pancreas of dogs treated with fractionated anterior pituitary extracts which failed to produce diabetic symptoms.

During the prolonged period of permanent diabetes, the islets of Langerhans may remain intact and show little change beyond loss of cytoplasmic granules in the beta cells, or they may undergo atrophy by a reduction to small groups of alpha cells, or by complete or partial replacement by hyaline material.

In dogs which become refractory to increased dosages of anterior pituitary extract and fail to exhibit permanent diabetic symptoms, there was evidence of hyperplasia in the islets of Langerhans.

X-ray crystallography and the chemistry of the steroids. I.

By J. D. BERNAL, F.R.S., D. CROWFOOT and I. FANKUCHEN. (*Received* 5 *July* 1939.)

A survey has been made of the X-ray crystallography of some eighty sterol derivatives belonging mainly to the cholesterol and ergosterol series but including also calciferol and other photo-derivatives of ergosterol and some higher plant and animal sterols. The measurements are recorded in four tables and include determinations of unit cell size, space group and some data on the crystal morphology and optics. In three cases, cholesteryl chloride, bromide and cholesteryl chloride hydrochloride, Patterson projections have also been derived from the intensities of the X-ray reflexions of the hol planes. These confirm earlier deductions on the shape and size of the sterol molecules, proving that these are roughly lath-shaped, 20 × 7 × 4 A, and the details of the patterns can also to some degree be correlated with the actual arrangement of the carbon atoms in the sterol ring system and with the positions of the chlorine and bromine atoms. The arrangement of the molecules in the crystal units is closely that given by the preliminary examination from the optic orientations and this has therefore been employed to suggest in each of the remaining sterol crystal structures the probable molecular arrangement.

Among the eighty compounds studied a number of different types of crystal structure appear. An attempt is made to group these in a general geometric classification depending upon the relative orientation of the molecular axes, thickness, width, and length to the crystallographic axes *a, b* and *c*. Altogether 104 different sterol structures are included in the classification and of these 77 fall into the second of the three main groups described above, which includes cholesteryl chloride and bromide and has been called the normal type of sterol structure.

The crystallographic measurements as a whole are discussed in their bearing on specific chemical problems under the following headings:

(*a*) *Characterization and identification.* The X-ray data have been applied particularly among the higher plant and animal sterols both to identify individual constituents (e.g. stigmasterol in phytosterol mixtures), to distinguish additional crystal forms (e.g. two types of cerevisterol) and to characterize new sterols and relate these to previously known compounds (e.g. a sterol from rubber).

(*b*) *Molecular weight determinations.* Molecular weight measurements have been carried out on coprosterone, ergotetraene, γ-spinasterol acetate, ergosterol H_2O, stigmasterol H_2O, γ-sitosterol H_2O and a sterol from rubber. In the case of crystals of cholestanol, ergostadiene triol and Δ^4-cholestene 7-ol, the measurements are used to estimate water of crystallization.

(*c*) *The stereochemistry of the carbon skeleton.* The X-ray measurements indicate that the general configuration of the sterol ring system must be flat but so far it has been impossible to correlate stereochemical changes at particular ring junctions with crystallographic changes, e.g. between rings C and D (α-ergostenol, β-ergostenol), B and C (lumisterol), A and B (coprostane, cholestane).

(*d*) *The effect of substituents on the crystallography of the sterols.*

(i) *The position of the hydroxyl group.* A hydroxyl group at C_3 of the sterol skeleton generally, but not invariably leads to double layer formation in the crystal structure and vice versa, a double layer crystal structure usually indicates the presence of a terminal hydroxyl group. Exceptions are cholestane-6-ol which shows a double layer, and pyrocalciferol which does not. Brassicasterol, cerevisterol, the spinasterols and the rubber sterol all probably have hydroxyl groups at C_3. The position of *i*-cholesterol (which shows one double layer) is obscure.

(ii) *The stereochemistry of the hydroxyl group at* C_3. It is not possible to distinguish at this stage between the two possible configurations of the hydroxyl group at C_3. In cholesteryl chloride and bromide, the chlorine and bromine atoms must lie closely in the plane of the ring system. α-Chlor-cholestane is correlated crystallographically with cholesteryl chloride.

(iii) *The position of the double bonds.* The introduction of either hydroxyl groups or halogens at the double bond system usually produces radical changes in the crystallography which makes simple comparison difficult. The Patterson analysis of cholesteryl chloride hydrochloride provides, however, definite evidence that the extra chlorine atom is at C_5. The crystallography of both the hydroxy- and maleic anhydride derivatives of ergosterol is in agreement with their present chemical formulae but provides no certain proof of the correctness of these.

(*e*) *A comparison of the crystallography of different sterols—monohydroxy compounds.* There is a group of sterols including ergosterol and many of the higher plant and animal sterols which show particularly close resemblances in crystal structure to one another. While inclusion in this group must indicate close similarity, both in sterol skeleton and molecular arrangement, deviations do not necessarily seem to have a chemical significance.

(*f*) *The structure of calciferol.* Calciferol, while showing certain differences from the characteristic sterol group mentioned above, also shows similarities particularly in *c* plane intensities. It seems unlikely therefore that the actual distribution of the atoms in the molecule differs considerably from that in ergosterol.

Many of the outstanding problems of the chemical structure of the sterols can only be settled by exact analysis. The present survey has indicated a number of compounds that are suitable for such treatment.

Band spectra of cathodo-luminescence. By S. T. Henderson. (*Communicated by N. F. Mott, F.R.S.—Received 7 July* 1939.)

A photographic method is used to examine the emission bands of various fluorescent materials excited by cathode rays. Single bands given by zinc or zinc-cadmium sulphides agree closely with the Gauss error curve, except at the outer edges where limits to the emission must occur. Approximate graphical analysis gives adequate resolution for more complex bands. Each activator metal produces a band in some characteristic position which varies only slightly with varying preparative methods and activator contents, except when the activator is reduced to very small amounts. The effects of lowering the temperature, and of changing to ultra-violet excitation are described.

A simple relation is demonstrated between band position and composition in the ZnS.CdS series, and the electronic transitions responsible are briefly considered in this case, and also for some manganese-activated materials.

The freezing-point of rhodium. By C. R. Barker and F. H. Schofield. (*Communicated by G. W. C. Kaye, F.R.S.—Received* 10 *July* 1939.)

The freezing-point of rhodium on the International Temperature Scale has been determined by measuring the ratio of brightness, for a certain wave-length, of black-body radiators held at the freezing-points of rhodium and gold, the latter being the basic point of the scale for all high temperatures. The brightness measurements were made by an optical pyrometer of the disappearing-filament type, sighted on the radiator, which, in the case of rhodium, consisted of a closed-end thoria tube projecting into an ingot of the metal. The ingot was contained in a thoria crucible, packed in thoria powder, and placed in an evacuated enclosure. It was heated by electric induction in such a way that it could be alternately melted or frozen at a convenient rate. The ratio of brightness was determined by the successive use of two rotating sectors, the first reducing the brightness of the radiator at the rhodium point so as to give an apparent temperature intermediate between the rhodium and gold points; and the second, when applied to a radiator at this intermediate temperature (about 1270° C), reducing its brightness to that corresponding with the gold point (1063° C). This two-stage reduction in brightness was necessitated by the fact that it is impracticable to cut and measure, with sufficient accuracy, a single sector giving the required ratio of brightness, which is of the order of 700 to 1 for the wave-length used. The purity of the two specimens of rhodium employed in the investigation, was checked by measurement of the ratio of electrical resistance, R_{100}/R_0.

The value found for the freezing-point, 1966 ± 3° C, is indistinguishable from the only previous one obtained by the same method, namely that of the National Bureau of Standards.

The $\lambda 3400$ bands of PH and PD.

By M. Ishaq and R. W. B. Pearse. (*Communicated by A. Fowler, F.R.S.—Received* 10 *July* 1939.)

The band of PD analogous to the λ 3400 band of PH has been photographed in the 4th order of a 10 ft. concave grating. An analysis of its rotational structure has been made and the corresponding band-spectrum constants evaluated. In order to compare the values of the constants with those of PH, the PH band has been photographed with the same dispersion and remeasured. The results are:

For the initial $^3\Pi_i$ state for PD: $B = 4\cdot175$ cm.$^{-1}$; $D = -1\cdot52 \times 10^{-4}$ cm.$^{-1}$; $A = -115\cdot5$ cm.$^{-1}$; while for PH: $B = 8\cdot025$ cm.$^{-1}$; $D = -5\cdot7 \times 10^{-4}$ cm.$^{-1}$; $A = -115\cdot5$ cm.$^{-1}$; for the final $^3\Sigma^-$ state for PD: $B = 4\cdot363$ cm.$^{-1}$; $D = -1\cdot20 \times 10^{-4}$ cm.$^{-1}$; while for PH: $B = 8\cdot412$ cm.$^{-1}$; $D = -4\cdot3 \times 10^{-4}$ cm.$^{-1}$.

A catalogue of wave numbers of the lines measured is given, together with their classification.

The infra-red absorption spectrum of methylamine vapour.

By C. R. Bailey, S. C. Carson and E. F. Daly. (*Communicated by C. K. Ingold, F.R.S.—Received* 10 *July* 1939.)

The infra-red absorption spectrum of methylamine vapour has been examined between 1 and $26\cdot5\mu$ with a prism spectrometer. With the assistance of Raman spectra obtained by other workers fundamental modes and combination tones have been assigned. A model for the methylamine molecule analogous to the D_{3n} model for ethane has been shown to offer a reasonable explanation of the spectra. With the inclusion of an indirectly determined low torsional frequency in methylamine, the assignment is capable of yielding a satisfactory calculated value for the specific heat.

PAGE

The properties of flow of liquid He II. By J. F. Allen and A. D. Misener . 467

Luminescence of mercury vapour along an α-ray pencil, and transfer of nitrogen excitation to mercury. By A. Luyckx 492

Dielectric loss due to polar molecules in solid paraffin wax. By D. R. Pelmore 502

Absorption of penetrating cosmic ray particles in gold. By J. G. Wilson 517

The electrical conductivity of thin films of mercury. By E. T. S. Appleyard and J. R. Bristow 530

Superconductivity of thin films. I. Mercury. By E. T. S. Appleyard, J. R. Bristow, H. London and A. D. Misener 540

The scattering of α-particles in helium. By S. Devons 559

Shower production by penetrating cosmic rays. By A. C. B. Lovell . 568

Index 583

A study of sensitized explosions

IV. The carbon monoxide-oxygen reaction catalysed by nitrogen peroxide

By E. J. Buckler and R. G. W. Norrish, F.R.S.

Department of Physical Chemistry, Cambridge

(*Received* 10 *March* 1939)

Introduction

The work of Hadman, Thompson and Hinshelwood (1932 *a*, *b*) has shown that the reaction between pure carbon monoxide and oxygen is characterized by a region of ignition above 650° C, bounded by upper and lower critical pressure limits outside which the rate of oxidation falls to negligibly small values in the dry gases. Sagulin, Kowalsky, Kopp and Semenoff (1930) have reported that the region of ignition of moist carbon monoxide is extended more than 200° C towards lower temperatures in the presence of 0·1 % nitrogen peroxide, although larger concentrations than this exert an anti-catalytic effect. Another aspect of the catalytic influence of nitrogen peroxide on the carbon monoxide-oxygen reaction is revealed by the work of Crist and Roehling (1935) and Crist and Calhoun (1936), who have found that steady reaction occurs in nitrogen peroxide sensitized mixtures at 527° C and 750 mm. total pressure. The rate of reaction varies with concentration of nitrogen peroxide in a manner shown by curve *B* in fig. 1, which has been taken from the paper by Crist and Roehling (1935).* This graph, as shown by Crist and Roehling (1935), can be represented as the sum of two simpler curves *A* and *C*, depicting respectively distinct catalytic functions of nitrogen peroxide. Curve *C* was shown to be explained by a mechanism in which nitrogen peroxide, by alternate oxidation and reduction, plays the part of an oxygen carrier in accordance with the following formal equations:

$$CO + NO_2 = CO_2 + NO,$$

$$2NO + O_2 = 2NO_2.$$

---

* For purposes of comparison with the data of this paper, the original ordinates of Crist and Roehling in fig. 1 have been converted to show the reaction velocity in mm. CO_2 formed per second.

These reactions were found to be homogeneous and independent of surface. Curve *A* on the other hand, which shows a maximum at about 0·36 mm. NO_2, represents a reaction which was somewhat affected by the nature and pretreatment of the vessel surface and which was ascribed to a chain mechanism in which nitrogen peroxide exerted simultaneously catalytic and anticatalytic effects. In considering the matter further, the present authors were struck by the similarity in form between curve *A* in fig. 1 and the curves reproduced in fig. 2 showing the sensitizing effect of nitrogen peroxide on the hydrogen-oxygen reaction obtained by Norrish and Griffiths (1933). In any discussion of the carbon monoxide-oxygen reaction it is also necessary to bear in mind that its mechanism is profoundly altered by the presence of traces of hydrogen or water (see Garner and his co-workers 1927–32; Bone 1931; Hadman *et al.* 1932*a*, *b*). In particular it has been found recently by Buckler and Norrish (1938) that in the presence of only 1 % hydrogen the ignition region for carbon monoxide is transferred to that characteristic of hydrogen, and that propagation and branching of reaction chains become

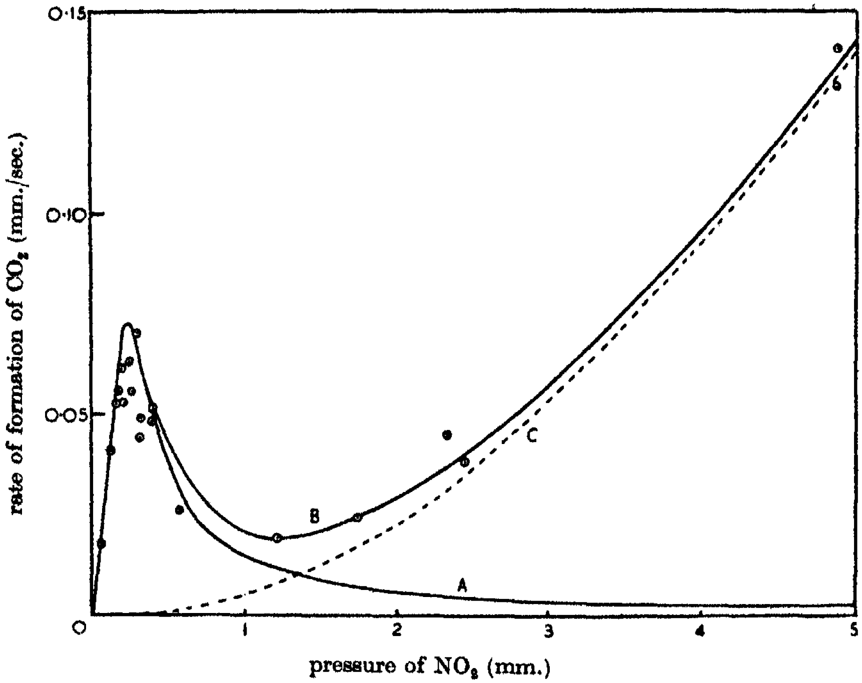

FIG. 1. Variation of rate of oxidation of carbon monoxide with concentration of nitrogen peroxide (Crist and Roehling 1935). Temperature 527° C; total pressure of $2CO + O_2 = 750$ mm. Hg.

possible over 150° C lower than in pure carbon monoxide and oxygen. Moreover, it was shown that ignition in CO-O_2-H_2 mixtures is controlled uniquely by the chain-branching processes responsible for ignition in oxy-hydrogen mixtures at these temperatures. The fact that traces of hydrogen can exert so profound an effect on the oxidation of carbon monoxide immediately raises the possibility that the anomalous behaviour of CO-O_2-NO_2 mixtures at low nitrogen peroxide concentrations shown in fig. 1 might be due to small quantities of hydrogen or water vapour present as impurity in the reactant gases.

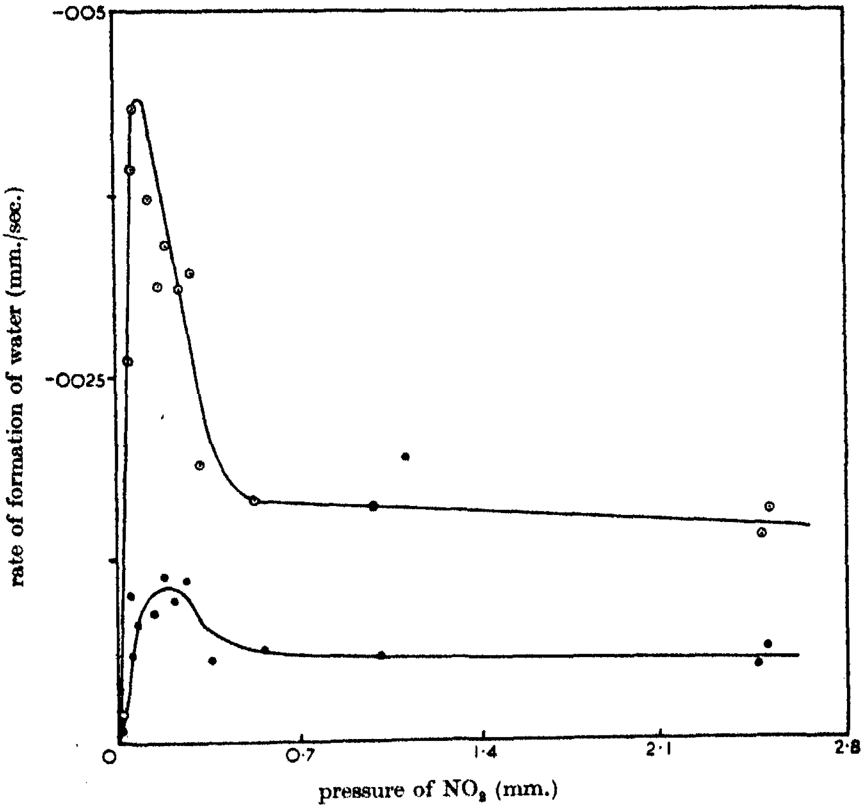

FIG. 2. Variation of rate of oxidation of hydrogen with concentration of nitrogen peroxide (Norrish and Griffiths 1933). Temperature 302° C; total pressure of $2H_2+O_2 = 150$ mm. Hg. ⊙ reaction in light; ● reaction in dark.

The object of the present work was to investigate in more detail the oxidation of carbon monoxide in the presence of small concentrations of nitrogen peroxide, to examine the influence of hydrogen on such mixtures, and further, to determine whether the maximum in curve *B* shown in fig. 1, obtained by Crist and Roehling (1935), could be ascribed to the presence of minute traces of hydrogen or water vapour.

It has been found that the rate of reaction in carbon monoxide-oxygen mixtures containing 0·25 mm. nitrogen peroxide but no hydrogen, prepared and dried by normal laboratory methods, becomes measurable above about 425° C. According to measurements made at 527° C the reaction velocity decreases steadily with decrease of total pressure, and there is no evidence of a region of ignition at low pressures.

However, when hydrogen is added to such CO-O_2-NO_2 mixtures, explosions may be obtained even at 357° C. These are preceded by induction periods which at first decrease and then increase with increasing concentrations of nitrogen peroxide. The results indicate that ignition in CO-O_2-NO_2-H_2 mixtures is conditioned under these circumstances by a chain-branching mechanism similar to that responsible for the nitrogen peroxide sensitized ignition of oxy-hydrogen mixtures (Foord and Norrish 1935). At these lower temperatures therefore, in the presence of hydrogen, the maximum in curve *B* of fig. 1 obtained by Crist and Roehling is replaced by a region of ignition bounded by upper and lower critical concentrations of nitrogen peroxide, while in the absence of hydrogen the catalytic effect of nitrogen peroxide is entirely eliminated.

Further experiments established that while dry CO-O_2-NO_2 mixtures do not ignite at low pressures at 500° C, addition of water vapour to the sensitized gases introduced a region of ignition similar to that found with traces of hydrogen. This provides an example of ignition catalysis produced by the combined influence of two substances, neither of which alone affects the ignition temperatures of carbon monoxide and oxygen. These results may be explained by the fact that water, while it cannot cause branching, catalyses the propagation of straight chains, and nitrogen peroxide, which does not assist chain propagation, readily gives rise to chain branching.

Experiments have been performed which eliminate the possibility of traces of hydrogen being the cause of the maximum in the curve shown in fig. 1, but since in the apparatus we employed it was not possible rigorously to eliminate the last traces of water vapour, we have been led to ascribe the catalytic maximum of the curve shown in fig. 1 to the joint action of water vapour and nitrogen peroxide. That the amount of water required to produce the effect is very minute may be gauged by the extreme sensitivity of the reaction at these temperatures to traces of free radicals containing hydrogen.

In the present work a further study has also been made of the induction period. As in the nitrogen peroxide sensitized ignition of hydrogen and oxygen, the present results enable one to draw the conclusion that ignition in chain reactions involves a thermal process which can become the limiting factor governing ignition.

EXPERIMENTAL METHOD

Apparatus

The apparatus used was identical with that described by us in a recent paper (Buckler and Norrish 1938), and consisted essentially of an electrically heated reaction vessel of quartz or pyrex, into which gas mixtures could be introduced from a separate mixing vessel. The pressure measurements were carried out by the use of two water-jacketed Bourdon gauges of the type described by Foord (1934), one of which employed the movement of a beam of light and the other the deflexion of a pointer for observing differences of pressure. For differential measurements the latter gauge was accurate to a pressure change of 0·02 mm., while both were sufficiently robust to withstand the shock of an explosion in the reaction vessel. A conical quartz reaction vessel 18 cm. long tapering from a diameter of 40 mm. to one of 4 mm. was used in all experiments on the ignition of mixtures containing water vapour or hydrogen. The steady reaction in dry hydrogen-free mixtures was studied in a pyrex reaction vessel 20 cm. long and 35 mm. diameter of volume 217 c.c.

For a purpose which will be described later, it was arranged that after undergoing reaction for some minutes, such mixtures could be withdrawn through a spiral cooled in liquid air and stored in a Toepler pump for use in subsequent experiments. Gases were prepared as described below, and stored in large soda-glass bulbs, and the final drying of every permanent gas or mixture was accomplished by passage through spirals cooled in liquid air.

Preparation of gases

Pure oxygen, hydrogen, carbon monoxide and nitrogen were obtained by methods previously described (Buckler and Norrish 1938). Nitrogen peroxide was prepared by heating lead nitrate in a stream of oxygen, passing the mixed gases over phosphorus peroxide and condensing the oxides of nitrogen in a trap cooled to − 80° C. Oxygen was bubbled through the liquid cooled to − 8° C for 3 hr. to remove traces of nitrous anhydride, and the residue was fractionally distilled *in vacuo*, the middle fraction being stored at − 80° C until required in a bulb connected to the main apparatus.

Practical methods

In the preparation of samples of gas containing accurately known small concentrations of nitrogen peroxide or hydrogen, a measured pressure of either sensitizer was first admitted to a subsidiary bulb and diluted with a large excess of oxygen. Requisite amounts of the dilute mixture were then admitted to the final reservoir, followed by extra carbon monoxide and oxygen.

Induction periods were measured with an ordinary stop-watch from the time of opening the tap between the final mixing vessel and the reaction vessel, to the time of appearance of a flash seen through the window in the entry tube or a movement of the beam of light from the mirror gauge.

The percentage combustion of an ignited mixture was conveniently determined by withdrawing the residual gases from the furnace through a spiral cooled in liquid air. The amount of carbon dioxide collected could be estimated from the pressure shown on the mirror gauge when the gas was allowed to expand into the volume occupied by the spiral, the gauge diaphragm and the connecting tubing. From a knowledge of the volume of the bulb of the reaction vessel, as little as 0·1 % combustion could be detected and measured in this way.

In certain experiments it was desirable to know whether the steady chain reaction between carbon monoxide, oxygen and nitrogen peroxide was due in any way to unavoidable traces of hydrogen introduced during preparation of the gases. It is reasonable to suppose that if hydrogen did participate in the propagation of reaction chains in such mixtures, it would itself be oxidized to water as the reaction proceeded. Accordingly, after reaction had continued for several minutes, the partially oxidized gases were withdrawn slowly through a spiral cooled in liquid nitrogen to remove traces of water vapour and nitrogen peroxide, and stored over mercury in the Toepler pump. Gases subjected to such pretreatment were then resensitized with nitrogen peroxide, and the rate of reaction compared with that obtained using "ordinary" gases.

EXPERIMENTAL RESULTS

The experimental evidence may be divided into two main groups. The first deals with the variation with experimental conditions of induction periods prior to ignition or slow reaction in mixtures of carbon monoxide and oxygen under the combined sensitizing influence of nitrogen peroxide and hydrogen. The second is an extension of the work of Crist and Roehling (1935) and Crist and Calhoun (1936) on the slow reaction occurring in hydrogen-free mixtures of carbon monoxide and oxygen in the presence of nitrogen peroxide alone.

Sensitization by hydrogen and nitrogen peroxide

The work of Gibson and Hinshelwood (1928), Thompson and Hinshelwood (1929), Norrish and Griffiths (1933), and Foord and Norrish (1935) has shown that nitrogen peroxide can reduce the temperature of ignition of oxy-hydrogen mixtures from above 460° C to below 350° C, while recent work by Buckler and Norrish (1938) has demonstrated that traces of hydrogen reduce the ignition temperatures of carbon monoxide and oxygen from above 650 to about 480° C. It is reasonable to suppose therefore that two sets of branching chain reactions are possible in mixtures of carbon monoxide, oxygen, hydrogen and nitrogen peroxide. Below 460° C explosions may be produced by the mechanism responsible for ignition in oxy-hydrogen mixtures sensitized by nitrogen peroxide, while above that temperature the branching chain reactions occurring during ignition of unsensitized hydrogen and oxygen may also come into play. Accordingly, comparable experiments have been performed at about 350° C and above 500° C to investigate the relative importance and interaction of these two mechanisms.

Effect of water vapour and hydrogen

In fig. 3 is shown the variation of induction periods with hydrogen pressure at 357° C and 150 mm. total pressure and at 500° C and 23·7 mm. total pressure in mixtures of $2CO + O_2$ containing constant partial pressures of nitrogen peroxide. The results are interesting in that an abrupt transition was observed from slow reaction to ignition as the hydrogen pressure was increased, without any accompanying discontinuity in the values of the induction periods. In both regions the induction periods were terminated by a sudden slight increase of pressure followed by ignition or reaction, after which the pressure fell as the products reassumed isothermal conditions. It is seen that the hydrogen pressure at which transition from slow reaction to ignition occurs is greatly reduced by increase of temperature, but both curves indicate that ignition becomes impossible in hydrogen-free mixtures.

A similar continuous variation of induction periods in passing from a region of slow reaction to one of ignition was obtained using water vapour instead of hydrogen as shown in fig. 4 which was obtained at 500° C and 22·2 mm. Hg total pressure. These results confirm those of Sagulin *et al.* (1930) that nitrogen peroxide reduces the ignition temperatures of moist carbon monoxide and oxygen, since the present experiments were performed 150° C below the ignition temperature of the pure gases. An unusual example is provided here of ignition catalysis produced in the presence of two

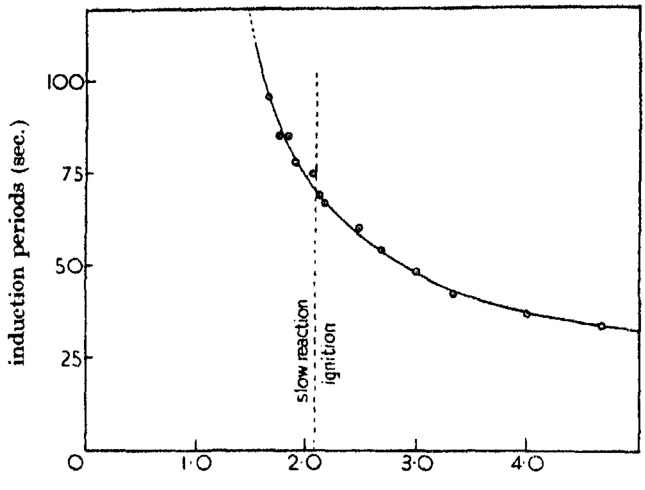

Temperature = 357° C; pressure of $2CO + O_2$ = 100 mm. Hg; pressure of NO_2 = 0·114 mm. Hg.

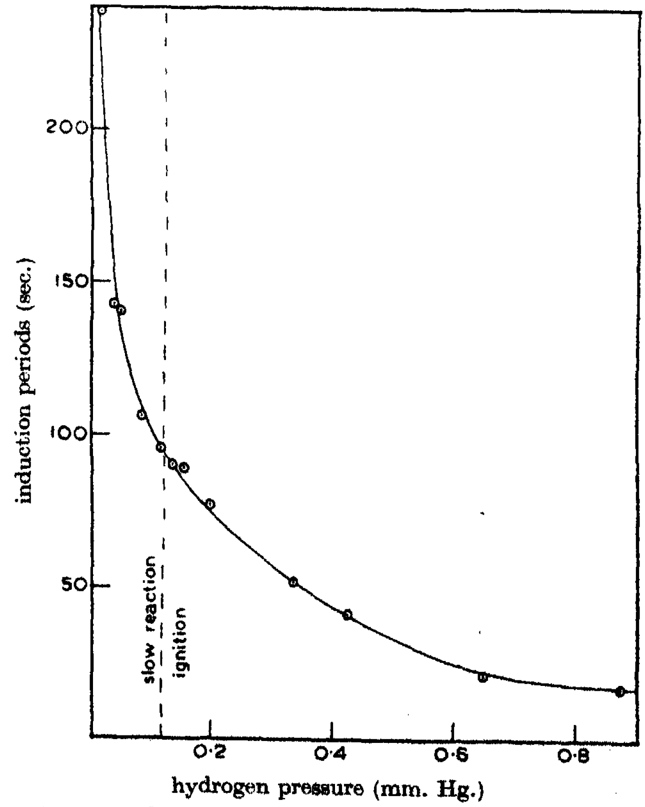

Temperature = 500° C; pressure of $2CO + O_2$ = 23·7 mm. Hg; pressure of NO_2 = 0·29 mm. Hg.

Fig. 3. Variation of induction periods with hydrogen pressure in mixtures of $2CO + O_2$ containing constant partial pressures of nitrogen peroxide.

substances, neither of which alone affects the ignition temperatures of the pure gases.

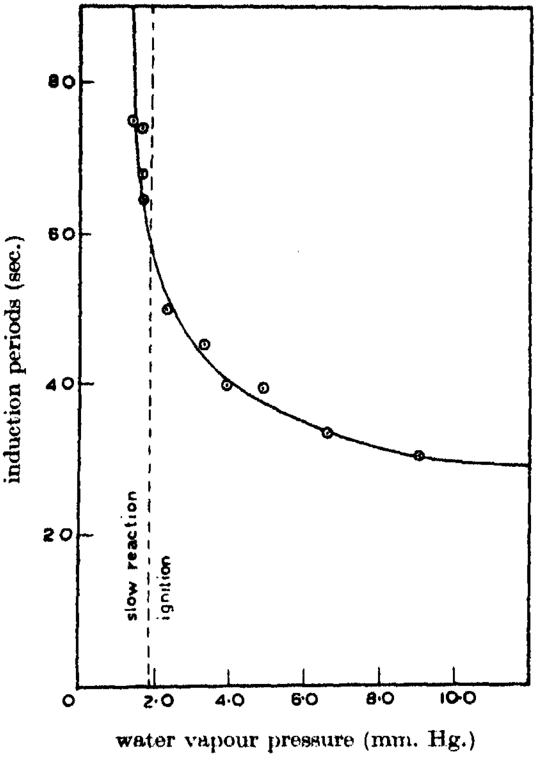

Fig. 4. Variation of induction periods with water vapour pressure. Temperature = 500° C; pressure of $2CO + O_2 = 22 \cdot 2$ mm. Hg; pressure of $NO_2 = 0 \cdot 27$ mm. Hg.

Effect of nitrogen peroxide

The effect of increasing concentrations of nitrogen peroxide on the induction periods prior to ignition or slow reaction in mixtures of $2CO + O_2$ at 150 mm. total pressure and 357° C is shown by the two curves of fig. 5, which were obtained using mixtures containing constant partial pressures of oxy-hydrogen gas of 5·0 mm. and 10·0 mm. respectively. The results are of similar form to those obtained by Foord and Norrish (1935) at the same temperature and total pressure using mixtures of hydrogen and oxygen, and demonstrate once more the dual role of nitrogen peroxide as catalyst and anti-catalyst. It may be noted as a difference in detail that while the curves obtained using oxy-hydrogen mixtures are characterized by an upper and a lower critical concentration of nitrogen peroxide between which explosion occurs and outside which the induction periods are terminated by slow reaction, the present results demonstrate only a lower critical limit of this nature, whereas the upper critical concentration appears to represent a boundary between a region of explosion and one of complete stability.

When the temperature was raised to 540° C it was noticed that a faint

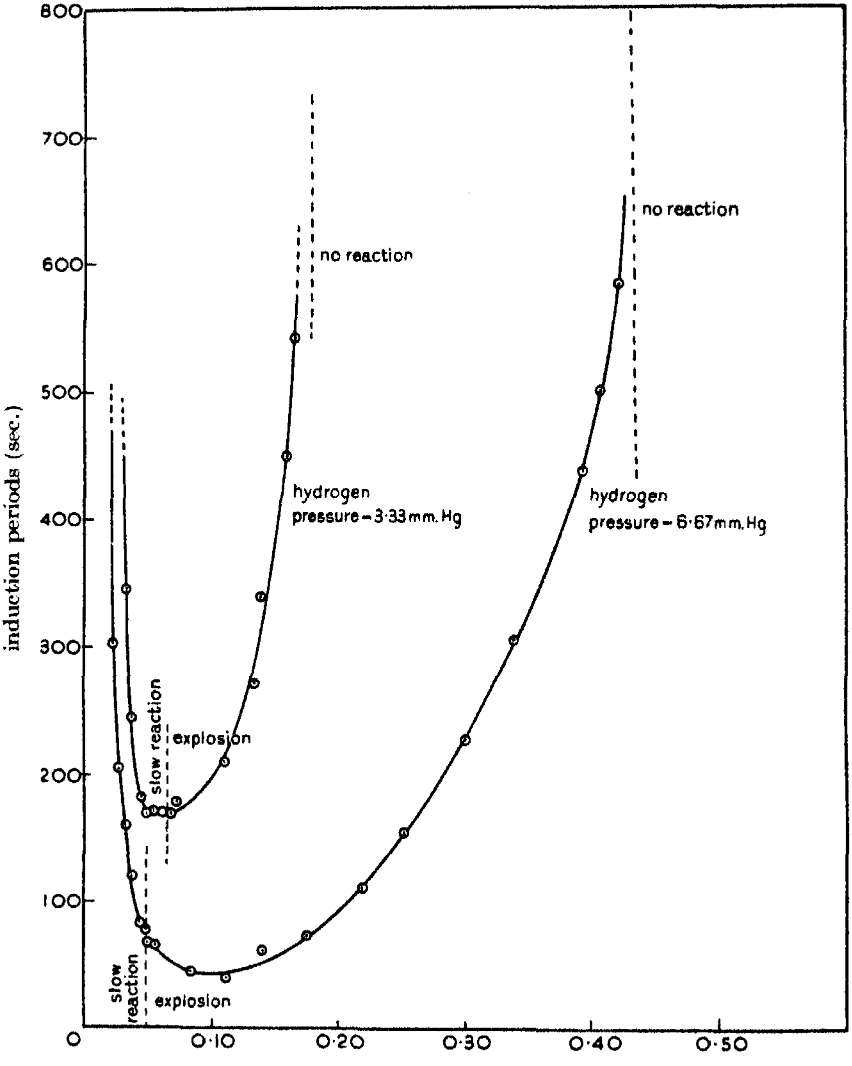

Fig. 5. Variation of induction periods with concentration of nitrogen peroxide in mixtures of carbon monoxide and oxygen containing constant partial pressures of hydrogen. Temperature = 357° C; pressure of $2CO + O_2$ = 150 mm. Hg.

blue flash occurred about 30 sec. after admission to the furnace of mixtures of $2CO + O_2$ containing nitrogen peroxide and no added hydrogen. The accompanying pressure changes were less than could be detected by the gauges, and the amount of carbon dioxide present in the gases after withdrawal proved to be negligible. The induction periods prior to the flash

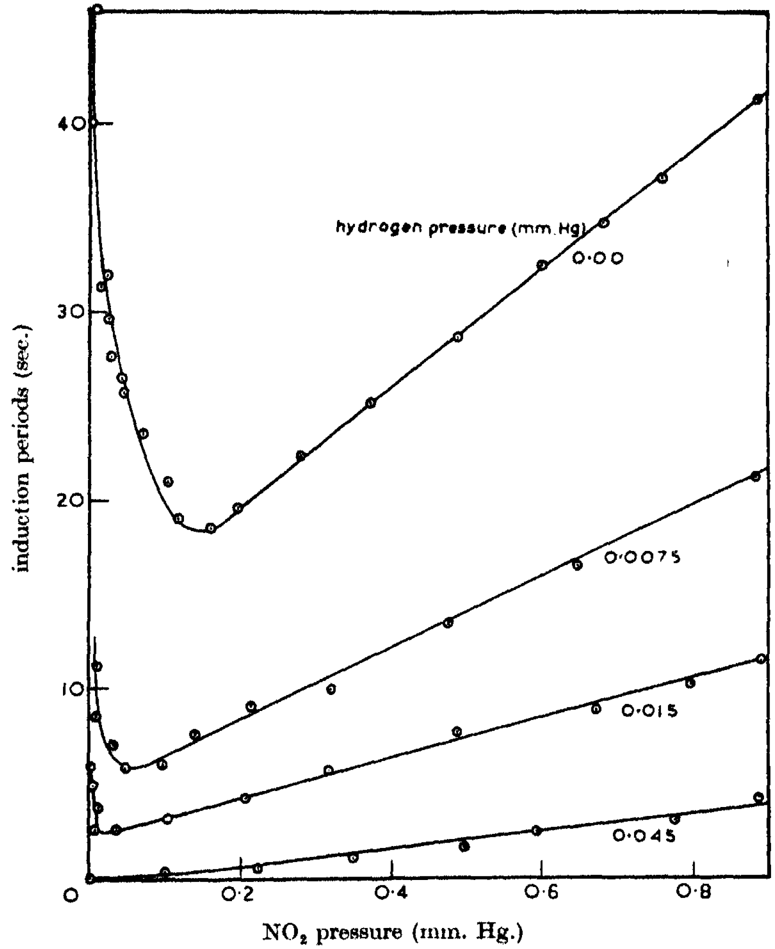

FIG. 6. Variation of induction periods with concentration of nitrogen peroxide in mixtures of carbon monoxide and oxygen containing constant partial pressures of hydrogen. Temperature = 540° C; pressure of $2CO + O_2$ = 70·0 mm. Hg.

varied with concentration of nitrogen peroxide in a manner shown in fig. 6 by the curve labelled Hydrogen pressure = 0·00 mm. The intensity of the flash was greatest near the minimum of the curve and decreased as the concentration of nitrogen peroxide was increased, until nothing could be detected above about 1·0 mm. NO_2. It was found that addition of only 0·01 % hydrogen reduced the induction periods considerably, as shown by the curve labelled Hydrogen pressure = 0·0075 mm., and also increased the intensity of the flash. In view of the extreme sensitivity of the reaction to traces of hydrogen it seems most probable that the faint blue flashes detected in mixtures containing no added hydrogen were due to presence of small quantities of this gas introduced during preparation of the carbon monoxide. However, the results themselves suggest that the carbon monoxide used in these experiments contained less than 1 part in 10,000 of hydrogen.

When the concentration of hydrogen was increased, each blue flash was accompanied by a marked decrease of pressure, until with a partial pressure of hydrogen exceeding 0·03 mm. the explosions produced over 70 % combustion. The remaining curves of fig. 6, obtained in mixtures of $2CO + O_2$ containing 0·015 mm. and 0·045 mm. of hydrogen respectively, demonstrate that at these higher temperatures appreciable concentrations of hydrogen reduce the induction periods to zero when no nitrogen peroxide is present, and mask the catalytic action of the latter sensitizer, leaving it with only a resultant inhibitory effect.

The effect of carbon monoxide and nitrogen

In fig. 7 are shown two curves expressing the variation of induction periods with total pressure at 380° C in mixtures containing 50 mm. of $2H_2 + O_2$ and 0·25 mm. NO_2 to which carbon monoxide and nitrogen respectively have been added as diluent gases. Since these two gases possess almost identical physical constants, the differences between the two sets of results must be ascribed to participation of carbon monoxide in the elementary processes leading up to ignition. It is seen that the induction periods obtained in mixtures diluted with carbon monoxide are shorter than those for corresponding mixtures containing nitrogen, and that the transition from explosion to slow reaction occurs at a higher total pressure in the former than in the latter system. The minimum in the curve expressing the variation of induction periods with total pressure in mixtures diluted with carbon monoxide indicates that this gas possesses a mild sensitizing influence which is not shown by nitrogen, and which cannot be due to any change in the thermal or physical characteristics of the system.

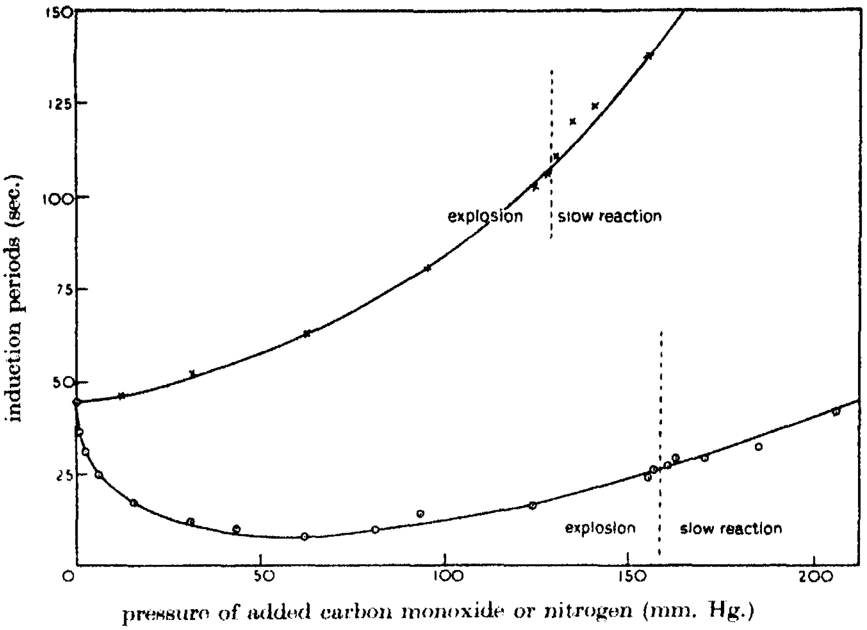

FIG. 7. The effects of added carbon monoxide and nitrogen on the NO_2-sensitized ignition of oxy-hydrogen mixtures. Temperature = 380° C; pressure of $2H_2+O_2$ = 50 mm. Hg; pressure of NO_2 = 0·25 mm. Hg. × dilution with nitrogen; ⊙ dilution with carbon monoxide.

Sensitization by nitrogen peroxide alone

The results of the preceding section indicate that nitrogen peroxide acts as an ignition catalyst to carbon monoxide-oxygen mixtures only in the presence of water vapour or hydrogen, and that above 500° C detectable effects are produced by very small amounts of the latter gas. In view of the fact that traces of hydrogen are often produced during preparation of carbon monoxide, the question arises whether the catalytic and anti-catalytic influence of nitrogen peroxide on the high-pressure oxidation of carbon monoxide observed by Crist and Roehling (1935) is also due to the presence of small quantities of hydrogen. Since no convenient direct method is available for the rigorous purification of carbon monoxide, it was decided to subject sensitized mixtures to partial oxidation, freeze out the condensable products with liquid nitrogen, and use the residual gases as a source of pure reactants.

The rate of oxidation of carbon monoxide at 527° C and 600 mm. total pressure was studied using "ordinary" and "purified" mixtures by admitting gases to a pyrex reaction vessel 35 mm. diameter in the following order. 200 mm. of pure dry oxygen was established in the reaction vessel and followed by an appropriate amount of a dilute nitrogen peroxide-oxygen mixture measured by the gauges to give some chosen concentration of nitrogen peroxide between 0 and 2 mm. The latter component was swept into the bulb of the reaction vessel and the total pressure increased to 600 mm. by admitting dry carbon monoxide, and subsequent reaction was followed on the gauges for about 20 min. The contents of the reaction vessel were then extracted slowly through a spiral cooled in liquid air and stored in a Toepler pump. The experiment was repeated and the unoxidized gases added to those already collected. 200 mm. of gas obtained in this way was readmitted to the reaction vessel followed by a suitable quantity of dilute NO_2-O_2 mixture and the total pressure increased to 600 mm. with more purified $2CO + O_2$. The rates of reaction of such mixtures, as measured by the decrease of pressure during the interval 10–20 min. from the time of admission, and the rates of oxidation of freshly prepared carbon monoxide are shown in fig. 8 over the range of concentrations of nitrogen peroxide from 0 to 20 mm. Hg.

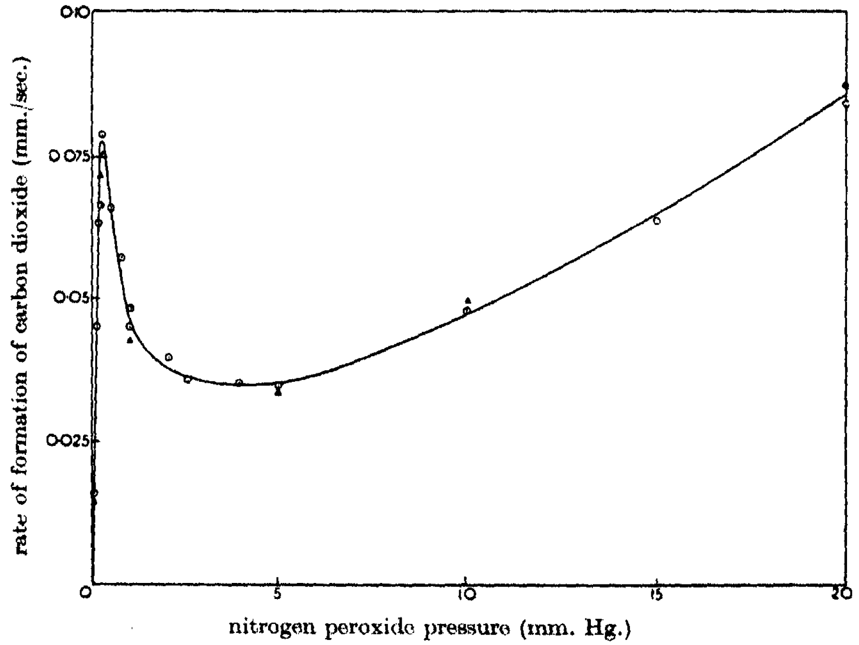

Fig. 8. The dependence of reaction rate in carbon monoxide-oxygen mixtures on concentration of nitrogen peroxide. Temperature = 527° C; total pressure = 600 mm. Hg. ⊙ "ordinary" mixtures; △ "purified" mixtures.

It is seen that no appreciable difference exists in the values for corresponding pairs of points, and that the dependence of reaction rate on concentration of nitrogen peroxide for both series of experiments can be expressed by the same curve. The results confirm those of Crist and Roehling (1935) in assigning to nitrogen peroxide a catalytic influence when its concentration is below 0·3 mm. or above about 2 mm., and a resultant inhibitory effect for intermediate values, and indicate that the elementary reactions responsible for these phenomena are not dependent on the presence of appreciable concentrations of molecular hydrogen. This evidence must not be taken as conclusive however, since in the preceding section it was shown that addition of only 0·01 % hydrogen at 540° C resulted in marked decrease of induction periods prior to the faint blue flashes observed in such mixtures at lower pressures. It will be realized also that the technique employed here does not include rigorous purification of the dilute nitrogen peroxide-oxygen mixture used for sensitizing the reactant gases, nor can it ensure exclusion of traces of water vapour from the system.

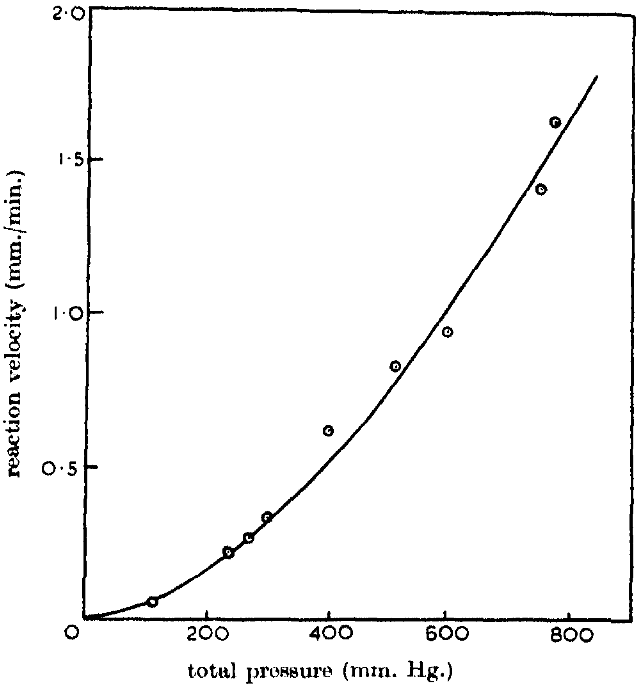

FIG. 9. Variation of reaction rate with total pressure. Temperature = 527°; pressure of NO_2 = 0·25 mm. Hg.

Since it is possible that later work may assign an independent mechanism to the catalytic influence of small concentrations of nitrogen peroxide on the slow reaction, it was decided to record the rate of sensitized oxidation in mixtures prepared by ordinary methods over a complete range of total pressures. In fig. 9 is shown the variation of reaction velocity with total pressure at 527° C in mixtures of $2CO + O_2$ containing 0·25 mm. of nitrogen peroxide. It is seen that the rate of reaction decreases steadily with decrease of pressure, giving no evidence of a region of ignition at low pressures.

Discussion

The results described in the present work and the relevant experimental evidence derived from other sources may be summarized as follows:

(1) In the presence of nitrogen peroxide the rate of oxidation of carbon monoxide prepared from ordinary sources becomes appreciable above 420° C. As the concentration of sensitizer is increased, the velocity of reaction at 527° C rises to a maximum at about 0·26 mm. NO_2, falls away to a minimum at about 1·5 mm. NO_2, and finally increases steadily as the pressure of nitrogen peroxide is increased above that value. This dependence of reaction rate on nitrogen peroxide concentration persists in mixtures which have been submitted to purification from traces of hydrogen as far as possible.

(2) The velocity of reaction in mixtures of carbon monoxide, oxygen and nitrogen peroxide decreases steadily with decrease of pressure at 527° C; nitrogen peroxide does not reduce the ignition temperatures of pure dry carbon monoxide and oxygen.

(3) Small concentrations of hydrogen reduce the ignition temperatures of pure carbon monoxide and oxygen from above 650° C to about 460° C, while addition of water vapour has no effect on the ignition temperatures.

(4) Ignition is possible below 350° C in mixtures of carbon monoxide, oxygen and nitrogen peroxide when hydrogen also is present, while explosions have been observed at 500° C when hydrogen is replaced by water vapour.

(5) Under conditions in which mixtures of carbon monoxide, oxygen and hydrogen do not ignite on entering the reaction vessel, addition of nitrogen peroxide gives rise to explosions preceded by induction periods which at first decrease and then increase with increasing concentrations of sensitizer, as shown in figs. 3 and 4.

(6) At temperatures sufficiently high to produce immediate ignition in mixtures of carbon monoxide, oxygen and hydrogen alone, the catalytic

action of nitrogen peroxide is masked leaving only a resultant inhibitory effect.

(7) Dilution of mixtures of hydrogen, oxygen and nitrogen peroxide with nitrogen lengthens the induction periods and ultimately converts ignition into slow reaction. When nitrogen is replaced by carbon monoxide the induction periods become generally shorter, and at first decrease and then increase as more diluent gas is added. The pressure of carbon monoxide required to suppress ignition is greater than the pressure of nitrogen required under otherwise similar conditions.

(8) An abrupt transition from ignition to slow reaction in mixtures of carbon monoxide, oxygen, hydrogen and nitrogen peroxide without any accompanying discontinuity in the values of the induction periods may be effected by dilution of the mixtures with inert gas or by suitable alterations in the concentration of either sensitizer.

These facts suggest that isothermal self-acceleration and explosion due to chain branching does not occur below 650° C in mixtures of carbon monoxide and oxygen sensitized by nitrogen peroxide alone. With the addition of traces of hydrogen to the CO-O_2-NO_2 system however, a new branching mechanism appears, and explosions preceded by induction periods can take place at temperatures more than 300° C below those required for ignition of pure carbon monoxide.

Previous work by Buckler and Norrish (1938) has shown that small quantities of hydrogen reduce the ignition temperatures of pure carbon monoxide and oxygen from above 650° C to about 460° C by introducing into the system the branching chain reactions responsible for explosion of oxyhydrogen mixtures. It is well known that nitrogen peroxide reduces the ignition temperatures of hydrogen and oxygen from above 460° C to about 300° C, hence it is reasonable to suppose that the catalytic influence of this substance on ignition in mixtures of carbon monoxide, oxygen, nitrogen peroxide and hydrogen is due to its ability to catalyse branching in the chain mechanism already made possible by hydrogen. It is concluded, therefore, that ignition in the present system between 300° C and 460° C is controlled by a chain-branching mechanism similar to that responsible for the nitrogen peroxide-sensitized explosion of hydrogen and oxygen, while at higher temperatures is regulated not only by this mechanism but also by the branching chain reactions occurring during explosion of oxy-hydrogen mixtures.

By incorporating the mechanism proposed by Foord and Norrish (1935) for the influence of nitrogen peroxide on the hydrogen-oxygen reaction into the theory developed by Buckler and Norrish (1938) for the ignition of mixtures of carbon monoxide and oxygen containing hydrogen, it is possible to formulate a scheme which will account satisfactorily for the influence of nitrogen peroxide on the latter system and explain the slight differences observed in the characteristics of reaction in H_2-O_2-NO_2 mixtures and in CO-H_2-O_2-NO_2 mixtures.

THEORY OF REACTION KINETICS

The general equation representing the rate of increase of centres in a chain reaction (Semenoff 1932; modified by Foord and Norrish 1935) is given by

$$\frac{dn}{dt} = \theta + \phi n - \delta n^2, \tag{1}$$

where θ = rate of production of chain centres by primary processes;
ϕ = difference between the probabilities of chain branching and deactivation exclusive of reactions of second order with respect to chain carrier concentration; and
δn^2 = rate of destruction of chain centres by self-neutralization processes.

Immediately after introduction of a mixture into the heated reaction vessel, the concentration of chain carriers increases exponentially until it attains a value n_c at which reaction becomes detectable. Shortly after this point an equilibrium is imposed on the number of chain centres owing to operation of self-neutralization processes. The induction period τ preceding detectable reaction may be derived from equation (1) as

$$\tau = \frac{1}{\phi}\log\left(1+\frac{n_c\phi}{\theta}\right), \tag{2}$$

while the equilibrium concentration of chain carriers is given by

$$n_e = \phi/\delta, \tag{3}$$

when ϕ^2 is large compared with $\delta\theta$.

The work of Foord and Norrish (1935) has shown that ignition sets in when the stable reaction consequent upon the equilibrium concentration of chain centres is sufficiently intense to impose adiabatic conditions in some favourable volume element of the reaction vessel. In other words, the general condition for ignition is

$$n_e > n_i, \tag{4}$$

where n_t is some critical concentration of chain centres, the value of which depends to some extent on the thermal characteristics of the gaseous mixture and the dimensions of the reaction vessel.

The following assumptions will be made in developing expressions for the dependence of induction periods on experimental conditions, the nomenclature being as closely as possible that employed by Foord and Norrish (1935).

Initiation of chains

Chains are initiated by primary processes such as

$$NO_2 = NO + O \quad (k_1). \tag{I}$$

Branching of chains

Oxygen atoms may be produced by either or both of the following chain-branching mechanisms:

(*a*) Above about 300° C a collision of an exothermic chain link and a nitrogen peroxide molecule may produce an oxygen atom without necessarily stopping the original chain, resulting in a nett branching if the oxygen atom starts a new chain or chains. The rate of production of chains by this mechanism may be represented as αnc, where

α = probability of chain branching,

n = concentration of chain centres,

c = concentration of nitrogen peroxide.

(*b*) Above 460° C a second mechanism of production of oxygen atoms may come into play

$$H + O_2 = HO + O.$$

The rate of this reaction may be written as $An[O_2]$, where A is the probability of the reaction.

Propagation of chains

Continued propagation of chains from oxygen atoms is possible only in the presence of molecular hydrogen by the reaction

$$O + H_2 = OH + H \quad (k_3), \tag{III}$$

followed by

$$OH + H_2 = H_2O + H,$$

$$OH + CO = CO_2 + H.$$

Chain ending

(*a*) Chains may be terminated by a suitable collision between a chain carrier and a nitrogen peroxide molecule at a rate given by βnc.

(*b*) Oxygen atoms may be removed by reaction with nitrogen peroxide

$$O + NO_2 = NO + O_2 \quad (k_2). \tag{II}$$

(*c*) Oxygen atoms may be removed by diffusion to the surface and by reactions such as

$$O + CO + M = CO_2 + M,$$

the rate of which together may be represented by $k_4[O]$.

(*d*) Other chain carriers may be removed by diffusion to the surface and by reactions such as

$$H + O_2 + M = HO_2 + M,$$

the rate of which may be represented by γn.

If the concentration of hydrogen is h, it follows that the instantaneous concentration of oxygen atoms is given by

$$[O] = \frac{k_1 c + \alpha nc + Anh[O_2]}{k_2 c + k_3 h + k_4}. \tag{5}$$

The rate of production of chain centres will be given by

$$\frac{dn}{dt} = k_3 h[O] - \beta nc - \gamma n - \delta n^2.$$

Substituting from equation (5) we obtain

$$\frac{dn}{dt} = \frac{k_1 k_3 hc}{k_2 c + k_3 h + k_4} + \left\{\frac{\alpha k_3 hc + Ak_3 h[O_2]}{k_2 c + k_3 h + k_4} - \beta c - \gamma\right\} n - \delta n^2, \tag{6}$$

which is of the same form as equation (1), where

$$\theta = \frac{k_1 k_3 hc}{k_2 c + k_3 h + k_4},$$

$$\phi = \frac{\alpha k_3 hc + Ak_3 h[O_2]}{k_2 c + k_3 h + k_4} - \beta c - \gamma. \tag{7}$$

Below 460° C the probability A of the reaction

$$H + O_2 = OH + O$$

becomes very small, and equation (7) simplifies to the same form as that deduced by Foord and Norrish (1935) for the value of the effective probability of chain branching in oxy-hydrogen mixtures sensitized by nitrogen peroxide. Above 500° C, however, the value of A is so large that in the presence of only small concentrations of hydrogen the term $Ak_3h[O_2]$, representing the rate of chain branching due to the presence of hydrogen, entirely predominates over the term αk_3hc, which represents the rate of chain branching by the less efficient mechanism involving nitrogen peroxide.

The effect of nitrogen peroxide

When the temperature is below 460° C the value of ϕ is given by

$$\phi = \frac{\alpha k_3 hc}{k_2c + k_3h + k_4} - \beta c - \gamma. \tag{8}$$

As shown by Foord and Norrish, insertion of this expression neglecting γ in equation (2) leads to the following equation for the induction periods prior to ignition or slow reaction:

$$\tau = \frac{c+k_5}{\beta c(k_6-c)} \log\left(1 + \frac{\beta n_c k_2(k_6-c)}{k_1k_3h}\right), \tag{9}$$

where

$$k_5 = \frac{k_3h+k_4}{k_2},$$

and

$$k_6 = \frac{\alpha k_3h - \beta k_3h - \beta k_4}{\beta k_2}.$$

This expression provides for a decrease of τ to a minimum value followed by an increase with increasing concentrations c of nitrogen peroxide in the range of conditions where ϕ is positive, and will account satisfactorily for the form of the curves shown in fig. 5.

The critical limits of nitrogen peroxide concentration between which induction periods are terminated by explosion will be determined by the values of c for which the value of ϕ given by the right-hand side of equation (8) exceeds a critical amount ϕ_c. It is to be expected that the critical intensity of reaction, determined according to equation (3) by ϕ_c, required to impose adiabatic conditions on the system, will be smaller the lower the thermal conductivity of the gaseous mixtures. Accordingly, the induction periods in the region of transition from ignition to slow reaction in sensitized mixtures of $2CO + O_2$ containing a small percentage of hydrogen should be much longer than those observed using oxy-hydrogen mixtures under similar conditions, since the thermal conductivity of the latter system is approximately four times that of the former. This is confirmed by a comparison of the curves shown in fig. 5 with those obtained by Foord and Norrish (1935) using sensitized mixtures of hydrogen and oxygen at the same temperature and total pressure. The upper critical limit of nitrogen peroxide in the latter system represents a boundary between a region of ignition and one of measureable slow reaction in which the induction periods have a duration of about 50 sec., while in the present system it is associated with a transition from a region of ignition preceded by induction periods up to 600 sec. to one in which steady reaction is so small that the length of the induction period and the moment at which chemical change begins cannot be determined.

When the temperature is raised above 500° C the value of $Ak_3h[O_2]$ in equation (7) entirely predominates over the αk_3hc term, and the value of ϕ in mixtures containing no nitrogen peroxide is positive when

$$\frac{Ak_3h[O_2]}{k_3h+k_4}>\gamma,$$

a condition which is fulfilled at low pressures by all but the most minute values of h. Under such circumstances mixtures of $2CO+O_2$ sensitized by hydrogen alone ignite immediately on admission to the heated reaction vessel. When nitrogen peroxide is also present its catalytic action is masked leaving only the resultant inhibitory effect, represented by the term βc, and the variation of induction periods with concentration of the latter sensitizer is given by

$$\tau=\frac{1}{X-\beta c}\log\left(1+n_c\frac{X-\beta c}{\theta}\right),$$

where X is a constant. This equation accounts satisfactorily for the form of the curve shown in fig. 6 for which the hydrogen pressure = 0·045 mm. Hg.

When the concentration of hydrogen is less than that required to produce immediate ignition in mixtures admitted to the reaction vessel it is possible to demonstrate the catalytic effect of nitrogen peroxide, as seen from the remaining curves of fig. 6. Under such circumstances, however, the concentration of hydrogen is so small that an insufficient number of free radicals is available to permit continued propagation of reaction chains, and chemical change is restricted to a feeble flash accompanied by a negligible degree of combustion.

The effect of hydrogen

Examination of equation (7) will show that in mixtures containing a constant partial pressure of nitrogen peroxide, the value of ϕ may be written

$$\phi=\frac{h}{k_7+k_8h}-k_9,$$

where $k_7=\dfrac{k_2c+k_4}{\alpha k_3c+Ak_3[O_2]}$, $k_8=\dfrac{k_3}{\alpha k_3c+Ak_3[O_2]}$ and $k_9=\beta c+\gamma$.

Variations in the logarithm term of equation (2) will not be important in determining the value of τ when ϕ has a finite positive value, and under such circumstances the variation of τ with hydrogen concentration is given by

$$\tau = \frac{\text{const.}}{\dfrac{h}{k_7 - k_8 h} - k_9}.$$

This equation predicts that the curve relating τ and h should be of approximately hyperbolic form, that τ should become small and constant as h is indefinitely increased, and that $\tau \to \infty$ when h is reduced below a finite positive value. Furthermore, it will be seen from equation (7) that as h is decreased the value of ϕ decreases steadily until, according to the general theory of ignition given by Foord and Norrish (1935), a point is reached at which the burst of reaction at the end of the induction periods is insufficient to establish adiabatic conditions and the concentration of chain centres settles down to a steady value due to operation of self-neutralization processes. The deductions are in complete agreement with the experimental results shown in the two diagrams of fig. 3, which were obtained at 357° C and 500° C respectively, using mixtures of $2CO + O_2$ containing constant concentrations of nitrogen peroxide.

The effect of water vapour

Addition of water vapour to mixtures of carbon monoxide and oxygen increases the velocity of steady oxidation but has no effect on the limits of ignition (cf. Hadman *et al.* 1932*a*, *b*; Sagulin *et al.* 1930; Cosslett and Garner 1930). It is evident therefore that while water vapour may supply free radicals necessary for continued propagation of reaction chains, it introduces no additional means of chain branching to carbon monoxide-oxygen mixtures. As was pointed out by von Elbe and Lewis (1937), the "water gas" reaction

$$CO + H_2O = CO_2 + H_2,$$

proposed by Hadman *et al.* (1932*a*) as the primary process in the catalytic action of water vapour, must be rejected, since the subsequent reaction

$$O + H_2 = OH + H$$

would lead to multiplication of chains. It may be supposed that water vapour gives rise to an equilibrium concentration of H atoms and OH radicals which facilitate the propagation of unbranched chains in carbon *monoxide-oxygen mixtures by the following series of reactions:*

$$CO + OH = CO_2 + H + 24\,\text{kcal.}$$

$$H + O_2 + M = HO_2 + M + 44\,\text{kcal.}$$

$$HO_2 + CO = CO_2 + OH + 66\,\text{kcal.}$$

It will be observed that since the thermodynamic equilibrium between H_2O, H and OH is not affected by the presence of CO, no chain branching reactions can result from the above mechanism.

However, the results shown in fig. 4 indicate that in the presence of nitrogen peroxide the reaction in moist carbon monoxide-oxygen mixtures assumes a self-accelerative character, manifested in the induction periods terminated by ignition. In such a system disruption of nitrogen peroxide into nitric oxide and oxygen atoms will occur by collision with excited chain carriers or exothermic chain links, and it may be supposed that subsequent multiplication of reaction chains may occur through the almost thermoneutral reaction

$$O + H_2O = 2OH.$$

Thus the process of branching made possible by nitrogen peroxide will derive its energy from the exothermic character of the carbon monoxide oxidation. It may be noted that if later experiments confirm that the maximum in the curve expressing dependence of reaction rate in CO-O_2-NO_2 mixtures on nitrogen peroxide concentration is due to the presence of water vapour, the kinetic mechanism outlined here would account satisfactorily for the form of the curves shown in fig. 8.

The effect of nitrogen and carbon monoxide

As shown in fig. 7 the induction periods prior to ignition of mixtures of hydrogen and oxygen sensitized by nitrogen peroxide are gradually increased by addition of nitrogen, while explosion is eventually replaced by slow reaction. These results confirm those of Foord and Norrish (1935) who suggest that the quenching of ignition by addition of inert gases is due to an increase in the number of ternary collisions involving recombination of chain centres. It will be seen by reference to equation (3) that an increase in δ will depress the equilibrium value n_e to which the concentration of reaction centres tends at the end of the induction periods. Addition of increasing amounts of inert gas will therefore eventually reduce the intensity of chemical change sufficiently to replace ignition by stable reaction. The effect of nitrogen in increasing the induction periods indicates also that it has some small influence in reducing the effective probability of chain branching.

It will be seen in fig. 7 that the induction periods of oxy-hydrogen mixtures sensitized by nitrogen peroxide and containing carbon monoxide, are generally shorter than those of similar mixtures in which carbon monoxide is replaced by the same quantity of nitrogen, while a greater pressure of the former gas is required than the latter to convert explosion into slow reaction. Since the physical constants of carbon monoxide and nitrogen are almost identical, any differences observed in the behaviour of mixtures containing these two gases must be ascribed to participation of carbon monoxide in the reaction chains. The initial decrease in the induction periods observed in mixtures diluted with increasing amounts of carbon monoxide suggests that in addition to its diluent effect, this gas also possesses a mild sensitizing action and tends to increase the probability of chain branching. It will be recalled that the mechanism of chain branching in this reaction involves disruption of nitrogen peroxide molecules by collision with excited chain carriers or exothermic chain links. Reference to the following table will show that carbon monoxide introduces into the system a series of elementary reactions which are more exothermic than any of the corresponding reactions involving hydrogen.

$H + O_2 + M = HO_2 + M + 44\,\text{kcal.}$	
$HO_2 + OH = H_2O + O_2 + 57\,\text{kcal.}$	$HO_2 + CO = CO_2 + OH + 66\,\text{kcal.}$
$OH + H_2 = H_2O + H + 15\,\text{kcal.}$	$OH + CO = CO_2 + H + 24\,\text{kcal.}$
$O + H_2 = OH + H + 3\,\text{kcal.}$	$O + CO + M = CO_2 + M + 127\,\text{kcal.}$

It is to be expected therefore that participation of carbon monoxide in the reaction chains will increase the proportion of collisions between excited chain carriers or exothermic chain links and nitrogen peroxide molecules resulting in disruption of the latter into nitric oxide and oxygen atoms. No new chain-branching reactions are introduced by carbon monoxide, but it is seen that its presence facilitates the existing mechanism of multiplication of reaction centres. In terms of the foregoing theory therefore, addition of increasing amounts of carbon monoxide at first increases the value of α in equation (9) and later decreases the value of ϕ and increases that of δ by inert gas effects of similar nature and order of magnitude to those exerted by nitrogen.

CONCLUSION

The results described above confirm the view that branching of reaction chains in mixtures of carbon monoxide, oxygen and nitrogen peroxide at temperatures below those required for ignition of pure carbon monoxide and oxygen is possible only when hydrogen or water vapour also is present. Traces of hydrogen reduce the ignition temperatures of carbon monoxide and oxygen from above 650 to about 470° C by introducing the branching chain mechanism responsible for ignition of oxy-hydrogen mixtures. Under the additional sensitising influence of nitrogen peroxide, ignition is possible in CO-O_2-H_2-NO_2 mixtures at 357° C, and appears to be controlled by the branching chain reactions responsible for the nitrogen peroxide-sensitized explosion of hydrogen and oxygen at this temperature.

It also appears that steady reaction may occur above 420° C at high pressures in CO-O_2-NO_2 mixtures which have been submitted to purification from traces of hydrogen. However, in view of the extreme sensitivity of the reaction to hydrogen or water vapour, it must at present remain undecided whether oxidation in mixtures of carbon monoxide and oxygen containing less than about 1·5 mm. NO_2 proceeds by an independent chain mechanism or whether it is conditioned by minute traces of such substances as hydrogen or water vapour which are known to catalyse chain propagation in such mixtures.

SUMMARY

It has been found that nitrogen peroxide does not sensitize the ignition of pure dry carbon monoxide and oxygen, but that under the combined influence of nitrogen peroxide and hydrogen explosions occur over 300° C below the temperatures required for ignition of the pure gases. The sensitized explosions are preceded by induction periods which at first decrease and then increase with increasing concentrations of nitrogen peroxide. The dependence of induction periods on concentration of hydrogen and presence of foreign gases has been studied and supports the view that explosion of CO-O_2-NO_2-H_2 mixtures is due to a chain branching mechanism similar to that occurring in the nitrogen peroxide sensitized ignition of hydrogen and oxygen. At 500° C explosions also occur in CO-O_2-NO_2 mixtures containing water vapour, by a chain mechanism in which it has been suggested that water catalyses chain propagation while nitrogen peroxide is responsible for chain branching.

The work of Crist and others has shown that nitrogen peroxide induces steady oxidation in mixtures of pure $2CO + O_2$ at 750 mm. total pressure and

527° C, and that its catalytic action falls into two parts: (1) a catalysis governed by the two homogeneous reactions

$$CO + NO_2 = CO_2 + NO,$$

$$2NO + O_2 = 2NO_2,$$

which are important when the concentration of nitrogen peroxide exceeds about 1·2 mm.; (2) a catalysis at lower concentrations of nitrogen peroxide which passes through a maximum and has the characteristics of a chain reaction. These results have been confirmed using mixtures purified from traces of hydrogen. It was shown that the catalytic and anti-catalytic effects of small concentrations of nitrogen peroxide in this reaction is not dependent on the presence of traces of hydrogen. However, in view of the extreme sensitivity of the reaction to the presence of the free radicals H and OH derived from water, which are known to catalyse the propagation of straight chains, it is believed that the catalysis has its origin in a branching reaction introduced by the nitrogen peroxide, identical in characteristics with that operating in the catalysis of oxy-hydrogen mixtures by nitrogen peroxide, i.e. by its dissociation through participation as a third body in some exothermic link of the chain. Also, if complete dryness were possible it is to be expected that the catalytic and anti-catalytic effects of nitrogen peroxide at small concentrations of the latter would disappear.

The results obtained using CO-O_2-NO_2-H_2 mixtures furnish another example of a reaction in which the probability of chain branching is small and under precise control, and support the view that the ultimate cause of ignition is a disturbance of thermal equilibrium in some favourable volume element of the reaction vessel.

REFERENCES

Bone, W. A. 1931 *J. Chem. Soc.* **1**, 338.
Buckler, E. J. and Norrish, R. G. W. 1938 *Proc. Roy. Soc.* A, **167**, 292.
Cosslett, V. E. and Garner, W. E. 1930 *Trans. Faraday Soc.* **26**, 190.
Crist, R. H. and Calhoun, G. M. 1936 *J. Phys. Chem.* **4**, 696.
Crist, R. H. and Roehling, O. C. 1935 *J. Amer. Chem. Soc.* **57**, 2196.
Foord, S. G. 1934 *J. Sci. Instrum.* **2**, 126.
Foord, S. G. and Norrish, R. G. W. 1935 *Proc. Roy. Soc.* A, **152**, 196.
Garner, W. E. and Bawn, C. E. H. 1932 *J. Chem. Soc.* p. 129.
Garner, W. E. and Hall, D. A. 1930 *J. Chem. Soc.* p. 2037.
Garner, W. E. and Johnson, C. H. 1927 *Phil. Mag.* **3**, 97.
Garner, W. E. and Roffey, F. 1929 *J. Chem. Soc.* p. 1123.
Gibson, C. H. and Hinshelwood, C. N. 1928 *Trans. Faraday Soc.* **24**, 559.

Hadman, G., Thompson, H. W. and Hinshelwood, C. N. 1932*a* *Proc. Roy. Soc.* A, **137**, 87.
— — — 1932*b* *Proc. Roy. Soc.* A, **137**, 97.
Norrish, R. G. W. and Griffiths, J. G. A. 1933 *Proc. Roy. Soc.* A, **139**, 147.
Sagulin, A., Kowalsky, A., Kopp, D. and Semenoff, N. 1930 *Z. phys. Chem.* B, **6**, 307.
Semenoff, N. 1932 *Phys. Z. Sowjet.* **1**, 725.
Thompson, H. W. and Hinshelwood, C. N. 1929 *Proc. Roy. Soc.* A, **124**, 219.

The mobility of alkali ions in gases

I. The attachment of water molecules to alkali ions in gases

By R. J. Munson and A. M. Tyndall, F.R.S.
H. H. Wills Physical Laboratory, University of Bristol

(*Received* 18 *April* 1939)

Introduction

Measurements of the mobility of gaseous ions carried out in the Wills Laboratory at Bristol have shown that a positive ion which at birth is a charged atom or molecule remains in its monomolecular state when the gas is pure. The relation between the mass of the ion and its mobility has been determined in a number of gases. In the presence of polar impurities each ion collects a cluster of molecules of impurity, so that it moves more slowly in an electric field. The purpose of this paper is to describe experiments made to study the formation of the clusters and the number of molecules they contain.

Early experimenters measured the mobility of clustered ions, but their values cannot be used for this purpose because the nature and concentration of the impurities present were unknown and uncontrollable. The only way of studying the problem is to use an apparatus made entirely of glass and metal, cleaned by a "bake out" and with tap grease and other contamination excluded. Controlled amounts of a known polar impurity can then be added to the pure gas. The experiments here described have been made at room temperature on the alkali positive ions in the inert gases with water vapour as the polar impurity.

METHOD AND PROCEDURE

The procedure adopted may be followed from fig. 1. S is a source of positive ions from a hot surface surrounded by a cooling jacket not shown in the figure. These ions are dragged through a grid G_1 into an "ageing" field E_1 between G_1 and G_2 maintained uniform by guard rings at intermediate potentials. The time spent by the ions in this region and hence the number of collisions they make with molecules of impurity when these are present will depend upon the values of the concentration, field, gas pressure and mobility. At G_2 they enter the mobility measuring chamber which we shall call the analyser. G_2 and G_3 diagrammatically represent shutters which periodically open and close with a frequency ν. The details of their action, which is electrical and not mechanical, are given in previous papers (Tyndall and Powell 1930).

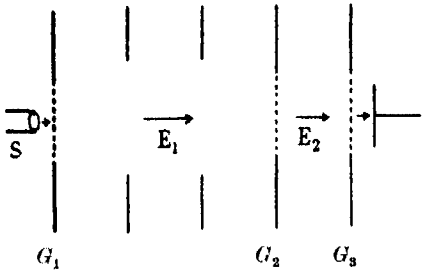

FIG. 1

When G_2 opens a thin layer of ions is transmitted and travels to G_3 in a steady uniform field E_2. If when this layer arrives G_3 is open, the ions pass on to the electrometer. If G_2 and G_3 work 180° out of phase, then the condition that the layers shall be transmitted through G_3 is that the ions shall travel from G_2 to G_3 in $\frac{1}{2}, \frac{3}{2}, \frac{5}{2}, \ldots$ periods of the oscillation. If, therefore, the electrometer current is plotted with ν a series of peaks are obtained which may be conveniently referred to by the optical analogy as orders in the mobility spectrum. If the ions in the layer are of more than one type, each type will give its own series of peaks. The conditions necessary to secure maximum resolving power for the separation of the component groups have already been discussed (Powell and Brata 1932).

Some earlier observations (Powell and Brata 1932) on sodium ions in nitrogen containing a trace of hydrogen gave evidence of the existence of an ion of mass 40 presumably due to the production of ammonia at the hot surface of the source and the attachment of one molecule to give an ion $Na^+(NH_3)$. Some indication was also obtained of the presence of a smaller number of ions with two ammonia molecules attached. It was therefore hoped that by varying either the life of the ion in the presence of water vapour impurity or the concentration of the impurity, the mobility spectrum might be used to watch the growth of a cluster up to its full complement of molecules. Unfortunately, it was impossible to construct the apparatus so that the time of measurement was small compared with the previous life of the ion. But, from the results given below, it will be seen that this has no serious consequences.

EXPERIMENTAL DETAILS

The dimensions of the apparatus were as follows:

$$SG_1 = 2\,\text{mm.},\quad G_1G_2 = 3\,\text{cm.},\quad G_2G_3 = 1\,\text{cm.}$$

The shutters G_1 and G_2 each consisted of grids 1 mm. apart. The external and internal diameters of the guard rings were 4 and 1 cm. respectively. The diameter of the pyrex container was 6 cm. The pressures employed were of the order of 4 to 2 mm. in Xe and of 25 to 5 mm. in He. The frequencies employed ranged from 120 to 2 kc.

To avoid contamination by vapours from tap grease which might contribute to the clusters, no taps were included in the apparatus except in the pumping plant. The admission of gas and of water vapour was all controlled by mercury U-tube cut-offs.

Previous experiments in this laboratory on alkali ions had been carried out with Kunsman sources. But some preliminary measurements with a Cs source of this type showed that it strongly decomposes water vapour, owing presumably to chemical action by its hot iron oxide surface. In one case in pure water vapour at a few mm. pressure, as much as 30 % decomposition occurred in a 10 min. run. With a lithium source it would have been even worse because a higher source temperature is necessary. Since it takes this time to make a mobility measurement, the use of such sources was therefore out of the question.

Blewett and Jones (1936) suggested a glass source for lithium ions which is far more satisfactory. We have successfully extended their method to the preparation of similar sources of all the other alkalis. The glass was a melt of Al_2O_3, SiO_2 and the oxide of the appropriate alkali in the proportions of 1 to 2 to 1 by weight produced by heating aluminium nitrate, alkali carbonate and powdered quartz with a blowpipe in a carbon crucible until the greater part of the CO_2 and water had been given off. The glass bead then formed was powdered and reheated several times. After a final powdering it was pasted into a tungsten spiral which had been flashed *in vacuo*, using water as a binder. A current through the spiral caused the powder to fuse into a bead of about 2 cu. mm. volume around the wire. After a preliminary ageing to remove ions of heavier alkalis, such sources gave pure and steady emission of the order of 2μA for hundreds of hours. Also, the 30 % decomposition recorded with a Kunsman source was reduced to 0·2 % with a caesium glass source and to 1 % with lithium. This reduction is no doubt due to the different nature of the surface and to its lower running temperature. But it was important that the products of even slight decomposition should not be allowed to accumulate in a succession of experiments. A tungsten spiral at yellow heat was therefore run in a side tube in another part of the apparatus. At its surface a balanced reversible reaction between oxygen, hydrogen and water will occur. By cooling the lower part of the tube containing the spiral in liquid oxygen so as to condense the water which is formed, practically the whole of the oxygen and hydrogen can be recombined. This treatment was of course carried out after and not during a mobility measurement. When the heating current was cut off and the liquid oxygen bath removed, the water content of the gas was restored to its original value by evaporation. The hot spiral also served another purpose by removing small traces of oxygen which accompany the emission of ions from this type of source. If these are allowed to accumulate they reduce the life of the source by oxidising the exposed parts of its tungsten leads.

DETERMINATION OF WATER CONCENTRATION

Only approximate estimations of most of the small concentrations of added water vapour can be given for the following reasons. When a small trace of water vapour was first admitted to the baked out apparatus no pressure was recorded because practically all of the water was taken up in an adsorbed film on the walls. For instance, in order to secure a vapour pressure of 0·007 mm. it was necessary to add between four and five times this amount to the apparatus. For the measurement of vapour pressure a McLeod gauge is not suitable because owing to increase of surface adsorption when the water vapour is compressed its full pressure is not recorded. A type of Rayleigh gauge, used by Schrader and Ryder (1919), with an optical level method of magnifying the movement of a mercury surface in a large U-tube was therefore employed, by which McLeod gauge readings were calibrated over a range of pressures; but the gauge was not as sensitive as could have been wished at the lower pressures which are therefore subject to some error. The lowest concentration was obtained by using a side tube containing ice immersed in a bath of CO_2 slush at −78° C so that the apparatus was filled with the pressure of saturated water vapour at this temperature. The value of this pressure given in standard tables is 0·0004 mm.

The procedure adopted was to add the vapour in the first case to an evacuated apparatus, measure its pressure and then add gas. The further assumption, which may not be justified, has to be made that the addition of gas does not alter the water vapour concentration by altering the conditions of its equilibrium with the adsorbed film. Another possible source of error may arise at low concentrations. When the source is running, the surfaces in its immediate neighbourhood may be slightly raised in temperature despite the surrounding cooling jacket. If so, some evaporation may take place from the adsorbed film and increase the concentration above its measured value in the region where ageing of the ion occurs.

RESULTS

Having selected a given concentration of water vapour a series of current frequency graphs were obtained for different values of ageing field E_1 and measuring field E_2. We shall first consider the results obtained when E_1 and E_2 were varied in the same proportion. In order to differentiate this case from others in which E_1 and E_2 were varied separately, this value of E_2 will be called E. In the general case, ions of lower mobility than that of the alkali ion were found, indicating the formation of a cluster. A typical case is shown in fig. 2 in which the value of the mobility of the Li^+ clustered ion in argon is plotted against E/p, where p is the pressure of the inert gas. These

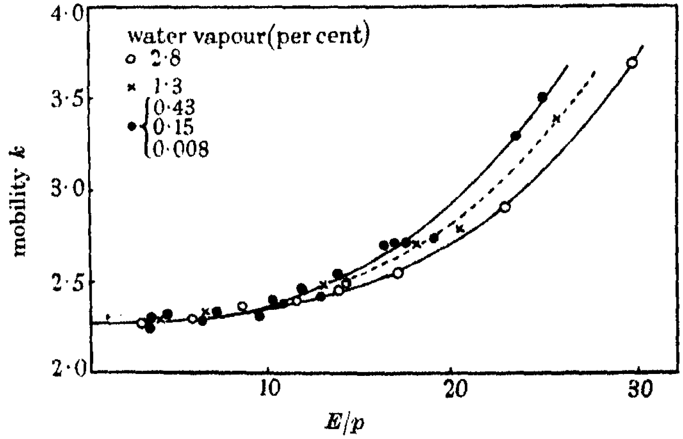

FIG. 2. Mobility of ions clustered in argon.

graphs were obtained with concentrations of water vapour varying from 0·008 to 2·8 %. The values of the mobility which are plotted are the measured values corrected for the fact that the presence of the water vapour slightly alters both the density and the dielectric constant of the gas. Blanc's reciprocal formula for mobility in mixed gases allows this correction to be made with reasonable accuracy provided the concentration of water is small. The correction for the lowest water concentration was negligible; for 1 % water it was 2·3 %.

The form taken by these graphs will be discussed later in the paper, but it will be noticed that whatever the concentration of water vapour they all converge to the same value of mobility at $E/p = 0$. We may conclude from this that an ion in thermal equilibrium with the gas acquires a cluster of water molecules, the size of which is independent of the concentration of water vapour within the limits used in these experiments. We may assume that as the cluster grows the binding energy for each additional water molecule decreases so that a state of dynamical equilibrium is finally reached, the size at any given instant fluctuating about a mean value. Table I gives the mobilities so obtained for all the alkali ions in all the inert gases with the exception of K^+ and Cs^+ in Kr. The values of the mobilities of the pure unclustered ions are also included for comparison. In a few cases the latter differ from those published earlier, but the differences are in the main very slight. It will be seen that all the alkali ions can collect a cluster in the presence of water.

TABLE I. VALUES OF MOBILITY OF ALKALI IONS

(*a*) Unclustered ions; (*b*) Clustered ions

	He		Ne		A		Kr		Xe	
Ion	(*a*)	(*b*)	(*a*)	(*b*)	(*a*)	(*b*)	(*a*)	(*b*)	(*a*)	(*b*)
Li	25·6	11·70	11·8	5·28	4·99	2·26	3·97	1·46	3·04	0·98
Na	24·2	11·15	8·70	5·25	3·23	2·25	2·34	1·43	1·80	0·94
K	22·9	11·85	8·0	5·26	2·81	2·19	1·98	—	1·44	0·92
Rb	21·4	12·8	7·18	5·38	2·40	2·10	1·57	1·37	1·10	0·87
Cs	19·6	13·4	6·50	5·48	2·23	2·18	1·42	—	0·97	0·83

In certain cases we may go further than this and deduce an upper limit to the number of water molecules in this cluster. In fig. 3 the relation found experimentally (Tyndall and others 1938) between the mobility k of an ion and its mass, M, is shown for the alkali ions in all the inert gases, k^2 being plotted with $1/M$. Langevin pictured an ion as being deflected by polarization forces due to the effect of its field on the gas molecules as well as making actual collisions with them. The polarizability of an inert gas atom increases with its mass. In the heavier gases the effect of the polarization forces is much more important than that of direct collision which results from the size of the colliding particles; but this is not the case in neon and helium. It has been previously shown that it is in accordance with this theory that in A, Kr and Xe, k^2 is approximately a linear function of $1/M$, while this is not so in Ne and He.

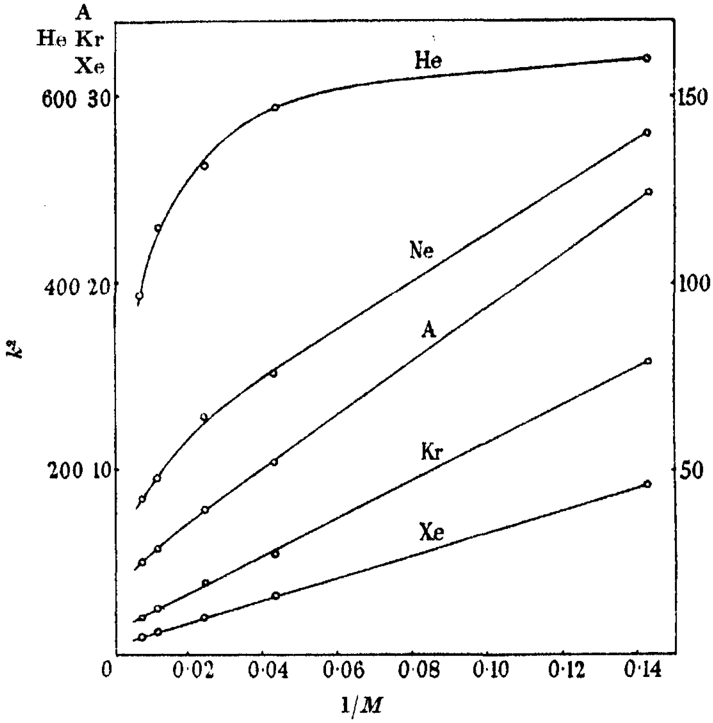

FIG. 3. Variation of mobility of alkali ions with the mass of the ion (M) in the inert gases.

In certain cases these graphs may be used as a type of mass spectrograph to determine the mass of other ions from their mobility. In the case of a clustered ion this is not justifiable because it cannot be assumed that its mobility is the same as that of a monatomic ion of the same mass. It will in fact be smaller, due to the increased size effect, the difference being least for the heavier gases and greatest for helium.

But if the value of the mobility of a clustered ion falls on the graph, the corresponding value of $1/M$ will set an *upper limit* to its mass expressed as that of the cluster, alkali ion $+ n\text{H}_2\text{O}$. Table II gives the values of n deduced in this way for a number of clustered ions in argon and krypton, and xenon.

The values for rubidium and caesium are doubtful, due to the error which necessarily arises in the estimation of a difference between two heavy masses as deduced from their mobilities. It will be seen from the rest that the value of n is of the order of six.

TABLE II. NUMBER OF WATER MOLECULES IN A CLUSTERED ION (UPPER LIMIT)

Gas	Li	Na	K	Rb	Cs
Argon	6·4	5·7	6·2	6·5 ?	2·5 ?
Krypton	5·9	5·8	—	4·6 ?	—
Xenon	6·4	6·6	6·4	6·3?	6·7 ?

In helium and neon the form of the graphs in fig. 3 is not such that extrapolation can be safely carried out and no estimate of n is therefore made. But an interesting result is shown in Table I in the columns of mobilities of clustered ions in these gases. In helium, in passing through the alkali series, the value of the mobility is a minimum with sodium ions, and Rb and Cs clustered ions both travel faster than those of lithium. A smaller effect in the same direction is found in neon and, unless the Rb value is in error, in argon also. This strongly suggests that as the size of the alkali ion increases the average number of water molecules it retains decreases owing to the decrease in the attractive field at its surface. In fact, it seems probable that the agreement at $n = 6$ for a number of ions in Table II is fortuitous and that if the size effect was allowed for, the value of n would vary in the same way in all gases. It is interesting to note that in electrolytes the mobility of the alkali ions increases with the atomic weight of the alkali.

It has also been shown (Tyndall 1938) that the classical theory of Langevin gives satisfactory quantitative agreement with experiment in the case of monatomic ions in the heavier inert gases. But to apply it to a cluster we must know the value of σ, its least distance of approach to a gas atom, and the calculation is sensitive to the value of σ chosen. A rough estimate gives $n = 4$ for Li^+ in argon instead of 6. It is interesting that Bernal and Fowler (1933) deduced this value for Li^+ in electrolytes. They also concluded that with Cs^+ the binding energy was not sufficient for the ion to form stable molecules with water. But in gases n cannot be zero because the mobility of the caesium ion is reduced when water is present.

Let us now return to fig. 2 and consider the results at higher values of the field. At high values of E and a low concentration of water vapour the ions will make very few collisions with water molecules. If the life of the ion in the mixture is gradually increased by reducing the field, we might have expected ions with 1, 2, 3 or more attached molecules to appear in succession and give evidence of their presence in the electrometer current frequency graph. It was found instead that, although some dozens of cases have been tested, the number of groups of ions present in detectable quantity were never more than two. At very high fields only one group existed in the form of unclustered alkali ions; at low fields again only one group, in this case all clustered. At intermediate values one of the two groups consisted of unclustered alkali ions and the other clustered.

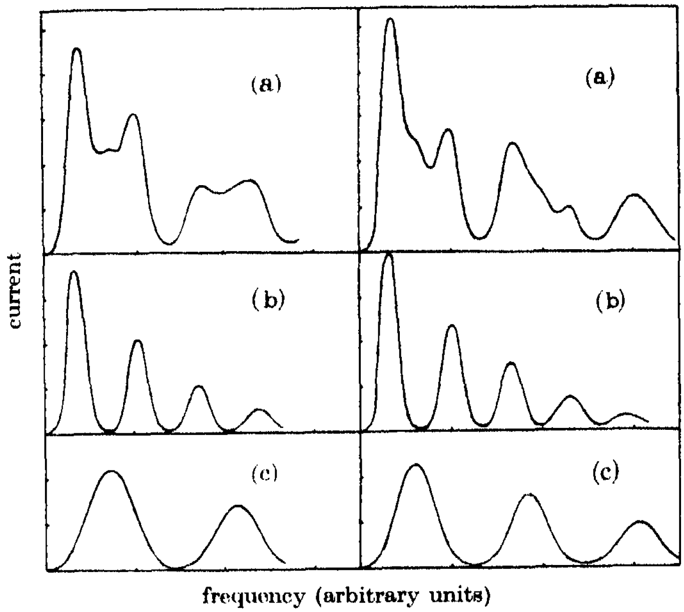

FIG. 4. Li^+ in $A + 0{\cdot}1\ \%\ H_2O$. FIG. 5. K^+ in $He + 0{\cdot}09\ \%\ H_2O$.

(*a*) experimental graphs. (*b*) and (*c*) components of experimental graphs.

Typical current frequency graphs are shown in figs. 4 and 5 for Li^+ in argon $+ 0{\cdot}1\ \%\ H_2O$ and K^+ in $He + 0{\cdot}09\ \%\ H_2O$. In each case the upper graph (*a*) is the experimental result; the experimental points are not shown because the graph follows them very closely even when plotted on a much larger scale. This graph may be analysed into the two groups, (*b*) $metal^+$ and (*c*) $metal^+(nH_2O)$, shown in the two lower graphs. The analysis is done by inspection but it is not arbitrary. Thus it is known where the unclustered ion should come on the frequency scale if it is present. If it appears to be present in one order then it must also be present in other orders of relative heights known with reasonable accuracy in a given apparatus. The frequency at which a given order of a clustered ion should occur is not known but when this simple analysis brings up a series of orders at frequencies in the ratio 1, 3, 5, 7, ..., and with peaks of the correct relative heights, one has confidence in saying that the mobility of the clustered ion is determined.

The presence of other groups of ions is not entirely excluded. Separate peaks with a height of 10 % or even less than that of the main peaks should have been detectable in the lower orders. But a similar group might well escape detection if its mobility was so near to that of a main group that the separate peaks were not resolvable in the lower orders. It can, however, be said that a large majority of the clustered ions are found in one mobility group.

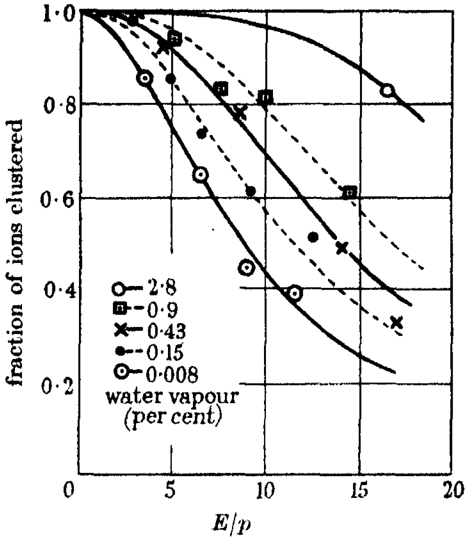

FIG. 6. Li^+ in argon.

Two effects occur as the value of the field is raised. First, the fraction of clustered ions in the stream decreases, the value at a given field depending upon the concentration of water vapour. A typical case is shown in fig. 6 for Li^+ in argon. At $E/p = 0$ the fraction is unity but subsequently falls rapidly at the low concentrations of water and less rapidly as the concentration is raised. Secondly, the mobility of the clustered ion rises with increase of field (fig. 2).

DISCUSSION AND FURTHER EXPERIMENTS

The simplest way of explaining these results is to assume that at a collision the probability of attachment of the first water molecule to the ion is much less than that of a subsequent molecule; but that having attached the first molecule, the cluster quickly builds up to a given size. At a given field a number of ions may reach and pass through the analyser without having clustered, in spite of the collisions they have made. This follows if the attachment of the first molecule required the presence of a third body to take off the excess energy liberated. If an alkali water molecule is then formed further attachment is far more probable, first, because the collision cross section is now increased and, secondly, because the excess energy may now be taken up in internal energy of the cluster, to be handed on in some later collisions with other molecules.

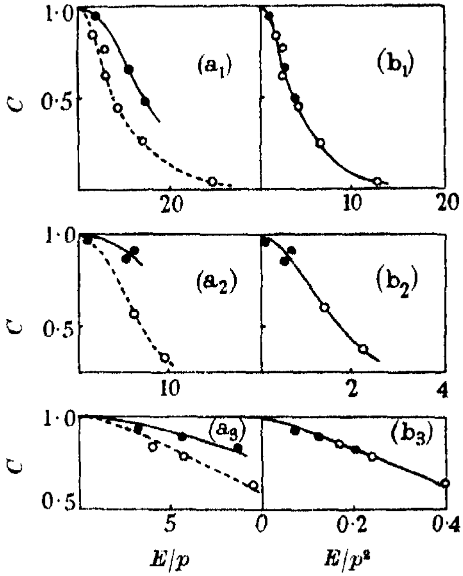

FIG. 7. a_1b_1, Li$^+$ in He; $p'(H_2O) = 1{\cdot}2 \times 10^{-4}$ mm.; p, ○ = 2·27, ● = 3·94 mm.
a_2b_2, K$^+$ in A; $p'(H_2O) = 2 \times 10^{-2}$ mm.; p, ○ = 4·30, ● = 9·03 mm.
a_3b_3, Na$^+$ in A; $p'(H_2O) = 2{\cdot}6 \times 10^{-2}$ mm.; p, ○ = 2·38, ● = 4·26 mm.

Since the fraction of water molecules in the gas is small the third body referred to would be a gas atom in nearly every case and for a given water concentration the probability of attachment should be proportional to the gas pressure, p. To test this conclusion some results are shown in fig. 7, a_1, a_2 and a_3, in which the value of the fraction of ions clustered (C) is plotted with E/p for two different values of p, the water concentration being kept constant. It will be seen that the fraction clustered increases with the gas pressure. Also, if the fraction is plotted against E/p^2 thereby reducing the results to a common gas pressure the points now lie on a common graph (fig. 7, b_1, b_2 and b_3), a result which is in quantitative agreement with the three body hypothesis. It is true that the graphs are not of a strict exponential form to be expected on this simple assumption but we do not feel that this vitiates the conclusion.

In order to explain the increase in mobility of the clustered ion with increasing field we make the following suggestion. At very low values of E/p the energy of thermal agitation of the ion is sensibly the same as that of the gas molecules in its neighbourhood. The number of molecules of water in the cluster will fluctuate about a mean value determined by the mean energy of the colliding particles, i.e. by the temperature; the number should fall with rise of temperature. At higher values of E/p the energy of drift of the ion in the direction of the field increases and its consequences can no longer be neglected. Thus at $E/p = 20$ a lithium ion in argon acquires a drift energy of 0·032 eV as compared with the normal energy of thermal agitation at room temperature of 0·034 eV. As an accompaniment of this drift energy it must also acquire a higher energy of thermal agitation, characteristic of a gas at a higher temperature and not of the gas in which it is moving. This increased energy may be expected to alter the equilibrium conditions so that the average number of water molecules attached to it decreases and its mobility consequently increases. It is therefore suggested that the rise in mobility which is found with increase of E/p (fig. 2) is due to a reduction in the average size which the cluster attains in its motion in the field. In fact, if the value of E/p is raised sufficiently the ion may not be able to retain any water molecules for an appreciable time so that no cluster is formed.

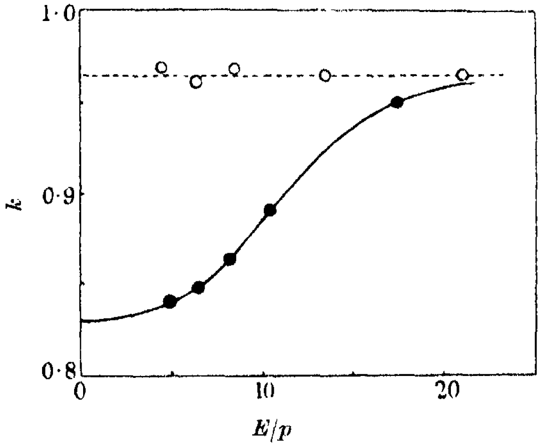

FIG. 8. ● Caesium ions in xenon + 0·6 % water vapour; ○ caesium ions in xenon.

Some support for this view for Cs^+ ions in Xe containing 0·6 % H_2O is given in fig. 8 in which the values of mobility of both clustered and unclustered ions are shown. It will be seen that as E/p increases the graph for clustered ions appears to merge gradually into the horizontal line for unclustered ions suggesting that the number of water molecules in the cluster then approaches zero.

Finally, it has been shown that the above results are not seriously influenced by the fact that the time spent in the analyser is not a negligible fraction of the life of the ion; in other words, by changes which may take place in the ion stream while it is being analysed. The probability of attachment within a distance d from the source is given by $1-e^{-\alpha d}$, where α depends upon the speed and the gas and water concentrations. The fractions plotted in fig. 6 refer to the composition of the ionic stream as it leaves the analyser. The relative numbers of clustered ions entering and leaving the analyser will depend upon the values of E_1 and E_2 used. If we apply this to the cases discussed above, where E_1 and E_2 were altered in the same ratio, $E_1 = 0{\cdot}66E_2$, it is found that the amount of clustering in the analyser itself should never be more than 8 %, the maximum occurring in the neighbourhood of 60 % clustering.

When E_1/E_2 is high the error would be greater and the results under these conditions have been discarded. When E_1 is low practically all the ions arrive at the analyser in the fully clustered state. By varying E_2 the change of mobility of the clustered ion as its speed is increased may then be studied. It is to be expected that owing to the accompanying increased thermal agitation the equilibrium size of the cluster would be reduced but that the number of clustered ions would not be sensibly reduced until they started to shed their last water molecule at high values of E_2. Without recording details, it may be said that full confirmation of this view has been obtained, the sharpness of the peaks observed indicating that equilibrium is attained very quickly after entry with the analyser.

But if a quantitative comparison is made between the observed amount of clustering at a given concentration and the amount to be expected on theoretical grounds, a serious discrepancy appears. Simple calculations from kinetic theory, neglecting the effect of attractive forces on the collision frequency, show that at the gas pressures and fields in use a three body collision during the life of the ion would in general be a rare occurrence. Thus for 0·005 % water in Xe at a pressure of 2·27 mm. the chance of a lithium ion making a three body collision is of the order of only 10^{-4} rising to 2×10^{-2} for 1 % water. The effect of the attractive field of the ion, ignored in this calculation, would be to produce a local concentration of gas and water molecules in the vicinity of the moving ion. But its domain would be very restricted, more so because most of the permanent dipoles of the water molecules are spinning so that the force falls off with the inverse fifth power of the distance except at very short distances. Consequently, although by introducing an attraction factor we might explain the results at high water concentrations, it does not seem possible to explain the relatively high probability of attachment at low concentrations without some considerable modification in our picture of the process.

It has already been mentioned that owing to some evaporation of a surface film near the source the low concentrations of water vapour may have been under-estimated and that additional collisions with water molecules may have taken place in the early life of the ion. But even if complete evaporation took place the pressure would not have been raised more than a few-fold and this factor is not enough to account for the results. Moreover, the graphs were not influenced by raising the field in the immediate neighbourhood of the source, between S and G_1, where the rise of surface temperature was greatest. This result also showed that the space charge in the neighbourhood of the source was not high enough to retain the ions for an appreciable time during which additional collisions could be made. The quantitative aspect of the problem is therefore still incomplete.

We wish to thank the Colston Research Society of the University of Bristol for a grant in aid of this work.

SUMMARY

The formation of clusters by the attachment of water molecules to alkali ions has been studied by measurements of the mobilities of these ions in the inert gases when small concentrations of water vapour are also present. In helium and neon the mobility of the clusters passes through a minimum as the mass of the alkali ion is increased. Thus the sodium clustered ion has the least and the caesium clustered ion the greatest mobility in the series, which suggests a decrease in the equilibrium number of attached molecules with increasing radius of the alkali atomic ion. In argon, krypton and xenon an *upper limit* of six molecules can be assigned to the number of water molecules in the cluster and the true number is probably less than six.

The process of clustering has been followed by passing the ions through an ageing field and then measuring their mobility. Only two groups of ions were found, one consisting of clustered ions and the other of unclustered, their relative numbers depending on the time spent in the ageing field and the concentration of water vapour in the gas. By varying the conditions the fraction of clustered ions could be varied from unity at very low ageing fields

to zero at high fields. These results follow if a three body collision between an ion, a gas molecule and a water molecule is necessary for the attachment of the first water molecule but that having attached the first molecule the cluster quickly builds up to a given size. Experimental work at different gas pressures supports this view.

With increasing field the energy of agitation of an ion must increase in association with its velocity of drift in the direction of the field. Since this is equivalent to a local higher temperature one would then expect a reduction in the number of water molecules that an ion can retain in attachment. It is found, in agreement with this view, that with increase of field the mobility of the clustered ion at a given gas pressure increases and gradually approaches that of the unclustered ion.

The paper contains a table of mobility values for all the alkali ions in all the inert gases, together with those for most of the water clusters of maximum size.

REFERENCES

Bernal and Fowler 1933 *J. Chem. Phys.* **1**, 515.
Blewett and Jones 1936 *Phys. Rev.* **50**, 464.
Powell and Brata 1932 *Proc. Roy. Soc.* A, **138**, 118.
Schrader and Ryder 1919 *Phys. Rev.* **13**, 321.
Tyndall 1939 *Mobility of positive ions in gases.* Camb. Univ. Press.
Tyndall and Powell 1930 *Proc. Roy. Soc.* A, **129**, 167.

The mobility of alkali ions in gases

II. The attachment of inert gas atoms to alkali ions

By R. J. Munson and K. Hoselitz
H. H. Wills Physical Laboratory, University of Bristol

(*Communicated by A. M. Tyndall, F.R.S.—Received* 18 *April* 1939)

During the course of some measurements of the mobility of lithium ions in xenon, it was observed that with small fields an ion of low mobility appeared in addition to the normal lithium ion. The first interpretation to suggest itself was that the molecules of a polar impurity in the gas were responsible for the formation of a clustered ion. But despite repeated attempts at purification this ion did not disappear, and since it could be partially suppressed by reducing the pressure or increasing the fields, it was not studied in detail at the time. However, during a later investigation by David and one of us (K. H., unpublished) with lithium ions in helium at liquid hydrogen temperature, conclusive evidence was obtained of a similar heavy ion at low fields. In this case there was no possibility of the ion picking up polar molecules of impurity since these would all be frozen out. The helium used was also claimed to be spectroscopically pure, so that undoubtedly the heavy ion arose from the attachment of helium atoms to the lithium ion. The polarizability of an inert gas atom increases with its atomic weight, so that on general grounds one would expect that the temperature range over which clusters of these atoms with a lithium ion could be detected would also increase with the atomic weight of the gas atom. The fact that clustered ions were observed in xenon at room temperature is therefore understandable, if they consisted of one or more xenon atoms attached to a lithium ion. Subsequent experiments were therefore undertaken in the other gases and the results are recorded and discussed below.

Experimental

The procedure followed was that given in Part I. In addition to the measuring tube there described, another one was used, which was specially designed for work at low temperatures and similar to the one used by Pearce (1936). The existence of clusters in certain cases was found from the analysis of the electrometer current-frequency curves. An example is given in fig. 1 (*a*) for lithium ions in xenon, the analysis into its components being shown in fig. 1 (*b*) and (*c*). As in the case where clusters arise from the presence of water vapour, only two groups were found, one (*b*) of clustered and the other (*c*) of unclustered lithium ions. By making an analysis of the ion stream over a range of values of E/p—using the notation of Part I—within which the cluster appeared, and extrapolating to $E/p = 0$, we can deduce the fraction C of ions clustered, and also the mobility of the cluster when the ions are in a state of thermodynamical equilibrium with their surroundings.

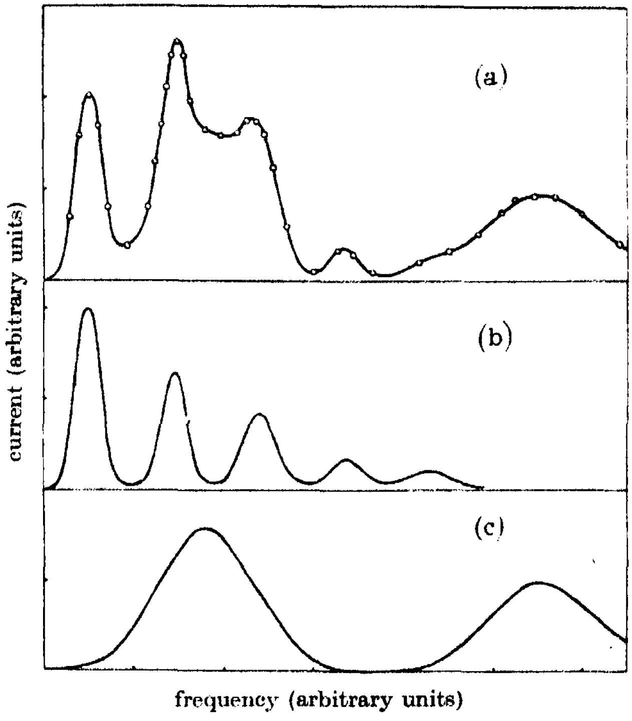

Fig. 1. Lithium ions in xenon at room temperature and low E/p. (*a*) Experimental graph; (*b*) and (*c*) components of experimental graph.

Table I gives the temperatures at which the clusters were looked for in the various gases and summarizes the results obtained for the equilibrium state at these temperatures. The ratio of the mobilities of the unclustered and clustered ions are given together with estimates of $C/1-C$. As stated in Part I, if the current carried by either ion was less than 10 % of the whole, it might have escaped detection. For instance, the statement that in neon at 195° K $C/1-C<1/10$, means that no clusters were detected at that temperature; similarly at 90° K in this gas, $C/1-C>10$ implies that no unclustered ions were observed. It will be seen that the greater the atomic weight of the gas atom, the higher is the temperature at which it will form a cluster with a lithium ion. An attempt was made to observe a cluster with potassium ions in argon, but without success even at liquid nitrogen temperature. Lithium ions in argon readily formed clusters at 195° K, so that evidently the difference in behaviour in these two cases is due to the difference in the sizes of the potassium and lithium ions.

TABLE I

Ion	Gas	Temp. ° K	$\dfrac{k_{\text{ion}}}{k_{\text{clust}}}$	$\dfrac{C}{1-C}$	n	r	$1/r(\Sigma_1^r D_r)$ eV
Li^+	He	20	1·10	>3	1·8	1	$>0{\cdot}016$
		77		$\fallingdotseq 1$		1	$\fallingdotseq 0{\cdot}07$
		90		<1		1	$<0{\cdot}08$
	Ne	90	1·98	>10	?	3 ?	$>0{\cdot}13$
		195		$<1/10$		1	$<0{\cdot}16$
	A	195	2·38	>10	2·7	2	$>0{\cdot}25$
		290		$<1/3$		1	$<0{\cdot}29$
	Kr	290	3·09	>10	2·6	2	$>0{\cdot}31$
		360		<2		1	$<0{\cdot}35$
	Xe	290	3·84	>20	2·6	2	$>0{\cdot}42$
K^+	A	77		$<1/10$		1	$<0{\cdot}06$

Following the argument given in Part I an upper limit to the average number of atoms attached to the ion, n, may be estimated in certain cases by neglecting the effect on its mobility of its increased size. Values of n so deduced are recorded in Table I, but it must be pointed out that these only apply at the temperatures given, since n must be a function of temperature.

In argon at 195° K and krypton and xenon at room temperature, the value of n lies between 2 and 3. It therefore seems reasonable to assume that when an allowance is made for the size effect, the probable number of gas atoms attached is 2. In neon it has previously been shown that the size effect is much more serious, and no reasonable estimate of n can be deduced. The size effect should be even larger in helium, so that the estimate given at 20° K, viz. 1·8, can only mean that the cluster contains on the average one atom.

In helium the limits set to $C/1-C$ are less definite than those in the other gases for the following reason. In neon, argon, krypton and xenon the resolving power of the apparatus is sufficient to give a distinct separation between the peaks produced by clustered and unclustered ions, so that both can be readily observed when present together. This was not possible in helium as only one set of peaks was found. The evidence for the existence of the cluster and an estimate of $C/1-C$ was indirect and obtained from the results shown in fig. 2, in which the mobility of the ion deduced from the peak frequency is plotted with E/p, at a temperature of 290° K in (*a*) and 20° K in (*b*).

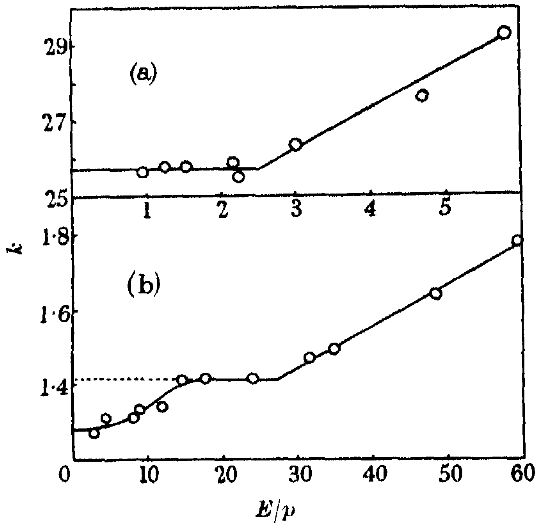

FIG. 2. (*a*) Li⁺ in He at 290° K; (*b*) Li⁺ in He at 20° K.

It has been shown by Mitchell and Ridler (1934) in nitrogen and by one of us (Munson unpublished) in the inert gases that the mobility of an ion is constant below a certain critical value of E/p above which it varies linearly with E/p. For this reason graph (*a*) at room temperature is interpreted as two straight lines intersecting at about $E/p = 2\cdot5$, although in this case the accuracy of the experimental points may not appear to justify it. At 20° K the graph is of the same type above $E/p = 17$ and since the unpublished work also shows that the critical value of E/p rises as the temperature falls, we are justified in assuming that the mobility measured between $E/p = 17$ and $E/p = 28$ is that of the unclustered ion at this temperature. Below $E/p = 17$ the mobility starts to decrease and then seems to tend again to a constant value near $E/p = 0$. This we assume to be the mobility of the clustered ion, although the value of the peak frequency from which it was derived may be slightly affected by the presence of some unclustered ions as well. However since there was a definite indication of a cluster at 77° K, it seems almost certain that there were very few unclustered ions at 20° K.

In Part I the role played by three body collisions in the mechanism of the formation of water clusters was discussed. In view of the fact that xenon readily forms clusters with lithium ions at room temperature, experiments were carried out both in helium and in argon using xenon as an impurity in place of water vapour. By this means conclusive evidence has been obtained that the xenon cluster is formed by a triple collision in which the third body can be a second xenon atom or either an argon or helium atom.

Let p denote the total pressure of the mixed gases, p' the partial pressure of xenon, and τ the time spent by a lithium ion in reaching the analyser. Then it can be shown that the fraction C of ions clustered on arrival at the analyser is given by

$$C = 1 - e^{-\beta\tau p'}, \tag{1}$$

where β may be a function of a number of quantities depending on the mechanism of attachment. If, for instance, a third body is necessary for cluster formation, and no atom but xenon can be effective in this way, then β is proportional to p', or if any atom can be effective β is proportional to p.

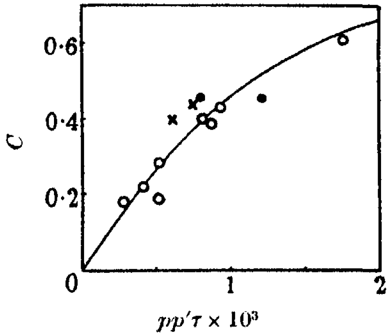

FIG. 3. ⊙ He+Xe; ● A+Xe; × Xe.

To test these conclusions p was varied from 15 to 3 mm. and p' from 0·4 to 2·5 mm. in the helium mixtures; in the argon mixtures the ranges of pressure were much smaller. Fig. 3 shows the observed value of C plotted against $pp'\tau$, the circles and dots referring to Lithium ions in He-Xe and A-Xe mixtures respectively, and the crosses in pure Xe. Considering the widely different conditions, the scatter of points around the smooth curve given by $C = 1 - e^{-6\times 10^3 pp'\tau}$ is small. Of the other possible expressions for β, none gave any agreement of this order; we therefore conclude that attachment must take place at triple collisions, and also that xenon, argon and helium atoms are equally effective as third bodies.

The latter result can also be expressed by saying that, for each of these atoms, the radius of the "sphere of action" in the attachment process has the same value. From the value of the constant 6×10^{-3} and the mean free path of an ion, one could deduce this radius, on the arbitrary assumption that, for a collision within such a sphere, the probability of attachment is unity. If the charge on the ion has no effect on its mean free path (which is, however, improbable), then the value of the radius is $7\cdot5 \times 10^{-8}$ cm.

THEORETICAL

Consider a system of n_1 ions and n_2 gas atoms enclosed in a volume v, and let $n_2 \gg n_1$. In general it will be possible for the ions and atoms to form clusters containing 1, 2, 3, ... atoms, when the temperature is low enough. When a cluster containing r atoms is in its ground state, let the energy required to remove the outermost atom be D_r. Then in order to break up the cluster completely, the energy which must be supplied is $(D_1 + D_2 + \ldots + D_r)$.

The problem of finding the equilibrium state of the system of ions, atoms and clustered ions is very complex, the complete solution requiring a knowledge of all the rotational and vibrational levels of all possible types of cluster. But from general consideration of diatomic molecules we should conclude that for clusters containing only one atom, the energy difference between the ground and first excited vibrational levels is large compared with that between the corresponding rotational levels, and also that the first excited vibrational level is so far above the ground state that for the temperatures used, practically all the clusters would be in their lowest vibrational state. This may not be true for clusters containing a number of atoms, but owing to the difficulties of calculation it will be assumed that the clusters remain in their vibrational ground state.

The spacing of the rotational levels of a cluster depends only on its moment of inertia, and in calculating this quantity it will be assumed that the nuclear separation of an ion and a gas atom attached to it is in all cases equal to the sum of their radii using the values given by Slater (1930). By this means it is found that in most of these experiments the average rotational quantum number of the clusters is high, so that a close approximation can be obtained to the free energy arising from rotation. We can now write down an expression for the free energy of the whole system, from which the equilibrium state at any temperature T can be deduced in the usual way.

If C_0 is the fraction of ions in the free state and C_r the fraction which has formed clusters containing r atoms, then when r is not greater than 3

$$\frac{C_r}{C_0} = \exp\left(\Sigma_1^r \frac{D_r}{K\tau}\right) \cdot \left[\left(\frac{h^2}{2\pi m K\tau}\right)^{\frac{3}{2}} N\right]^r \left(\frac{M+rm}{M}\right)^{\frac{3}{2}} \left(\frac{2\pi^3 I_r K\tau}{h^2}\right), \qquad (2)$$

where M, m are the masses of the ion and gas atom respectively, I_r the maximum moment of inertia of an r-atom cluster, $N = n_2/v$ and h and K have their usual significance.

For the particular case of the helium cluster at 20° K, when the temperature is so low that most of the clusters are not rotating

$$\frac{C_r}{C_0} = \exp\left(\Sigma_1^r \frac{D_r}{K\tau}\right) \cdot \left[\left(\frac{h^2}{2\pi m K\tau}\right)^{\frac{3}{2}} N\right]^r \left(\frac{M+rm}{M}\right)^{\frac{3}{2}}. \tag{3}$$

By inserting the values of the constants outside the exponential term it can be shown that when the temperature is sufficiently high for the fraction of clusters with one atom only ($r = 1$) to be small, then the fraction of the heavier clusters is quite negligible.

Using the experimental data given in Table I, where $C = \Sigma C_r$ and $1 - C = C_0$, we may now apply equation (2) to assign upper and lower limits to the dissociation energies of the clusters in He, Ne, A and Kr. In Xe, results at only one temperature are available, and the data thus give only a lower limit. The value which is taken for r is the average number of atoms in the cluster. When C is sufficiently large this is given by the value of n, except in the case of neon at 90° K, and here r is given at a guess the value 3. When C is small r is assumed to be unity. The results obtained are given in Table I in the column headed $1/r(\Sigma_1^r D_r)$ and it will be observed that there is a fairly close agreement between the upper and lower limits for the neon, argon and krypton clusters and that the value of the dissociation energy rises with increasing polarizability of the gas atom. This suggests also that the value of D_r is approximately independent of r, or in other words, that the interaction between the atoms in a cluster is small.

The force of interaction between an ion and a gas atom could in principle be calculated by wave mechanics, but the calculations have not been made. In their absence, it is possible to obtain a check on the above estimates of dissociation energy, in the case of the union of an alkali ion and an inert gas atom of similar structure, by making use of some calculations of Lennard-Jones (1931). He expressed the force between two neutral atoms in terms of inverse powers of the distance between their centres and evaluated the force constants. When one of these atoms is replaced by an ion, it is assumed, following Hassé and Cook (1931), that the force is the same except for the addition of an inverse fifth power term due to polarization. In this way the value obtained for the dissociation energy of a Li^+-He molecule is 0·057 eV, and of K^+-A molecule 0·058 eV. Comparison with the data given in Table I shows that the estimates in helium by the two methods are in satisfactory agreement. The one experimental result for potassium ions gives an upper limit of 0·06 eV.

We wish to express our thanks to Professor Tyndall for his continued interest and advice, and to Professor Mott for helpful discussions during the course of the work.

SUMMARY

Evidence of the attachment of inert gas atoms to a lithium ion has been obtained in all the inert gases. The condition necessary for attachment is that the energy of thermal agitation of the ion and of gas atoms through which it moves must not exceed a given value which depends upon the dissociation energy of the molecule so formed. At low values of field/pressure (E/p) when the ion is in thermal equilibrium with the surrounding gas an appreciable fraction of the Li ions in He are of the form Li^+, n(He) at 20° K; the fraction is much smaller at 90° K and zero at room temperature. The value of n is not more than two and more probably nearer unity. In neon practically all the ions show attachment at 90° K and none at 195° K. The corresponding temperature limits in argon are 195° K and 290° K. In Xe and Kr every ion collects at least one and probably two gas atoms at room temperature. In some cases there is evidence that n increases as the temperature is reduced. On the other hand, potassium ions collect no gas atoms in argon at 195° K, doubtless because the dissociation energy must be less than for lithium ions owing to the larger size of the potassium ion.

If the value of E/p is raised, these molecular ions tend to disappear owing to the increased thermal energy of the ion which is associated with its drift in the field. From estimates made of the fraction of ions which are molecular at a given temperature, upper and lower limits have been set to the values of the dissociation energy of a lithium ion and gas atom. It is found that the value increases with the mass of the gas atom, i.e. with its polarizability; it ranges from about 0·07 eV in helium to 0·33 in krypton and is $>0{\cdot}42$ in xenon.

REFERENCES

Hassé and Cook 1931 *Phil. Mag.* **12**, 554.
Lennard-Jones 1931 *Proc. Phys. Soc.* **43**, 461.
Mitchell and Ridler 1934 *Proc. Roy. Soc.* A, **146**, 911.
Pearce 1936 *Proc. Roy. Soc.* A, **155**, 490.
Slater 1930 *Phys. Rev.* **36**, 64.

The mobility of alkali ions in gases

III. The mobility of alkali ions in water vapour

By R. J. Munson

H. H. Wills Physical Laboratory, University of Bristol

(*Communicated by A. M. Tyndall, F.R.S.—Received* 18 *April* 1939)

It is known that in electrolytes at infinite dilution the mobility of an alkali ion increases with its mass and this has been attributed by some to a decrease in its degree of hydration as the size of the alkali atom increases. In Part I evidence was obtained, at least in helium and neon, that the average number of water molecules which are attached to an alkali ion when water is present as an impurity also decreases as the atomic weight of the ion increases. As a natural corollary to this work a determination of the mobility of the alkali ions in pure water vapour has been undertaken and is here described.

The method and apparatus of Part I was used. The nature of the ion from the source was first verified by running it in a pure gas which was then pumped off and water vapour introduced. The results are shown in fig. 1, where the mobility of the ion is plotted with E/p. For the sake of clearness the results for Rb^+ are excluded from the graph except at low values of E/p. The remainder of the Rb^+ graph follows more or less that for Na^+.

Extrapolating to $E/p = 0$ it is seen that the mobilities of the ions are all low suggesting that they exist as clusters. The mobility decreases slightly as the mass of the alkali atom increases, the values at $E/p = 0$ being: Li 0·725, Na 0·715, K 0·705, Rb 0·700, Cs 0·695. As E/p is raised the mobilities increase, but the order is changed. At $E/p = 45$ they all have about the same mobility and above this value K^+ has the greatest and Li^+ the least mobility.

These graphs can be qualitatively explained as follows: Following on the discussion in Part I we may assume that the mean number of water molecules attached to an ion depends on its energy of thermal agitation. At $E/p = 0$ the cluster is in equilibrium with the surrounding vapour at room temperature. With rising E/p its energy of thermal agitation rises and this may lead to a decrease in the average number of attached molecules. But the extent to which water molecules are shed will depend upon their dissociation energy. We may assume that the value of the dissociation energy will be greatest for lithium and least for caesium ions because the radius of the atomic ion increases with mass through the alkali series. As E/p increases we may therefore expect lithium clusters to be stable over a wider range of E/p than those of the higher alkalis. In agreement with this view it will be seen that the mobility of the Li^+ ion remains approximately constant until E/p about 55, above which it starts markedly to rise. In the case of the other alkalis the early constant part either holds over a more limited range or is absent altogether.

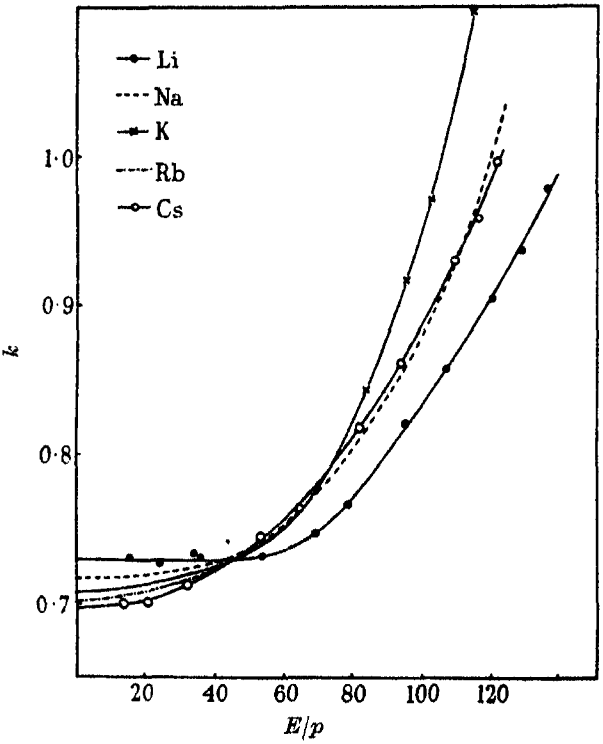

Fig. 1

But the effect of a reduction in the size of the cluster on the mobility of the ion depends upon the alkali. In Langevin's expression for the mobility of an ion, the mass of the ion M appears in a factor $(1+m/M)^{\frac{1}{2}}$, where m is the mass of a gas molecule, in this case water vapour. When the ion is clustered $M = M_0 + nH_2O$, where M_0 is the mass of the alkali atom. As M_0 increases the effect of changing n by a given amount decreases; it will be far less for caesium ($M_0 = 133$) than for lithium ($M_0 = 7$). A change in n will be accompanied by a change in the collision cross-section of the ion. The effect of this on the mobility will again be greatest for lithium and least for caesium clusters of the same water content. Consequently, whereas the lithium cluster is relatively stable, its mobility tends to rise relatively suddenly when it starts to diminish in size. At the other end of the scale the caesium cluster breaks down much more easily but with a more gradual effect on its mobility. The other ions lie between these two extremes with potassium ions showing the greatest mobility of the series at higher values of E/p. Presumably at a still higher value of E/p, sufficient to prevent any attachment of water molecules to the ions the order would change again. But the incidence of glow discharge from edges of the electrodes at high fields prevented a test of this conclusion.

At the same time we cannot ignore the possibility that at higher values of E/p the mobility of an ion of a given mass is no longer independent of E/p and that the shape of the graphs may thereby be affected. This effect has been referred to in Part II. But it clearly does not set in below a value of E/p about 55 for lithium ions in water vapour. Consequently, since the ions of the other alkalis, like those of lithium, also possess an envelope of attached water molecules, it is perhaps unlikely that the critical value of E/p at which the mobility undergoes this type of change would differ greatly through the series.

Since in pure water vapour the mobility of the alkali ions decreases with increasing mass of alkali atoms, their behaviour is quite different from that of water-clustered alkali ions in helium and neon and in electrolytic solutions. Though no quantitative analysis is possible at present, these differences call for comment. First, the conditions of equilibrium of a water-clustered ion in a gas differ from those in water vapour itself. Thus if by chance a water cluster in a gas loses a water molecule it has to await another favourable collision with a water molecule before recovery. The time taken before this occurs will depend on the water concentration and the dissociation energy. On the other hand, in water vapour itself every collision is one with a water molecule, so that a water molecule may leave at one collision and be replaced even at the next. Consequently quite temporary attachments may play an important part in determining its speed, and though the binding energy of a water molecule to a caesium ion is less than to a lithium ion, its effect on the relative mobilities may be masked by the frequency of these temporary attachments.

The mechanism in liquids is probably different again. Here we may picture the ion as in contact with the surrounding water molecules throughout its path. When the dissociation energy is small, as with caesium ions, the ion may be thought of as jumping from one molecule to the next and thus slipping through the liquid without the envelope of firmly attached molecules which would accompany a lithium ion. It is therefore not surprising that an alkali ion in water vapour behaves different from one in solution.

It is known that Langevin's expression based on the assumption of an inverse fifth power law of attraction between an ion and a gas molecule can be applied with reasonable quantitative success to the case of alkali ions in the inert gases. If it is to be applied to these ions in water vapour it is necessary to assume that the same law of force holds, in spite of the permanent dipole of the water molecule. This assumption may not be seriously in error, because most of the dipoles are spinning and any orientation of the dipoles which may occur at short apsidal distances is limited by the increased radius of the clustered ion. On the other hand, we do not know what figure to assign to the number of water molecules in the cluster; its mass and effective diameter are therefore both uncertain. But it may be of interest to record that if it be assumed that a lithium ion is unclustered in water vapour, its calculated mobility is 1·21 compared with the experimental value of 0·725. Whereas if it be given a cluster of six molecules (see Part I) and the diameter of the ion assumed to be that of the lithium ion plus two water molecules, then the calculated mobility is 0·75. Though this may appear to give good agreement with experiment, the value, six, cannot be taken as an estimate of the size of the cluster, because the expression is not mass sensitive when M is much greater than m. Detailed calculations using other clusters and other ions are therefore unjustifiable. It can, however, be assumed that for lithium ions n is certainly not zero and is probably greater than three or four.

SUMMARY

Determinations of the mobility of alkali ions in water vapour show that at low values of field/pressure (E/p) the mobility decreases slightly with increase in mass of the alkali atom. This sequence changes entirely when E/p is considerably increased. The latter result is qualitatively explained by the gradual break up of the cluster of molecules attached to the ion as its kinetic energy increases; the variation of the mobility with increasing E/p will depend upon the energy of dissociation of a water molecule from an alkali ion and upon the fractional change in the mass of an ion caused by the loss of a water molecule from the cluster, both of which depend upon the nature of the alkali ion under consideration. The results at low E/p are briefly discussed in comparison with the behaviour of alkali ions in liquids and of water-clustered ions in gases.

Natural convection in liquids

By O. A. Saunders

*Clothworkers Reader in Applied Thermodynamics at
Imperial College of Science and Technology*

(*Communicated by Sir Henry Tizard, F.R.S.—Received* 1 *March* 1939)

Theory of natural convection

Lorenz (1881) gave a solution to the problem of natural convection set up near a heated vertical plate, in which he assumed that the surfaces of equal fluid velocity and equal fluid temperature are parallel to the plate. Experiments show, however, that this is not the case.

Schmidt and Beckmann (1930) suggested applying the approximations of the boundary layer theory, and Pohlhausen (1930) showed how the partial differential equations thus obtained could be transformed into equations with a single independent variable. Five boundary conditions required to be satisfied in Pohlhausen's problem, three at the plate and two at infinity. Owing to the slow convergence of the terms, Pohlhausen found it impracticable to solve the equations in series for these boundary conditions. He therefore used measurements by Schmidt and Beckmann of the normal gradients of temperature and velocity in air very close to a heated plate, to obtain two more boundary conditions at the plate. Starting with the five given boundary conditions at the plate he obtained a solution in series of the equations for air, which was found to satisfy the conditions at infinity.

Pohlhausen considered air only. His method cannot be used for other fluids because the gradients of velocity and temperature near the plate have not been measured except for air; and it would not be safe to assume that the boundary conditions based on experiments in air are valid for other fluids.

In what follows, approximate solutions are given which are entirely theoretical and do not depend on measured temperature and velocity gradients. They may therefore be applied to any fluid, including air, giving theoretical values for the temperature and velocity gradients, and hence also the heat transfer and the friction drag at the plate.

Approximate theoretical solution

The equations of motion and of heat flow are

$$u\frac{\partial u}{\partial x}+v\frac{\partial u}{\partial y} = \nu\frac{\partial^2 u}{\partial y^2}+g\beta\theta, \tag{1}$$

$$u\frac{\partial \theta}{\partial x}+v\frac{\partial \theta}{\partial y} = \frac{k}{c}\frac{\partial^2 \theta}{\partial y^2}, \tag{2}$$

where u and v are the velocity components in the x and y directions, the x-axis being vertical and the y-axis horizontal and at right angles to the plate, θ being the temperature at any point, ν the kinematic viscosity, k the thermal conductivity, c the specific heat per unit volume at constant pressure, and β the coefficient of change of density (ρ) with temperature, defined by

$$\rho_0 = \rho(1+\beta\theta),$$

where ρ_0 is the density at $\theta = 0$.

In deriving these equations the usual approximations of boundary layer theory are made, i.e. $\partial^2 u/\partial x^2$ is neglected in (1) and $\partial^2\theta/\partial x^2$ in (2), and the equation of horizontal motion is ignored. These approximations are justified if the thicknesses of the velocity and temperature boundary layers are both small compared to the height of the plate. In natural convection, since it is the difference between the temperature at any point and the temperature at a great distance from the plate which causes the motion, the velocity boundary layer cannot be thinner than the temperature boundary layer; but in the case of a fluid of low conductivity and high viscosity the velocity boundary layer might extend beyond the temperature boundary layer.

The fluid density, which is assumed to be constant when writing the terms on the left-hand sides of equations (1) and (2), has been divided into both sides of the equations. The density is also assumed constant in the equation of continuity

$$\frac{\partial u}{\partial x}+\frac{\partial v}{\partial y} = 0. \tag{3}$$

Finally, the pressure at any point in the fluid is assumed to be equal to the hydrostatic pressure, calculated for the fluid outside the boundary layer, where the temperature may be taken arbitrarily as zero, since the equations are linear in θ.

In the problem to be considered the motion is assumed to be two-dimensional in a vertical plane normal to the plate, the origin of the rectangular axes being taken in the bottom edge of the plate. Thus the boundary conditions are $u = v = 0$ and $\theta = \theta_0$ when $y = 0$, for all x, and $u = v = \theta = 0$ at infinity, θ_0 denoting the plate temperature, assumed to be uniform.

It is convenient to replace all lengths, velocities, and temperatures by their dimensionless ratios to fixed units. Choose l, the vertical length of the plate, and θ_0, its temperature, as the units of length and temperature; the unit of velocity may be chosen arbitrarily since only zero values are specified in the boundary conditions, and on taking it as equal to k/cl, equations (1), (2) and (3) become

$$\frac{1}{Pr}\left(u\frac{\partial u}{\partial x}+v\frac{\partial u}{\partial y}\right) = \frac{\partial^2 u}{\partial y^2}+Gr\,Pr\,\theta, \tag{4}$$

$$u\frac{\partial \theta}{\partial x}+v\frac{\partial \theta}{\partial y} = \frac{\partial^2 \theta}{\partial y^2}, \tag{5}$$

$$\frac{\partial u}{\partial x}+\frac{\partial v}{\partial y} = 0, \tag{6}$$

where x, y, u, v, θ are now dimensionless, and Gr denotes the so-called Grashof number $[\equiv (g\beta\theta_0 l^3)/\nu^2]$, and Pr the Prandtl number $(\equiv c\nu/k)$.

It will be noted that Gr and Pr do not occur in (5) and (6). Since, at positions very near the surface, the terms on the left-hand side of (4) are small because u and v are small, and the term $Gr\,Pr\,\theta$ is greater nearer the surface, it might be expected that the gradients of u and θ near the surface would depend mainly on the product $Gr\,Pr$, provided Pr, which occurs in the denominator of the left-hand side, is not too small. Experiments confirm this, as described later.

Let
$$\xi = \left(\frac{3Gr\,Pr}{4}\right)^{\frac{1}{4}}\frac{y}{x^{\frac{1}{4}}}, \tag{7}$$

$$\psi = \left(\frac{64Gr\,Pr}{27}\right)^{\frac{1}{4}} x^{\frac{3}{4}}\zeta, \tag{8}$$

where $u = \partial\psi/\partial y$, $v = -\partial\psi/\partial x$, ψ being the stream function, and ζ and θ are functions of ξ. This transformation, which is the same as Pohlhausen's except for the constants, clears the equations of x and y, giving, after some reduction,

$$\zeta_3+\frac{1}{Pr}(\zeta\zeta_2-\tfrac{2}{3}\zeta_1^2)+\theta = 0, \tag{9}$$

$$\theta_2+\zeta\theta_1 = 0, \tag{10}$$

the suffixes denoting differentiation with respect to ξ.

The velocities u and v are given by

$$u = \left(\frac{64 Gr\, Pr}{27}\right)^{\frac{1}{2}} x^{\frac{1}{2}} \zeta_1, \tag{11}$$

$$v = -\left(\frac{3Gr\, Pr}{4}\right)^{\frac{1}{4}} x^{-\frac{1}{4}} \zeta + \left(\frac{Gr\, Pr}{12}\right)^{\frac{1}{4}} y x^{-\frac{1}{2}} \zeta_1. \tag{12}$$

Hence the boundary conditions are $\zeta = \zeta_1 = 0$ and $\theta = 1$ when $\xi = 0$, i.e. at all points on the x-axis, and $\zeta_1 = \theta = 0$ when $\xi = 0$, which, for finite values of y, corresponds to the y-axis.

Since ξ does not occur explicitly in (9) and (10), their order may be reduced by changing the variables to $\theta_1 (\equiv p)$ and θ. From (10), if suffixes attached to p denote differential coefficients with respect to θ, $\zeta = -p_1$. And differentiating ζ to obtain $\zeta_1 (= -pp_2)$, ζ_2, ζ_3, etc., and substituting in (9), we get

$$Pr(p^3 p_4 + 3p^2 p_1 p_3 + p^2 p_2^2 + pp_1^2 p_2 - \theta) - pp_1^2 p_2 - p^2 p_1 p_3 + \tfrac{2}{3} p^2 p_2^2 = 0. \tag{13}$$

The boundary conditions are satisfied if $p_1 = p_2 = 0$ when $\theta = 1$, and $p = 0$ when $\theta = 0$.

It will be noted that for finding the heat transfer at the plate the value of p at $\theta = 1$ is required. Equation (13), with p and θ as variables, is therefore suitable for finding the heat transfer by approximate solution. On the other hand, for finding the drag at the surface, which depends on p_2 and p_3, the approximate solution of (13) must be differentiated, involving greater errors.

The simplest polynomial with one undetermined constant, which satisfies the boundary conditions, is

$$p = A_1[(1-\theta)^3 - 1]. \tag{14}$$

By making this satisfy (13) at the mid-point of the range of θ, i.e. $\theta = \frac{1}{2}$, we find

$$A_1 = \left\{\frac{4Pr}{21(1+6Pr)}\right\}^{\frac{1}{4}}. \tag{15}$$

In fig. 1, curve 1, A_1 is shown plotted against Pr. The solution satisfies the differential equation at $\theta = 0$ but not at $\theta = 1$. A second approximate solution may be obtained by assuming

$$p = A_2[B(1-\theta)^4 + (1-B)(1-\theta)^3 - 1], \tag{16}$$

which satisfies the boundary conditions, and choosing A_2 and B so as to satisfy the differential equation at $\theta = 1$ and $\theta = \frac{1}{2}$. Eliminating B, the equation for A_2 reduces to

$$(1-336A_2^4)\,[(2{,}654{,}208A_2^{12}+48{,}960A_2^8-1{,}584A_2^4+4)\,Pr \\ +539{,}136A_2^{12}+22{,}176A_2^8+336A_2^4-1]+73{,}728A_2^{12}=0. \qquad (17)$$

Values of A_2 satisfying (17) are plotted against Pr in fig. 1, curve 2.

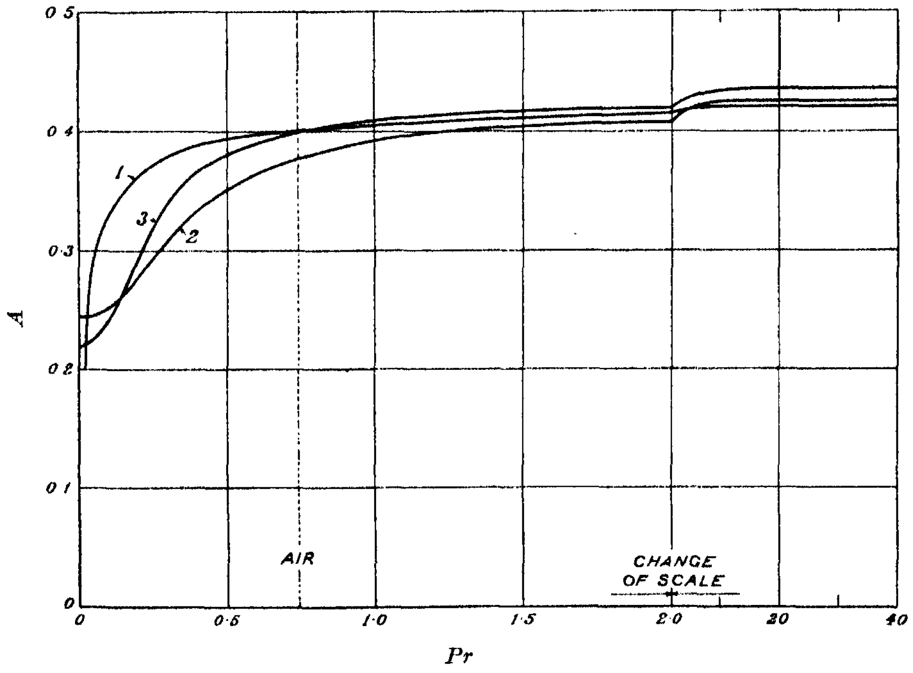

FIG. 1. Approximate values of A (see equation (21)).

Obtaining further approximate solutions by taking polynomials of higher degree which satisfy the equation at more points, or by using the least square deviation method, involves very heavy numerical work because of the complicated equation. A third approximate solution may be found relatively easily, however, by assuming

$$p = A_3[C(1-\theta)^5+D(1-\theta)^4+(1-C-D)\,(1-\theta)^3-1], \qquad (18)$$

which satisfies the boundary conditions, and choosing A_3, C, and D so as to satisfy the differential equation at $\theta = 1$ and at $\theta = \frac{1}{2}$, and the differentiated differential equation at $\theta = 1$. The first and last of these conditions give respectively

$$24A_3^4D = -1 \quad \text{and} \quad 120A_3^4C = 1. \qquad (19)$$

The second condition, on substituting for C and D in terms of A_3 from (19), reduces to

$$\begin{aligned} Pr[5{\cdot}35\times10^{15}A_3^{16}-1{\cdot}037\times10^{14}A_3^{12}-4{\cdot}28\times10^{12}A_3^{8} \\ +1{\cdot}465\times10^{10}A_3^{4}-1{\cdot}284\times10^{7}]+8{\cdot}95\times10^{14}A_3^{16} \\ +2{\cdot}837\times10^{13}A_3^{12}+1{\cdot}52\times10^{12}A_3^{8}-5{\cdot}58\times10^{9}A_3^{4}+4{\cdot}94\times10^{6}=0. \end{aligned} \tag{20}$$

Values of A_3 satisfying (20) are shown in fig. 1, curve 3.

It will be seen that for $Pr > 0{\cdot}73$ (the value for air) the three approximations are within less than $\pm 3\,\%$ of their mean value, although over part of the range of Pr the second and third differ more than the first and second. The only fluid for which Pr is less than 0·73 is mercury ($Pr = 0{\cdot}03$), for which the first and third approximations are respectively about 10 % above, and 10 % below the second.

It is, of course, not possible to say with certainty from fig. 1 how accurate the approximate solutions are, but it appears likely that curve 3 is within a few per cent of the exact solution. The curves show that A is practically constant for Prandtl numbers above about 10.

Case of air ($Pr = 0{\cdot}73$)

The values of A for air, taken from fig. 1, curves 1, 2 and 3, are respectively 0·402, 0·379 and 0·400, all of which are slightly below the value 0·418* taken by Pohlhausen from Schmidt and Beckmann's experiments.

The approximate solutions give distributions of temperature and velocity within the boundary layer, and these are compared with Pohlhausen's accurate solution in figs. 2 and 3. The curves 1, 2 and 3 in fig. 2 were obtained from equations (14), (16) and (18) respectively, by plotting $1/p(\equiv \partial\xi/\partial\theta)$ against θ, and integrating graphically to find ξ in terms of θ. The corresponding curves in fig. 3 were obtained by differentiating the approximate solutions so as to obtain $\zeta_1(=-pp_2)$ in terms of θ, and using equation (11) and fig. 2 to obtain $u\Big/\sqrt{\dfrac{4Gr\,Pr\,x}{3}}$ as a function of ξ.

---

* The results of the author's experiments (Saunders 1936) on the heat loss from vertical plates in a pressure chamber, which were expressed in dimensionless form taking $k = 5{\cdot}7\times10^{-5}$ c.g.s. units for air at 43° C (*International Critical Tables*), give $A = 0{\cdot}46$. According to more recent data (Kannuluik and Martin 1934; Hercus 1934; Gregory and Archer 1933; Sherratt and Griffiths 1939), however, the best value of k at 43° C is $6{\cdot}5\times10^{-5}$ c.g.s. units. Using this value the author's results give $A = 0{\cdot}416$, which agrees with Schmidt and Beckmann's value, but is slightly above the values from the approximate theory.

Squire's approximate solution

In the recently published book, *Modern Developments in Fluid Dynamics*, reference is made to a new method of approximate solution of the problem of natural convection due to a vertical plate given by Squire (unpublished) based on the equations of momentum and energy of the boundary layer as a whole. His results are given for comparison in figs. 2 and 3.

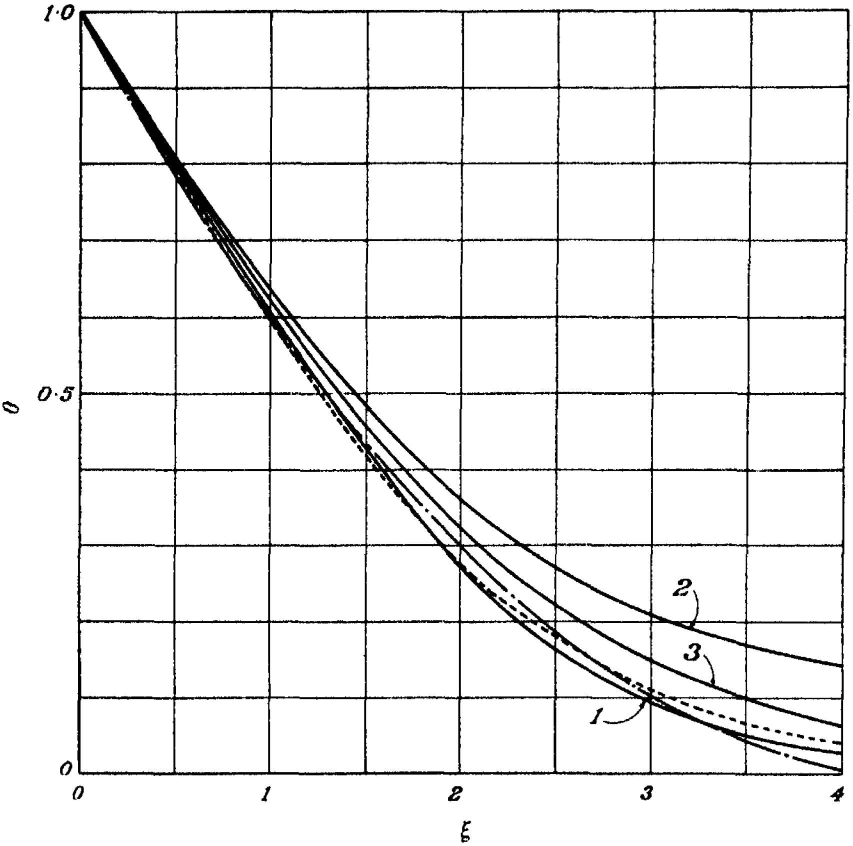

Fig. 2. Comparison between approximations for the temperature distribution in air and Pohlhausen's solution. ——— approximate theoretical solutions for air. ····· Pohlhausen's solution for air. —·— Squire's solution for air.

Mean heat transfer at the plate

The mean rate of heat transfer per unit area, H, for the plate of height l, is given by

$$H = -\frac{k\theta_0}{l}\int_0^1 \left(\frac{\partial\theta}{\partial y}\right)_{y=0} dx = \frac{k\theta_0}{l}\left(\frac{64 Gr\, Pr}{27}\right)^{\frac{1}{4}}\left(\frac{\partial\theta}{\partial\xi}\right)_{\xi=0},$$

where x, y, θ are dimensionless, as already defined.

Hence
$$\frac{Hl}{k\theta_0} = C(Gr\,Pr)^{\frac{1}{4}}, \tag{21}$$
where
$$C = 1{\cdot}241\,A.$$

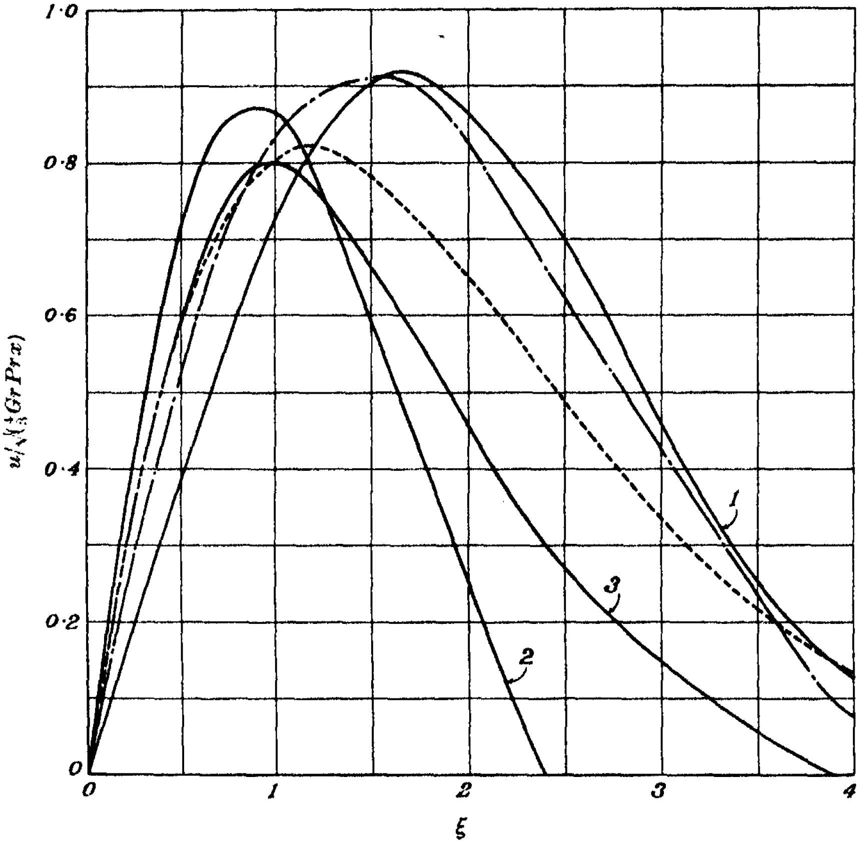

FIG. 3. Comparison between approximations for the velocity distribution in air and Pohlhausen's solution. ——— approximate theoretical solutions for air. ----- Pohlhausen's solution for air. —·— Squire's solution for air.

Range of validity of theory

The theory would be expected to break down when the flow becomes turbulent, which experiments with air show to occur when $Gr\,Pr$ exceeds about 2×10^9. It would also be expected that the theory would cease to be applicable for plates below a certain height, since the approximations of the boundary layer theory would not be justified. Experiments with air show this to be the case for values of $Gr\,Pr$ below about 10^3.

COMPARISON BETWEEN THEORY AND EXPERIMENTS WITH FLUIDS OTHER THAN AIR

The only experiments on natural convection due to a vertical plate in a liquid are those of Lorenz who, in 1934, measured the mean heat loss from a plate 12 cm. high in oil. Colburn and Hougen (1932), and Montsinger (1932), measured the heat losses to surrounding water from a vertical cylinder and a copper block respectively, but these shapes cannot strictly be compared with a vertical plate. The temperature and velocity in the fluid near the heated surface have not been measured for fluids other than air.

Lorenz expressed his results in the form of equation (21), giving $C = 0{\cdot}56$ for values of $Gr\,Pr$ between 10^7 and 10^9, which agrees well with the approximate theoretical value, $0{\cdot}54$ $(= 1{\cdot}241A)$, from fig. 1, curve 3, for Prandtl numbers above 10, which would include the oil used by Lorenz.

Experiments in air have shown that unsteadiness of flow begins at the top of the plate for a value of $Gr\,Pr$ equal to about 2×10^9, but this may not be true for other fluids, because of their different Prandtl numbers.

The following experiments were thought worth trying:

(1) Measurements of the loss from a heated vertical plate in mercury, for which $Pr = 0{\cdot}03$. For no other fluid is Pr appreciably below $0{\cdot}73$, the value for air, all other liquids having higher values than air. So far as the author knows, the heat loss by natural convection in mercury has not previously been investigated. Comparison between the approximate theory and experiments with mercury is thus of special interest.

(2) Measurements of the loss from a heated vertical plate in water, for both streamline and turbulent flow conditions, and comparison between the critical conditions at which unsteadiness of flow begins in water, and the corresponding known conditions for air.

HEAT LOSS FROM A VERTICAL PLATE IN MERCURY

Two electrically heated steel plates were used, of heights 2·8 and 4·65 cm., each of width 3·0 cm. These were small enough not to require more mercury than was conveniently available and yet gave values within the range of $Gr\,Pr$ for which the approximate theory is known to hold good for air. Fig. 4 shows the arrangement of the apparatus with the larger plate in position. The mercury filled a steel dish 18 × 20 cm. to a depth of 9 cm., the top of the heated plate being about 2·5 cm. below the mercury surface. Cooling water was circulated around the dish to keep the temperature of the mercury from rising.

Some difficulty was experienced in making an electric heater to give sufficient heat to the steel plate. Eventually a length of about 20 cm. of nichrome tape was wound into a flattened coil the size of the plate and was embedded in fireclay. The plate was pressed into contact with the surface of the fireclay before it set, the tape being just below the fireclay surface.

The larger plate had two thermocouples inserted in small holes drilled horizontally in its thickness, with junctions at the middle of the top and bottom halves of the plate. The smaller plate had one thermocouple at the middle.

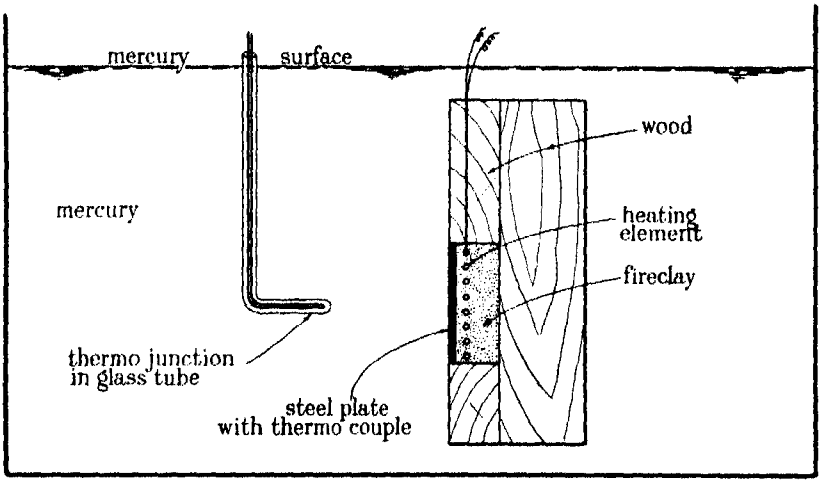

Fig. 4

In some preliminary experiments the heat input was maintained constant and, after allowing sufficient time for the various temperatures to become steady, the temperature of the mercury was explored with a movable thermocouple in a glass tube. It was found to be practically uniform horizontally but varied vertically, the greatest drop from the level of the top of the plate to the level of the bottom being 5 % of the mean difference between the temperatures of the plate and of the mercury. This was partly due, however, to non-uniformity of the plate temperature, the top couple reading up to about 8 % higher, relative to the mercury, than the bottom one. The effective temperature of the mercury was taken as the value at a point 4 cm. away along the normal from the middle of the plate. The mean of the two thermocouple readings was taken as the temperature of the larger plate, and the reading at its middle as the temperature of the smaller plate.

Fig. 5 shows a series of results obtained by changing the heat input every 10 min., which was found long enough for the temperatures to become steady. Several other sets of readings were taken for both ascending and descending series of inputs, with varying amounts of extra wood and cork at the back and sides to reduce the heat loss by conduction, and with freshly cleaned mercury and a freshly polished surface on the steel plate. The differences in the heat loss found in these experiments were very little greater than the differences between repeat readings, and it has not been thought

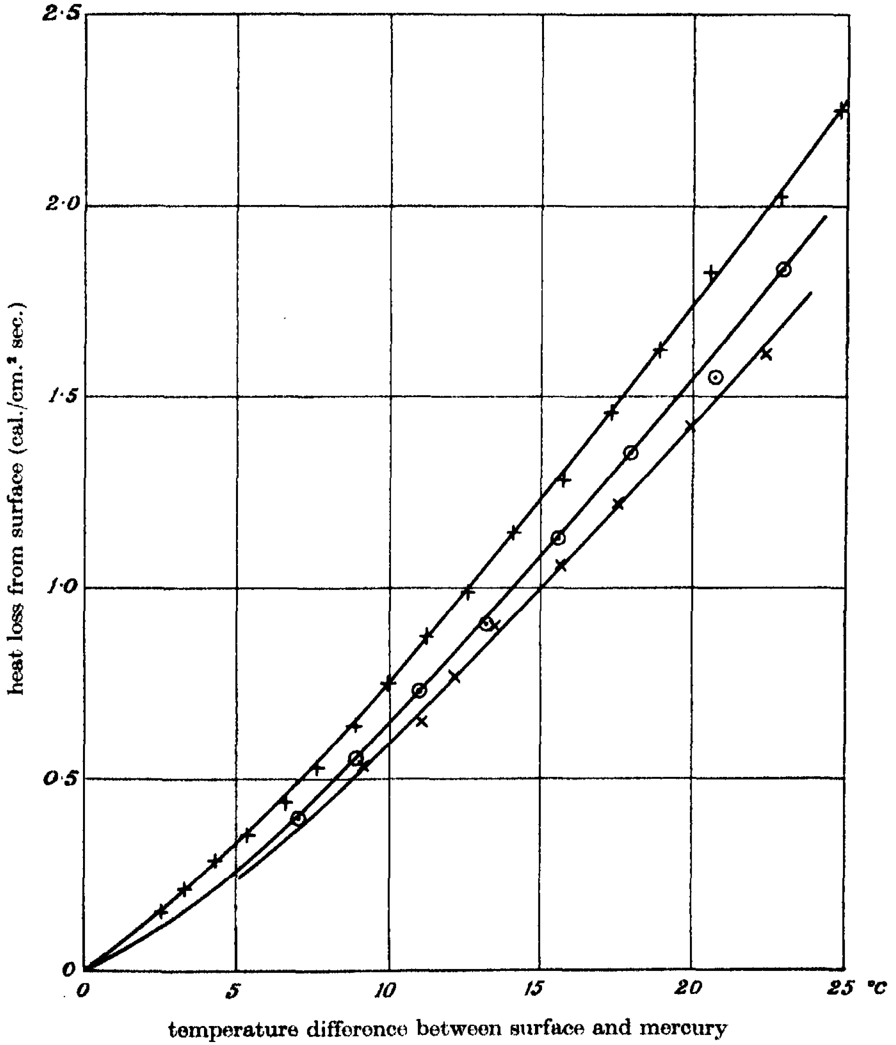

FIG. 5. Experimental results for the heat loss in mercury. × vertical plate, 4·65 cm. high; ⊙ vertical plate, 2·80 cm. high; + horizontal cylinder, 1·25 cm. diameter.

worth while to give all the results. Most of the readings gave points within ± 5 % of those in fig. 5.

Fig. 6 shows the results expressed in dimensionless co-ordinates. For mercury at 20° C, $k = 0{\cdot}02$ and $\beta gc/k\nu = 3510$; at 40° C, $k = 0{\cdot}02$ and $\beta gc/k\nu = 3690$, c.g.s. units in each case.

The dotted line shows the approximate theory, taken from fig. 1, curve 3,

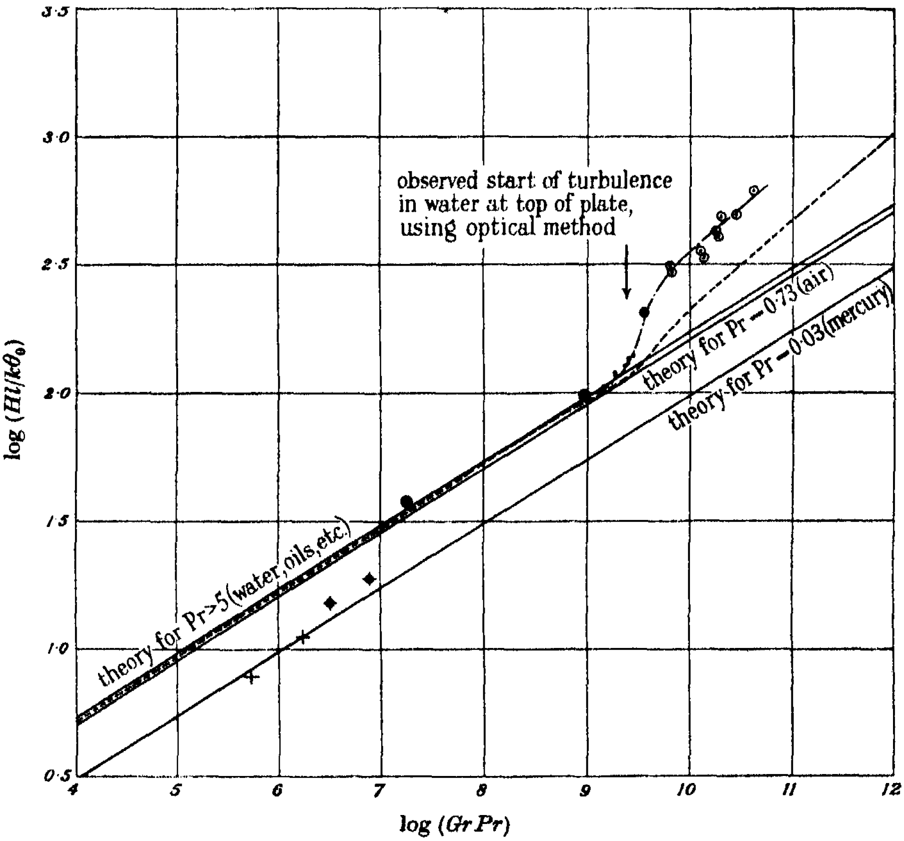

FIG. 6. Experimental and theoretical results for the heat loss from a vertical plate in air, water and mercury.

—— approximate theory (streamline flow).
• experiments in water with plate 30·5 cm. high.
⊙ experiments in water with plate 61 cm. high.
+ experiments in mercury with plate 2·80 cm. high.
✦ experiments in mercury with plate 4·65 cm. high.
◎ experiments in oil by Lorenz, plate 12 cm. high.
----- experiments in air by author (Saunders 1936).

which agrees quite well with the experiments. The experimental results may be expressed by a formula similar to (21) with $C = 0{\cdot}31$ for the smaller plate and $C = 0{\cdot}35$ for the larger plate. The two plates ought, of course, to give the same value of C. The theoretical values from the first, second and third approximations are 0·328, 0·30 and 0·28; the best agreement with the average of the two experiments is thus given by the first approximation.

HEAT LOSS FROM A VERTICAL PLATE IN WATER

Two plates were used, of heights 61 and 30·5 cm., each 30·5 cm. wide and made of aluminium 0·5 cm. thick. Electric heating elements of resistance tape, insulated on both sides by sheets of mica, were sandwiched between the aluminium and wood 2·5 cm. thick. The wood projected 2·5 cm. from the edges of the plate, and was built up flush with the front face of the aluminium. All the surfaces of the wood were coated with waterproof paint.

The heating elements for the larger plate were divided into four, and for the smaller plate into two, equal sections one above the other. Copper-eureka thermocouples were embedded in each section in horizontal grooves cut in the front face of the aluminium, and the grooves were filled in with lead. The thermo-junctions were at the middle of each section, and the currents in the different sections were adjusted so that all the couples gave nearly the same readings, and the plate temperature could be taken as uniform.

The plate was suspended in a water tank of height 160 cm. and horizontal section 25 by 61 cm., the top of the plate being about 30 cm. below the surface of the water. Preliminary runs were made to find the ratios of the currents in the various sections, which gave a uniform plate temperature.

In each main experiment the water was first thoroughly stirred. The heat was then turned on and the thermocouple readings taken over a period of time, during which readings of the temperature of the water at several positions were also taken with thermocouples, the leads of which were coated with hard varnish to prevent electrical leakage. It was found that the mean plate temperature reached a nearly constant value in about 15 min., after which it continued to rise very slowly. The temperature of the water at the top of the tank rose steadily and an increasing vertical gradient of temperature was set up in the water. As soon as readings had been taken for the first nearly constant condition, the heat input was altered to a higher value, and a second set of readings obtained. This was repeated several times, until the vertical temperature gradient in the water became too great, after which the whole apparatus was allowed to cool before another experiment was started. In some cases an experiment was ended because too many air bubbles were formed on the plate.

It was decided to reject all readings taken when the temperatures in the water opposite the top and bottom edges of the plate differed by more than 10 % of the difference between the mean plate and water temperatures. Under these conditions the water temperature was very nearly uniform horizontally at any level, except close to the plate.

The cold water entering the boundary layer is known to be drawn mainly from the region of the bottom edge of the plate, but some enters at other levels. Two thermocouples were therefore used to measure the effective water temperature, one being opposite the bottom edge and the other opposite the mid-level, and their mean was taken.

In order to allow for the heat loss through the wood, three pairs of differential thermocouples were embedded in the wood of the larger plate, the two junctions of each pair being at different depths along a line drawn normal to the surface. The leads were brought out along slanting holes drilled nearly parallel to the surface of the wood, so that they should lie as nearly as possible along isothermals. The three pairs of junctions were at positions along the vertical bisector of the plate, respectively 15, 30, and 45 cm. from the top edge. The couples were calibrated in position by placing a second plate, identical with the first, so that the two aluminium faces were in contact. Equal inputs were then supplied to each plate and, assuming half the total input to pass through the wood attached to each plate, three curves were plotted for each plate relating the heat flow through the wood to the differential reading of each of the three pairs of thermo-junctions. Hence three separate values of the heat loss through the wood, which ought to agree, were given from the calibration curves. Actually they were found to differ slightly, but as they were always less than 8 % of the total input it was thought justified to take a mean value. For the smaller plate the heat loss through the wood was assumed to be the same percentage of the input as for the larger plate.

A typical series of results is given in Table I. The values of the physical constants for water were reckoned at the mean of the plate and water temperatures, which in the case of the larger plate differs considerably for the different experiments; for this reason the results have not been shown in a graph of heat loss against temperature difference, as was done in the case of the results for mercury.

In fig. 6 the results are expressed in dimensionless co-ordinates. The approximate theoretical solution for water ($Pr > 5$) is shown by the full line. The results for the smaller plate agree well with the theory, but those for the

TABLE I. RESULTS FOR WATER

Mean temperature difference between plate and water ° C	Mean of plate and water temperatures ° C	Total heat input to plate cal./cm.² sec.	Net heat loss from plate cal./cm.² sec.	$\frac{\beta g c}{k\nu}$ 1/cm.³ ° C.	k cal./cm. sec. ° C.	log $Gr\,Pr$	log $Hl/k\theta_0$	Type of flow
Plate height, l, 30·5 cm.								
4·1	19·8	$24·8 \times 10^{-3}$	$23·4 \times 10^{-3}$	$1·50 \times 10^{4}$	$1·38 \times 10^{-3}$	9·24	2·10	Steady
5·5	21·4	34·0	32·2	1·68	1·39	9·42	2·11	,,
3·9	19·4	20·3	19·0	1·45	1·37	9·20	2·04	,,
4·0	19·4	20·5	19·1	1·45	1·37	9·22	2·03	,,
3·8	19·7	19·4	18·1	1·49	1·38	9·21	2·02	,,
3·5	20·0	18·5	17·3	1·52	1·38	9·18	2·04	,,
4·7	20·2	27·1	25·5	1·54	1·38	9·21	2·08	,,
6·4	19·9	39·8	37·7	1·51	1·38	9·44	2·11	Unsteady
3·9	18·5	20·1	18·7	1·35	1·37	9·17	2·03	Steady
4·7	20·3	28·2	26·6	1·56	1·38	9·32	2·10	,,
5·5	20·7	34·4	32·6	1·60	1·39	9·40	2·11	Unsteady
6·4	20·3	42·2	40·1	1·56	1·38	9·45	2·14	,,
6·9	20·3	45·8	43·5	1·56	1·38	9·48	2·15	,,
Plate height, l, 61 cm.								
1·7	14·7	$9·35 \times 10^{-3}$	$8·1 \times 10^{-3}$	$0·92 \times 10^{4}$	$1·33 \times 10^{-3}$	9·55	2·33	Unsteady
2·5	17·1	19·5	18·0	1·18	1·35	9·82	2·51	,,
2·6	17·7	19·6	18·1	1·24	1·35	9·86	2·50	,,
3·8	19·3	38·7	36·7	1·43	1·37	10·09	2·63	,,
5·5	16·0	47·6	45·1	1·05	1·34	10·11	2·57	,,
5·9	16·5	47·6	45·1	1·11	1·34	10·17	2·54	,,
6·3	18·8	64·5	61·4	1·37	1·37	10·29	2·64	,,
6·5	19·0	64·6	61·5	1·38	1·37	10·31	2·62	,,
6·3	20·3	74·0	71·0	1·56	1·38	10·34	2·70	,,
7·1	24·6	87·0	83·8	1·98	1·42	10·50	2·71	,,
7·4	30·1	110·0	106·0	2·52	1·46	10·63	2·78	,,

Note. The values of the physical constants for water are taken from Landolt and Bornstein's *Physikalisch-Chemische Tabellen*.

larger plate are higher than the theory, owing, as shown below, to turbulence.

Observations of type of flow by optical method

Observations of the type of flow near the plate were made by an optical method. This, which has been described elsewhere (Saunders and Fishenden 1935), consists in observing the angular deflexion of a beam of light passing parallel to, and very near, the heated plate, brought about by refraction due to the temperature gradients in the fluid. A horizontal beam of light from a carbon arc several metres away entered and left the tank through glass windows in the narrow vertical sides, and the angular deflexion due to the heated plate was observed on a screen. For steady streamline motion the deflexion shown on the screen for any point on the plate was constant, but for unsteady flow it varied with time.

With the smaller plate steady motion was observed over the whole height at temperature differences below about 5° C, above which unsteadiness occurred starting at the top. With the larger plate the motion was unsteady except near the bottom edge. The critical value of $Gr\,Pr$ at which unsteadiness was first observed was about 2×10^9, which is practically the same as the corresponding value for air.

Owing to the unsteadiness of the flow it is not surprising that the results for the larger plate do not agree with the streamline theory. For fully developed turbulent flow the heat transfer per unit area would be expected to be practically independent of distance up the plate, and the slope of the curve in fig. 6 would thus be one in three. The experimental points for the larger plate, which are based on the mean heat transfer for the whole plate, suggested a slope somewhat steeper than one in three, especially for the lower points. This is probably due to the flow near the lower part of the plate, which is partly streamline and partly in the transition stage between streamline flow and turbulence.

The results in fig. 6 for air ($Pr = 0{\cdot}73$) and water ($Pr \doteqdot 7{\cdot}0$), when the flow is not streamline, suggest that the mean curve is higher the higher the Prandtl number. By taking a line of slope one in three through the experimental points for the larger plate in water, it is found that

$$\frac{Hl}{k\theta_0} = 0{\cdot}17(Gr\,Pr)^{\frac{1}{3}}$$

for values of $Gr\,Pr$ above about 10^{10}, and for a mean value of Pr equal to about 7·0.

The corresponding equation from the experimental curve for air ($Pr = 0{\cdot}73$) is

$$\frac{Hl}{k\theta_0} = 0{\cdot}10(Gr\,Pr)^{\frac{1}{4}}.$$

The work was carried out in the Mechanical Engineering Department of Imperial College and the author wishes to thank Professor C. H. Lander for his help and interest in the work. He is also indebted to the Clothworkers Company for financial assistance which enabled the work to be carried out.

REFERENCES

Colburn and Hougen 1932 See W. J. King 1932 *Mech. Engng*, p. 347.
Gregory and Archer 1933 *Phil. Mag.* **15**, 301.
Hercus and Sutherland 1934 *Proc. Roy. Soc.* A, **145**, 599.
Kannuluik and Martin 1934 *Proc. Roy. Soc.* A, **144**, 496.
Lorenz 1881 *Ann. Phys., Lpz.*, **13**, 582.
— 1934 *Z. tech. Phys.* **15**, 362.
Montsinger 1932 See W. J. King 1932 *Mech. Engng*, p. 367.
Pohlhausen 1921 *Z. angew. Math. Mech.* **1**, 115.
— 1930 *Tech. Mech. Thermodynam., Berl.*, **1**, 391.
Saunders 1936 *Proc. Roy. Soc.* A, **157**, 278.
Saunders and Fishenden 1935 *Engineering*, **139**, 483.
Schmidt and Beckmann 1930 *Tech. Mech. Thermodynam., Berl.*, **1**, 341.
Sherratt and Griffiths 1939 *Phil. Mag.* **27**, 68.

The excitation of γ-radiation in processes of proton capture

By S. C. Curran, *St John's College*
and J. E. Strothers, *Newnham College*
The Cavendish Laboratory, Cambridge

(*Communicated by W. L. Bragg, F.R.S.—Received* 5 *April* 1939)

1. Introduction

It is found that many light elements emit γ-radiation during bombardment by protons of high energy. Excitation curves relating the intensity of the emitted γ-radiation with the energy of the incident protons do not increase smoothly with increasing bombarding voltage, but show, in most instances, pronounced maxima. The resonance character of these excitation curves is most naturally explained by assuming that the γ-radiations arise in the process of capture of protons by nuclei, and measurements of the quantum energies of these radiations lend general support to the assumption that the γ-rays have this origin. In a previous paper (Curran, Dee and Petržílka 1938) the results of an investigation of the process of proton capture by the four light elements, beryllium, boron, carbon and fluorine, have been given. The experiments have now been extended to include the five elements lithium, sodium, magnesium, phosphorus and chlorine. The form of the excitation curve for the intensity of the capture γ-radiation has been determined for incident protons of energy up to 10^6 eV, and in each case the quantum energy of the radiation has been measured. An attempt has also been made to detect the capture of protons by deuterium but no definite evidence of the occurrence of this process could be obtained.

2. The experimental arrangement and detecting apparatus

The experiments were carried out in the Cavendish High Voltage Laboratory, using the Philips generator and the associated discharge tube installation from which beams of ions with energies up to $1 \cdot 1 \times 10^6$ eV are available. The targets were under the bombardment of protons, separated from the rest of the ion beam by magnetic analysis. The system used for the detection of the γ-rays emitted from the targets consisted of a pair of thin-walled Geiger-Müller counters. The capture γ-radiation ejected from an aluminium plate Compton electrons, photoelectrons and electron pairs and some of these passed through both counters causing real coincidences. The high sensitivity and low natural effect of this arrangement render it suitable for the detection of weak resonances. The range distribution of the electrons can be determined by placing absorbing screens between the counters and observing the number of coincidences as a function of the thickness of absorber, and the end-point of the absorption curve so obtained gives a measure of the maximum quantum energy of the γ-ray. The Geiger-Müller counters were coupled to an improved amplifying circuit having a resolving time for coincidences of approximately 10^{-6} sec. In all other respects the experimental arrangement and method of procedure were the same as those described in the earlier paper (Curran *et al.* 1938). Some features of the detecting system are described elsewhere (Curran and Petržílka 1939).

3. PREPARATION OF THE TARGETS

Lithium targets of the desired thickness were prepared by burning the metal in air and collecting the oxide on a clean copper surface. Sodium targets were obtained by evaporation of solutions of sodium bromide. The purity of this compound had been established by observations of the groups of α-particles and protons which were emitted from the salt under deuteron bombardment. Thin targets of metallic magnesium were deposited on copper by evaporation of the pure metal *in vacuo*, but for experiments in which thick targets were required, magnesium was burned in air and the products of combustion collected upon clean copper. The agreement between the results which were obtained with these two different types of target showed that the oxygen and nitrogen present in the latter case did not yield any measurable intensity of γ-radiation. Red phosphorus compressed into the pitted surface of a copper block proved to be sufficiently stable under bombardment with protons to serve as a suitable target. Evaporation of alcoholic solutions of analytically pure copper chloride gave suitable "chlorine" targets. Targets of heavy ice were obtained by the condensation of heavy water vapour upon a copper block which was cooled with liquid air.

4. EXPERIMENTAL RESULTS

(*a*) *Heavy hydrogen*

According to mass values the process

$$ {}^1\mathrm{H} + {}^2\mathrm{H} = {}^3\mathrm{He} + h\nu \qquad (1) $$

is exoergic with $h\nu = 5{\cdot}39 \times 10^6$ eV for zero bombarding energy of the proton. A target of heavy ice was bombarded with protons with energies from $0{\cdot}5 \times 10^6$ to $1{\cdot}0 \times 10^6$ eV. The detecting system was placed as close as possible to the target. A very low intensity of γ-radiation, showing no evidence of resonance characteristics, was observed. The yield of γ-quanta per incident proton appeared from the results of these experiments to be less than 10^{-11}. It is possible that this extremely small positive effect might arise from the bombardment of heavy ice by deuterons originating in the target itself and deriving their energy from the incident protons.

(*b*) *Lithium*

Hafstad and Tuve (1935) measured the yield of γ-rays from lithium and found two very sharp resonances at 440 and 850 kV. Further work however failed to confirm the existence of the peak at 850 kV (Hafstad, Heydenburg and Tuve 1936) but produced evidence of a high intensity of γ-radiation in the neighbourhood of 1000 kV (Rumbaugh and Hafstad 1936). Later work by Herb, Kerst and McKibben (1937) indicated the presence of a broad resonance at about 1000 kV instead of the previously reported peak at 850 kV. Working at lower voltages Bothe and Gentner (1937) observed a resonance peak at a bombarding voltage of 200 kV. We have examined the excitation curve from 350 to 1000 kV with the results shown in fig. 1. In an attempt to increase the homogeneity of the resolved proton beam a slit was introduced into the target tube. Curve 1 shows the results which were obtained with the improved resolution; in curve 2, taken without the defining slit and with a thicker target, the results were extended to 1000 kV. The points on the figure show values observed in several different runs. It may be seen that these results give no evidence either of a peak in the excitation curve at 850 kV or of any marked increase in the yield of γ-radiation near 1000 kV. Herb *et al.* (1937) report that the peak intensity at the upper resonance level near 1000 kV occurs between 1020 and 1200 kV according to the thickness of the target, and this peak would not therefore have been obtained in the present experiments in which the bombarding voltage did not exceed 1000 kV. The published curves of these workers however indicate a yield of γ-radiation at 1000 kV of between 50 and 100 % of the maximum yield at 440 kV. According to the present experiments, the intensity at 1000 kV is only 15 % of that at 440 kV. It is hoped to extend the measurements to higher voltages in the near future.

Capture of protons by ^{6}Li might be expected to lead to the formation of radioactive ^{7}Be (Rumbaugh, Roberts and Hafstad 1938):

$$^6\mathrm{Li} + {}^1\mathrm{H} = {}^7\mathrm{Be} + h\nu. \qquad (2)$$

The failure to observe any resonances other than that at 440 kV seems to indicate that the above process does not take place with protons of energy less than 1000 kV, since it has been established that this resonance is due to the process

$$^7\mathrm{Li} + {}^1\mathrm{H} = {}^8\mathrm{Be} + h\nu. \tag{3}$$

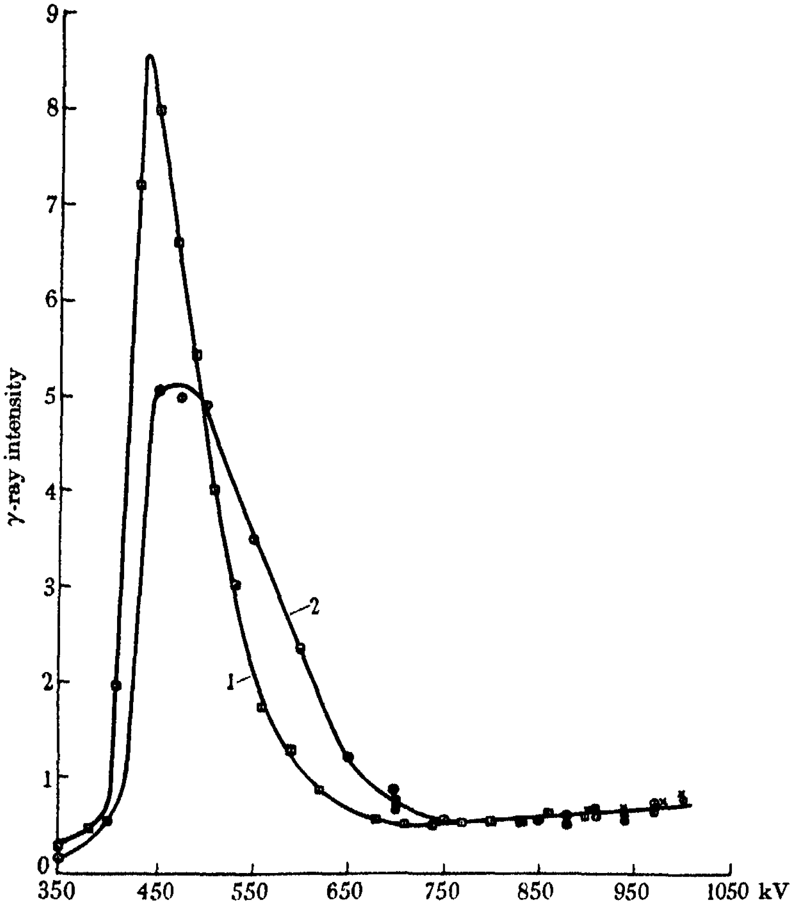

FIG. 1

It is possible that the very intense radiation emitted according to equation (3) might conceal any weaker effect produced in proton capture by ^{6}Li but an alternative method of detection of the occurrence of the process (2) is available in the investigation of the formation of radioactive ^{7}Be. Long bombardment (of the order of 200 μA-hr.) of lithium targets at voltages as high as 950 kV did not produce any measurable quantity of ^{7}Be. Calculations based upon the actual experimental arrangements used prove that the yield of capture γ-quanta per incident proton must be less than $2{\cdot}5 \times 10^{-10}$.

Many determinations (Crane, Delsasso, Fowler and Lauritsen 1935; Delsasso, Fowler and Lauritsen 1936; Gaerttner and Crane 1937; Delsasso, Fowler and Lauritsen 1937) of the quantum energies of the γ-radiation emitted in process (3) have been made, but the results which have been obtained are somewhat contradictory. Whereas there is general agreement in assigning an upper limit to the quantum energy of about $17{\cdot}0 \times 10^6$ eV, the quantum energies of the softer components have not been definitely established.

Two thin-walled counters were used in the manner described above to determine the quantum energy of the γ-radiation emitted from the target under bombardment with protons of energy $0{\cdot}6 \times 10^6$ eV. Using the relationship established in previous work (Curran *et al.* 1938) the end-point of the absorption curve at 32·0 mm. of aluminium corresponds to a quantum energy of $18{\cdot}6 \times 10^6$ eV, whereas from mass values the expected energy release is $17{\cdot}6 \times 10^6$ eV. These values are in agreement within the experimental accuracy of the determination. The "half-value thickness" obtained from the curve indicates (Mitchell and Langer 1937) a quantum energy of $16{\cdot}8 \times 10^6$ eV. This result suggests that only a small percentage of softer radiation can be present.

(*c*) *Sodium*

Herb *et al.* (1937) detected the emission of γ-radiation from targets of metallic sodium bombarded with protons of energies between $0{\cdot}9 \times 10^6$ and $2{\cdot}0 \times 10^6$ eV. One broad resonance was observed extending from 1150 to 1320 kV. Gentner (1937), working at low voltages, found a sharp resonance at 305 kV. We have investigated the emission of γ-radiation in the process

$$^{23}\mathrm{Na} + {}^{1}\mathrm{H} = {}^{24}\mathrm{Mg} + h\nu, \tag{4}$$

and have detected between 400 and 920 kV six resonances, not hitherto reported. From curves 1 and 2 of fig. 2, the peak values for these resonances are seen to be at 425, 525, 590, 690, 755 and 875 kV. These two curves are representative of a series, all of which exhibited the same characteristics. Curve 1 was obtained with the defining slit in front of the target in order to increase the homogeneity of the proton beam, but the peaks are not more clearly resolved. The abundance of resonances in this region of bombarding voltages indicates the close spacing of the excitation levels of the magnesium nucleus at about 11×10^6 eV above the ground state.

The maximum quantum energy to be expected in the process defined by equation (4) is, according to accepted mass values (Livingstone and Bethe 1937) and for protons of energy $0{\cdot}75 \times 10^6$ eV, $11{\cdot}6 \times 10^6$ eV. Gentner (1937), by the "half-value thickness" method, obtained the value $8{\cdot}3 \times 10^6$ eV and suggested that the process of de-excitation occurred by the successive emission of two or more quanta.

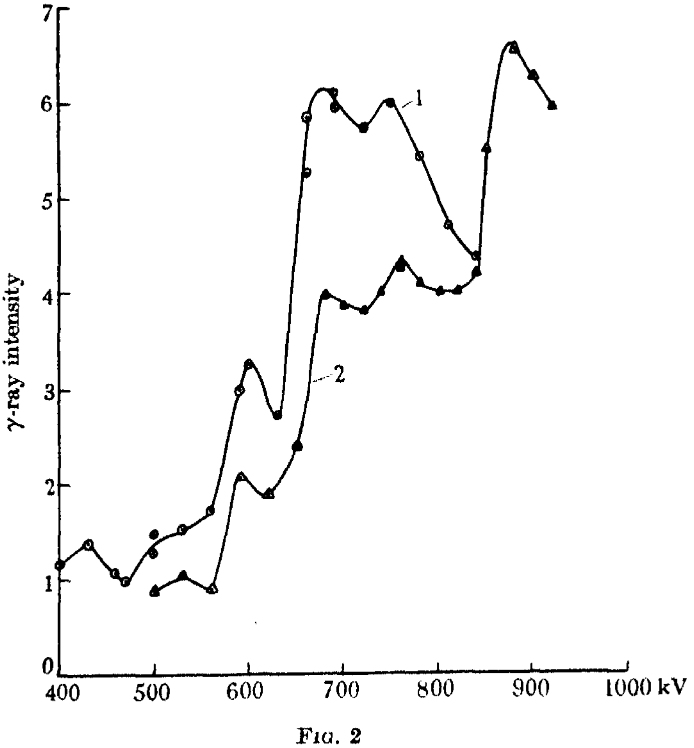

Fig. 2

In curves 1 and 2, fig. 3, the results of absorption measurements are shown. The range of the secondary electrons (18·2 mm. of aluminium) corresponds to a value of $h\nu = 11{\cdot}2 \times 10^6$ eV. This agreement with the calculations from the accepted mass values proves that the excited ^{24}Mg nucleus may return to the ground level with the emission of a single quantum of γ-radiation. The possibility, however, of transitions to intermediate states of excitation with the emission of softer radiations is supported by the observation that the "half-value thickness" of 3·5 mm. of aluminium indicates a quantum energy of $6{\cdot}5 \times 10^6$ eV.

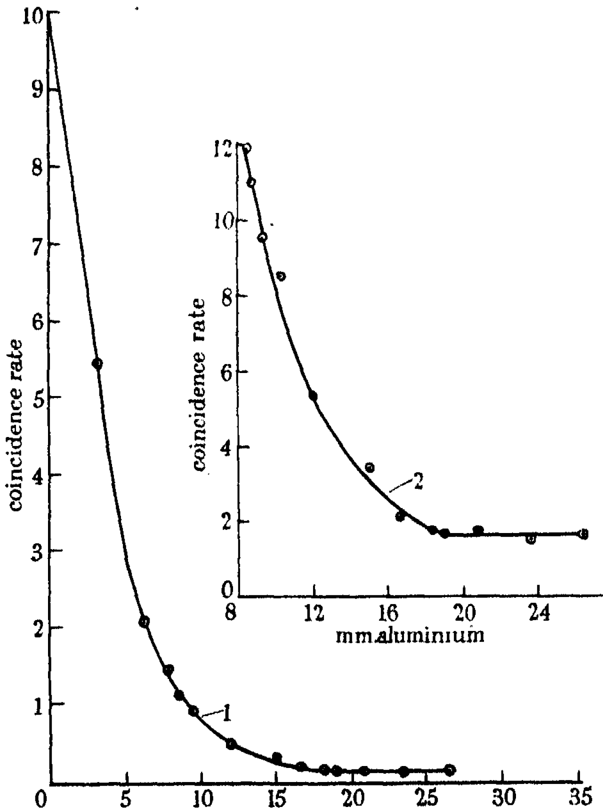

FIG. 3

(*d*) *Magnesium*

The three known isotopes of magnesium ^{24}Mg, ^{25}Mg and ^{26}Mg are of relative abundance 77·4, 11·5 and 11·1 % respectively. Capture of a proton by the most abundant isotope would lead to the formation of the unknown element ^{25}Al. In the case of the two heavier isotopes capture might be expected to take place according to the reactions:

$$^{25}\text{Mg}+{}^{1}\text{H} = {}^{26}\text{Al}+h\nu, \tag{5}$$

$$^{26}\text{Mg}+{}^{1}\text{H} = {}^{27}\text{Al}+h\nu. \tag{6}$$

Bombardment of sodium with alpha-particles leads to the formation of a radioactive element of half-life approximately 7 sec. which is presumed to be ^{26}Al,

$$^{23}\text{Na}+{}^{4}\text{He} = {}^{26}\text{Al}+{}^{1}\text{H}. \tag{7}$$

The subsequent decay of the ^{26}Al takes place with the emission of positrons of maximum energy $1{\cdot}8 \times 10^6$ eV (Frisch 1934),

$$^{26}\mathrm{Al} = {}^{26}\mathrm{Mg} + e^{+}. \tag{8}$$

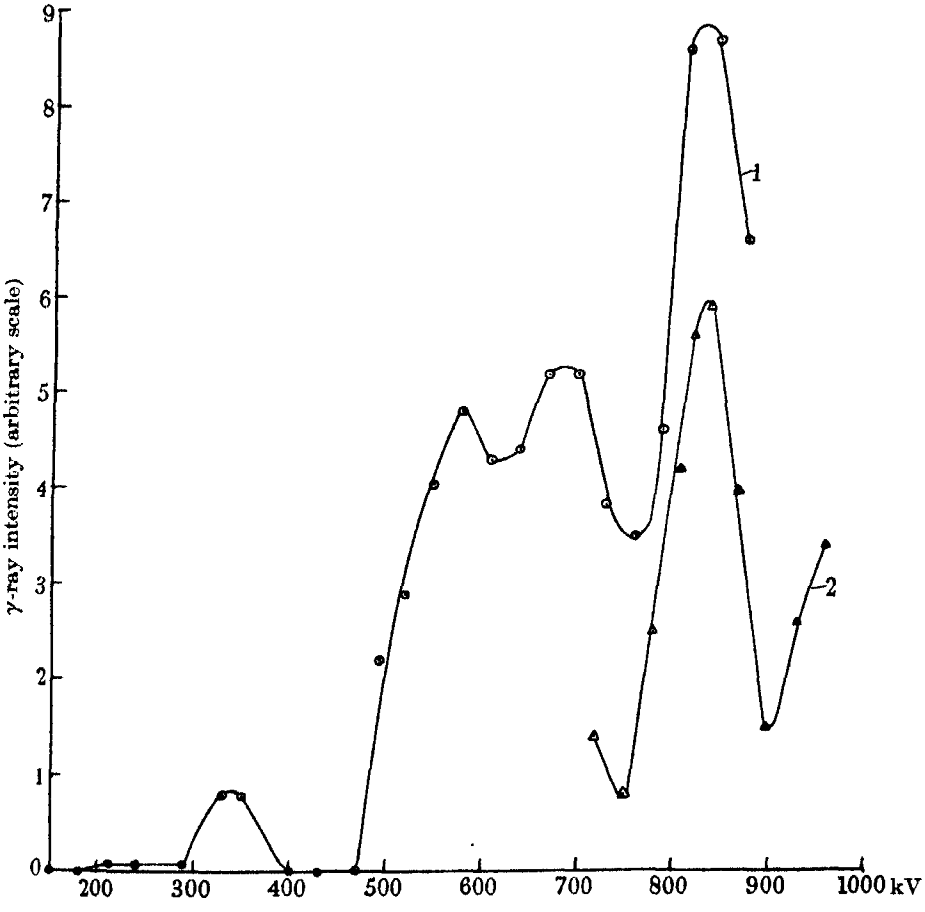

FIG. 4. Curve 1, magnesium oxide; curve 2, magnesium.

When magnesium targets were bombarded by protons, coincidences produced by the secondary electrons released by the capture γ-rays were detected with the standard arrangement of two Geiger-Müller counters. Although of weak intensity, the yield curve for the γ-radiation revealed at least three well-defined maxima. In an attempt to inspect the excitation function more closely, a single Geiger-Müller counter was employed and the results of this measurement are shown in curve 1 of fig. 4, where resonance peaks occur at 580, 680 and 825 kV. It is possible that the small peak at 340 kV may also result from the bombardment of magnesium but its weak intensity precluded decisive experiments. In the region of higher voltages the γ-emission was sufficiently intense for coincidence counting methods to be employed successfully in its detection, and curve 2 of fig. 4 was obtained. This curve indicates the existence of another resonance peak in the neighbourhood of 1000 kV.

A possible method of differentiating between the effects due to the two isotopes ^{25}Mg and ^{26}Mg is available in the study of the excitation function for the production of ^{26}Al from ^{25}Mg according to equation (5). This reaction has not previously been reported, but it was found that magnesium targets became radioactive under proton bombardment, the half-life of the radioactive element being approximately 7 sec., in agreement with the period of the radioactivity produced by α-particle bombardment of sodium and interpreted as due to the formation of ^{26}Al according to equation (7). The investigation of the excitation function for the production of ^{26}Al from ^{25}Mg was carried out as follows. For each value of the bombarding energy the proton beam was allowed to fall upon the target for a period of 15 sec. The beam was switched off and starting 5 sec. after cessation of bombardment, the decay of the activity of the target was followed by means of a thin-walled Geiger counter placed in front of a thin aluminium window near the target. From the decay curves obtained in this way the initial intensity of the radioactivity at each bombarding voltage was calculated and this is plotted as a function of bombarding voltage in fig. 5. Curve 1 indicates the existence of five resonance peaks at 180, 410, 480, 575 and 825 kV. Curve 2 shows the results of a more detailed study of the peak at 825 kV, a thinner metallic target being employed. Repeated measurements of the yield from different targets were made between the limits 350 and 650 kV (curves 3 and 4) and they agree in showing evidence of the existence of three resonances within this region of bombarding voltage. The differences in the relative intensities of the peaks in these sets of observations may be due to differences in target thickness and actual experimental difficulties in the measurements of proton current, etc. As a check on the process giving rise to the resonances of fig. 5, the period of the radioactivity was determined at four different bombarding voltages, 350, 430, 650 and 850 kV; average values of the half-life so obtained were 7·2, 8·5, 7·7 and 7·25 sec. respectively.

From consideration of the method of detection it is obvious that the peaks of fig. 5 must be due to capture by the isotope ^{25}Mg. The question remains as to which of the two isotopes ^{25}Mg and ^{26}Mg is involved in the production of the peaks of fig. 4. In view of the agreement in position and relative intensity it would seem reasonable to assign the common resonance at 825 kV to ^{25}Mg. Having made this assumption it may be deduced that the other established resonances at 580, 680 and 1000 kV (fig. 4) must arise

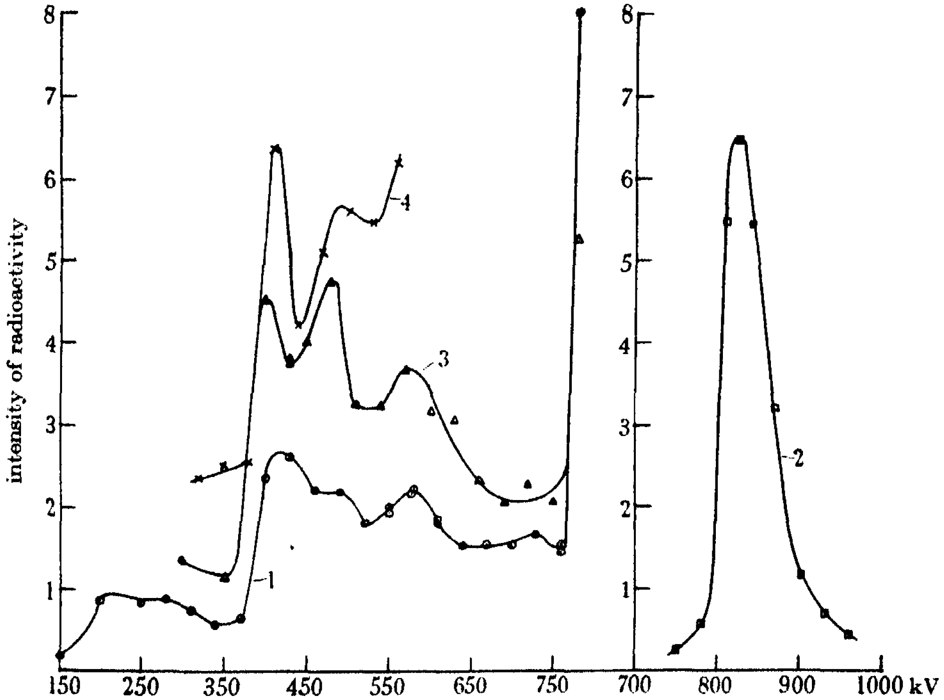

Fig. 5

from capture by ^{26}Mg. Thus from considerations of position in the voltage scale the only ambiguous case is the resonance at 580 kV which is almost coincident with the resonance at 575 kV due to ^{25}Mg (fig. 5). However if we assume proportionality between radioactive intensity and emitted γ-ray intensity it can be shown that the peak at 580 kV in fig. 4 must be ascribed to ^{26}Mg. The ratio of the intensity of induced radioactivity at the resonance peaks 575 and 825 kV is found to be 1 : 25, while, on the other hand, for the capture γ-rays, the ratio of the peak intensities at 580 and 825 kV is 14 : 25. It would appear correct therefore to allocate the resonance at 580 kV to ^{26}Mg. Comparison of curves 2 of figs. 4 and 5 indicates that the resonance effect at about 1000 kV is due to the same isotope since there is no evidence of it in the yield function of the radioactivity. The argument used here would be invalid if the numbers of γ-quanta emitted per capture changed violently from peak to peak, but such a possibility seems very improbable. The results may therefore be summarized in the form shown in Table I.

TABLE 1

Isotope	Resonance peak voltages (kV)
^{25}Mg	180, 410, 480, 575, 825
^{26}Mg	580, 680, 1000

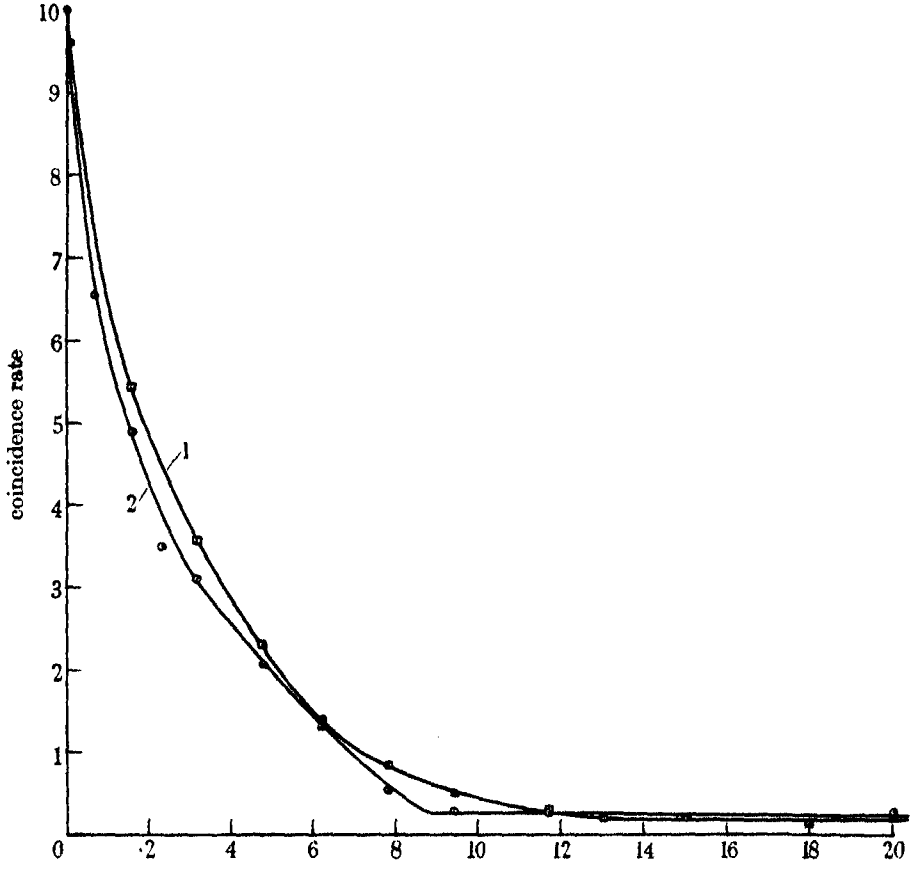

FIG. 6

Further evidence in support of these conclusions may be obtained from measurements of the quantum energy of the γ-rays released in the capture process. At a bombarding potential of 850 kV the capture γ-radiation must be due almost entirely to ^{25}Mg. Absorption measurements made at this voltage are shown in curve 1, fig. 6, and the end-point at 13·0 mm. of aluminium corresponds to a quantum energy $h\nu = 8{\cdot}0 \times 10^6$ eV, while the "half-value thickness" indicates a quantum energy of $4{\cdot}0 \times 10^6$ eV, suggesting that the γ-radiation is heterogeneous. From equation (5), using probable mass values (see below), the calculated value of $h\nu$ is $(9{\cdot}1 \pm 2{\cdot}72) \times 10^6$ eV; the experimental value lies within the limits of error.

If the bombarding potential of the proton beam is 620 kV, the isotope responsible for the release of a large percentage of the γ-radiation is ^{26}Mg, and curve 2 of fig. 6 shows the results of measurements obtained at this voltage. The end-point at 8·8 mm. of aluminium is equivalent to a quantum energy of $5{\cdot}6 \times 10^6$ eV and the half-value thickness corresponds to a quantum energy of $3{\cdot}0 \times 10^6$ eV, which again suggests the presence of softer radiations. According to equation (6) for protons of energy 620×10^3 eV the quantum energy $h\nu$ is equal to $(8{\cdot}1 \pm 1{\cdot}2) \times 10^6$ eV, while the end-point of curve 2, fig. 6 indicates a value of $5{\cdot}6 \times 10^6$ eV for the maximum energy release. There is therefore a minimum discrepancy of $1{\cdot}3 \times 10^6$ eV between the experimental and calculated values and this may indicate that transitions between the excited state of ^{27}Al at about $6{\cdot}9 \times 10^6$ eV and the ground state may not occur. Support for this view of the process would be found in the existence of an excited state of the ^{27}Al nucleus at about $1{\cdot}3 \times 10^6$ eV. By α-particle bombardment of ^{24}Mg an excitation level of ^{27}Al at $0{\cdot}98 \times 10^6$ eV has been found (Duncanson and Miller 1934) and γ-rays from ^{27}Mg of about $1{\cdot}0 \times 10^6$ eV quantum energy have been detected (Henderson 1935; Richardson 1938).

Using the absorption method an estimate has been made (fig. 7) of the maximum energy of the positrons emitted by ^{26}Al according to equation (7). At a bombarding potential of 825 kV a strong source of positrons is available. The observed end-point at 2·85 mm. of aluminium when corrected for the thickness of the counter wall and of the target tube corresponds to a β-ray energy of $2{\cdot}2 \times 10^6$ eV (Widdowson 1939). The mass value of ^{26}Al used in the above calculation of the energy release in equation (5) was deduced from this value of the positron energy (see also Livingstone and Bethe 1937).

The total number of positrons emitted from a target of magnesium oxide after bombardment with a known proton current for a known period of time was measured, due allowance being made for the geometry of the apparatus, absorption by the counter walls, decay of the radioactivity during bombardment and so on. The yield of positrons per incident proton (reactions 5 and 7) was thus found to be $0{\cdot}75 \times 10^{-11}$ at 410 kV, and at 825 kV this is increased to $1{\cdot}5 \times 10^{-10}$. The assumption that for each proton captured by ^{25}Mg two quanta are emitted seems reasonable in view of the observed "half-value thickness" and therefore the yields of γ-quanta per incident proton are $1{\cdot}5 \times 10^{-11}$ and $3{\cdot}0 \times 10^{-10}$ at 410 and 825 kV respectively. From the ratios of the radioactive intensities at the resonance peaks (Table II) the yields of γ-quanta per proton at various bombarding voltages may be calculated in the case of ^{25}Mg.

TABLE II

Resonance voltage $\times 10^{-3}$	180	410	480	575	825
Intensity	0·3	1·0	0·8	0·8	20·0

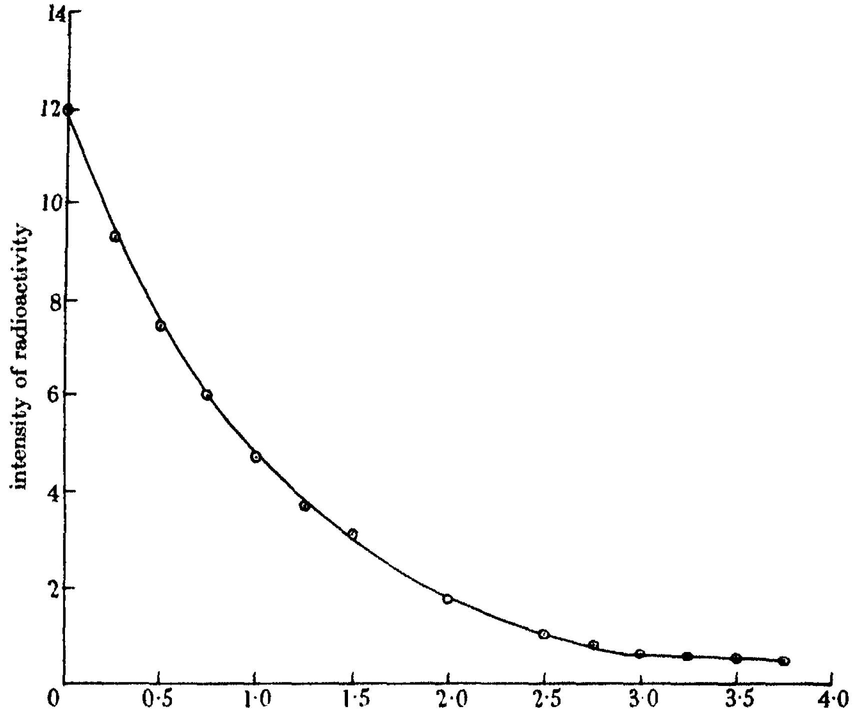

FIG. 7

From curve 1 of fig. 4 it is possible to deduce the yields of γ-quanta per proton at the resonance peaks at 580 and 680 kV arising from capture by ^{26}Mg. It is apparent that the ratios of the intensities of the peaks at 580, 680 and 825 kV are 11 : 12 : 20. From the yield at 825 kV previously calculated ($3{\cdot}0 \times 10^{-10}$) the yields in the case of ^{26}Mg are $1{\cdot}9 \times 10^{-10}$ and $2{\cdot}1 \times 10^{-10}$ at the lower voltages. These figures are corrected for the variable efficiency of the counters with γ-ray energy and it is assumed that, in the case of ^{26}Mg, as in the case of ^{25}Mg, two quanta per disintegration are emitted.

(*e*) *Phosphorus*

Substituting accepted mass values in the equation

$$^{31}\mathrm{P} + {}^{1}\mathrm{H} = {}^{32}\mathrm{S} + h\nu, \tag{9}$$

it appears that the capture of protons by phosphorus is exoergic to the extent of $(9{\cdot}45 \pm 0{\cdot}076) \times 10^6$ eV for zero energy of the incident proton. We have found that the γ-radiation emitted in this process is of weak intensity, and for the investigation of its excitation function a single Geiger-Müller counter was employed. The results of this measurement are shown in fig. 8, from which it is apparent that the threshold value of the voltage for γ-emission is 350 kV. The excitation curve obtained by using a thick target shows four rather broad resonances having maxima at 460, 580, 700 and 950 kV.

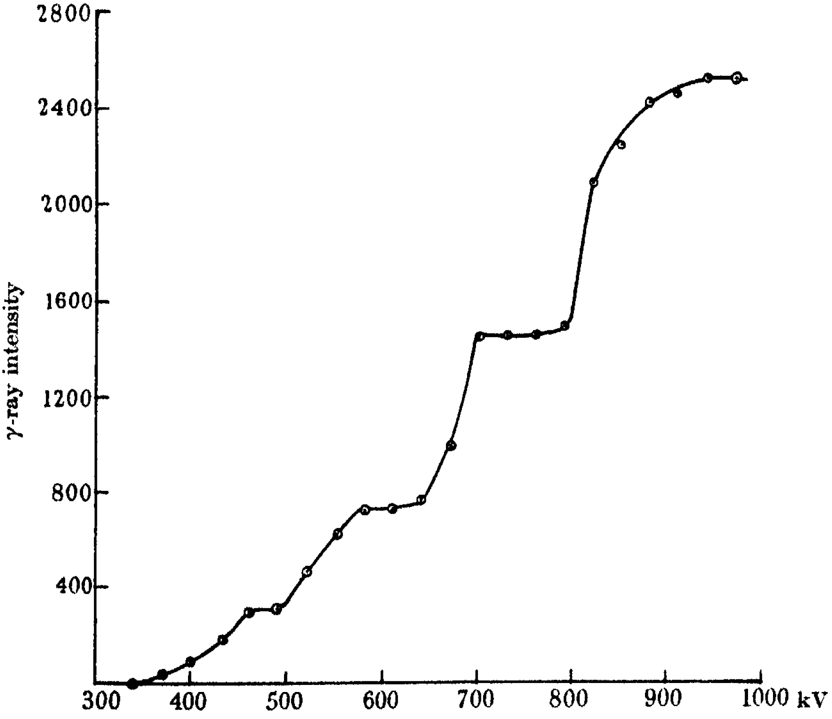

FIG. 8

The energy of the capture γ-radiation for a proton energy of 850×10^3 eV was measured in the usual manner. On account of the weak intensity of the γ-rays the absorption curve was not followed in detail beyond a thickness of 12 mm. of aluminium but it indicated that the end-point could not be less than this value and that therefore the maximum energy release is at least $7{\cdot}5 \times 10^6$ eV. The mixed nature of the radiation is apparent from the "half-value thickness" of 1·45 mm. of aluminium which corresponds to a quantum energy of 3×10^6 eV. It is evident from these figures that only a small proportion of the radiation can have an energy approaching the calculated maximum value of $10{\cdot}3 \times 10^6$ eV.

The formation of excited ^{28}Si nuclei in the reaction

$$^{31}\mathrm{P} + {}^{1}\mathrm{H} = {}^{28}\mathrm{Si} + {}^{4}\mathrm{He} \tag{10}$$

may give rise to γ-radiation of about 3×10^6 eV, but the resonant nature of the excitation function (fig. 8) and the evidence of the emission of γ-rays of an energy greater than $7{\cdot}0 \times 10^6$ eV prove that the greater part of the emitted radiation arises in the capture process.

(*f*) *Chlorine*

Evidence for the emission of γ-radiation from chlorine under bombardment with protons was obtained in the course of experiments designed to check that the effects observed when using sodium chloride targets were actually due to sodium. The emission of γ-rays from copper chloride targets was also detected and the intensity of the γ-radiation as a function of the bombarding voltage was followed from 500 kV, the lowest voltage at which a detectable intensity was obtained. From the observations shown in fig. 9 it appears that the intensity of the γ-radiation increases nearly exponentially with some indication of the presence of three broad resonances at 650, 800 and 1000 kV.

Absorption measurements for the radiation gave an end-point at 24·0 mm. of aluminium, corresponding to a maximum quantum energy of $14{\cdot}5 \times 10^6$ eV. The equation

$$^{37}\mathrm{Cl} + {}^{1}\mathrm{H} = {}^{38}\mathrm{A} + h\nu \tag{11}$$

indicates, using generally accepted mass values (Livingstone and Bethe 1937), and taking into account the bombarding energy of the proton, $0{\cdot}9 \times 10^6$ eV, a value of $h\nu = 12{\cdot}1 \times 10^6$ eV. These two values of the quantum energy are within the specified limits of accuracy of the mass determinations. The "half-value thickness" of 2·2 mm. of aluminium corresponds to a quantum energy of $4{\cdot}9 \times 10^6$ eV, indicating that the radiation is heterogeneous. Possibly γ-radiation might be emitted as a result of the formation of excited nuclei of ^{32}S according to the process

$$^{35}\mathrm{Cl} + {}^{1}\mathrm{H} = {}^{32}\mathrm{S} + {}^{4}\mathrm{He}. \qquad (12)$$

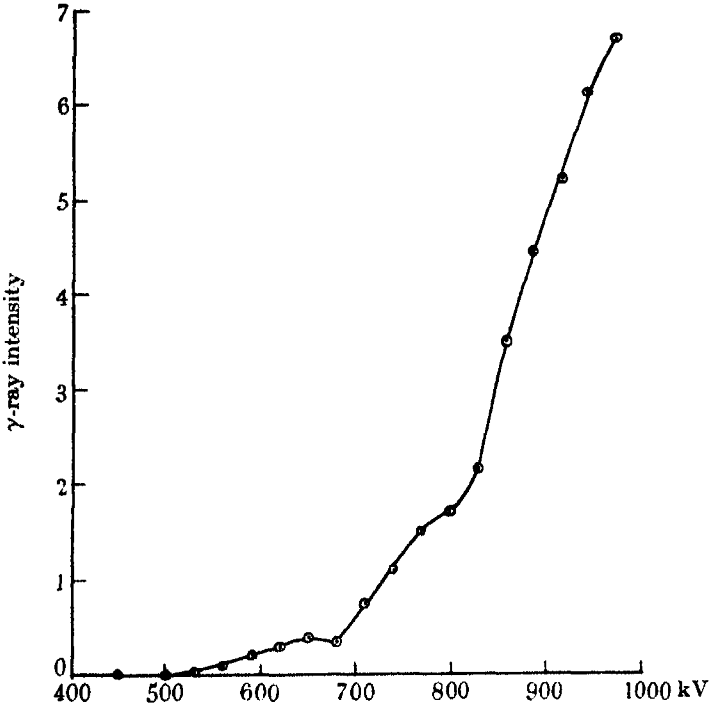

FIG. 9

The full quantum energy to be anticipated from this process is $2{\cdot}4 \times 10^6$ eV for an energy of incident protons of $0{\cdot}9 \times 10^6$ eV but the limits of accuracy in the determination of mass values allow this energy release to be as high as $3{\cdot}4 \times 10^6$ eV. In view of the difference between these values and those which were obtained it seems reasonable to assume that the radiation which has been observed in this experiment is the capture γ-radiation arising from process (11).

The authors wish to thank Mr P. I. Dee for his continued interest and helpful advice during the course of this work. The authors are pleased to express their indebtedness to the Caird Trustees (S. C. C.), to the Department of Scientific and Industrial Research and Newnham College (J. E. S.) for the grant of awards during tenure of which the above research was carried out.

SUMMARY

The excitation functions for the γ-radiations emitted by the elements deuterium, lithium, sodium, magnesium, phosphorus and chlorine under proton bombardment have been determined for energies of the incident protons from 0 to 10^6 eV.

Resonance peaks, hitherto unobserved, have been found in the excitation curves for incident protons of the energies given below.

^{23}Na : 425, 525, 590, 690, 755, 875×10^3 eV,
^{25}Mg : 180, 410, 480, 575, 825×10^3 eV,
^{26}Mg : 580, 680, 1000×10^3 eV,
^{31}P : 460, 580, 700, 950×10^3 eV,
^{37}Cl : 650, 800, 1000×10^3 eV.

In the case of ^{7}Li no evidence of any resonance peak other than that at 440 kV could be obtained. No capture γ-radiation could be detected during the bombardment of ^{6}Li and deuterium with protons of energies up to 10^6 eV.

The yield of γ-radiation was measured in the case of ^{25}Mg and ^{26}Mg, the values obtained being $3{\cdot}0 \times 10^{10}$ quanta per proton at 825 kV (^{25}Mg) and $2{\cdot}1 \times 10^{-10}$ for ^{26}Mg at 680 kV.

The energy of the capture γ-radiation was measured in each case from observations of the end-points of the absorption curves which were obtained by placing aluminium sheets between the pair of Geiger-Müller counters used for the detection of the γ-rays.

REFERENCES

Bothe and Gentner 1937 *Z. Phys.* **104**, 685.
Crane, Delsasso, Fowler and Lauritsen 1935 *Phys. Rev.* **48**, 125.
Curran, Dee and Petržílka 1938 *Proc. Roy. Soc.* A, **169**, 269.
Curran and Petržílka 1939 *Proc. Camb. Phil. Soc.* **35**, 309.
Delsasso, Fowler and Lauritsen 1936 *Phys. Rev.* **50**, 389.
— — — 1937 *Phys. Rev.* **51**, 391.
Duncanson and Miller 1934 *Proc. Roy. Soc.* A, **146**, 396.
Frisch 1934 *Nature, Lond.*, **133**, 721.
Gaerttner and Crane 1937 *Phys. Rev.* **51**, 49, 58.
Gentner 1937 *Z. Phys.* **107**, 354.
Hafstad and Tuve 1935 *Phys. Rev.* **48**, 306.
Hafstad, Heydenburg and Tuve 1936 *Phys. Rev.* **50**, 504.
Henderson 1935 *Phys. Rev.* **48**, 855.
Herb, Kerst and McKibben 1937 *Phys. Rev.* **51**, 691.

Livingstone and Bethe 1937 *Rev. Mod. Phys.* **9**, no. 3.
Mitchell and Langer 1937 *Phys. Rev.* **52**, 137.
Richardson 1938 *Phys. Rev.* **53**, 124.
Rumbaugh and Hafstad 1936 *Phys. Rev.* **50**, 681.
Rumbaugh, Roberts and Hafstad 1938 *Phys. Rev.* **54**, 657.
Widdowson 1939 *Proc. Phys. Soc.* **51**, 19.

Fine structure of the Raman lines of carbon tetrachloride

By A. C. Menzies

University College, Southampton

(*Communicated by R. Whiddington, F.R.S.—Received* 18 *April* 1939)

Symmetry considerations

Assuming first of all for simplicity that the four chlorine atoms are identical, the greatest symmetry the CCl_4 molecule could have is T_d. This would lead us to anticipate four fundamentals, ν_1, ν_2, ν_3, ν_4 belonging to normal modes A_1, E, F_2, F_2, respectively, using Placzek's (1934) nomenclature. A_1 is the total symmetric normal mode, and so ν_1 is polarized in the Raman effect, and inactive in the infra-red. A_1 is a singlet mode. E is a doublet mode and ν_2 is depolarized in the Raman effect, while it is inactive in the infra-red. F_2 is a triplet mode and ν_3 and ν_4 are depolarized in the Raman effect and are also active in the infra-red.

If the Raman spectrum of CCl_4 is examined under coarse dispersion, lines are observed at 217, 314, 459 cm.$^{-1}$, identified as ν_2, ν_4 and ν_1 respectively. Two at 760 and 790 cm.$^{-1}$ are usually regarded as the result of resonance degeneracy between ν_3 and $(\nu_1+\nu_4)$, both in the mode F_2.

Theoretical quantitative calculations

The pentatomic model with symmetry T_d has been calculated by Dennison (1926) using central forces, and Schaefer (1930) has applied Dennison's results to the special case of CCl_4. Urey and Bradley (1931) have worked out the formulae for a model in which in addition to valence forces a repulsion between corner atoms is postulated. Rosenthal (1934) has made general calculations and continued them later with Voge (1936). Wu and Sutherland (1938) have deduced what the isotope fine-structure should be for each of the four primary Raman lines.

Experimental observation of fine structure

Langseth (1931) examined the fine structure of the lines. ν_2 and ν_3 appeared to the eye as doublets, when weak exposures were made, but stronger exposures caused the doublet structure to disappear. ν_1 had the most interesting structure—he was able to resolve it clearly into three components, with separations of the order expected on the basis of an isotope explanation. He measured the separation directly from the plate—this may be expected to err in the direction of an under-estimate on account of the overlapping of the components. He estimated the relative intensities by eye, as in the ratio 10 : 10 : 5. This makes the first component too strong—one would have anticipated 8 : 10 : 5, assuming an abundance-ratio of 3 : 1. Langseth suggested that it might arise from the overlaying of weak rotational branches.

This disagreement prompted the reinvestigation of the fine structure of the line, making a quantitative determination of the relative intensities instead of an eye estimation.

EXPERIMENTAL

The carbon tetrachloride ("Analar" from British Drug Houses) was contained in a demountable Raman tube, like a polarimeter tube with screwed ends, with a side tube convenient for filling. This type of tube is particularly convenient for aligning. The light was provided by two Cooper-Hewitt glass mercury lamps (M 12). These lamps are relatively feeble but the mercury lines are sharp—a necessity for fine-structure work. The lamps were placed above and below the tube respectively, and the light was concentrated on the tube by two pieces of 1 in. towel rail used as cylindrical lenses. Lamps, rails and tube were all carried by a metal frame, so that the tube could easily be removed and replaced without the necessity of realignment.

The spectrograph was made in the departmental workshop, using girders and wood left over from construction of the new laboratory. It has 3 in. diameter lenses, and two 60° high dispersion glass prisms of size to match. The aperture of the main camera is $f/20$; the lens is mounted in the place of the horn on an Edison-Bell phonograph mechanism, the excellent screw providing means for accurate focusing. This mechanism also allows the lens to be swung aside on its mounting, when its place is taken by an *f*/3 astronomical camera. With this, small spectrograms can be taken in one-fiftieth of the time, for adjusting purposes.

The spectrograph is housed in a room kept at an air temperature constant to $\frac{1}{10}$° C, and the light is brought in from an adjoining room through a hole in the wall. The dispersion is about 6 A/mm. near 4358 A.

The spectra were analysed by a recording microphotometer also made in the departmental workshop, from designs partly original and partly helped by conversations with D. H. Follett of Messrs Adam Hilger Ltd., at the time when they were designing their microphotometer. It uses an inextensible steel tape to link the two trolleys bearing the spectrum plate and the recording plate. The trolleys are of stainless steel riding on ball bearings in V grooves. Cobalt-chrome magnets are used to form "infinitely variable" rebates for retaining the plates in position on the trolleys. The light-sensitive detector is a sperrschicht cell, actuating a galvanometer with 2 sec. period.

Intensity marks were put on the plate by transferring it to another spectrograph specially set up permanently for the purpose. Five spectra of known intensity ratios are printed on the plate simultaneously, using a method employing thin prisms, which will be described in detail in another place.

Ilford "Zenith 700" plates were used; these were found by trial to be faster for the purpose than the more commonly employed Ilford "Double Xpress" plates. The intensity marks were arranged to take 24 hr. to print so that the Raman exposures of about 50 hr. should not be disproportionately long. This avoids a prolific source of error in intensity measurements.

RESULTS

The lines ν_2 and ν_4 were each not resolved clearly; the doublets mentioned by Langseth were not obtained, either by weak or by strong exposures. ν_2 had in some pictures an envelope which suggested that it had a doublet or triplet structure.

ν_1 in some twenty photographs was clearly triple and the highest frequency component was in all cases less intense than the one next to it, instead of the equality found by Langseth. A typical curve for ν_1 excited by 4047 A, converted into an intensity scale, is given in the figure.

It was attempted unavailingly to resolve this pattern, using the conventional diffraction maximum shape. It was then decided to approach the problem experimentally, and an envelope was obtained for the exciting line (4047 A). This had a half-intensity width of about 1·7 cm.$^{-1}$, but this was too "thin". In case the lines were being widened through insufficient constancy of temperature or of pressure (for which latter no correcting device was at work) the envelope was found for the 4108 A mercury line, recorded at the same time in the same spectrum, and this had a half intensity width of 1·6 cm.$^{-1}$, so that the matter was fortunately not to be explained in this way.

It seemed possible that in the Raman scattering act, whether due to anharmonicity, pressure or other effects in the liquid, the lines might be broadened. This was tested on benzene and the total symmetric vibration line at 992 cm.$^{-1}$ was accordingly photographed and microphotometered with the same set-up. The small satellite due to $C_5^{12}C^{13}H_6$ was clearly visible, and the half intensity width of the main line was found to be 3·5 cm.$^{-1}$, although it was being excited by 4047 A with a half-intensity width only half as great. (It is interesting to compare this result with that of Grassmann (1933) who found for the benzene 992 cm.$^{-1}$ line a half-intensity width of 3·6 cm.$^{-1}$, while Carelli and Went (1932) found 16 cm.$^{-1}$. This observation confirms that of Grassmann, but he considered that the Raman line was not wider than the exciting line itself.)

Assuming that a similar broadening was at work in the case of the CCl_4 total-symmetric line, an attempt was made to fit components having the same shape as the benzene line to the ν_1 envelope. In order to select from all the possible solutions the most likely one, certain constraints were imposed on the solution:

(*a*) that components should have the same half-intensity width,

(*b*) that the components should be equidistant,

(*c*) that the chief aim should be to fit the upper part of the envelope, where the accuracy can be presumed to be higher. In this way a reasonable fit was found with components I, II and III of the figure. The areas were found by weighing pieces of card of the same shape.

If $n : 1$ is the abundance ratio of Cl^{35} to Cl^{37}, an elementary calculation shows that the relative intensities of components having respectively four, three, two, one, no Cl^{35} atoms should be $n^4 : 4n^3 : 6n^2 : 4n : 1$, so that I/II is $n/4$, and II/III is $2n/3$. These give in the particular case analysed values 3·26 and 3·04 for n with a mean value 3·15. [The estimated error is about 5 %.]

To make the comparison envelope, IV has been put in to conform with this value of n and so has no experimental significance.

The separations of the three components are each 3·3 cm.$^{-1}$, which are of the right order but a little higher than the theoretical values which are calculated by Wu and Sutherland, 3·2 cm.$^{-1}$ from Rosenthal and Voge's formula and 3·1 cm.$^{-1}$ from Urey and Bradley's formula. Langseth found 3·10 and 3·28 for the separations between I and II and between II and III respectively.

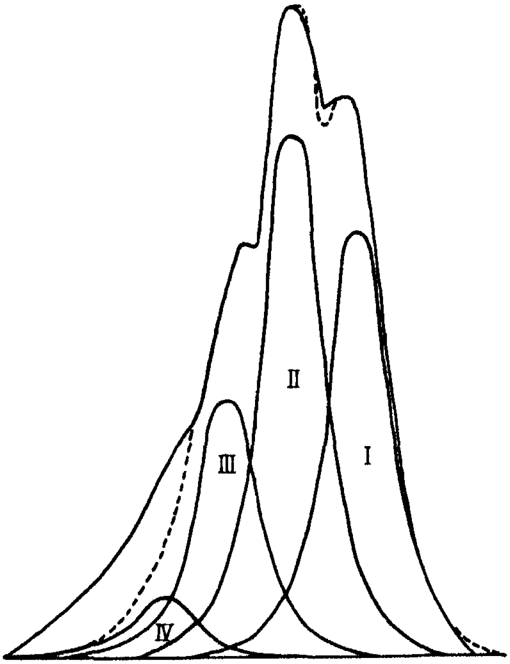

FIG. 1. Outer firm lines, experimental intensity curve for 459 cm.$^{-1}$ line of CCl_4; inner firm lines, empirical curves for isotope components; broken line, curve obtained by summing empirical component curves.

CONCLUSION AND SUMMARY

The intensities in the fine structure of the Raman line corresponding to the total symmetric vibration in CCl_4 have been examined quantitatively and are consistent with a chlorine isotope explanation, since the analysis leads to an abundance ratio of about 3·15, in good agreement with Aston's value from mass spectra.

The total symmetric vibration Raman line (992 cm.$^{-1}$) in benzene, and the components of the 459 cm.$^{-1}$ line in CCl_4, are considerably wider than the exciting line.

REFERENCES

Carelli and Went 1932 *Z. Phys.* **76**, 276.
Dennison 1926 *Phil. Mag.* **1**, 195.
Grassmann 1933 *Z. Phys.* **82**, 767.
Langseth 1931 *Z. Phys.* **72**, 350.
Placzek 1934 *Handbuch der Radiologie*, **6**, 2.
Rosenthal 1934 *Phys. Rev.* **45**, 538; **46**, 730.
Schaefer 1930 *Z. Phys.* **60**, 586.
Urey and Bradley 1931 *Phys. Rev.* **38**, 1969.
Voge and Rosenthal 1936 *J. Chem. Phys.* **4**, 137.
Wu and Sutherland 1938 *J. Chem. Phys.* **6**, 114.

Theory of electrical breakdown in ionic crystals.* II

By H. Fröhlich

H. H. Wills Physical Laboratory, University of Bristol

(*Communicated by N. F. Mott, F.R.S.—Received* 24 *April* 1939)

1. INTRODUCTION

Recently a theory of electrical breakdown in solids has been developed (Fröhlich 1937).† This theory is based on the idea that electrical breakdown is a phenomenon due to the acceleration of electrons, as has been suggested by von Hippel (1935) and others. The critical field strength at which the breakdown occurs has been calculated in the following way:

In strong external electrical fields, there are always some electrons in the conduction levels of an ionic crystal. These electrons, which are not in thermal equilibrium with the lattice, may be brought into these levels by cold emission or by some similar "pulling out" mechanism. Such an electron will make collisions with the lattice vibrations and thus lose per second a certain energy $B(E)$, which depends upon its kinetic energy E. On the other hand, it will gain per second an energy $A(E, F)$ from the external field F. Now it has been shown in I that B decreases but that A increases with increasing energy E. Thus there exists always an energy E'

---

[*] Based on report L/T 105 of the British Electrical and Allied Industries Research Association (E.R.A.).

[†] In the following quoted as I.

for which $A = B$. An electron with energy E less than E' will, on the average over several collisions, lose energy, whereas an electron with E greater than E' will gain more and more energy.

Now it was shown in I that $E' \propto 1/F$. Thus weak fields, for which E' is greater than the energy $\mathscr{T}$ required to excite* an ion of the crystal, will lead to a stationary state, as discussed in more detail in another paper (cf. Fröhlich 1939). If, however, F is so big that E' is less than $\mathscr{T}$, the field will continuously increase the number of electrons capable of ionization. This will finally lead to a breakdown. Thus it was concluded that the breakdown field F has to be calculated from the condition† $E'(F) = \mathscr{T}$.

The actual calculation of the breakdown field could be carried out quantitatively for diatomic polar crystals (alkali halides). This was possible because of two facts: first, the internal polarization caused by the heat movement of the ions may be calculated from the charges and masses of the ions, the residual ray frequencies and the lattice constant (cf. Born and Göppert-Mayer 1933). Secondly, the interaction between an electron and the lattice vibrations may be calculated from the above-mentioned polarization. This would not be possible for non-polar lattices. For complicated polar crystals, however, the second fact is still true, whereas a calculation of the "internal" polarization from the charges and masses of the ions, etc. would be mathematically very difficult.

It is the aim of this paper to show that a quantitative formula for the breakdown field of any kind of polar crystal may be derived by using the optical properties of the crystal in the infra-red for the determination of the "internal" polarization. The following calculations will show that, according to this formula, the breakdown field of a polar crystal is completely determined by its optical properties in the infra-red and ultraviolet, and by its molecular volume.

2. THE LATTICE VIBRATIONS

The purpose of this paragraph is to calculate the electrical polarization due to the heat movement of the ions from the optical behaviour of the crystal in the infra-red. It is well known that each polar crystal has a certain number of proper frequencies, $\nu_1, \nu_2, \ldots, \nu_i, \ldots, \nu_r$ in the infra-red, the so-called residual, or Reststrahlen, frequencies. If the crystal vibrates with a certain frequency ν_i, an electrical polarization $\mathbf{P}_{\nu_i}$ is induced, which at a given instant of time is a function of the space co-ordinates. This function may be expanded as a Fourier series. Each term of this series has the form

---

* If an ion is excited, only a small energy is required to ionize it. This energy may, therefore, be supplied from collisions with slow electrons.

† A detailed discussion of this condition is given in a recent paper (Fröhlich 1939).

$$\text{const.}\times\cos[(\mathbf{w},\mathbf{r})+2\pi\nu_i t],$$

where $\mathbf{w}$ is a wave-vector. Thus we may speak of an expansion as a series of polarization waves. There are longitudinal and transversal polarization waves, but it will be shown in § 3 that we need only consider the longitudinal waves.

The most general polarization $P(\mathbf{r},t)$ will be obtained by a superposition of polarization waves of all possible wave-lengths and frequencies. Thus

$$P(\mathbf{r},t) = \Sigma_{w\nu_i}P_{\mathbf{w}\nu_i},$$

$$P_{w\nu_i} = \frac{1}{(2V)^{\frac{1}{2}}}[p_{\mathbf{w}\nu_i}e^{i(\mathbf{w},\mathbf{r})}+p^*_{\mathbf{w}\nu_i}e^{-i(\mathbf{w},\mathbf{r})}], \tag{1}$$

where

$$p_{w\nu_i} = \text{const.}\times e^{2\pi i\nu_i t} \tag{2}$$

and V is the volume of the crystal.

We have now to calculate the total energy as a function of the coefficients $p_{w\nu_i}$. Then may be deduced the strength of each polarization wave from quantum mechanics and thermodynamics.

The energy of each wave $(\mathbf{w},\nu_i)$ may be divided up into potential and kinetic energy. Since the oscillators are supposed to be harmonic, the density of the potential energy U_P must be proportional to $P^2_{w\nu_i}$

$$U_P = \tfrac{1}{2}c_iP^2_{w\nu_i}\sim\cos^2[(\mathbf{w},\mathbf{r})+2\pi\nu_i t]. \tag{3}$$

Then the kinetic energy is proportional to

$$\sin^2[(\mathbf{w},\mathbf{r})+2\pi\nu_i t]$$

with the same constant factor as in the case of the potential energy. Integrating over the whole of space, we find the total energy of one wave (using equation (1))

$$H_{w\nu_i} = 2c_ip_{w\nu_i}p^*_{w\nu_i}.$$

The meaning of the constants c_i will be determined below. We shall first transform the expression for $H_{w\nu_i}$ into a canonical form. For this purpose, we define the canonical co-ordinates $X_{w\nu_i}$ and $Y_{w\nu_i} = M_i\dot{X}_{w\nu_i}$ (cf. equation (2)) by

$$2\pi\nu_i\left(\frac{M_i}{c_i}\right)^{\frac{1}{2}}X_{w\nu_i} = p_{w\nu_i}+p^*_{w\nu_i}, \tag{4}$$

$$\frac{1}{(c_iM_i)^{\frac{1}{2}}}Y_{w\nu_i} = i(p_{w\nu_i}-p^*_{w\nu_i}). \tag{5}$$

This leads to

$$H_{w\nu_i} = \frac{Y^2_{w\nu_i}}{2M_i}+2\pi^2\nu_i^2M_iX^2_{w\nu_i}, \tag{6}$$

i.e. to the Hamilton function of an harmonic oscillator with frequency ν_i and mass M_i. The introduction of a mass is not necessary and has only been made in order to give X and Y the dimensions of a length and a momentum respectively, thus making them equal to the X and Y used in I. We shall see below that M_i does not occur in any of our final results.

From equation (6) we obtain the total energy H by summing over all wave numbers and frequencies

$$H = \Sigma_{w\nu_i} H_{w\nu_i}.$$

There remains the determination of the factors c_i. For this purpose we proceed in the following way: We assume the crystal to be in a constant external electric field F. Let ϵ be the dielectric constant of the crystal. Then $\epsilon F^2/8\pi$ will be the density of the electrical energy. Since $F^2/8\pi$ is the energy of the field alone, the density of the elastic energy of the dielectric is given by

$$\frac{(\epsilon-1)F^2}{8\pi} = \frac{FP}{2}, \tag{7}$$

where

$$P = \frac{\epsilon-1}{4\pi}F$$

is the polarization of the dielectric. Equation (7) may be derived more directly if we consider that e^*F is the force acting on a charge e^*. Assuming this charge to be bound elastically, P/e^* is its displacement (per unit volume) and consequently $\frac{1}{2}FP$ its contribution to the density of the elastic energy. In our case, the total polarization is the sum of the contributions of the ions, P_0 (due to their polarizability) and the contributions P_i of the different oscillators with natural frequencies $\nu_i\,(i = 1, 2, \ldots, r)$. Thus

$$P = P_0 + \Sigma_{i\geqslant 1} P_i. \tag{8}$$

The polarizability $(\epsilon-1)/4\pi$ is made up in a similar way

$$\epsilon - 1 = (\epsilon_0 - 1) + \Sigma_{i\geqslant 1}(\epsilon_i - 1), \tag{9}$$

where $\epsilon_0 - 1$ is the contribution of the ions and $\Sigma(\epsilon_i - 1)$ that of the oscillators. From the definition of the polarizability, it follows that

$$F = \frac{4\pi}{\epsilon_0 - 1}P_0 = \frac{4\pi}{\epsilon_1 - 1}P_1. \tag{10}$$

Inserting equation (8) into equation (7), and making use of equation (10) we find for the energy density of the dielectric

$$\frac{\epsilon-1}{8\pi}F^2 = \frac{2\pi}{\epsilon_0 - 1}P_0^2 + 2\pi\Sigma_{i\geqslant 1}\frac{P_i^2}{\epsilon_i - 1}.$$

Thus the oscillators with frequency ν_i give a contribution $2\pi P_i^2/(\epsilon_i - 1)$ which must be equal to the density of the potential energy, equation (3), assumed above for these oscillators. Thus we find

$$c_i = \frac{4\pi}{\epsilon_i - 1}. \tag{11}$$

This means that $1/c_i$ is the contribution of the oscillators ν_i to the total polarizability.*

The constants ϵ_i can be determined experimentally from the optical constants n, κ of the crystal. From the theory of dispersion, it follows† that

$$n^2 - \kappa^2 = \epsilon(\nu) = \epsilon_0 + \Sigma_{i \geqslant 1} \frac{(\epsilon_i - 1)\, \nu_i^2}{\nu_i^2 - \nu^2}. \tag{12}$$

Here, ν is the frequency of the light for which the optical constants are measured and $\epsilon(\nu)$ is the dielectric constant for this frequency. ϵ_0 is the contribution due to the polarizability of the ions which is independent of ν, if ν is small compared with the first electronic absorption frequency ν_0 (in general in the ultra-violet).

If we choose ν such that $\nu_1 \ll \nu \ll \nu_0$, ϵ_0 is simply given by

$$\epsilon_0 = n^2, \quad \nu_1 \ll \nu \ll \nu_0.$$

A further simplification of equation (12) is obtained for $\nu = 0$. In this case, $\epsilon(\nu)$ becomes the ordinary static dielectric constant, and equation (12) becomes identical with equation (9), which may be written in the form

$$\epsilon - \epsilon_0 = \Sigma_{i \geqslant 1}(\epsilon_i - 1). \tag{13}$$

The left-hand side of this equation can be evaluated from the observed dielectric constant and from the refractive index in the visible region. Thus, if there is only one residual frequency ν_1, $\epsilon_1 - 1$ is known too. But if the crystal has more residual frequencies, the ϵ_i's have to be determined from optical measurements in the infra-red.

---

* In the above consideration it was assumed that the potential energy of a polarization wave is entirely made up of what we have called elastic energy. As has been shown by Fröhlich and Mott (1939) this is only true in the case of transverse waves and of *short* longitudinal waves. Only short longitudinal waves are, however, important for the scattering of electrons of an energy of several electron-volts.

† Neglecting the Lorenz-Lorentz force (cf. Mott and Littleton 1938).

3. INTERACTION BETWEEN ELECTRON AND LATTICE VIBRATIONS

Let $\phi_{w\nu_i}$ be the electrical potential produced by one polarization wave with wave number w and frequency ν_i. Then $e\phi_{w\nu_i}$ is the interaction energy of this wave with the electron. Hence we obtain the total interaction energy W by summing over all w and ν_i

$$W = e\Sigma\phi_{w\nu_i},$$

$\phi_{w\nu_i}$ is determined by the equation

$$\nabla^2\phi_{w\nu_i} = 4\pi \operatorname{div} \mathbf{P}_{w\nu_i}.$$

From this equation it follows that only longitudinal waves have an electrical interaction with an electron. Inserting $P_{w\nu_i}$ from equation (1), we obtain

$$\phi_{w\nu_i} = -\frac{4\pi i}{(2V)^{\frac{1}{2}}\, w}\left(p_{w\nu_i} e^{i(\mathbf{w},\mathbf{r})} - p^{*}_{w\nu_i} e^{-i(\mathbf{w},\mathbf{r})}\right),$$

or, making use of equations (4), (5) and (11),

$$\phi_{w\nu_i} = \frac{4\pi^2\nu_i}{w}\left(\frac{(\epsilon_i-1)\,M_i}{2\pi V}\right)^{\frac{1}{2}}\left\{X_{w\nu_i}\sin(\mathbf{w},\mathbf{r}) + \frac{Y_{w\nu_i}}{2\pi\nu_i M_i}\cos(\mathbf{w},\mathbf{r})\right\}.$$

This expression becomes identical with the interaction energy of an electron with a polarization wave deduced in I, equation (10), if we put

$$\epsilon_i - 1 = \frac{e^2}{2\pi a^3 M_i \nu_i^2}, \qquad (14)$$

for X and Y have in both cases the same meaning.† Thus we obtain the matrix elements in the same way as in I. The matrix element for the absorption of a quantum $h\nu_i$, for instance, is given by

$$M_{kk',w\nu_i} = \frac{2\pi e}{w}\left[\frac{\epsilon_i - 1}{4\pi V}\,h\nu_i n_{w\nu_i}\right]^{\frac{1}{2}}.$$

Here k and k' are the wave-vectors of the electron before and after the collision, and $n_{w\nu_i}$ is the number of quanta $h\nu_i$ with which the oscillator $(\mathbf{w}, \nu_i)$ is excited. We see that the matrix element does not contain the mass M_i, as was to be expected.

The matrix element for emission is the same as for absorption, if we replace $n_{w\nu_i}$ by $1 + n_{w\nu_i}$.

---

† This expression for $\epsilon_i - 1$ is identical with that obtained in Born's theory for a diatomic crystal, if M_i is the reduced mass.

From the matrix elements, we can calculate the time of relaxation τ in a similar way to that used in I. The only essential difference is that we have now to sum over the different frequencies ν_i. We thus obtain

$$\frac{1}{\tau} = \Sigma_{i\geqslant 1}\frac{1}{\tau_{0i}}\phi_i(T), \tag{15}$$

where

$$\phi_i(T) = 1+\frac{2}{e^{h\nu_i/kT}-1}. \tag{16}$$

Here, T is the temperature and τ_{0i} is the time of relaxation for $T = 0$, due to the oscillations with frequency ν_i

$$\frac{1}{\tau_{0i}} = \frac{1}{8\sqrt{2}}\frac{e^2h\nu_i(\epsilon_i-1)\,w_{0i}^2}{m^{\frac{1}{2}}E^{\frac{3}{2}}}, \quad E > \frac{1}{8}\frac{\hbar^2w_{0i}^2}{m}. \tag{17}$$

$$\frac{1}{\tau_{0i}} = \pi\sqrt{2}\frac{e^2\nu_i(\epsilon_i-1)\,m^{\frac{1}{2}}}{\hbar E^{\frac{1}{2}}}, \quad E < \frac{1}{8}\frac{\hbar^2w_{0i}^2}{m}. \tag{17a}$$

Here, E is the kinetic energy of the electron, and w_{0i} is the maximum wave number of the polarization waves with the frequency ν_i.

In a similar way, one can calculate the energy B, transferred per second from the electron to the lattice vibrations. According to the previous paper, I, § 5, the contribution of the vibrations with the frequency ν_i is given by

$$B_i = \frac{h\nu_i}{\tau_{0i}}\frac{8mE}{\hbar^2w_{0i}^2}\log\gamma_i, \tag{18}$$

$$\gamma_i = \frac{E^{\frac{1}{2}}w_{0i}}{(2m)^{\frac{1}{2}}\pi\nu_i}. \tag{19}$$

Therefore

$$B = \Sigma B_i. \tag{20}$$

4. THE BREAKDOWN FIELD

According to I (cf. § 1 of the present paper), the breakdown field F has to be calculated from the condition

$$A(E,F) = B(E), \quad E = \mathscr{T}.$$

Here, A is the energy, transferred per second from the field to the electron, i.e.

$$A = \frac{e^2F^2\tau(E)}{m}.$$

B is the energy, transferred per second from the electron to the lattice, given by equations (20) and (18).

Introducing τ from equations (15) and (17), we obtain

$$eF = \left(\frac{mB}{\tau}\right)^{\frac{1}{2}}_{E=\mathscr{T}} = \frac{\pi}{2}\frac{(mh)^{\frac{1}{2}}e^2}{\mathscr{T}}\left\{\Sigma_{i\geqslant 1}(\epsilon_i - 1)\, w_{0i}^2 \nu_i \phi_i(T) \times \Sigma_{i\geqslant 1}(\epsilon_i - 1)\, \nu_i^2 \log \gamma_i\right\}^{\frac{1}{2}}. \tag{21}$$

We still have to calculate the wave numbers w_{0i}. These are in our present theory the only quantities which are in a direct connexion with the atomic structure of the dielectric medium. They have to be determined from the fact that the total number of the mechanical degrees of freedom of the oscillators must be $3N$, if N is the number of atoms in the crystal. Since in an atomic theory the w_{0i}'s would be completely determined by the lattice structure, w_{0i} must be roughly the same (w_0) for all frequencies ν_i. We thus obtain

$$3N = \frac{3V}{(2\pi)^3}\frac{4\pi}{3}w_0^3 r$$

or

$$w_0 = \left(\frac{6\pi^2 n}{r}\right)^{\frac{1}{3}} \simeq 2^{\frac{1}{3}}\pi\left(\frac{n}{r}\right)^{\frac{1}{3}}.$$

Here, r is the number of different residual frequencies ν_i of the crystal and $n = N/V$, the number of atoms per cm.^{3}.

The energy $\mathscr{T}$ will, as in I, be taken from the wave-length λ_0 of the first maximum of the ultra-violet absorption band

$$\mathscr{T} = \frac{hc}{\lambda_0}.$$

Thus, we finally obtain

$$eF = \frac{\pi^2 e^2 m^{\frac{1}{2}}}{2^{\frac{2}{3}} c h^{\frac{1}{2}}}\frac{\lambda_0 n^{\frac{1}{3}}}{r^{\frac{1}{3}}}\left\{\sum_{i=1}^{r}(\epsilon_i - 1)\,\nu_i\phi_i(T) \times \sum_{i=1}^{r}(\epsilon_i - 1)\,\nu_i^2 \log\gamma_i\right\}^{\frac{1}{2}}.$$

5. DISCUSSION

We shall first write down the above expression for F in different units. We shall express F in V/cm. and the other quantities in units described below. We then obtain

$$F = 5{\cdot}0 \times 10^4\left(\frac{dz}{Gr}\right)^{\frac{1}{3}}\lambda_0\left\{\sum_{i=1}^{r}\frac{\epsilon_i - 1}{\lambda_i}\phi_i(T) \times \sum_{i=1}^{r}\frac{\epsilon_i - 1}{\lambda_i^2}\log\gamma_i\right\}^{\frac{1}{2}}\text{V/cm.} \tag{22}$$

Here, λ_0 is the wave-length of the maximum of the first ultra-violet absorption in Ångströms, the λ_i's are the residual wave-lengths in μ, d is the density in g./cm.^{3}, G the molecular weight, z the number of atoms per molecule,

r the number of different residual wave-lengths; $\phi_i(T)$ is a temperature factor, given by equation (16), and the ϵ_i's have to be determined from optical measurements in the infra-red, as described in § 2 (cf. equations (12) and (13)); $\log \gamma_i (\sim 6)$ is given by equation (19).

It should be mentioned that in the case of a diatomic crystal ($r = 1$) the above expression is identical with that obtained in I, if $\epsilon_i - 1$ is substituted from equation (14).

Dependence on temperature

Assuming that there exists only *one* frequency ν_i, of residual rays, the temperature factor of F is given by

$$\phi_i^{\frac{1}{2}}(T)$$

(cf. equation (16)). This dependence on T should, however, hold only up to a temperature T_0, where a complete change in the mechanism of the breakdown occurs. T_0 is usually not less than 100° C.

In Table I we shall give the value of $\phi_i^{\frac{1}{2}}$ at room temperature ($T = 300°$) for different residual wave-lengths λ_i. Note that $\phi_i(0) = 1$.

TABLE I. $\sqrt{\{\phi_i(T)\}}$ AT $T = 300°$

λ_i in μ	10	20	30	40	50	60	80	100	120
$\sqrt{\{\phi_i(300)\}}$	1·01	1·10	1·23	1·37	1·51	1·64	1·87	2·08	2·28

From this table we see that F should have an appreciable temperature dependence below T_0 for substances with $\lambda_i \gtrsim 30\mu$, e.g. for the alkali halides, which have residual wave-lengths up to 120μ. For most of the other polar crystals, however, as, for instance, for silicates with λ_i's between 10 and 20μ, F should depend only very little on temperature.

In agreement with this prediction, measurements on mica which were recently carried out by W. Hackett* in a temperature range between 80 and 400° K lie between the theoretical curves for $\lambda = 10\mu$ and $\lambda = 20\mu$, but diverge at greater temperatures in accord with the results of A. M. Thomas (1936). For alkali halides, the only measurements existing at present are some by A. E. W. Austen* on KBr which show a strong decrease of F with decreasing T in qualitative but not quantitative agreement with theory.

---

* Kindly communicated by the E.R.A. to the author before publication (cf. Austen and Hackett 1939).

Absolute values of the electric strength

Equation (22) allows the quantitative calculation of F if all experimental data are obtainable. In the simple case of the alkali halides ($z = 2$) with only one residual wave-length, equation (22) is reduced to

$$F = 1{\cdot}64 \times 10^5 \left(\frac{d}{G}\right)^{\frac{1}{2}} \lambda_0 \frac{\epsilon - \epsilon_0}{\lambda_1^{\frac{1}{2}}} \sqrt{\{\phi_1(T)\}}\ \mathrm{V/cm.}, \tag{23}$$

if one makes use of equation (13), and of $(\log \gamma_i)^{\frac{1}{2}} = 2{\cdot}6$ (cf. I).

As mentioned above, this is identical with the equation for F in I, if one inserts for $\epsilon - \epsilon_0$ the value given in Born's theory (cf. Born and Göppert-Mayer 1933, p. 646).

The experimental data for ϵ, ϵ_0 and λ_i may be taken from a table given in the article by Born and Göppert-Mayer (1933, p. 647). For ϵ, two sets of experimental values will be taken, those of Kyropoulos and those of Errera. The F-values calculated in this way will be distinguished by an index K or E. For λ_0 we shall use the same values as in I. In Table II we compare the theoretical values of F for $T = 300°$ K with the experimental values of von Hippel (1935). Since in von Hippel's experiments F lies in the 100 direction, whereas the breakdown occurs in the 110 direction, we have still to multiply the F-value of equation (23) by a factor $\sqrt{2}$ as discussed in I.

TABLE II. F_{100} IN 10^5 V/CM. FOR $T = 300°$ K

		NaCl	NaBr	NaI	KCl	KBr	KI	RbCl	RbBr	RbI
					Theory					
F	K.	16	15	—	9·4	7·7	8·2	7·7	5·8	6·5
	E.	15	13	14	8·9	7·3	6·3	8·4	5·4	4·7
					Experimental					
		15	10	8	8	7	6	7	6	5

This dependence on the direction means that we have to assume $m_{110} < m_{100}$ and $m_{110} \sim m$ where m_{110} and m_{100} are the *effective* masses in the 110 and 100 directions respectively. For very small kinetic energies of an electron ($k \sim 0$) this would not be possible because of the cubic symmetry of the crystal. The energies near $\mathcal{T}$ (5–10 eV), however, lie in most cases in a higher Brillouin zone where such a behaviour may very well be expected since high effective mass means potential barrier between the atoms and, as pointed out by von Hippel (1935), the potential barrier in the 100 direction is much higher than in the 110 direction.

There is still a rather big uncertainty in the experimental values for ϵ which enters in the theoretical formula for F. Nevertheless, the agreement with experiment seems to be still better than with the formula used in I, which contains Born's theoretical formula for $\epsilon - \epsilon_0$ instead of the experimental value for this magnitude, used here.

We shall now calculate the theoretical values of F for quartz and mica. Quartz has four residual wave-lengths (cf. Schäfer and Matossi 1930) of which we shall use only the two strongest $\lambda_i = 8{\cdot}4\mu$, $\lambda_2 = 20{\cdot}5\mu$. This should involve only a small error in the calculation of F. Since for quartz $\epsilon = 4{\cdot}6$ and $\epsilon_0 = 2{\cdot}3$ (cf. Landolt-Börnstein *Tables*), we find, according to equation (13),

$$\epsilon - \epsilon_0 = (\epsilon_1 - 1) + (\epsilon_2 - 1) = 2{\cdot}3. \tag{24}$$

The values of $\epsilon_1 - 1$ and $\epsilon_2 - 1$ should be determined from infra-red measurements. Unfortunately, the experiments available at present (cf. Schäfer and Matossi 1930) do *not* allow a determination of ϵ_1 and ϵ_2. It seems, however, that the assumption $\epsilon_1 = \epsilon_2$ is not in contradiction with experiment. If, therefore, we choose (cf. equation (24)) $\epsilon_1 - 1 = \epsilon_2 - 1 = 1{\cdot}15$, we obtain with $\lambda_0 = 1200$ A (cf. Landolt-Börnstein *Tables*)

$$F = 3{\cdot}3 \times 10^6\,\mathrm{V/cm}.$$

for crystalline quartz if the field lies in the direction in which the breakdown occurs. On the other hand, the assumption that only the shortest residual wave, $\lambda_1 = 8{\cdot}4\mu$ is of importance gives an upper limit for F, i.e.

$$F < 7{\cdot}4 \times 10^6\,\mathrm{V/cm}.$$

Reliable experimental values are not available at present.

For mica the strong residual wave-lengths are the same as for quartz. The experimental values for the dielectric constant lie between 7·1 and 7·7, whereas $\epsilon_0 = 2{\cdot}5$. Thus, we have to replace equation (24) for quartz by

$$\epsilon - \epsilon_0 = (\epsilon_1 - 1) + (\epsilon_2 - 1) = \begin{matrix} 5{\cdot}2 \\ 4{\cdot}6 \end{matrix}.$$

Since there are no experiments available for even a rough determination of ϵ_1 and ϵ_2, we shall first assume $\epsilon_1 = \epsilon_2$ as has been done for quartz. Furthermore, there is no experimental value for λ_0. Since both quartz and mica are silicates, and since in both cases the refractive indices in the visible, $n = \sqrt{\epsilon_0}$, are nearly the same, it seems that λ_0 should have nearly the same value in both cases (probably due to the SiO_2 group). In this way we obtain F between $6{\cdot}6 \times 10^6$ and $7{\cdot}5 \times 10^6\,\mathrm{V/cm}$. for mica. It should be emphasized, however, that owing to the uncertain experimental values of $(\epsilon_1 - 1)/(\epsilon_2 - 1)$ and of λ_0, the theoretical value for F contains the same uncertainty.

The work of Thomas (1936) gave values up to 8×10^6 V/cm. for clear muscovite mica. Since then preliminary further results communicated by the E.R.A. have given greater values up to about 10 or 11×10^6 V/cm., while values up to 13 or 14×10^6 V/cm. for impulse voltages have recently been communicated from the National Physical Laboratory. In an earlier paper and in correspondence with the E.R.A., von Hippel has quoted values of 10×10^6 V/cm. for mica of thickness $3{\cdot}5\mu$. Work on thin films of mica still in progress by the E.R.A. gives values of the same order or rather higher for such thicknesses. Accordingly the theoretical values quoted are of the right order but appear somewhat low. It is possible to give a theoretical upper limit for the electric strength, by calculation on the assumption that ν_1 is the only important residual frequency ($\lambda_1 = 8{\cdot}4\mu$). This limit turns out to be 15×10^6 V/cm. which is greater than the experimental figures quoted. Further infra-red data could clear up the outstanding uncertainties.

Dependence on thickness

As already mentioned in I the breakdown field should increase with decreasing thickness t, if t is of the order of a few mean free paths ($\sim 10^{-5}$ cm.). A lower limit for F is easily obtained from the fact that the total voltage, applied to the dielectric, must be greater than the excitation energy $\mathscr{T}$

$$F > \mathscr{T}/t.$$

For mica, for instance, $\mathscr{T} = 10$ V, and, therefore, $F > 10/t$ V/cm. This lower limit for F surpasses the value of F for thick layers at $t \sim 1{\cdot}5 \times 10^{-6}$ cm. We should, however, expect the beginning of the increase of F already at $t \sim 10^{-5}$ cm., since the mean free path is about 10^{-6} cm.

Experimental work by A. E. W. Austen* on thin films of mica, and kindly communicated by the E.R.A. to the author has confirmed the existence of this phenomenon.

SUMMARY

Following the ideas on electrical breakdown developed in a previous paper, a formula for the breakdown field strength is derived which holds for any kind of polar crystal.

---

* To be published later (cf. Austen and Hackett 1939).

This formula makes possible the quantitative calculation of the breakdown field from the optical properties of the dielectric, the dielectric constant and from the molecular volume.

The breakdown field F has been calculated for the alkali halides for quartz and for mica. Satisfactory agreement with experimental values, when they exist, is obtained.

It follows from the theory that F should be practically independent of temperature in the case of silicates, in agreement with experiment. For the alkali halides, however, F should increase with increasing temperature.

For films thinner than about 10^{-5} cm., F should increase with decreasing thickness.

REFERENCES

Austen and Hackett 1939 *Nature, Lond.*, **143**, 637.
Born and Göppert-Mayer 1933 *Handbuch der Physik*, 2nd ed. **24**/2, 623.
Fröhlich 1937 *Proc. Roy. Soc.* A, **160**, 230.
— 1939 *Phys. Rev.* (in the Press).
Fröhlich and Mott 1939 *Proc. Roy. Soc.* A, **171**, 496.
von Hippel 1935 *Ergebn. exakt. Naturw.* **14**, 79.
Mott and Littleton 1938 *Trans. Faraday Soc.* **34**. 485.
Schäfer and Matossi 1930 *Das Ultrarote Spektrum.* Berlin.
Thomas 1936 *Brit. Elect. Allied Ind. Res. Ass.*, Rep. D/T22.

The formation of HeH^+ molecules

BY MARJORIE B. M'EWEN, PH.D.
Demonstrator in Physics

AND F. L. ARNOT, SC.D.
Lecturer in Natural Philosophy
The University of St Andrews

(*Communicated by H. S. Allen, F.R.S.—Received* 24 *April* 1939)

INTRODUCTION

Although a particle of apparent mass number 5, attributed to the singly-charged helium hydride molecule HeH^+, has been detected in mass-spectrographic work in mixtures of helium and hydrogen (Hogness and Lunn 1925) and has indeed been used to determine the mass of the deuteron by its position with respect to $H^2H^2H^{1+}$ (Bainbridge 1933), yet no study of the conditions leading to its formation has previously been made. In view of the fact that no evidence of the existence of this molecule has been obtained from spectroscopic work it was desirable that a detailed investigation of the peak appearing at mass number 5 should be made, its molecular form definitely established and its mode of formation investigated.

APPARATUS

The mass spectrograph previously used by Arnot and Milligan (1936) and by Arnot and M'Ewen (1939) for similar investigations of the formation of mercury and helium molecules was employed. The details of the construction of the ionization chamber and magnetic analyser are given in the above papers.

Electrons from a tungsten filament were accelerated to a nickel gauze anode E_1 by a potential V_0 applied between the centre of the filament and E_1. Positive ions formed between E_1 and a second gauze E_2 were drawn through E_2 by a potential V_1 and then further accelerated to the slit in the top of the collimating tube by a potential V_2. Except where otherwise stated the values of V_0, V_1 and V_2 were set equal to 28, 10 and 190 V respectively. The filament emission for all the curves shown, except those in fig. 3 for which it was varied, was 1 mA. A potential of 40 V was applied between the Faraday cylinder and the analyser to prevent the ejection of electrons from the Faraday cylinder by metastable helium atoms. This precaution was shown to be necessary in the work on helium (Arnot and M'Ewen 1939).

For the ion-analysis curves in fig. 1, the hydrogen and helium were mixed in known proportions in a flask of 1 l. capacity, and from there were admitted to the ionization chamber through a fine glass capillary leak and liquid air trap. Subsequently the two gases were admitted through separate leaks and then mixed before entering the ionization chamber through a liquid air trap. The composition of the mixture could be varied by altering the pressure of the gases in the two storage flasks. Preliminary tests were carried out to determine the pressures at which it was necessary to store the gases in the flasks so that the partial pressures of the two gases in the ionization chamber changed at the same rate when the flasks were cut off and pumping continued. The pressure variation curves shown in fig. 2 were thus obtained with a mixture of constant composition throughout the pressure range used. The total pressure in the ionization chamber, except of course for the curves of fig. 2, had values ranging from $2{\cdot}5 \times 10^{-3}$ to $3{\cdot}0 \times 10^{-3}$ mm. of Hg for the different curves. The residual gas pressure in vacuum runs was always below 10^{-6} mm. of Hg.

RESULTS

(1) *Analysis of the ions*

Fig. 1 shows a set of positive ion analysis curves for various mixtures of hydrogen and helium, the bottom curve (*e*) being a run in vacuum. We see from curve (*a*) that no trace of an HeH^+ peak is obtained in pure hydrogen. When the gas is a mixture of hydrogen and helium containing 50 % or 90 % of helium we see from curves (*b*) and (*c*) that a well-marked HeH^+ peak appears. When only pure helium is admitted to the ionization chamber we see from curve (*d*) that the HeH^+ peak is barely detectable. It does not completely disappear because, as shown by the vacuum run (*e*), there is still a slight amount of hydrogen present.

In addition to the He^+ peak observed in curves (*b*), (*c*) and (*d*) when helium is mixed with the hydrogen, we observe the well-known H_3^+, H_2^+, H^+ and H_{2-1}^+ peaks, the latter being due to dissociation of an H_2^+ ion on entering the magnetic field. These peaks have been fully investigated in previous positive ion studies (Smyth 1931) and so require no comment here.

A careful search at mass number 6, where a peak was observed by

Hogness and Lunn (1925) and attributed by them to HeH_2^+, revealed no sign of any particles of this mass.

(2) *Variation of peaks with pressure*

In the previous work on the formation of mercury and helium molecules we have shown how it is possible to distinguish between ions formed directly by electron impact involving a single collision and ions formed by a secondary attachment or dissociation process subsequent to the initial ionization and hence due to two collisions by observing the variation in the height of the peaks with change in pressure. When the ions are formed by direct ionization of an atom or molecule the curve rises linearly with increase of pressure until scattering and neutralization of the ions

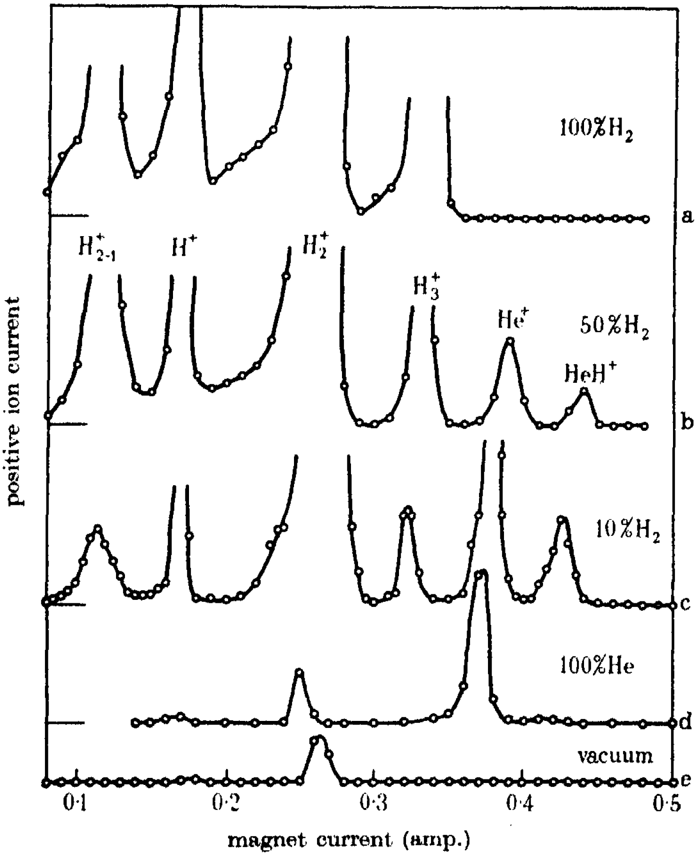

FIG. 1. Positive ion analysis curves for various mixtures of hydrogen and helium, showing presence of HeH⁺ molecule.

by the gas in the analyser causes the curve to decrease as the pressure is further increased. When the ions are formed by a secondary process involving a second collision the curve goes on rising until a considerably higher pressure is reached, because then the number of ions formed is proportional to the square of the pressure.

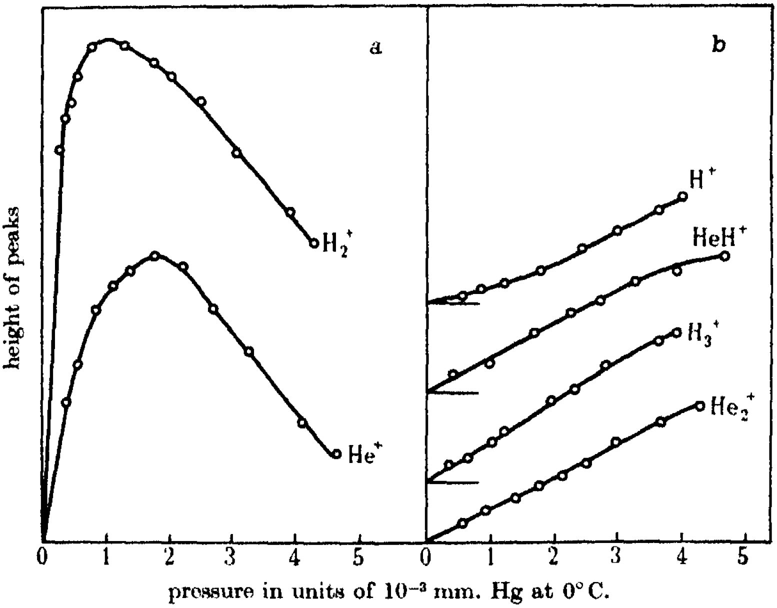

FIG. 2. Pressure variation curves for hydrogen and helium peaks. (*a*) Primary ions formed by direct electron impact in a single collision. (*b*) Ions formed by a secondary process involving a second collision of the primary ion with an atom or molecule.

Fig. 2 shows the variation in the height of the various peaks of fig. 1 with pressure. The sharp rise and fall of the curves for H_2^+ and He^+ in fig. 2*a* are typical of ions formed by direct electron impact in a single collision. The fact that the curves of fig. 2*b* are all increasing with rise of pressure over the pressure range where the directly formed H_2^+ and He^+ curves are decreasing shows that these ions H^+, HeH^+, H_3^+ and He_2^+ are all dependent for their formation upon a higher power of the pressure than that which governs the formation of the H_2^+ and He^+ ions. They are all in fact dependent upon the square of the pressure, the second collision resulting in dissociation, dissociation and attachment, or in simple attachment. For the hydrogen ions the processes are

$$H_2^+ + H_2 \rightarrow H^+ + H + H_2, \tag{1}$$

$$H_2^+ + H_2 \rightarrow H_3^+ + H, \tag{2}$$

as shown by previous investigators (Smyth 1931). We have previously shown (1939) that the He_2^+ ion is formed by the attachment of a metastable He atom to a normal He atom according to the process

$$He'(1s2s,\ {}^3S) + He(1s^2,\ {}^1S_0) \rightarrow He_2^+(1s\sigma^2 2p\sigma,\ {}^2\Sigma_u^+) + \epsilon.$$

We shall show later that the HeH^+ ion under investigation in this work is formed by the process

$$H_2^+ + He \rightarrow HeH^+ + H.$$

At this stage we can say from the evidence of fig. 2 that the HeH^+ ion is definitely not formed by direct ionization of an HeH molecule, but is formed by a secondary attachment process.

(3) *Variation of the peaks with filament emission and with electron energy*

Fig. 3 shows the variation in the height of the HeH^+ peak with filament emission. The linear dependence on emission shows that the number of HeH^+ ions formed is proportional to the first power of the emission, and hence that in the attachment process only one of the two particles involved is excited or ionized, the other particle being in the normal state. A linear dependence on filament emission is also obtained for the He^+, H_2^+ and H^+ ions as would be expected.

Fig. 4 shows the variation in the height of the peaks with electron energy, from which it will be seen that the HeH^+ ionization sets in simultaneously with the H_2^+ and H^+ ionization and definitely before the electrons have acquired sufficient energy to form He^+ ions. This shows that the helium atom involved in the attachment process leading to the formation of the HeH^+ ion is a neutral atom, and further that the HeH^+ ions arise from an ionized hydrogen atom or molecule.

THE PROCESS OF FORMATION OF THE MOLECULE

The magnetic analysis curves of fig. 1 together with the pressure variation curves of fig. 2 show quite definitely that HeH^+ molecules exist and that they are formed by an attachment process. The fact that the HeH^+ ionization varies with the first power of the filament emission, as shown in fig. 3, proves that in the attachment process only one of the particles involved is excited or ionized. Finally, the evidence of fig. 4 shows that the hydrogen particle involved in the attachment process is ionized, not merely

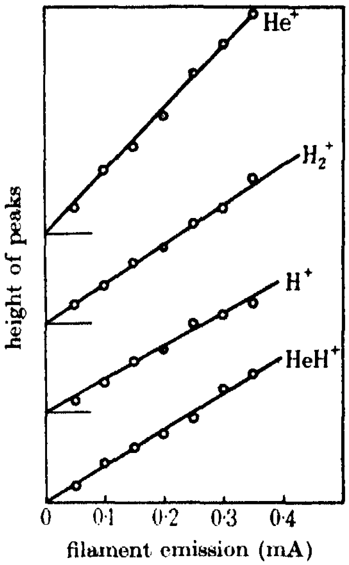

FIG. 3. Showing variation in heights of peaks with filament emission.

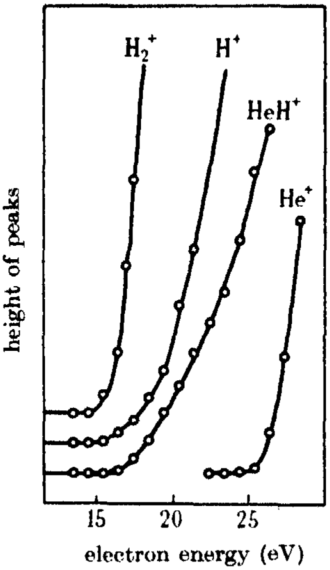

FIG. 4. Showing that the HeH$^+$ ionization sets in simultaneously with the hydrogen molecular and atomic ionization.

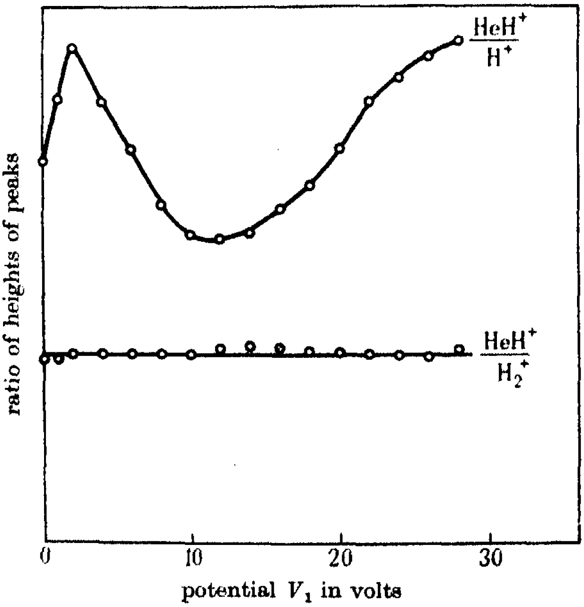

FIG. 5. Showing that the HeH$^+$ ions are formed from H_2^+ ions and not from H$^+$ ions.

excited, and that the helium atom is neutral. We thus have the two following processes to consider:

$$H_2^+ + He \rightarrow HeH^+ + H, \tag{3}$$

$$H^+ + He \rightarrow HeH^+. \tag{4}$$

It is well known that H^+ is formed by the secondary process (1) and therefore (4) represents a tertiary process. Consequently, if the HeH^+ ions were formed according to (4) we should expect the number of HeH^+ ions to vary with the cube of the pressure, and therefore the HeH^+ curve in fig. 2*b* should be markedly different from the three other curves for H^+, H_3^+ and He_2^+ ions which are all dependent upon the square of the pressure. The similarity of the HeH^+ curve in fig. 2*b* to the three secondary process curves indicates that the HeH^+ ions are also due to a secondary process, and hence are formed according to (3).

Conclusive evidence that (3) is the effective process was obtained as follows. The total potential $V_1 + V_2$ accelerating the ions into the analyser was maintained constant while V_1 itself was varied. This altered the conditions in the ionization chamber and hence the relative heights of the various peaks. The variation in the height of the HeH^+, H_2^+ and H^+ peaks with V_1 was obtained and the ratios HeH^+/H^+ and HeH^+/H_2^+ plotted in fig. 5. We see that the number of HeH^+ ions is directly proportional to the number of H_2^+ ions and bears no simple relation to the number of H^+ ions. This shows that the HeH^+ ions are formed by the secondary process (3) and not by the tertiary process (4).

We would expect (3) to be the effective process on theoretical grounds, for the relative kinetic energy of the two colliding particles would have to be radiated in process (4), and it is known that radiative processes are very inefficient compared to those in which the excess energy can be carried away by a material particle such as the H atom in process (3).

The evidence presented above shows conclusively that the helium hydride ion HeH^+ is formed by the process

$$H_2^+ + He \rightarrow HeH^+ + H,$$

which involves dissociation of the H_2^+ ion into H^+ and H together with association of H^+ and He to form the molecule. The energy required to dissociate the H_2^+ ion is 2·6 eV (Smyth 1931) and the energy liberated by the association of H^+ and He into HeH^+ is given by Coulson and Duncanson (1938) from a comparative study of the wave functions of HeH^+ as certainly lying between 0·61 and 2·10 eV, the most probable value being about 1·5 eV. An earlier theoretical calculation by Beach (1936) gave a value of 2·02 eV. Accepting the value 1·5 eV, there is an energy deficiency in the above process of 2·6 − 1·5 = 1·1 eV which must be obtained from the kinetic energy of the H_2^+ ion.

In fig. 6 are shown the potential energy curves for the ground state and the ionized state of the hydrogen molecule taken from Smyth (1931). Coulson and Duncanson (1938) give the energy of dissociation of HeH^+ as 1·5 eV, and the equilibrium internuclear distance of the lowest vibrational state as 0·764 A. Their work also shows that the ground state of the normal HeH molecule is unstable. From these data we have drawn approximate potential energy curves for the ground state and the ionized state of the HeH molecule.

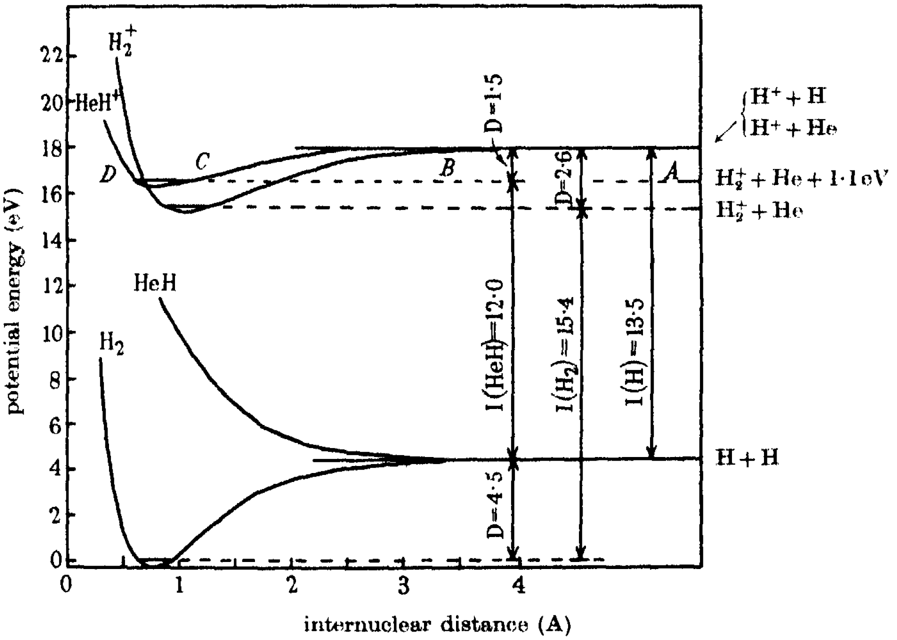

FIG. 6. Potential energy curves for the ground states and ionized states of H_2 and HeH.

The total energy, kinetic plus potential, of an H_2^+ ion and an He atom at a large distance apart approaching each other with a relative kinetic energy of 1·1 eV is represented by the line *AB* lying 1·1 eV above the lowest vibrational state of the H_2^+ molecule. As the H_2^+ ion and He atom approach each other, the total energy of the system remains constant as shown by the horizontal line *ABCD*. When the internuclear distance has been reduced to a value between *C* and *D* the quasi-molecule H_2^+He rearranges itself into a stable molecule HeH^+ in the lowest vibrational state *CD* and a free H atom which has just sufficient energy to get clear of the HeH^+ molecule. If the approaching particles have a relative kinetic energy greater than 1·1 eV the ejected H atom carries off any energy in excess of that of the quantized state in which the molecule is formed. It will be seen from fig. 6 that the ionization potential of the HeH molecule is 12 V.

SUMMARY

An investigation of the formation of the singly-charged helium hydride molecule HeH^+ has been made by means of a mass spectrograph. It is found that the molecule is formed by a collision between a singly-charged hydrogen molecule and a normal helium atom in which the hydrogen molecule is dissociated. The process is

$$H_2^+ + He \rightarrow HeH^+ + H.$$

For this process to be energetically possible the colliding particles must have kinetic energy in excess of the difference between the energy of dissociation of H_2^+ (2·6 eV) and that of HeH^+, which Coulson and Duncanson find from a wave-mechanical treatment to be about 1·5 eV. The kinetic energy of the H_2^+ ion must therefore be greater than 1·1 eV. The ionization potential of the HeH molecule is found to be 12 V. No evidence of the existence of a HeH_2^+ molecule was found.

REFERENCES

Arnot and M'Ewen 1939 *Proc. Roy. Soc.* A, **171**, 106.
Arnot and Milligan 1936 *Proc. Roy. Soc.* A, **153**, 359.
Bainbridge 1933 *Phys. Rev.* **44**, 57.
Beach 1936 *J. Chem. Phys.* **4**, 353.
Coulson and Duncanson 1938 *Proc. Roy. Soc.* A, **165**, 90.
Hogness and Lunn 1925 *Phys. Rev.* **26**, 44.
Smyth 1931 *Rev. Mod. Phys.* **3**, 347.

Diffraction of X-rays by crystals at elevated temperatures

By G. D. Preston, M.A., *National Physical Laboratory*

(*Communicated by C. H. Desch, F.R.S.—Received* 28 *April* 1939)

[Plates 1–5]

1. Introduction

During an investigation of age-hardening of an alloy of aluminium with 4 % copper, a large number of Laue photographs was taken and attention was directed to certain anomalous streaks on these photographs which altered as the process of hardening took place (Preston 1938). In addition to these streaks, which were associated with the chemical change in the crystal, there were others which did not seem to change with the hardness and which were also present on photographs of aluminium. A further investigation showed that when a single crystal of the alloy or of pure aluminium was photographed at a temperature of about 550° C, the intensity of these streaks was greatly increased. The purpose of the present paper is to give a description of this effect which has now also been observed in crystals of rocksalt, periclase, diamond and zinc. The presence of streaks running through the normal reflexions is a commonplace on Laue photographs; they were observed 25 years ago by Friedrich (1913) in photographs of KCl and NaCl. Ten years later Faxén (1923), in a theoretical investigation of the effect of temperature on the intensity of X-ray reflexion, referred to Friedrich's observations and suggested that an attempt should be made to correlate these streaks with the temperature of the crystal. So far as I am aware this suggestion has never been carried out. The experiments described below show that Faxén was correct in his surmise that the streaks are connected with the temperature of the crystal.

2. Experimental

The experimental arrangement used to obtain Laue photographs at elevated temperatures was very simple. The crystal to be examined was usually in the form of a wire or rod about 1 mm. diameter and from 3 to 15 mm. long. It was mounted with the aid of a little refractory cement in a small silica holder attached to a metal base which fitted the goniometer of the X-ray spectrograph. The silica holder gave some thermal insulation between the crystal and the spectrograph. The heating element consisted of a silica tube 8 mm. diameter in which a small hole was cut to admit a narrow pencil of X-rays, and diametrically opposite this a larger hole to allow the egress of rays diffracted through angles up to 40° to the incident beam. The silica tube was wound with nickel-chromium wire, the winding extending about 15 mm. on either side of the apertures in the tube and being carried as close to these as possible. The temperature was measured by a thermocouple of iron-constantan wire, the junction being placed as close as possible to the crystal. The recorded temperature is not a true measure of the temperature of the specimen, but it was impossible to attach the couple to the aluminium crystal without risk of damaging the latter. Accurate temperature measurement was, in the present case, of less importance than protecting the specimen from strains. In the experiments with aluminium it was found that the recorded temperature was about 50° C less than the temperature of the specimen, which began to melt when the couple indicated a temperature of 610° C. The temperatures recorded for the other crystals can only be taken as a very rough approximation.

The Laue photographs here reproduced have all been taken with a silver target operated at 60 kV peak. The distance from specimen to film is in all cases 5 cm. The use of intensifying screens and duplitized X-ray film has made it possible to obtain photographs with exposures of 10 min. with polychromatic radiation and of 30 min. with monochromatic radiation. The former is equivalent to an exposure of about 5 hr. without the screens. All the photographs described have been taken with the crystal stationary.

3. DESCRIPTION OF RESULTS

(*a*) *Aluminium*

The specimen consisted of a crystal grown by the strain-anneal method in a wire 1 mm. diameter. A piece about 15 mm. long was mounted in the silica holder and annealed at 500° C to remove any strain introduced in cutting off the specimen and subsequent manipulation. The orientation of the crystal was such that a [110] axis was nearly parallel to the axis of the wire, so that photographs were obtained with the X-ray beam parallel to [001], [$\bar{1}$10] and [$\bar{1}$11], the axis of the wire being in all cases nearly parallel to the vertical axis of the spectrometer. The photographs are reproduced in figs. 1–3 (Plates 1–3). Fig. 1 *a*, taken at room temperature, shows, in addition to the intense Laue spots, four diffuse spots symmetrically arranged about the centre and about 1·3 cm. from it; also eight diffuse spots about 2·5 cm. from the centre. In fig. 1*b*, taken at 500° C, the intensity of these diffuse spots is very greatly increased, while the Laue spots are much fainter than in the room temperature photograph. A projection of the photograph showed that the four inner diffuse spots corresponded roughly to Laue reflexions of indices (801), the eight outer ones to (4(12)3). In the conditions in which the photograph was obtained (λ min. = 0·20 A), the presence of these reflexions would require the side of the cubic unit to be doubled, assuming that the spots are produced by the shortest wave-length present in the beam. Actually these spots are almost entirely due to the silver characteristic radiation, $\lambda = 0{\cdot}56$ A, as is proved by the photograph, fig. 1*c*, taken with monochromatic Ag $K\alpha$ radiation, with the crystal at 500° C and in the same orientation as in figs. 1*a* and *b*. A photograph similar to fig. 1*c* was obtained at room temperature, but the spots were very faint.

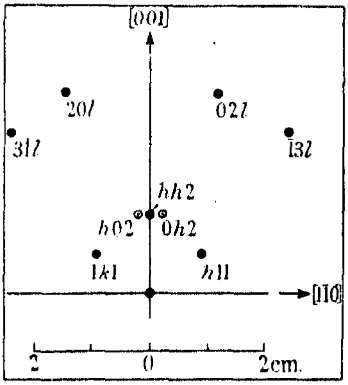

FIG. 4

The photographs obtained with the incident beam parallel to [110] are shown in fig. 2*a* at room temperature, and in fig. 2*b* at 500° C. Here again the diffuse spots increase in intensity as the temperature is raised; they are here also due to the silver characteristic radiation. A tracing of the photograph obtained with monochromatic radiation is shown in fig. 4. In this case the imperfection of the monochromator was shown up; the spectrograph slits transmit a wave-length band extending ± 0·05 A on either side of the silver $K\alpha$ line, so that Laue spots are produced on the photograph. From their presence we can form a very rough estimate of the relative intensities of the diffuse reflexions and the normal Laue reflexions. The band of white radiation could just be faintly seen in a rotation photograph of the crystal in which the silver $K\alpha$ reflexions were quite black. The intensity of this band cannot exceed one-thirtieth of the silver $K\alpha$, yet it produces Laue spots which are at least thirty times as intense as the diffuse spots produced by the silver $K\alpha$. The intensity of the latter is therefore not one-thousandth of the normal reflexions. This estimate is necessarily very rough but indicates the very feeble nature of the effect we are considering.

With the X-ray beam parallel to $[\bar{1}11]$ a pattern of diffuse spots is obtained, showing threefold symmetry, much more intense at 500° C than at room temperature (figs. 3*a*, *b*). That the diffuse spots here are again due to the silver characteristic was proved by using monochromatic radiation.

(*b*) *Rocksalt and periclase*

These two crystals are structurally similar and, to a first approximation at least, the effects produced by heating are so nearly identical that they may here be considered together. The rocksalt specimen was in the form of a small rod obtained by cleavage from a large crystal of unknown, but probably natural, origin. The rod, at first about 15 × 2 × 3 mm., was partly dissolved away in water to get rid of any defects on the surface or edges produced in handling. The periclase was a small crystal separated from a mass of fused magnesia prepared in the Ceramics Section of the Metallurgy Department. Both crystals gave very good Laue reflexions and both showed the presence of diffuse spots which become more intense as the temperature is raised. Photographs of rocksalt with the incident beam parallel to [100] are shown in fig. 5*a*, room temperature, and in fig. 5*b* at 500° C (Plate 4). Figs. 6*a* and *b* (Plate 5) are of magnesium oxide with the incident beam parallel to [110]. Comparison of these photographs with those of aluminium show certain differences.

The room-temperature photograph of rocksalt seems to be identical with those described by Wadlund (1938), who states that he obtained a similar effect with potassium chloride, but failed to obtain it with mica, fluorite, gypsum and calcite. The photographs reproduced here show that the intensity of the diffuse spots is dependent on the temperature of the crystal.

(*c*) *Diamond*

I am indebted to Mr Shaw for the loan of a stone of 0·35 carat (72·4 mg.) which was roughly cut to the shape of an irregular octahedron. At room temperature Laue photographs were taken with the incident beam parallel to [100], [110] and [111]; no diffuse spots were present, but the background scattering gave the impression of not being of uniform intensity. There seemed to be a cruciform space of less intense blackening near the central spot in the [100] and [110] photographs. At 500° C the [100] and [111] photographs showed no appreciable change, but in the [110] orientation four faint diffuse streaks were visible.

4. ANALYSIS OF DIFFRACTION PATTERN PRODUCED BY ALUMINIUM

The Laue photographs are too complex to afford much information about the nature of the effect we are observing. The photograph, fig. 1*c*, taken with a beam of monochromatic silver radiation, $\lambda = 0{\cdot}56$ A, parallel to a [001] axis, is the simplest and will be dealt with first. It closely resembles the two-dimensional diffraction pattern which would be given by a single net of atoms arranged at the corners and centres of a square net of 4·09 A side, the parameter of aluminium at 500° C. Zachariasen (1938) has suggested that the pattern observed by Wadlund in rocksalt is due to a simple cross-grating, but I believe that this conclusion is erroneous, at any rate for the aluminium pattern, for the following reasons: (i) the positions of the spots are not correct, (ii) spots which ought to be present are not observed, (iii) spots are observed for which two indices must be fractional.

If we imagine the crystal to be set up with the X-ray beam parallel to [001] and choose a pair of axes on the photograph parallel to [100] and [010] then the co-ordinates (x, y) of a diffraction maximum from a square net (of side a) perpendicular to [001] are

$$\frac{x}{D} = \lambda h/\sqrt{\{a^2 - \lambda^2(h^2 + k^2)\}}$$

and

$$\frac{y}{D} = \lambda k/\sqrt{\{a^2 - \lambda^2(h^2 + k^2)\}},$$

where D is the distance from specimen to photographic film. Putting $\lambda = 0{\cdot}56$ A, $a = 4{\cdot}09$ A, the values of (x, y) for integral values of (h, k) are calculated and plotted as shown in fig. 7. Here all the points of intersection of the hyperbolas $h = \text{const.}$ and $k = \text{const.}$ represent the positions of maxima which would be produced by a square net of atoms of side a. The points marked by full or open circles are those for which $(h+k)$ is even, and would be produced by a net of the type which exists on the cube faces of aluminium; i.e. two nets of side 4·09 A intermeshed, and one having its origin at the centre of the other; it is a square net of side $a/\sqrt{2}$. The points which are observed in fig. 1*c* have been marked with full circles: they have indices (20) and (31); (33) if present is very weak. The values of (x, y) for the points (20) and (31) are as follows:

	Calc.		Obs.	
	$2x$	$2y$	$2x$	$2y$
20	2·91	0	2·75	0
31	4·65	1·55	4·8	1·6

The difference between calculated and observed values is small, but rather larger than can be accounted for by experimental error.

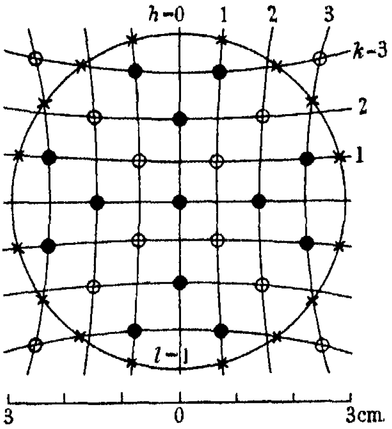

FIG. 7

If the pattern really arose from the presence of single sheets of atoms in the crystal we should have all points for which $(h+k)$ is even represented in the photograph. They are not all present; (11), (22), (40) and (42) are absent and (33) is very weak. In addition to these absences there are others. We cannot suppose that the particular cube axis along which the incident beam travels is favoured, and if nets exist perpendicular to it there will also be nets perpendicular to the other two cube edges. These nets will give rise to maxima lying at the intersection of the circles $l = 1$, $l = 2$ (fig. 7) with the two sets of hyperbolas $h = \text{const.}$ and $k = \text{const.}$ Thus the net perpendicular to [100], i.e. a (100) plane of the lattice, would give reflexions where the circle $l = 1$ cuts the hyperbolas $k = 1$, $k = 3$; the condition that $k+l$ must be even cutting out the reflexion at $k = 2$. These points and the corresponding ones for the net (010) are marked with crosses in fig. 7; none of them is observed.

Turning now to the photograph (fig. 2) taken with the incident beam parallel to a [110] axis the four spots arranged in pairs on either side of the vertical axis will have indices of the type ($h11$) with $h = -0{\cdot}75$, on the cross-grating view. They fall close to the calculated position. The point lying on the vertical axis must have indices of the type (hhl) and calculation shows that its position is consistent with the values $h = 0{\cdot}2$, $l = 2$. Two of the indices are fractional, which is quite inconsistent with the idea that a cross-grating is responsible for the production of the spots. The cross-grating should produce a pair of spots of indices (0·4, 0, 2) one on either side of the vertical axis as indicated in fig. 4.

In photographs of an alloy of aluminium with 4 % by weight of copper aged at room temperature, the points (0·4, 0, 2) are quite definitely observed; the points missing from fig. 1*c* are also present. In this case we are justified in inferring that the pattern is due to the separation of copper atoms on (100) planes of the crystal which thus produce the diffraction effects characteristic of a two-dimensional grating. The temperature spots in the pure aluminium must be assigned to a different cause; the resemblance of the patterns to cross-grating spectra is misleading. The fact that the intensity of the spots increases as the temperature of the crystal is raised suggests that their presence is connected with the temperature vibrations of the lattice. The frequency of the atomic vibrations is of the order of 10^{13} per sec. and is small compared with the frequency of the X-rays, about 5×10^{18} per sec. Thus in a time of the order of 10^{-15} sec. an atom will have described one hundredth of its orbit while in the same time a train of 5000 X-rays will have been diffracted by it. So far as the X-rays are concerned the atoms may be regarded as being at rest, but slightly displaced from the positions of exact geometrical regularity. The displacement corresponding to a particular frequency of the lattice vibration will be a periodic function of the position of the atoms. The effect of this wave-like disturbance of the regularity of the lattice is to produce a series of "ghosts" associated with the normal spectra; if the disturbance consists of a very large number of lattice waves these will produce a continuous faint background on the Laue photographs. The experiments described above show that this background is not of uniform intensity but possesses well-marked maxima. The simplest explanation of the presence of these maxima is to suppose that the thermal vibrations are of such a nature that the crystal is divided up into small groups of atoms; in each group the face-centred arrangement is accurately maintained, but neighbouring groups have slightly different spacings due to a wave of dilatation, or are inclined at a small angle to the average direction of the crystal as a result of a wave of shear. The smallest group would consist of an atom and three of its neighbours; the atoms at the points (000), $(0\frac{1}{2}\frac{1}{2})$, $(\frac{1}{2}0\frac{1}{2})$ and $(\frac{1}{2}\frac{1}{2}0)$. These will contribute to the amplitude of the diffracted ray, in a direction defined by (hkl), terms of the type

$$F = 1 + \cos \pi(h+k) + \cos \pi(k+l) + \cos \pi(l+h),$$

$$G = \sin \pi(h+k) + \sin \pi(k+l) + \sin \pi(l+h),$$

the intensity being proportional to the sum of the squares of these two quantities. The numbers (hkl) which define the direction of the diffracted ray are to be thought of as varying continuously and are not confined to integral values. They are, however, subject to one restriction, namely that the point in reciprocal space which they define must lie on the sphere of reflexion. For the photograph fig. 1*c*, for instance, the relation

$$h^2 + k^2 + \left(l - \frac{a}{\lambda}\right)^2 = \frac{a^2}{\lambda^2}$$

defines one of the numbers h, k, l when two of them are chosen.

The group of four atoms considered above can be used to build up the face-centred lattice which can be regarded as groups of four placed at the corners of a simple cubic cell. A more natural group to take would be an atom and its twelve neighbours. The analogous expressions for this group do not differ much from F and G; for the sake of simplicity the values of F^2 have been taken as representing approximately the way in which these functions vary and their values have been computed along lines such as $h = 0$, $h = 1$, $h = k$ on the different photographs. The neglect of the G term does not introduce any serious error so far as consideration of the salient features of the photographs is concerned; its inclusion would be necessary if we proposed to discuss any detail. In fig. 8 the value of F^2 is shown along the lines $h = 0$, $h = 1$ and $h = k$ of fig. 1*c* or fig. 7. At the top of fig. 8 scales showing the values of (hkl) are included and the observed spots are marked by a cross (+). In figs. 8*a* and *b* the points for which (hk) is approximately (20) and (31) occur as well-marked peaks on the F^2 curve. Fig. 8*c* shows F^2 along the line $h = k$; the larger of the three peaks corresponds to $(hk) = (33)$ and is only observed as a very faint reflexion. The two smaller peaks are not observed; the discrepancy arises from the choice of the group of four atoms, if a larger group had been chosen these two peaks would have disappeared from the curve. Fig. 9 refers to the photographs with the X-ray beam parallel to [110] and shows the variation of F^2 along the lines $h = 0$ and $h = k$. Here again there is evidence that the group of four atoms is too small; the smaller peak in fig. 9*a* corresponds to the point (0*h*2) of fig. 4; it is really a shoulder of the peak (*hh*2) of fig. 9*b*. The larger group would reduce the intensity of this shoulder and leave the peak (*hh*2) as observed. Fig. 10 shows the F^2 curves for the lines $h = k$ and $h = 0$ of the photographs with the X-ray beam parallel to [111], fig. 3. The agreement with the observed reflexions is quite good. It will be noticed that on the left-hand side of fig. 10*a* both *h* and *k* are fractional.

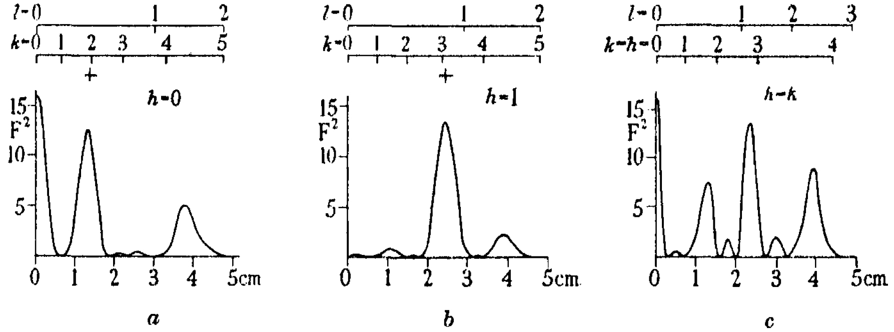

a *b* *c*

FIG. 8

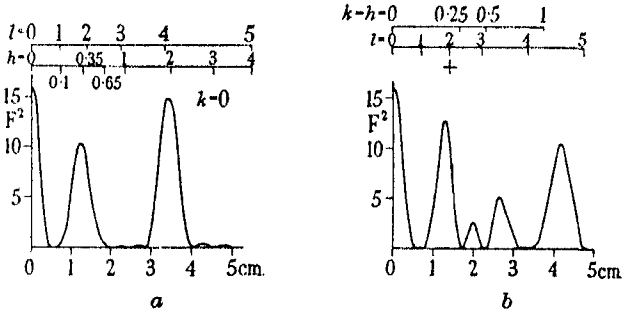

a *b*

FIG. 9

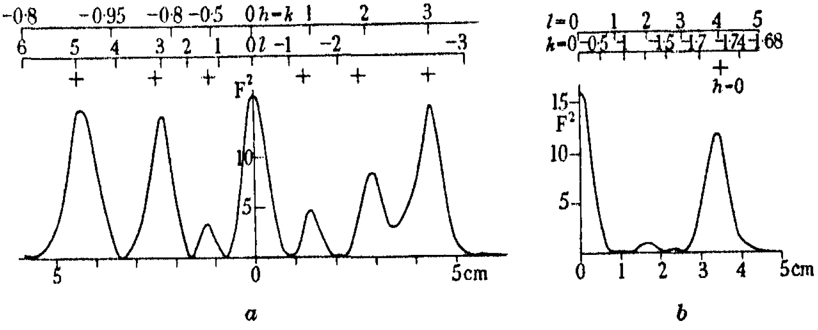

a *b*

FIG. 10

It has been mentioned above that the positions of the reflexions are not quite consistent with the view that they arise from a cross-grating. The question arises whether on the view now put forward the positions of the spots correspond accurately with the maxima of the function F^2 and G^2. The intensity of reflexion is

$$I = F^2 + G^2 = 4(1 + \cos \pi h \cos \pi k + \cos \pi k \cos \pi l + \cos \pi l \cos \pi h)$$

for the group of four atoms considered above. For the group of thirteen atoms, consisting of an atom and its twelve neighbours, the intensity is $(I-3)^2$ so that the maxima of this group occur in the same places as those of the group of four atoms. The intensity I has a maximum value, 16, when hkl are integers, all even or all odd; $I \equiv 0$ if hkl are integers, mixed even and odd. We are concerned with the value of I on the sphere of reflexion; let hkl be three integers, all even or all odd, defining a point in space near to the surface of the sphere of reflexion. If $(h+e, k+f, l+g)$ is a neighbouring point such that e, f, g are small compared with unity, it can be shown that the change, δI, of I in passing from (hkl) to $(h+e, k+f, l+g)$ is

$$\delta I = -4\pi^2(e^2+f^2+g^2).$$

The contours of equal values of I surrounding the maxima are spheres so that the maxima of I on the sphere of reflexion are found where the line joining a point such as hkl to the centre of the sphere of reflexion intersects the surface of the sphere of reflexion. In the case of the photograph fig. 1c with the X-ray beam parallel to [001] the co-ordinates of the maxima on the plate are now

$$\frac{x}{D} = \frac{h}{\frac{a}{\lambda} - l}, \quad \frac{y}{D} = \frac{k}{\frac{a}{\lambda} - l},$$

where h, k, l are integers, all even or all odd, defining a point in reciprocal space near the surface of the sphere of reflexion. The numerical values are as follows:

	Calc.		Obs.	
hkl	$2x$	$2y$	$2x$	$2y$
200	2·78	0	2·75	0
311	4·84	1·61	4·8	1·6

The agreement is well within the limits of error and the discrepancy noted in connexion with the cross-grating is removed. It should be observed that in the above table (200) and (311) are not the indices of the reflecting points; they lie near to but not on the sphere of reflexion.

The work has been carried out in the Metallurgy Department of the National Physical Laboratory under the supervision of Dr C. H. Desch, to whom I am indebted for his continual interest and encouragement. The earlier part of the investigation was made during the time when Professor W. L. Bragg was Director of the Laboratory, and I have had the great advantage of discussing the results with him on several occasions; it is a great pleasure to acknowledge his assistance. Most of the experimental work has been carried out under my direction by Mr J. Trotter, and I am glad to record my appreciation of the care which he has bestowed on the work.

SUMMARY

A description is given of certain diffuse spots which appear on Laue photographs of single crystals of aluminium, rocksalt and periclase; these spots do not belong to the normal Laue pattern and their intensity increases as the temperature of the crystal is raised to about 500° C. Analysis of the photographs of aluminium leads to the conclusion that the presence of the diffuse spots can be explained by the thermal vibrations of the lattice, which break the crystal up into groups, consisting probably of an atom and its twelve neighbours. The thermal vibrations cause the interatomic distances to vary slightly from one group to another so that new diffraction maxima, characteristic of the group of atoms, are produced.

REFERENCES

Faxén 1923 *Z. Phys.* **17**, 266.
Friedrich 1913 *Phys. Z.* **14**, 1082.
Preston 1938 *Proc. Roy. Soc.* A, **167**, 526.
Wadlund 1938 *Phys. Rev.* **53**, 843.
Zachariasen 1938 *Phys. Rev.* **53**, 844.

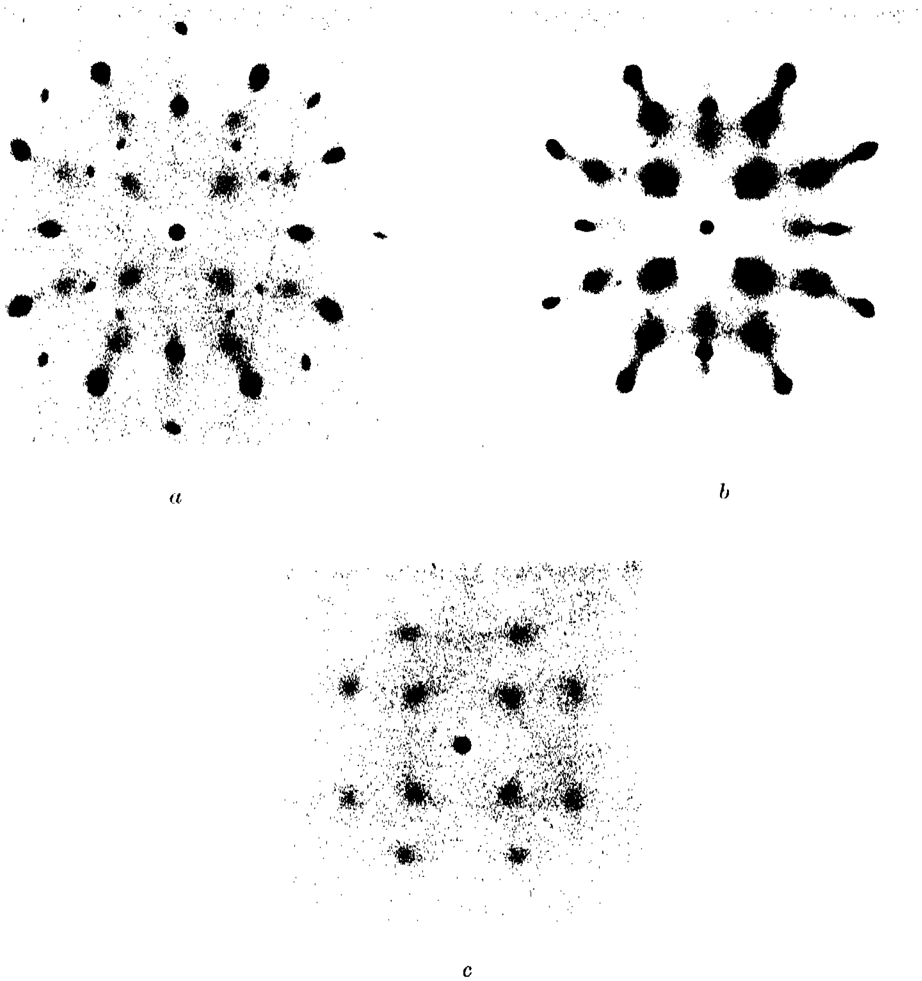

a

b

c

Fig. 1. Aluminium. X-rays parallel to [001], [110] vertical, reduced to two-thirds original size.

a, room temperature; *b*, 500° C; *c*, 500° C monochromatic Ag $K\alpha$ radiation.

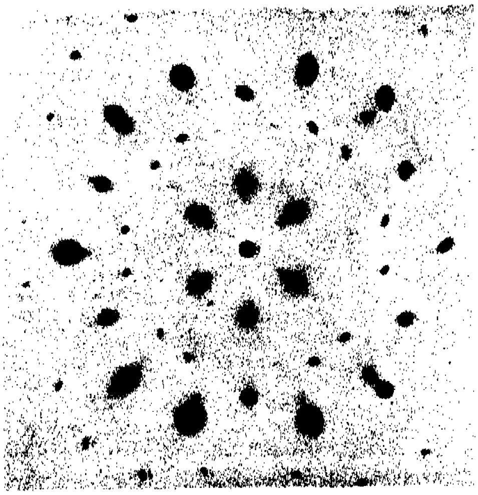

a

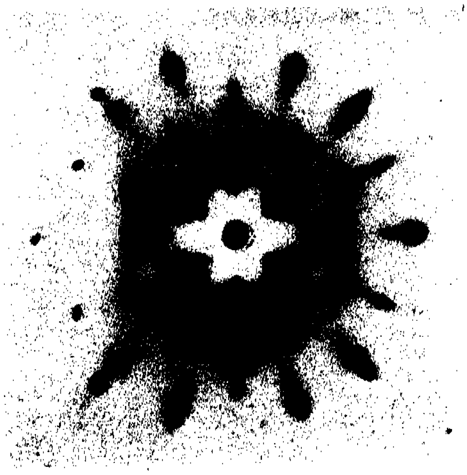

b

Fig. 2. Aluminium. X-rays parallel to [110], [001] vertical, reduced to two-thirds original size.

a, room temperature; *b*, 500° C.

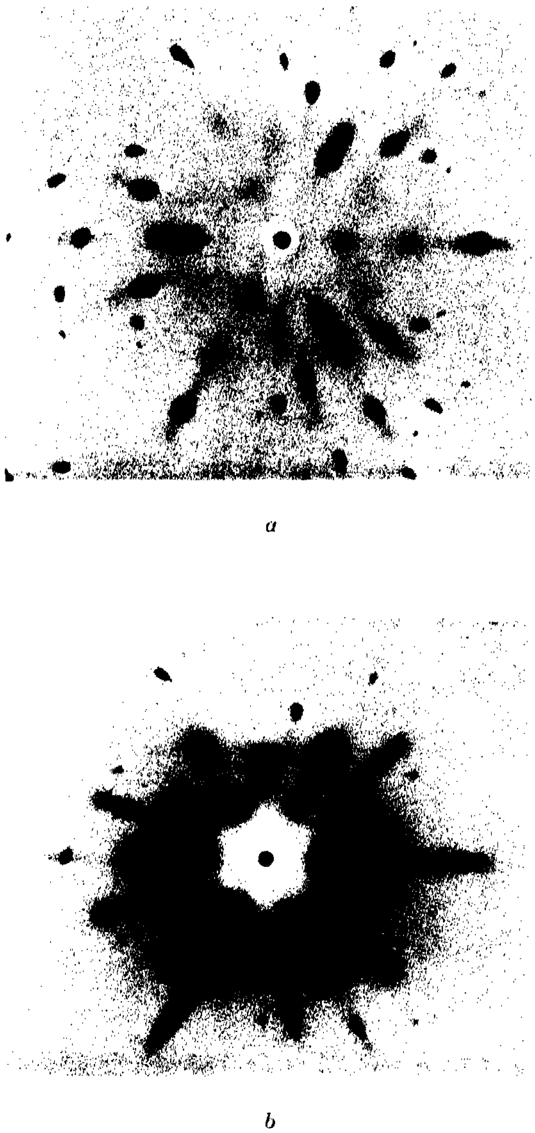

FIG. 3. Aluminium. X-rays parallel to [110], [110] vertical, reduced to two-thirds original size.

a, room temperature; *b*, 500° C.

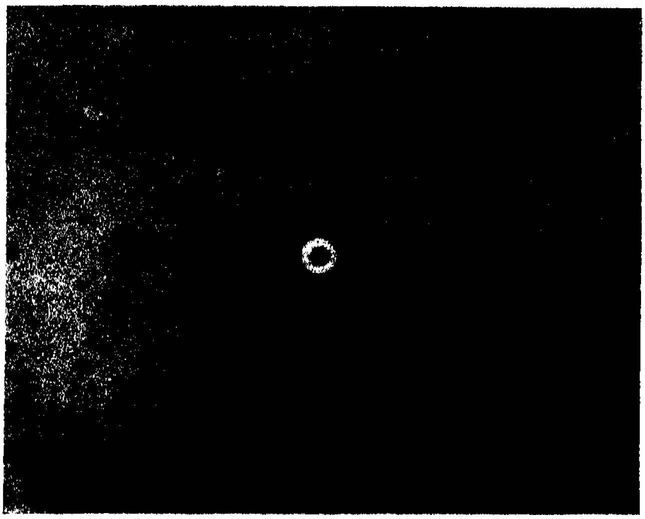

a

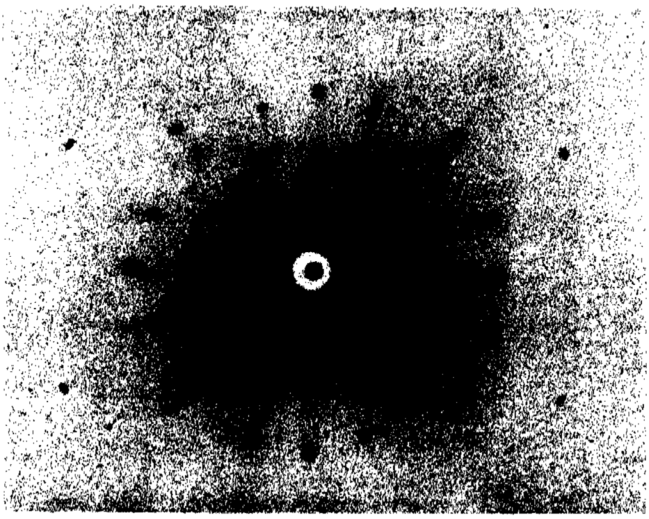

b

Fig. 5. Sodium chloride. X-rays parallel to [001], [100] vertical, reduced to two-thirds original size.

a, room temperature; *b*, 500° C.

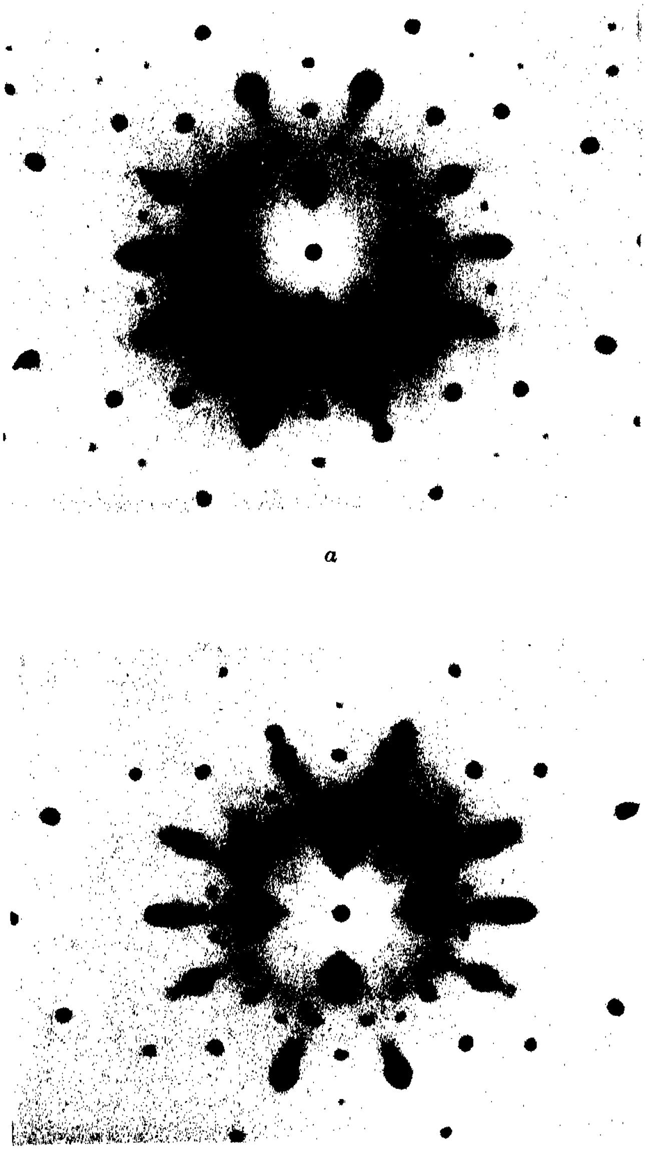

a

b

Fig. 6. Magnesium oxide. X-rays parallel to [110], [001] vertical, reduced to two-thirds original size.

a, room temperature; b, 500° C.

Resonance phenomena in the scattering of α-particles by some light nuclei

By S. Devons, M.A.

Senior Rouse Ball Student, Trinity College, Cambridge

(*Communicated by W. L. Bragg, F.R.S.—Received* 1 *May* 1939)

I. Introduction

The early experiments of Chadwick and Bieler (1921) and Rutherford and Chadwick (1927) showed that it was possible, in the case of light nuclei, to observe deviations from the classical-coulomb scattering laws by using the α-particles from radioactive sources. The departure from the classical scattering was found to be most marked at large energies, the ratio of the actual to the classical scattering appearing to increase very rapidly with energy for the most energetic particles used. Later experiments by Riezler (1932, 1935) extended these early observations, but also showed that in one case, the large angle (150°) scattering by carbon, the departure from classical scattering does not become uniformly greater for increasing energy of the α-particle, for large α-particle energies, but shows a marked maximum at 5 MeV. This result was subsequently interpreted by Wentzel (1934) as a resonance phenomena.

In the experiments of Riezler the resolution with respect to energy of the scattered particles was rather low. In addition the scattering was not observed at a sufficiently large and closely spaced series of energies to decide whether or not the ratio to classical scattering did increase continuously with increasing α-particle energy, for very fast particles, in cases other than carbon. In the case of carbon itself, the maximum in the scattering ratio was rather broad (about 1 MeV) and it was not possible in view of the low resolution of the experiments to decide the real width of the resonance maximum. Since the experiments described here were carried out, observations of the scattering of α-particles in oxygen and neon have been published by Brubaker (1938). In both these cases resonance phenomena are in evidence, but even in these experiments the resolution with respect to energy was not very high and the spacing of the observations not as close as is desirable.

According to the present theory of nuclear structure the scattering ratio for α-particles and light nuclei should show marked resonance phenomena with varying α-particle energy in the same way as the cross-section for disintegration by α-particles. Numerous experiments on the disintegration of light nuclei by α-particles have shown that resonance phenomena occur for α-particle energies of between 4 and 8 MeV, and that the widths of these resonances are of the order 0·1 MeV in most cases and the spacing of the resonances usually of the order 0·5 MeV apart. It would be of interest, then, to obtain more complete data concerning the variation of the scattering ratio with energy in order to ascertain under what circumstances resonances similar to those observed in disintegration experiments are observable in scattering experiments. A more detailed theoretical discussion of the conditions required in order to observe resonance in scattering is given below. The main experimental conditions required are a high energy resolution and a large scattering angle, in so far as these conditions can be obtained without too large a sacrifice in the intensity of the scattered beam of particles.

II. EXPERIMENTAL METHOD

In order to obtain a high resolution with respect to energy all the elements studied were used in the form of gases. In this way the scattering of α-particles in helium, carbon (as C_2H_2), nitrogen, oxygen, fluorine (as CF_4) and neon was investigated. The experiments with helium were carried out by the usual annular ring method and will be described in a separate communication. In the other cases this experimental method does not allow of high energy resolution at large scattering angles and a somewhat different geometrical arrangement was therefore used. A diagrammatic cross-section of the apparatus employed is shown in fig. 1.

The source S is an active deposit of Ra (B + C), etc. of about 40 millicuries on a small polished platinum or nickel button 3 mm. in diameter. A beam of α-particles from this source is defined by the circular aperture A, 5 mm. in diameter, covered by a mica window of stopping power equivalent to 7 mm. of air. The distance SA is 4·5 cm. The pressure of air between S and A can be adjusted and measured on a mercury manometer. In this way the energy of the α-particles in the scattering region can be altered by small and exactly known amounts. In addition mica screens can be introduced in front of the source in order to produce large differences in the α-particle energy or to cut off the α-particles completely in order to measure the "natural" count. The beam of α-particles passes into the gas to be investigated, contained in the brass cylinder C, and at a pressure varying between 5 and 40 cm. according to the gas being used and the energy of the α-particles.

The scattered α-particles which are detected are defined by the annular slits S_1, S_2 which define both the range of scattering angles and the effective target for scattering (shown shaded in fig. 1). The mean scattering angle is 90° and the range of scattering angles about 10°. The effective thickness of the scattering target corresponds to about 1·0 mm. of air stopping power. All the particles passing through the slits S_1, S_2 enter the annular ionization chamber formed by the plates P, Q. The collecting electrode P is supported by a sulphur ring to the case of the apparatus and the connexion to the grid of the first valve is insulated by means of a quartz plug. This ionization chamber is suitable for counting α-particles in the presence of quite strong

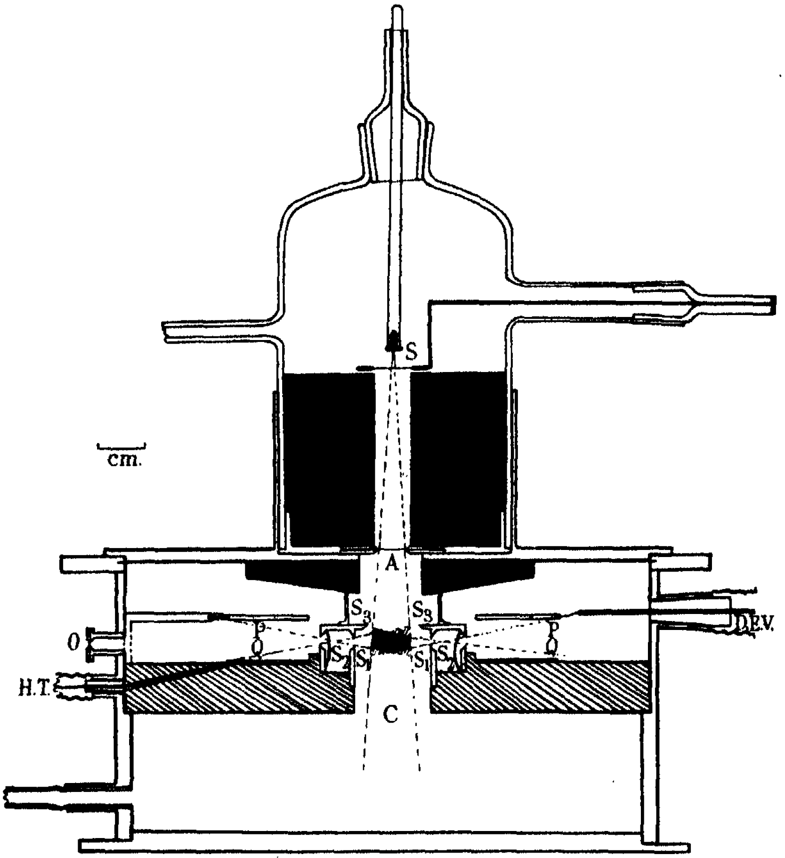

FIG. 1. Apparatus.

γ-ray sources for voltages of the plate Q above about 250 V. In the actual experiments Q was maintained at 300 V. The background effect due to the presence of the strong γ-ray source S is reduced to a minimum by placing as much lead as possible between P, Q and S (the lead is shown black in fig. 1); and also by constructing the plates P, Q of thin aluminium (0·5 mm. thick). All the slits S_1, S_2 were made of aluminium in order to reduce extraneous scattering. The auxiliary slit S_3 is placed in such a position that it is necessary for an α-particle to be scattered three times from a solid surface in order to enter the ionization chamber without being scattered from the gas.

Extraneous scattering can be measured by filling the scattering chamber with helium. The range of the α-particles scattered at angles of 80° or more from helium nuclei is so small that these particles are unable to enter the ionization chamber and be recorded. Any observed scattering in this case must then be due to scattering from the slits or to multiple scattering in the gas. The actual observed effect in this case is found to be negligible.

The size of the impulses produced by scattered α-particles traversing the ionization chamber varies from about twice to four times the height of the background, according to the pressure of gas, but does not vary by more than 50 % for a particular gas pressure. The variation is much less for all but the smallest α-particle energies used. It is therefore possible to separate the impulses produced by α-particles from those that might be produced by disintegration protons entering the ionization chamber. A small aperture O covered with mica of 3 mm. stopping power can be used to introduce α-particles of known range into the ionization chamber and thus enable the "bias" on the amplifier to be adjusted.

All the scattering measurements were made at one fixed range of angles, the mean scattering angle being 90°. This angle was chosen since attention was primarily directed towards measuring the variation of scattering cross-section with *energy*, and the energy resolution of this type of apparatus is greatest for a scattering angle of 90°.

Brubaker (1938) has recently used an arrangement similar to that described here for the measurement of the scattering of α-particles in oxygen, neon and argon. The annular ionization chambers used by Brubaker were of a toroidal shape with a loop of wire round the axis of the toroid as the collecting electrode. This construction seems rather more elaborate than that described above and possesses further disadvantages. First, the background of such ionization chambers in the presence of γ-rays is usually higher than for an ionization chamber with plane electrodes owing to the large potential gradient near the surface of the wire. Secondly, the ionization produced by particles entering the toroid depends quite considerably on the exact direction of the particles, since the field in such an ionization chamber is not even approximately uniform. In Brubaker's experiments the size of the α-particle impulses recorded varied from twice to eight times the background height and it was therefore impossible to avoid counting some disintegration protons or to miss counting some of the scattered α-particles entering the ionization chamber.

Two sets of experiments were carried out with each element studied. In the first of these the variation of the number of scattered particles with α-particle energy was observed, the observations for the whole range of α-particle energies being carried out with each α-particle source prepared. In the second set of experiments the scattering was measured for only one or two α-particle energies, with each source, after which the gas being investigated was pumped out and replaced by argon at a pressure corresponding to the same stopping power per cm. of path. The scattering in argon was then measured for a series of energies, including the energies for which the scattering in the other gas had been measured. From the variation of the scattering with energy (–Number of scattered particles proportional to $(\text{Energy})^{-2}$) in the case of argon it was found that for α-particle energies up to about 5 MeV the scattering in argon is classical. It is possible then to calculate the expected scattering in any gas for the classical case, knowing the actual scattering in argon. The ratio of the classical to the actual scattering is therefore determined for a few energies by the second set of observations. This together with the first set of experiments gives the variation of the scattering cross-section (in terms of the ratio to classical scattering) for the whole range of energies.

In the results given below the errors indicated are for *relative* values of the scattering cross-sections. The absolute values are liable to additional error up to about 10% on account of the uncertain purity of the argon used. In addition the values of the scattering at the lowest energies are liable to be too low owing to straggling and small angle scattering of the α-particles in the gas between the source and the scattering volume. This straggling etc. will give rise to different effects in the case of argon and the lighter nuclei owing to the difference in the velocities of the scattered α-particles (with the same primary energy) in the two cases.

III. EXPERIMENTAL RESULTS

Carbon. The gas used in this case was acetylene (C_2H_2) obtained from a solution of the gas in acetone. The latter was removed by passing the mixed gas and vapour through a multiple U-tube immersed in a slush of solid CO_2, at which temperature the relative amount of acetone in the gaseous mixture is negligible. In counting the scattered α-particles the "bias" of the counter was adjusted so as not to count recoil hydrogen nuclei. The results of the experiments are shown in fig. 2.

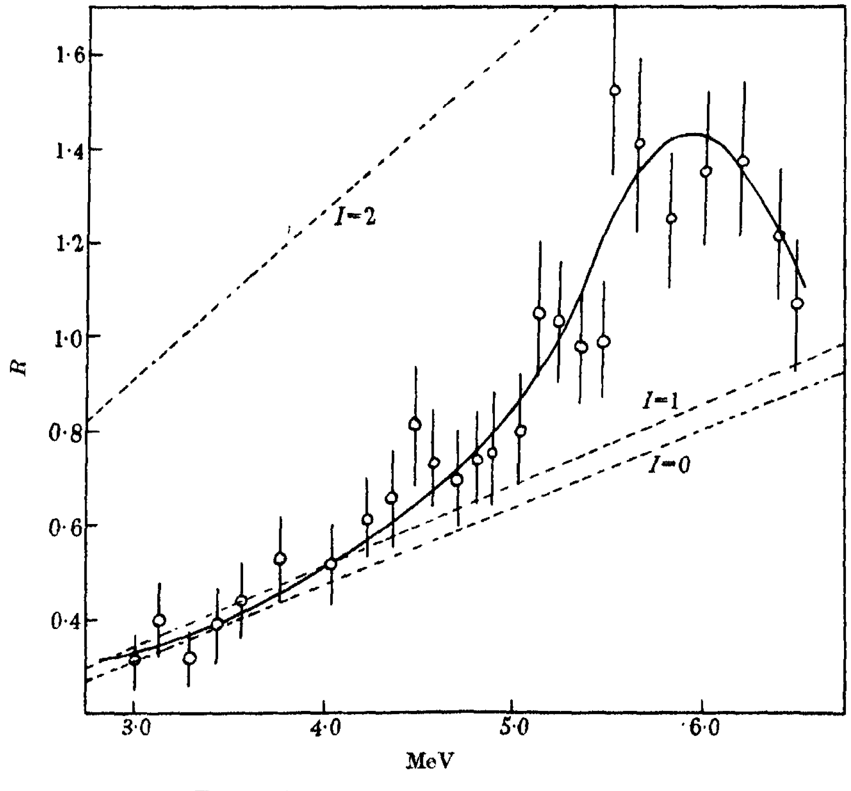

Fig. 2. Scattering of α-particles by carbon.

The scattering was observed for two ranges of energies, from 3·0 to 5·0 MeV and 4·5 to 6·5 MeV, a different gas pressure being used in the two ranges. The observations were made at energies about 0·2 MeV apart so that with the resolution used (about 0·1 MeV) even sharp resonances of sufficient intensity should have been observed. Between 60 and 200 particles were counted at each energy, the scattered intensity being rather small in this case.

The errors shown in fig. 2 are derived from the statistical fluctuations in the number of particles counted. The dotted lines represent the maximum anomalies in the scattering that are theoretically possible for compound nuclei (i.e. scattering nucleus plus the scattered α-particle) having total angular momentum (or spin) equal to 0, 1, 2, etc. quantum units. The significance of these maximum values is discussed below.

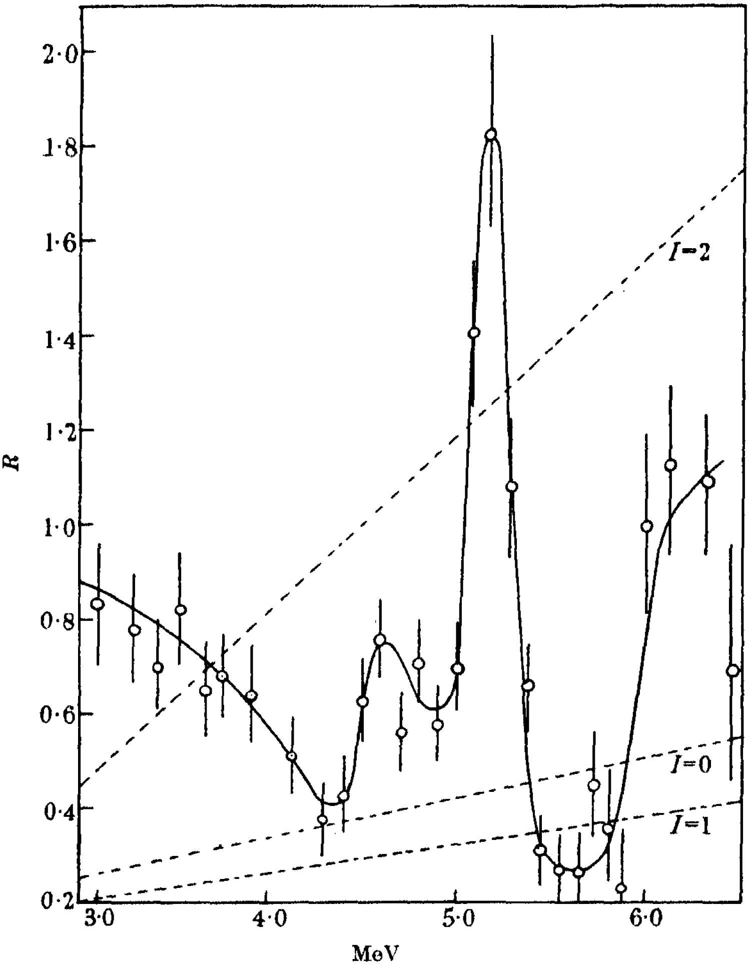

FIG. 3. Scattering of α-particles by nitrogen.

Nitrogen. The scattering has been observed for energies of 3·0–6·5 MeV. The results are shown in fig. 3. Nitrogen is disintegrated by fast α-particles according to the reaction

$$N^{14} + He^{4} = O^{17} + H^{1},$$

so that it was necessary in the experiment to arrange the "bias" on the counter so as not to count the disintegration protons.

In calculating the theoretical maxima for scattering, the simplifying assumption was made that the compound nuclei had total angular momentum equal to the orbital momentum of the α-particle on collision, or in other words the spin of the nitrogen nucleus was neglected. The true theoretical maximum will usually be smaller than the approximate value, but the exact difference depends on the manner in which the orbital momentum of the α-particle and the spin of the scattering nucleus combine.

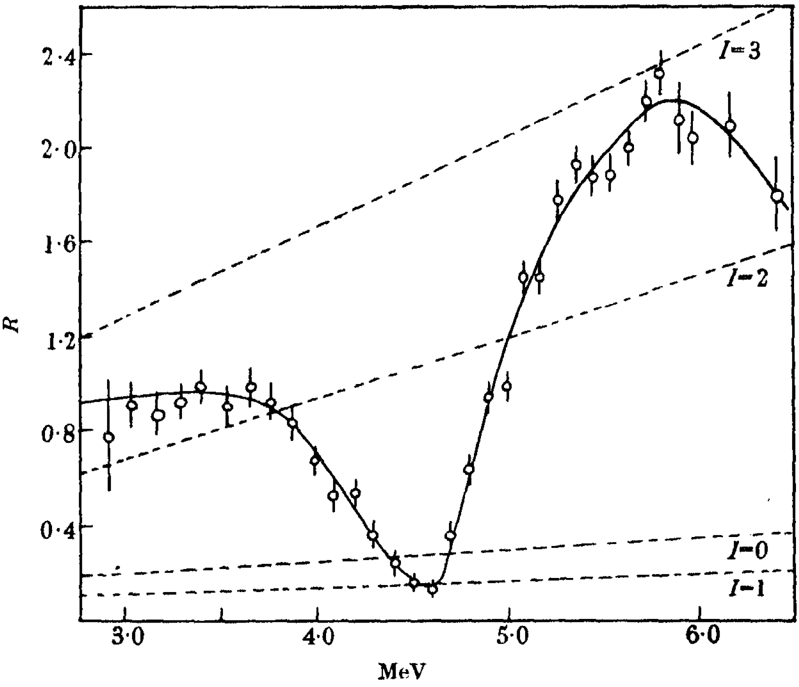

FIG. 4. Scattering of α-particles by oxygen.

Oxygen. The scattering in oxygen has been observed for energies of 2·8–6·2 MeV the results being shown in fig. 4. As in the case of carbon the scattering nucleus possesses zero spin so that the assumption that the spin of the compound nucleus is equal simply to the orbital momentum of the α-particle gives the correct values for the theoretical scattering maxima.

Fluorine. The scattering was observed for α-particle energies of 2·7–6·0 MeV. The gas used was carbon tetrafluoride.* The same considerations with regard to disintegration protons and angular momenta are applicable in this case as with nitrogen. An allowance has been made in this case for the scattering due to the carbon present. This has been made by using the results of the experiments on the scattering in acetylene. The actual contribution of the carbon nuclei to the observed scattering is only a few per cent. The results of the experiments with CF_4 are shown in fig. 5.

---

* I wish to express my thanks to Professor O. Ruff (Breslau) who kindly supplied the carbon tetrafluoride used in these experiments.

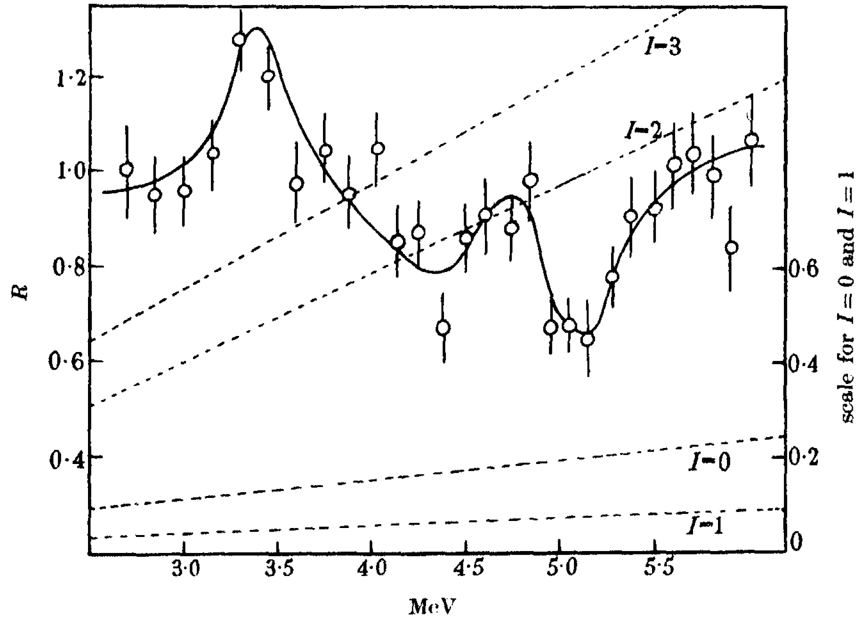

FIG. 5. Scattering of α-particles by fluorine.

Neon. A few experiments have been carried out using neon as scattering gas, the range of α-particle energies covered being 2·6–4·9 MeV. Disintegration protons are present in this case. The results are shown in fig. 6.

The scattering of α-particles in both neon and oxygen has been studied by Brubaker (1938) for several scattering angles. The result of these experiments is discussed below together with the results presented here. The scattering in argon has been used throughout in order to find the actual values of the scattering in other cases as a ratio to the Rutherford scattering. This scattering in argon is assumed to be classical. In order to verify this, in the range of α-particle energies for which the scattering in argon has been used as a comparison standard, the variation of the number of scattered particles (N) with energy (E) was observed. It is found that, in accordance with the assumption of classical scattering the quantity NE^2 is constant. The actual values obtained for this quantity in a typical experiment with argon (after the scattering had been measured in some other gas with the particular α-particle source) are shown in fig. 6. Such experiments with argon were usually made after a scattering experiment in a particular gas in order to check that the straggling was not exceptionally large for the source being used.

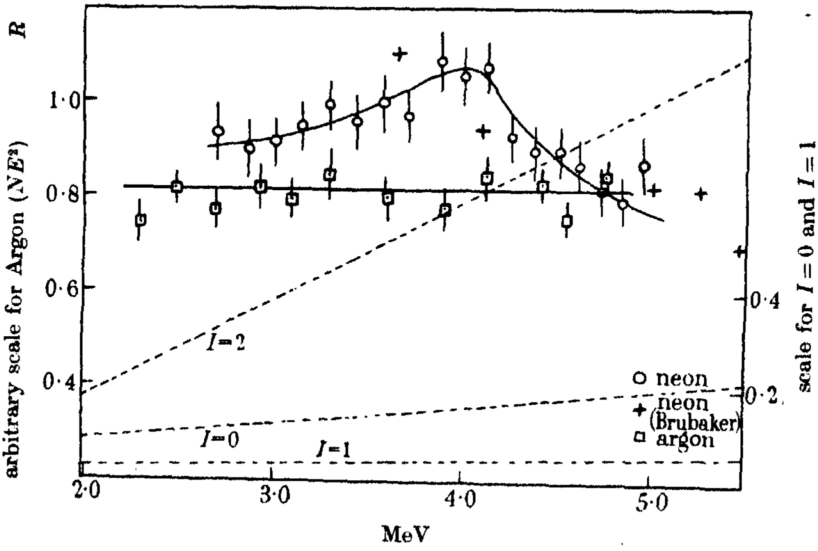

FIG. 6. Scattering of α-particles by neon and argon.

IV. THEORETICAL

It has been shown by Bethe (1937), by applying the dispersion theory of Breit and Wigner (1936) and Bethe and Placzek (1937) to the special case of elastic scattering that the anomalies in the scattering ratio due to a single resonance level can be expressed approximately in the form

$$R = 1+\frac{\rho^2}{(E-E_r)^2+\frac{1}{4}\gamma_{rI}^2}, \tag{1}$$

R is the ratio of the scattering due to the resonance level (which is denoted by the subscripts, r, I) to the classical-coulomb scattering; E is the energy of the scattered particles; γ_{rI} the total width of the excited level of the compound nucleus formed by the scattered particle + scattering nucleus; ρ is given by the equation

$$\rho = (2I+1)\,\lambda\,\frac{\gamma^{s}_{rI}}{2}\,\frac{Mv^2\sin^2\frac{\theta}{2}}{e^2zZ}\,P_I(\cos\theta), \tag{2}$$

in the case when both the scattering nucleus and the scattered particles have zero intrinsic spin. I is the total angular momentum (spin) of the compound nucleus and is equal, in this special case, to the orbital angular momentum of the scattered particle; λ is the de Broglie wave-length of the scattered particles; γ^{s}_{rI} is the partial width of the level r, I, with respect to the process of elastic scattering only, γ_{rI} referring to the width for all possible modes of disintegration of the compound nucleus. M, v, ze are the reduced mass, velocity and charge of the scattered particle, Ze the charge of the scattering nucleus and θ the reduced angle of scattering.

Equation (1) illustrates the theoretically expected resonance nature of the scattering process, R passing through maxima when the energy of the incident α-particle equals the resonance energy E_r.

The conditions that are theoretically necessary in order to observe resonances are at once apparent from equations (1), (2). In order that R should be large when E is equal to E_r the partial width for elastic scattering should be a large fraction of the total width of the level, v and θ should be large and Z small, i.e. resonance scattering is most likely to be observed for large angle scattering by light nuclei which have a small probability of disintegration by the particles employed. In cases where the incident particle can either be scattered elastically or produce a disintegration of the bombarded nucleus, the relative widths of the excited state of the compound nucleus for the two processes depend chiefly on the energy available for the processes and the relative potential barriers for the scattered and disintegration particles.

For α-particle energies equal to, or less than, the height of the potential barrier, only levels of the compound nucleus with small spin will be effective in producing resonances in scattering, since the potential barrier for charged particles with large angular momentum is much higher than for those with zero angular momentum, and the penetrability of the barrier consequently smaller. The term γ^{s}_{rI} is directly proportional to the penetrability of the barrier and the anomaly in the scattering contains the factor $(\gamma^{s}_{rI})^2$. Hence resonance effects produced by particles with large orbital momentum will only be observable for energies large compared with the potential barrier. In addition, quite independently of the barrier effect, only those particles with angular momentum quantum number, l, such that

$$l\lambda \leqslant r \qquad (3)$$

(λ is the de Broglie wave-length of the particles and r the radius of the nuclear forces) will be strongly affected by the short-range nuclear forces. Thus one would expect in general a rapid rise in the scattering cross-section with energy for high energies owing to the increase in the effect of the particles with large orbital momentum. Furthermore, the total, as well as the effective level density, increases with energy and this contributes to large scattering at high energies. It would seem then that resonance in scattering is most likely to be observed with particles of energy of the order of the height of the potential barrier of the scattering nucleus.

The approximate theoretical maximum for the anomaly in the scattering due to resonance obtained by putting $E = E_r$ and $\gamma^s_{rl} = \gamma_{rl}$ in equation (2), is

$$R_{\max} = \frac{4(2l+1)^2}{e^4 z^2 Z^2} \frac{P_l^2(\cos\theta)\, h^2 v^2}{\operatorname{cosec}^4\left(\frac{\theta}{2}\right)}. \tag{4}$$

This expression applies only to the case when both the scattering nucleus and scattered particle have zero intrinsic spin. In the case of α-particles and nuclei with non-zero spin the calculation of the theoretical scattering requires the additional knowledge of the spin of the compound nucleus in addition to the orbital angular momentum of the scattered particle. The above expression for $R_{\max}$ refers only to the resonance scattering of α-particles with a particular orbital momentum. The actual scattering observed will include in addition the ordinary coulomb scattering contribution from particles with all angular momenta. The values of $R_{\max}$ shown in figs. 2–6 refer to the resonance scattering only. The particular results obtained for α-particle scattering are discussed below.

Carbon. The compound nucleus formed in this case is O^{16}, so that resonance in scattering will be caused by excitation levels in this nucleus. The curve showing the relation between R and α-particle energy (fig. 2) shows a rather broad maximum for an energy of 5·8 MeV. The scattering of α-particles in carbon has been studied previously by Riezler (1932) using a scattering angle of 150°. Riezler found a maximum scattering cross-section corresponding to $R = 15$ at an energy of about 5·4 MeV. The anomaly (which is, within experimental error, at the same energy as the maximum found here) at both angles of scattering is consistent with an excitation level of O^{16} with energy 11·3 MeV* above the ground state, and with spin, I, of one quantum unit. This level seems to be broad, half-width of the order 0·5 MeV. In this case the width of the level must be due entirely to re-emission of the α-particle, i.e. scattering, since the only other process energetically possible is γ-ray emission. For orbital momentum of the α-particle of one, the barrier height of the carbon nucleus is considerably less than 5·8 MeV, so that it is not difficult to understand the resonance being broad. There is some indication of other resonances at lower energies but more data would be required to confirm their existence. A peculiarity of the scattering in the present case is that the value of R does not seem to approach one, even at energies of about 3 MeV. Further experimental data, particularly at lower α-particle energies, is required to confirm and investigate this effect.

---

* This is obtained by using the accepted values for the masses of O^{16}, He^4 and C^{12}.

Nitrogen. The scattering ratio shows a marked and rather narrow resonance at an energy of 5·2 MeV and another less definite one at 4·6 MeV. For sufficiently energetic α-particles, the compound nucleus formed in this case, F^{18}, can disintegrate into O^{17} and a proton or F^{17} and a neutron. Since both these processes are endo-thermic, the energy of the proton or neutron is not so large as to make the partial width, with respect to α-particle emission, of levels of F^{18} small compared with the total level width. It seems reasonable then, to attribute the resonance at 5·2 MeV to particles with orbital momentum of two, although in this case momentum will not be equal necessarily to the spin of the compound nucleus owing to the intrinsic spin of the N^{14} nucleus. The width of the level seems consistent with this α-particle energy and momentum.

Resonances for the emission of protons when nitrogen is disintegrated by α-particles have been observed by several investigators. There seems no indication that these resonances occur at the same energy as the resonances for scattering, a result which is quite consistent with the theoretical view that the resonances for the two processes are competitive. Resonances in the neutron reaction have been observed (Funfer 1938) but at energies greater than those for which scattering has been investigated.

Oxygen. The scattering ratio at 90° in oxygen seems to be very small indeed for an α-particle energy of about 4·6 MeV. A zero cross-section for elastic scattering at a particular angle is theoretically possible only if scattering is the only process energetically allowed, a condition which is very nearly obeyed in the present case.

The scattering maximum at 5·8 MeV corresponds to a level in Ne^{20} with an excitation energy of 9·4 MeV and the size of the anomaly indicates a spin value for the level of at least two (O^{16} itself has a zero spin). Brubaker has investigated the scattering in oxygen at several angles. There is a marked point of inflexion in Brubaker's curve at an energy of 5·8 MeV for the scattering at 88°, a result in good agreement with the maximum found here. Brubaker also finds a minimum in the cross-section for 88° scattering at 4·6 MeV, as found here. However the region between 4·0 and 5·0 MeV has not been investigated fully by Brubaker and consequently the *very small* cross-section at 4·6 MeV was not found.

Excitation levels of Ne^{20} in this energy region have been investigated by Bonner* (1939) by studying the energies of the neutrons in the reaction

$$F^{19} + H^2 = Ne^{20} + n^1.$$

Bonner finds several neutron groups including three of energies 1·4, 2·6, and 11·1 MeV respectively corresponding to Ne^{20} left with excitation energy of $10{\cdot}1 \pm 0{\cdot}3$ and $9{\cdot}0 \pm 0{\cdot}3$ MeV in two cases and in the ground state in the third case. It seems then that the state of Ne^{20} observed in scattering resonance is also excited in the above reaction.

Fluorine. There seems evidence of resonances at energies of 3·5 and 4·7 MeV. No definite angular momenta can be assigned to these resonances owing to the fact that the ratio of the scattering to the disintegration widths for the levels is unknown. In addition the spin of F^{19} is not zero.

Resonances for proton emission in the reaction

$$F^{19} + He^4 = Ne^{22} + H^1$$

have been found by Chadwick and Constable (1931) for α-particle energies of 4·1 and 3·7 MeV. It is possible that within experimental error the resonance for disintegration at 3·7 MeV and for scattering at 3·5 MeV correspond to the same excited level of Na^{23}. If this were so the partial width of this level for scattering would be considerably smaller than the total width.

No resonances have been established for the reaction

$$F^{19} + He^4 = Na^{22} + n^1.$$

Neon. In the range of energies studied, there seems to be no definite resonance in the scattering by neon at 90°. Brubaker, however, finds a resonance for an α-particle energy of 6·3 MeV with an experimental half-width of about 0·3 MeV, corresponding to a level of Mg^{24}. The resonance seems to be present at the smaller angles of scattering used (53° and 65° 30′) but not at the scattering angles of 88° and 104°. It seems necessary to account for this resonance by α-particles of orbital momentum three at least. This large momentum is not improbable for such a large energy α-particle, especially as the resonance appears rather narrow.

In all the cases considered scattering resonances have been found to occur, but the number of such resonances seems rather small. This result can very probably be attributed to the following causes. First, resonances for energies smaller than the barrier heights would be narrow and the anomalies small compared with coulomb scattering. The accuracy and resolution of experiments using natural α-particle sources makes it impossible to look for these low energy resonances. Secondly, the energy range between the barrier height and the available maximum α-particle energy (the same order as the probable level spacing) is so small as to make the observation of many resonances improbable. In most cases, in fact, one resonance is found in this region. Removal of the limitations of intensity, resolution, or energy would probably make it possible to find many more levels.

---

* I am indebted to T. W. Bonner for informing me of his results.

I am indebted to Trinity College for a research studentship which has made it possible for this work to be done, and to Dr N. Feather for some helpful discussion.

SUMMARY

The scattering of α-particles at 90° has been investigated for the elements carbon, nitrogen, oxygen, fluorine, neon and argon. The scattering substance was in the form of a gas and the scattered particles were detected by means of an annular chamber and linear amplifier.

Resonances in the scattering have been found for α-particle energies as follows:

Carbon: 5·7 MeV,
Nitrogen: 4·6, 5·2 MeV,
Oxygen: 5·8 MeV,
Fluorine: 3·5, 4·7 MeV,
Neon: —.

The results are discussed with relation to the interpretation of scattering on the "many-body" theory of the nucleus and also in connexion with other experimental data on scattering and disintegration. The results are not of a very high accuracy, owing to low intensity and resolution of the α-particle sources used.

REFERENCES

Bethe 1937 *Rev. Mod. Phys.* **9**, 174 (§ 71).
Bethe and Placzek 1937 *Phys. Rev.* **51**, 450.
Bonner 1939 Unpublished.
Breit and Wigner 1936 *Phys. Rev.* **49**, 519.

Brubaker 1938 *Phys. Rev.* **54**, 1011.
Chadwick and Bieler 1921 *Phil. Mag.* **42**, 923.
Chadwick and Constable 1932 *Proc. Roy. Soc.* A, **135**, 48.
Funfer 1938 *Ann. Phys., Lpz.*, **32**, 313.
Riezler 1931 *Proc. Roy. Soc.* A, **134**, 154.
— 1935 *Ann. Phys., Lpz.*, **23**, 198.
Rutherford and Chadwick 1927 *Phil. Mag.* **4**, 605.
Wentzel 1934 *Z. Phys.* **90**, 754.

Thermal diffusion in mixtures of the inert gases

By B. E. Atkins,* R. E. Bastick and T. L. Ibbs
Physics Department, University of Birmingham

(*Communicated by M. L. E. Oliphant, F.R.S.—Received* 8 *May* 1939)

Since the independent prediction of the thermal diffusion effect by Chapman (1916) and by Enskog (1911) and its experimental verification by Chapman and Dootson (1917), the general nature of the phenomenon has been extensively studied by a number of workers, and its power in giving information on intermolecular fields has been demonstrated. The present work deals with all the binary mixtures of helium, neon, argon, krypton and xenon. These mixtures of inert gases are of special interest owing to the simplicity of the monatomic molecules. A few pairs of these gases had previously been examined by us (Ibbs and Grew 1931) as part of the general investigation of the effect, but it seemed desirable to work through the whole group systematically so that the behaviour could be studied under practically identical conditions.

EXPERIMENTAL METHOD

The method employed followed the general principles which we have previously used in some of our experiments, but certain modifications were introduced because of the small quantities of krypton and xenon which were available and of the low thermal conductivity of these gases. The apparatus consisted of two vessels joined by a short connecting tube. The "hot side" was a cylindrical glass bulb *A* (fig. 1) of volume about 4 c.c., surrounded by a steam jacket *J*. Below this was placed a Shakespear katharometer used for the gas analysis, one cell C_1 of volume about 1 c.c. forming the "cold side". The connecting tube between the hot and cold sides was made as short as possible so as to produce a steep temperature gradient. A water jacket *W*, served to protect the katharometer block from the effects of the steam jacket. There was a wax joint between the short glass tube and the water jacket, and a lead washer *L*, formed the joint between the water jacket and the katharometer block. The lead washer was compressed by means of the screws *S*.

---

* It is sad to report that Dr B. E. Atkins was killed in an accident in Switzerland in February 1939.

The thermal separation was investigated in all these experiments with the "cold side" at about room temperature, and the "hot side" at the temperature of the steam.

Mixtures of two gases of known proportions by volume were made in a gas burette, and after being allowed to stand for about an hour to become uniform, were admitted through the tap *T* into the diffusion apparatus before the steam was applied. In this way a "katharometer reading" was obtained and a series of such readings for mixtures of different proportions gave the calibration curve for a pair of gases. In practice it was convenient to measure the thermal separation for each mixture immediately after its calibration point had been obtained. About twelve different mixtures of each pair were examined. All the measurements were made at a pressure of 20 cm. of mercury instead of at atmospheric pressure as in previous experiments. This provided a satisfactory means of reducing the quantity of gas required in the experiments, and it introduced no fundamental change in the method. Previous experiments (Ibbs, Grew and Hirst 1929) have shown that the thermal separation is independent of the pressure over a considerable range of pressure, as would be expected from the theory. When steam was admitted to the jacket the rise in temperature tended to increase the pressure of the gas in the bulb, but by leaving the tap *T* open for a short time, a quantity of gas was allowed to return to the burette in order to keep the pressure at 20 cm. This avoids any error in the katharometer readings due to change in pressure. Leaving the tap open

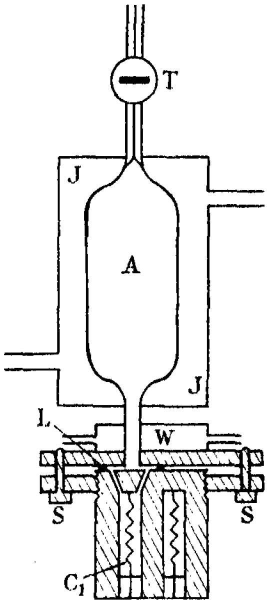

FIG. 1. Apparatus.

in this way for a short time caused no error in the thermal separation as the bore of the tap T, and of its connecting tube, were narrow.

The katharometer measured the change in concentration of the gas on the cold side. For many of the pairs of gases examined this change could be regarded as complete in about 3 min., for some of the heavier pairs, such as argon-xenon, and argon-krypton, the time required was about 9 min. Thus a longer time is required for the heavier and more slowly moving molecules. For krypton-xenon 15 min. had to be allowed.

The thermal separation, i.e. the total change in concentration on the hot and cold sides, had to be obtained from the observed change in concentration on the cold side. In previous experiments the volume of the side where the effect was observed had been small compared with the volume of the other vessel, with the result that most of the thermal separation occurred on the small side. The small change in concentration on the other side could then be calculated from the relative volumes and temperatures of the two sides. Any uncertainty in these volumes would have only a small effect on the final result. In the present case it is difficult to assign definite volumes to the hot and cold sides, and the volume of the connecting tube becomes important. As the change in concentration on the hot side will now be relatively large, a new method was necessary to obtain it.

The method adopted was to make thermal diffusion experiments with pairs of common gases, hydrogen-nitrogen, hydrogen-carbon dioxide, and hydrogen-argon, using exactly the same apparatus and conditions as for the inert gases. The small bulb of the hot side, of volume about 4 c.c., was then replaced by a large bulb of volume 85 c.c., and the experiments repeated under the same conditions of temperature, with steam on the hot side, and the cold side at room temperature. With this arrangement the change in concentration on the small cold side is measured, the change on the large hot side is calculated, and an accurate value of the total separation obtained. This total separation can then be compared with the measured cold side separation using the small hot bulb, and the factor obtained by which the cold side separation must be multiplied to convert it to total separation. For the first part of the work when xenon-helium, xenon-neon, and xenon-argon were investigated, this factor was 1·15, for later work when a new hot bulb was used the factor was 1·47. For krypton-xenon mixtures a special katharometer was used which will be described later.

For this work greater accuracy than had previously been necessary was required in measuring changes in concentration, and special care had to be taken in keeping the bridge current constant. In previous work it had been sufficient to use a milliammeter for this purpose. The change in concentration of a gas mixture produced by thermal diffusion alters its thermal conductivity which in turn affects the temperature and resistance of the platinum helix in the katharometer cell. The small change in the bridge current which is thus produced cannot generally be detected by a milliammeter. The method adopted was to use the milliammeter for a rough adjustment of the current, and to make the final adjustment by balancing the potential difference due to the current flowing through a fixed resistance, with that of a standard Weston cadmium cell. The usual bridge current of 0·1 amp. was generally used, but for mixtures of low thermal conductivity, e.g. krypton-argon, it was more satisfactory to work with a smaller current of 0·082 amp. For such mixtures the helix in the gas mixture was much hotter than the helix in air. This caused difficulty in keeping the galvanometer readings steady during thermal diffusion measurements, as any small change in room temperature would upset the balance of the bridge. The effects of this unbalanced condition can be reduced by decreasing the current in the bridge.

Special arrangement for krypton-xenon mixtures

This difficulty is greatest for krypton-xenon mixtures, in which the thermal conductivity is very low for all proportions of the gases. As the thermal separation for these mixtures is also very small, special arrangements are required for its measurement. It was decided to use an unsymmetrical katharometer, i.e. one in which one helix is longer than the other. By choosing helices of suitable length, and putting the shorter one in the sealed cell in air, and the longer one in the gas of low conductivity, it can be arranged for the two wires to be at the same temperature.

The conditions for compensating for the difference in thermal conductivity of the gases in the two cells in order to obtain a more stable arrangement, have been investigated by Daynes (1933). Considering the case of two lengths of thin platinum wire in similar cells, he concludes that the temperature of the two wires will be the same, and hence the katharometer is least sensitive to change in temperature of the block, when

$$\frac{L_1}{\;} = \sqrt{\frac{K_2}{K_1}},$$

where L_1 and L_2 are the lengths of the two platinum wires, and K_1, K_2 are the thermal conductivities of the gases in the two cells. Thus if the thermal conductivities are known, the conditions for stability can be found.

It was decided to arrange for the bridge to be balanced with krypton in the open cell, and air in the sealed cell. Although no measurements of the thermal conductivity of krypton were available an approximate value was obtained by measuring the current and potential drop in each helix of a symmetrical katharometer with air in one cell and krypton in another. In this way the resistance, temperature, and heat losses in each helix can be obtained. This enabled relative values of the thermal conductivities of air and krypton to be calculated. It was concluded that to give equality of temperature the length of the wire in krypton must be 1·90 times the length of the wire in air. A katharometer with the lengths in this ratio was found to work very satisfactorily for krypton-xenon, argon-xenon, and argon-krypton mixtures. This was more sensitive, and the galvanometer readings were steadier than with the symmetrical arrangement. It is interesting to note that from these calculations the thermal conductivity of krypton is roughly one-quarter that of air.

An alternative arrangement for obtaining stability would be to use a symmetrical katharometer with krypton in the sealed cell. This method of using gases other than air in the sealed cell has been successfully used by us in other work.

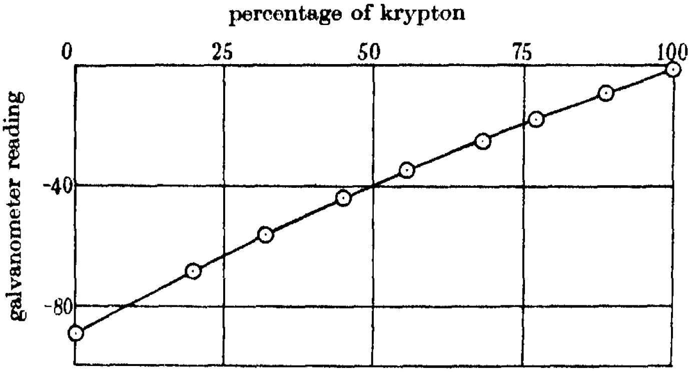

Fig. 2. Calibration curve for krypton-xenon mixtures.

The calibration curve for krypton-xenon mixtures using the asymmetrical katharometer is shown in fig. 2. As all the mixtures have a thermal conductivity less than for krypton, all the galvanometer deflexions are shown as negative. By using this curve the thermal separation on the cold side for krypton-xenon mixtures could be obtained, but it was necessary to know the factor by which this separation must be multiplied to obtain the total separation for the new arrangement. In this case it was not possible to follow the method, already described, of finding this factor by obtaining the cold side separation for mixtures of common gases, e.g. hydrogen-nitrogen, hydrogen-carbon dioxide, hydrogen-argon, for which the total separation was already known. As mixtures of these pairs of gases have all a relatively high thermal conductivity, it is impossible in this case to obtain a balance point on the bridge. The calculation of the total separation for krypton-xenon mixtures was made by using the thermal diffusion results previously obtained for xenon-argon mixtures with the symmetrical katharometer, and comparing them with the results using the asymmetrical katharometer for this pair. Because of the low thermal conductivity, the cold side separation in xenon-argon mixtures could be measured with the asymmetrical katharometer, and from the known total separation the factor by which the cold side separation must be multiplied to give the total separation was obtained. The factor was in this case 1·66, which is greater than for the symmetrical katharometer as the cell had a larger volume. By multiplying the measured cold side separation for krypton-xenon mixtures by this factor the total separation was obtained.

The Shakespear katharometer provides a powerful and convenient method of analysing mixtures of the inert gases, in experiments such as these, where numerous observations are required.

Purification of the gases

In the course of the experiments it was necessary to purify all the inert gases. After measurements had been made on a pair of gases they had to be separated so that they could again be used. This involved a good deal of work in repeated fractionations. The usual technique using bulbs containing charcoal immersed in liquid air, or cooled pentane, was employed.

The best test of the purity of the gases for our purpose was to examine a single gas, without admixture, for thermal diffusion. If the impurities in a gas produce no appreciable thermal separation it can be regarded as sufficiently pure. The nature of the impurity is important. For example, a small amount of helium as an impurity in neon will have less effect than it will have in argon, krypton, or xenon.

EXPERIMENTAL RESULTS

All the pairs of gases were examined under practically the same experimental conditions, the thermal separation being measured between room temperature (T_2 absolute) and the boiling point of water (T_1 absolute). In order to allow for small variations in these temperatures the separations are obtained for comparative purposes for $\log_{10}(T_1/T_2) = 0{\cdot}112$ corresponding to temperatures of 100 and 15° C. With the small differences in temperature involved, the separation can safely be regarded for this purpose as proportional to $\log_{10}(T_1/T_2)$. A graph of the relation between the separation and the proportions of the two gases was obtained for each pair of gases. Typical curves are shown in fig. 3 for mixtures of helium-krypton, neon-krypton and argon-krypton. It will be seen that in each case the points can be well represented by a smooth curve.

For each pair of gases considered, a table is given showing the separation taken from a number of points on the smooth separation-concentration curve. In general the method of measurement tends to give the greatest accuracy for the mixtures containing the smaller proportions of the lighter gas, so that the results for such mixtures have often been selected as being more reliable than the others.

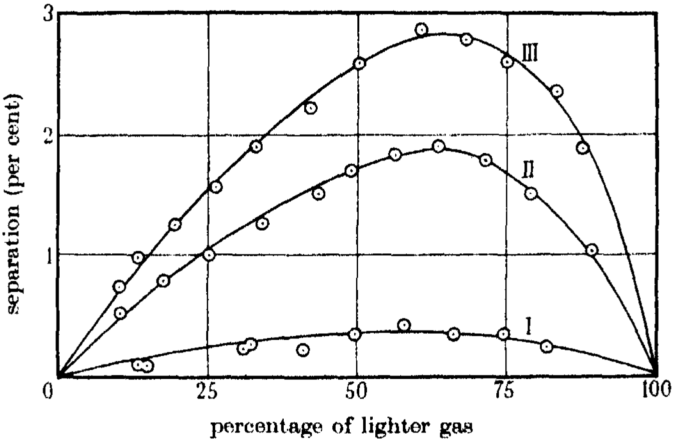

FIG. 3. Relation between separation and concentration. I, argon-krypton; II, neon-krypton; III, helium-krypton.

The experimental value of the coefficient of thermal *separation* k_t is obtained from the relation

$$\Delta\lambda_1 = -\Delta\lambda_2 = -k_t \log\frac{T_1}{T_2},$$

where $\Delta\lambda_1$ is the change in concentration produced by a temperature gradient between T_1 and T_2 in a mixture containing the proportion by volume λ_1 of the heavier gas; $\Delta\lambda_2$ is the corresponding change in the proportion λ_2 of the lighter gas ($\lambda_1+\lambda_2=1$). From the ratio of the molecular masses m_1/m_2 and of the molecular diameter σ_1/σ_2 of the two gases, an expression can be obtained giving the theoretical values of k_t for molecules behaving as rigid elastic spheres. Although the values of k_t depend upon the proportions of the two gases in the mixture, the ratio

$$R_T = \frac{k_t\,\text{experimental}}{k_t\ \text{rigid elastic spheres}},$$

can, to a considerable degree of accuracy, be regarded as a constant for the pair of gases. This important ratio gives information on the molecular fields of the two unlike molecules. A separate investigation of the possible variation of R_T with concentration is being made.

(i) *Helium-neon.* Ten mixtures were examined. The katharometer calibration curve was almost a straight line which shows that there is little variation in the sensitivity of the instrument. The graph of the relation between separation and concentration has its maximum separation of 2·6 % at about 60 % of helium. Table I gives the separation and the corresponding values of k_t and R_T for five points on this graph.

TABLE I. VALUES OF k_t AND R_T FOR HELIUM-NEON MIXTURES

% He	% Sep.	k_t(exp.)	k_t(r.e.s.)	R_T
20	1·37	0·0531	0·0655	0·81
30	1·87	0·0724	0·0919	0·79
40	2·23	0·0864	0·1099	0·79
50	2·50	0·0970	0·1220	0·79
60	2·59	0·1004	0·1257	0·81

Mean value of $R_T = 0{\cdot}80$.

The values of R_T are high, and in general agreement with our previous results, and with those more recently obtained by Blüh, Blüh, and Puschner (1937). This is the "hardest" of the pairs of molecules examined.

By inserting the values $m_1/m_2 = 5{\cdot}06$ and $\sigma_1/\sigma_2 = 1{\cdot}21$ in the general formulae, the following expression is obtained for k_t rigid elastic spheres:

$$k_t = \frac{5}{2}\left(\frac{0{\cdot}255\lambda_1 + 0{\cdot}313\lambda_2}{3{\cdot}062 + 1{\cdot}713\lambda_1/\lambda_2 + 1{\cdot}046\lambda_2/\lambda_1}\right).$$

(ii) *Helium-argon.* Eleven mixtures of different proportions were examined. The separation-concentration curve has a maximum separation of 2·6 % at about 65 % helium. Table II gives the separation and the corresponding values of k_t and R_T for five points on this curve.

TABLE II. VALUES OF k_t AND R_T FOR HELIUM-ARGON MIXTURES

% He	% Sep.	k_t(exp.)	k_t(r.e.s.)	R_T
10	0·65	0·0250	0·0369	0·68
20	1·23	0·0476	0·0711	0·67
30	1·70	0·0660	0·1018	0·65
40	2·09	0·0810	0·1280	0·63
50	2·40	0·0931	0·1484	0·63

Mean value of $R_T = 0{\cdot}65$.

The value of R_T is lower than for helium-neon mixtures, as argon is a "softer" molecule than neon.

Using the values $m_1/m_2 = 10{\cdot}00$ and $\sigma_1/\sigma_2 = 1{\cdot}68$,

$$k_t \text{ rigid elastic spheres} = \frac{5}{2}\left(\frac{0{\cdot}286\lambda_1 + 0{\cdot}244\lambda_2}{2{\cdot}140 + 1{\cdot}879\lambda_1/\lambda_2 + 0{\cdot}448\lambda_2/\lambda_1}\right).$$

(iii) *Helium-krypton.* Eleven mixtures of different proportions were examined. The separations are large, because of the large value of m_1/m_2, and reach a maximum separation of about 2·8 % in mixtures containing about 63 % of helium. Table III gives the separation and the corresponding values of k_t and R_T for five points on the separation-concentration curve (fig. 3, III).

TABLE III. VALUES OF k_t AND R_T FOR HELIUM-KRYPTON MIXTURES

% He	% Sep.	k_t(exp.)	k_t(r.e.s.)	R_T
30	1·75	0·0677	0·105	0·64
40	2·20	0·0852	0·133	0·64
50	2·58	0·1000	0·156	0·64
60	2·79	0·1080	0·172	0·63
70	2·76	0·1068	0·176	0·61

Mean value $R_T = 0{\cdot}63$.

The value of R_T is a little less than for helium-argon mixtures as krypton is a "softer" molecule than argon.

Using the values $m_1/m_2 = 20{\cdot}99$ and $\sigma_1/\sigma_2 = 1{\cdot}90$,

$$k_t \text{ rigid elastic spheres} = \frac{5}{2}\left(\frac{0{\cdot}239\lambda_1 + 0{\cdot}145\lambda_2}{1{\cdot}297 + 1{\cdot}557\lambda_1/\lambda_2 + 0{\cdot}210\lambda_2/\lambda_1}\right).$$

(iv) *Helium-xenon.* Fourteen mixtures of different proportions were examined. The thermal separation is the largest attained in the experiments, and this may be expected from the very large value of m_1/m_2. A maximum separation of 3·15 % is obtained in mixtures containing about 70 % of helium. Table IV gives the separation and the corresponding values of k and R_T for five points on the separation-concentration curve.

TABLE IV. VALUES OF k_t AND R_T FOR HELIUM-XENON MIXTURES

% He	% Sep.	k_t(exp.)	k_t(r.e.s.)	R_T
10	0·53	0·0211	0·0376	0·56
20	1·06	0·0422	0·0733	0·57
30	1·55	0·0618	0·1071	0·58
40	2·03	0·0810	0·1375	0·59
50	2·53	0·1007	0·1613	0·62

Mean value of $R_T = 0{\cdot}59$.

In spite of the large thermal separation, the value of R_T is lower than for helium-krypton mixtures. Thus in the four pairs of gases already considered there has been a progressive decrease in the values of R_T as the gas molecules mixed with helium became "softer".

The calibration curve shows that the katharometer is very sensitive to small quantities of helium in xenon, and that the sensitivity of the instrument decreases rapidly as the proportion of helium increases.

Using the values $m_1/m_2 = 32{\cdot}90$ and $\sigma_1/\sigma_2 = 2{\cdot}24$,

$$k_t \text{ rigid elastic spheres} = \frac{5}{2}\left(\frac{0{\cdot}220\lambda_1 + 0{\cdot}099\lambda_2}{0{\cdot}899 + 1{\cdot}433\lambda_1/\lambda_2 + 0{\cdot}113\lambda_2/\lambda_1}\right).$$

(v) *Neon-argon.* Ten mixtures of different proportions were examined. The thermal separation is less than for the mixtures containing helium, the smaller mass ratios m_1/m_2 being a contributing factor. The separation-concentration curve is almost symmetrical, and shows a maximum separation of 1·2 % in mixtures containing about 58 % of neon. Table V gives the separation and the corresponding values of k_t and R_T for five points on the separation-concentration curve.

TABLE V. VALUES OF k_t AND R_T FOR NEON-ARGON MIXTURES

% Ne	% Sep.	k_t(exp.)	k_t(r.e.s.)	R_T
20	0·60	0·0233	0·0448	0·52
30	0·85	0·0339	0·0621	0·53
40	1·05	0·0407	0·0750	0·54
50	1·18	0·0457	0·0831	0·55
60	1·21	0·0467	0·0850	0·55

Mean value of $R_T = 0{\cdot}54$.

This value of R_T is in satisfactory agreement with the value 0·53 previously obtained by Ibbs and Grew for this pair.

Using the values $m_1/m_2 = 1{\cdot}98$ and $\sigma_1/\sigma_2 = 1{\cdot}39$,

$$k_t \text{ rigid elastic spheres} = \frac{5}{2}\left(\frac{0{\cdot}241\lambda_1 + 0{\cdot}237\lambda_2}{3{\cdot}616 + 2{\cdot}368\lambda_1/\lambda_2 + 1{\cdot}214\lambda_2/\lambda_1}\right).$$

(vi) *Neon-krypton.* Eleven mixtures were examined. The thermal separation is greater than for neon-argon mixtures, and the separation-concentration curve shows a maximum separation of 1·8 % in mixtures containing about 63 % of neon. Table VI gives the separation and the corresponding values of k_t and R_T for five points on the separation-concentration curve (fig. 3, II).

TABLE VI. VALUES OF k_t AND R_T FOR NEON-KRYPTON MIXTURES

% Ne	% Sep.	k_t(exp.)	k_t(r.e.s.)	R_T
20	0·84	0·0325	0·0649	0·50
30	1·15	0·0445	0·0916	0·49
40	1·44	0·0558	0·1132	0·49
50	1·72	0·0667	0·1285	0·52
60	1·90	0·0735	0·1359	0·54

Mean value of $R_T = 0·51$.

The value of R_T is less than for neon-argon mixtures, as the "softer" molecule krypton has been substituted for argon.

Using the values $m_1/m_2 = 4·15$ and $\sigma_1/\sigma_2 = 1·57$,

$$k_t \text{ rigid elastic spheres} = \frac{5}{2}\left(\frac{0·322\lambda_1 + 0·325\lambda_2}{3·194 + 2·260\lambda_1/\lambda_2 + 0·839\lambda_2/\lambda_1}\right)$$

(vii) *Neon-xenon.* Thirteen mixtures were examined. Although the mass ratio m_1/m_2 is greater than for neon-krypton mixtures, the thermal separation is less, owing to the effect of substituting the "softer" molecule xenon for krypton. The separation-concentration curve is very unsymmetrical as would be expected from the large mass ratio. It is difficult to estimate the position of the maximum of the curve, but the greatest separation is probably about 1·7 % in mixtures containing approximately 70 % of neon. Table VII gives the separation and the corresponding values of k_t and R_T for five points on the curve.

TABLE VII. VALUES OF k_t AND R_T FOR NEON-XENON MIXTURES

% Ne	% Sep.	k_t(exp.)	k_t(r.e.s.)	R_T
20	0·67	0·0284	0·0697	0·41
30	0·99	0·0419	0·0999	0·42
40	1·26	0·0536	0·1258	0·43
50	1·49	0·0633	0·1459	0·43
60	1·69	0·0716	0·1582	0·45

Mean value of $R_T = 0·43$.

The values of R_T are considerably less than for neon-krypton mixtures. Using the values $m_1/m_2 = 6·51$ and $\sigma_1/\sigma_2 = 1·85$,

$$k_t \text{ rigid elastic spheres} = \frac{5}{2}\left(\frac{0·343\lambda_1 + 0·296\lambda_2}{2·652 + 2·290\lambda_1/\lambda_2 + 0·532\lambda_2/\lambda_1}\right).$$

(viii) *Argon-krypton.* Ten mixtures were examined. The separations are small owing to the small mass ratio, and also to the "softness" of the intermolecular fields. The separation-concentration curve is nearly symmetrical as would be expected from the small mass ratio, and the maximum separation of 0·4 % occurs in mixtures containing about 58 % of argon. Table VIII gives the separation and the corresponding values of k_t and R_T for five points on the curve (fig. 3, I).

TABLE VIII. VALUES OF k_t AND R_T FOR ARGON-KRYPTON MIXTURES

% A	% Sep.	k_t(exp.)	k_t(r.e.s.)	R_T
40	0·294	0·0114	0·0725	0·16
50	0·353	0·0137	0·0782	0·18
60	0·397	0·0154	0·0718	0·21
70	0·368	0·0143	0·0711	0·20
80	0·297	0·0116	0·0566	0·20

Mean value of $R_T = 0·19$.

The effect of the small separation is seen in the low value of R_T.

Using the values $m_1/m_2 = 2·10$ and $\sigma_1/\sigma_2 = 1·13$,

$$k_t \text{ rigid elastic spheres} = \frac{5}{2}\left(\frac{0·206\lambda_1 + 0·240\lambda_2}{3·653 + 1·931\lambda_1/\lambda_2 + 1·539\lambda_2/\lambda_1}\right).$$

(ix) *Argon-xenon.* Thirteen mixtures were examined. The separations are small, but owing to the larger mass ratio, they are greater than for argon-krypton mixtures. The maximum separation of 0·475 % occurs in mixtures containing about 58 % of argon. Table IX gives the separation and the corresponding values of k_t and R_T for five points on the separation-concentration curve.

TABLE IX. VALUES OF k_t AND R_T FOR ARGON-XENON MIXTURES

% A	% Sep.	k_t(exp.)	k_t(r.e.s.)	R_T
30	0·328	0·0134	0·0833	0·16
40	0·414	0·0170	0·1011	0·17
50	0·460	0·0189	0·1124	0·17
60	0·483	0·0198	0·1158	0·17
70	0·436	0·0179	0·1096	0·16

Mean value of $R_T = 0·17$.

Although the separations are greater than for argon-krypton mixtures, the value of R_T is lower, as would be expected by the substitution of xenon for krypton.

Using the values $m_1/m_2 = 3·29$ and $\sigma_1/\sigma_2 = 1·33$,

$$k_t \text{ rigid elastic spheres} = \frac{5}{2}\left(\frac{0·282\lambda_1 + 0·317\lambda_2}{3·425 + 2·075\lambda_1/\lambda_2 + 1·124\lambda_2/\lambda_1}\right).$$

(x) *Krypton-xenon.* Owing to the low thermal conductivity of each of these gases the special arrangements, already described, were required in the measurements. The thermal separation is extremely small. This is due to the small mass ratio and more particularly to the "softness" of the two molecules. With such a small separation the degree of accuracy of the measurements was reduced. In this case it was better to make a number of measurements on one mixture of the pair, rather than to work on mixtures of different proportions. Ten measurements were therefore made on a mixture containing 45 % of krypton, and the mean separation taken. The results are given in Table X.

TABLE X. VALUES OF k_t AND R_T FOR A MIXTURE OF KRYPTON AND XENON

% Kr	% Sep.	k_t(exp.)	k_t(r.e.s.)	R_T
45	0·098	0·0041	0·0532	0·08

This is the smallest value of R_T we have obtained. The separation is less than one tenth of what would occur for rigid elastic spheres. The behaviour of the molecules is therefore approaching that of Maxwellian molecules for which thermal separation would disappear.

Using the values $m_1/m_2 = 1{\cdot}57$ and $\sigma_1/\sigma_2 = 1{\cdot}18$,

$$k_t \text{ rigid elastic spheres} = \frac{5}{2}\left(\frac{0{\cdot}156\lambda_1 + 0{\cdot}162\lambda_2}{3{\cdot}673 + 2{\cdot}081\lambda_1/\lambda_2 + 1{\cdot}537\lambda_2/\lambda_1}\right).$$

CONSIDERATION OF RESULTS

The most striking feature of the results is the consistent decrease in the values of R_T as heavier molecules are substituted in the mixtures for lighter ones. This is well shown in the summary given in Table XI, where values of R_T are given above the diagonal line. In all cases as we go down a column, or from left to right, R_T decreases.

The change in R_T means that there is a change in the nature of the forces acting between the unlike molecules in collision. The simplest way of considering these forces is to regard the molecules as behaving like point centres of repulsive force. Thermal diffusion and viscosity experiments have shown that the molecules can be regarded as behaving in this way. Whatever may be the complexity of the actual forces operating the success of this simple representation is rather remarkable.

The relation between the repulsive force index, S_{12}, and R_T is given by the following formula which is due to Chapman†

$$R_T = \frac{13}{10}\left(\frac{S_{12}-5}{S_{12}-1}\right).$$

TABLE XI. VALUES OF R_T AND REPULSIVE FORCE INDEX FOR MIXTURES OF THE INERT GASES

	He	Ne	A	Kr	X
He		0·80	0·65	0·63	0·59
Ne	11·4		0·54	0·51	0·43
A	9·0	7·9		0·19	0·17
Kr	8·7	7·6	5·7		0·08
X	8·3	7·0	5·6	5·3	
Radon*	7·3				

R_T thermal separation ratio

S_{12} repulsive force index

The values of S_{12} calculated in this way from R_T are given below the diagonal line in Table XI. There is, of course, a decrease in S_{12} going downwards or from left to right along the columns; the greatest value being 11·4 for helium-neon and the lowest 5·3 for krypton-xenon. Thus there is a wide range of molecular behaviour extending from very hard down to almost Maxwellian. The value of S_{12} for helium-radon shown at the foot of the first column was obtained by Dr G. E. Harrison (1937), who has worked in this laboratory on thermal diffusion in mixtures containing small concentrations of radon, using radioactive methods of measurement. It is interesting to note that the value is lower than for helium-xenon; showing that the more massive radon molecule is softer than the xenon molecule. Thus radon comes, as might be expected, at the end of the sequence of the inert gases.

---

* Obtained by Dr G. E. Harrison.

† In previous calculations of S_{12} we have used an approximate expression omitting the factor 13/10. This results in high values of S_{12}. The factor 13/10 is introduced to allow for the fact that Chapman's first approximation to k_t rigid elastic spheres is lower than the true value.

The values of S_{12} for unlike molecules, obtained from thermal diffusion experiments, may be compared with the values of S_{11} for simple unmixed gases given by viscosity. Over a considerable range of temperature the coefficient of viscosity of a gas varies as a power of the absolute temperature, which means that the molecules can again be represented as point centres of repulsive force obeying an inverse power law. Thus if η_1 and η_2 represent the viscosity of a gas at temperatures T_1 and T_2, then

$$\frac{\eta_1}{\eta_2} = \left(\frac{T_1}{T_2}\right)^n.$$

The repulsive force index S_{11} is obtained from n by the relation

$$n = \frac{S_{11}+3}{2(S_{11}-1)}.$$

The value of n can be found practically by plotting $\log \eta$ against $\log T$ and finding the slope of the curve. The value of the repulsive force index can be regarded as constant over a region of temperature where the slope of the graph is constant.

This method has been applied to a number of viscosity measurements on the inert gases (Rankine 1910; Nasini and Rossi 1928; Trautz and Binkele 1930; Trautz and Zink 1930; Trautz and Heberling 1934) and the values of S_{11} shown in Table XII have been obtained for the range of temperature 0° to 100° C.

TABLE XII. REPULSIVE FORCE INDEX S_{11} OBTAINED FROM VISCOSITY

	He	Ne	A	Kr	X
S_{11}	15·3	13·5	7·4	6·3	5·2

This shows a decrease in S_{11} with increasing molecular weight corresponding to the decrease in S_{12} which has been found for mixtures of the inert gases from thermal diffusion. The increasing softness of the molecules as the mass becomes greater is thus a fundamental property of the monatomic molecules. As the complexity of the structure increases, the molecules behave less like rigid elastic spheres. This regularity of behaviour suggests that a complete description of the intermolecular forces might be obtained in terms of the electronic constitution, thus obtaining a correlation between the molecular structure and the behaviour of the gas in bulk in the ordinary gas phenomena. Various attempts in this direction have been made to calculate the forces between molecules by means of quantum mechanics, a summary of which has been given by Lennard Jones (1931).

A comparison of the values of S in Tables XI and XII shows that the values obtained from viscosity are in general higher than those obtained from thermal diffusion, and this is particularly so in the case of the lighter molecules. Thus the numerical values of S_{12} obtained from thermal diffusion cannot be regarded as the "mean" of the values of S_{11} for the separate gases. This may be due to approximations used in the theory in calculating S_{12} for thermal diffusion, or it may be due to a real physical difference in the nature of the collision processes involved. This appears to need further theoretical consideration. It seems very unlikely that the low values of S_{11} in thermal diffusion can be due to a systematic experimental error in measuring k_t.

In conclusion we should like to express our thanks to Dr F. W. Aston for the valuable advice which he has given on the manipulation of the inert gases, and for lending us a quantity of the rarer gases; and also to Professor S. Chapman for his friendly encouragement throughout the course of the work.

SUMMARY

Measurements of thermal separation have been made in all the binary mixtures of helium, neon, argon, krypton, and xenon; using the Shakespear hot-wire method of gas analysis. By applying Chapman's theory the repulsive force index S_{12} of the intermolecular field has been obtained for each pair. The results show a wide and orderly range of molecular behaviour, the values of S_{12} extending from 11·4 for helium-neon to 5·3 for krypton-xenon. In all cases there is a decrease in the value of S_{12} as a heavier molecule is substituted for a lighter one in a mixture. The successive monatomic molecules thus become "softer" as their mass increases, i.e. their behaviour becomes less like that of rigid elastic spheres. This conclusion is in general agreement with the information given by viscosity on the molecular fields of the single gases. A comparison with Harrison's thermal diffusion value of S_{12} for helium-radon, obtained by using radioactive methods of measurement, shows that the massive radon molecule takes its proper place in the sequence as the "softest" of the group.

REFERENCES

Blüh, G., Blüh, O. and Puschner, M. 1937 *Phil. Mag.* **24**, 1103–14.
Chapman, S. 1916 *Proc. Roy. Soc.* A, **93**, 1–20.
Chapman, S. and Dootson, F. W. 1917 *Phil. Mag.* **33**, 248–53.

Chapman, S. and Hainsworth, W. 1924 *Phil. Mag.* **48**, 594–607.
Daynes, H. A. 1933 *Gas analysis by measurement of thermal conductivity.* Camb. Univ. Press.
Enskog, D. 1911 *Phys. Z.* **12**, 533–9.
Harrison, G. E. 1937 *Proc. Roy. Soc.* A, **161**, 80–94.
Ibbs, T. L. 1925 *Proc. Roy. Soc.* A, **107**, 470–86.
Ibbs, T. L. and Grew, K. E. 1931 *Proc. Phys. Soc.* **43**, 142–55.
Ibbs, T. L., Grew, K. E. and Hirst, A. A. 1929 *Proc. Phys. Soc.* **41**, 456–75.
Lennard Jones, J. E. 1931 *Proc. Phys. Soc.* **43**, 461–82.
Nasini and Rossi 1928 *Gazz. chim. ital.* **58**, 433–42.
Rankine, A. O. 1910 *Proc. Roy. Soc.* A, **84**, 181–92.
Trautz, M. and Binkele, H. E. 1930 *Ann. Phys., Lpz.*, **5**, 561–80.
Trautz, M. and Heberling, R. 1934 *Ann. Phys., Lpz.*, **20**, 118–20.
Trautz, M, and Zink, R. 1930 *Ann. Phys., Lpz.*, **7**, 427–52.

Vacuum wave-length measurements in the iron spectrum by means of the reflection echelon grating

BY W. EWART WILLIAMS AND A. MIDDLETON
King's College, London

(*Communicated by O. W. Richardson, F.R.S.—Received* 29 *December* 1937)

[Plates 6–8]

1. INTRODUCTION

As is well known, the determination of the wave-length of a spectral line is made by comparing it with another line of known wave-length. In the most precise measurements the comparison is made directly with the red line of cadmium which forms the spectroscopic standard of wave-length. It is not always convenient to use this primary standard, and at the instance of the International Astronomical Union a number of investigators have independently determined the wave-lengths of selected lines in the spectrum emitted from an iron arc under specified conditions. The committee of the Union has drawn up tables giving the values of these lines which are recognized as secondary standards and which are distributed fairly uniformly throughout the spectrum. As substandards, their wave-lengths are required to as high a degree of precision as possible.

Apart from considerations of standards, accurate wave-length measurements are now required for an entirely different purpose. The spectral lines of many elements have been arranged in series, and a comparatively simple formula expresses the frequency or the difference between the term values. Occasionally the difference between the experimental and calculated values is so large that the "perturbation" becomes obvious from the roughest measurements, but in general they are small and only precision measurements will show their existence and significance.

Hitherto, the Fabry-Perot interferometer has been the only accurate method available for obtaining the wave-length of one spectral line in terms of another. No spectral line can be strictly monochromatic; it has a line width and an energy or intensity distribution with wave-length that is dependent on the nature of the emitter and the physical conditions of the discharge. This distribution may be further complicated by the presence of other lines—due to the existence of isotopes, hyperfine structure components or incipient Stark effect splitting—which are not "resolved" or separated from the line which we wish to measure. The best we can do in such a case is to attempt to find the centre of gravity of the group. It can be mathematically shown that the Michelson interferometer method will, in general, give a spurious value for the centre of gravity of an asymmetric line and experimental investigation has verified this. The ordinary ruled grating has too low a resolving power to justify its use in precision measurements. It is an axiom, often neglected by spectroscopists, that the degree of accuracy which may be obtained is directly proportional to the resolving power of the instrument employed, since we are rarely certain that we are dealing with simple symmetrical lines.

Up to the present our standard has been the wave-length of red cadmium in air of a specified condition, and the comparison measurements have been made in air. When the lines to be measured are in the red region, any variation in the physical or chemical condition of the air, causing the wave-lengths to alter, will substantially produce a corresponding change in the standard, but if the lines are in the ultra-violet region the air of the laboratory should be maintained at standard conditions or a somewhat uncertain set of corrections has to be applied.

It is now generally accepted that the vacuum frequencies of spectral lines—which are the quantities required in spectroscopic calculations—are not known to the same degree of accuracy as the determinations of the air wave-lengths. The uncertainty is partly due to difficulties in completely specifying the laboratory air—its temperature, humidity, CO_2 content, etc.—and partly due to errors in the generally accepted dispersion curves for "normal" air.

Following on the development of the reflection echelon grating, details of which have been previously given (Williams 1931), an entirely new method of precision wave-length measurement has been evolved. The wave-length comparisons are made *in vacuo* so that the results can be directly linked up, when required, with the vacuum wave-lengths observed in the Lyman-Schumann regions. The main purpose of this investigation, and of the following one of Williams and Drinkwater, has been to test the possibilities of the method and to obtain fresh values for the frequencies of secondary standards.

2. EXPERIMENTAL METHOD AND PROCEDURE

The basis of the method for wave-length comparison consists of the addition of *two* reflecting mirrors (Williams 1933) which form an integral part with the echelon, and afford reference lines or directions which correspond to constant path differences.

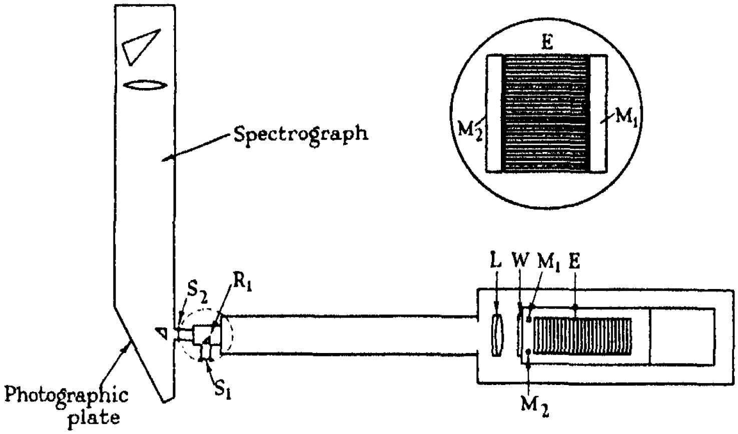

FIG. 1

The optical system employed is shown diagrammatically in fig. 1. The light from the slit S_1 of the auxiliary unit is reflected by the prism R_1, and on emerging from the achromatic lens L passes through the quartz window W to fall on the echelon E and its associated mirrors M_1 and M_2 as a parallel beam. The arrangement of these mirrors can be seen from the inset which shows a front view. The mirrors are plane silica strips, 8 × 40 mm. and about 7 mm. thick, and are surface platinized. By means of screw adjustments they can be tilted as required. The echelon has 40 plates of 1 mm. step and approximately 6·87 mm. thick. The reflected and diffracted light is brought to a focus by L on the vertical slit S_2 of the Hilger E 1 quartz spectrograph. This separates out the composite pattern on the tilted photographic plate.

The head carrying the slit S_1 and the right-angled prism can be rotated on the optical axis of the collimator. During the present work it was rotated through 90° from the position shown so that the slit S_1 was immediately below and parallel to the plane of the paper. In the diagram the rotating head is shown in this position merely for convenience of illustration.

When the echelon steps are horizontal (and the mirror strips vertical) the patterns obtained on the photographic plate from four well-separated wave-lengths will be similar to fig. 2. $A_1A_2A_3\ldots B_1B_2B_3$ are images of the slit S_1 formed by the mirrors M_1 and M_2. By suitably tilting these mirrors the images can be obtained at any desired point. Usually they are arranged close to and symmetrical with the echelon patterns. C_1 and D_1 represent the mth and $(m-1)$th orders for a line of known wave-length λ_1; similarly, C_2 and D_2 are consecutive orders for another line of wave-length λ_2. In some cases only one order of a line is seen on the plate; C_3 of λ_3 is an example of such single-order position.

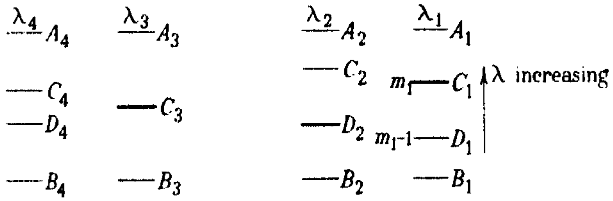

FIG. 2

The path difference measured in wave-lengths corresponding to a direction A_1 is given by (m_1+f_1), where f_1 is the ratio A_1C_1/C_1D_1. Similarly, the order of interference at A_2 is (m_2+f_2), where $f_2 = A_2C_2/C_2D_2$. In the case of λ_3, although the interorder distance cannot be directly measured it can be easily determined if it is known for any other wave-length, say λ_1. Since the angular separation of orders for an echelon varies directly as the wave-length, the interorder distance for λ_3 becomes

$$C_1D_1 \times \frac{\lambda_3}{\lambda_1} \times \frac{A_3B_3}{A_1B_1}.$$

The last term takes account of the varying magnification of the spectrograph for different wave-lengths. If the distance A_3C_3 is divided by this value given above we get f_3, the fractional part of λ_3.

Since the direction of the reflected image from the mirror M_1 is the same for all wave-lengths and the angle of incidence on the echelon is similarly constant, then

$$(m_1+f_1)\lambda_1 = (m_2+f_2)\lambda_2 = (m_3+f_3)\lambda_3 = K.$$

The approximate value of the integer m_1 is given by dividing twice the plate thickness by the wave-length. If the wave-lengths λ_1, λ_2 and λ_3 are accurately known and f_1, f_2 and f_3 found from measurements of the plate, the *exact* value of m_1 can be readily found by choosing that integral value (approximately $2t/\lambda_1$) which will give the correct fractional parts for λ_2

and λ_3. The method now becomes exactly the same as developed by Benoit for the Fabry-Perot interferometer. The wave-length of a fourth line λ_4 must be known beforehand to sufficient accuracy that K/λ_4 cannot be in error by an integer. If its fractional part f_4 is measured the exact wave-length is given by $K/(m_4+f_4)$.

The focal length of L is approximately 170 cm., so that with an echelon of 1 mm. step the interorder distance in the red region is approximately 1 mm., reducing to about one-half this amount at 3000 A. With very sharp lines such as the satellites of mercury lines the limit of accuracy of measurement is that of the photomeasuring micrometer. For this purpose a special modification of the Hilger L1 micrometer was designed by one of us (W.E.W.) which has a 2 cm. scale cross-slide inclined at a convenient angle for continuous measurements. The micrometer reads to 0·001 mm. by means of a vernier, and this gives a measurement of the fractional part to 0·001 in the red end and about half this value at 3000 A. Since the order of interference is approximately 22,000 in the red and twice this value at 3000 A, the apparatus is capable of comparing wave-lengths to within about one part in 20×10^6 in any part of the spectrum. It cannot, however, be too strongly emphasized that this standard of accuracy is only obtainable with really sharp lines. In general, spectral lines are not sufficiently narrow that one can make full use of the resolving and dispersive power of the system. In some earlier preliminary experiments, one of us (W.E.W.), in conjunction with T. T. Thomas, carried out some measurements on the wave-lengths of certain satellites of various mercury lines which are themselves complex. In this instance the interference pattern of the satellite would be equally as sharp as the mirror image, and no difficulty was experienced in measuring the distance from the line to the mirror image to within 0·001 mm. By rotating both the primary slit and the echelon unit through 90° so that the dispersion of the echelon is horizontal and in the same plane as that of the E1, a 2½ times magnification of the whole pattern is obtained because the photographic plate is inclined to the optical axis of the spectograph. The increased magnification did not in this case materially reduce the consistency of settings, and we estimated that our standard of accuracy was approximately doubled; that is, the utmost limits of our apparatus was about one part in 40×10^6, which corresponds at 6000 A to 0·00015 A. With broader lines, this increased magnification, instead of improving the accuracy actually appeared to lessen it. This is in agreement with observations in other fields of optics that accuracy of setting in the case of a hazy ill-defined object is materially reduced when too great a magnification is employed.

Since one obtains three or four images of each spectral line by this method (two mirror images and one or two diffractional orders) it would not be practical to use parallel dispersions to increase the magnification in the case of a rich spectrum such as iron. A quartz-fluorspar achromatic doublet corrected for spherical aberration has been designed for placing in an extension tube between the echelon rotating head and the slit of the E 1 to give a variable magnification up to 3. With this magnification the brightness of the final image decreases to one-ninth, but even apart from this, experience shows that its use is only justified with extremely sharp lines.

If instead of using the Rayleigh expression for resolving power we define the *separating power* of an optical instrument as the smallest wave-number difference between two lines that can be resolved, we get $\delta\nu = \frac{1}{2Nt}$ cm.$^{-1}$, where N is the number of plates and t is the plate thickness in cm. This value is independent of the wave-length and for our instrument should be 0·018 cm.$^{-1}$. Two components of a mercury line with a separation of 0·023 cm.$^{-1}$ are clearly separated, so that the practical resolving power of the instrument is substantially equal to the theoretical value. A very real practical advantage of the reflection echelon over the Fabry-Perot interferometer is that the echelon remains in permanent adjustment and, thanks to the vacuum chamber in which it is placed, long (10–15 hr.) exposures on weak lines give equally sharp definition as 5 min. exposures on strong lines.

Originally the object of this investigation was to determine the vacuum frequencies of the secondary standard iron lines emitted by a Pfund arc as specified by the International Astronomical Union. We were reluctantly forced to the conclusion that while by continual practice concordant results could be obtained, we could not satisfy ourselves that the results were in reality accurate. With practice, one can set on the same part of a fringe with remarkable consistency, but there is no evidence to show that it is the centre of gravity of the line.

The only point of difference between our usage of the Pfund arc and the usual one was that instead of taking the light from a central zone of the arc 1–1·5 mm. in width, the area we employed was approximately a thousand times smaller. If anything, this should have further reduced any pole effect, but we actually found that the widths of the lines was of the order of a hundred times greater than the accuracy of setting. We are of the opinion that the observer is not justified in attempting to measure a line to an accuracy greater than about one-twentieth of half the width of the line at half intensity, whether the line width is due to the source or due to low resolving power of the optical instrument employed. If one is prepared to make an accurate microphotometric record of the intensity distribution in the line, it becomes another matter, and a higher standard of accuracy can be justifiably expected.

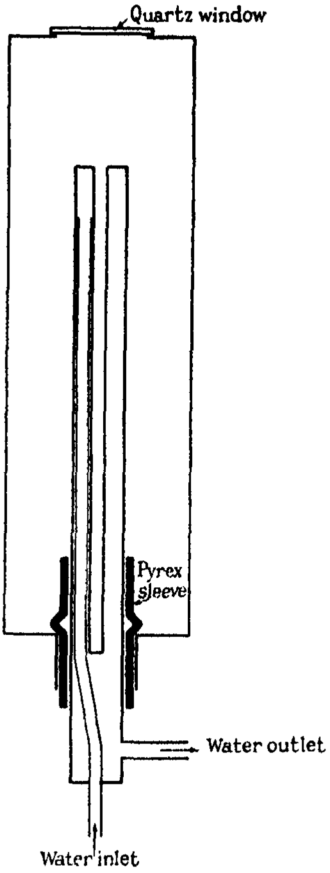

FIG. 3

The obvious way to secure more homogeneous spectral lines would be to excite the substance in a Schüler discharge tube. This would be successful with most elements, but with iron it becomes a different matter. Iron sputters so slowly that iron cathodes are normally used in Schüler tubes so that only the spectra of the substance and of the carrier gas (usually helium) are photographed. After a number of trials, including attempts to use a hot cathode, the design shown in fig. 3 was evolved.

The anode is a heavy brass tube 2 ft. long and 3 in. in diameter with an annular ring at the top 1½ in. internal diameter. A quartz window 2 in. in diameter is fixed to it by means of sealing wax. The lower end of the cylinder is fitted with a brass cap as shown. The cathode is a steel tube 16 in. long, $\frac{9}{32}$ in. internal and $\frac{3}{8}$ in. external diameters. This tube, one end of which is closed, is welded at the other end to an outer steel tube 20 in. long and $\frac{7}{8}$ in. external diameter. Fitted to the bottom of this tube are two other tubes for cooling purposes. The inlet tube is carried to within 1 in. of the top of the cathode and is made elliptical in section so as to fit between the outer wall of the cathode and the inner wall of the large tube. A pyrex glass sleeve insulates the anode from the cathode and a sealing wax joint is made over the brass tube, the pyrex sleeve and the projecting iron tube to make the tube vacuum tight. The outer anode tube was also cooled by about 40 turns of composition tubing. The cooling systems for the cathode and anode were connected in series with a short length of a few inches of heavy rubber tubing, the water resistance was sufficiently high that no measurable current leakage occurred with a potential difference of 1600 V. The discharge tube was "conditioned" for some days with a current of 4 amp. and a potential of 900 V, the ballast resistance absorbing the remaining 700 V being in the form of radiator (electric fire) elements running at dull red heat in another room which contained the D.C. generator. A fairly strong flow of water was essential to dissipate the 3·6 kW without local boiling. After a few days the hydrogen lines became much fainter and the iron lines proportionately stronger. With a current of 4 amp. the iron lines were definitely broader than with 2 amp., but a reduction of the current to 1 amp. showed little material narrowing of the lines so that most of the exposures were made with a current of 2 amp. It is of interest to note in passing that this current is between ten and twenty times greater than normally used in the Schüler type of discharge.

3. Comparison between the spectra obtained from the arc and the Schüler tube

In figs. 4–6 of Plates 6, 7 are shown the line spectra obtained from the two types of discharge. The Schüler tube spectrum in each case is the central portion with the arc spectrum on either side. The times of exposure have been chosen so that the average intensity should be approximately equal. The extremely strong lines in the central strip are those of helium—the carrier gas—and do not concern us here. Some of the lines are relatively much stronger in the Schüler discharge than in the arc, while other lines are much reduced or even missing altogether.

If a table is made of the lines in this region which are reduced in the Schüler tube, the term levels which occur most frequently are (in Catalan's notation) the $a\,^5P_3$, $a\,^5P_2$, $a\,^5P_1$, $a\,^3P_2$, $a\,^5F_4$, $a\,^5F_3$, $a\,^5F_2$ and $a\,^5F_1$ levels. The majority of the lines which are reduced in intensity are those which show small pressure displacements belonging chiefly to the *a* and *b* groups.

The term levels involved in the case of enhanced lines are chiefly the $a\,^5D_4$, $b\,^3P_2$, $a\,^5D_2$, $a\,^3F_4$ and the $a\,^5D_3$ levels. We have not made any exhaustive comparison of the lines as the subject lies outside the scope of our investigation, but it appears that a careful comparison with different carrier gases in the tube (argon, neon and krypton as well as helium) might help in the assignation of other term values not yet identified.

4. Results

Our vacuum wave-length values are compared directly with that of the red line of cadmium emitted from a water-cooled Schüler tube containing a cadmium (95%)-silver (5 %) cathode approximately 15 cm. long and 1 cm. internal diameter. The D.C. discharge was maintained at 125 mA. Several

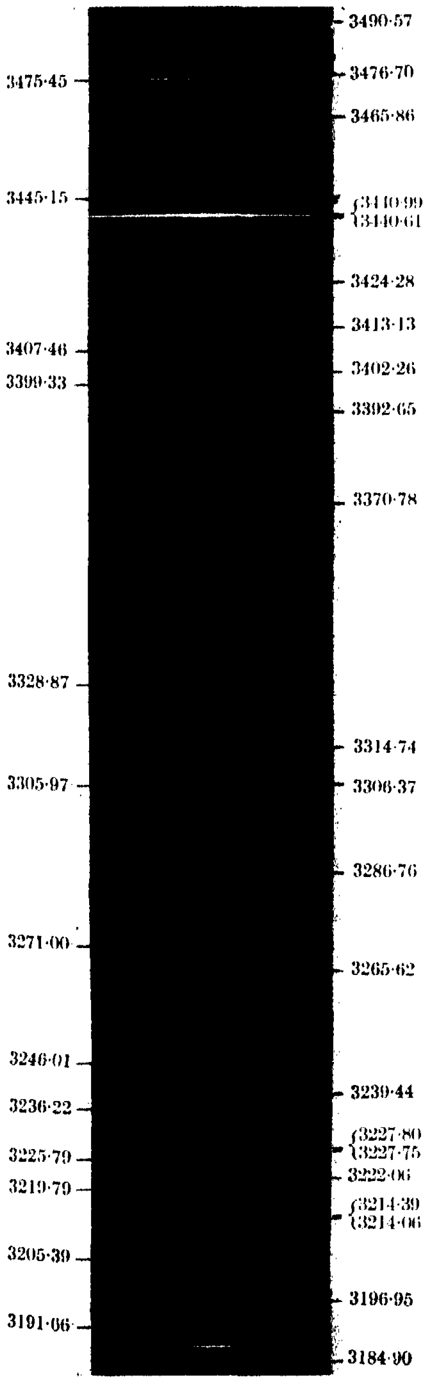
3490·57
3475·45
3476·70
3465·86
3445·15
3440·99
3440·61
3424·28
3413·13
3407·46
3402·26
3399·33
3392·65
3370·78
3328·87
3314·74
3305·97
3306·37
3286·76
3271·00
3265·62
3246·01
3239·44
3236·22
3227·80
3227·75
3225·79
3222·06
3219·79
3214·39
3214·06
3205·39
3196·95
3191·06
3184·90

Fig. 4

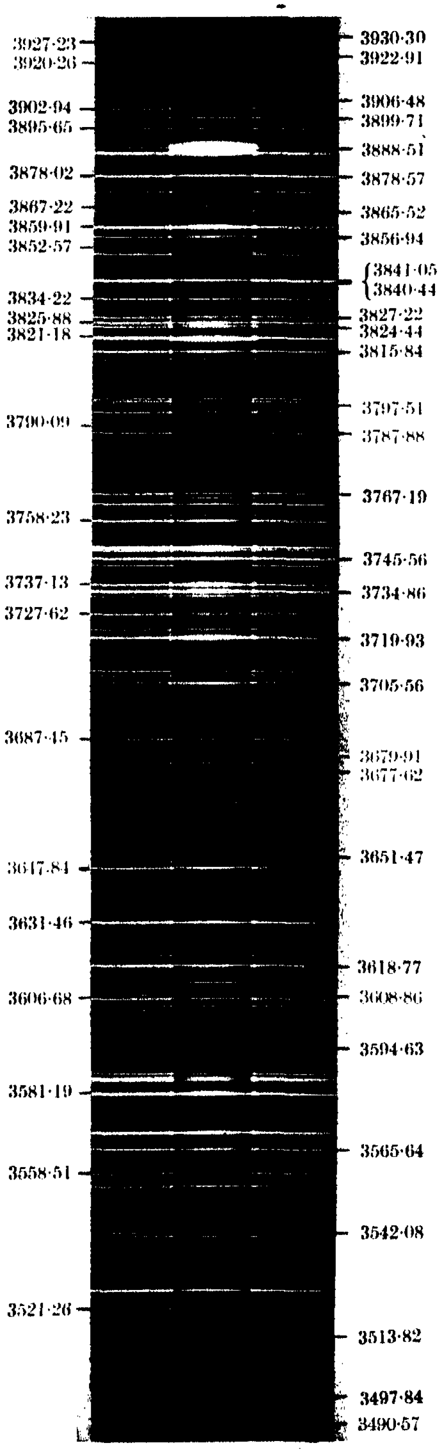
3927·23
3930·30
3920·26
3922·91
3902·94
3906·48
3895·65
3899·71
3888·51
3878·02
3878·57
3867·22
3865·52
3859·91
3856·94
3852·57
3841·05
3840·44
3834·22
3827·22
3825·88
3824·44
3821·18
3815·84
3797·51
3790·09
3787·88
3767·19
3758·23
3745·56
3737·13
3734·86
3727·62
3719·93
3705·56
3687·45
3679·91
3677·62
3651·47
3647·84
3631·46
3618·77
3606·68
3608·86
3594·63
3581·19
3565·64
3558·51
3542·08
3521·26
3513·82
3497·84
3490·57

Fig. 5

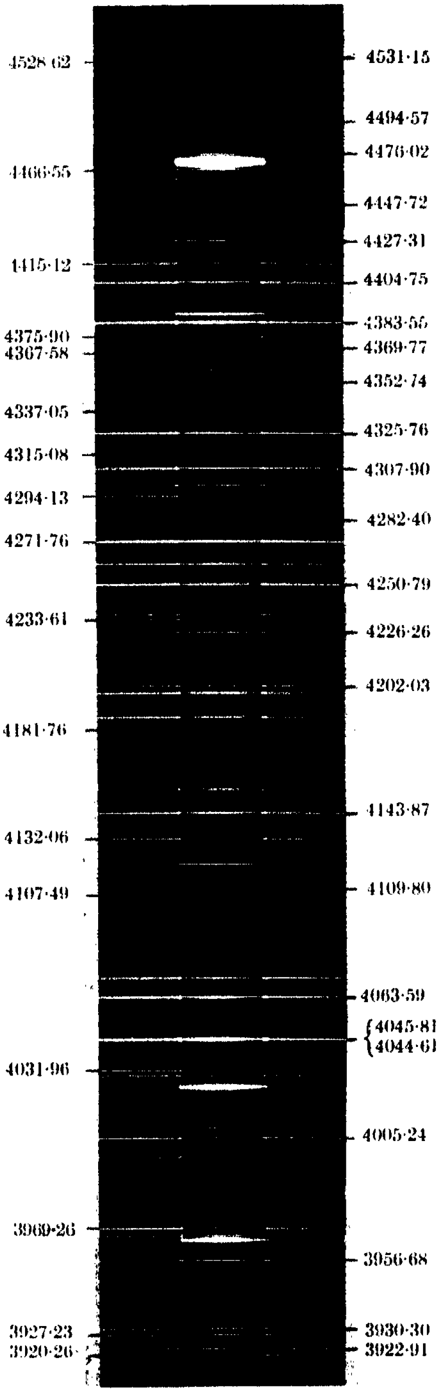
4528·62
4531·15
4494·57
4476·02
4466·55
4447·72
4427·31
4415·12
4404·75
4383·55
4375·90
4367·58
4369·77
4352·74
4337·05
4325·76
4315·08
4307·90
4294·13
4282·40
4271·76
4250·79
4233·61
4226·26
4202·03
4181·76
4143·87
4132·06
4109·80
4107·49
4063·59
4045·81
4044·61
4031·96
4005·24
3969·26
3956·68
3927·23
3930·30
3920·26
3922·91

Fig. 6

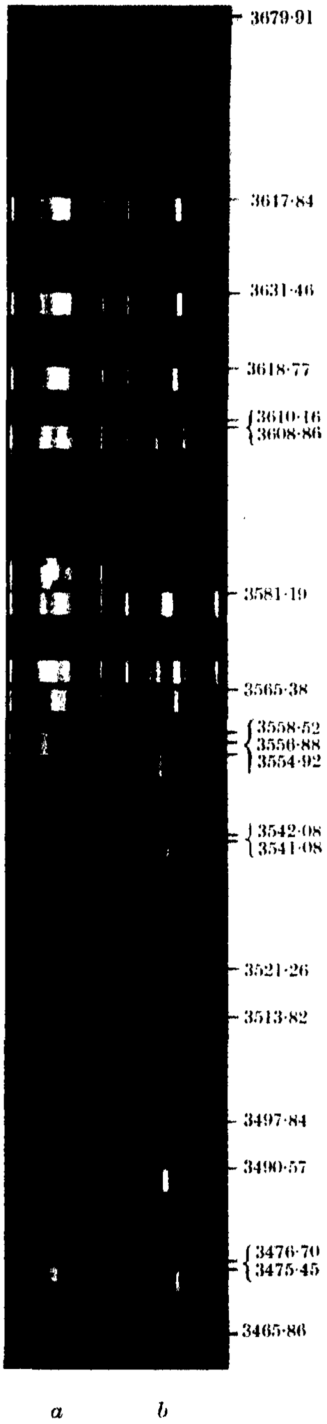
3679·91
3617·84
3631·46
3618·77
3610·16
3608·86
3581·19
3565·38
3558·52
3556·88
3554·92
3542·08
3541·08
3521·26
3513·82
3497·84
3490·57
3476·70
3475·45
3465·86
a
b

FIG. 7

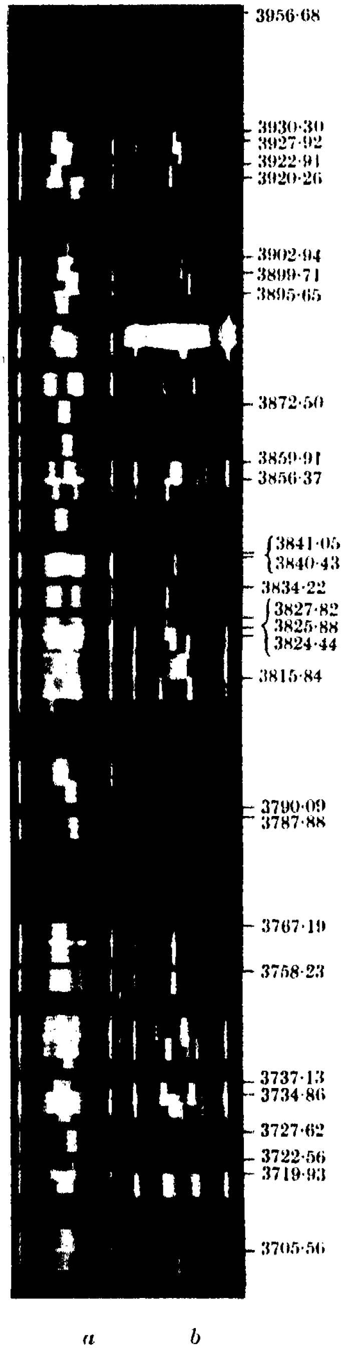
3956·68
3930·30
3927·92
3922·91
3920·26
3902·94
3899·71
3895·65
3872·50
3859·91
3856·37
3841·05
3840·43
3834·22
3827·82
3825·88
3824·44
3815·84
3790·09
3787·88
3767·19
3758·23
3737·13
3734·86
3727·62
3722·56
3719·93
3705·56
a
b

FIG. 8

comparisons were made with the A.E.G. and the G.E.C. hot-cathode argon-filled cadmium lamps. Even when run at lower currents than the rated value the lines from these lamps were not as sharp as in the hollow-cathode discharge. No difference in wave-length could be detected, but since the fractional part could be determined with greater precision and certainty with the Schüler tube, in spite of the extra labour involved, the latter source was always used.

The vacuum wave-length standard we have chosen is $\lambda_{\text{vac}} = 6440{\cdot}2498$A. This is obtained from the standard spectroscopic value $\lambda_{\text{air}} = 6438{\cdot}4696$A, together with Sears and Barrell's (1934) value for the refractive index of normal air at this wave-length, 1·00027649. The refractive indices calculated from the formulae of Pérard (1934) and Kösters and Lampe (1934) are practically identical with the value of Sears and Barrell (1934), but a large discrepancy occurs if the formula of Meggers and Peters (1918) is chosen. In any case, if in the future some other value comes to be accepted as the vacuum wave-length of this line our results can be easily scaled to suit the new value.

The procedure adopted for a plate for measurement was to set the apparatus for best focus for the red cadmium, and an exposure time chosen so that the mirror images would just show clearly on the plate. The cadmium tube was then replaced by the iron one and four or six exposures made, the plate holder being moved down a suitable amount after each exposure. Finally, a second exposure with the cadmium tube was made. When no difference could be detected in the fractional parts for the red cadmium line exposures, the plate could be used for measurement.

Since the E 1 spectrograph uses a single component objective the light is parallel when falling on the prism for one wave-length only. In consequence, as can be shown from geometrical optics, the prism introduces a considerable amount of astigmatism, and while the tilt and curvature of the plate have been chosen for good focus of a vertical slit image, the astigmatism is so pronounced that either an entirely fresh tilt and plate curvature have to be adopted for good horizontal focusing, or the echelon image has to be focused to a plane inside the E 1 slit to compensate for this astigmatism. If this is done, the now broad lines in the vertical plane retain their sharpness, but the echelon image has to be refocused for different ranges on the plate. The difficulty would be eliminated if a spectrograph with achromatic objectives were employed, but the effective dispersion would be reduced about 2½ times.

The various iron exposures would generally consist of different exposure times for a given range and different focusing positions for different ranges.

In order to test the degree of concordance obtainable, three independent sets of plates were taken, the apparatus being completely readjusted in between each set. The values obtained are given in the table below.

TABLE I. VACUUM WAVE-LENGTHS OF IRON LINES

1st group	2nd group	3rd group
4428·5512	0·5511	0·5509
4326·9788	0·9786	0·9784
4064·7408	0·7412	0·7409
3931·4090	0·4087	0·4089
3929·0308	0·0309	0·0309
3921·3668	0·3669	0·3672
3828·9068	0·9068	0·9072
3826·9648	0·9650	0·9653
3825·5270	0·5272	0·5272
3759·2996	0·2998	0·3000

The maximum difference from the mean is 0·0003 A, the average value being 0·00012 A, so that we are of the opinion that in this region we are fully justified in giving these wave-lengths to eight significant figures. The justification for this is basically due to the much narrower lines that we have to measure than if an air arc was used. In passing it might be noted that once such a source is fitted up it needs no attention by way of replacements but is always ready for use.

Figs. 7, 8, Plate 8, are the echelon patterns for the air arc (*a*) and the Schüler tube (*b*), with a magnification factor of approximately 7·5. The outer lines are mirror images of the slit which form the reference marks, the echelon pattern being contained within them. Unfortunately the arc pattern for the longer wave region is somewhat over-exposed in comparison with *B*, so that the discrepancy between the standards is over-emphasized, but if anything the converse is true for the shorter range. It will be evident that ill-defined and reversed lines in the arc spectrum are often relatively sharp in the Schüler discharge.

The second and third columns of Table II denote the observed vacuum wave-length and wave number with $\lambda\,6440{\cdot}2498$ A as the vacuum wave-length of the red cadmium line. The fourth column is the value of the wave-length in normal air calculated from the following formula of Kösters and Lampe (1934) suitably modified to correspond to standard conditions:

$$(n-1)\,10^6 = 272{\cdot}749 + \frac{1{\cdot}502}{\lambda^2} + \frac{0{\cdot}01834}{\lambda^4},$$

λ being the vacuum wave-length expressed in microns. The fifth column is

TABLE II

1	2	3	4	5	6	7
Ref. no.	Vacuum wave-length	Wave number	Calculated normal air wave-length	Previous value of air-arc wave-length corrected for pressure	Source of λ for 5	Transition involved Catalan's notation
1	5372·9847	18611·630	$5371{\cdot}490_{5}$	0·491 S	1	$8A-18B$
2	5228·6435	19125·420	$5227{\cdot}188_{0}$	0·189 0·188 S	1 1	$12A-31B$ $19A-63B$
3	5173·0379	19331·001	$5171{\cdot}597_{0}$	0·596 S	1	$11A-29B$
4	5168·9276	19346·373	$5167{\cdot}487_{7}$	0·488 S	1	$11A-30B$
5	4529·8844	22075·617	$4528{\cdot}614_{1}$	0·615 S	1	$14A-55B$
6	4428·5511	22580·748	$4427{\cdot}307_{5}$	0·311 $0{\cdot}306_{5}$ S	1	$2A-\ 8B$ $27B-67C$
7	4416·3620	22643·070	$4415{\cdot}121_{6}$	0·122 S	1	$13A-52B$
8	4405·9868	22696·390	$4404{\cdot}749_{2}$	0·749 S	1	$12A-50B$
9	4377·1597	22845·864	$4375{\cdot}929_{7}$	0·931 S	1	$1A-\ 7B$
10	4326·9786	23110·814	$4325{\cdot}761_{8}$	0·764 $0{\cdot}761_{5}$ S	1	$1A-\ 9B$ $13A-55B$
11	4133·2220	24194·199	$4132{\cdot}056_{0}$	0·058 S	1	$13A-59B$
12	4064·7410	24601·813	$4063{\cdot}592_{9}$	0·594	2	$12A-59B$
13	3931·4089	25436·174	$3930{\cdot}295_{6}$	0·298 S	1	$3A-17B$
14	3929·0309	25451·569	$3927{\cdot}918_{3}$	0·921 S	1	$4A-18B$
15	3924·0214	25484·060	$3922{\cdot}910_{1}$	0·913 S	1	$2A-16B$
16	3921·3670	25501·311	$3920{\cdot}256_{4}$	0·259 S	1	$5A-19B$
17	3861·0042	25899·997	$3859{\cdot}909_{5}$	0·912 S	1	$1A-16B$
18	3857·4626	25923·779	$3856{\cdot}368_{6}$	0·372 S	1	$2A-18B$
19	3842·1354	26027·193	$3841{\cdot}045_{4}$	$0{\cdot}048_{5}$ S	1	$13A-64B$
20	3841·5250	26031·328	$3840{\cdot}435_{2}$	0·437 S	1	$9A-40B$
21	3835·3084	26073·522	$3834{\cdot}220_{2}$	0·223 S	1	$8A-38B$
22	3828·9069	26117·114	$3827{\cdot}820_{3}$	$0{\cdot}822_{5}$ S	1	$12A-63B$
23	3826·9650	26130·367	$3825{\cdot}878_{9}$	0·882 S	1	$7A-36B$
24	3825·5271	26140·188	$3824{\cdot}441_{4}$	0·443 S	1	$1A-17B$
25	3816·9226	26199·116	$3815{\cdot}839_{1}$	0·840 S	1	$11A-62B$
26	3791·1669	26377·102	$3790{\cdot}090_{1}$	0·093 S	1	$9A-44B$
27	3788·9542	26399·506	$3787{\cdot}878_{0}$	0·881 S	1	$10A-45B$
28	3759·2998	26600·698	$3758{\cdot}231_{3}$	0·233 S	1	$8A-43B$
29	3738·1939	26750·886	$3737{\cdot}130_{9}$	0·132 S	1	$2A-22B$
30	3735·9247	26767·135	$3734{\cdot}862_{2}$	0·865 S	1	$6A-37B$
31	3728·6780	26819·157	$3727{\cdot}617_{4}$	0·619 S	1	$8A-45B$
32	3720·9915	26874·557	$3719{\cdot}932_{9}$	0·934 S	1	$1A-21B$
33	3688·5040	27111·262	$3687{\cdot}453_{8}$	0·456 S	1	$6A-41B$
34	3680·9599	27166·826	$3679{\cdot}911_{7}$	0·914 S	1	$1A-22B$
35	3648·8813	27405·660	$3647{\cdot}841_{3}$	0·842 S	1	$7A-48B$
36	3632·4969	27529·273	$3631{\cdot}461_{2}$	0·462 S	1	$8A-50B$
37	3619·7988	27625·845	$3618{\cdot}766_{4}$	0·767 S	1	$9A-52B$
38	3609·8880	27701·690	$3608{\cdot}858_{1}$	0·859 S	1	$10A-54B$
39	3566·3965	28039·507	$3565{\cdot}377_{6}$	0·379 S	1	$8A-53B$
40	3522·2674	28390·803	$3521{\cdot}260_{1}$	0·262 S	1	$7A-53B$

Table II (*continued*)

1 Ref. no.	2 Vacuum wave-length	3 Wave number	4 Calculated normal air wave-length	5 Previous value of air-arc wave-length corrected for pressure	6 Source of λ for 5	7 Transition involved Catalan's notation
41	3514·8212	28450·949	3513·815$_8$	0·818 S	1	6*A*–51*B*
42	3498·8397	28580·904	3497·838$_4$	0·843 S 0·8406	1 3	4*A*–27*B*
43	3477·6962	28754·669	3476·700$_3$	0·704 S 0·7023	1 3	5*A*–28*B*
44	3466·8523	28844·609	3465·859$_2$	0·862 S 0·8610	1 3	4*A*–28*B*
45	3414·1091	29290·218	3413·129$_5$	0·131 S 0·1306	4 3	15*A*–126*B*
46	3408·4355	29338·974	3407·457$_3$	0·459 S 0·4579	4 3	14*A*–122*B*
47	3287·6982	30416·418	3286·750$_8$	0·752 0·7507	4 3	14*A*–143*B*

the previously accepted value of the normal wave-length of the standard air arc corrected to a vacuum arc by means of Babcock's (1928) equations for term depressions due to pressure. The letter S in this column denotes that the particular wave-length is recommended as a secondary standard by the International Astronomical Union. The reference number in the sixth column, given below, indicates the source from which the wave-length value has been taken; these are

(1) *Trans. Int. Astr. Un.* **3**, Table I, 1929.

(2) Catalan, M. A. (1930) "Estructura del espectro del hierro." *An. Soc. esp. Fís. Quim.* **28**, 1239.

(3) Meggers, W. F. and Humphreys, C. J. (1937) *Bur. Stand. J. Res.* **18**, 543–63.

(4) *Trans. Int. Astr. Un.* **4**, Table 6, 1933.

The transitions involved are given in column 7 in Catalan's notation for ease of printing. The double values occurring in lines 2, 6 and 10 are due to the different pressure corrections that have to be applied according to which transition is supposed to occur. No evidence of widening was found in these lines, so that the probability is that in the Schüler discharge the intensity of one or other is negligibly small.

The following Table III gives the energy level differences from four of the lines, which, assuming the combination principle, afford some test of the accuracy of the work. Comparison with the results of others is not fully justifiable in view of the uncertainties in the dispersion curves of normal air.

TABLE III. ENERGY LEVEL DIFFERENCES

Line	Transition	Wave number
3859	$1A-16B$	25899·997
3922	$2A-16B$	25484·060
		415·937
3679	$1A-22B$	27166·826
3737	$2A-22B$	26750·886
		415·940
3679	$1A-22B$	27166·826
3859	$1A-16B$	25899·997
		1266·829
3737	$2A-22B$	26750·886
3922	$2A-16B$	25484·060
		1266·826

It is interesting to note that if the wave number of line 3737 be increased by 0·003 cm.$^{-1}$, which corresponds to a reduction of wave-length of 0·0004 A, the energy level differences given in the above table would exactly correspond.

5. ACKNOWLEDGEMENTS

We wish to acknowledge our indebtedness to the Royal Society for providing funds for the construction of the necessarily expensive equipment, and allowing us to use it. One of us (W. E. W.) is further indebted to the trustees of the Leverhulme Fellowship for a Fellowship, during a part of the tenure of which this work was carried out.

In conclusion, it gives us great pleasure to thank Professor O. W. Richardson, F.R.S., for the co-operation and help we have received throughout the work.

6. SUMMARY

The vacuum wave-lengths of 47 iron lines have been determined directly against the red cadmium standard by means of a new method employing a reflection echelon in vacuum so that no corrections for the refractive index of normal air need be made. By using a Schüler type hollow-cathode source, much narrower lines are obtained than is possible with an iron arc, and the concordance of independent determinations justify the values being given to eight significant figures. The work is being extended further to the ultra-violet.

REFERENCES

Babcock, H. D. 1928 *Astrophys. J.* **67**, 240–61.
Kösters, M. W. and Lampe, H. 1934 *Phys. Z.* **35**, 223–4.
Meggers, W. F. and Peters, C. G. 1918 *Bull. U.S. Bur. Stand.* **14**, 687.
Pérard, A. 1934 *Trav. Bur. int. Poids Mes.* **19**, 1–127.
Sears, J. E. and Barrell, H. 1934 *Philos. Trans.* A, **233**, 143–216.
Williams, W. E. 1931 *Nature, Lond.*, **127**, 816–17.
— 1933 *Proc. Phys. Soc.* **45**, 699–723.

The infra-red absorption spectrum of tetra-deuteroethylene

By G. K. T. Conn and G. B. B. M. Sutherland

Laboratory of Physical Chemistry, Cambridge

(*Communicated by R. G. W. Norrish, F.R.S.—Received* 23 *January* 1939)

The ethylene molecule possesses twelve fundamental modes of vibration of which seven have been identified with certainty from its infra-red absorption and Raman spectra. The remainder have been tentatively assigned in different ways by different authors, and much uncertainty exists regarding their true values. The present investigation was undertaken with a view to obtaining new information on a closely related spectrum which might enable one to discriminate between those assignments. An equally important reason was that the ethylene molecule has been made the subject of many theoretical investigations in attempts to find a suitable representation for the force field within a polyatomic molecule. Such theories may best be tested by seeing how closely they predict the frequencies of the isotopic molecule. In some cases it is necessary to know a few of the frequencies of the isotopic molecule, in addition to those of the normal molecule, to obtain all the constants of the force field. The remaining isotopic frequencies may then be predicted and their verification used as a test. This work was made possible largely through the kind co-operation of Professor de Hemptinne of the University of Louvain, who supplied us with the specimen of C_2D_4 used (de Hemptinne, Jungers and Delfosse 1938). He and his colleagues were simultaneously investigating the Raman spectra of the various deuteroethylenes with a similar object in view. The sample we employed was estimated to have a light hydrogen content of not more than 10 %.

EXPERIMENTAL

The absorption spectrum was investigated over the range 1·0–19·0μ. In the preliminary survey of the spectrum a constant deviation prism spectrometer was used with 60° prisms of sylvine, fluorite and quartz. The regions of absorption were then explored under high dispersion using a prism-grating spectrometer of the Pfund-Hardy type. In the present work the thermocouple used as detector was connected directly to a Paschen moving-magnet galvanometer of internal resistance 12Ω and sensitivity of the order of 10^{-10} amp./cm. at 1 m. An echelette grating of 4800 lines to the inch, ruled by Barker on a nickel surface was used to cover the region 3–6μ; while a grating of 1200 lines to the inch ruled on a tin surface, was used over the region 6–14μ, the second order being employed from 6 to 9·5μ, and the first order for the longer wave-lengths.

The absorption cell used was in all cases a pyrex tube 12 cm. long and 4 cm. diameter flanged at the ends. In general, rock-salt end-plates sealed by means of "porcenam" paint were used. For the observations covering the region 14–19μ end-plates of sylvine were used.

Examination under low dispersion

The region 1–3μ was investigated using a quartz prism and a pressure of C_2D_4 of 12 cm. of Hg in the absorption cell. Between 1 and 2·8μ no evidence of strong absorption was found. Beyond 2·8μ it appeared there was a region of strong absorption, the centre lying somewhere about 3·3μ. As this is a region of quartz absorption a satisfactory curve of the C_2D_4 absorption in this region was not obtained.

With a pressure of 12 cm. Hg of C_2D_4 in the absorption cell, the region 4–13·5μ was explored using the sylvine prism. The curve of percentage absorption plotted against wave-length so obtained is shown in fig. 1. It will be seen that absorption bands are indicated at 4·5, 6·7, 8 and 9μ while beyond 12μ the percentage absorption increases rapidly. This last region of strong absorption was investigated several times under reduced pressure (4·3 cm. Hg) and as a result the absorption curve illustrated in fig. 2 was obtained. This curve is the result of three independent determinations of the absorption in this region and indicates a very strong band with a broad Q-branch centred about 13·8μ.

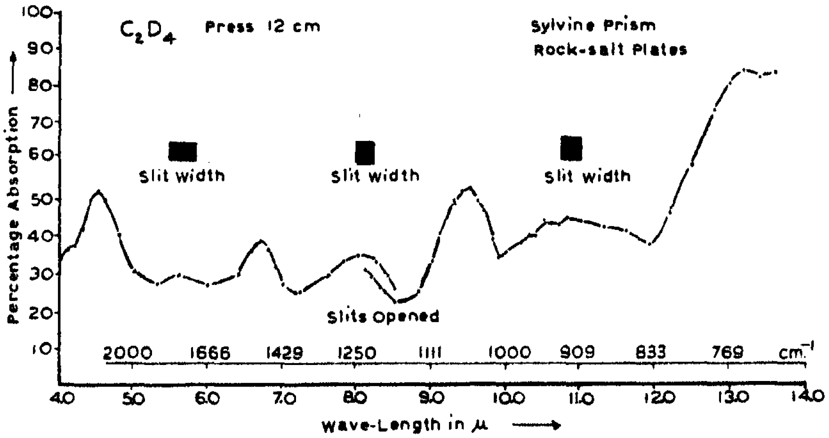

FIG. 1

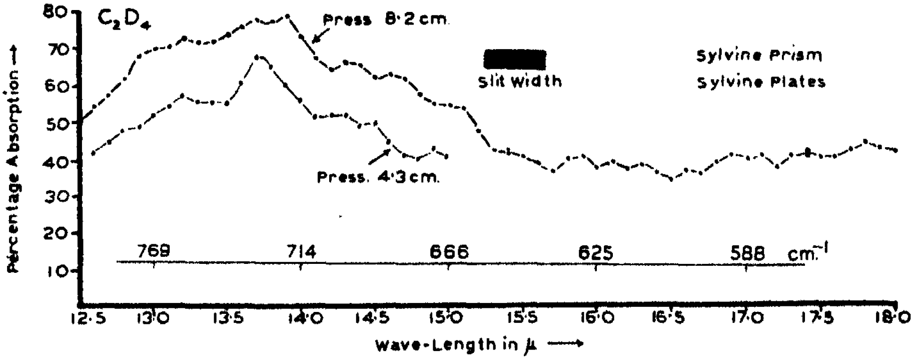

FIG. 2

The region 14–19μ was investigated using sylvine plates and a C_2D_4 pressure of 8·3 cm. Hg. This region was covered with some care but no evidence of further absorption in this region was obtained.

Investigation under high resolution

3·3μ region. In investigating the contour of the band observed in this region the absorption was plotted from 3 to 4μ as already observed. The absorption cell, fitted in this case with sylvine plates, contained C_2D_4 under a pressure of 8·2 cm. Hg. The contour obtained (fig. 3) is the result of three independent plots of the absorption. It will be seen that the band shows a definite Q-branch with slight asymmetry in the long wave-length side. There are also indications of a fine structure in the "P"-branch. The separation of the 'P" and "R" branches is of the order of 143 cm.$^{-1}$, so that it is clear that there is more than one absorption band in this region. The head of the Q-branch lies at $3{\cdot}367 \pm 0{\cdot}002\mu = 2970 \pm 2$ cm.$^{-1}$. The slit width used corresponded to 4 cm.$^{-1}$ in this region.

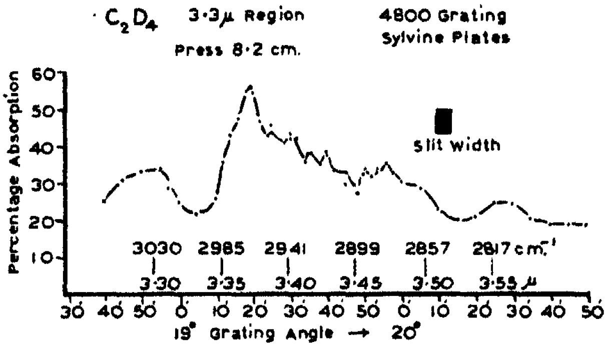

Fig. 3

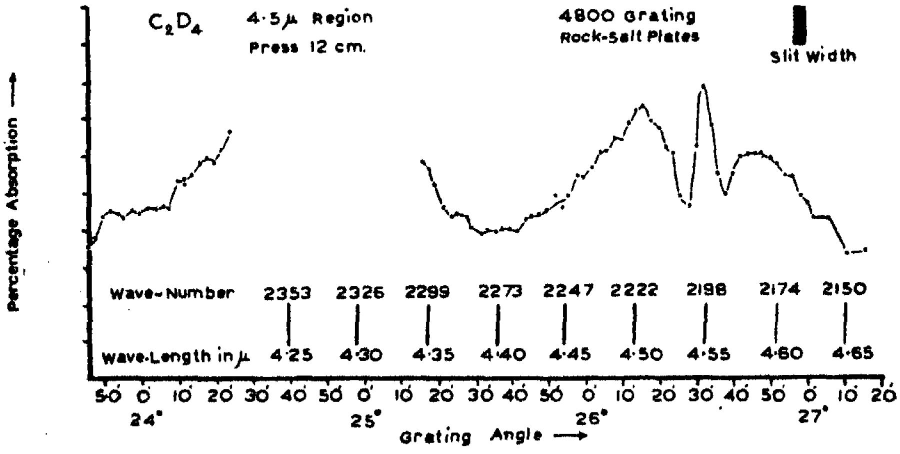

Fig. 4

4·4μ region. The pressure used in this case was 12 cm. Hg, and the slit widths were 3 cm.$^{-1}$. It was found that there were two bands in this region. One of these showed a strong Q-branch at $4{\cdot}547 \pm 0{\cdot}002\mu = 2199 \pm 1{\cdot}2$ cm.$^{-1}$; there were also indications of fine structure in the R-branch. The P–R separation was 41·2 cm.$^{-1}$. The contour obtained is shown in fig. 4. Evidence of a second band in the region of 4·3μ was also obtained. Unfortunately, owing to strong absorption due to atmospheric CO_2 in the neighbourhood of 4·26μ, it was found impossible to plot the absorption of C_2D_4 under high resolution. The attempt to resolve these two bands was therefore made under low dispersion using a fluorite prism. The result is shown in fig. 5. For this purpose the pressure in the absorption cell was lowered to 3·8 cm. Hg to cut down the broadening of the bands. It will be seen that the two bands have been resolved. Fig. 5 shows also a plot of the available energy. The figure reproduced is the best of a series of attempts to determine the position of this shorter wave-length band. A smooth curve has been drawn through the points obtained. (It will be seen that, of course, the atmospheric CO_2 absorption, cut down the available energy very markedly just over the interesting region so that an accurate plot could only be obtained with difficulty.) The centre of the band is at a wave-length which is certainly not greater than 4·28μ (2336 cm.$^{-1}$) and not less than 4·22μ (2370 cm.$^{-1}$) and is probably in the neighbourhood of 4·25μ (2353 cm.$^{-1}$). We may conclude that the centre of this region of absorption is about

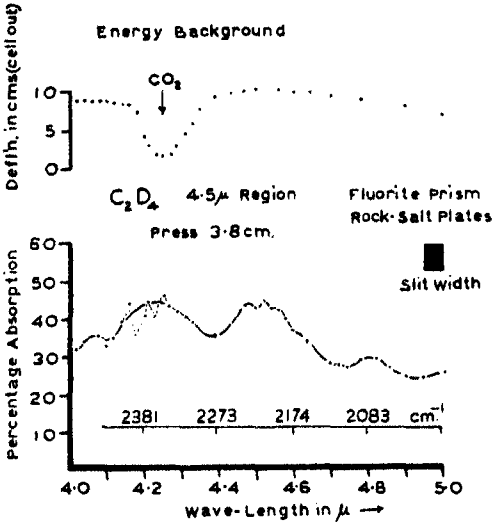

Fig. 5

$$4{\cdot}25 \pm 0{\cdot}02\mu = 2353 \pm 10\,\text{cm.}^{-1}.$$

It is unfortunate that the contour of this band cannot be obtained. It might be expected to show "*P*" and "*R*" branches with no *Q* (see Discussion).

6·7μ region. This region was investigated using the 1200 grating in the second order. The pressure of C_2D_4 was 15·3 cm. Hg. As this band falls on the long wave-length side of a very strong water doublet centred at 6·26μ, water vapour in the atmosphere gives rise to a fluctuating background which makes accurate observation somewhat troublesome. For this reason several points on the *R*-branch are not shown as these coincided with strong water lines and were unreliable. However, by increasing the pressure and opening the slits to 1·0 mm. (5·5 cm.$^{-1}$) a satisfactory curve of the absorption in this region was obtained (see fig. 6). The band has a very sharp *Q*-branch, the position of the maximum of absorption being

$$6{\cdot}679 \pm 0{\cdot}005\mu = 1497{\cdot}3 \pm 1{\cdot}1 \text{ cm.}^{-1}.$$

Owing to the flat-topped nature of the *P* absorption the *P*-*R* separation can only be estimated very roughly as 50 cm.$^{-1}$. In fig. 6, as in figs. 7 and 9 which follow, regions of maximum absorption are given in duplicate. Such duplicate curves were obtained under similar conditions and are inserted as comparative evidence of different determinations of the position of absorption maxima.

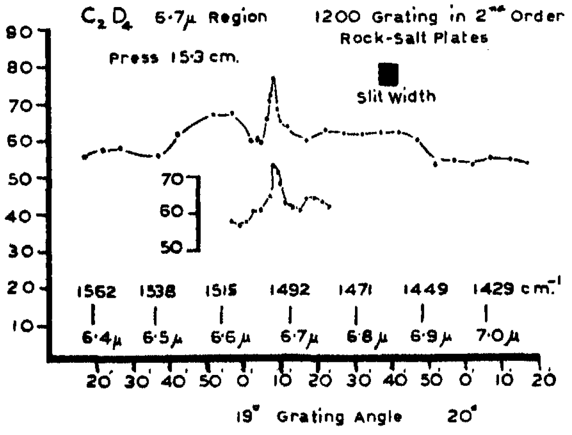

FIG. 6

8·0μ region. The absorption in this region was weak and in order to bring up the contour of the band the pressure was increased to 21·5 cm. Hg. The slit widths used were 2 cm.$^{-1}$. The contour of the band is shown in fig. 7. The centre of the *Q*-branch is at $7{\cdot}741 \pm 0{\cdot}001\mu = 1291{\cdot}8 \pm 0{\cdot}8$ cm.$^{-1}$.

9·5μ region. The gas pressure was 12·0 cm. Hg and the slit widths were 3·5 cm.$^{-1}$. The band (fig. 8) shows *P*, *Q* and *R* branches, the centre of the

Q-branch lying at $9{\cdot}254 \pm 0{\cdot}005\mu = 1080{\cdot}6 \pm 0{\cdot}7$ cm.$^{-1}$. The P-R separation is approximately 52 cm.$^{-1}$.

14μ region. The band in this region was much the strongest of all. The contour of this band was obtained under low dispersion (see above). The P-R separation in this case is about 58 cm.$^{-1}$. When examined under high resolution at a gas pressure of 3·8 cm. Hg with slit widths of 3 cm.$^{-1}$, the broad Q-branch showed two maxima of absorption (fig. 9). This doublet structure has been checked several times. The positions of the two maxima

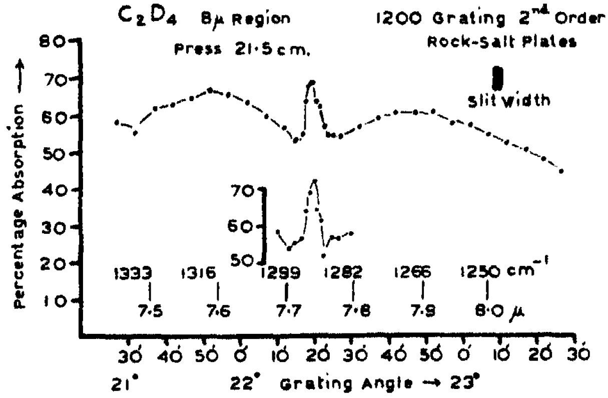

FIG. 7

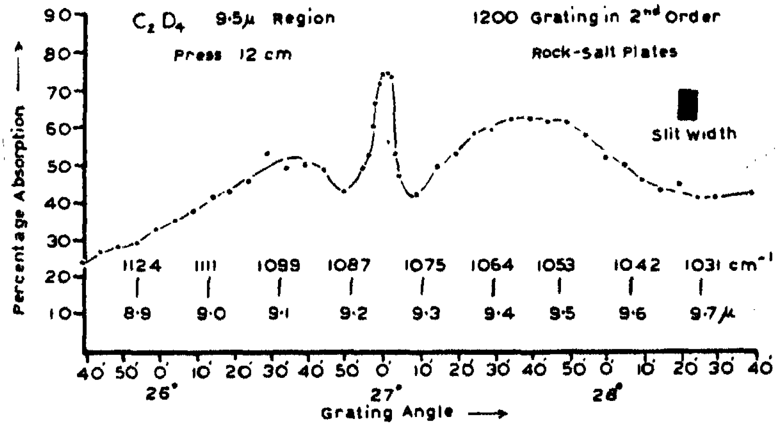

FIG. 8

are $$13{\cdot}757 \pm 0{\cdot}01\mu = 726{\cdot}9 \pm 0{\cdot}6 \text{ cm.}^{-1},$$

and $$13{\cdot}857 \pm 0{\cdot}01\mu = 721{\cdot}6 \pm 0{\cdot}6 \text{ cm.}^{-1}.$$

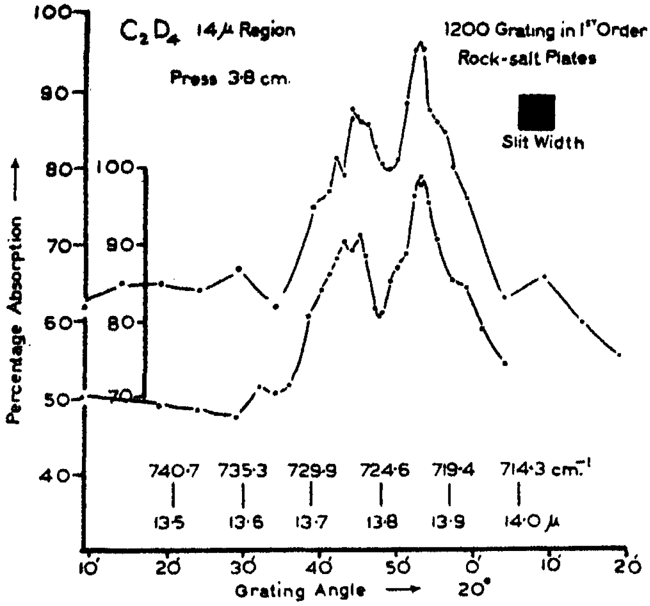

FIG. 9

DISCUSSION

The vibration spectrum of light ethylene C_2H_4

Before entering on a discussion of the above results it is necessary to review briefly our knowledge and the present interpretations of the vibration spectrum of C_2H_4. The data are summarized in Table II. The fundamental modes of vibration of the accepted planar model of ethylene are represented in fig. 10. The notation is a descriptive one based on the symmetry properties of the vibrations. This has been introduced, as hitherto authors have tended to adopt arbitrary numerical notations of their own which renders correlation extremely difficult. It is to be hoped that some such method of descriptive notation will soon become standardized. The principles on which it is based are essentially an extension of earlier notations of Mecke (1932) combined with the methods of symmetry groups:

ν denotes a vibration in which the motions of the atoms are essentially along the bonds joining the atoms;

δ denotes a vibration in which the motions of the atoms are essentially perpendicular to the bonds;

$+$ denotes that a reflection of the co-ordinates in a certain plane of symmetry leaves the vibration unaltered;

TABLE I. VIBRATION SPECTRUM OF C_2D_4

Centre of absorption in cm.$^{-1}$	722	727	1081	1292	1497	2199	2353	2970
Pressure in cm. Hg	3·8		12	21·5	15·3	12	3·8	8·2
Character	Q		Q	Q	Q	Q	?	Q
Raman frequencies in liquid in cm.$^{-1}$	780		981		1515	2251	2304	
Intensity	0		1·5		15	15	0·2	

Absorption data: this paper.
Raman data: de Hemptinne, Jungers and Delfosse (1938).

TABLE II. VIBRATION SPECTRUM OF C_2H_4*

Absorption centre (in gas) in cm.$^{-1}$	847	950	1444	1724	1890	2047	2326	2988	3107
Intensity	Very weak	Very strong	Strong	Very weak	Medium	Weak	Weak	Strong	Strong
Character	?	Broad Q	Sharp Q	?	Sharp Q	Sharp Q	?	Sharp Q	No Q

Raman lines:											
in gas (cm.$^{-1}$)	—	1343	—	1626	1656	2880	—	3020	—	3240	3272
in liquid (cm.$^{-1}$)	943	1341	1601	1621	1653	2870	2997	3008	3075	3230	3263
Intensity	Weak diffuse	Very strong	Very weak	Very strong	Weak	Weak	Very weak	Very strong	Weak diffuse	Very weak	Very weak

Absorption data: Levin and Meyer (1928); Coblentz (1905).
Raman data: Bhagavantam (1936); Dickinson, Dillon and Rassetti (1929); Glockler and Renfrew (1938); Bonner (1936).

* We have omitted frequencies over 4000 cm.$^{-1}$ which are obviously overtone or combination bands and do not come under consideration at the moment.

− denotes that the same operation alters the phase of the vibration by half a period.

The three planes of symmetry are:

(1) through the centre of symmetry and perpendicular to the C–C axis of the molecule;

(2) through the C–C axis and perpendicular to the plane of the molecule;

(3) the plane of the molecule.

It will be noticed that this still leaves two modes of vibration undifferentiated. We are, therefore, forced to introduce our sole numerical convention which is that when two or more vibrations are undifferentiated through their symmetry or physical properties* then the lowest one (numerically) of the set will be denoted by a suffix $_0$, the next by a suffix $_1$ and so on.

Selection rules

The selection rules for fundamental combination bands, which may be deduced by the methods of Tisza (1933), are very conveniently expressible in the above notation. Thus for a vibration to be active in absorption it must be antisymmetrical with respect to only one of the three planes, i.e. either $\omega(-++)$, $\omega(+-+)$ or $\omega(++-)$. These correspond to changes of electric moment respectively along the least, middle, and greatest axes of inertia. In order to find whether a combination or overtone band is active we multiply corresponding characters of the components together with the rule that

+ multiplied by + gives +
+ ,, − ,, −
− ,, − ,, +

e.g. $\omega(++-)+\omega(---)$ gives $\omega(--+)$, which would therefore be inactive in absorption.

The rules for the Raman-active frequencies are equally simple. Here one must have the vibration antisymmetric with respect to two or else none of the planes. The advantages of such a notation in which the activity of a combination band is at once clear by inspection are too obvious to require further comment.

To avoid needless discussion we shall simply remark that there is no controversy regarding the assignment of the three $(+++)$ frequencies, the two (− + +) frequencies, the δ(+ + −) frequency and ν(+ − +), the generally accepted values for which have been entered on fig. 10. The first frequency about which difference of opinion has existed is ν(− − +). Mecke (1932) and Teller and Topley (1935) have associated it with the Raman frequency at 3230 cm.$^{-1}$; later authors have preferred to assign it to the slightly stronger line at 3075 cm.$^{-1}$. More recently, Glockler and Renfrew (1938) have suggested that the earlier interpretation is the correct one as the Raman frequency at 3075 cm.$^{-1}$ is observable only in the liquid whereas that at 3230 cm.$^{-1}$ is observed both in the gas and in the liquid. They suggest that the Raman frequency 3075 cm.$^{-1}$ is really the frequency which appears strongly in the infra-red of the gas at 3107 cm.$^{-1}$, the difference being due to the change of state. We shall discuss the value of this

---

* It is not always possible to make the easy classification into valency and deformation vibrations which we have been able to do here. We suggest that the symbol ω be used to denote a vibration, the character of which is unspecified.

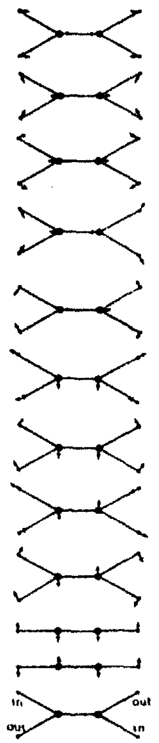

	Assignments	
	C_2H_4	C_2D_4
$\nu_0(+ + +)$	1626	1515
$\nu_1(+ + +)$	3020	2251
$\delta(+ + +)$	1343	981
$\nu(- + +)$	2988	2199
$\delta(- + +)$	1444	1081
$\nu(+ - +)$	3107	2353
$\delta(+ - +)$	(1020)	(727)
$\nu(- - +)$	(3075)	2304
$\delta(- - +)$	(1030)	(844)
$\delta(+ + -)$	950	722
$\delta(- + -)$	943	780
$\delta(- - -)$	(700)	(500)

FIG. 10. Normal modes of vibration of ethylene molecule. Assignments in brackets are still open to question.

fundamental frequency later. The next frequency $\delta(- - -)$ is very difficult to identify as it is inactive both in absorption and in scattering. It can only be deduced from combination bands or from data on specific heats. It has been assigned a value between 750 and 800 cm.$^{-1}$ by Eucken and Parts (1933) on the basis of their specific heat measurements. This assumes the allocation of the remaining frequencies made by Mecke. Any modification of his assignment must, therefore, affect this value. There remain three frequencies, viz. $\delta(+ - +)$, $\delta(- - +)$ and $\delta(- + -)$. These may be taken with $\delta(+ + -)$ and visualized as essentially the oscillations of the two CH_2 groups with respect to one another as units, the first two in the plane of the molecule, the latter two in and out of the plane of the molecule. The assignments suggested for them by the various authors are listed in Table III.

TABLE III. CONTROVERSIAL FREQUENCIES IN ETHYLENE

Frequency	Mecke (1932)	Bonner (1936)	Teller and Topley (1935)	Thompson and Linnett (1937)	Mannebach and Verleysen (1937)
$A\ \delta(+ - +)$	1100	950	730	950	950
$R\ \delta(- - +)$	970	950	1160	1160 (or 950)	950
$A\ \delta(+ + -)$	950	940	950	—	—
$R\ \delta(- + -)$	940	1100	1097	—	—

These are based on the experimental data in Table II and on different proposals for the internal force fields. Confining ourselves for the moment to the experimental data, we might remark that there is no justification for assigning the Raman line at 943 cm.$^{-1}$ to $\delta(- - +)$ in preference to $\delta(- + -)$ or vice versa. Both frequencies are permitted in the Raman effect. It is impossible in the present state of our knowledge to say which would be the more intense. The infra-red absorption band at $10{\cdot}5\mu$ has a very definite and intense Q-branch. Of the two frequencies $\delta(+ - +)$ and $\delta(+ + -)$, the latter only may be expected to exhibit a Q-branch (cf. Dennison 1931). There is, therefore, no ambiguity in this case. We must assign the value 950 cm.$^{-1}$ to $\delta(+ + -)$. The contour of $\delta(+ - +)$ ought to resemble that of the infra-red band at 3107 cm.$^{-1}$ since this fundamental possesses the same symmetry, i.e. it should show a doublet structure. There is no other band in the ethylene spectrum except the weak one at 847 cm.$^{-1}$ which might be assigned to this fundamental. The authors who have assigned the value 950 cm.$^{-1}$ to this fundamental have assumed that it overlies the band due to $\delta(+ + -)$. Until more details of the rotational structure are available, and these have been explained in detail, it is not possible to say whether this is the case or not. It certainly is a possibility which cannot be discarded. It will be observed that although the assignments differ in detail they have one property in common. The sums $\delta(+-+)+\delta(--+)$ and $\delta(++-)+\delta(-+-)$ add up to either about 1900 or 2050 cm.$^{-1}$. The reason for this is that there are two absorption bands, the Q-branches of which are at exactly those frequencies. The structure of those bands is such that the vibrations corresponding to them must have the symmetry $(-++)$ and since these are the only two simple combinations of the twelve fundamentals which will give frequencies of this order of magnitude, any assignment of these four fundamentals must satisfy this requirement.

There are, however, other weak bands which seem to have been neglected in any discussion of the fundamental frequencies. These lie at 847, 1724 and 2326 cm.$^{-1}$. It is unfortunate that the contours of those bands are not known and, in the case of the latter two, will be difficult to obtain, since they coincide with strong atmospheric absorption due respectively to water and carbon dioxide. Even though the contour is unknown, the mere existence of those bands is sufficient proof that none of the above assignments is satisfactory since none will give a simple explanation of them as combination bands.

The vibration spectrum of heavy ethylene (C_2D_4)

We can now consider the interpretation of our experimental results and particularly what light they can throw on the above difficulties. It is convenient to summarize first the relations which may be expected between the corresponding frequencies in the isotopic molecules. These may be derived from the equations of Mannebach and Verleysen (1937) or from Redlich's (1935) general theory. They relate the products of corresponding frequencies as follows:

$$\frac{\Pi(+++)_H}{\Pi(+++)_D}=\frac{m_D}{m_H};\quad \frac{\Pi(--+)_H}{\Pi(--+)_D}=\sqrt{\frac{m_D\mu'_D}{m_H\mu'_H}};$$

$$\frac{\Pi(-++)_H}{\Pi(-++)_D}=\frac{\Pi(+-+)_H}{\Pi(+-+)_D}=\sqrt{\frac{m_D\mu_D}{m_H\mu_H}};$$

$$\frac{\delta(++-)_H}{\delta(++-)_D}=\sqrt{\frac{\mu_D}{\mu_H}};\quad \frac{\delta(-+-)_H}{\delta(-+-)_D}=\sqrt{\frac{\mu''_D}{\mu''_H}};$$

$$\frac{\delta(---)_H}{\delta(---)_D}=\sqrt{\frac{m_D}{m_H}},$$

where

$$\frac{1}{\mu_{\mathrm{H}}} = \frac{1}{m_{\mathrm{H}}} + \frac{2}{M_{\mathrm{C}}},$$

$$\frac{1}{\mu'_{\mathrm{H}}} = \frac{1}{m_{\mathrm{H}}} + \frac{2}{M_{\mathrm{C}}}\left\{1 + \frac{4l^2}{L^2} + \frac{4l}{L}\cos\frac{\alpha}{2}\right\},$$

$$\frac{1}{\mu''_{\mathrm{H}}} = \frac{1}{m_{\mathrm{H}}} + \frac{2}{M_{\mathrm{C}}}\left\{1 + \frac{2l}{L}\cos\frac{\alpha}{2}\right\}^2,$$

and similarly for μ_{D}, μ'_{D} and μ''_{D}. Here also m_{H} is the mass of a hydrogen atom, M_{C} is the mass of a carbon atom, l is the CH distance, L is the CC distance, α the HCH angle. The values of the last three are known with sufficient accuracy for our purpose (Penney 1937).

The assignment of the four fundamentals, $\delta(+\,+\,-)$, $\nu(-\,+\,+)$, $\delta(-\,+\,+)$ and $\nu(+\,-\,+)$, to the absorption bands with centres respectively at 722, 2190, 1081 and 2353 cm.$^{-1}$ is so obvious as hardly to need further discussion. The contours and intensities are correct: the numerical values of the first three give excellent agreement when substituted in the above isotopic relations. In the case of $\nu(+\,-\,+)$ it is not possible to apply that check since $\delta(+\,-\,+)$ is unlocated. It seems to us that the location of this frequency is the crux of the whole ethylene problem. At first it seemed a good opportunity to test the various potential functions since each of these gave a rather different value for $\delta(+\,-\,+)_{\mathrm{D}}$ on the assumption that $\delta(+\,-\,+)_{\mathrm{H}}$ was at 950 cm.$^{-1}$. These are tabulated below:

TABLE IV

	Mannebach and Verleysen (1937)	Tchang (1938)	Bonner (1936)	Thompson* and Linnett (1937)	Fox and Martin (1938)
$\delta(+\,-\,+)_{\mathrm{D}}$	678	693	757	742	670

Bands were looked for in all of these regions without success although it should be recalled that since $\delta(+\,-\,+)$ is weak in C_2H_4 it will probably also be weak in C_2D_4. The combination and overtone bands observed in C_2D_4 do not give much help at this stage and we shall return to them later. What is significant is that the band at 722 cm.$^{-1}$ appears to be double. There is a distinct second Q-branch at 727 cm.$^{-1}$. It is extremely difficult to find an interpretation of this band unless it be the missing fundamental. Such a low frequency cannot be a summation band: it turns out that it cannot be interpreted as a difference band either, assuming that the fundamentals have the values in Table VII. One other possibility would have been that it was $2\delta(+ + -) - \delta(+ + -)$ but such a difference band would be expected to lie on the low frequency side of the main fundamental and would hardly have such an intensity at ordinary temperatures.

---

* In a letter to *Nature* (1937) giving our preliminary results we quoted 1016 cm.$^{-1}$ as this value. This was due to a slip in Thompson and Linnett's paper in a table where they give a correlation of their results with Mannebach and Verleysen's.

There is one serious objection to this assignment—the presence of a Q-branch. This would be forbidden on a strict application of Dennison's (1931) patterns for the structure of the bands of an asymmetrical rotator. Now those certainly seem to hold qualitatively in the case of C_2H_4, but it should be remembered that for C_2D_4 the moments of inertia are larger and consequently more rotational levels will be excited. Since Dennison's calculations only go up to $J = 4$, we cannot rely on them completely. The very important case of the two analogous vibrations in formaldehyde should be compared. These are essentially due to the oscillations of the CH_2 group as a unit (*a*) in the plane of the molecule but perpendicular to the symmetry axis, (*b*) in and out of the plane of the molecule. These have been identified by Ebers and Nielsen (1937) (*a*) at 1278 cm.$^{-1}$, (*b*) at 1165 cm.^{1} and each exhibits a Q-branch owing to rotational coupling between the neighbouring frequencies. When we recall that the oxygen atom is spectroscopically practically equivalent to a CH_2 group it is more than plausible that the corresponding bands in ethylene should resemble those in structure.

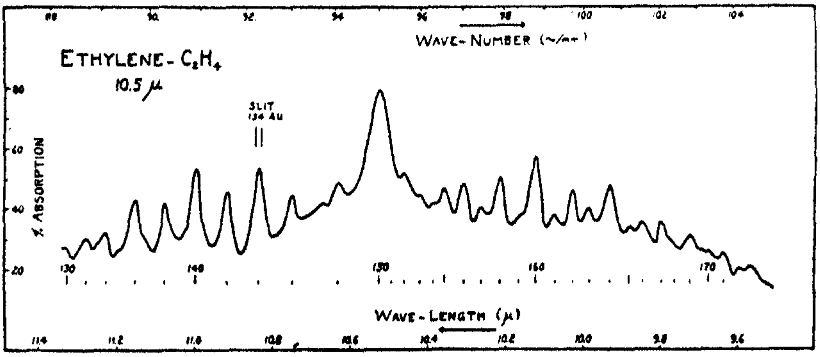

FIG. 11

Accepting this value of 727 cm.$^{-1}$ for $\delta(+ - +)$ in C_2D_4 we now use the isotopic equations to find its value in C_2H_4. We find the value 1017 cm.$^{-1}$. That this value is at least a reasonable one may be seen by an examination of the absorption of C_2H_4 in this region. The absorption curve due to Levin and Meyer (1928) is reproduced in fig. 11. It should be noted that the R side of the band extends over 100 cm.$^{-1}$ (from 950 to 1050 cm.$^{-1}$) whereas the *P* side extends only over 70 cm.$^{-1}$. This is very unusual; one normally finds the positive side covers a smaller frequency range than the negative because of the convergence due to interaction between rotation and vibration. The abnormal extension of the C_2H_4 band at 10·5μ on the high frequency side is an indication that another weak band is overlapping there. Taking the value 1020 cm.$^{-1}$ as a sufficiently good approximation for $\delta(+-+)_H$ the value of $\delta(--+)_H$ must be either 1030 or 880 cm.$^{-1}$ according to the interpretation of the bands at 2045 and 1900 cm.$^{-1}$. The former of those alternatives is to be preferred (*a*) because the weaker of the two combination bands at 2047 cm.$^{-1}$ is more likely to be derived from the weaker of the two fundamentals, (*b*) because the alternative assignment leads to anomalies and contradictions, as the reader may readily verify, (*c*) because the consequent assignments of $\delta(++-)_D$ and $\delta(-+-)_D$ give excellent agreement, as we shall now show.

Starting from the assumption that

$$\delta(++-)_H = 950\ \text{cm.}^{-1} \quad \text{and} \quad \delta(-+-)_H = 940\ \text{cm.}^{-1},$$

we obtain from the isotopic equations

$$\delta(++-)_D = 720\ \text{cm.}^{-1} \quad \text{and} \quad \delta(-+-)_D = 782\ \text{cm.}^{-1}.$$

Experimentally, a strong absorption band with a *Q*-branch is found at 722 cm.$^{-1}$, a Raman line at 780 cm.$^{-1}$, and a combination band in the infra-red at 1497 cm.$^{-1}$ having the contour expected for $\delta(++-)+\delta(-+-)$.

It remains to evaluate $\delta(--+)_D$, since the weak combination band in C_2D_4 which corresponds to the band at 2047 cm.$^{-1}$ in C_2H_4 has not been picked up with the limited amount of gas at our disposal. We therefore use the isotopic equations quoted and the values $\nu(--+)_H = 3060$ cm.$^{-1}$, $\nu(--+)_D = 2304$ cm.$^{-1}$ and $\nu(--+)_H = 1030$ cm.$^{-1}$. This yields $\delta(--+)_D = 844$ cm.$^{-1}$. The results of this discussion are summarized in Table V below:

TABLE V

	$\delta(+-+)$	$\delta(--+)$	$\delta(++-)$	$\delta(-+-)$
C_2H_4	1020	1030	950	940
C_2D_4	727	844	722	780

Confirmation of these assignments can best be sought by seeing whether hitherto unexplained bands in the spectra of C_2H_4 can now be accounted for as simple combination bands compatible with the selection rules. In doing so, however, it must be remembered that the assignments of $\nu(--+)$

and $\delta(---)$ are still open to question. In estimating $\delta(--+)_D$ we took the former to be 3070 cm.$^{-1}$ as opposed to the other possible value of 3272 cm.$^{-1}$. This has still to be justified. The combination bands are tabulated below with their characteristics as far as known; alongside each are put the possible interpretations consistent with the selection rules. It will at once be observed that no interpretation is offered for the very weak absorption found by Coblentz (1905) at 847 cm.$^{-1}$. It cannot be fitted into the present scheme as a reasonable difference band; the only explanation is that it is a fundamental. This seems very unlikely in view of the observation of Levin and Meyer (1928) that "although slight general absorption existed in this region, no fine structure could be found". Until further investigation shows this to be a real band with structure resembling the other ethylene bands, we must conclude that its presence was due to impurity. The assignment given to 1601 cm.$^{-1}$ has already been suggested by Glockler and Renfrew (1938). The interpretation of the additional Raman line at 1653 cm.$^{-1}$ requires that $\delta(---)$ be lowered to about 700 cm.$^{-1}$. The same applies in the interpretation of the frequency at 3263 cm.$^{-1}$. The excellent agreement obtained in the interpretation of the band at 4515 cm.$^{-1}$ is regarded as a strong proof that $\nu(--+)$ lies at 3070 cm.$^{-1}$ and not 3263 cm.$^{-1}$ and explains why that value was chosen above in the estimation of $\delta(--+)_D$. The only other assignments requiring discussion are the alternatives proposed for the absorption at 4324 cm.$^{-1}$. Of the two, $\delta(+++)+3\delta(+-+)$ seems

TABLE VI. INTERPRETATION OF C_2H_4 SPECTRUM

Position	Character	Interpretation	Predicted
847	Very weakly active in absorption. Contour structureless	Impurity	—
1601	Very weak in Raman	$\nu_0(+++)$ for $C^{12}C^{13}H_4$	1601
1653	Weak in Raman	$\delta(---)+\delta(++-)$	1650
1724	Very weak in absorption. Contour unknown	$\delta(---)+\delta(--+)$	1730*G*
2326	Weak in absorption. Contour unknown	$\delta(+-+)+\delta(+++)$	2363*M*
3230	Very weak in Raman	$2\nu_0(+++)$	3252
3263	Very weak in Raman	$2\{\delta(---)+\delta(++-)\}$	3300
4307	Very weak in absorption. Doublet	$\delta(+-+)+2\nu_0(+++)$	4272*M*
4324	Weak in absorption. Doublet?	$\delta(+++)+3\delta(+-+)$	4403*M*
		$\nu(-++)+\delta(+++)$	4350*L*
4515	Weak in absorption. Doublet	$\nu(--+)+\delta(-++)$	4519*M*
4729	Very weak in absorption. Doublet	$\nu(+-+)+\nu_0(+++)$	4733*M*

The letters *L*, *M* and *G* in the last column indicate that the change of electric moment is respectively along the least, middle or greatest axis of inertia.

the more likely, since $\delta(+\,+\,+)+\delta(+\,-\,+)$ has presumably already been observed at 2326 cm.$^{-1}$, while the other assignment means assuming that a very weak absorption near the centre of the band is a Q-branch. We are now in a position to interpret the spectrum of C_2D_4.

There are only three bands to be considered, the small amount of C_2D_4 available militating against the detection of more combination frequencies. Of these we have already discussed the band at 1497 cm.$^{-1}$. The other low frequency band at 1292 cm.$^{-1}$ is more difficult to interpret; the only possible combination of C_2D_4 frequencies which is active in absorption in this region is $\delta(-\,-\,-)+\delta(-\,-\,+)$. This should be close to 1344 cm.$^{-1}$ if we take $\delta(-\,-\,-)_D$ as being $1/\sqrt{2}$ times $\delta(-\,-\,-)_H$ (700 cm.$^{-1}$) and $\delta(-\,-\,+)_D$ equal to 844 cm.$^{-1}$. Since neither of the latter two values are experimental one cannot expect too close agreement. On the other hand, the possibility that this weak band is due to the presence of some C_2HD_3 and $C_2H_2D_2$ cannot be ruled out. There was about 10 % of H present and one of the most prominent bands of any of the mixed molecules would be that due to the deformation vibration of the CHD group. This is known to lie just under 1300 cm.$^{-1}$ from investigations on Raman spectra (de Hemptinne *et al.* 1938). The remaining band at 2970 cm.$^{-1}$ is readily interpreted as

$$\nu(+\,+\,+)+\delta(+\,+\,-),$$

although this should only be regarded as the assignment for the strong Q-branch at this point. The width of the absorption in this region is such that other combination bands must be present such as

$$\nu(-\,-\,+)+\delta(-\,-\,-),$$

but without a knowledge of the contours there is little point in going through the possible combinations.

TABLE VII. COMBINATION BANDS IN C_2D_4 SPECTRUM

Position	Character	Interpretation	Predicted
1292	Very weak in absorption Q	C_2HD_3 or	1262
		$\delta(-\,-\,-)+\delta(-\,-\,+)$	1344*G* (approx.)
1497	Weak in absorption Q	$\delta(+\,+\,-)+\delta(-\,+\,-)$	1502*L*
2970	Medium intensity in absorption Q	$\nu(+\,+\,+)+\delta(+\,+\,-)$	2981*G*

GENERAL CONCLUSIONS

The main conclusion to be drawn from the above results and discussion is that the fundamental frequencies of ethylene are not yet definitely settled. It is quite certain that all the current assignments are wrong; moreover, the question whether the new set of fundamentals proposed here is the correct one or not will best be settled by more experimental work on the weak combination bands in both C_2H_4 and C_2D_4. Calculations, even with the most complex sort of potential function, are in danger of being a waste of time until more experimental data are available. In this connexion we would refer to a recent publication by Fox and Martin (1938) in which the authors claim to have established the frequency $\delta(--+)$ for C_2H_4 at 1215 cm.$^{-1}$. Their argument is very doubtful for two reasons. First it is based on the assumption that $\delta(+-+) = 950$ cm.$^{-1}$, an assumption which we have shown is completely unjustified. Secondly, the potential function takes no account of interactions between the two CH_2 groups (i.e. terms of the form $\Delta\phi_1\Delta\phi_2$ in their function are neglected). Yet in the analogous oscillations of the CH_2 groups out of the plane $\delta(++-)$ and $\delta(-+-)$ such a type of interaction term is very appreciable. Finally, the values they assume make it quite impossible to explain the band at 2047 cm.$^{-1}$.

We have actually considered the possibility of $\delta(--+)$ being approximately equal to 1200 cm.$^{-1}$ but for a different reason. If one takes the weak band as 847 cm.$^{-1}$ as $\delta(+-+)$ then $\delta(--+)$ would have to be at 1200 cm.$^{-1}$ in order to account for the band at 2047 cm.$^{-1}$. The objections to such an assignment are:

(1) those raised earlier to treating 850 cm.$^{-1}$ as a fundamental,

(2) it gives $\delta(+-+)_D = 600$ cm.$^{-1}$ and so leaves the Q-branch at 727 cm.$^{-1}$ unexplained,

(3) it makes the specific heat much too high unless of course $\delta(---)$ is made very much higher.

These objections, while strong, are not quite sufficient to rule out this as a possible assignment since it may be verified by the reader that practically all the combination bands can be accounted for, provided a judicious choice of the value of $\delta(---)$ is made. Incidentally, the question of the specific heat is another objection which may be raised against our proposed assignment, since it yields values fairly consistently above the experimental ones by about 1 %. This is possibly not so serious as it sounds since Eucken and Parts (1933), after choosing $\delta(---)$ to fit their lower range of values of C_p, found that for higher temperatures the experimental values were consistently about 1 % lower than the theoretical ones.

It remains to test the various potential functions which have been proposed for ethylene on such of the frequencies of C_2D_4 as can be assigned without doubt. This is done in Table VIII. It should be remembered that this is a test of an assignment of frequencies (see Table III) as well as a test of a potential function. Actually, however, the variation in the assignment applies only to $\delta(+\,-\,+)$ and $\delta(+\,+\,-)$ and, in our table only to $\delta(+\,-\,+)$ since $\delta(+\,+\,-)$ is in a class by itself. Thus it appears from the infra-red data there is little to choose between three of the four functions proposed but that Linnett and Thompson's function is definitely very poor. For completeness one should include the Raman frequencies, but these have already been discussed by de Hemptinne and his co-workers (1938). Moreover, we are convinced that a detailed discussion of potential functions is rather unprofitable until the assignment of the three doubtful frequencies $\delta(+\,-\,+)$, $\delta(-\,-\,+)$ and $\delta(-\,-\,-)$ has been accomplished with absolute certainty.

TABLE VIII. VALUES OF C_2D_4 VIBRATION FREQUENCIES PREDICTED ON VARIOUS THEORIES

Mode of vibration	Mannebach and Verleysen (1937)	Sutherland and Dennison (1935)	Bonner (1936)	Thompson and Linnett (1937)	Observed value
$\nu(-\,+\,+)$	2153 (1·9)	2220 (0·9)	2150 (1·9)	2101 (3·7)	2199
$\delta(-\,+\,+)$	1073 (0·8)	1055 (2·5)	1071 (0·8)	1187 (10·6)	1081
$\nu(+\,-\,+)$	2325 (1·2)	—	2305 (2·3)	2323 (1·2)	2353 ± 10
$\delta(+\,+\,-)$	—	720 (0·3)	505 (29)	—	722

Figures in brackets give percentage difference between calculated and observed values.

This research was made possible through the receipt of certain grants which we now gratefully acknowledge. In the construction of the spectrometer and its accessories generous grants were made to one of us (G.B.B.M.S.) by the Royal Society, and from the Rouse Ball Fund by Trinity College, while the other author is indebted to Sidney Sussex College and to the Department of Scientific and Industrial Research for maintenance grants.

APPENDIX

Table giving the chief notations used for the vibration frequencies of ethylene

Descriptive notation			Numerical notation			Symmetry type	
Conn and Sutherland (1939)	Mecke (1932)	Teller and Topley (1935)	Sutherland and Dennison (1935)	Thompson and Linnett (1937) Fox and Martin (1938)	Manneback and Verleysen (1936)	Tisza (1933)	Kohlrausch (1938)
$\nu_0(+++)$	$\nu_0(\pi, s)$	ν_t^{CC}	ν_8	ν_3	ν_3	A_{1g}	A_{1g}
$\nu_1(+++)$	$\nu_1(\pi, s)$	ν_t^{CH}	ν_2	ν_1	ν_1	A_{1g}	A_{1g}
$\delta(+++)$	$\delta(\pi, s)$	$\nu_t^{CH_2}$	ν_4	ν_2	ν_2	A_{1g}	A_{1g}
$\nu(-++)$	$\nu(\pi, a)$	ν_x^{CH}	ν_1	ν_4	ν_4	A_{2u}	B_{3u}
$\delta(-++)$	$\delta(\pi, a)$	$\nu_\alpha^{CH_2}$	ν_3	ν_5	ν_5	A_{2u}	B_{3u}
$\nu(+-+)$	$\nu(\sigma, a)$	ν_β^{CH}	ν_5	ν_6	ν_8	B_{1u}	B_{2u}
$\delta(+-+)$	$\delta(\sigma, a)$	ν_β^{M}	ν_9	ν_7	ν_9	B_{1u}	B_{2u}
$\nu(--+)$	$\nu(\sigma, s)$	$\nu_{\alpha\beta}^{CH}$	ν_6	ν_8	ν_6	B_{2g}	B_{1g}
$\delta(--+)$	$\delta(\sigma, s)$	$\nu_{\alpha\beta}^{M}$	ν_{10}	ν_9	ν_7	B_{2g}	B_{1g}
$\delta(++-)$	$\delta'(a)$	ν_γ^{M}	ν_{11}	—	—	B_{2u}	B_{1u}
$\delta(-+-)$	$\delta'(s)$	$\nu_{\alpha\gamma}^{M}$	ν_{12}	—	—	B_{1g}	B_{2g}
$\delta(---)$	$\delta(a)$	$\nu_{\alpha\beta\gamma}^{M}$	ν_7	—	—	A_{1u}	A_{1u}

REFERENCES

Bhagavantam, S. 1936 *Nature, Lond.*, **138**, 1096.
Bonner, L. G. 1936 *J. Amer. Chem. Soc.* **58**, 34.
Coblentz, W. W. 1905 *Publ. Carneg. Instn*, **35**.
Dennison, D. M. 1931 *Rev. Mod. Phys.* **3**, 280.
Dickinson, R. G., Dillon, R. T. and Rassetti, F. 1929 *Phys. Rev.* **34**, 582.
Delfosse, J. M. 1935 *Ann. Soc. Sci. Brux.* **55**, 114.
Ebers, E. S. and Nielsen, H. H. 1937 *J. Chem. Phys.* **5**, 823.
— — 1938 *J. Chem. Phys.* **6**, 311.
Eucken, A. and Parts, F. 1933 *Z. phys. Chem.* B, **20**, 184.
Fox, J. J. and Martin, A. E. 1938 *Proc. Roy. Soc.* A, **167**, 257.
Glockler, G. and Renfrew, M. M. 1938 *J. Chem. Phys.* **6**, 170 and 409.
Hemptinne, M. de, Jungers, J. and Delfosse, J. M. 1938 *J. Chem. Phys.* **6**, 319.
Kohlrausch, K. W. L. 1938 *Der Smekal-Raman-Effekt.*
Levin, A. and Meyer, C. F. 1928 *J. Opt. Soc. Amer.* **16**, 137.
Mannebach, C. and Verleysen, A. 1936 *Ann. Soc. Sci. Brux.* **56**, 349.
— — 1937 *Ann. Soc. Sci. Brux.* **57**, 31.
Mecke, R. 1932 *Z. phys. Chem.* B, **17**, 1.
Nielsen, H. H. 1937 *J. Chem. Phys.* **5**, 818.
Penney, W. G. 1937 *Proc. Roy. Soc.* A, **158**, 306.
Redlich, O. 1935 *Z. phys. Chem.* B, **28**, 371.
Redlich, O. and Tompa, H. 1937 *J. Chem. Phys.* **5**, 529.
Sutherland, G. B. B. M. and Dennison, D. M. 1935 *Proc. Roy. Soc.* A, **148**, 250.
Sutherland, G. B. B. M. and Conn, G. K. T. 1937 *Nature, Lond.*, **140**, 644.
Tchang, Yong-Li 1938 *Ann. Soc. Sci. Brux.* **58**, 87.
Tisza, L. 1933 *Z. Phys.* **82**, 48.
Teller, E. and Topley, B. 1935 *J. Chem. Soc.* p. 885.
Thompson, H. W. and Linnett, J. W. 1937 *J. Chem. Soc.* p. 1376.

Some observations on cosmic rays using a large randomly operated cloud chamber

By E. J. Williams

University College of Wales, Aberystwyth, formerly Leverhulme Foundation Fellow and Lecturer, University of Liverpool

(*Communicated by J. Chadwick, F.R.S.—Received* 13 *March* 1939)

[Plates 9, 10]

Cloud-chamber photographs of cosmic rays obtained with a counter-controlled chamber do not represent the normal relative frequency of the different types of particles and of particles of different energy present in this radiation. There is, for instance, a strong bias in favour of "shower" electrons, while low-energy particles, owing to their limited effective range, are under represented. A knowledge of the true statistical distribution of events in cosmic rays is now becoming desirable, and this can only be obtained from photographs of tracks produced during random expansions. For this, and for certain other reasons, it was considered worth while to revert to the use of the randomly operated chamber for certain cosmic-ray investigations.* The main objection to its use, viz. its very low efficiency, may be overcome by increasing the size of the chamber. The average number of cosmic-ray tracks recorded per expansion increases roughly as the fourth power of the linear dimensions of the chamber, and it was estimated that a chamber about a foot in diameter and a foot deep would on the average record one or two cosmic-ray tracks every photograph. A cloud chamber of these dimensions was constructed and was found to fulfil expectations. In this paper an account of it is given and of some results obtained by its use. These results are of a preliminary nature. More extensive observations on the various effects discussed will be made with a still larger chamber which is now under construction.

The results given in this paper are mainly concerned with the relative number and the spectrum of cosmic-ray particles with energy below 10^8 V—the region of energy where a counter-controlled chamber exerts most strongly its selective action. The evidence for mesotrons ("heavy electrons") obtained earlier by Williams and Pickup (1938) was obtained in experiments with the chamber described here. A fuller account of certain details connected with this work is given in the present paper, together with a discussion of the relative number of slow mesotrons in cosmic rays at sea-level. I wish to thank Mr Pickup for his permission to reproduce here the mesotron tracks observed in our work.

---

* Schneider has recently (1938) published an account of observations made with a randomly operated chamber, the method being chosen for much the same reasons as those we have mentioned here. The results obtained by him will be referred to later in this paper.

1. DESCRIPTION OF CLOUD CHAMBER

The essential parts of the cloud chamber used in the present work are shown in fig. 1. The main compartment *A*, where the tracks are formed, is cylindrical, about 30 cm. in diameter and 30 cm. long. Before an expansion is made the rubber diaphragm *B* is close to the perforated brass plate *C*, the valve *D* is shut and the reservoir *E* partially evacuated. To operate an expansion the catch *F* is knocked in the direction of the arrow. This opens the valve, and the rubber diaphragm falls on to the perforated brass plate *G*. Most of the photographs were taken with ethyl alcohol vapour as condensant, the expansion ratio for which is about 1·16.

The side of *C* facing *A* is covered with black velvet, which prevents irregular motion of the gas in *A* during an expansion and provides a dark background for the tracks. The camera used had lenses of focal length, *f*, of 12 cm., and an aperture of *f*/5·8. It was focused on the plane *J* between the magnetic field coils *H*. With a magnification of 0·28, such as was chosen, the effective depth of focus was about 5 cm.

To avoid distortion of the tracks by convection currents it is very important that the walls of the chamber be kept at a uniform temperature (cf. Blackett and Wilson 1937), a variation of half a degree or so being the limit tolerable. In view of this the brass formers containing the field coils (the inside of which are within 2 cm. of the chamber walls) were kept at room temperature by passing water through the copper tubes *K* soldered to the side of the formers. With this precaution the distortion of the tracks (the estimate of which is described in the next section on the spectrum) corresponded in general to a radius of curvature (in the chamber) greater than 7 m., i.e. to a dip in an arc 10 cm. long of less than 0·18 mm. Convection currents set up as the result of the expansion are confined, during the sensitive time of the chamber, to a region close to the walls and do not give any trouble.

A mechanical method of timing the various events in the operation of the chamber proved quite satisfactory. With the arrangement used the timing could be reproduced at long intervals with an accuracy of at least 0·01 sec. This reproducibility is important, especially when the chamber is used for determining decay periods of long-lived radioactive substances, and it is doubtful if an electrical method of timing would be equally reliable. The chamber described here has been used for this purpose, the radioactive substance being mounted inside the chamber as shown in the figure (Walke, Williams and Evans 1939).

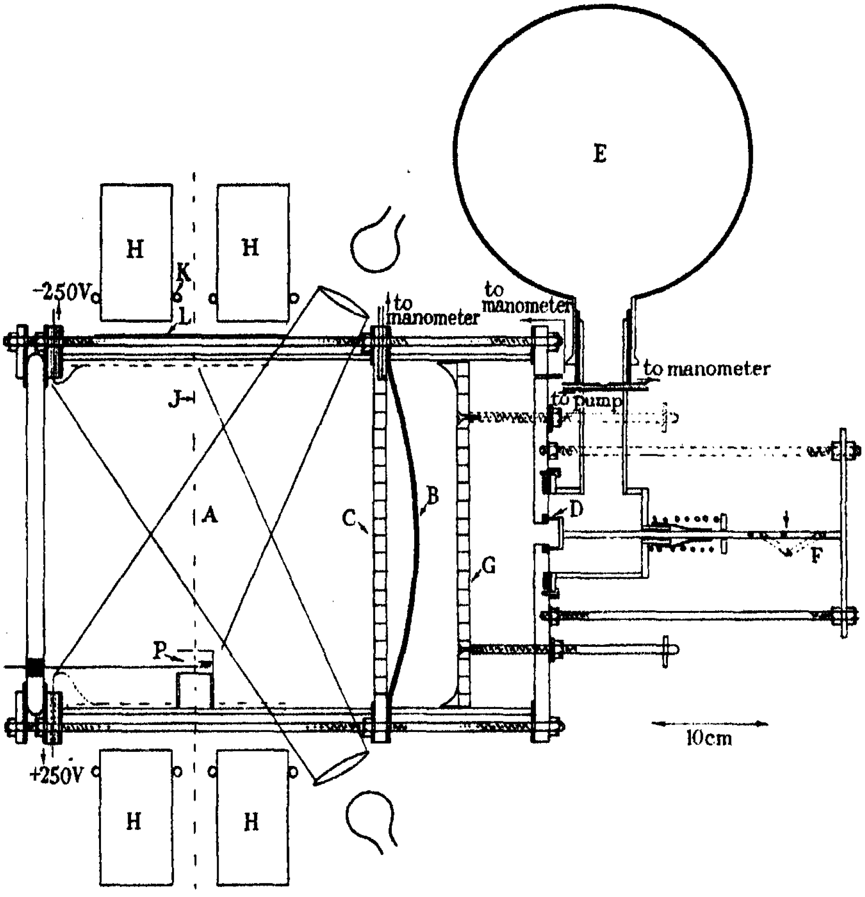

Fig. 1. Diagram of cloud chamber.

The interval of time after an expansion during which the supersaturation remains sufficient to cause condensation on ions—the sensitive time of the chamber—was determined by counting the tracks from a radioactive source which was uncovered at different times after the expansion, the expansion ratio used being the maximum consistent with not giving a general cloud. It was found to be about 0·4 sec., which is about 20 times greater than the sensitive time of an ordinary sized chamber about 4 cm. deep.

In a note to be published elsewhere (Williams 1939) it is shown that if we neglect the motion of the gas near the walls due to local turbulence set up during the expansion, or to convection currents, the sensitive time of a chamber is

$$\tau = 0{\cdot}77(\rho C/k\,\overline{\gamma - 1}^2)\,(V/S)^2\,(\delta r/r)^2, \tag{1}$$

where ρ is the density of the gas in the chamber, C its specific heat at constant pressure, γ the ratio of its specific heats, and k its thermal conductivity. V is the volume of the chamber after expansion and S the total surface area. $(1+r)$ represents the expansion ratio, and δr the difference between the expansion ratio which is just sufficient to give tracks and that which begins to give general cloud. For an ordinary sized chamber, say 4 cm. deep and 16 cm. diameter, (V/S) is about 1·3 cm. For the large chamber described here its value is about 4 cm. Thus according to (1) the latter should have a 10 times greater sensitive time. This is in rough agreement with the relative values actually observed.

For oxygen or air, at normal pressure, the absolute value of τ according to (1) is

$$30(V/S)^2\,(\delta r/r)^2, \quad = 500(\delta r/r)^2$$

for the present chamber. The value of $(\delta r/r)$ corresponding to the observed value of τ, viz. 0·4 sec., is therefore 0·03. This estimate agrees, at least in order of magnitude, with the actual value of $(\delta r/r)$. Specific observations on the latter were not made. This agreement indicates that the effects of air currents and of radiation left out in the derivation of (1) do not increase appreciably the conduction of heat from the walls. It should be noted that in (1) it is also assumed that the expansion itself is adiabatic. This is in effect satisfied provided the expansion takes a time small compared with τ, which was the case in the present experiments.

The average number, N, of cosmic-ray tracks recorded in a cloud-chamber photograph is approximately equal to $nA\tau$, where n is the number of cosmic-ray particles/sq. cm./sec., and A is the area of the horizontal projection of the volume of the chamber photographed. $A = dD$, where d is the diameter of the region photographed, and D is the depth of focus. At sea-level n is about 0·03. For the present chamber $d \sim 24$, $D \sim 5$, $\tau \sim 0{\cdot}4$. Thus $N \sim 1{\cdot}5$, which agrees roughly with the observed value. The large sensitive time and volume of the chamber also makes it a very sensitive detector of radiations from radioactive substances.

It should be noted that the use of a large chamber to give a long sensitive time ensures that during this time convection currents set up by the warming of the gas do not reach far from the walls of the chamber. In this respect besides providing a large sensitive volume the method is much superior to that in which the sensitive time is increased by following the main expansion (in a smaller chamber) by another expansion made at such a rate as to maintain the necessary supersaturation. The latter method (as has been shown by Bearden (1935) and Frisch (1935)) is quite effective in increasing the sensitive time, and could, of course, be incorporated in the present chamber to give a still larger sensitive time.

2. ENERGY SPECTRUM OF COSMIC-RAY PARTICLES BELOW 3×10^8 V

All tracks with a photographed length (projected on the plane of the chamber) greater than 9 cm. were included in these measurements. All tracks shorter than this, through leaving the field of view* or becoming blurred by going out of focus, were left out on account of the greater uncertainty in their curvature. This uncertainty arises from their finite thickness, and sometimes from distortion produced by motion of the gas in the chamber, which takes place when the temperature of the walls is not sufficiently uniform. For a long track this distortion is not equivalent to a uniform curvature. It is generally localized to a portion of the track and therefore detectable as such. In nearly all cases, however, the curvature was calculated from the deviation of the middle point of the track from the straight line joining its ends. No diffused tracks, i.e. tracks which passed through the chamber before the expansion, were included in the measurements. The number of tracks which thus qualified for inclusion in the spectrum was about 600. For the majority of these (series A), the magnetic field used was about 2200 G, and it was about 1000 G for the remainder (series B).

The tracks were divided into five groups corresponding to the following ranges of energy (E), expressed in electron-volts: 3×10^6–10^7, 10^7–3×10^7, 3×10^7–10^8, 10^8–3×10^8, $> 3 \times 10^8$. Assuming the particles to have a velocity close to that of light, which is the case for practically all cosmic-ray particles, we have $E = 300\,H\rho$. Of the 356 tracks in series A with energy greater than 10^8 V it was not possible in the case of about 40 of them to determine whether the energy exceeded 3×10^8 V or not, i.e. to distinguish between the last two divisions. The 320 tracks or so for which this distinction was possible were distributed between the two divisions in the ratio of 1 to 3·5, and the procedure adopted for the above 40 tracks was to apportion them between the two divisions in the same ratio. No attempt was made to distinguish between the last two divisions for the tracks in series B. It may be assumed that above 3×10^6 V electrons from radioactive substances do not make any contribution. The results are given in Table I.

---

* The field of view does not extend to the walls of the chamber. The scattering from the glass walls of the light which enters the chamber limits the effective region for tracks to a cylinder of diameter about 24 cm.

TABLE I

Series	No. of particles with energy, E, in the interval					
	3×10^6–10^7	10^7–3×10^7	3×10^7–10^8	10^8–3×10^8	$> 3 \times 10^8$	Total
A (2200 G)	37	39	40	79 (40)	277 (316)	472
B (1000 G)	7	7	8	60		82

There is no significant difference between the distributions for the two series, which indicates that up to 10^8 volts a field of 1000 gauss produces a fairly accurately measurable curvature. For about one-half of the photographs in series A there was 1 cm. of lead immediately above the chamber. An analysis of the results shows that such lead has no appreciable effect on the spectrum. In the absence of this lead about two-thirds of the tracks had to traverse about 5 cm. of copper in order to enter the chamber, the remainder encountering only light building material in entering the chamber from the outside atmosphere.

It may be noted that the ratio of 3·5 to 1 of the numbers in the last two groups signifies an upper limit to the average error in the curvature $\sigma(=1/\rho)$ of $\sigma_m \sim (1/700)$ radians per cm. ($\rho_m \sim 700$ cm., $E_m \sim 4{\cdot}5 \times 10^8$ V). This estimate is obtained on the supposition that the observed curvature of the tracks in the two groups is entirely spurious, to be attributed for example to distortion of the tracks by air-motion. Though of course this is not the case it is certain that some tracks with energy greater than 3×10^8 V have been included in the group 10^8–3×10^8. In fact it is the number in this group that is subject to the greatest uncertainty, for below 10^8 V the curvature is so large that the fractional error in its measurement is comparatively small, while in the group above 3×10^8 V the number of particles is so large that even if all the particles recorded between 10^8 and 3×10^8 were transferred to it the percentage increase in the number would only be about 20. For the purpose of the discussion to follow we shall assume that in the series A the true number of tracks above 3×10^8 is the directly recorded number plus 39. This correction is obtained on the assumption that the excess of the number in the group 10^8–3×10^8 over the number expected by extrapolation of the distribution below 10^8 V is due to the inclusion of particles whose true energy is above 3×10^8 V. The modified numbers are given in brackets in Table I.

Observations have previously been made by Danforth and Lipmann (1934), and by Schneider (1938) on the relative number of very low energy cosmic-ray particles ($< 10^7$ V), using a randomly operated cloud chamber as in the present experiments. They find that electrons with energy between 3×10^6 and 10^7 V constitute nearly 10 % of all cosmic-ray particles. This is in satisfactory agreement with the present value of 8 %.

The energy spectrum from about 5×10^8 to 2×10^{10} V has been measured by Blackett (1937).* The present data serve to extend the spectrum down to 3×10^6 V. The combined results are given in Table II, and represented graphically in fig. 2.

TABLE II

E_1	E_2	f
3×10^6	10^7	0·079
10^7	3×10^7	0·084
3×10^7	10^8	0·086
10^8	3×10^8	(0·084)
3×10^8	10^9	0·142
10^9	3×10^9	0·276
3×10^9	10^{10}	0·173
10^{10}	3×10^{10}	0·051
3×10^{10}	∞	0·024

In the table f represents the ratio of the number of particles with energy between E_1 and E_2 to the total number with energy greater than 3×10^6 V. In the figure the ordinates represent log (df/dE), where df is the ratio of the number with energy between E and $E + dE$ to the total number with energy greater than 3×10^6 V, E being measured in 10^8 V. The energy is plotted logarithmically along the other axis, so that a negative slope of γ means that in that region $(df/dE) \propto E^{-\gamma}$.

Cosmic-ray particles are now believed to consist mainly of electrons and the newly discovered mesotrons. The latter constitute the penetrating component of cosmic-ray radiation. With this interpretation of cosmic rays it follows from the measurements of Blackett and Wilson on the energy loss by cosmic-ray particles in metal plates, that above about 3×10^8 V the particles are nearly all mesotrons. On the other hand below about 10^8 V

---

* Blackett's results do not extend much below 5×10^8 V, because of the selective action in this region of the counter-controlled chamber used in his experiments, as discussed in the introduction to this paper. This selectivity does not apply above about 5×10^8 V because particles of such energy generally appear singly, and the probability of recording "single" particles is practically independent of their energy.

In Blackett's measurements tracks inclined at an appreciable angle to the vertical are also excluded by the counter-control, though included in the present measurements. This difference however does not affect the main significance of the combined results.

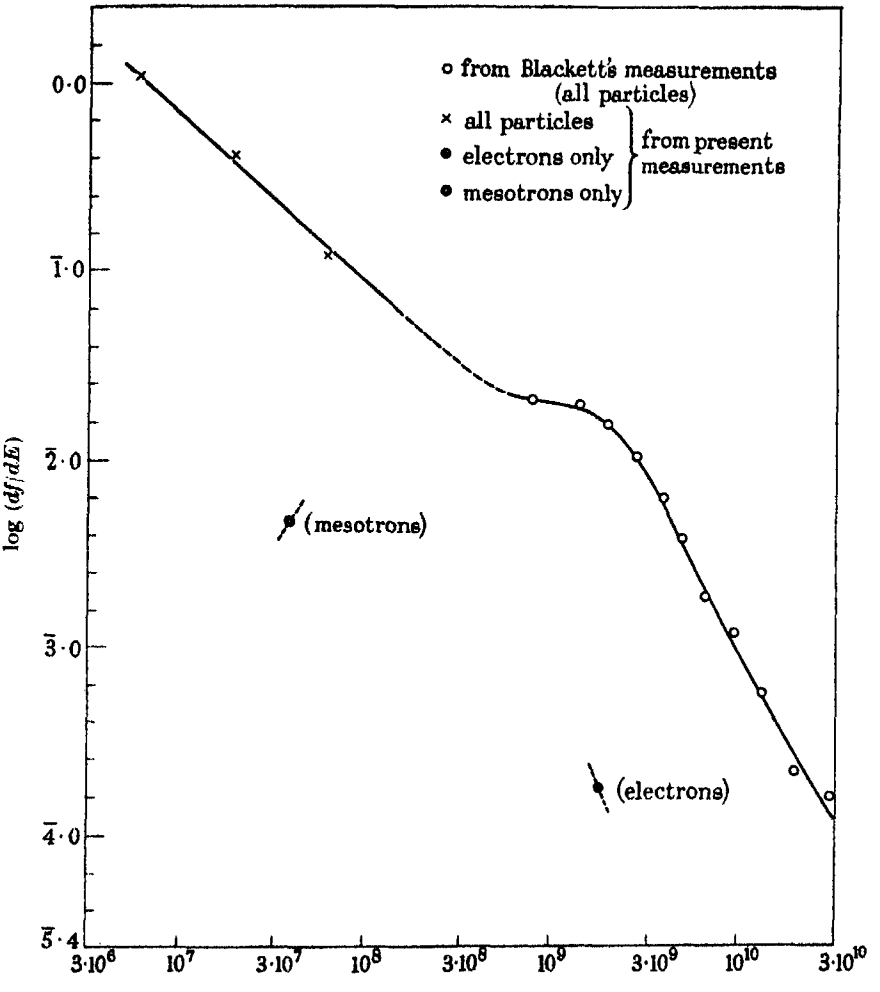

FIG. 2. Energy spectrum of cosmic-ray particles at sea-level. df = fractions of particle above 3×10^6 V with energy between E and $E + dE$.

the energy loss and specific ionization are characteristic of electrons. There is accordingly a fairly sharp transition from electrons to mesotrons between 10^8 and 3×10^8 V. Thus if the distribution of electrons and that of mesotrons were plotted separately the former would be represented by the curve in fig. 2 below about 10^8 V, the latter by this curve above 3×10^8 V. Little is known about the distribution of mesotrons below 10^8 V where electrons predominate. Included in the photographs examined here for the spectrum are those which revealed the tracks of two or three slow mesotrons reported earlier by Williams and Pickup (1938). These tracks give a rough idea of the number of mesotrons with $E \sim 3 \times 10^7$ V.* The result is represented by a double circle in the figure and corresponds to an intensity of about 1 % of the electron intensity at the same energy. The theoretically expected number of low energy mesotrons is considered in § 4.

The electron spectrum well above 10^8 V where mesotrons predominate may be inferred from the frequency of showers as has already been done by Blackett (1938). The showers observed in the present experiments are discussed in the next section (§ 3). Their number and size indicate that the number of electrons with energy between 10^9 V and 3×10^9 V is of the order of 0·003 of the total number of particles. This value, which is represented by the crossed circle in the figure, is about 0·01 of the mesotron intensity at the same point.

The ratio, R, of the number of electrons to the number of mesotrons is a quantity of interest. According to the present measurements 25 % of all the particles have energy less than 10^8 V, and from the evidence cited above these are practically all electrons. 67 % of the particles have energy greater than 3×10^8 V and we have seen that only about 1 or 2 % of these are electrons. Of the remaining 8 %, between 10^8 and 3×10^8 V, half may be assumed to be electrons and half mesotrons. Thus approximately 30 % of all the particles are electrons, and 70 % are mesotrons, which gives $R \sim 0{\cdot}4$. This result agrees in order of magnitude with the ratio of the soft component to the hard component as estimated from absorption experiments using counters. A close comparison in this respect is not possible, as the observations of different workers, using the counter method, do not lead to concordant results.

The absorption of electrons in the atmosphere is so high that those observed at sea-level have to be attributed to a secondary action of the penetrating component, i.e. of the mesotrons. One process in which electrons can thus be produced, pointed out by Bhabha (1938), is that in which a mesotron in a close collision with an atomic electron communicates to it a large amount of energy ("knock-on" collisions). The theoretical value of the average number of electrons which accompany the cosmic-ray mesotrons at sea-level due to this process, is about 0·3 per mesotron.* If electrons with energy less than 3×10^6 V are excluded, as in the present experiments, the relative number of electrons due to the knock-on process is appreciably less than 0·3, being only about 0·10–0·14 for light elements and still less for heavy elements.† The observed ratio is about 0·4, so that the knock-on process accounts for only about one-third of the observed number of electrons. Recently Euler and Heisenberg (1938) have shown that the spontaneous disintegration of a mesotron to an electron and a neutrino—which is to be expected if mesotrons are identified with the heavy "quanta" of Yukawa's theory of nuclear forces—accounts satisfactorily for certain outstanding anomalies in the absorption of mesotrons in the atmosphere. They show further that this disintegration gives rise to a fairly strong electronic component. Assuming a decay period for the mesotron of 2×10^{-6} sec.—a value in accord with the absorption anomalies—Euler and Heisenberg find that the number of electrons in air at sea-level due to the disintegration process is about 0·3 per mesotron. This, together with the contribution of 0·10–0·14 from the knock-on process, would account satisfactorily for the number of electrons observed in the present experiments. It must however be remembered that the estimate of the number of disintegration electrons made by Euler and Heisenberg refers to cosmic radiation in the open air. The presence of solid material above the chamber in the present experiments, particularly the copper of the magnetic field coils, appreciably reduces the number of disintegration electrons, and it is not unlikely that some other process for the production of electrons by mesotrons will have to be assumed in order to account for the number of electrons observed.

---

* It must be remembered that E represents 300 $H\rho$, and therefore not the energy itself for slow particles. Taking the mass of the mesotron to be 180 electron masses, a mesotron with $E \sim 3 \times 10^7$ has an energy of $4{\cdot}5 \times 10^6$ V.

---

* The estimate of this number may be made without much difficulty. The simplifying factor is that the rate of loss of energy by a fast electron is nearly independent of its energy. By virtue of this the total length of electron track arising from the production by the penetrating particle of a secondary electron of energy, Q, is practically the same whether the energy Q is dissipated into ionization by this electron itself, or by other fast electrons to which it may give rise through the cascade process of shower formation. Thus, in calculating the average number of electrons of *all* energies accompanying a mesotron, the difficulties involved in a quantitative treatment of the cascade process may be obviated. Some calculations along these lines will be described elsewhere, and the details of the estimates quoted above. The results obtained differ appreciably from those obtained by Bhabha (1938), especially for light elements. In Bhabha's calculations the details of the cascade process are worked out, and large errors may have thus been incurred.

† These estimates assume that the electrons are in equilibrium with the mesotrons. Now the change in the average number of electrons per mesotron when cosmic radiation passes from one material to another is closely related to the change in the total ionization due to this radiation. From the results of the observations on the latter it may be inferred that during such a transition the number of electrons remains very nearly between the equilibrium values for the two materials. The present estimates made on the above assumption of equilibrium are therefore not inapplicable to the present experiments—in which appreciable amounts of material of different atomic numbers lie above the chamber.

Regarding the form of the energy distribution of the electrons it will be seen from fig. 2 that below about 10^8 V log (df/dE) varies linearly with log E. The line is inclined at $-45°$ which corresponds to $(df/dE) \propto E^{-1}$. It is however likely that this simple form of the distribution is accidental, being a resultant effect of different and independent factors, and we shall not discuss it further here.

Tracks of cosmic-ray electrons are reproduced in figs. 3–5 (Plate 9). About 30 % of the electron tracks are either associated with each other in pairs or accompany the nearly straight tracks of mesotrons. Examples of each kind are reproduced. The majority of electron tracks are not obviously associated with other tracks *in the chamber*.

3. ELECTRON SHOWERS

Five showers consisting of seven or more electron-tracks were observed in the 1000 or so photographs taken. Though this number is small, it exceeds the total number of showers observed in previous observations made with a randomly operated chamber, and it is sufficient to give a rough idea of the relative frequency of showers in cosmic rays.

The tracks in one of these showers (reproduced in fig. 6, Plate 9) are nearly parallel, and are widely spaced, indicating an origin not in the immediate neighbourhood of the chamber. It is probable that the tracks observed in the chamber form only part of a much bigger shower which may be of the type recently observed by Auger, Maze and Grivet-Meyer (1938) using widely spaced counters. The electrons traverse the chamber obliquely, and as a result their energy cannot be accurately measured.

The other four showers have their origin in the material immediately surrounding the chamber. They are, in all probability, produced by the cascade process. Two of these showers are reproduced in figs. 7 and 8 (Plate 9). From the number of such showers the number of high energy electrons in cosmic rays at the levels concerned may be deduced. This has been done by Blackett (1938) using Heitler's theoretical results for the cascade process, and estimating the relative frequency of showers from counter experiments. There is, however, some uncertainty as to the number of electrons in the showers which a given counter arrangement records. It is therefore of interest that the number of showers observed in the present experiments with a randomly operated chamber confirms in order of magnitude the number deduced from counter experiments. Of the four showers mentioned above three appeared in the photographs taken with 1 cm. of lead over the chamber. These have 8, 8 and 11 tracks respectively, the tracks being sharp. The total number of sharp tracks in the same series was about 700. Thus the ratio of the number of showers with 8 or more tracks to the total number of tracks is about 0·004. According to the results of counter experiments by Montgomery and Montgomery (1935) this ratio, under 1 cm. of lead, is about 0·001. There is thus rough agreement, though the present results indicate that the actual relative number of showers somewhat exceeds the number deduced from counter experiments.*

4. TRACKS PROVIDING EVIDENCE FOR MESOTRONS

The most direct evidence for the existence of mesotrons has come from the observation in cloud-chamber experiments of tracks whose momentum and specific ionization are theoretically compatible only if we assume the particle to have a mass considerably greater than that of an electron but still much less than that of a proton. Examples of such tracks have been obtained by several workers, including E. Pickup and myself. The experiments of the latter, which were made with the large cloud chamber described in § 1, have been described in a communication to *Nature* (1938). Three or four tracks were observed which could not be attributed to protons or electrons. In the above communication these were labelled *a*, *b*, *c*, and *d*, a reproduction of *d* being given. Track *d* is again reproduced here, and a reproduction of *a* is also given.

Track d (figs. 13, 14, Plate 10). This is the one which, of those observed by Williams and Pickup, provides the most conclusive evidence for the mesotron. Its momentum deduced from the curvature is about 70*mc*, where *c* is the velocity of light, and *m* is the mass of an electron. An electron with this momentum would have a velocity close to that of light, and its specific ionization would be characteristic of fast electrons. The ionization along *d* is, however, about 3 times that along fast electrons, so that an electronic origin is ruled out. In fig. 14 (Plate 10) a portion of *d* is reproduced alongside the track of a fast electron, and the large difference in ionization is readily seen. A proton with the same ionization as *d* would have a momentum and therefore radius of curvature about 10 times greater than that observed.* But before we can use this result to rule out a proton we must be sure that the observed curvature of *d* cannot have been spuriously produced by motion of the gas in the chamber. This in fact is the crucial question regarding this type of evidence for the mesotron, and it was not until track *d* was obtained that we were absolutely sure that it could be answered negatively. Regarding the effect of air motion, to quote from the earlier report by Williams and Pickup: "Photographs taken in the same 'run' happened to have tracks of fast particles in the same part of the chamber, and these showed that spurious curvature, which, of course, exists to *some* extent, was not more than about one-twentieth of the curvature of the track *d*. Moreover, the spurious curvature was in the opposite direction to that of the latter. Old tracks passing through before the expansion showed obvious distortion, but even for these the extent of the corresponding spurious curvature was small and again in the opposite direction to that of *d*." We might mention also that the curvature of *d* is about 15 times the upper limit to the average spurious curvature for *all* the photographs as estimated in § 2. There is thus no possibility that the curvature of *d* is spurious, and accordingly a proton cannot have been the responsible particle.

---

* The presence of the copper coils above the lead in the present experiments would not be expected to increase the frequency of showers of the size concerned.

The curvature and ionization of *d* are compatible only with a particle with a mass of about one-tenth the mass of the proton. It is not possible to deduce an accurate value of the mass of the responsible particle from the experimental data. One obtains its momentum fairly accurately from the magnetic field and the radius of curvature of the track ($H\rho$). The velocity is estimated from the specific ionization, and it is this which is subject to most error. In track *d* the spots along the track represent (with one or two exceptions) primary ions, but they are so close that the number per cm. is difficult to count. Two procedures were adopted in estimating the specific ionization. In one the number of distinguishable spots along the track was counted, and a correction then made for unresolved spots to obtain the true number of primary ions per cm. Denoting the latter by I and the uncorrected number by I_0 then,

$$I = \sigma^{-1} \log_e (1 - I_0 \sigma)^{-1}, \qquad (2)$$

where σ is a parameter representing the resolving power, and is comparable with the width of the track. For the part of *d* in focus $I_0 = 25$ and $\sigma = 0{\cdot}03$, giving $I = 46$. A check on this number was obtained by the second procedure. In a length l of track the average number of ions, i.e. of "free paths", is Il. The mean free path is I^{-1}, so that the average number of free paths greater than g cm. in a length l is

---

* Alternatively a proton with the observed curvature would have a velocity of $0{\cdot}04c$ and accordingly a specific ionization about 100 times that of fast electrons and 30 times that of *d*. Furthermore, a proton with a velocity of $0{\cdot}04c$ would have a range of only about 4 cm. in the chamber, while *d* has a range of at least 20 cm. (which is its observed length in the chamber).

$$n = Ile^{-Ig}. \tag{3}^*$$

Large free paths appear as gaps in the track, the true gap being of course the observed gap plus a quantity roughly equal to the width of the track. In 8 cm. of the track d there are 6 gaps greater than 0·08 cm., thus $8Ie^{-0\cdot08I} = 6$, giving $I = 53$ in fair agreement with the more direct method. This second method is more powerful than would appear at first sight. It is not very tedious if one counts only the big gaps, and though the number of such gaps is small the exponential term varies so rapidly with I that there is no large statistical error. The biggest error actually comes from the measurement of the gap length.

Measurements on 5 electrons with velocities between 0·8 and 0·97c taken under the same conditions as track d gave an average primary ionization (reduced to 0·96c) of $14\cdot1 \pm 1$. The gas in the chamber in the experiments was a mixture of hydrogen and air in approximately equal proportions by volume, and this result is consistent with the primary ionization in hydrogen and in air as observed by Williams and Terroux (1930). From the work of the latter, and some other considerations, the primary ionization may be taken to vary as $\beta^{-1\cdot4}$. Accordingly the velocity of the particle responsible for track d is $0\cdot96(14\cdot1/46)^{1/1\cdot4}c = 0\cdot41c$. The radius of curvature of d is 55 cm. and the magnetic field used was 2300 G. This gives $H\rho = 1\cdot26 \times 10^6$, which corresponds to a momentum of $73mc$, where m represents electronic mass, and c the velocity of light. If μ is the mass of the particle its momentum is $\mu\beta c(1-\beta^2)^{-1/2}$. Equating this to $73mc$, and substituting 0·41 for β we have $\mu = 160m$. The probable error is estimated to be about 15 %.

Track a (fig. 15, Plate 10). This track has a much greater specific ionization than an electron of the same curvature, while a proton with the same ionization would be practically straight having a curvature about 10 times less. Of the tracks obtained by Mr Pickup and the writer it ranks next to d in the conclusiveness of its evidence for a "new" particle. Its average radius of curvature is 110 cm., and though there is a slight flattening in the middle

---

[*] It is of interest to calculate from this the expected number of large gaps in tracks of fast electrons in air. For this case the value of I is about 22 (Williams and Terroux 1930). It follows then from the above formula that in 10 cm. of track there is a probability of about 0·5 of a gap greater than 3 mm. Such gaps therefore do not necessarily mean inefficient condensation on ions, if they do not occur more frequently than about once every 10 or 20 cm.

the deviation of the track from a circle of this curvature is well within the upper limit to the distortion curvature resulting from air motion, as estimated in § 2. This slight flattening, therefore, does not signify any abnormal air motion in this particular expansion. On the other hand, the deviation of the track from a straight line—which is practically what the path of a proton giving the same specific ionization would be—corresponds to about 7 times the upper limit to the average curvature due to air motion. There is thus little possibility that the responsible particle is a proton. This possibility, however, cannot be ruled out with the same certainty as in the case of track *d*, and it was not until *d* was obtained (some eight months after *a*) that it was considered safe to demand a "new" particle to account for tracks of this type.

The greater density of ionization along *a* than along *d*, which is mainly due to the gas being air instead of an air-hydrogen mixture, prevents a measure of the ionization along *a* by direct counting. It can only be done by the "gap" method. In 13 cm. of the track there are 5 gaps greater than 0·5 mm. Hence from equation (3) the specific primary ionization is 115. The ionization along tracks of million-volt electrons ($\beta \sim 0{\cdot}96$) in the same gas was found to be 23. Hence, as in the calculations for *d*, the velocity of the particle responsible for *a* is $0{\cdot}96(23/115)^{1/1{\cdot}4}c = 0{\cdot}30c$. This velocity, and its momentum of $65mc$, give a mass equal to $\{65(1-0{\cdot}30^2)^{\frac{1}{2}}/0{\cdot}30\}m = 210m$,* with a probable error of about 20 %.

The particle responsible for the track *c*, mentioned in the earlier report, passed through the chamber before the expansion, the ions having diffused appreciably before condensation. Under these conditions tracks are generally distorted quite appreciably by air motion, and track *c* actually did not have a uniform curvature. Accordingly the identification of the track as that of a mesotron is not quite certain.

The following table contains a summary of the two tracks *a* and *d*.† In view of the much greater accuracy of the data for *d* the value of the mass deduced from this alone may be taken as the best value yielded by the present work. I_m denotes the specific ionization of a million-volt electron ($\beta = 0{\cdot}96$).

---

* In the earlier report the relativistic correction $(1-0{\cdot}30^2)$ was omitted and the estimated mass was $220m$.

† The track *b* mentioned in the earlier report by Mr Pickup and the writer indicates a mass of about $600m$, which is much greater than the above values given by tracks *a* and *d*. The difference between the observed curvature of *b* and that of a proton with the same density of ionization corresponds to a radius of curvature of about 250 cm., which is about one-third the upper limit to the average spurious radius of curvature estimated in § 2. This, however, does not leave enough margin of error to rule out a proton as the responsible particle. In any case, if it is not another "new" particle, it is far more likely to be the track of a proton than that of a particle of mass around $200m$. The spurious radius of curvature to make it conform to the latter would be less than 100 cm.

Track	ρ	$H\rho \times 10^5$	(I/I_m)	Momentum ÷ mc	Velocity ÷ c	Mass ÷ m
d	55	1·26	3·3	73	0·41	160 ± 30
a	110	1·10	5	65	0·30	210 ± 60

In the course of investigations of certain induced activities, using the cloud chamber described in this paper, Mr F. C. Thompson recently obtained a photograph of another track with too much curvature for a proton, and too much ionization for an electron. The ionization and curvature indicate a mass of about $200m$, in satisfactory accord with the values in the above table.

It is of interest to compare the observed number of tracks distinguishable as those of mesotrons with the total number of cosmic-ray tracks observed. Confining the estimates to sharp tracks, that is to particles passing through the chamber after the expansion, the number of distinguishable mesotrons in *all* the photographs taken using the present chamber (including those taken in investigations of induced radioactivity) is three, viz. tracks a and d and the above-mentioned track obtained by Mr Thompson. The total number of sharp cosmic-ray tracks in the same photographs is about 2500. To be distinguishable from fast electrons it may be assumed that the velocity of a mesotron must be less than about $0{\cdot}5c$—corresponding to an ionization about $2\frac{1}{2}$ times greater than that of a fast electron. The data accordingly means that at sea-level a fraction of the order of 0·001 of all ionizing cosmic-ray particles are slow mesotrons, i.e. with a velocity less than $0{\cdot}5c$.

Let $N(T)\,dT$ be the number of mesotrons with energy between T and $T+dT$ at sea-level, and $\alpha N(T)\,dT$ the number at a height above sea-level (i.e. above the chamber) equal to the range, R', of mesotrons of energy T. Let dT/dx denote the rate of loss of energy when the energy is T. Then if R is the range of a mesotron of velocity $0{\cdot}5c$, and if slow mesotrons are not created as such, the expected number at sea-level with velocity less than $5{\cdot}0c$ is approximately

$$N_s = \alpha N(T)\,(dT/dx)\,R. \tag{4}$$

Taking T as 5×10^8 V and assuming that for this and lower energies there is no process of energy loss other than ionization $R' \sim 250$ g./cm.^{2}, and α is about 1·5. Also $dT/dx \sim 2 \times 10^6$ V/g./cm.^{2} for this value of T, and $R \sim 1{\cdot}2$ g./cm.^{2}. From the discussion in § 2 the number of mesotrons per 10^6 V in the region of 5×10^8 V is about 0·0002 of the total number, S, of cosmic-ray particles. Therefore from (4)

$$N_s = 1{\cdot}5 \times 0{\cdot}0002 \times S \times 2 \times 1{\cdot}2 = 0{\cdot}0007 \times S.$$

The spontaneous disintegration of a mesotron, for which there is now considerable evidence (Euler and Heisenberg 1938; Blackett 1939), and which is not allowed for in (4) reduces the number of slow mesotrons, under the conditions of the present experiments, by about 40 %.* Thus we would expect about 4 slow mesotrons every 10,000 cosmic-ray particles. This agrees in order of magnitude with the observed number of slow mesotrons. The latter is too small to give much significance to the actual ratio of about 3 to 1 of observed to calculated.

[*Note added in proof*, 28 *June*. Maier-Leibnitz (1939) recently reported observing 5 mesotrons coming to the end of their range in a cloud chamber, the chamber being operated in such a way as to give it a sensitive time of about one second (slow expansions, cf end of § 1). The observed number of mesotron-ends is much greater than would be expected from the number of slow mesotrons (velocity $< 0{\cdot}5c$) observed in the experiments described here. As Maier-Leibnitz shows, the theoretical ratio of the number of mesotron-ends observed in a cloud chamber to the number of slow mesotrons observed (assuming *very* slow mesotrons are not created as such) is equal to the ratio of the average length of the track of a slow mesotron traversing the chamber, l say, to the range of a slow mesotron, i.e. R of equation (4). R is about 1·2 g./cm.^{2}, while for the chamber used by Maier-Leibnitz and also the present chamber l is about 10 cm. of air at N.T.P., $\sim 0{\cdot}01$ g./cm.^{2}. Accordingly, in the present experiments in which 3 slow mesotrons have been observed, the expectation of a mesotron-end was $3(l/R) \sim 0{\cdot}03$ only. The total length of cosmic-ray track in Maier-Leibnitz' experiments was about $3{\cdot}5 \times 10^4$ cm. of normal air, and in the present experiments about $2{\cdot}5 \times 10^4$ cm. The number of mesotron-ends to be expected in Maier-Leibnitz' experiments from the number of slow mesotrons observed in the present experiments is therefore about 0·04. The reported number of 5 cannot be reconciled with this,

---

* The fraction of mesotrons of initial energy $x \times \mu c^2$ which reach the end of their range without disintegrating is $e^{-\gamma}$ where γ is approximately

$$(\mu c/\tau F)\,\{\log\,(x+\sqrt{(1+x^2)})-x/\sqrt{(1+x^2)}\}.$$

μ is the mass of the mesotron, τ its "rest" decay period, and $F\beta^2$ is the rate of loss of energy per cm. of a mesotron of velocity βc. F increases slowly with β, but this may be neglected in an approximate calculation. For air at N.T.P. $F \sim 2000$ V/cm. Taking $\mu = 160m$, and $\tau = 2 \times 10^{-6}$ sec., the fraction of mesotrons of initial energy $5{\cdot}10^8$ V which reach the end of their range in air (N.T.P.) is about 40 %, while about 60 % of those with initial energy $2{\cdot}4 \times 10^8$ V reach the end of their range. The presence of solid material around the chamber (including superincumbent building material) increases the fraction reaching the end of their range, and this is allowed for in the estimate quoted in the above text.

unless it is assumed that *very* slow mesotrons are created as such by more energetic particles.]

The work described in this paper was carried out at the University of Liverpool, and I wish to thank Professor J. Chadwick for suggestions and advice during its progress. I am also indebted to Mr E. Pickup and Mr G. R. Evans for their assistance in the work.

SUMMARY

An account is given of a large Wilson cloud chamber, about 30 cm. deep and 30 cm. diameter. Such a chamber has a sensitive time of nearly half a second, and this, together with its large effective volume, makes it a very sensitive detector of weak radiations. The results of certain cosmic-ray observations made with this chamber are described. "Counter-control" was not used, the intrinsic efficiency of the chamber ensuring, on the average, at least one cosmic-ray track for photograph. In the absence of counter-control the photographs represent the true statistical distribution of different cosmic-ray events. Results for the energy distribution of cosmic-ray particles below 3×10^8 V are thus obtained, and also some indications of the relative frequency of showers and of slow penetrating particles (mesotrons). Certain details of earlier work by Williams and Pickup on heavily ionizing tracks, which provided evidence for mesotrons, are also given in this paper. Some of the photographs taken are reproduced.

REFERENCES

Auger, Mazo and Grivet-Meyer 1938 *C.R. Acad. Sci., Paris*, **206**, 1721.
Bearden 1935 *Rev. Sci. Instrum.* **6**, 256.
Bhabha 1938 *Proc. Roy. Soc.* A, **164**, 257.
Blackett 1937 *Proc. Roy. Soc.* A, **159**, I.
— 1938 *Proc. Roy. Soc.* A, **165**, II.
— 1939 *Nature, Lond.*, **142**, 992.
Blackett and Wilson 1937 *Proc. Roy. Soc.* A, **160**, 304.
Danforth and Lipmann 1934 *J. Franklin Inst.* **73**, 217.
Euler and Heisenberg 1938 *Ergebn. exakt. Naturw.* **17**, 1.
Frisch 1935 *Naturwissenschaften*, **23**, 166.
Maier-Leibnitz 1939 *Z. Phys.* **112**, 569.
Montgomery and Montgomery 1935 *Phys. Rev.* **48**, 786.
Schneider 1938 *Phys. Rev.* **53**, 615.
Walke, Williams and Evans 1939 *Proc. Roy. Soc.* A, **171**, 360.
Williams 1939 *Proc. Camb. Phil. Soc.* (in the Press).
Williams and Pickup 1938 *Nature, Lond.*, **141**, 684.
Williams and Terroux 1930 *Proc. Roy. Soc.* A, **126**, 289.

DESCRIPTION OF PLATES 9, 10

PLATE 9

FIG. 3. *a* and *b* represent an electron pair. Energy of $a = 9 \times 10^7$ V, of $b = 2{\cdot}4 \times 10^7$. *c* is an electron track (energy 8×10^6) not associated with *a* and *b*. *e* is probably a mesotron track (energy 10^9 V). *d* and *f* are "old" tracks, probably of mesotrons (energy $> 6 \times 10^8$ V). $H = 2200$ G.

FIG. 4. *a* and *b* represent an electron pair (energies 5×10^7 and 7×10^7). *d* is probably an unassociated electron (energy 7×10^7).

FIG. 5. *a* is probably a mesotron track (energy $> 6 \times 10^8$), and *b* an electron track produced by *a* (energy $= 1{\cdot}5 \times 10^7$). *c* is an independent track, probably of a mesotron (energy $> 4 \times 10^8$). $H = 1000$ G.

FIG. 6. *a*, *b*, *c*, *d*, *e*, *f*, *g* are nearly parallel electron tracks, probably representing a portion of a more extensive shower. Energies $> 10^8$ V. $H = 600$ G.

FIG. 7. Shower of 8 tracks. 3 have energy $< 3 \times 10^7$, and 5 energy $> 3 \times 10^7$. Gas is mixture of hydrogen and air. $H = 200$ G.

FIG. 8. An old shower of 7 tracks. 5 are positive electrons with energy less than 10^8 V. 2 have energy $> 10^8$ V, sign of charge uncertain. $H = 2200$ G.

FIG. 9. Shows a secondary electron (energy $= 2{\cdot}5 \times 10^5$) produced in the gas by a fast mesotron (energy $> 3 \times 10^8$). $H = 1000$ G.

FIG. 10. Associated tracks of high energy. The tracks are practically straight, corresponding to an energy greater than $1{\cdot}0 \times 10^9$ V, and probably greater than $1{\cdot}5 \times 10^9$ V. Stereoscopic reproduction showed that the tracks are in the same plane within the experimental error of about 0·3°. The angle between them in their own plane is 3°, corresponding to an intersection in the ceiling of the room about 1 m. above the chamber.

FIG. 11. Track of a heavy particle which probably starts in the gas.

FIG. 12. Example of occasional α-tracks produced in gas of chamber. In this case the particle passed through before the expansion, the positive and negative components being separated. Range about 4 cm. standard air and probably due to radon "contamination".

PLATE 10

FIGS. 13–15. Tracks providing evidence for existence of mesotrons (from earlier work of Williams and Pickup). Full details given in § 4.

FIG. 16. Tracks of "slow" cosmic-ray proton. Energy $1{\cdot}4 \times 10^7$ V. Radius of curvature $= 450$ cm. ($H = 600$ G.) About 8 tracks of slow protons were observed (with velocity less than $0{\cdot}5c$). The total number of cosmic-ray tracks observed being about 2000, it follows that slow protons constitute a fraction of the order of 0·004 of the total number. This is of the same order of magnitude as the relative number of slow protons observed by other workers using a counter-controlled chamber. This is to be expected since slow protons ($v \sim 0{\cdot}4c$) have sufficient range to operate the counter system (which is not generally the case for slow mesotrons). It may be inferred from the observed number of slow protons that the majority of cosmic ray particles with energy below about 5×10^9 volts are not protons.

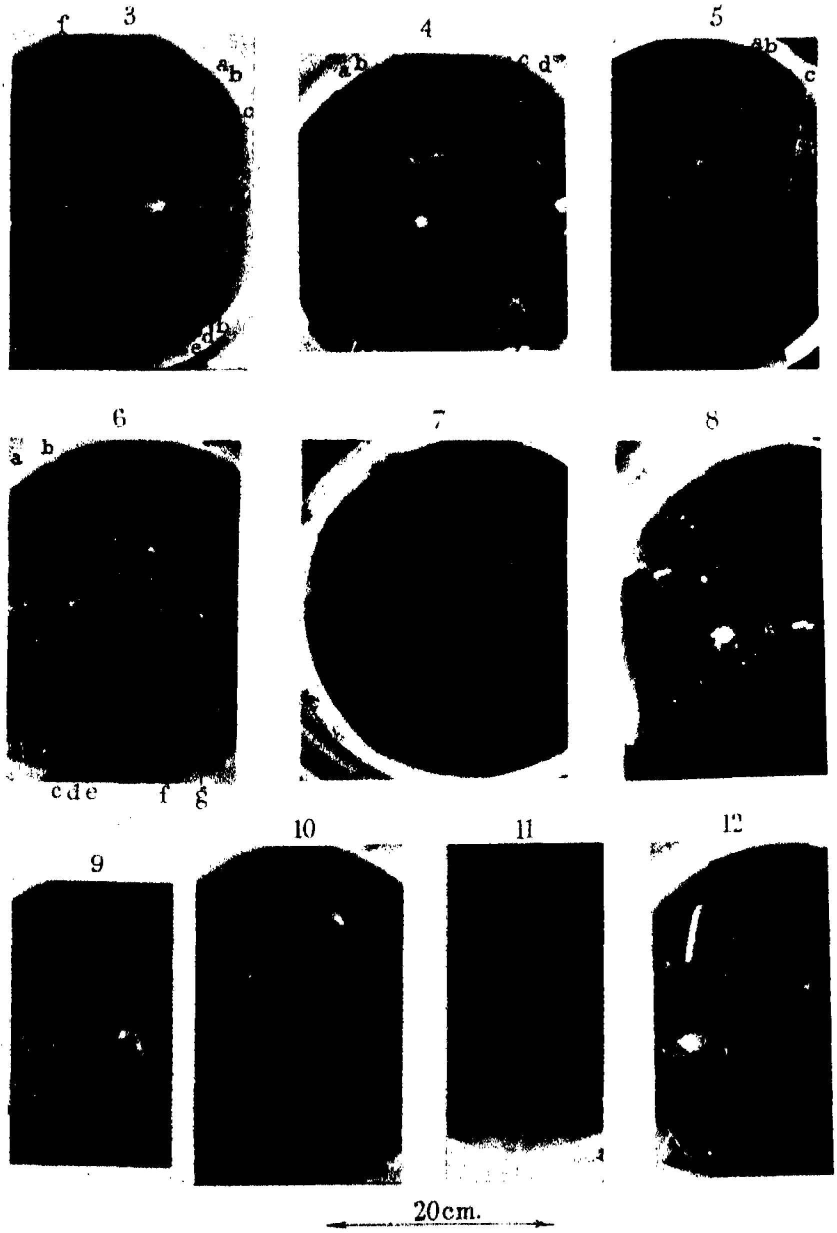

FIGS. 3–12

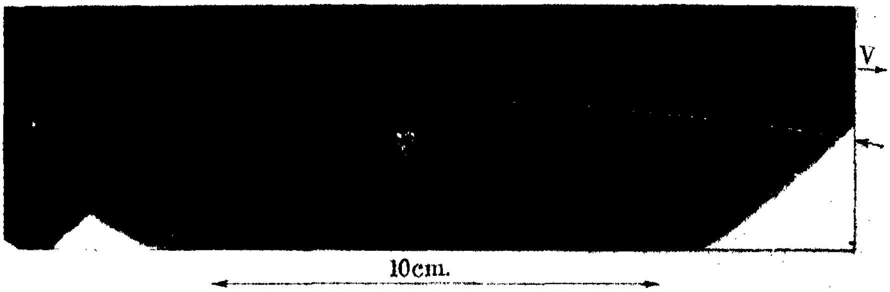

Fig. 13

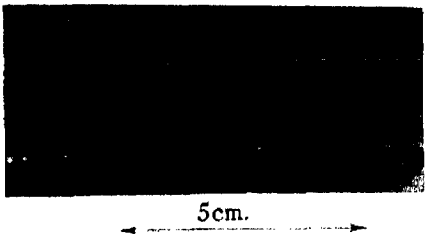

Fig. 14

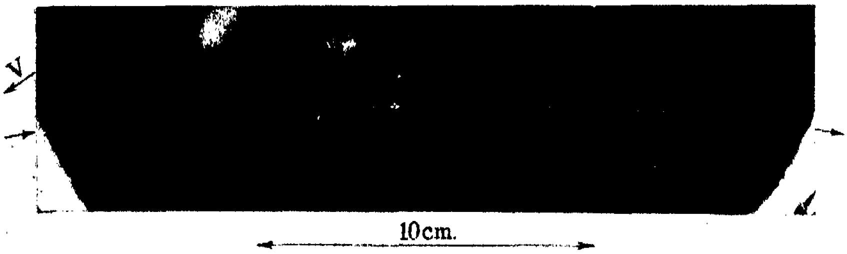

Fig. 15

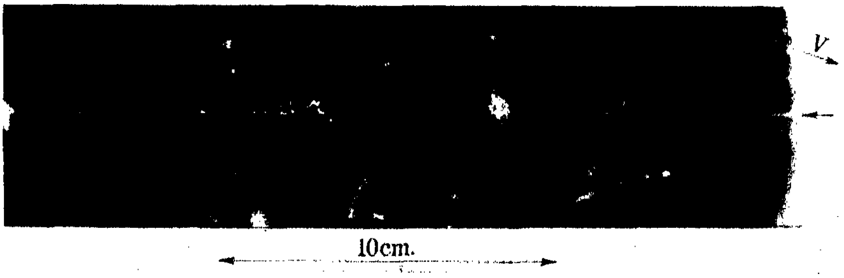

Fig. 16

The two-dimensional hydrodynamical theory of moving aerofoils. III

By Rosa M. Morris, B.Sc.

(*Communicated by G. I. Taylor, F.R.S.—Received* 17 *March* 1939)

1. In the previous papers of this series (Morris 1937, 1938; referred to subsequently as "I" and "II") I have developed a general expression for the velocity potential of the two-dimensional fluid motion surrounding an infinite cylinder of general shape, moving in any manner perpendicular to its axis, in inviscid and incompressible fluid. From this expression I derived in "I" the kinetic energy of the fluid when the circulation is zero and in the more general case the forces and couple on the cylinder, including also in "II" the effect of a trail of vortices extending downstream from an assumed trailing edge at the rear of the cylinder. In a brief discussion at the end of "II" the general formulae obtained were reduced for the case of an aerofoil of small thickness and small symmetrical camber, but using the particular hydrodynamical assumptions made by Wagner in his theory of accelerated motions; according to which the circulation associated with the trail is just sufficient to cancel the general circulation round the aerofoil. This was done in order to obtain comparison with the only previous attempt to calculate the effects of rotation and acceleration.

In view of the difficulties inherent in any attempt to generalize Wagner's theory and also of the fact that his fundamental assumption of zero total circulation probably holds, if at all, only at the beginning of the motion, it seemed advisable to divide the general discussion of the dynamics of the aerofoil into two stages. In the first of these, with which the present paper is mainly concerned, the basis is that of the older general theory which omits the trailing wake and its effects altogether, but includes a circulation defined in terms of the velocity of the cylinder by the usual Joukowski condition at the trailing edge. In the second stage an independent effort is to be made to estimate the effect of various kinds of trailing vortices on the general motion of the aerofoil.

We have therefore examined in some detail one case of the older general theory—the Joukowski aerofoil—where the expressions for the force and couple can be obtained in finite form and therefore to any desired degree of accuracy, so that their dependence on the thickness and camber can be defined. These results are then applied—following a suggestion kindly made to me by Professor G. I. Taylor—in the discussion of the important question of the stability of a simple rectilinear motion of the aerofoil. In a final paragraph we have attempted to derive the corresponding formulae for a special case of Wagner's theory, replacing the trail by a single average vortex whose general effect is the same, but the results obtained serve only to emphasize the unsatisfactory nature of the assumptions underlying the theory and suggest a further investigation, which it is hoped will form the subject of a later communication, of the relative motion of the aerofoil and trailing vortices and its influence on the interaction between them. Pending this further investigation it seems useless attempting to develop in any further detail the general trail theory.

2. When the cylinder cross-section is defined by the relation

$$z = x+iy = e^{-i\xi} \sum_{n=0}^{\infty} a_n e^{ni\xi}, \tag{2·1}$$

and the origin $z = 0$ is moving with velocity $w = u+iv$, whilst the cylinder is rotating about its length with angular velocity ω, the components of the resultant force on the cylinder are determined in the notation of "I" and "II" by the formula

$$\begin{aligned} Y+iX = {} & -\pi\rho i\{A\dot{\bar{w}} - 2\bar{B}\dot{w} - i\dot{\omega}\bar{D}\} - \pi\rho\omega\{A\bar{w} - 2\bar{B}w - i\omega\bar{D}\} \\ & -\rho\dot{K}\left\{\bar{a}_0 + \sum_{n=2}^{\infty} \bar{a}_n\right\} + \rho\bar{w}K - \rho i\omega K\bar{a}_1, \end{aligned} \tag{2·2}$$

whilst the couple about the origin is

$$\begin{aligned} \Gamma = {} & -\pi\rho C\dot{\omega} - \tfrac{1}{2}\pi\rho i\{D\dot{\bar{w}} - \bar{D}\dot{w}\} + \pi\rho i\{\bar{B}w^2 - B\bar{w}^2\} - \tfrac{1}{2}\pi\rho\omega\{\bar{D}w + D\bar{w}\} \\ & -\tfrac{1}{2}\rho\dot{K}\sum_{n=1}^{\infty}(b_n + \bar{b}_n) + \tfrac{1}{2}\rho K\{a_1\bar{w} + \bar{a}_1 w\}. \end{aligned} \tag{2·3}$$

In these formulae the constants A, B, C, ... are defined in terms of the coefficients in the equation (2·1) of the cross-section curve by the equations

$$\left.\begin{aligned} A &= a_0\bar{a}_0 + \sum_{n=1}^{\infty} na_{n+1}\bar{a}_{n+1}, \\ B &= a_0 a_2, \qquad C = \sum_{n=1}^{\infty} nb_n\bar{b}_n, \\ D &= b_1 a_0 + \sum_{n=1}^{\infty} n\bar{b}_n a_{n+1}, \\ \bar{D} &= \bar{b}_1\bar{a}_0 + \sum_{n=1}^{\infty} nb_n\bar{a}_{n+1}; \end{aligned}\right\} \tag{2·4}$$

wherein $$b_r = \sum_{n=0}^{\infty} a_{n+r}\bar{a}_n,$$

and bars over a complex quantity denote the conjugate quantity.

The circulation K is defined in terms of the velocity of the cylinder by Joukowski's condition for finite velocity at the trailing edge, which in our case gives

$$\frac{iK}{2\pi} = \bar{a}_0 w e^{i\zeta_t} - \sum_{n=2}^{\infty} (n-1)\, a_n \bar{w} e^{(n-1)i\zeta_t} + i\omega \sum_{n=0}^{\infty} n b_n e^{ni\zeta_t}, \tag{2·5}$$

where we have used ζ_t for the value of ζ at the sharp edge of the aerofoil: this is of course a singular point for the transformation $z = z(\zeta)$, so that at this point $z'(\zeta_t) = 0$ or

$$-a_0 e^{-i\zeta_t} + \sum_{n=2}^{\infty} (n-1)\, a_n e^{(n-1)i\zeta_t} = 0.$$

The equation (2·5) can therefore be written in the form

$$\frac{iK}{2\pi} = \bar{a}_0 w e^{i\zeta_t} - a_0 \bar{w} e^{-i\zeta_t} + i\omega \sum_{n=0}^{\infty} n b_n e^{ni\zeta_t}. \tag{2·6}$$

Now ζ_t relates to a point on the curve of cross-section of the aerofoil, so that it must be real. It follows then that

$$\left(\frac{d\bar{z}}{d\zeta}\right)_{\zeta=\zeta_t} = -i\sum_{n=0}^{\infty} (n-1)\, \bar{a}_n e^{-(n-1)i\zeta_t} = \overline{\left(\frac{dz}{d\zeta}\right)}_{\zeta=\zeta_t} = 0,$$

so that at $\zeta = \zeta_t$ $$\left(z\frac{d\bar{z}}{d\zeta} + \bar{z}\frac{dz}{d\zeta}\right)_{\zeta=\zeta_t} = \left\{\frac{d(z\bar{z})}{d\zeta}\right\}_{\zeta=\zeta_t} = 0.$$

This implies that $$\sum_{n=1}^{\infty} n\{b_n e^{ni\zeta_t} - \bar{b}_n e^{-ni\zeta_t}\} = 0. \tag{2·7}$$

Separating the Joukowski condition in the form (2·6) into its real and imaginary parts we get

$$\frac{K}{2\pi} = -i(\bar{a}_0 w e^{i\zeta_t} - a_0 \bar{w} e^{-i\zeta_t}) + \tfrac{1}{2}\omega \sum_{n=0}^{\infty} n(b_n e^{ni\zeta_t} + \bar{b}_n e^{-ni\zeta_t}), \tag{2·8}$$

and $$\tfrac{1}{2}\omega \sum_{n=1}^{\infty} n(b_n e^{ni\zeta_t} - \bar{b}_n e^{-ni\zeta_t}) = 0.$$

The last equation is satisfied independently of ω on account of the condition (2·7), and therefore the Joukowski condition reduces to a single equation. Our surmise on p. 355 in "II" is therefore wrong.

3. The Joukowski aerofoil is defined by the transformation

$$z = ae^{-i\zeta} + \frac{b^2}{z_0 + ae^{-i\zeta}}, \quad |z_0| < a, \tag{3·1}$$

the origin being taken at the centre of the circle from which the aerofoil is transformed. This can be written in the form

$$z = ae^{-i\zeta} + \frac{b^2}{a} e^{i\zeta} \sum_{n=0}^{\infty} (-)^n \frac{z_0^n}{a^n} e^{ni\zeta}, \tag{3·2}$$

so that $$a_0 = a, \quad a_1 = 0, \quad a_2 = b^2/a,$$

and for $n > 2$ $$a_n = (-)^n \frac{b^2}{a} \frac{z_0^{n-2}}{a^{n-2}}.$$

From these we deduce that

$$b_0 = \frac{a^4 + b^4 - a^2c^2}{a^2 - c^2}, \quad b_1 = \frac{-b^4 z_0}{a(a^2 - c^2)},$$

where $c^2 = z_0\bar{z}_0$, and for $n > 1$

$$b_n = \sum_{r=0}^{\infty} a_{n+r}\bar{a}_r = (-)^n \frac{b^2}{a^n} z_0^{n-2} \left\{ a^2 + \frac{b^2 z_0^2}{a^2 - c^2} \right\}.$$

The area S of the aerofoil section, which in the general case is given by

$$S = -\pi \sum_{n=0}^{\infty} (n-1) a_n \bar{a}_n,$$

is in this case $$\pi a^2 \left\{ 1 - \frac{b^4}{(a^2 - c^2)^2} \right\}.$$

To determine the forces and couple we want the following constants:

$$\pi A = \pi \left\{ a_0 \bar{a}_0 + \sum_{n=1}^{\infty} n a_{n+1} \bar{a}_{n+1} \right\} = 2\pi a^2 - S,$$

$$B = b^2,$$

$$C = \frac{a^2 b^4 (2a^2 - c^2)}{(a^2 - c^2)^2} + \frac{a^2 b^8 c^2}{(a^2 - c^2)^4} + \frac{b^6 (2a^2 - c^2)(z_0^2 + \bar{z}_0^2)}{(a^2 - c^2)^3},$$

$$D = \frac{-2b^4 z_0}{a^2 - c^2} - \frac{a^2 b^4 z_0}{(a^2 - c^2)^2} - \frac{a^2 b^6 \bar{z}_0}{(a^2 - c^2)^3}.$$

We also want the values of

$$\bar{a}_0+\sum_{n=2}^{\infty}\bar{a}_n = a+\frac{b^2}{a+\bar{z}_0},$$

and $$\sum_{n=1}^{\infty}(b_n+\bar{b}_n) = -\frac{b^4(z_0+\bar{z}_0)}{a(a^2-c^2)}$$

$$+\sum_{n=2}^{\infty}(-)^n\frac{b^2}{a^2}\left[\left(a^2+\frac{b^2z_0^2}{a^2-c^2}\right)\frac{z_0^{n-2}}{a^{n-2}}+\left(a^2+\frac{b^2\bar{z}_0^2}{a^2-c^2}\right)\frac{\bar{z}_0^{n-2}}{a^{n-2}}\right],$$

and also $$a_0b_1 = -b^4z_0/(a^2-c^2).$$

For the Joukowski condition we want

$$\sum_{n=1}^{\infty}n(b_ne^{ni\zeta_t}+\bar{b}_ne^{-ni\zeta_t}),$$

where ζ_t is the value of ζ at the trailing edge. This is given by

$$z_0+ae^{i\zeta_t} = -b,$$

so that this expression can be reduced to

$$\frac{b^2}{a^2-c^2}[b(z_0+\bar{z}_0)+z_0^2+\bar{z}_0^2]+4b^2+3b(z_0+\bar{z}_0)+2c^2.$$

To the first order in x_0, y_0 and c, since

$$b^2 = a^2-2bx_0-c^2 = a^2-2ax_0,$$

these various constants reduce to

$$S = 4\pi ax_0;$$

$$A = 2a(a-2x_0);$$

$$B = a(a-2x_0),\quad A = 2B;$$

$$C = 2a^3(a-4x_0);$$

$$D = -4a^2x_0-2a^2iy_0,\quad D' = -4a^2x_0,\quad D'' = -2a^2y_0;$$

$$\bar{a}_0+\sum_{n=2}^{\infty}\bar{a}_n = 2a-3x_0+iy_0;$$

$$\sum_{n=1}^{\infty}(b_n+\bar{b}_n) = 2a(a-4x_0);$$

$$a_0b_1 = -a^2z_0,$$

$$\sum_{n=1}^{\infty}n(b_ne^{ni\zeta_t}+\bar{b}_ne^{-ni\zeta_t}) = 4a^2.$$

4. Inserting these values in the general expressions (2·2) and (2·3) for the complex force and the couple, and using $D = D' + iD''$, we derive the following expressions

$$X = S\rho\dot{u} - 2\pi\rho(a^2-b^2)\,\dot{u} + \pi\rho\dot{\omega}D'' - S\rho\omega v + 2\pi\rho(a^2+b^2)\,\omega v$$

$$+\pi\rho\omega^2 D' + \tfrac{1}{2}i\rho\dot{K}\left(\frac{b^2}{a+\bar{z}_0} - \frac{b^2}{a+z_0}\right) - \rho K v, \qquad (4\cdot 1)$$

$$Y = S\rho\dot{v} - 2\pi\rho(a^2+b^2)\,\dot{v} - \pi\rho\dot{\omega}D' + S\rho\omega u - 2\pi\rho(a^2-b^2)\,\omega u$$

$$+\pi\rho\omega^2 D'' - \tfrac{1}{2}\rho\dot{K}\left(2a + \frac{b^2}{a+z_0} + \frac{b^2}{a+\bar{z}_0}\right) + \rho K u, \qquad (4\cdot 2)$$

$$\Gamma = -\pi\rho C\dot{\omega} + \pi\rho D''\dot{u} - \pi\rho D'\dot{v} - \tfrac{1}{2}\rho\dot{K}\sum_{n=1}^{\infty}(b_n + \bar{b}_n)$$

$$-4\pi\rho b^2 uv - \pi\rho\omega\{D'u + D''v\}. \qquad (4\cdot 3)$$

Assuming the Joukowski condition at the trailing edge, we have seen that K must satisfy the equation

$$\frac{K}{2\pi} = -i(\bar{a}_0 w e^{i\zeta_t} - a_0 \bar{w} e^{-i\zeta_t}) + \tfrac{1}{2}\omega \sum_{n=1}^{\infty} n(b_n e^{ni\zeta_t} + \bar{b} e^{-ni\zeta_t}),$$

which reduces to

$$\frac{K}{2\pi} = 2uy_0 - 2v(b + x_0)$$

$$+\tfrac{1}{2}\omega\left[\frac{b^2}{a^2-c^2}\{b(z_0+\bar{z}_0) + z_0^2 + \bar{z}_0^2\} + 4b^2 + 3b(z_0+\bar{z}_0) + 2c^2\right].$$

To the first order in x_0, y_0, c, this condition reduces to

$$\frac{K}{2\pi} = 2uy_0 - 2av + 2a^2\omega. \qquad (4\cdot 4)$$

Using this value for K and also the first-order values of the constants, the expressions for the forces and couple on the aerofoil are

$$X = 4\pi\rho a y_0\,\dot{v} - 6\pi\rho a^2 y_0\,\dot{\omega} - 4\pi\rho y_0 uv$$

$$-8\pi\rho a x_0\,\omega v + 4\pi\rho a v^2 - 4\pi\rho a^2 x_0\,\omega^2, \qquad (4\cdot 5)$$

$$Y = 4\pi\rho a(a - x_0)\,\dot{v} - 8\pi\rho a y_0\,\dot{u} - 8\pi\rho a^2(a - 2x_0)\,\dot{\omega}$$

$$-2\pi\rho a^2 y_0\,\omega^2 + 4\pi\rho y_0 u^2 - 4\pi\rho a uv + 4\pi\rho a^2\omega u, \qquad (4\cdot 6)$$

$$\Gamma = 6\pi\rho a^3(a - 4x_0)\,\dot{\omega} - 6\pi\rho a^2 y_0\,\dot{u} + 4\pi\rho a^2(a - 3x_0)\,\dot{v}$$

$$-4\pi\rho a(a - 2x_0)\,uv + 4\pi\rho a^2 x_0\,\omega u + 2\pi\rho a^2 y_0\,\omega v. \qquad (4\cdot 7)$$

5. The usual theory giving the numerical details for the lift, drag and moment for an aerofoil moving in a uniform rectilinear motion, is of course based on a statical theory which assumes the aerofoil to be at rest in a uniform stream. It is however easy to show that our theory gives identical results even under more general circumstances than those usually adopted.

Let us then first assume that the cylinder is moving forwards with a uniform velocity U at a finite angle of attack α. In such a case

$$u = U\cos\alpha, \quad v = -U\sin\alpha, \quad w = Ue^{-i\alpha}, \tag{5·1}$$

and the angular velocity and all the accelerations are zero. The components of the force on the aerofoil thus reduce to

$$X = \rho KU\sin\alpha, \quad Y = \rho KU\cos\alpha, \tag{5·2}$$

whilst in the quite general case

$$\Gamma = \pi\rho i(\bar{B}w^2 - B\bar{w}^2).$$

If $B = |B|e^{2i\epsilon}$, this means that

$$\Gamma = 2\pi\rho\,|B|\,U^2\sin 2(\alpha+\epsilon). \tag{5·3}$$

The usual notation for the position of the trailing edge is such that $\zeta_t = \pi - \beta$ so that the Joukowski condition in the quite general case is

$$\frac{K}{2\pi} = -i\bar{a}_0 we^{i(\pi-\beta)} + ia_0\bar{w}e^{-i(\pi-\beta)} \tag{5·4}$$

$$= i\bar{a}_0 we^{-i\beta} - ia_0\bar{w}e^{i\beta},$$

or taking a_0 real, which is always possible by proper choice of axes,

$$\frac{K}{2\pi} = 2a_0 U\sin(\alpha+\beta).$$

The drag on the aerofoil is therefore zero, whilst the lift is

$$L = X\sin\alpha + Y\cos\alpha = \rho KU$$

$$= 4\pi\rho a_0 U^2\sin(\alpha+\beta), \tag{5·5}$$

and the moment round the centre is

$$\Gamma = 2\pi\rho\,|B|\,U^2\sin 2(\alpha+\epsilon). \tag{5·6}$$

The centre of pressure, or the point on the "chord" where the single resultant of the pressures acts, is also readily determined as soon as we know the position of the chord.

These formulae are so far quite general, being restricted only by the assumptions about the fluid motion which we have made. It is of course doubtful whether the hydrodynamical assumptions of simple circulation hold at large angles, even when we have, as in the Joukowski aerofoil, a well rounded leading edge.

6. For the Joukowski aerofoil we have

$$B = b^2, \quad \epsilon = 0, \quad a_0 = a,$$

and therefore $$L = 4\pi\rho a U^2 \sin(\alpha+\beta),$$

whilst $$\Gamma = 2\pi\rho b^2 U^2 \sin 2\alpha.$$

The line of action of the resultant force is given by

$$Xy - Yx + \Gamma = 0,$$

and with the origin at the centre of the circle as we have taken it, the chord is the line $y = -y_0$. The centre of pressure is therefore the point

$$(x_\rho, y_\rho) = \left(\frac{Xy_0+\Gamma}{Y}, -y_0\right).$$

The distance of this centre along the chord from the trailing edge will be

$$x_\rho + 2b + x_0 = 2b + x_0 + (Xy_0+\Gamma)/Y,$$

which is $$2b + x_0 + y_0 \tan\alpha + \frac{b^2 \sin\alpha}{a \sin(\alpha+\beta)}. \qquad (6\cdot1)$$

This increases as α increases, so that as the angle of attack is increased the centre of pressure moves forward. This is usually taken to imply an approach to instability of the aerofoil, but the problem of stability seems to be more involved because increasing angle of attack involves the introduction of an angular velocity and changing circulation, so that all the terms in the lift, drag, and moment must be introduced.

7. The general question of longitudinal stability has been tackled in two different ways. There are first the general dynamical discussions originated by Lanchester (1906) and Bryan (1911) and continued and extended by Bairstow (1913, 1920) and others, Glauert (1927) and more recently B. M. Jones (1935). In these the hydrodynamical reactions—reduced to a force with components X, Y and a couple Γ—are assumed to be determinate

functions of the velocities of the moving aerofoil, so that for longitudinal stability discussions they may be expanded in the approximate forms

$$\left.\begin{aligned} X &= X_0 + X_p p + X_q q + X_\omega \omega, \\ Y &= Y_0 + Y_p p + Y_q q + Y_\omega \omega, \\ \Gamma &= \Gamma_0 + \Gamma_p p + \Gamma_q q + \Gamma_\omega \omega, \end{aligned}\right\} \tag{7·1}$$

where p, q, ω denote the small oscillatory deviations of the velocity components from their stationary values. The criterion for stability determined in the usual way from the equations of motion, can then be expressed in terms of known constants of the aerofoil and the coefficients X_0, X_p, X_q, X_ω etc.

These discussions however, while they may be to some extent useful in an empirical sort of way, fall short of a complete theory as they provide no complete theoretical basis for the determination of the coefficients or any justification for the assumption that they represent the complete effect even under the most ideal conditions. Here however our discussion to some extent —but still incompletely—fills the gap. We have in fact from the general values in paragraph 2:

$$\begin{aligned} Y + iX = &-\pi\rho i\{A\dot{\bar{w}} - 2\bar{B}\dot{w} - i\dot{\omega}\bar{D}\} - \pi\rho\omega\{A\bar{w} - 2\bar{B}w - i\omega\bar{D}\} \\ &\qquad - \rho\dot{K}\left\{\dot{\bar{a}}_0 + \sum_{n=2}^{\infty}\bar{a}_n\right\} + \rho\dot{\bar{w}}K - \rho i\omega K\bar{a}_1, \end{aligned}$$

$$\begin{aligned} \Gamma = &-\pi\rho C\dot{\omega} - \tfrac{1}{2}\pi\rho i\{D\dot{\bar{w}} - \bar{D}\dot{w}\} + \pi\rho i\{\bar{B}w^2 - B\bar{w}^2\} \\ &\qquad - \tfrac{1}{2}\rho\omega\{\bar{D}w + D\bar{w}\} - \tfrac{1}{2}\rho\dot{K}\sum_{n=1}^{\infty}(b_n + \bar{b}_n) + \tfrac{1}{2}\rho K\{\dot{\bar{a}}_1 w + a_1\bar{w}\}, \end{aligned}$$

whilst according to the equation (2·8)

$$\frac{K}{2\pi} = -i\{\bar{a}_0 w e^{i\zeta_t} - a_0\bar{w}e^{-i\zeta_t}\} + \tfrac{1}{2}\omega\sum_{n=1}^{\infty} n(b_n e^{ni\zeta_t} + \bar{b}_n e^{-ni\zeta_t}).$$

If now we wish to discuss the stability of the uniform rectilinear motion with velocity U at an angle of attack α, we assume that the aerofoil is moving forward with a velocity $U+p$, p being the small part of the forward velocity which varies. We also suppose that there is small vertical oscillation q and small angular oscillation θ, and that p, q and θ are so small that we can neglect squares and products of them. We have then

$$\begin{aligned} u &= (U+p)\cos\alpha - U\theta\sin\alpha + q\sin\alpha, \\ v &= -(U+p)\sin\alpha - U\theta\cos\alpha + q\cos\alpha, \\ \omega &= \dot{\theta}. \end{aligned}$$

The first two of these equations are equivalent to

$$w = u + iv = \{U + p + i(q - U\theta)\}\, e^{-i\alpha},$$

so that

$$\dot{w} = \{\dot{p} + i(\dot{q} - U\omega)\}\, e^{-i\alpha}.$$

Adopting now a notation similar to that introduced in paragraph 5, using however the general value of K given above, and retaining only first order terms in the small quantities p, q, ω, θ, we have

$$\begin{aligned} Y + iX = {} & -\pi\rho i\{Ae^{i\alpha}(\dot{p} - i\dot{q}) - 2\bar{B}e^{-i\alpha}(\dot{p} + i\dot{q} - 2iU\omega) - \bar{D}i\dot{\omega}\} \\ & - 4\pi\rho k' a_0\{\dot{p}\sin(\alpha+\beta) - (\dot{q} - U\omega)\cos(\alpha+\beta) + k\dot{\omega}/2a_0\} \\ & + 4\pi\rho a_0 e^{i\alpha} U\{(U + 2p)\sin(\alpha+\beta) - (q - U\theta)\, e^{i\alpha+i\beta}\} \\ & + 2\pi\rho k\omega U e^{i\alpha} - 4\pi\rho i \bar{a}_1 a_0\, \omega U \sin(\alpha+\beta), \end{aligned}$$

and

$$\begin{aligned} \Gamma = {} & -\pi\rho C\dot{\omega} - \tfrac{1}{2}\pi\rho i\{De^{i\alpha}(\dot{p} - i\dot{q}) - \bar{D}e^{-i\alpha}(\dot{p} + i\dot{q})\} \\ & + \pi\rho i\{(U^2 + 2Up)(\bar{B}e^{-2i\alpha} - Be^{2i\alpha}) + 2iU(q - U\theta)(\bar{B}e^{-2i\alpha} + Be^{2i\alpha})\} \\ & - 2\pi\rho a_0 \sum_{n=1}^{\infty}(b_n + \bar{b}_n)\{\dot{p}\sin(\alpha+\beta) - (\dot{q} - U\omega)\cos(\alpha+\beta) + k\dot{\omega}/2a_0\} \\ & - 2\pi\rho a_0 U\{(U + 2p)\sin(\alpha+\beta)(a_1 e^{i\alpha} + \bar{a}_1 e^{-i\alpha}) \\ & \qquad\qquad - (q - U\theta)\, e^{i\alpha}(a_1 e^{i\alpha+i\beta} + \bar{a}_1 e^{-i\alpha-i\beta})\} \\ & + \pi\rho k\omega U\{a_1 e^{i\alpha} + \bar{a}_1 e^{-i\alpha}\}, \end{aligned}$$

where

$$k = \tfrac{1}{2}\sum_{n=0}^{\infty}(-)^n n\{b_n e^{-ni\beta} + \bar{b}_n e^{ni\beta}\}; \quad k' = \bar{a}_0 + \sum_{n=2}^{\infty}\bar{a}_n.$$

These expressions determine, under the ideal conditions we have assumed, exact values for all the coefficients X_p, X_q, …, but they show at once that the simple values (7·1) are far from giving a complete account of the reaction involved. Our expressions for X, Y, Γ involve in fact not only all the terms shown in (7·1) but also terms in the accelerations of the type $X_{\dot{p}}\dot{p}$ and also, what is more important perhaps, terms in the angular displacement of the type $X_\theta\theta$. In his discussion B. M. Jones realizes that the simpler relations are incomplete in so far as the acceleration terms are concerned, and he endeavours to remedy this defect as regards the moment equation and its dependence on $\dot{q}$, but as in all previous discussions very little more than a general idea that the component must exist is advanced as a reason for its inclusion. That such a procedure is not always free from criticism can be seen from our form of this particular term. Using $D = |D|\, e^{i\delta}$ and

$$E = 2\sum_{n=1}^{\infty}(b_n + \bar{b}_n),$$

our analysis shows in fact that

$$\Gamma_{\dot q} = -\pi\rho\{|D|\cos(\alpha+\delta) - E\cos(\alpha+\beta)\},$$

whilst the term in $\dot p$, which is neglected, has a coefficient

$$\Gamma_{\dot p} = \pi\rho\{|D|\sin(\alpha+\delta) - E\sin(\alpha+\beta)\}.$$

These are of the same order of magnitude unless the angle of attack α and the angle β are both small.

Our general form of the approximate relations of course render the discussion of the stability problem much more complicated, and for the present we shall content ourselves with two comparatively simple cases. In the first of these the aerofoil will be assumed to be a flat plate, and in the second a first approximation to the nearly flat Joukowski aerofoil for which we now have the values of the coefficients concerned.

8. We therefore examine in some detail the general problem of the stability of the previous uniform rectilinear motion, but restricting ourselves first to the simplest approximation obtained by assuming that the aerofoil is a flat plate. Taking all quantities per unit length of the plate, the general equations of motion are of the form

$$M(\dot u - \omega v - y_G\dot\omega - x_G\omega^2) = X + X_1, \tag{8·1}$$

$$M(\dot v + \omega u + x_G\dot\omega - y_G\omega^2) = Y + Y_1, \tag{8·2}$$

$$I_G\dot\omega = G_G + \Gamma + Xy_G - Yx_G. \tag{8·3}$$

Here M is the mass, (x_G, y_G) the co-ordinates of the centroid and I_G the moment of inertia of the plate about the centroid. X_1, Y_1 and G_G are the external forces and couple acting on the plate—provided by the propellers, steering and gravity—whilst X, Y, Γ are the hydrodynamic forces determined above. In the case of the flat plate these reduce to

$$\begin{aligned} X &= 4\pi\rho a v^2, \\ Y &= 4\pi\rho a^2\dot v - 8\pi\rho a^3\dot\omega - 4\pi\rho a u v + 4\pi\rho a^2\omega u, \\ \Gamma &= -6\pi\rho a^4\dot\omega + 4\pi\rho a^3\dot v - 4\pi\rho a^2 u v. \end{aligned}$$

Inserting in these expressions the values of u and v given in the previous paragraph, we find at once that

$$X_{\dot p} = X_{\dot q} = X_{\dot\omega} = 0;$$

$$X_p = 8\pi\rho a U\sin^2\alpha; \quad X_q = -4\pi\rho a U\sin 2\alpha; \quad X_\omega = 0;$$

$$X_\theta = 4\pi\rho a U^2\sin 2\alpha; \quad X_0 = 4\pi\rho a U^2\sin^2\alpha;$$

whilst

$$
\begin{aligned}
&Y_{\dot{p}} = -4\pi\rho a^2 \sin\alpha; \quad Y_{\dot{q}} = 4\pi\rho a^2 \cos\alpha; \quad Y_{\dot{\omega}} = -8\pi\rho a^3;\\
&Y_p = 8\pi\rho a U \sin\alpha \cos\alpha; \quad Y_q = -4\pi\rho a U \cos 2\alpha; \quad Y_\omega = 0\\
&Y_\theta = 4\pi\rho a U^2 \cos 2\alpha; \quad Y_0 = 4\pi\rho a U^2 \sin\alpha \cos\alpha;
\end{aligned}
$$

and similarly

$$
\begin{aligned}
&\Gamma_{\dot{p}} = -4\pi\rho a^3 \sin\alpha; \quad \Gamma_{\dot{q}} = 4\pi\rho a^3 \cos\alpha; \quad \Gamma_{\dot{\omega}} = -6\pi\rho a^4;\\
&\Gamma_p = 4\pi\rho a^2 U \sin 2\alpha; \quad \Gamma_q = -4\pi\rho a^2 U \cos 2\alpha; \quad \Gamma_\omega = -4\pi\rho a^3 U \cos\alpha;\\
&\Gamma_\theta = 4\pi\rho a^2 U \cos 2\alpha; \quad \Gamma_0 = 4\pi\rho a^2 U^2 \sin\alpha \cos\alpha.
\end{aligned}
$$

It is probably, however, simpler at the moment to interpret our equations directly without introducing these coefficients. Doing this the equations (8·1), (8·2) and (8·3) become

$$M(\dot{u} - \omega v - y_G \dot{\omega} - x_G \omega^2) = 4\pi\rho a v^2 + X_1, \tag{8·4}$$

$$(M - 4\pi\rho a^2)(\dot{v} + \omega u) + M x_G \dot{\omega} + 8\pi\rho a^3 \dot{\omega} - M y_G \omega^2 = -4\pi\rho a u v + Y_1, \tag{8·5}$$

$$
\begin{aligned}
&(I_G + 6\pi\rho a^4)\dot{\omega} - 8\pi\rho a^3 x_G \dot{\omega} - 4\pi\rho a^2 (a - x_G)\dot{v}\\
&\qquad = G_G - 4\pi\rho a (a - x_G) u v + 4\pi\rho a y_G v^2 - 4\pi\rho a^2 x_G \omega u,
\end{aligned} \tag{8·6}
$$

or with the special values of u, v and using D for the operator d/dt these reduce to

$$
\left.
\begin{aligned}
&(M \cos\alpha\, D - 8\pi\rho a U \sin^2\alpha)\, p + (M \sin\alpha\, D + 4\pi\rho a U \sin 2\alpha)\, q\\
&\qquad - (M y_G D^2 + 4\pi\rho a U^2 \sin 2\alpha)\,\theta - 4\pi\rho a U^2 \sin^2\alpha - X_1 = 0,\\
&\{(M - 4\pi\rho a^2) \sin\alpha\, D + 4\pi\rho a U \sin 2\alpha\}\, p\\
&\qquad - \{(M - 4\pi\rho a^2) \cos\alpha\, D + 4\pi\rho a U \cos 2\alpha\}\, q\\
&\qquad\quad - \{(M x_G + 8\pi\rho a^3) D^2 - 4\pi\rho a U^2 \cos 2\alpha\}\,\theta\\
&\qquad\qquad + 4\pi\rho a U^2 \sin\alpha \cos\alpha + Y_1 = 0,\\
&\{4\pi\rho a^2 (a - x_G) \sin\alpha\, D - 4\pi\rho a (a - x_G)\, U \sin 2\alpha - 8\pi\rho a y_G\, U \sin^2\alpha\}\, p\\
&\quad - \{4\pi\rho a^2 (a - x_G) \cos\alpha\, D - 4\pi\rho a (a - x_G)\, U \cos 2\alpha - 4\pi\rho a y_G\, U \sin 2\alpha\}\, q\\
&\qquad + \{(I_G + 6\pi\rho a^4 - 8\pi\rho a^3 x_G) D^2 + 4\pi\rho a^3\, U \cos\alpha\, D\\
&\qquad - 4\pi\rho a (a - x_G)\, U^2 \cos 2\alpha - 4\pi\rho a y_G\, U^2 \sin 2\alpha\}\,\theta\\
&\qquad\quad - G_G - 4\pi\rho a (a - x_G)\, U^2 \sin\alpha \cos\alpha - 4\pi\rho a y_G\, U^2 \sin^2\alpha = 0,
\end{aligned}
\right\} \tag{8·7}
$$

and in these equations, following the usual practice, the finite terms are assumed to balance among themselves.

9. If now we write

$$M' = M - 4\pi\rho a^2,$$

$$I' = I_G + 6\pi\rho a^4 - 8\pi\rho a^3 x_G,$$

$$G_G = -I_G n^2\theta,$$

the solution of the above equation for θ is

$$\theta = \Theta e^{\lambda t},$$

where Θ is a constant and λ is a root of an equation which can be written in the form

$$(a''b - ab'')(a'c - ac') - (a'b - ab')(a''c - ac'') = 0. \qquad (9\cdot1)$$

In this equation the expressions $a, b, c, a', b', c', a'', b'', c''$ are defined by the following relations

$$a = M\lambda\cos\alpha - 8\pi\rho a U\sin^2\alpha;$$

$$b = M\lambda\sin\alpha + 4\pi\rho a U\sin 2\alpha;$$

$$c = -(My_G\lambda^2 + 4\pi\rho a U^2\sin 2\alpha);$$

$$a' = -(M'\lambda\sin\alpha + 4\pi\rho a U\sin 2\alpha);$$

$$b' = M'\lambda\cos\alpha + 4\pi\rho a U\cos 2\alpha;$$

$$c' = (Mx_G + 8\pi\rho a^3)\lambda^2 - 4\pi\rho a U^2\cos 2\alpha;$$

$$a'' = 4\pi\rho a^2(a - x_G)\lambda\sin\alpha - 4\pi\rho a(a - x_G)U\sin 2\alpha - 8\pi\rho a y_G U\sin^2\alpha;$$

$$b'' = -\{4\pi\rho a^2(a - x_G)\lambda\cos\alpha - 4\pi\rho a(a - x_G)U\cos 2\alpha - 4\pi\rho a y_G U\sin 2\alpha\};$$

$$c'' = I'\lambda^2 + 4\pi\rho a^3 U\lambda\cos\alpha + I_G n^2 - 4\pi\rho a(a - x_G)U^2\cos 2\alpha - 4\pi\rho a y_G U^2\sin 2\alpha.$$

For our purpose it is more convenient to write the equation for λ in the form*

$$c''(a'b - ab') + a''(b'c - bc') + b''(ac' - a'c) = 0. \qquad (9\cdot2)$$

---

* In transforming the equation (9·1) to (9·2) we have rejected a factor $a = 0$. In reality this means that the biquadratic equation (9·2) should really be a quintic and then there is always a positive real root

$$\lambda = 8\pi\rho a U\sin^2\alpha / M\cos\alpha.$$

This value of λ is always very small in practice, but it means that, at least at high speeds, there is always a small element of instability in the motions: this probably merely means either that the approximations adopted are not entirely satisfactory or that the theory really requires the viscous drag to account completely for stability under otherwise suitable conditions. Any drag additional to that included above would of course tend to counterbalance this instability and even a term due to a trailing wake might be sufficient.

Before attempting to solve this equation, or to express the condition for the reality of the roots, which is what we are really after, we must notice that under the conditions of practical aerodynamics it will simplify considerably. In fact the value of $\rho a U$ will always in practice be numerically much smaller than the value of $M\lambda$ so that each bracket in (9·2) is of the same order. But then since a'' and b'' are both very small compared with c'' we assume that the last two terms are completely negligible compared with the first. The equation (9·2) then reduces simply to

$$I'\lambda^2 + 4\pi\lambda\rho a^3 U \cos\alpha + I_G n^2 - 4\pi\rho a(a - x_G)\, U^2 \cos 2\alpha - 4\pi\rho a y_G\, U^2 \sin 2\alpha = 0. \tag{9·3}$$

This reduction of course is equivalent to the usual extraction of the main root of the usual biquadratic period equation obtained in these discussions, the root which corresponds to what is called the phugoid oscillation of the aerofoil.

Physically our approximations seem to imply that it is the rotational terms that are the governing factors in the stability. If the motion is to be stable the values of λ given by equation 9·3 must of course be complex. This means that

$$4I'[I_G n^2 - 4\pi\rho a(a - x_G)\, U^2 \cos 2\alpha - 4\pi\rho a y_G\, U^2 \sin 2\alpha] > 16\pi^2\rho^2 a^6 U^2 \cos^2\alpha,$$

or

$$I_G n^2/U^2 > 4\pi\rho a(a - x_G) \cos 2\alpha + 4\pi\rho a y_G \sin 2\alpha + \frac{16\pi^2\rho^2 a^6 \cos^2\alpha}{I_G + 6\pi\rho a^4 - 8\pi\rho a^3 x_G}. \tag{9·4}$$

The last term on the right-hand side is very small compared with the remaining terms and we can therefore say that the condition for stability is simply

$$I_G n^2/U^2 > 4\pi\rho a(a - x_G) \cos 2\alpha + 4\pi\rho a y_G \sin 2\alpha. \tag{9·5}$$

An important point to notice is that we have now a single criterion for stability. When there is oscillation the exponential factor in the amplitude of the harmonic oscillation which is

$$\exp[-2\pi\rho a^3\, Ut \cos\alpha/I']$$

always represents a decay; in the discussions based on the incomplete equations this factor may under certain conditions represent an increasing amplitude and this is interpreted as implying instability as much as does a pure exponential solution.

We can now see in what manner the position of the centre of gravity will affect the stability, and also whether the position of the centre of pressure in any way influences it. From the expression in paragraph 6 for the position of the centre of pressure, we see that for a flat plate it is at the point $x = a$, and remains unaltered whatever the angle of attack. If $\alpha < \pi/4$ so that $\cos 2\alpha$ and $\sin 2\alpha$ are both positive, then as the centre of gravity moves forward the first term on the right-hand side decreases, and when the centre of gravity is in front of the centre of pressure it becomes negative. It appears then that the further forward the centre of gravity, the greater the stability. This may however only be true up to a certain point because we must remember that the term $I_G n^2$ will also depend on the position of the centre of gravity, $-I_G n^2\theta$ being the moment of the external forces about the centre of gravity, so that as x_G increases $I_G n^2$ will decrease and thus the possibility of stability will decrease. The second term on the right-hand side indicates that the lower the centre of gravity the greater the stability. We notice also that if y_G is positive the stability increases as the angle of attack decreases from zero.

10. Having reduced the equation for λ in the case of the flat plate to the comparatively simple form above, we now turn to the question of the stability of the thin aerofoil, to see in what manner the thickness and camber may influence the stability. To work out the equations from the beginning would be much too tedious, especially considering the fact that we ultimately only take very approximate forms. By tracing back the terms remaining in the period equation (8·3), we notice that it is only necessary to calculate the θ term in the last equation of motion. That is, we want the θ term in the equation

$$I_G\dot{\omega} = G_G + \Gamma + Xy_G - Yx_G,$$

where now

$$X = 4\pi\rho a y_0 \dot{v} - 6\pi\rho a^2 y_0 \dot{\omega} - 4\pi\rho y_0 uv$$
$$- 8\pi\rho a x_0 \omega v + 4\pi\rho a v^2 - 4\pi\rho a^2 x_0 \omega^2,$$

$$Y = 4\pi\rho a(a - x_0)\dot{v} - 8\pi\rho a y_0 \dot{u} - 8\pi\rho a^2(a - 2x_0)\dot{\omega}$$
$$- 2\pi\rho a^2 y_0 \omega^2 + 4\pi\rho y_0 u^2 - 4\pi\rho a uv + 4\pi\rho a^2 \omega u,$$

$$\Gamma = 6\pi\rho a^3(a - 4x_0)\dot{\omega} - 4\pi\rho a^2 y_0 \dot{u} + 4\pi\rho a^2(a - 3x_0)\dot{v}$$
$$- 4\pi\rho a(a - 2x_0) uv + 4\pi\rho a^2 x_0 \omega u + 2\pi\rho a^2 y_0 \omega v,$$

where u, v, ω have the same values as for the flat plate. The equation for λ is then

$$\begin{aligned}&\{I_G + 6\pi\rho a^3(a-4x_0) + 6\pi\rho a^2 y_0 y_G - 8\pi\rho a^2(a-2x_0)\,x_G\}\,\lambda^2\\ &\quad-\{4\pi\rho a^2 y_0\,U\sin\alpha + 4\pi\rho a^2(a-3x_0)\,U\cos\alpha - 4\pi\rho a y_0 y_G\,U\cos\alpha\\ &\qquad\qquad + 8\pi\rho a x_0 y_G\,U\sin\alpha - 4\pi\rho a x_0 x_G\,U\cos\alpha - 8\pi\rho a y_0 x_G\,U\sin\alpha\}\,\lambda\\ &\quad+\{I_G n^2 - 4\pi\rho a(a-3x_0)\,U^2\cos 2\alpha - 4\pi\rho y_0 y_G\,U^2\cos 2\alpha\\ &\qquad\qquad - 4\pi\rho a y_G\,U^2\sin 2\alpha - 4\pi\rho y_0 x_G\,U^2\sin 2\alpha + 4\pi\rho a x_G\,U^2\cos 2\alpha\} = 0,\end{aligned}$$

and the condition for stability is therefore simply

$$I_G n^2/U^2 > 4\pi\rho\{a(a-3x_0-x_G)+y_0 y_G\}\cos 2\alpha + 4\pi\rho\{a y_G + y_0 x_G\}\sin 2\alpha.$$

The camber of the aerofoil depends on the value of y_0 and therefore we see that an increase in camber means a reduction in stability in all cases. The thickness of the aerofoil depends on the value of x_0 so that if we assume that the actual mass of the body is so great that the position of the centre of gravity is not appreciably changed by increasing the thickness of the fore-end of the wing-section, then an increase of thickness or bluntness of the fore-end means an increase of the stability. If, however, as x_0 increases x_G also increases, then, unless α is very small so that $\sin 2\alpha$ is very small, the last term on the right-hand side will represent an influence for decreasing stability, although it may not even then override the influence of the first term.

These results agree with those obtained by other writers, although generally speaking they are much more precise than those obtained previously. Glauert (1919), in a discussion of the stability of the phugoid oscillation, concludes that stability can be most easily secured by a forward movement of the centre of gravity relative to the wing structure, and later (1929) he states more precisely in relation to a hinged aerofoil that for a hinged position further forward than 0·25 of the chord, the damping moment changes sign at very low frequencies and the oscillation of the aerofoil will be maintained by an unstable damping moment.

Later Higgins (1934), concludes that satisfactory stability usually occurs when the centre of gravity is between 25 and 20 % of the chord from the leading edge, and that given two aeroplanes of like characteristics at high speeds, the low wing aeroplane with its high centre of gravity would be less stable, and the high wing aeroplane too stable at low speeds.

The range of variation shown by these results seems to emphasize our point that the critical point for stability is not the centre of pressure on the wing (except in the flat plate), although it is a point near this centre. Too close an analogy between our precise results and those obtained in the previous general dynamical discussions cannot however be expected because while we have been able to generalize the previous discussions in certain directions we have not yet been able to include the effect of the viscous drag which is included in the empirical coefficients of the dynamical theory. There are however indications that it may still be possible to generalize our theory in this direction, but such generalization would take us too far from our path at the moment.

11. When the above discussion was completed it was hoped to be able to carry it through also on the basis of Wagner's theory, in a simplified and tractable form. Assuming that the aerofoil is the simple flat plate and that the trail of vortices from the back edge can be replaced by a single average vortex with the same effect, we can of course use the results of "II" to deduce the forces. If the circulation round the plate is K and the strength of the vortex $-K$, so that the total circulation is zero, then the expressions for the force and couple assume in the general case the following forms:

$$\begin{aligned} Y+iX = & -\pi\rho i\{A\dot{w}-2\bar{B}\dot{w}-i\dot{\omega}\bar{D}\}-\pi\rho\omega\{A\bar{w}-2\bar{B}w-i\omega\bar{D}\} \\ & +\rho\dot{K}\left\{\bar{z}_0-\bar{a}_0 e^{i\bar{\zeta}_s}+\bar{a}_0 e^{i\zeta_s}-\sum_{n=0}^{\infty}\bar{a}_n\right\} \\ & +\rho i\bar{a}_0 K\{\dot{\zeta}_s e^{i\zeta_s}-\dot{\bar{\zeta}}_s e^{i\bar{\zeta}_s}\}+\rho i\bar{a}_0\,\omega K(e^{i\bar{\zeta}_s}-e^{i\zeta_s}), \end{aligned} \tag{11·1}$$

$$\begin{aligned} \Gamma = & -\pi\rho C\dot{\omega}-\tfrac{1}{2}\pi\rho i\{D\dot{\bar{w}}-\bar{D}\dot{w}\}+\pi\rho i\{\bar{B}w^2-B\bar{w}^2\} \\ & -\tfrac{1}{2}\pi\rho\omega\{\bar{D}w+D\bar{w}\}+\tfrac{1}{2}\rho\dot{K}\sum_{n=1}^{\infty}(b_n e^{ni\zeta_s}+\bar{b}_n e^{-ni\bar{\zeta}_s}-b_n-\bar{b}_n) \\ & -\tfrac{1}{2}\rho K\left[\frac{d}{dt}(z_s\bar{z}_s)-i\left\{\dot{\zeta}_s\sum_{n=1}^{\infty}nb_n e^{ni\zeta_s}-\dot{\bar{\zeta}}_s\sum_{n=1}^{\infty}n\bar{b}_n e^{-ni\bar{\zeta}_s}\right\}\right] \\ & -\tfrac{1}{2}\rho a_0 K\bar{w}(e^{-i\zeta_s}-e^{-i\bar{\zeta}_s})-\tfrac{1}{2}\rho\bar{a}_0 Kw(e^{i\bar{\zeta}_s}-e^{i\zeta_s}), \end{aligned} \tag{11·2}$$

wherein $z_s = z(\zeta_s)$ is the position of the representative vortex, and the constants A, B, ... have the same values as before. In the case of the flat plate these reduce to

$$\begin{aligned} Y+iX = & -4\pi\rho a^2\dot{v}+4\pi\rho a^2 i\omega v-2\rho a\dot{K}+\rho\dot{K}\{\bar{z}_s-ae^{i\bar{\zeta}_s}+ae^{i\zeta_s}\} \\ & +\rho iaK\{\dot{\zeta}_s e^{i\zeta_s}-\dot{\bar{\zeta}}_s e^{i\bar{\zeta}_s}\}+\rho ia\omega K(e^{i\bar{\zeta}_s}-e^{i\zeta_s}), \end{aligned} \tag{11·3}$$

$$\begin{aligned} \Gamma = & -2\pi\rho a^4\dot{\omega}-4\pi\rho a^2 uv-\rho a^2\dot{K}+\tfrac{1}{2}\rho a^2\dot{K}(e^{2i\zeta_s}-e^{-2i\bar{\zeta}_s}) \\ & -\tfrac{1}{2}\rho K\left[\frac{d}{dt}(z_s\bar{z}_s)-2ia^2\{\dot{\zeta}_s e^{2i\zeta_s}-\dot{\bar{\zeta}}_s e^{-2i\bar{\zeta}_s}\}\right] \\ & +\tfrac{1}{2}\rho a\bar{w}K(e^{-i\zeta_s}-e^{-i\bar{\zeta}_s})-\tfrac{1}{2}\rho awK(e^{i\bar{\zeta}_s}-e^{i\zeta_s}). \end{aligned} \tag{11·4}$$

It is, however, impossible to make further progress with these formulae owing to our ignorance of the motion of the vortex itself. In Wagner's discussion the vortices, once they are shed are assumed to remain at rest, and the theory then assumes a definite form with

$$\dot{z}_s = -w - i\omega z_s.$$

But the difficulty about this assumption is that we know that a vortex near a cylinder does not remain at rest; if it is close to the cylinder it moves in fact very fast. When it is at a distance from the cylinder it can of course remain stationary but only because the reaction between it and the cylinder is negligible. Before therefore we can make any progress on these lines it seems necessary to examine in some detail the actual motion of the vortices in the neighbourhood of the cylinder, so that we can allow properly for these motions in the forces they exert on the cylinder. Such an investigation will, it is hoped, form the subject of a further communication on this subject.

SUMMARY

This paper follows two previous ones on the general hydrodynamical problem of the two-dimensional motion of a cylinder in inviscid incompressible fluid. The general formulae obtained in these papers are here reduced for the special case of the Joukowski aerofoil, where the coefficients assume simple finite forms. The formulae obtained are then applied to a determination of the lift, moment and centre of pressure in uniform rectilinear motion, and also to a discussion of the dynamics of the small oscillation about such rectilinear motion. A simple condition is then obtained for the stability of this rectilinear motion, showing the effects of thickness, camber and angle of attack on this important property of the aerofoil.

REFERENCES

Bairstow, L., Jones, B. M. and Thomson, B. A. 1913 *Rep. Memor. Adv. Comm. Aero., Lond.*, no. 77.
Bairstow, L. 1920 *Applied aerodynamics.*
Bryan, G. H. 1911 *Stability in aviation.* Macmillan and Co.
Glauert, H. 1919 *Rep. Memor. Adv. Comm. Aero., Lond.*, no. 638.
— 1927 *Rep. Memor. Adv. Comm. Aero., Lond.*, no. 1093.
— 1929 *Rep. Memor. Adv. Comm. Aero., Lond.*, no. 1242.
Higgins, G. J. 1934 *Tech. Notes Nat. Adv. Comm. Aero., Wash.*, no. 511.
Jones, B. M. 1935 *Aerodynamic theory*, **5**. Berlin.
Lanchester, F. W. 1906 *Aerodonetics.*
Morris, R. M. 1937 *Proc. Roy. Soc.* A, **161**, 406.
— 1938 *Proc. Roy. Soc.* A, **164**, 346.

The lower limiting crystallite size and internal strains in some cold-worked metals

By W. A. Wood

Physics Department, National Physical Laboratory, Teddington, Middlesex

(*Communicated by G. W. C. Kaye, F.R.S.—Received* 27 *April* 1939)

[Plates 11–14]

In recent X-ray work on the structure of a metal after cold-working (Wood 1935), and similarly after fatigue stressing (Gough and Wood 1936), it was shown that when a metal consisting of annealed perfect grains received any permanent deformation, then the grains were dispersed into crystallites with orientations departing widely from the crystallographic orientations of the parent grains. It is possible to set an upper limit to the size of the crystallites in the following manner. With the back-reflexion technique as used in the work, the X-ray photograph of a stationary annealed specimen shows isolated clear-cut reflexion spots which lie on the diffraction rings corresponding to the Bragg reflexion angles. Deformation of the metal causes the spots to extend into continuous arcs owing to the increase in number of independently reflecting units produced with various orientations in the reflecting volume. It can be shown, by calibrating for known grain sizes, that the formation of a continuous line by multiplication and coalescence of the reflexion spots in this way requires an increase in number which can only be brought about by a decrease in size of the units to about 10^{-4} cm. The *continuity* of the diffraction arc indicates therefore that the crystallites must be less than about 10^{-4} cm. It is then possible to set a lower limit to the crystallite size from consideration of the Scherrer effect by which the radial breadth of the continuous diffraction arc depends on the particle size according to a formula of the type $\delta B = 0{\cdot}9\lambda/t \cos\theta$, where δB is the increase in breadth due to the fine-grain effect, t the linear particle size, and θ the reflexion angle. The effect becomes appreciable only when the particle size is less than 10^{-4} cm.; thus in the present experiments a barely noticeable increase in width of 0·1 mm. on the photographic plate would occur in the (420) ring of aluminium, using cobalt K-radiation, if the crystallite size decreased to $0{\cdot}8 \times 10^{-4}$ cm.; but the breadth would increase by about 1 mm. at 10^{-5} cm. and by 1 cm. at 10^{-6} crystallite size, thus constituting a sensitive indication of any reduction in size below the value of 10^{-4} cm. fixed as upper limit. It is found, however, that the broadening of the diffraction line produced by the breakdown of the grains under progressive deformation of a metal never exceeds a definite maximum. On these grounds, the author has pointed out that the limited broadening, whether due to the fine-grain effect or the alternative possibility of lattice distortion or any other cause, automatically sets a lower limit to the size of the crystallites formed on deformation; also, that the striking contrast on the one hand between the ease with which the grains are dispersed into crystallites immediately after deformation and, on the other, the subsequent impossibility, even after the most severe deformation, of breaking them down below about 10^{-5} cm., the value corresponding to the order of maximum line-broadening observed, indicates that the crystallite must be regarded as a fundamental unit of the metallic grain.

The present work brings out the following new observations in connexion with the line-broadening effect and the lattice dimensions of the metal. Taking as example copper, for which the line-broadening is particularly well marked, it is shown that the diffraction rings broaden to a definite maximum, and then on further working diminish in width to an equally characteristic minimum. At the same time, the lattice dimensions of the crystallites change, having an expanded value when the diffraction ring is most diffuse and a contracted value when the line breadth decreases. Moreover, the expanded value is greater and the contracted value is less than what may be termed the standard lattice parameter provided by the large perfect grains of the normal annealed state. The crystalline condition of the cold-worked metal is therefore marked by two extremes: (*a*) a comparatively stable state which is characterized by a contracted lattice and a certain line broadening, and (*b*) a less stable state (since it is upset by continued deformation), characterized by an expanded lattice and an abnormally diffuse line breadth. This latter state therefore throws some light on the nature and extent of the distortion which can be transmitted to and retained by the metallic lattice during overall deformation of a specimen. Also the comparative instability of this state explains the well-known phenomenon that it is possible largely to recover the original hardness, tensile or fatigue properties of a deformed metal by mild heat treatment at temperatures much below those required to renew the properties by recrystallization through annealing (Gough 1924). The reversion from (*b*) to (*a*) is therefore referred to as "recovery", being associated with the removal only of the observed internal strains from the lattice, and being thereby distinguished from recrystallization which proceeds by the reconstitution of new grains. Finally, since the lattice distortion is accompanied by expansion of the lattice, the recovered state with its contracted lattice must give the amount of residual line broadening due only to the Scherrer effect and therefore the corresponding lower limit of the crystallite size. Although major importance is attached to these expansion and recovery effects, in view of the association of lattice distortion with structure-sensitive physical properties, the observed contraction of the lattice is itself of some interest in apparently indicating that the surface atomic layers must be taken into account in X-ray work on fine grains. In large crystals, the surface normally plays no part in X-ray observations, but in the crystallites of 10^{-4} to 10^{-5} cm. size the surface layers begin to form an appreciable proportion of the whole volume, presumably exerting a surface tension analogous to the effects calculated by Lennard-Jones for ionic lattices.

Measurements of the above changes are given for the reasonably ductile metals Cu, Ag, Ni, Al, Mo and Fe in a condition of high purity. At the same time the results of a determination of the lower limiting crystallite size are recorded.

1. COPPER (PURITY 99·999 %)

Specimens were machined to approximately 3 cm. long and rectangular cross-section $0{\cdot}5 \times 0{\cdot}3$ mm., and then annealed *in vacuo* until the grains were about 10^{-1} to 10^{-2} cm. in size and gave quite sharp reflexion spots. After etching they were cold-rolled into strip and X-rayed after every 1 % reduction up to 10 % (reckoned on the original thickness) and then after every 5 % approximately up to 99 %. The rolling process was preferred because the flat surface of the strip lends itself most easily to accurate comparison of line breadth and lattice spacings, but drawing into wire and extrusion give the same effects.

The specimens were examined in a back-reflexion spectrometer designed for precision work of this type. The incident beam passes through a hole in the centre of a flat film and is diffracted backwards, forming full circles concentric with the beam. Photographs were taken with the specimen stationary, its surface perpendicular to the beam, also when oscillating ± 10° about that position. The point of the method is that the diameter of the diffraction ring at the large diffraction angles involved is most sensitive to small changes in lattice spacing, whilst at the same time least sensitive to slight differences in distance of specimen to film. Also the variation of line breadth with particle size is greatest for large values of θ.

These breadths, B, were measured by a Moll microphotometer. The minimum breadth, B_0, due to the finite slit system and the arrangement of the apparatus, was taken as that given by the annealed specimens photographed under the same conditions, the specimens being oscillated to give the continuous line necessary for measurements; this minimum was also checked by photographs of specimens of ZnO and ZnS obtained with a particle size just small enough to give continuous lines. The difference $B-B_0$ then gave the increase δB to be substituted in the Scherrer formula, this procedure being considered accurate enough in view of the assumptions implicit in the deduction of the formulae of this type.

First, typical photographs are reproduced in order to illustrate the order of the effects referred to above, and then the quantitative results are summarized.

(i) *Expansion effect.* Fig. 1 (Plate 11) of the annealed state shows the separate sharp reflexion spots of the initially large perfect grains. Fig. 2 (Plate 11), taken after 4 % reduction, shows the transition to continuous arcs and the beginnings of diffusion, indicating the onset of the crystallite formation; the inner ring is the (400) $\alpha_1\alpha_2$ doublet and the outer single ring the (331) β. Fig. 3 (Plate 11), after 80 % reduction, shows the diffraction rings in the abnormally diffuse condition and also the increase in diameter of the inner ring. The reflexion angle θ is 83·2° for the inner (400) ring (cobalt K-radiation being used), and 77·7° for the outer (331) ring. The difference in these values of θ is sufficient to render the diameter of the (400) ring much more sensitive than the (331) to a lattice change; therefore, when such changes occur, the distance between the two rings should decrease. This relative shift of the two rings is clearly demonstrated by comparison with the preceding fig. 2, despite the difference in diffusion of the rings in the two cases. Fig. 3 is interesting because there is no source of experimental movement that would produce the same effect. Moreover, the bodily shift of the (400) ring serves to demonstrate that the internal strain or distortion which can be imposed on the lattice is of the nature of an expansion, for the ring is made up of reflexions from the three mutually perpendicular (400), (040) and (004) planes, and all these directions must have increased.

(ii) *Recovery effect.* Fig. 4 (Plate 11) shows the diffraction rings after the same specimen has been reduced further in thickness to 85 %. The photograph shows directly that the diameter of the (400) ring has contracted and at the same time the radial diffusion of the rings has decreased. The further deformation has removed the previous expansion from the lattice, thus producing recovery without recrystallization. The abnormal diffusion associated with the expansion effect is attributed to irregularities in such expansion and not to any appreciable further breakdown of the crystallites: otherwise, on recovery, it would be difficult to explain why the crystallites should again increase in size to the arbitrary value corresponding to the characteristic line breadth of the recovered state. After the initial changes accompanying breakdown, the diffusion and expansion effect reached a maximum after about 8 % reduction, being followed by a recovery at 10 %; the processes then alternated as the deformation of the specimen continued. The line breadth decreased to the same value during each recovery; it is therefore reasonable to conclude that this residual broadening is due to the fine-grain effect only, and affords a measure of the lower limiting crystallite size.

Finally, a comparison is shown between the lattice spacing of the recovered state and the initial condition. For this purpose, the photograph of the latter shows the diffraction rings as continuous lines obtained by oscillation of the specimens in order that the position of the diffraction spots should be measurable and represent the true diffraction angle. The initial condition is given in fig. 5*a* and the recovered in fig. 5*b* (Plate 11), and the shift is shown relative to the calibration edges *A*, *B* which correspond to the edges *A*, *B* of the preceding photographs, the fig. 5 having been enlarged (approximately 2·8 times) to bring out the effect. The relative movement is clearly visible despite the diffused $\alpha_1\alpha_2$ doublet in the recovered state, and is in the direction corresponding to contraction of the lattice.

(iii) *Quantitative measurements.* As shown by the photographs reproduced, the magnitude of the observed shifts of the rings is of such an order that the diffusion effects do not interfere with a reasonably accurate determination of the corresponding lattice changes. The absolute value of the unit cell of the initial annealed material was measured at the same time, but major importance is attached to the deviations from this value since they are relative changes occurring under fixed experimental conditions and therefore measurable with greater accuracy. The contraction effect is reckoned from the initial normal spacing, but the expansion given below is the change reckoned from the spacing of the recovered state since that change represents the total amount of internal strain which can be imposed on the lattice.

Lattice spacing of the annealed copper ...	$3{\cdot}608_6 \times 10^{-8}$ cm.
Maximum contraction in recovered state ...	0·06 %
Maximum expansion in distorted state ...	0·27 %
Lower limiting crystallite size	$0{\cdot}7 \times 10^{-5}$ cm.

2. Silver (purity 99·999 %)

The changes in copper have been described in some detail so that for the remaining metals it is necessary only to summarize the results, whilst merely drawing attention to outstanding peculiarities.

For silver, measurements were made on the (331) and (420) rings using cobalt K-radiation, and on the (422) ring using nickel K-radiation. Figs. 6*a* and *b* (Plate 12), after 65 and 70 % reduction respectively, illustrate first the distortion and then the recovery after continued working. The rings are matched along a diameter to show the difference caused by the variation in lattice spacing; at the same time, the improvement in resolution is shown by the fact that the $\alpha_1\alpha_2$ doublets, which are not resolved in fig. 6*a*, are however definitely discernible in fig. 6*b*. Up to about 70 % reduction, in these experiments, the changes observed in the silver were similar to those described for copper, the recovered state being apparently stable at room temperature. But after heavier deformation recovery from the distorted state becomes more violent and complete recrystallization is observed. This is shown by a specimen after 90 % reduction, which gave a photograph similar to fig. 6*a* immediately after rolling, but after standing at room temperature for about a week gave the completely different type reproduced in fig. 7*a*, Plate 12 (fig. 7*b* is the initial annealed state for comparison). This type of recovery thus results in recrystallization to an imperfectly annealed condition. After further deformation, the recrystallization occurred spontaneously on rolling and the corresponding X-ray photographs then showed the reflexion spots from the fresh grains superposed on continuous rings. This marked tendency for recrystallization probably explains why, as indicated below, the magnitude of the observed expansion effect is much less for silver than for copper. The results of the measurements were as follows:

Lattice spacing of the annealed silver	$4{\cdot}077_9 \times 10^{-8}$ cm.
Maximum contraction in recovered state ...	0·03 %
Maximum expansion in distorted state ...	$0{\cdot}04_5$ %
Lower limiting crystallite size	$0{\cdot}8 \times 10^{-5}$ cm.

3. Nickel (purity 99·97 %)

For nickel, the degree of line broadening was definitely less than in the preceding cases; otherwise the changes are similar to those observed for copper and call for no special comment. The measurements were made on the (420) ring using copper K-radiation and are summarized below:

Lattice spacing of the annealed nickel ...	$3{\cdot}517_0 \times 10^{-8}$ cm.
Maximum contraction in recovered state ...	0·07 %
Maximum expansion in distorted state ...	0·13 %
Lower limiting crystallite size	$1{\cdot}2 \times 10^{-5}$ cm.

4. ALUMINIUM (PURITY 99·99 %)

Pure aluminium is known to be spontaneously self-recovering during cold working, and for this reason was found not to exhibit the changes described for the copper and silver. Dehlinger first showed that the line-broadening effect was negligible for aluminium (Dehlinger 1930), and concluded that no lattice distortion was produced on deformation. At the same time it is found that the metal exhibits the formation of continuous arcs from the diffraction spots of the annealed state. Therefore, in the present view, the absence of the line broadening means that the upper and lower limits approach and narrow down the crystallite size very definitely to about 10^{-4} cm. The main point of interest noted in the aluminium was in connexion with the angular spread of the orientations of the crystallites. In the commercially pure metal, the continued deformation produces a completely random orientation which is then followed, after severe working, by the formation of a "fibre structure" brought about by the assumption of a preferred orientation of the crystallites relative to some axis in the specimen. In the very pure metal examined this process did not occur, as shown by the photographs reproduced. Fig. 8 (Plate 13), from a particularly large-grained specimen after 6 % reduction, shows the formation of diffraction arcs from the usual diffraction spots characterizing the initial state; the photograph shows a maximum of intensity on the arc, indicating that the majority of the crystallites do not depart widely in orientation from the parent grain. Now fig. 9 (Plate 13), after 99·6 % reduction, shows that even after this severe working the crystallites are never oriented completely at random. The intensity maxima in this case are not due to a "fibre structure" since they are found to be differently placed when a photograph is taken from another point on the same surface of the specimen; also the effect is observed at each intermediate stage in reduction. In the pure metal therefore it is not possible to impose any appreciable cold-work effects, not even to the extent of first producing the random distribution of crystallites.

5. MOLYBDENUM (PURITY 99·95 %)

Measurements were made on the (321) ring using nickel K-radiation. Compared with Cu, Ag and Ni, the degree of line broadening is small, although the observed lattice changes are of the same order. With those metals it was possible definitely to say that when the diffraction ring became abnormally diffuse then the lattice expanded, and vice versa, but this is not so obvious in the case of molybdenum owing to the smaller line broadening, and consequently it is not possible to conclude directly that the expansion from the standard spacing marks the distorted state and the contraction the recovered state, especially since the changes occur quickly on deformation. Figs. 10*a* and *b* (Plate 13), taken after 1 and 6 % reduction respectively show the order of the difference between the two extremes, the former being in excess of the standard spacing of the annealed initial state and the latter below. These photographs were taken using a slit instead of a pinhole source during oscillation of the specimen so that the ring is in focus only along the diameter perpendicular to the slit, although the whole ring was photographed; the photographs are cut along this diameter and the diffraction rings are matched at one end to illustrate the displacement at the other. The slit covers a larger surface of the specimen and by its use, it is shown that the effects observed are not purely local. Fig. 10*b* also shows the order of the maximum radial diffusion of the lines, there being little change on further deformation of the metal. Since the lattice changes occur without appreciable variation in definition of the line, it is reasonable to conclude that the actual broadening which is observed is due only to the Scherrer effect. The measurements were as follows:

Lattice spacing of the annealed molybdenum ...	$3{\cdot}140_3 \times 10^{-8}$ cm.
Maximum contraction	0·05 %
Maximum expansion from contracted state ...	0·10 %
Lower limiting crystallite size	$2{\cdot}2 \times 10^{-5}$ cm.

6. IRON (PURITY 99·96 %)

Measurements were made on the (310) ring using cobalt K-radiation. It was found that the iron exhibited even less of the line-broadening effect than molybdenum so that the same conclusions apply. The lattice changes are of the same order, as shown by figs. 11*a* and *b* (Plate 14) taken after 20 and 90 % reduction respectively; the former corresponds to a lattice spacing less than and the latter to one greater than the standard for the

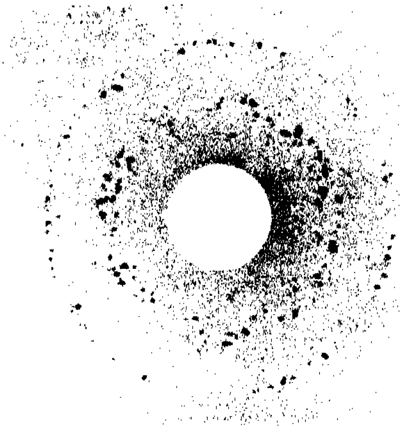

FIG. 1. Cu, annealed.

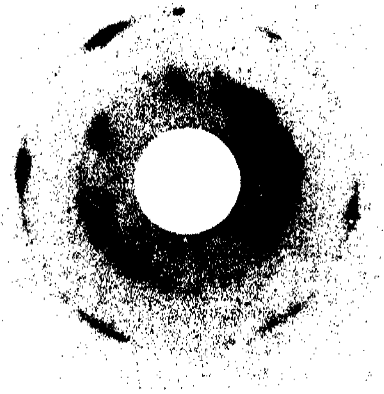

FIG. 2. Cu, 4% reduction.

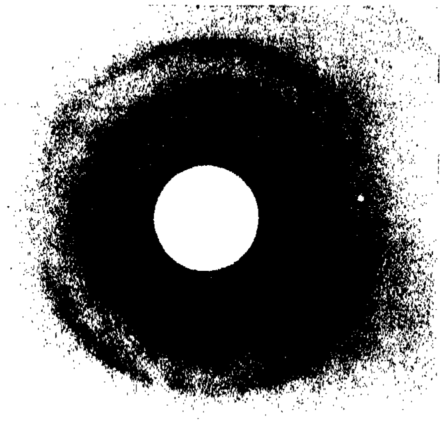

FIG. 3. Cu, 80% reduction.

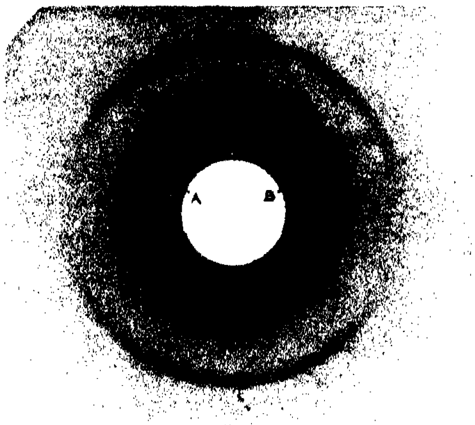

FIG. 4. Cu, 85% reduction.

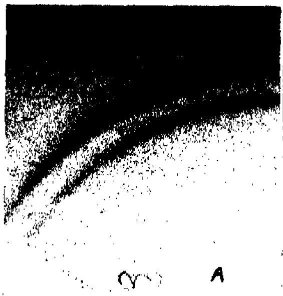

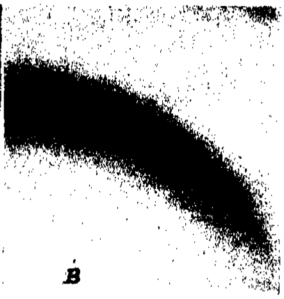

FIG. 5*a*. Initial state. FIG. 5*b*. Recovered state.

Copper: FIG. 3 shows the expansion of the inner ring towards the outer ring due to lattice expansion effect; fig. 4 shows the contraction on recovery caused by further cold working; figs. 5*a* and 5*b* show a difference between the recovered and initial state.

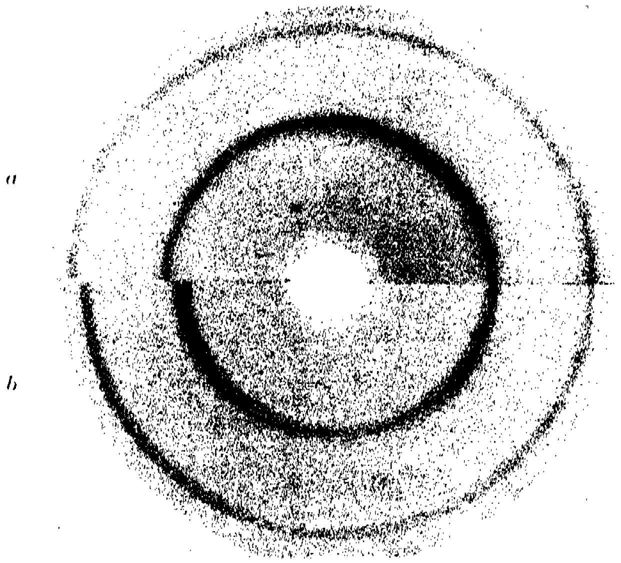

Fig. 6*a*. 65% reduction. Fig. 6*b*. 70% reduction.

Silver: Figs. 6*a*, 6*b* show the difference in diameter of the diffraction rings between the expanded and recovered states.

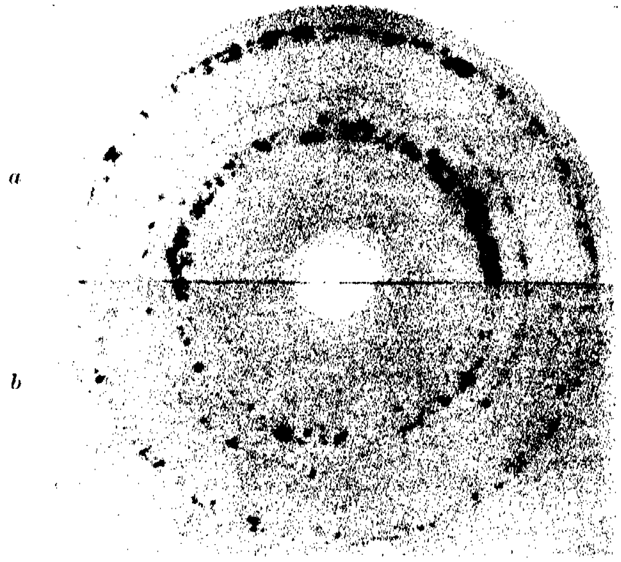

Fig. 7*a*. 90% reduction. Fig. 7*b*. Initial.

Silver: Fig. 7*a* shows the recrystallisation on severe working to initial condition as shown by 7*b*.

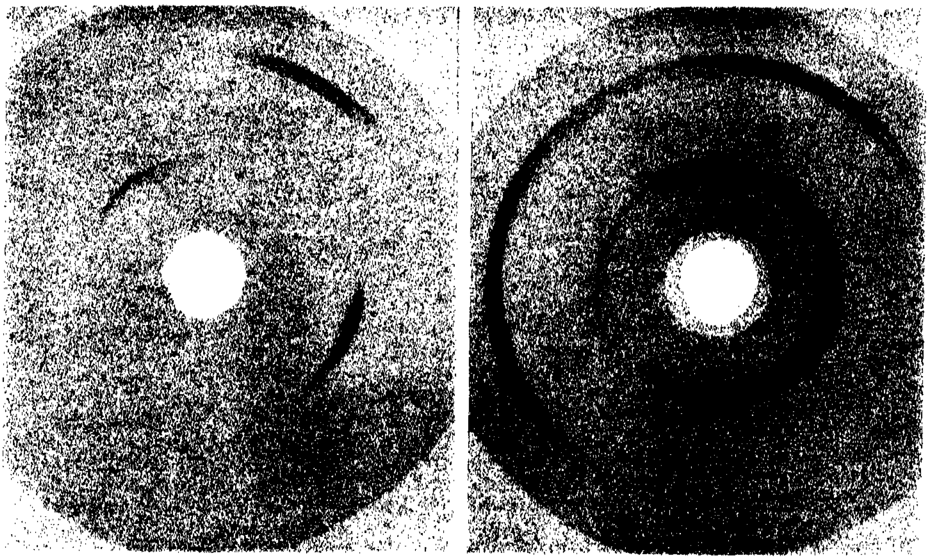

FIG. 8. Al, 6% reduction. FIG. 9. Al, 98·6% reduction.

FIGS. 8, 9 show that a complete ring is not produced even after heavy cold working of pure aluminium.

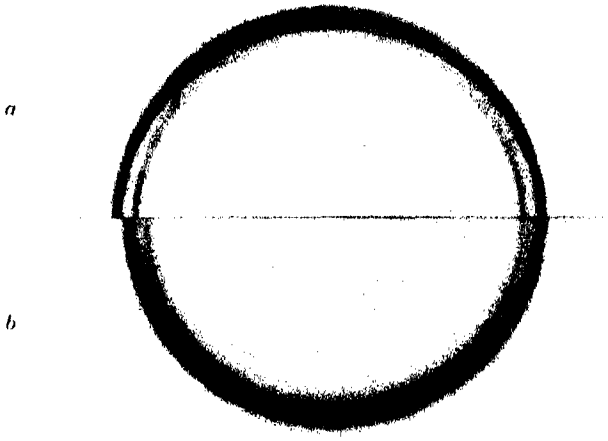

FIG. 10*a*. Molybdenum, 1% reduction. FIG. 10*b*. 6% reduction.

FIGS. 10*a*, 10*b* show the difference in diameter of the diffraction ring between expanded and recovered states of molybdenum lattice.

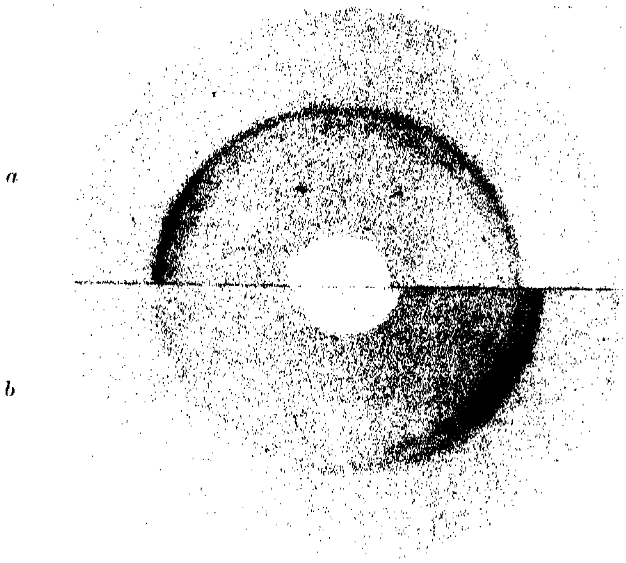

FIG. 11*a*. Iron, 20% reduction. FIG. 11*b*. 90% reduction.

FIGS. 11*a*, 11*b* show difference in diameter of diffraction ring between expanded and recovered states of iron lattice.

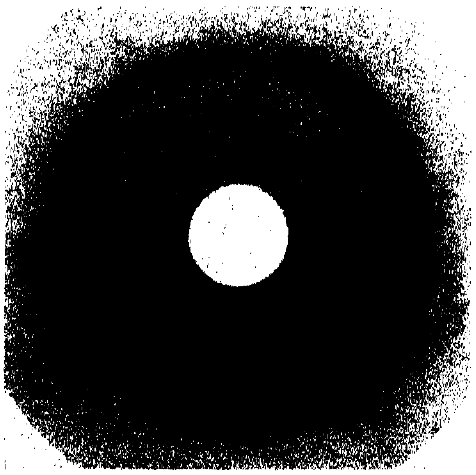

FIG. 12 shows the much greater line broadening effect in a carbon steel compared with that in pure iron above.

annealed condition. These photographs were chosen for reproduction in order to illustrate the negligible difference in line broadening despite the great difference in degree of deformation of the specimen.

A comparison of some interest is afforded by the results of similar tests on the deformation of a 0·1 % carbon steel. Fig. 12 (Plate 14) shows the same diffraction ring, photographed under the same conditions as the pure iron, after the steel had been reduced by about 40 %, sufficient to produce the maximum degree of line broadening. It will be seen, on comparison with fig. 11, that the diffusion of the diffraction ring is quite of a different order from that of the pure iron. This observation serves to demonstrate the function of the carbon on the "X-ray structure" of the iron lattice in lowering the permissible limit of crystallite size, and thus extending the potential range of the structure-sensitive properties.

The measurements on the iron were as follows:

Lattice spacing of the annealed iron	$2{\cdot}861_0 \times 10^{-8}$ cm.
Maximum contraction	0·05 %
Minimum expansion from contracted state ...	0·10 %
Lower limiting crystallite size	$3{\cdot}2 \times 10^{-5}$ cm.

DISCUSSION

One of the points arising from the above work is the question of the relation of the crystallite formation to the grains and grain boundaries which are observed in metallographic examination. It is clear that even in the early stages of deformation each grain is dispersed into very differently oriented crystallites. On the other hand, the changes seen under the microscope are confined essentially to some elongation of the grain boundaries and the appearance of the slip lines with their apparent parallelism and regularity. Various investigators have shown that the periodicity of the slip lines reaches the order of 10^{-4} cm., that is, the same order as the size of the independently reflecting crystallites shown by the X-rays. This points to the probability that the crystallites correspond to the sections into which the grain is divided by the lines of slip. It is then necessary, however, to account for the very different orientations which must be produced amongst the crystallites in one grain in order to explain the observed transition from a single reflexion spot to an elongated arc and finally a practically complete ring. (The formation of the ring is of course enhanced in the polycrystalline metal because normally the ring consists initially of more than one reflexion spot; but the results on the aluminium, shown in figs. 8 and 9, which are from a particularly large-grained specimen giving initially only a single reflexion spot, and similar work in progress on single metallic crystals, indicate that the orientations of the crystallites in the one grain must vary by at least 20–30°, and probably more in a metal which is not spontaneously self-annealing.) Now it is well known, from the work of Taylor, Elam, Mark, Polanyi and others, that if a crystal is constrained to deform in a definite direction, the action of slip causes a rotation of the crystallographic orientation relative to the axis of the applied stress. This leads to the interpretation of the X-ray results that the apparently parallel sections between the slip lines formed in a single metallic grain extending in a given direction must elongate by considerably different amounts in order to produce the internal rotations of their crystallographic orientation to the extent observed.

A further point is the apparent difficulty of reconciling the above lower limit to the crystallite size of 10^{-4} to 10^{-5} cm. for a metal of given purity with the Beilby layer shown by the electron-diffraction work of Finch and others to be amorphous when produced during the mechanical polishing of a metallic surface. The logical conclusion from the X-ray work is that any amorphous state is definitely unstable, especially so in view of the observation of the recovery effects associated with continued cold working. A solution may perhaps be found in the result, illustrated by the steel photograph fig. 12, Plate 14, that the lower limit is decreased by the introduction of impurity, which presumably inhibits the processes of recovery and recrystallization. A similar result to that of the steel is found in work on the crystallite size of electrodeposited metals (Wood 1931), which are usually coprecipitated with oxide, hydroxide or gases, and on nitrided steel (Wood 1933) where highly dispersed precipitates of nitrides are formed. It may be, therefore, that the intimate contact with the polishing media introduces sufficient impurity into the surface of the polished metal to account for the amorphous film, but in that case the layer must be regarded as quite artificial and not characteristic of the metal itself.

Finally, the changes show that the metal accommodates itself to external deformation by the dispersion into and relative movements of the crystallites, but that this process is accompanied, in the general case, by the incidence of measurable internal strains in the lattice. The results suggest that the former corresponds to the property of ductility but is possible only because of the instability of the distorted lattice and the observed recovery effect which permits the deformation to be progressively repeated without causing brittle fracture. It is not possible in view of the present incomplete state of the theory of the metallic lattice to calculate the internal stresses corresponding to the maximum expansion effect, and, although it can hardly be fully correct to utilize the known constants of volume elasticity for the purpose, it is satisfactory to note that if this is done the equivalent stresses come out to be of the same order as the breaking stresses of the bulk material.

The author desires to thank Dr G. W. C. Kaye, F.R.S., in whose department the work was undertaken, for his interest in these researches, and Mr M. G. Harwood for considerable assistance in the experimental work.

SUMMARY

An X-ray examination has been made of the changes in crystalline structure during the progressive cold working of pure Cu, Ag, Ni, Al, Mo and Fe. It is shown that the grains are dispersed into a fundamental unit (crystallite) characterized by a lower limiting size ranging from 10^{-4} cm. for Al to $0 \cdot 7 \times 10^{-5}$ cm. for Cu. This size is deduced from the broadening of appropriate diffraction lines. It is further shown, in the general case of copper, that on continued cold working the diffraction lines broaden to a maximum and then diminish in width to a definite value, the two processes alternating on further working. At the same time, the lattice dimensions of the crystallites change, having an expanded value when the line is most diffuse and a contracted value when the line breadth decreases. These changes are measured and indicate that the condition of the cold worked metal is marked by two extremes, (i) a comparatively stable state with a contracted lattice and minimum line broadening giving the lower limiting crystallite size, and (ii) a less stable state characterized by an expanded lattice and an abnormally diffuse line breadth which represents the extent and nature of the distortion transmitted to and retained by the metallic lattice during continued deformation.

REFERENCES

Dehlinger, U. 1930 *Z. Kristallogr.* **44**, 241.
Gough, H. J. 1924 *Fatigue of metals.* E. Benn.
Gough, H. J. and Wood, W. A. 1936 *Proc. Roy. Soc.* A, **154**, 510.
Wood, W. A. 1931 *Phil. Mag.* **12**, 853.
— 1933 *Phil. Mag.* **16**, 719.
— 1935 *Trans. Faraday Soc.* **31**, 1248.

Calculated wave functions and energy values for X-ray terms of potassium

By W. A. Thatcher, M.Sc.

(*Communicated by D. R. Hartree, F.R.S.—Received* 28 *April* 1939)

1. Introduction

Calculations of approximate wave functions, carried out by the method of the self-consistent field (Hartree 1928), have now been made for a number of atoms and ions, and energy values of terms of the optical spectrum, based on these calculations, have been made in a few cases (for example, McDougall 1932). But, apart from the work considered in the present paper, the calculations for ions have all been for atoms ionized in the outermost group; no calculations of wave functions for atoms ionized in an inner group, and consequently no proper calculations of X-ray energies, have previously been made.

It has been found empirically that the calculated value of the energy parameter ϵ appearing in the equation for the radial wave function of an inner group is in very close agreement with the observed value of ν/R for the corresponding X-ray term, but it is by no means clear why the agreement should be as close as it is, since the two quantities are really not directly comparable, as has already been pointed out (see, for example, Hartree 1928, pp. 116–17, 123 and Hartree 1933, pp. 288–90). The value of ϵ in the equation for the radial wave function $P(nl)$ would be the energy required to remove an electron from that wave function if the rest of the atom were a static field of force, unaffected by the removal of that electron. Actually the atom is a configuration of electrons which changes when one of them, particularly an inner one, is removed. Further, the interaction energy of any one electron with the rest of the atom includes exchange terms as well as the direct Coulomb interaction which is all that is taken into account in considering any one electron as in the field of the rest of the atom regarded as a static field.

It seemed desirable to make some self-consistent field calculations for an atom ionized in an inner group for two reasons; first in order to obtain some quantitative data regarding the alteration of the outer wave functions when an electron is removed from an inner group, and secondly to enable proper calculations to be made of X-ray energy levels, allowing for this alteration of the wave functions of the outer group on removal of an inner electron, and for exchange, by calculating the total energy of the whole atom in two appropriate states, and taking the difference.

The present paper is concerned with the calculation of the wave functions and energies for potassium. Other X-ray phenomena to which the results could be applied are the Auger effect, in the usual treatment of which (see, for example, Burhop 1935) the disturbance of the remainder of the atom due to the removal or transition of an inner electron is neglected, and X-ray dispersion, in which a similar approximation is commonly made.

For specifying electron configurations of an atom ionized in an inner group, it is convenient to adopt a notation which specifies the wave functions, occupied in the normal state of the atom, which are unoccupied in the state under consideration. Using a notation suggested by White (1934, pp. 309, 310) we will indicate the absence of an electron in a normally occupied (nl) wave function by the symbol $(nl)^{-1}$. For example, a potassium atom with its normal configuration except for the absence of one K electron may be described by the symbol $\mathrm{K}^{+}(1s)^{-1}$.

The configurations for which wave functions have been calculated, and are given in this paper, are, in this abbreviated notation and in the usual full notation,

$$\mathrm{K}^{+2}[(1s)^{-1}(4s)^{-1}] = \mathrm{K}^{+2}[(1s)^{1}(2s)^{2}(2p)^{6}(3s)^{2}(3p)^{6}]$$

and

$$\mathrm{K}^{+2}[(2p)^{-1}(4s)^{-1}] = \mathrm{K}^{+2}[(1s)^{2}(2s)^{2}(2p)^{5}(3s)^{2}(3p)^{6}].$$

Energy calculations have been made for these two configurations and also for the normal state of the K^{+} ion, namely

$$\mathrm{K}^{+1}[(4s)^{-1}] = \mathrm{K}^{+1}[(1s)^{2}(2s)^{2}(2p)^{6}(3s)^{2}(3p)^{6}],$$

for which wave functions were already available (Hartree 1934).

2. SELF-CONSISTENT FIELDS FOR K^{+2} IONS

For $\mathrm{K}^{+2}[(1s)^{-1}(4s)^{-1}]$, the solution was started from a set of estimates of the contributions to Z supplied by Hartree. The successive approximations to the self-consistent field were taken to such a stage that the maximum difference between estimated and calculated contributions to Z for each group was less than 0·015, and the corresponding maximum difference for the total Z was less than 0·03. For $\mathrm{K}^{+2}[(2p)^{-1}(4s)^{-1}]$ the solution was carried out as a variation on that for the $(1s)^{-1}(4s)^{-1}$ configuration; this gave values of the radial wave functions P, each of which was the sum of the corresponding value for the $(1s)^{-1}(4s)^{-1}$ configuration and a variation.

As a check, a final calculation was made starting from these as estimates. For this configuration the maximum differences between estimated and final Z's were 0·01 in any one contribution and 0·025 in the total.

Tables I–IV give the results of these calculations. Tables I and III give the unnormalized radial wave functions $P(nl)$, the ϵ parameters and values of the normalization integral $\int_0^\infty P^2(nl)\,dr$; Tables II and IV give the contributions to Z, and the total $2Z_p$, in the same form as the corresponding results for $K^+(4s)^{-1}$ (Hartree 1934).

Table I. $K^{++}(1s)^{-1}\,(4s)^{-1}$ wave functions

Table of P/r^{l+1} for small r

r	$(1s)$	$(2s)$	$(2p)$	$(3s)$	$(3p)$
0·00	100·00	100·00	100·00	100·00	100·00
0·005	90·96	90·84	95·38	90·84	95·38
0·01	82·72	82·35	90·98	82·33	90·96
0·015	75·22	74·47	86·81	74·42	86·79
0·02	68·39	67·21	82·85	67·13	82·79

Table of P

r	$(1s)$	$(2s)$	$(2p)$	$(3s)$	$(3p)$
0·00	0	0	0	0	0
0·005	0·455	0·454	0·0024	0·454	0·002
0·01	0·827	0·824	0·0091	0·823	0·009
0·015	1·128	1·117	0·0195	1·116	0·020
0·02	1·368	1·344	0·0331	1·343	0·033
0·03	1·698	1·627	0·0679	1·621	0·068
0·04	1·872	1·724	0·1101	1·711	0·110
0·05	1·936	1·680	0·1570	1·658	0·156
0·06	1·923	1·530	0·2065	1·495	0·205
0·07	1·856	1·301	—	—	—
0·08	1·756	1·017	0·3070	0·955	0·303
0·10	1·505	+0·356	0·4021	+0·267	0·394
0·12	1·239	−0·345	0·4867	−0·455	0·471
0·14	0·992	−1·021	0·5580	−1·139	0·532
0·16	0·779	−1·634	0·6151	−1·741	0·575
0·18	0·603	−2·163	0·6584	−2·239	0·602
0·20	0·461	−2·601	0·6889	−2·623	0·612
0·22	0·349	−2·950	0·7078	−2·892	0·607
0·24	0·263	−3·214	0·7166	−3·051	0·590
0·26	0·196	−3·401	0·7169	−3·111	0·560
0·28	0·146	−3·520	0·7100	−3·079	0·521
0·30	0·108	−3·580	0·6973	−2·969	0·473

TABLE I (*continued*)

Table of P

r	$(1s)$	$(2s)$	$(2p)$	$(3s)$	$(3p)$
0·35	0·050	−3·530	0·6469	−2·414	0·326
0·40	0·023	−3·292	0·5810	−1·587	+0·155
0·45	0·010	−2·954	0·5094	−0·615	−0·027
0·50	0·005	−1·576	0·4386	+0·403	−0·207
0·6	0·001	−1·841	0·3120	2·325	−0·536
0·7	0·000	−1·248	0·2114	3·869	−0·799
0·8	—	−0·817	0·1403	4·942	−0·988
0·9	—	−0·520	0·0912	5·576	−1·108
1·0	—	−0·325	0·0581	5·848	−1·171
1·2	—	−0·119	0·0231	5·649	−1·173
1·4	—	−0·044	0·0090	4·937	−1·077
1·6	—	−0·016	0·0034	4·072	−0·942
1·8	—	−0·005	0·0013	3·236	−0·797
2·0	—	−0·002	0·0005	2·504	−0·660
2·2	—	−0·001	0·0002	1·904	−0·537
2·4	—	—	0·0001	1·426	−0·431
2·6	—	—	—	1·055	−0·343
2·8	—	—	—	0·774	−0·270
3·0	—	—	—	0·563	−0·211
3·2	—	—	—	0·407	−0·164
3·4	—	—	—	0·292	−0·127
3·6	—	—	—	0·209	−0·097
3·8	—	—	—	0·148	−0·074
4·0	—	—	—	0·105	−0·056
4·5	—	—	—	0·044	−0·028
5·0	—	—	—	0·018	−0·014
5·5	—	—	—	0·007	−0·006
6·0	—	—	—	0·003	−0·003
6·5	—	—	—	—	−0·0014
7·0	—	—	—	—	−0·0006
7·5	—	—	—	—	−0·0003
8·0	—	—	—	—	−0·0001
ϵ_{nl}	286·13	30·93	26·74	4·426	3·169
$\int_0^\infty P^2(nl)dr$	0·3685	4·462	0·18265	34·25	1·6553

TABLE II. $K^{++}(1s)^{-1}(4s)^{-1}$ CONTRIBUTIONS TO Z AND TOTAL $2Z_p$

	Contributions to Z					
r	$(1s)^1$	$(2s)^2$	$(2p)^6$	$(3s)^2$	$(3p)^6$	Total $2Z_p$ $(2v_0 = -115{\cdot}2)$
0·00	1·000	2·000	6·000	2·000	6·000	38·000
0·005	0·999	—	—	—	—	37·421
0·01	0·993	1·999	6·000	2·000	6·000	36·851
0·015	0·980	1·995	—	—	—	36·288
0·02	0·958	1·992	6·000	1·999	6·000	35·736
0·03	0·895	1·985	—	—	—	34·682
0·04	0·805	1·968	5·997	1·997	6·000	33·691
0·05	0·709	1·962	5·990	—	—	32·757
0·06	0·605	1·950	5·980	1·994	5·998	31·881
0·07	0·512	—	—	—	—	31·039
0·08	0·422	1·943	5·938	1·992	5·992	30·233
0·10	0·276	1·928	5·852	1·990	5·985	28·702
0·12	0·173	1·926	5·720	1·990	5·970	27·272
0·14	0·102	1·921	5·542	1·989	5·951	25·934
0·16	0·061	1·906	5·310	1·986	5·932	24·662
0·18	0·034	1·873	5·046	1·982	5·912	23·471
0·20	0·019	1·822	4·741	1·976	5·881	22·370
0·22	0·010	1·752	4·419	1·966	5·858	21·355
0·24	0·004	1·666	4·082	1·955	5·828	20·425
0·26	0·002	1·565	3·745	1·945	5·802	19·565
0·28	0·001	1·462	3·416	1·934	5·781	18·781
0·30	—	1·347	3·092	1·924	5·765	18·067
0·35	—	1·058	2·347	1·902	5·733	16·535
0·40	—	0·796	1·723	1·889	5·723	15·293
0·45	—	0·581	1·232	1·885	5·722	14·253
0·5	—	0·405	0·861	1·884	5·720	13·354
0·6	—	0·185	0·395	1·872	5·670	11·818
0·7	—	0·082	0·171	1·814	5·502	10·496
0·8	—	0·028	0·071	1·698	5·199	9·339
0·9	—	0·014	0·028	1·535	4·801	8·328
1·0	—	0·004	0·010	1·342	4·326	7·464
1·2	—	0·000	0·002	0·950	3·314	6·151
1·4	—	—	—	0·618	2·384	5·292
1·6	—	—	—	0·379	1·643	4·767
1·8	—	—	—	0·223	1·094	4·445
2·0	—	—	—	0·137	0·709	4·255
2·2	—	—	—	0·070	0·450	4·145
2·4	—	—	—	0·038	0·281	4·081
2·6	—	—	—	0·020	0·172	4·044
2·8	—	—	—	0·011	0·105	4·023

TABLE II (*continued*)

	Contributions of Z					Total $2Z_p$
r	$(1s)^1$	$(2s)^2$	$(2p)^6$	$(3s)^2$	$(3p)^6$	$(2v_0 = -115{\cdot}2)$
3·0	—	—	—	0·005	0·063	4·011
3·2	—	—	—	0·003	0·036	4·005
3·4	—	—	—	0·001	0·021	4·002
3·6	—	—	—	0·001	0·012	4·000
3·8	—	—	—	0·000	0·007	4·000
4·0	—	—	—	—	0·004	etc.
4·5	—	—	—	—	0·001	—

TABLE III. $K^{++}(2p)^{-1}\,(4s)^{-1}$ WAVE FUNCTIONS

Table of P/r^{l+1} for small r

r	$(1s)$	$(2s)$	$(2p)$	$(3s)$	$(3p)$
0·00	100·00	100·00	100·00	100·00	100·00
0·005	90·96	90·85	95·38	90·84	95·38
0·01	82·74	82·40	90·99	82·37	90·99
0·015	75·27	74·58	86·84	74·52	86·82
0·02	68·49	67·35	82·91	67·25	82·86

Table of P

r	$(1s)$	$(2s)$	$(2p)$	$(3s)$	$(3p)$
0·00	0	0	0	0	0
0·005	0·4548	0·454	0·0024	0·454	0·0024
0·01	0·8274	0·824	0·0091	0·824	0·0091
0·015	1·1290	1·119	0·0195	1·118	0·0195
0·02	1·3698	1·347	0·0332	1·345	0·0331
0·03	1·7016	1·635	0·0680	1·629	0·0680
0·04	1·8799	1·740	0·1104	1·727	0·1102
0·05	1·9484	1·706	0·1578	1·684	0·1572
0·06	1·9394	1·567	0·2080	1·532	0·2067
0·08	1·7820	1·078	0·3110	1·015	0·3071
0·10	1·5383	+0·4365	0·4090	+0·346	0·4015
0·12	1·2760	−0·250	0·4995	−0·366	0·4838
0·14	1·0304	−0·922	0·5766	−1·047	0·5506
0·16	0·8161	−1·538	0·6400	−1·664	0·6007
0·18	0·6368	−2·075	0·6897	−2·168	0·6341
0·20	0·4913	−2·528	0·7264	−2·570	0·6507

TABLE III (*continued*)

Table of P

r	($1s$)	($2s$)	($2p$)	($3s$)	($3p$)
0·22	0·3756	−2·895	0·7514	−2·864	0·6523
0·24	0·2850	−3·179	0·7656	−3·049	0·6401
0·26	0·2150	−3·388	0·7705	−3·137	0·6154
0·28	0·1610	−3·528	0·7676	−3·134	0·5799
0·30	0·1180	−3·610	0·7581	−3·048	0·5353
0·35	0·0575	−3·604	0·7131	−2·550	0·3922
0·40	0·0270	−3·400	0·6483	−1·768	0·2201
0·45	0·0125	−3·082	0·5753	−0·822	+0·0339
0·50	0·0057	−2·717	0·5007	+0·184	−0·1544
0·6	0·0012	−1·980	0·3636	2·120	−0·5054
0·7	0·0002	−1·371	0·2530	3·707	−0·7935
0·8	0·0000	−0·904	0·1711	4·834	−1·0061
0·9	—	−0·583	0·1132	5·518	−1·1464
1·0	—	−0·369	0·0737	5·831	−1·2218
1·2	—	−0·142	0·0302	5·684	−1·2451
1·4	—	−0·053	0·0118	5·004	−1·1566
1·6	—	−0·019	0·0047	4·156	−1·0194
1·8	—	−0·007	0·0018	3·328	−0·8685
2·0	—	−0·002	0·0007	2·589	−0·7231
2·2	—	−0·001	0·0003	1·976	−0·5921
2·4	—	−0·000	0·0001	1·487	−0·4784
2·6	—	—	0·0000	1·106	−0·3823
2·8	—	—	—	0·815	−0·3028
3·0	—	—	—	0·595	−0·2380
3·2	—	—	—	0·432	−0·1858
3·4	—	—	—	0·311	−0·1442
3·6	—	—	—	0·223	−0·1113
3·8	—	—	—	0·159	−0·0854
4·0	—	—	—	0·113	−0·0653
4·5	—	—	—	0·048	−0·0329
5·0	—	—	—	0·019	−0·0162
5·5	—	—	—	0·008	−0·0078
6·0	—	—	—	0·003	−0·0037
6·5	—	—	—	0·001	−0·0017
7·0	—	—	—	0·000	−0·0008
7·5	—	—	—	—	−0·0004
8·0	—	—	—	—	−0·0002
8·5	—	—	—	—	−0·0001
ϵ_{nl}	271·93	29·90	25·33	4·358	4·115
$\int_0^\infty P^2(nl)\,dr$	0·3815	4·706	0·21860	34·63	1·8752

TABLE IV. $K^{++}(2p)^{-1}\,(4s)^{-1}$ CONTRIBUTIONS TO Z AND TOTAL $2Z_p$

	Contributions to Z					Total $2Z_p$
r	$(1s)^2$	$(2s)^2$	$(2p)^5$	$(3s)^2$	$(3p)^6$	$(2v_0 = -144{\cdot}9)$
0·00	2·000	2·000	5·000	2·000	6·000	38·00
0·005	1·998	2·000	5·000	2·000	6·000	37·28
0·01	1·987	1·999	5·000	2·000	6·000	36·58
0·015	1·962	1·997	5·000	2·000	6·000	35·89
0·02	1·921	1·994	5·000	1·999	6·000	35·23
0·03	1·79	1·98	5·00	2·00	6·00	33·99
0·04	1·62	1·97	5·00	2·00	6·00	32·86
0·05	1·43	1·96	4·99	2·00	6·00	31·83
0·06	1·23	1·95	4·98	1·99	6·00	30·90
0·07	1·04	1·94	4·97	1·99	6·00	30·04
0·08	0·86	1·93	4·94	1·99	5·99	29·24
0·10	0·57	1·93	4·88	1·99	5·99	27·77
0·12	0·36	1·93	4·80	1·99	5·97	26·43
0·14	0·22	1·93	4·66	1·99	5·96	25·19
0·16	0·13	1·91	4·49	1·95	5·93	24·04
0·18	0·08	1·88	4·29	1·98	5·91	22·97
0·20	0·04	1·84	4·06	1·97	5·88	21·97
0·22	0·02	1·78	3·81	1·97	5·86	21·05
0·24	0·01	1·70	3·54	1·96	5·83	20·19
0·26	0·01	1·60	3·27	1·94	5·80	19·40
0·28	0·00	1·50	3·00	1·93	5·78	18·66
0·30	—	1·39	2·73	1·92	5·76	17·99
0·35	—	1·11	2·11	1·90	5·73	16·54
0·40	—	0·85	1·58	1·89	5·72	15·34
0·45	—	0·63	1·15	1·88	5·71	14·34
0·50	—	0·45	0·82	1·88	5·71	13·47
0·6	—	0·21	0·39	1·87	5·67	11·95
0·7	—	0·09	0·18	1·82	5·53	10·66
0·8	—	0·04	0·08	1·71	5·27	9·50
0·9	—	0·02	0·03	1·55	4·89	8·48
1·0	—	0·01	0·01	1·37	4·44	7·61
1·2	—	—	—	0·98	3·44	6·28
1·4	—	—	—	0·65	2·51	5·41
1·6	—	—	—	0·40	1·75	4·84
1·8	—	—	—	0·24	1·17	4·50
2·0	—	—	—	0·13	0·77	4·30
2·2	—	—	—	0·07	0·49	4·18
2·4	—	—	—	0·04	0·31	4·10
2·6	—	—	—	0·02	0·19	4·06
2·8	—	—	—	0·01	0·19	4·04
3·0	—	—	—	0·00	0·07	4·02
3·2	—	—	—	—	0·04	4·01
3·4	—	—	—	—	0·03	4·00
3·6	—	—	—	—	0·02	4·00
3·8	—	—	—	—	0·01	—

It is interesting to compare the results for K^{+2} $[(1s)^{-1}(4s)^{-1}]$ with those for K^{+} $(4s)^{-1}$ and Ca^{++} $(4s)^{-2}$ (D. R. Hartree and W. Hartree 1935); this comparison can be made best in terms of the contribution to Z or in terms of the normalized wave functions. Starting from the K^{+} ion in its normal state $(4s)^{-1}$, the removal of an electron from a $(1s)$ wave function results in a shrinkage of the wave functions of the L and M shells, and this shrinkage is so marked that the $(3s)$ and $(3p)$ wave functions of the K atom, ionized in the $(1s)$ group, are much more like the corresponding wave functions of the normal state of Ca^{++} than like those of K^{+}.

3. ENERGY VALUES, GENERAL FORMULAE

The energy of an atomic state, in terms of the radial wave functions $P(nl)$ of the different (nl) groups and the numbers of the electrons in these groups, can be obtained by Slater's (1929) method. If the functions $P_N(nl\,|\,r)$ are a set of normalized wave functions, satisfying the condition of orthogonality

$$\int_0^\infty P_N(nl\,|\,r)\,P_N(n'l\,|\,r)\,dr = 0 \quad (n' \neq n) \tag{1}$$

for each l, and if

$$\rho(nl, n'l'\,|\,r) = P_N(nl\,|\,r)\,P_N(n'l'\,|\,r), \tag{2}$$

$$Z_k(nl, n'l'\,|\,r) = r^{-k}\int_0^r r_1^k \rho(nl, n'l'\,|\,r_1)\,dr_1, \tag{3}$$

$$Y_k(nl, n'l'\,|\,r) = Z_k(nl, n'l'\,|\,r) + r^{k+1}\int_r^\infty r_1^{-(k+1)}\rho(nl, n'l'\,|\,r_1)\,dr_1, \tag{4}$$

Slater's method gives the total energy as the sum of multiples of the integrals

$$I(nl) = -\frac{1}{2}\int_0^\infty P_N(nl\,|\,r)\left[\frac{d^2}{dr^2} + \frac{2N}{r} - \frac{l(l+1)}{r^2}\right]P_N(nl\,|\,r)\,dr, \tag{5}$$

$$F_k(nl, n'l') = \int_0^\infty r^{-1}\rho(nl, nl\,|\,r)\,Y_k(n'l', n'l'\,|\,r)\,dr, \tag{6}$$

$$G_k(nl, n'l') = \int_0^\infty r^{-1}\rho(nl, n'l'\,|\,r)\,Y_k(nl, n'l'\,|\,r)\,dr. \tag{7}$$

For the configurations with which this paper is concerned, the coefficients of these integrals are given in the last three columns of Table VII.

The wave functions $P(nl)$, obtained by the method of the self-consistent field without exchange, do not satisfy the orthogonal condition (1) exactly, but, as pointed out by McDougall (1932, § 4 (a)), Slater's formulae can be applied if, for each l, the radial wave functions $P(nl)$ are replaced by a set of independent, mutually orthogonal, linear combinations. It is most convenient in practice to form these linear combinations by leaving the wave function of lowest n unaltered, for each l, and modifying the others in order of increasing n so as to make each orthogonal to those of lower n. In the present work the wave functions $P(2s\,|\,r)$, $P(3s\,|\,r)$ and $P(3p\,|\,r)$ require this modification. McDougall (1932, § 4 (*a*)) has given the appropriate orthogonal combinations of normalized P functions, but for the present work unnormalized wave functions were used, and the expressions involved are somewhat different.

We will write $P(nl\,|\,r)$ for the wave functions calculated without exchange such as those tabulated in Tables I and III, and

$$N^2(nl) = \int_0^\infty P^2(nl\,|\,r)\,dr. \tag{8}$$

Also we will write $P_1(nl\,|\,r)$ for the corresponding member of the set of orthogonal linear combinations, and

$$N_1^2(nl) = \int_0^\infty P_1^2(nl\,|\,r)\,dr, \tag{9}$$

so that the normalized orthogonal wave functions to be used in (1) to (7) are

$$P_N(nl\,|\,r) = P_1(nl\,|\,r)/N_1(nl). \tag{10}$$

Also we will write

$$S(nl, n'l) = \int_0^\infty P(nl\,|\,r)\,P_1(n'l\,|\,r)\,dr \quad (n > n') \tag{11}$$

Since the functions P_1 are constructed in the order of increasing n, it follows that when constructing $P_1(nl\,|\,r)$, the functions $P_1(n'l\,|\,r)$ for $n' < n$ are already determined, so that $S(nl, n'l)$ can be found for $n' < n$.

For $l = 0$, the required set of orthogonal functions is given by

$$\left.\begin{aligned} P_1(1s\,|\,r) &= P(1s\,|\,r),\\ P_1(2s\,|\,r) &= P(2s\,|\,r) - \frac{S(2s, 1s)}{N_1^2(1s)}P_1(1s\,|\,r),\\ P_1(3s\,|\,r) &= P(3s\,|\,r) - \frac{S(3s, 2s)}{N_1^2(2s)}P_1(2s\,|\,r) - \frac{S(3s, 1s)}{N_1^2(1s)}P_1(1s\,|\,r), \end{aligned}\right\} \tag{12}$$

and correspondingly, for $l = 1$,

$$\left.\begin{aligned} P_1(2p\,|\,r) &= P(2p\,|\,r),\\ P_1(3p\,|\,r) &= P(3p\,|\,r) - \frac{S(3p, 2p)}{N_1^2(2p)}P(2p\,|\,r). \end{aligned}\right\} \tag{13}$$

The normalizing integrals are

$$\left.\begin{aligned} N_1^2(1s) &= N^2(1s), & N_1^2(2p) &= N^2(2p), \\ N_1^2(2s) &= N^2(2s)-\frac{S^2(2s,1s)}{N_1^2(1s)}, & N_1^2(3p) &= N^2(3p)-\frac{S^2(3p,2p)}{N_1^2(2p)}, \\ N_1^2(3s) &= N^2(3s)-\frac{S^2(3s,2s)}{N_1^2(2s)}-\frac{S^2(3s,1s)}{N_1^2(1s)}. & & \end{aligned}\right\} \qquad (14)$$

Values of $N_1^2(nl)$ and $S(nl,n'l)$ for the two K^{+2} ions considered in this paper, and for the normal state of the K^+ ion, are given in Table V. For K^+ the values of $P(np\,|\,r)$ and $N^2(np)$ already tabulated (Hartree 1934) are given for $(P/r^2)_{r=0}=500$. These quantities have been divided by 5 and 25 respectively in deriving the results for K^+ in Table V, so that these results should be comparable to those for K^{+2}.

TABLE V. COEFFICIENTS $S(nl,\, n'l)$ USED IN FORMING ORTHOGONAL LINEAR COMBINATIONS $P_1(nl\,|\,r)$, AND NORMALIZATION INTEGRALS $N_1^2(nl) = \int_0^\infty P_1^2(nl\,|\,r)\,dr$ FOR THESE ORTHOGONAL WAVE FUNCTIONS

Table of $S(nl,n'l)$

$(nl)\,(n'l)$	$\mathrm{K}^{++}(1s)^{-1}\,(4s)^{-1}$	$\mathrm{K}^{++}(2p)^{-1}\,(4s)^{-1}$	$\mathrm{K}^{+}(4s)^{-1}$
$(1s)\,(2s)$	0·0143	0·0149	0·0145
$(1s)\,(3s)$	−0·0766	−0·0754	−0·0749
$(2s)\,(3s)$	0·193	0·162	0·222
$(2p)\,(3p)$	0·0037	0·0063	0·0109

Table of $N_1^2(nl)$

(nl)	$\mathrm{K}^{++}(1s)^{-1}\,(4s)^{-1}$	$\mathrm{K}^{++}(2p)^{-1}\,(4s)^{-1}$	$\mathrm{K}^{+}(4s)^{-1}$
$(1s)$	0·3686	0·3815	0·3816
$(2s)$	4·461	4·701	4·901
$(3s)$	34·23	34·61	40·25
$(2p)$	$0{\cdot}1826_5$	0·2186	$0{\cdot}2328_0$
$(3p)$	1·6552	1·8722	2·4546

As already mentioned, the integrals required in the calculation of the energy were evaluated using unnormalized wave functions. For instance, the integral $F_k(nl,n'l')$ was evaluated in the form

$$\int r^{-1}Y_k(nl,nl\,|\,r)\,P_1^2(n'l'\,|\,r)\,dr/N_1^2(nl),$$

division by the appropriate normalizing factor being done after the integral had been evaluated. This procedure was suggested by Hartree and Black (1933) from their experience of similar work for oxygen. The main advantage is that, using unnormalized P's for which $(P/r^{l+1})_{r=0}$ is the same for each configuration considered, the contribution to the integral for small r, which is often the most troublesome to evaluate to adequate accuracy, is very nearly the same for all configurations, so can be done once for all, the corresponding contribution for other configurations being found by a variation method.

4. THE I INTEGRALS

The I integrals (5) provide the largest contributions to E. As is usually the case, it is convenient to substitute for d^2P/dr^2 in $I(nl)$ from the equation satisfied by $P(nl)$, which, for the self-consistent field without exchange, is

$$\left[\frac{d^2}{dr^2}+\frac{2}{r}Z_p(nl\,|\,r)-\epsilon_{nl}-\frac{l(l+1)}{r^2}\right]P(nl\,|\,r)=0, \tag{15}$$

where $Z_p(nl\,|\,r)/r$ is the potential at radius r of the field which, in this approximation, is considered to act on an electron in an (nl) wave function.

If $P(nl) = P_1(nl)$, as it is for $(1s)$ and $(2p)$ in the present case, then

$$2I(nl) = -\epsilon_{nl}-\frac{2}{N_1^2(nl)}\int_0^\infty P_1^2(nl\,|\,r)\,\frac{N-Z_p(nl\,|\,r)}{r}\,dr. \tag{16}$$

The modifications introduced by the use of the linear combinations (12), (13) have been given by McDougall for normalized P's and P_1's; the use of unnormalized wave functions merely affects the coefficients of certain of the integrals.

Writing, for brevity,

$$T(nl,n'l) = \frac{2S(nl,n'l)}{N_1^2(nl)\,N_1^2(n'l)}\int_0^\infty P_1(nl\,|\,r)\,P_1(n'l\,|\,r)\,\frac{Z_p(nl\,|\,r)-Z_p(n'l\,|\,r)}{r}\,dr, \tag{17}$$

the results are

$$\left.\begin{aligned}
2I(2s) &= -\epsilon_{2s}-\frac{2}{N_1^2(2s)}\int_0^\infty P_1^2(2s\,|\,r)\,\frac{N-Z_p(2s\,|\,r)}{r}\,dr+T(2s,1s),\\
2I(3s) &= -\epsilon_{3s}-\frac{2}{N_1^2(3s)}\int_0^\infty P_1^2(3s\,|\,r)\,\frac{N-Z_p(3s\,|\,r)}{r}\,dr+T(3s,2s)+T(3s,1s)\\
&\qquad -\frac{2S(3s,2s)\,S(3s,1s)}{N_1^2(3s)\,N_1^2(2s)\,N_1^2(1s)}\int_0^\infty P_1(1s\,|\,r)\,P_1(3s\,|\,r)\,\frac{Z_p(2s\,|\,r)-Z_p(1s\,|\,r)}{r}\,dr\\
&\text{(compare McDougall 1932, formula (4·18)),}\\
2I(3p) &= -\epsilon_{3p}-\frac{2}{N_1^2(3p)}\int_0^\infty P_1^2(3p\,|\,r)\,\frac{N-Z_p(3p\,|\,r)}{r}\,dr+T(3p,2p).
\end{aligned}\right\} \tag{18}$$

Following the method of Hartree and Black (1933, § 6) a good check on the evaluation of these integrals can be obtained as follows. Let

$$D(nl \mid r) = N - Z_p(nl \mid r) - \Sigma_{n'l'} q(n'l') Y_0(n'l', n'l' \mid r) + Y_0(nl, nl \mid r), \quad (19)$$

where $q(n'l')$ is the number of occupied wave functions in the $(n'l')$ group. The functions $Y_0(n'l', n'l' \mid r)$ have to be evaluated for the calculation of the F integrals, and so do not have to be calculated specially, and $D(nl \mid r)$ is small, since it is only different from zero on account of the difference between $P(nl \mid r)$ and $P_1(nl \mid r)$, and the departures of $P(nl)$ from the exact solution of the equations of the self-consistent field (see Hartree and Black 1933, p. 324). Then

$$2I(nl) = -\epsilon_{nl} - \Sigma_{n'l'} 2q(n'l') F_0(nl, n'l') + 2F_0(nl, nl) - \frac{2}{N_1^2(nl)} \int_0^\infty D(nl \mid r) P_1^2(nl \mid r)\, dr \quad (20)$$

(see Hartree and Black 1933, formula (19)). When the F_0 integrals have been calculated, this checks the value of the integral in $I(nl)$. It is not satisfactory for use as the standard method of calculating $I(nl)$, as there is a danger of accumulation of errors in summing the multiples of the F_0's, but it is useful as a check of the values calculated from (18). The closeness of the check is shown by Table VI.

TABLE VI. CHECK OF $I(nl)$ INTEGRALS

		A $-[2I(nl)+\epsilon(nl)]$ from (16), (18)	B $-[2I(nl)+\epsilon(nl)]$ from (20)	$B-A$
$K^{++}(1s)^{-1}(4s)^{-1}$	$(1s)$	75·07	75·05	−0·02
	$(2s)$	56·43	56·40	−0·03
	$(2p)$	60·11	60·14	0·03
	$(3s)$	27·83	27·83	0·00
	$(3p)$	26·40	26·39	−0·01
$K^{++}(2p)^{-1}(4s)^{-1}$	$(1s)$	89·16	89·16	0·00
	$(2s)$	56·64	56·68	0·04
	$(2p)$	60·30	60·33	0·03
	$(3s)$	27·71	27·76	0·05
	$(3p)$	26·04	26·09	0·05
$K^{+}(4s)^{-1}$	$(1s)$	93·51	93·46	−0·05
	$(2s)$	59·33	59·31	−0·02
	$(2p)$	63·06	63·04	−0·02
	$(3s)$	27·55	27·57	0·02
	$(3p)$	24·86	24·91	0·05

5. EVALUATION OF THE Y_k FUNCTIONS AND THE F_k AND G_k INTEGRALS

Hartree and Black (1933, § 7) give two equations from which to calculate the functions $Y_k(nl, n'l' \mid r)$, namely,

$$\left.\begin{aligned}\frac{d}{dr}Y_k(nl,n'l'\mid r) &= -\frac{1}{r}[(k+1)Y_k(nl,n'l'\mid r)-(2k+1)Z_k(nl,n'l'\mid r)],\\ \frac{d}{dr}Z_k(nl,n'l'\mid r) &= \rho(nl,n'l'\mid r)-\frac{k}{r}Z_k(nl,n'l'\mid r),\end{aligned}\right\} \quad (21)$$

and they give modifications convenient for large r and for small r. The functions Z_k, however, are not required except as intermediate steps in the evaluation of the Y_k's and it is possible to eliminate them entirely and work directly from ρ to Y_k. Eliminating Z_k between equations (21) gives

$$\frac{d^2}{dr^2}Y_k(nl,n'l'\mid r) = -\frac{2k+1}{r}\rho(nl,n'l'\mid r)+\frac{k(k+1)}{r^2}Y_k(nl,n'l'\mid r), \quad (22)$$

which is a particularly convenient form for numerical integration since it is a second order equation with the first derivative absent.

The terminal conditions are

$$\left.\begin{aligned}&Y_k(nl,n'l'\mid 0) = 0,\\ &r^kY_k(nl,n'l'\mid r) \to \text{constant as } r \to \infty,\end{aligned}\right\} \quad (23)$$

so that there is not a complete set of initial conditions for starting the solution of equation (22) from either end of the range. However, it is a linear equation, so can be solved by evaluating any particular integral satisfying the boundary condition at $r = 0$ and finally adding a multiple of the complementary function r^{k+1} to satisfy the condition at infinity (the other complementary function r^{-k} does not satisfy the condition at the origin). If the evaluation of the particular integral becomes unsatisfactory, due to the presence of a large multiple of the complementary function in the solution, the numerical work can often be lightened by adding or subtracting a suitable multiple of it at an intermediate stage in the integration.

To see the effect on $Y_k(nl, n'l' \mid r)$, obtained in this way, of a rounding off or other error in the course of the integration, suppose that the solution of (22), obtained by numerical integration, differs from the exact solution satisfying the conditions (23) by $y_k(r)$. If this discrepancy arises from a single error in the interval of integration r_1 to $r_1 + \delta r$, then for these and later values of r, its behaviour will be given by

$$y_k(r) = Ar^{-k} + Br^{k+1}. \quad (24)$$

Let the error be 0 at $r = r_1$ and x at $r = r_1 + dr$. Then, substituting in (24)

$$x = Ar_1^{-k}[\{1+(\delta r/r_1)\}^{-k} - \{1+(\delta r/r_1)\}^{k+1}] = -(2k+1)\,Ar_1^{-k}\,\delta r/r_1 + O[(\delta r)^2].$$

The term Br^{k+1} is corrected for in the choice of the complementary function to fit the condition at infinity, so the residual error at $r > r_1$ is

$$Ar^{-k} = -x(r_1/r)^k\,(r_1/\delta r)/(2k+1)$$

approximately. Similarly for $r < r_1$, the difference Br^{k+1} in the complementary function required to satisfy the condition at infinity introduces an error

$$x(r/r_1)^{k+1}\,(r_1/\delta r)/(2k+1)$$

approximately. Thus the effects of a rounding off error on the final values of Y_k, after addition of a multiple of the complementary function r^{k+1} to satisfy the condition at infinity, is greatest at the place where the error occurs and decreases to zero at $r = \infty$ (except for $k = 0$) and at $r = 0$. The greatest value of $(r_1/\delta r)$ in practice is of the order of 20, except for the first few intervals for which one or two extra figures are retained in any case, when it may be greater; the fact that the greatest effect of the error may be as much as 20 times the magnitude of the error itself shows the need for carrying out the numerical work to rather a high nominal accuracy if this method is used.

When working with the unnormalized wave functions $P_1(nl\,|\,r)$ it may be convenient to replace $\rho(nl, n'l'\,|\,r)$ in (22) by $P_1(nl\,|\,r)\,P_1(n'l'\,|\,r)$. Then $Y_k(nl, n'l'\,|\,r)$ must be replaced by

$$N_1(nl)\,N_1(n'l')\,Y_k(nl, n'l'\,|\,r).$$

The relation

$$aF_k(nl, n'l') - bF_k(nl, n''l'')$$

$$= \frac{1}{N_1^2(nl)}\int_0^\infty r^{-1}\,P^2(nl\,|\,r)\,[aY_k(n'l', n'l'\,|\,r) - bY_k(n''l'', n''l''\,|\,r)]\,dr$$

is sometimes useful in the evaluation or checking of the values of the F_k integrals. It is a generalization of a relation used by Hartree and Black (1933, p. 327). The most useful values are $a = b = 1$ and $a = N_1^2(n'l')$, $b = N_1^2(n''l'')$.

To save computation, it is often convenient to work with the differences between the various quantities occurring in the evaluation of the integrals F_k and G_k for the different configurations, rather than doing the work for each configuration independently. If the symbol Δ is used to indicate such a difference, we have, for example, from (22)

$$\frac{d^2}{dr^2}\Delta Y_k(nl, n'l' \mid r) = -\frac{2k+1}{r}\Delta\rho(nl, n'l' \mid r) + \frac{k(k+1)}{r^2}\Delta Y_k(nl, n'l' \mid r).$$

This, or the corresponding equation involving the product $P_1(nl \mid r)\, P_1(n'l' \mid r)$ of unnormalized wave functions in place of $\rho(nl, n'l' \mid r)$, has been used to a considerable extent in the present work.

Also, using barred symbols to refer to one configuration and unbarred symbols for another, we have, for unnormalized P's,

$$N_1^2(nl)\, F_k(nl, n'l') - \bar{N}_1^2(nl)\, \bar{F}_k(nl, n'l')$$
$$= \int_0^\infty r^{-1}[P_1^2(nl \mid r)\, Y_k(n'l', n'l' \mid r) - \bar{P}_1^2(nl \mid r)\, \bar{Y}_k(n'l', n'l' \mid r)]\, dr. \quad (25)$$

The integrand of (25) is small compared with the integrand in the integral for $N_1^2 F_k$ for either configuration separately, so that the integral in (25) is easier to evaluate than the corresponding integral for F_k of either configuration separately.

If (25) is used, it is necessary to do the complete integrations, for the integrals F_k required, for one configuration; the corresponding integrals for other configurations can then be found by evaluation of the differences (25). Further, the smoothness of the differences of the integrand of (25) provides a good check on the calculation of the products $P_1^2 Y_k/r$. A similar method can be used for the integrals G_k.

The values of the required I, F and G integrals for the three configurations considered, and the coefficients of these integrals* in the formula for $2E$, the total energy in terms of the ionization energy of the hydrogen atom, are given in Table VII.

The calculations have been carefully checked, and it is hoped that no errors, other than those due to the accumulation of rounding-off errors, are present in the final results. The accuracy of the final energy values is, of course, limited by the effects of the rounding-off errors in the different stages of the calculation leading to these values. By the variation principle, deviations of the values of the radial wave functions P from the exact solution of the equations of the self-consistent field only affect the energy values to a small extent. The main source of uncertainty in the final

---

* Since $G_k(nl, nl) = F_k(nl, nl)$, the contributions to the values of $2E$ which formally come from integrals of the type $G_k(nl, nl)$ have been included with those coming from the corresponding F_k integrals, in this table and in Table VIII.

E values arises from the calculation of the F_k and G_k integrals, some of which occur with large coefficients in the energy formula (see Table VII), and particularly of the I integrals which are the largest (and so most affected by errors in the normalization integrals) and the most troublesome to evaluate.

TABLE VII. VALUES OF I, F_k AND G_k INTEGRALS, AND COEFFICIENTS OF THESE INTEGRALS IN THE FORMULA FOR $2E$, THE TOTAL ENERGY IN RYDBERG UNITS

	Value			Coefficient in formula for $2E$		
Integral	K^{++} $(1s)^{-1}$ $(4s)^{-1}$	K^{++} $(2p)^{-1}$ $(4s)^{-1}$	K^{+} $(4s)^{-1}$	K^{++} $(1s)^{-1}$ $(4s)^{-1}$	K^{++} $(2p)^{-1}$ $(4s)^{-1}$	K^{+} $(4s)^{-1}$
$2I(1s)$	$-362\cdot10$	$-361\cdot11$	$-360\cdot81$	1	2	2
$2I(2s)$	$-87\cdot38_4$	$-86\cdot59_0$	$-86\cdot04_1$	2	2	2
$2I(2p)$	$-86\cdot84_7$	$-85\cdot63_4$	$-85\cdot00_4$	6	5	6
$2I(3s)$	$-32\cdot23_1$	$-32\cdot03_7$	$-30\cdot61_4$	2	2	2
$2I(3p)$	$-29\cdot57_6$	$-30\cdot16_0$	$-26\cdot73_3$	6	6	6
$F_0(1s, 1s)$	11·797	11·591	11·584	0	2	2
$F_0(1s, 2s)$	3·318	3·225	3·180	4	8	8
$F_0(1s, 2p)$	$3\cdot794_3$	3·643	3·563	12	20	24
$F_0(1s, 3s)$	$1\cdot098_7$	1·092	1·011	4	8	8
$F_0(1s, 3p)$	$1\cdot019_0$	1·002	0·882	12	24	24
$F_0(2s, 2p)$	2·372	2·312	2·266	2	2	2
$F_0(2s, 2p)$	2·579	2·445	2·391	24	20	24
$F_0(2s, 3s)$	0·970	0·963	0·904	8	8	8
$F_0(2s, 3p)$	0·911	0·897	$0\cdot803_5$	24	24	24
$F_0(2p, 2p)$	$2\cdot743_5$	2·636	2·570	30	20	30
$F_0(2p, 3s)$	$0\cdot985_5$	0·972	$0\cdot914_5$	24	20	24
$F_0(2p, 3p)$	0·928	0·908	$0\cdot813_5$	72	60	72
$F_0(3s, 3s)$	0·7376	0·7310	0·6814	2	2	2
$F_0(3s, 3p)$	0·7048	0·6952	0·6302	24	24	24
$F_0(3p, 3p)$	0·6757	0·6631	0·5893	30	30	30
$F_2(2p, 2p)$	1·282	1·244	1·201	−12/5	− 8/5	−12/5
$F_2(3p, 3p)$	$0\cdot337_5$	0·388	$0\cdot273_5$	−12/5	−12/5	−12/5
$G_0(1s, 2s)$	0·268	0·340	0·254	− 2	− 4	− 4
$G_0(1s, 3s)$	$0\cdot061_5$	0·063	0·054	− 2	− 4	− 4
$G_1(1s, 2p)$	0·588	0·542	0·516	− 2	−10/3	− 4
$G_1(1s, 3p)$	$0\cdot056_5$	0·051	0·040	− 2	− 4	− 4
$G_0(2s, 3s)$	0·062	0·059	0·053	− 4	− 4	− 4
$G_1(2s, 2p)$	1·482	1·427	1·420	− 4	−10/3	− 4
$G_1(2s, 3p)$	0·036	0·038	0·026	− 4	− 4	− 4
$G_1(2p, 3s)$	0·072	0·071	$0\cdot065_5$	− 4	−10/3	− 4
$G_0(2p, 3p)$	0·025	0·035	$0\cdot030_5$	−12	−10	−12
$G_2(2p, 3p)$	0·067	0·067	0·052	−24/5	− 4	−24/5
$G_1(3s, 3p)$	0·461	0·408	$0\cdot410_5$	− 4	− 4	− 4

The accuracy of the values of $2I(nl)+\epsilon_{nl}$ can be judged roughly by reference to the checks of the values of this quantity given in Table VI. The values of ϵ_{2s} and ϵ_{2p} should be accurate to 0·005 and those of ϵ_{1s} to 0·03; the coefficient of $I(1s)$ in the formula for $2E$ is only 2, so that the uncertainty in ϵ_{1s} does not give a large contribution to that in $2E$. The normalization integrals $N_1^2(nl) = \int_0^\infty P_1^2(nl)\,dr$ should all be accurate to 1 part in 4000.

Estimates of the effects of these and other possible uncertainties on the values of $2E$ suggest that the probable error (in the sense in which the term is used in the theory of errors) of the difference $\Delta(2E)$ between the values of $2E$ for two different configurations is about 0·5. It is only possible to estimate this quantity rather roughly, but this gives an idea of the order of accuracy of the final results.

6. SPIN AND RELATIVITY CORRECTIONS

For light atoms, the spin and relativity corrections to the energy values are small, and nearly cancel. The expressions for these corrections have been given by Hartree (1928, § 7).

The relativity correction $\Delta\epsilon_{\rm rel}$ is

$$\Delta\epsilon_{\rm rel} = \tfrac{1}{4}\alpha^2\int_0^\infty\left[\epsilon_{nl}-\frac{2Z_p(nl\,|\,r)}{r}\right]^2 P_N^2(nl\,|\,r)\,dr, \tag{26}$$

where $\alpha^2 = (2\pi e^2/ch)^2 = 1/18800.$

The spin correction $\Delta\epsilon_{\rm spin}$ is

$$\Delta\epsilon_{\rm spin} = \alpha^2\mathbf{l}\,.\,\mathbf{s}\left[\int_0^\infty r^{-3}\,Z(nl\,|\,r)\,P_N^2(nl\,|\,r)\,dr\right], \tag{27}$$

where $Z(nl\,|\,r)/r^2$ is the field which, in the self-consistent field approximation, is considered to be acting on an electron in an (nl) wave function at a distance r from the nucleus. For $l \neq 0$ the factor $\mathbf{l}\,.\,\mathbf{s}$ in (27) has the values

$$\begin{aligned}\mathbf{l}\,.\,\mathbf{s} &= \tfrac{1}{2}l \quad \text{for} \quad j = l+\tfrac{1}{2}\\ &= -\tfrac{1}{2}(l+1) \quad \text{for} \quad j = l-\tfrac{1}{2}.\end{aligned}$$

For $l = 0$, (27) becomes indeterminate, as the integral becomes infinite and $\mathbf{l}\,.\,\mathbf{s} = 0$. But in this case the spin correction can be obtained by comparison with that for the corresponding term of a hydrogen-like atom with the same nuclear charge N.

Let $P_{(H)N}(ns\,|\,r)$ be the normalized hydrogen-like wave function in the field of the same nucleus, and $\Delta\epsilon_{(H)\text{spin}}$ the spin correction to ϵ for the hydrogen-like atom. Then, since the large contributions to the integral in (27) come from the immediate neighbourhood of the origin,

$$\frac{\Delta\epsilon_{\text{spin}}}{\Delta\epsilon_{(H)\text{spin}}} = \left[\operatorname*{Lt}_{r\to 0} \frac{P_N(ns\,|\,r)}{P_{(H)N}(ns\,|\,r)}\right]^2.$$

Or, if $P(ns\,|\,r)$, $P_{(H)}(ns\,|\,r)$ are unnormalized wave functions with

$$\operatorname*{Lt}_{r\to 0}\,[P(ns\,|\,r)/r] = \operatorname*{Lt}_{r\to 0}\,[P_{(H)}(ns\,|\,r)/r],$$

then
$$\frac{\Delta\epsilon_{\text{spin}}}{\Delta\epsilon_{(H)\text{spin}}} = \frac{\int_0^\infty P^2_{(H)}(ns\,|\,r)\,dr}{\int_0^\infty P^2(ns\,|\,r)\,dr}.$$

For $(1s)$,
$$\Delta\epsilon_{(H)\text{spin}} = \alpha^2 N^4,$$

so
$$\Delta\epsilon_{\text{spin}}(1s) = \alpha^2 N^4 \int_0^\infty P^2_{(H)}(1s\,|\,r)\,dr \Big/ \int_0^\infty P^2(1s\,|\,r)\,dr.$$

Spin and relativity corrections have only been applied for the missing $(1s)$ and $(2p)$ electrons of the K^{++} ions, since the differences between those corrections for the occupied wave functions in the different configurations are negligible.

7. Results and discussion

The contribution to $2E$ from the different kinds of integrals, and from spin and relativity corrections, and values of $2E$ themselves, for the different configurations are summarized in Table VIII. The energy difference

$$2E[K^{+2}, (1s)^{-1}(4s)^{-1}] - 2E[K^{+}, (4s)^{-1}],$$

is the calculated value of (ν/R) for the K absorption edge of the X-ray spectrum, and so is directly comparable with an experimentally observable quantity. Similarly the two values of

$$2E[K^{+2}, (2p)^{-1}(4s)^{-1}] - 2E[K^{+}, (4s)^{-1}], \tag{28}$$

for the two different values of the spin correction give the calculated values of (ν/R) for the L_{II}, L_{III} edges, and the values of

$$2E[K^{+2}, (1s)^{-1}(4s)^{-1}] - 2E[K^{+2}, (2p)^{-1}(4s)^{-1}],$$

give the calculated values of (ν/R) for the $K\alpha$ doublet. Comparison of these quantities with the observed values (from Siegbahn 1931, Tables 47, 167, 176*b*) is made in Table VIII, and the values of the ϵ parameters in the calculation of the self-consistent field (without exchange) for K^+ are also given.

TABLE VIII. VALUES OF $2E$ AND CONTRIBUTIONS THERETO, AND COMPARISON WITH OBSERVATION

Contribution from	$K^{++}(1s)^{-1}(4s)^{-1}$		$K^{++}(2p^{-1}(4s)^{-1}$		$K^+(4s)^{-1}$
I integrals		−1299·87		−1568·60	−1625·35
F_k integrals		278·42		399·85	440·57
G_k integrals		−11·67		−12·01	−12·28
Relativity correction	for $(1s)^{-1}$	8·60	for $(2p)^{-1}$	0·16	—
Spin correction	for $(1s)^{-1}$	−7·78	for $(2p)^{-1}$	0·13 −0·06$_5$	— —
Total $2E$		−932·3		−1180·5 −1180·7	−1197·3 —

	Calc.		Obs.			Obs. − Calc.	K^+, ϵ_{nl}
$2E[K^{++}(1s)^{-1}(4s)^{-1}]$ $-2E[K^+, (4s)^{-1}]$	265·0		265·6		(K edge)	−0·6	267·3$_5$
$2E[K^{++}, (2p)^{-1}(4s)^{-1}]$ $-2E[K^+, (4s)^{-1}]$	16·8 16·6	0·19$_5$	21·7 21·5	0·21	(L_{II} edge) (L_{III} edge)	−4·9	21·97
$2E[K^{++}, (1s)^{-1}(4s)^{-1}]$ $-2E[K^{++}(2p)^{-1}(4s)^{-1}]$	248·2 248·4		243·9 244·1		($K\alpha_2$) ($K\alpha_1$)	−4·3	—

The calculated value of (ν/R) for the K edge is in surprisingly good agreement with the experimental value. The discrepancy, 0·6, is almost within the limits of the accuracy of the calculations, and is only about 8 times greater than the discrepancy in the similarly calculated ionization energy of He, whereas the ionization energy itself is about 140 times that for He. There is a greater discrepancy in the position of the L_{II}, L_{III} edges, and this suggests that the extreme closeness of the agreement for the K edge is to a certain extent accidental. The value of ϵ_{2p} for K^+ is actually in better agreement with the position of the $L_{II,III}$ edges than is the properly calculated ionization energy (28); a similar result was found for the ionization energy of He calculated on the basis of the same approximation to structure of a many-electron atom. The calculated value 0·19$_5$ of the L_{II}–L_{III} spin doublet separation is in good agreement with the observed value 0·21 (Siegbahn 1931, Table 167).

Comparison of the values of the various I, F_k, G_k integrals for the different configurations shows the considerable extent to which the perturbation of the outer groups contributes to the total energy change on removal of an electron from an inner group. It has seemed worth while to carry out these calculations in full for one case, in order to find the magnitude of these perturbations and to take them into account in the calculation of energies. But the numerical work involved is fairly extensive; in the calculation of the energies for the three configurations with which this paper is concerned, 114 integrals were calculated and solutions of (22) evaluated for 72 different $Y_k(nl, n'l' \mid r)$ functions, exclusive of checks which involved the calculation of about 50 % more such integrals. For a heavier atom, the amount of work involved would be substantially greater, and might become prohibitive.

In conclusion, I wish to thank Professor Hartree, at whose suggestion this work was undertaken. He supplied the initial estimates for the calculation of the self-consistent field, supervised the early part of the work, and gave from time to time valuable practical contributions to its progress.

SUMMARY

Self-consistent field calculations, without exchange, have been made for two states of the potassium atom ionized in an inner group, namely for the configurations

$$K^{+2}[(1s)^1(2s)^2(2p)^6(3s)^2(3p)^6],$$

and

$$K^{+2}[(1s)^2(2s)^2(2p)^5(3s)^2(3p)^6].$$

The results are given in this paper. The perturbation of the wave functions of the outer electron groups on removal of an electron from an inner grant is found to be considerable, so that, for example, the $(3s)$ and $(3p)$ wave functions of a K atom ionized in the $(1s)$ group are more like those of a normal Ca atom than like those of a normal K atom. The results may be applied to take this perturbation into account in the theory of the Auger effect or of X-ray dispersion.

The application made in the present paper is to the calculation of X-ray ionization energies. The total energies of these configurations and of the normal state of K^+ have been calculated by Slater's method, and the calculated values of ν/R for the K, L_{II} and L_{III} edges and $K\alpha$ doublet obtained and compared with the observed values. The agreement is very good for the K edge and good for the K lines but less so for the L edges.

A new method of evaluating one of the quantities, $Y_k(nl, n'l' \mid r)$ required in the evaluation of the energy integrals is given.

REFERENCES

Burhop 1935 *Proc. Roy. Soc.* A, **148**, 272–84.
Hartree 1928 *Proc. Camb. Phil. Soc.* **24**, 89–132.
— 1933 *Proc. Roy. Soc.* A, **141**, 282–301.
— 1934 *Proc. Roy. Soc.* A, **143**, 506–17.
Hartree and Black 1933 *Proc. Roy. Soc.* A, **139**, 311–35.
Hartree, D. R. and W. 1935 *Proc. Roy. Soc.* A, **149**, 210–31.
McDougall 1932 *Proc. Roy. Soc.* A, **138**, 550–79.
Siegbahn 1931 *Specktroskopie der Rontgenstrahlen*, Zweite auflage. Berlin: Springer.
Slater 1929 *Phys. Rev.* **34**, 1291–322.
White 1934 *An introduction to atomic spectra.* New York: McGraw Hill.

The friction of clean metals and the influence of adsorbed gases. The temperature coefficient of friction

BY F. P. BOWDEN AND T. P. HUGHES

Laboratory of Physical Chemistry, Cambridge

(*Communicated by C. H. Desch, F.R.S.—Received* 2 *May* 1939)

Experiments on electron diffraction and electron emission, as well as optical and other methods, have made it abundantly clear that, when a solid is cleaned in air by any ordinary method, its surface is still covered by a film of oxide, water vapour, and other adsorbed impurities. The surface film is often several molecular layers in thickness. Any complete theory of friction must take this film into consideration. Most experiments on the friction of metals are not made with metallic surfaces at all, but with a metal coated with this surface film. If a lubricant is used it is not added to the metal directly, but is superimposed on the film of contaminant.

Recent papers (Bowden and Leben 1939; Bowden and Tabor 1939) have described an investigation of the kinetic friction between unlubricated metal surfaces which had been cleaned in air. The experiments show that sliding may not be continuous. The motion may proceed in jerks and large fluctuations may occur in the friction and in the surface temperature. The real area of contact between the metals is very small and corresponding fluctuations occur in it during sliding. The results suggest that metallic contact occurs only locally at the points of the surface irregularities. These contacts are usually few in number and their size is large compared with the dimensions of a molecule. The exact nature of the metallic junction depends on the relative physical properties of the metals, and the frictional resistance may be due to the surface irregularities of one metal ploughing through the other or to a cohesion and welding at the points of contact. The molecular field of force at the surface of a solid may be profoundly modified by the addition of even a single adsorbed layer, so that, on the above view the presence of this surface film should have a large influence on the friction.

It is difficult to remove the last adsorbed film and to maintain a clean surface, and few measurements of the friction of clean metals have been published. Jacob (1912), and Shaw and Leavey (1930) have heated metals *in vacuo* to clean them and found that the static friction increased. Their results were variable, however, and a comparison of their cleaning technique with that necessary to obtain photoelectrically clean surfaces indicates that their surfaces did not approach a really clean state. Holm, Guldenpfennig, Holm and Stormer (1931) observed that adhesion occurred between metals if they had been cleaned previously by heating to a high temperature in a good vacuum. This adhesion was maintained in the presence of a rare gas, hydrogen, or nitrogen, but disappeared on the introduction of oxygen. Later, Holm and Kirschstein (1936), using the tilt method of measuring the static friction, found that the forces necessary to cause motion between two degassed metals were very great. Since the surfaces were degassed by heating them together to a high temperature, it was not certain whether the adhesion was caused by an initial high temperature welding or not. On the other hand, Pöschl (1930, p. 71) has stated that when surfaces are cleaned in a good vacuum the sliding friction between them decreases and becomes vanishingly small.

This paper describes an attempt to measure the kinetic friction between naked metals. A new method of measuring the kinetic friction is described, and the experiments show that the removal of the surface film from a metal surface causes a very large increase in the sliding friction. The coefficient of friction between thoroughly outgassed metals was more than twenty times as great as that observed with metals "cleaned" in the ordinary way. The addition of a trace of some gases reduced this friction, while others had little or no effect.

The effect of temperature on the coefficient of friction was also investigated. Unless great precautions were taken the results were very variable, and the friction appeared sometimes to increase and sometimes to decrease with temperature. This erratic behaviour was due to traces of surface contaminants. When the surfaces were carefully cleaned the results were reproducible and reversible and the coefficient of friction showed a small but regular decrease as the temperature rose. These observations have an important bearing on the theory of friction.

EXPERIMENTAL

Method

If a body of mass m slides along a surface and the only retarding force is the friction, the equation of motion may be written

$$\frac{d^2x}{dt^2} = -\mu g,$$

where d^2x/dt^2 is the rate of deceleration, μ is the coefficient of friction, and g is the gravitational constant. The value of the coefficient of friction may then be obtained from the rate of deceleration of the sliding body.

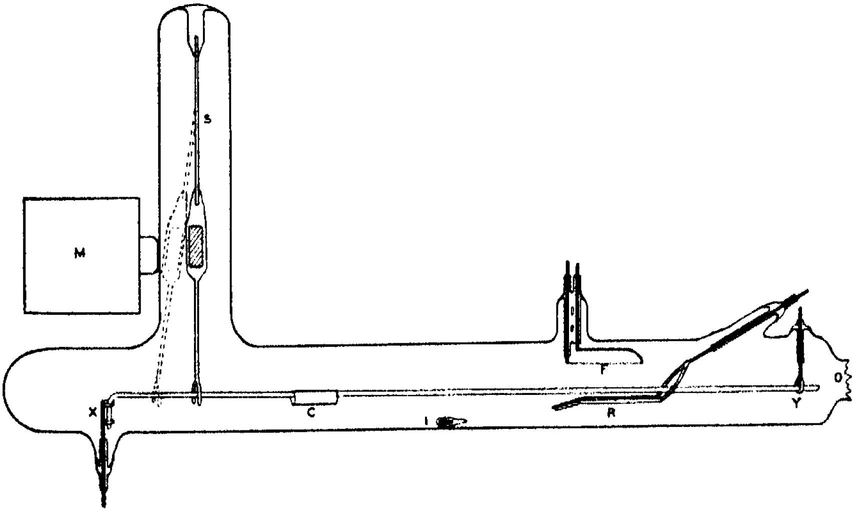

FIG. 1. The friction apparatus.

The apparatus used is shown in fig. 1. The sliding body was a small hollow cylinder of metal which hung on a lower cylindrical surface of smaller diameter. This cylinder was projected along the lower surface by a spring, and its motion was recorded photographically. The experimental curve showing the relation between the time and the distance slid was a parabolic one and the deceleration at any time could be calculated from the slope of the parabola at that point. This gave a measure of the average coefficient of kinetic friction over any short interval of time. The results showed that μ was sensibly constant over a range of sliding speeds from 100 cm./sec. down to very low speeds. In addition, it was found that if the spring was bent to the same extent for each kick, the product μ into d, the distance slid, was constant for a particular spring and cylinder over a variety of surfaces. When an apparatus had been calibrated for a particular spring and cylinder, the friction of the cylinder on the lower surface could be obtained immediately from the distance d, since μ is inversely proportional to this distance. In practice, the apparatus was calibrated by measuring μd, and the friction corresponding to any distance of sliding was evaluated from this. Successive values of d varied by about 5 % for low frictions, but the experimental error was greater for the very small values of d corresponding to high frictions.

The friction apparatus

Fig. 1 shows the general arrangement used to measure the friction. The cylinder C was projected along the lower surface by the pyrex or tungsten spring S. The end of the spring was forked and transmitted the impulse to both sides of the upper part of the cylinder; in this way any tendency of the cylinder to leave the lower surface during the sliding was reduced to a minimum. The spring was bent to the same extent for each kick by pulling the piece of soft iron, sealed in the pyrex, against the wall of the containing tube by means of the electromagnet M. The distance slid by the cylinder was read on a scale placed parallel to the lower surface. The cylinder could be moved about and turned over quite conveniently by small pieces of iron I sealed in glass and which were controlled from outside by an electromagnet held in the hand.

The lower surface was usually a thin foil of the metal, and was supported on a quartz rod of diameter 0·5 mm. This foil was wrapped around the rod with the seam underneath, so that the part of its surface where sliding occurred was quite smooth. The metal was degassed by passing a suitable heating current through it. The two nickel loops X, which held the quartz rod in a vertical position, made electrical contact with one end of the foil, while the single loop Y made contact at the other end. This loop Y only fitted loosely around the rod, and both the rod and foil could undergo thermal extension. In the case of metals sliding on tungsten the lower surface was a tungsten wire kept under tension and degassed by an electric current. The upper cylinder was degassed apart from the lower surface on the molybdenum rails R. In this position it was heated by 2000 or 5000 V electrons from the filament *F*. Both metal surfaces were kept at a temperature just below that at which excessive evaporation sets in during the final stages of degassing.

The surfaces were cleaned and rubbed with 000 emery paper and no further polishing was attempted. A microscopic examination showed that after degassing the fine scratches due to the emery were replaced by small pits and elevations. This change in the physical state of the surface had comparatively little effect on the friction. Experiment showed that the kinetic friction on both surfaces was approximately the same when they were contaminated in the air.

The apparatus was attached to the vacuum system at *O*. By means of two mercury diffusion pumps in parallel, backed by a Hyvac pump, the pressure was maintained below 10^{-6} mm. during the friction measurements. At first the pressure was measured by an ionization gauge, but this was later replaced by a sensitive type of Pirani gauge, since the former possessed marked "gettering" properties in oxygen atmospheres. Both these gauges were calibrated by a Macleod gauge. No grease was used on the apparatus side of the liquid air traps.

Of the gases used, oxygen was generated by heating a tube of potassium permanganate, nitrogen by heating a tube containing a coarsely ground mixture of potassium dichromate and ammonium chloride, and hydrogen was diffused into the apparatus from coal gas through a heated palladium tube. In order to introduce small quantities of these gases, three-way taps of a special design were used as pipettes in series with an expansion chamber in between them.

The absolute friction was determined from the photographed deceleration curve of the sliding cylinder. The shadow of the cylinder was arranged to pass along the narrow slit of a camera during the movement of the cylinder. When a moving film was used in the camera, a distance-time curve was obtained. The time markings were made by intercepting a parallel beam of light with a sectored disk rotated on a synchronous motor. In this way a series of sharp lines was obtained representing time intervals of 0·003 sec.

Results

The change in the friction due to the removal of surface films

The frictional behaviour as the surface films were removed was studied for the following pairs of metallic surfaces; nickel sliding on tungsten, nickel on nickel, copper on copper, and gold on gold. The usual procedure was to measure the friction, and to separate the surfaces and to heat them in a vacuum for a certain length of time. The surfaces were then allowed to cool, quickly placed in contact, and the friction again measured.

Nickel on tungsten. When the surfaces were "cleaned" in air and the apparatus was first assembled, the value of the coefficient of friction was about $\mu = 0{\cdot}3$. This is in reasonable agreement with the values for metal surfaces usually obtained by other methods. When the apparatus was evacuated the friction rose to $\mu = 0{\cdot}5$. This was probably due to the removal of the more volatile surface contaminants. On heating the wire alone with the cylinder resting upon it, a further increase to $\mu = 0{\cdot}7$ was observed. Finally the wire and cylinder were separated and heated at as high a temperature as possible. The tungsten was heated to *ca.* 1650° K and the nickel to *ca.* 1300–1400° K. They were then allowed to cool, were placed in contact and the friction rapidly measured. The process was then repeated several times. The friction continued to increase with prolonged heating and finally after several hours it reached a maximum of *ca.* $\mu = 6{\cdot}0$ (see fig. 2*a*). If the clean surfaces were allowed to stand at room temperature in a vacuum of about 10^{-5} to 10^{-6} mm. a steady decrease in the friction was observed. This decrease occurred in a few minutes and was probably due to the gradual contamination of the surfaces by the residual gas in the apparatus (see later).

Nickel on nickel. When the foil was heated with the cylinder resting on it the friction rose from $\mu = 0{\cdot}6$ to $\mu = 1{\cdot}9$. When the surfaces were separated and cleaned by prolonged heating to over 1300° K, the friction rose to a maximum value of $\mu = 4{\cdot}6$ (fig. 2*b*). No further increase was noted when hydrogen was admitted to the red hot surfaces (see later).

Copper on copper. The initial friction was about $\mu = 0{\cdot}5$. After heating for several hours at a bright red heat, it rose to a maximum value of $\mu = 4{\cdot}8$ (fig. 2*c*).

Gold on gold. The results on gold were not very reproducible. This may be due to the softness of the metal. Before degassing the friction was about $\mu = 0{\cdot}6$, and after prolonged degassing it rose gradually to a value of about $\mu = 4{\cdot}5$ (fig. 2*d*).

Degree of cleanness of the surfaces. There is no simple method of determining the nature or the amount of any impurity which may remain on a metal surface. However, in the case of tungsten some information is available. Langmuir and Villars (1931) have shown that the oxide film on this metal begins to evaporate at 1500° K. Later, Roberts (1935) made a thorough study of the conditions under which the surface of this metal may be cleaned, and found that a tungsten wire had to be heated in excess of 2000° K before the oxide film was completely removed. Bosworth and

Rideal (1937) have observed that the fraction of a tungsten surface which remains covered by adsorbed oxygen at 1600° K is only 0·3. Since the last adsorbed molecules will presumably be in the cracks and cavities in the surface, it is possible that the surface of this metal was almost clean in the above experiments as far as the friction measurements are concerned. More recently Van Cleave (1938) has found that a rapid removal of the first oxygen film on tungsten only set in at 1750° K. In the case of other metals less is known and the closeness of approach to a really clean surface can only be guessed at from a comparison with the technique used in photoelectric work. In these friction experiments the heating was continued in a good vacuum for some hours and the rate of gas evolution became immeasurably small. The temperature was kept as high as possible and considerable evaporation of the metal took place. The possibility that

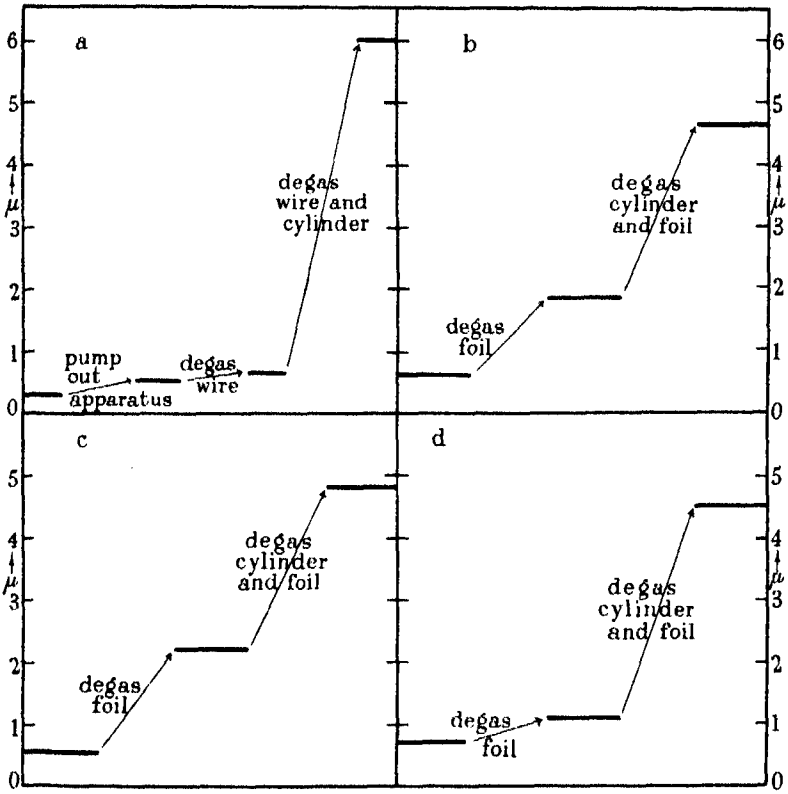

FIG. 2. The influence of degassing on the friction. (*a*) Nickel sliding on tungsten, (*b*) nickel on nickel, (*c*) copper on copper, (*d*) gold on gold.

the more strongly bound surface films were not removed cannot be excluded, but it is probable that the surfaces approached the clean state.

The influence of adsorbed gas on the friction

After the metals had been thoroughly outgassed and the friction had attained its maximum value, the pumps were turned off, a trace of gas was admitted, and the friction was immediately measured. The surfaces were at room temperature during the entry of the gas into the friction apparatus.

(*a*) *The effect of oxygen.*

Nickel on tungsten. When a trace of oxygen, enough to give a pressure of 10^{-3} mm., was admitted to the clean surfaces, there was a rapid fall in the friction from $\mu = 6{\cdot}0$ to $\mu = 1{\cdot}6$. The effect is shown in fig. 3*a*. The time of this change was too brief to be measured with any accuracy, but it was certainly about the order of a second or two. On standing, the friction showed a further slow decrease with time, and successive kicks also caused it to decrease slightly. The admission of larger quantities of oxygen gave similar results.

Nickel on nickel. The effect of admitting a relatively large quantity of oxygen (about 1 mm.) is shown in fig. 3*b*. The fall in the friction was slower than in the case of nickel on tungsten, and only became marked after a number of kicks had been made. The change in the friction appears to be the result of a slower oxidation process which is accelerated by the actual sliding process. This fall continued for several hours, but even when the metal was heated in oxygen to form a visible oxide film the value of the coefficient of friction, $\mu = 3{\cdot}0$, was high and showed comparatively little further change on standing.

Copper on copper. The introduction of oxygen at a pressure of a few mm. caused a rapid fall in the friction from $\mu = 4{\cdot}8$ to $\mu = 2{\cdot}4$, as in fig. 3*c*. After this there was a further slow fall to $\mu = 1{\cdot}9$ on standing for some hours. When a visible oxide film was made by heating the surface in oxygen, the friction fell to $\mu = 0{\cdot}75$.

Gold on gold. The addition of a trace of oxygen caused an immediate reduction in the friction from about $\mu = 4{\cdot}3$ to $\mu = 3{\cdot}2$. The addition of larger quantities of oxygen had a similar effect. The further slow fall with time in the case of the other metals was only slight in the case of gold. After standing for half an hour the friction was still $\mu = 3{\cdot}2$, and even after 16 hours it had only fallen to $\mu = 2{\cdot}8$, as in fig. 3*d*.

(*b*) *The effect of hydrogen.*

Hydrogen was admitted to clean surfaces of all the metals investigated, but no change was observed in the friction. In each case the friction remained at its high value. In fact, hydrogen was found to be very effective in removing oxide films when they were present, and experiment showed that the highest frictions were most stable when the residual gas in the apparatus was hydrogen.

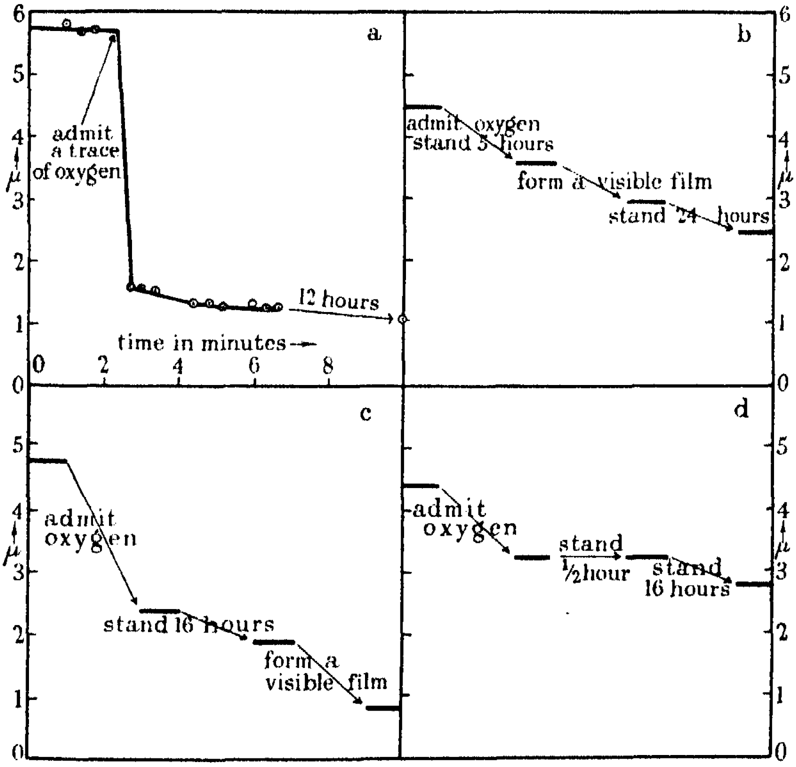

FIG. 3. The influence of oxygen on the friction of clean metals. (*a*) Nickel sliding on tungsten, (*b*) nickel on nickel, (*c*) copper on copper, (*d*) gold on gold.

(*c*) *The effect of nitrogen.*

Provided that the nitrogen was carefully purified and was free from oxygen it had no influence on the friction of the metals investigated. Nitrogen was found to give the same friction as oxygen for nickel sliding on tungsten if there was a trace of oxygen in the gas; it was without any influence if the oxygen had been removed by passing the gas over a heated tungsten filament.

(*d*) *The effect of mercury vapour.*

If the clean metals were allowed to stand overnight in a vacuum with no liquid air on the trap, a large reduction in the friction occurred because of contamination by mercury vapour. In the case of copper the friction was reduced to $\mu = 0{\cdot}7$ after standing overnight, and this value was not changed by subsequent sliding. The other metals, however, only showed a reduction in the friction as the result of the sliding process itself. Each successive kick lowered the value of the friction until it fell to about $\mu = 0{\cdot}5$. When the mercury vapour was partially removed by replacing liquid air on the trap, a small increase in the friction resulted.

The influence of temperature on the friction of clean metals

There is some uncertainty as to the effect of temperature on the friction of metals. Hardy and Doubleday (1922) have shown in the case of a lubricated surface that a small rise in temperature had little effect on the static friction. Jacob (1912) and Shaw and Leavey (1930) have attempted to measure the effect of temperature on the static friction of unlubricated surfaces. The results were rather irregular; the static friction appeared sometimes to increase and sometimes to decrease as the temperature rose. No measurements on the influence of temperature on kinetic friction have yet been published.

The apparatus described in this paper was very suitable for studying the effect of temperature over a wide temperature range. The lower surface was maintained at the required temperature by the passage of a suitable heating current through it. The temperature was measured by an optical pyrometer. After the upper cylinder had been degassed, it was placed on the lower surface and heated by conduction. For this reason the actual temperature at the points of contact was not known with great accuracy, but it is probable that the temperature of the surface layers at these points was not very different from that of the lower surface.

Results.

Unless elaborate precautions were taken to degas the metals very thoroughly, the results obtained were very erratic and unreproducible. In some cases the friction increased and in others it decreased as the temperature rose. A typical series of results under these conditions is shown in fig. 4. The variability of the results is due to the influence of the removal of surface films superimposed on any purely thermal effect.

If the surfaces were first thoroughly outgassed and a good vacuum was maintained the results became reproducible and reversible. The results for nickel on tungsten, nickel on nickel, copper on copper, and gold on gold are in fig. 5 *a*, *b*, *c* and *d*. In each case the friction decreased as the temperature rose. The effect is slight and the friction falls to about half its value when the temperature is raised 1000° C. Gold showed little change until a temperature of about 600° C was reached, when the friction rose suddenly to a very high value of $\mu = 20$ or 30. The effect was not due to a ploughing in of the cylinder edges into the lower surface, for a cylinder with bevelled edges gave the same result.

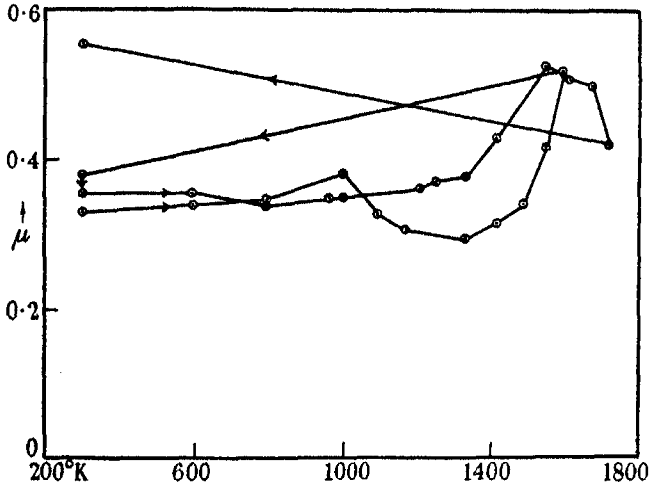

Fig. 4. The influence of temperature on the friction between incompletely degassed surfaces of nickel and tungsten.

Discussion

Clean metals

It is clear from these results that the removal of the surface films from a metal surface has a profound effect on the friction. In every case the friction showed a large increase, and the coefficient of kinetic friction could be nearly twenty times as great as the value normally obtained between metals "cleaned" in air in the ordinary way. The frictional force between unlubricated metals is usually a small fraction of the normal load, but if the surfaces are cleaned in a vacuum the frictional force may be four to six times as great as the normal load. It should be emphasized that this force is not merely that required to start motion (static friction), it continues to act while the surfaces are in rapid motion. The actual value of the coefficient of friction between the degassed metals appeared to differ slightly, but in view of the very considerable experimental errors involved for the highest frictions, it may be concluded that they were all of the same order of magnitude. The possibility that a trace of surface contaminant still remained cannot be excluded, and it is possible that the friction might rise to still higher values if the surfaces could really be obtained as naked metal.

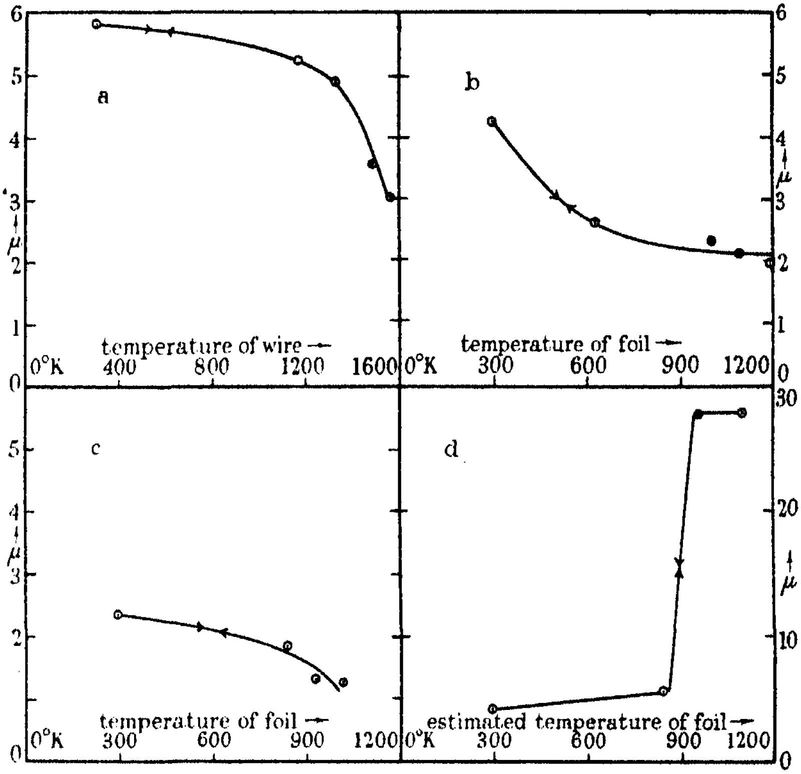

FIG. 5. The influence of temperature on the friction between clean metal surfaces. (*a*) Nickel sliding on tungsten, (*b*) nickel on nickel, (*c*) copper on copper, (*d*) gold on gold.

In spite of the great friction the sliding bodies behaved in a fairly reproducible manner and gave uniform deceleration curves. The results showed that, within the limits of experimental error, the friction was independent of the velocity from 100 cm./sec. down to very low speeds.

These observations lend strong support to the view that friction is due to molecular adhesion at the points of contact between the sliding metals. Under normal conditions the presence of adsorbed films will reduce the field of force at the surface of the metal. When this film is removed the strength of the field is increased, the metals are able to approach together more closely, and the molecular interaction and adhesion are very much greater.

The influence of gases

The effect of admitting various gases to the clean surfaces is very striking. In every case oxygen caused a relatively great reduction in the friction. In the case of nickel sliding on tungsten, for example, the admission of a trace of oxygen was followed by a rapid fall in the friction from $\mu = 6{\cdot}0$ to $\mu = 1{\cdot}6$. The time required for this fall to occur was too rapid for it to be measured, but it appeared to be less than a second or two. The friction could only be restored to its initial high value by evacuating the apparatus and reheating the metals to a high temperature. Roberts (1935) has shown that if oxygen is admitted at a low pressure (10^{-3} to 10^{-4} mm.) to a clean tungsten surface at room temperature, the surface is immediately covered by the gas. The oxygen forms a chemisorbed layer on the surface, and may only be completely removed by heating the metal to a very high temperature. This result has an important bearing on the frictional experiments and suggests that the initial fall in the friction after a trace of oxygen has been admitted to a tungsten surface is due to the rapid formation of the chemisorbed primary film. After the rapid initial change there is a further slow fall in the friction, which is probably due to the slow building up of a thicker oxide layer. The thicker this layer becomes, the more efficiently is any welding between the surfaces prevented, until, when the oxide reaches a certain depth, the value of μ would correspond to the friction between the completely oxidized surfaces. The effect of oxygen on the friction of the other metals was similar in nature to that for nickel on tungsten, but the effect was not so great in all cases. The rate of oxidation of a metal surface and the thickness of the resulting oxide layer naturally vary from one metal to another. The influence of oxygen on the friction would then be greater for the more easily oxidizable metals such as tungsten and copper and less for the more resistant metals such as nickel and gold, as was noted in the results. It is also possible that differences between the molecular force fields might give rise to differences in their adhesive and frictional properties, apart from the actual thickness of the oxide film.

When hydrogen or nitrogen were admitted to the clean metals there was no appreciable fall in the friction, even on prolonged exposure. The work of Roberts (1935) and Van Cleave (1938) has shown that both these gases form chemisorbed films on tungsten, but it seems that such films can possess little or no frictional properties on the metals. This result is in harmony with the observations of Holm and Kirschstein (1936) that oxygen decreased the adhesion between metals, while hydrogen and nitrogen did not.

An interesting effect was observed with most of the metals. If the cylinder was kicked along the wire a number of times the friction fell to a somewhat lower value. The act of sliding the surfaces together apparently causes a reduction in the friction. The observation was frequently made in low pressures of oxygen, where the sliding process resulted in a certain amount of frictional oxidation at the points of contact between the surfaces, presumably as the result of frictional heating, lattice distorsion and deformation. The effect was also observed during all stages of the degassing, and was particularly marked when the surfaces had been standing overnight in mercury vapour. In some cases the effect may be attributed to a slight smoothing of the surface by the removal of small projections formed during the degassing process. Where the effect is large, however, it suggests that it is due to the sliding process assisting to smear a contaminant over the surface. Even if the surface itself is clean there will still be gases and other impurities dissolved within the metal and held between the grain boundaries beneath the surface. The sliding process causes a tearing and distortion of the metal to a considerable depth (Beare and Bowden 1935), so that these impurities are liberated and can come to the surface. Strong support to this suggestion is given by the behaviour of the pressure during the early stages of degassing. When the cylinder was kicked along the wire the Pirani gauge showed a momentary but definite increase in pressure, showing that an appreciable volume of gas had been liberated.

Most clean metals are easily "wetted" by mercury, and the observed reduction in the friction suggests that a mercury film is smeared over the surface by the sliding process. Whether the large reduction in the friction is due to a weakening of the metallic junctions by amalgamation, or whether it is due to a thin liquid film of mercury is not certain.

The effect of surface films

Although the kinetic friction is reduced by the primary film of oxygen it does not fall to the low values normally observed in air until comparatively thick layers of oxide are built up on the surface. A similar effect was observed with a fatty acid vapour (Bowden and Hughes 1938). The adsorption of a single layer of the vapour on the outgassed metal reduced the friction but it did not fall to the values usually observed for boundary lubricated surfaces ($\mu = 0{\cdot}1$–$0{\cdot}2$) until a comparatively thick film had condensed on the surface.

Hardy's work has shown very clearly the importance of the first adsorbed film and he suggests that the *static* friction is due entirely to the molecular interaction between the primary film on each surface.

This work supports the view (Beare and Bowden 1935) that in the case of kinetic friction the primary film is not enough. The surface irregularities on the solid penetrate even the best lubricant film and when sliding occurs the solid is torn and distorted to a considerable depth beneath the surface. Excess lubricant must be present so that it can move in and repair the damage, and polymolecular layers are necessary before a substance can act as an effective boundary lubricant for moving surfaces.

It is probable that the oxide layer reduces the friction between unubricated metals by weakening the metallic junctions between the surfaces. The results of earlier papers (Bowden and Leben 1939; Bowden and Tabor 1939) suggest that the junctions are of three main types. With the first type the irregularities of the harder metal penetrate the surface of the other, and the friction is the force required to drag these projections through the softer metal. If an oxide layer is present on the surfaces the penetration, and hence the friction, will not be so great. The second and third types of junction are due to the adhesion and metallic welding between the surfaces, and this will be greatly reduced by the presence of an oxide film. Experiments have shown that the electrical resistance across the metal contact is, for different metals, proportional to the specific resistance of the metal. This shows that the conductivity is mainly due to the metal itself. The presence in the junctions of very thin fragments of the oxide layer would, however, have only a small effect on the electrical resistance so that their presence might not be apparent from the conductivity measurements. These oxide fragments would have a profound effect on the mechanical strength of junctions and would weaken them considerably. Unless the oxide layer is very thick it is not able to prevent metallic contact, the surface irregularities break through it during sliding. It does, however, reduce the extent and the intimacy of the contact, and so reduces the friction. It is fortunate for engineering practice that metal surfaces are usually dirty.

The influence of temperature

It is clear that the variable results obtained with metals which have not been thoroughly outgassed are due to surface contamination. The changes in the composition of this film on heating will cause frictional changes which are so great that they mask any effect due to temperature alone. This erratic behaviour may explain some of the conflicting results for static friction which were obtained by earlier workers. When the surface had been thoroughly outgassed, however, the results were reversible and reproducible and for nickel on tungsten, nickel on nickel and copper on copper the friction falls slightly as the temperature rises. The fact that the measurements were reversible, i.e. that the friction returned to its original value as the surfaces were cooled down, is important, since it shows that the frictional decrease was due to the temperature alone and not to any irreversible change in the structure of the surface. The fact that the friction *decreased* as the temperature rose also suggests that the surfaces were reasonably clean. If contaminating films were present, a high temperature would diminish their concentration and cause an increase in the friction.

The decrease in the coefficient of friction for most metals was only a few per cent for a temperature rise of 100°. This small effect is in harmony with the view that friction may be due to the tearing of the metal at the local points of contact. It has been suggested that the surface irregularities separating the metals flow plastically under the applied load until their area is sufficient to enable them to support it. At high temperatures the mechanical strength of the metals is considerably reduced so that, for a given load, the total cross-section of the junctions must be greater. Since the mechanical strength of the metal has fallen off proportionately, however, the force required to break them will be approximately the same and the friction may be nearly independent of temperature.

Gold was exceptional; at a temperature of *ca.* 600° C the friction rose suddenly to a very high value of $\mu = 20$ or 30. This effect is probably due to the pronounced softening of the gold at this temperature so that the metal flows readily and the surfaces are welded together over a large area.

We wish to express our thanks to the Trustees of the Ramsay Memorial Fund for a Fellowship (T. P. H.), and to the Royal Society and Chemical Society for grants for apparatus.

SUMMARY

A method is described for measuring the kinetic friction between metal surfaces which have been freed from the oxide and surface films which are normally present. The removal of the films has a profound effect and the kinetic friction between the outgassed metals may be twenty times greater than that observed for the same metals cleaned in air.

The addition of a trace of oxygen to the clean metal causes an immediate reduction in the friction. Adsorbed hydrogen and nitrogen have little or no effect. Although the friction is reduced by a single film it is clear that

polymolecular layers are necessary before a substance can act as an effective boundary lubricant for moving surfaces.

The temperature coefficient of friction between clean metals was determined over a wide temperature range. Most of the metals investigated show a small but regular decrease in the kinetic friction as the temperature rises. If the temperature causes excessive softening of the metal the friction may rise to a high value.

REFERENCES

Beare, W. G. and Bowden, F. P. 1935 *Phil. Trans.* A, **234**, 329–54.
Bosworth, R. C. L. and Rideal, E. K. 1937 *Physica*, N.S. **4**, 925–40.
Bowden, F. P. and Hughes, T. P. 1938 *Nature, Lond.*, **142**, 1039–40.
Bowden, F. P. and Leben, L. 1939 *Proc. Roy. Soc.* A, **169**, 371–91.
Bowden, F. P. and Tabor, D. 1939 *Proc. Roy. Soc.* A, **169**, 391–413.
Hardy, W. B. and Doubleday, I. 1922 *Proc. Roy. Soc.* A, **101**, 487–92.
Holm, R., Guldenpfennig, F., Holm, E. and Stormer, R. 1931 *Wiss. Veröff. Siemens-Konz.* **10** (4), 20–64.
Holm, R. and Kirschstein, B. 1936 *Wiss. Veröff. Siemens-Werken*, **15** (1), 122–7.
Jacob, C. 1912 *Ann. Phys., Lpz.*, **38**, 126–48.
Langmuir, I. and Villars, D. S. 1931 *J. Amer. Chem. Soc.* **53**, 486–97.
Pöschl, Th. 1930 *The physics of solids and fluids*, by Ewald, Pöschl and Prandtl. London: Blackie.
Roberts, J. K. 1935 *Proc. Roy. Soc.* A, **152**, 445–80.
Shaw, P. E. and Leavey, E. W. 1930 *Phil. Mag.* **10**, 809–22.
Van Cleave, A. B. 1938 *Trans. Faraday Soc.* **34**, 1174–7.

The mechanism of sliding on ice and snow

BY F. P. BOWDEN AND T. P. HUGHES

Laboratory of Physical Chemistry, Cambridge

(*Communicated by C. H. Desch, F.R.S.—Received* 2 *May* 1939)

INTRODUCTION

The preceding paper has shown that the sliding friction between metals decreases in a regular manner as the temperature is raised, provided that the chemical nature of the surface layers remains unchanged. The behaviour of the friction at temperatures near the melting-point was not investigated. Most metals become very soft at these high temperatures, and the irregularities which normally separate the two surfaces now collapse, so that a comparatively large area of contact is developed. Since the frictional force is the resultant of the minute adhesions acting across the real area of contact, we should expect that the friction between two such surfaces would be very great. The friction between two gold surfaces sliding together has been observed to increase to very high values where the metal becomes soft.

With solids of different physical properties, however, there is the further possibility that a surface layer of solid may be melted, either by pressure melting or by frictional heating, when the mass of the solid is still frozen and hard. If the melted fluid is present in sufficient quantity and possesses a low viscosity, the conditions may become those of lubricated sliding and lead to a large reduction in the friction. This effect would naturally be most marked for those substances which retain their rigid character at temperatures close to the melting-point, and which give a liquid of low viscosity on melting. Ice is a solid which has these properties, and it is well known that the friction of solids on ice and snow is very low. The suggestion has often been made that, in skating or ski-ing, the surfaces are lubricated by a layer of water formed by pressure melting (e.g. Reynolds 1901, p. 737), but few measurements of any sort have been made either to support or to disprove this suggestion.

Pressure melting. Experience shows that ski slide quite readily on snow at $-20°$ C. If we consider that the ski makes contact with the snow over the whole of its under surface (neglecting the tip), the pressure for an average man of 75 kg. weight on ski of area 5000 cm.^{2} is 15 g./cm.^{2}. This pressure can only form a water layer if the snow were at $-0.00012°$ C or a higher temperature. The real area of contact is of course less than the apparent area. In the case of metals the real area may be a minute fraction of the apparent area of contact, and the mutual pressure between the two surfaces may be the flow pressure of the metal (Holm 1929; Bowden and Tabor 1939). With a powder such as snow, which can pack down and conform to the shape of the ski, we might expect the area of contact to be greater—perhaps not less than 1/1000 of the area of the ski. If this were the case then the pressure is still only great enough to melt snow at $-0.12°$ C. In order to have a sufficient pressure to melt snow at the low temperature of $-20°$ C, the real area of contact must be less than 0·031 cm.^{2}, i.e. about 1/100,000 of its apparent area.

These calculations of the pressure melting are made on the assumption that the pressure is applied equally to the solid and to the liquid phases. Poynting (1881) has pointed out that if the pressure is applied to the solid alone, the lowering of the melting-point is about 11½ times as great. This effect and its bearing on flow pressures has been discussed by Johnston (1912) and Jeffreys (1935). We cannot, on theoretical grounds rule out the pressure-melting theory, but if it is true it means that the real area of contact is extremely small. The pressure itself is, of course, not sufficient to cause melting. Heat must be supplied from some source which is at a higher temperature than that corresponding to the equilibrium melting pressure.

Melting due to frictional heating. There is, however, another possible cause of surface melting, that is the frictional heat liberated at the sliding interfaces. Earlier work (Bowden and Ridler 1936; Bowden and Hughes 1937) has shown that this frictional heat may raise the surface temperature of sliding metals to a high value and may cause local melting and flow of the solids. In the case of a ski sliding on ice at $-20°$ C, for example, if the coefficient of friction is $\mu = 0.05$ the amount of frictional heat liberated when the ski moves forward a distance of 1 cm. is given by

$$Q = \frac{\mu M g}{J} = \frac{0\cdot05 \times 37\cdot5 \times 981 \times 1000}{4\cdot18 \times 10^7} = 0\cdot044 \text{ cal.}$$

This heat is concentrated at the points of contact of the snow crystals. If the ski were making intermittent rubbing contact over its whole area, this heat would be sufficient to raise from -20 to 0° C and to melt a layer over 6 mol. in thickness over this area. In actual fact, the real area of contact must be very much less, and the heat is concentrated at the points of contact of the snow crystals. Again we do not know the real area of contact, but if the area of contact is taken as 0·1 cm.^{2}, then the thickness of the water layer melted would be $5{\cdot}5 \times 10^{-3}$ cm. or $1{\cdot}7 \times 10^{5}$ molecular layers. It is clear that a great part of the heat must be lost by conduction from the points of contact to the surrounding snow and to the ski. These crude calculations cannot be taken very seriously but they do show that the frictional heat liberated is considerable, and that the retention of a small fraction of it may be sufficient to cause local melting at the points of contact of the snow or ice crystals.

This paper describes an investigation of the experimental laws which govern the friction of solids sliding on ice and snow. The work shows that these laws bear a general resemblance to those observed for other solids, but there are important differences. Experiments were undertaken to determine whether a water layer is formed at all, and if so, whether it is due to pressure melting or to frictional heating. The results show that at very low temperatures (– 140° C) the friction of ice is high, and is of the same order as that observed for other unlubricated solids. At higher temperatures, however, the friction decreases and there is evidence that partial lubrication by a water film may occur. The results suggest, that, although pressure melting plays some part, the low friction observed for rapidly moving solids on ice and snow is due in a large measure to the melting of a water layer by frictional heating.

EXPERIMENTAL

The experiments were carried out in an ice cave dug out of the ice above the Research Station at the Jungfraujoch, 3346 m. in Switzerland. The temperature of the cave never rose above – 3° C. Since the air is very pure at these altitudes, the danger of contamination of the surfaces by grease and vapour was very slight.

The apparatus used to study the friction is shown in fig. 1. It is similar in principle to that previously described by Bowden and Ridler (1936). A horizontal turntable (C) of copper carried the lower surface of ice or snow. This turntable was hollow, and could be filled with cooling agents such as solid carbon dioxide or liquid air, so that the film of ice on top of it could be cooled to any desired temperature. The upper sliding surface (I) was attached to the arm (A). The other end of this arm was held in gimbals (G) so that the sliding surface could move freely in a horizontal or a vertical plane. The load was applied by fitting weights in the cup (L). When the lower surface rotated the frictional force between the two surfaces would tend to drag the upper surface with it. This movement was prevented by a fine thread fastened to the upper slider at Z, and attached at the other end to a flat spring. The deflection of this spring gave a measure of the frictional force between the two surfaces. It was measured by a beam of light reflected from a mirror attached to the spring.

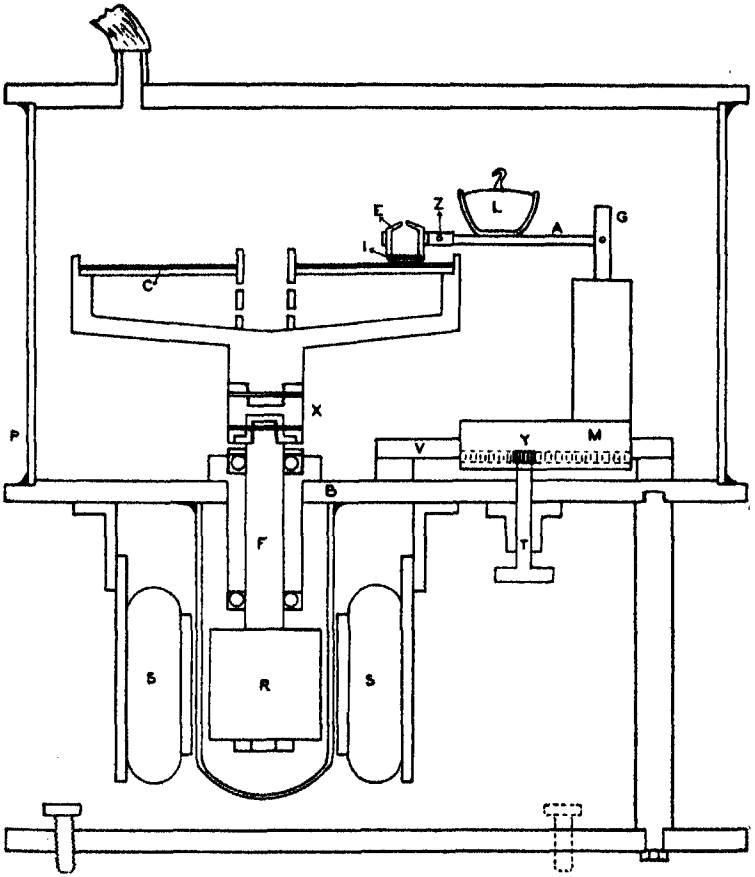

FIG. 1. The friction apparatus

The gimbals were mounted on the brass block (*M*) which could slide along the brass rail (*V*). This block was fitted underneath with a rack strip, and could be propelled along the rail by means of a small pinion (*Y*) on the tap (*T*). This sliding block also carried the vertical flat spring used for measuring the friction, and this was so arranged that its scale reading was not affected during the sliding of the block. When the tap (*T*) was turned, the upper slider (*I*) moved nearer to the centre of the turntable, so enabling the surfaces to run in a fresh track.

The apparatus was so designed that the sliding surfaces were completely enclosed in the glass cylinder (*P*) which could then be evacuated. The turntable (*C*) was connected to the rotor (*R*) of an induction motor by the vertical steel shaft (*F*). These two metal components were thermally insulated from one another by the block of vulcanite (*X*) secured by tapered pins. The rotor was separated from the stator (*S*) of the induction motor by a glass sheath sealed on to the flat steel base plate (*B*). This arrangement enabled the lower surface to be rotated in a vacuum. A number of experiments on the friction of ice surfaces were carried out in the absence and in the presence of air. No difference in the behaviour was observed, showing that the air of the laboratory caused no appreciable contamination of the surfaces.

RESULTS

The friction of ice on ice

The lower surface of ice was formed by running a film of water on to the turntable and allowing it to freeze. The table was then set in rotation and the ice surface was planed smooth with a small plane. The small upper ice surface (*I*) was frozen on to a copper plate which formed the base of an ebonite cylinder (*E*).

The influence of load on the friction.

The sliding speed was maintained constant at *ca.* 400 cm./sec. and the effect of load on the friction was investigated. Fig. 2, curve *a*, shows the results obtained with ice cooled to -3° C. Over a certain range of loads (0–200 g.) there was a linear relation between the frictional force *F* and the applied load *W* showing that the coefficient of kinetic friction μ_k was constant. In this case μ_k was equal to 0·032. At higher loads the curve became concave to the *W* axis showing that μ_k decreased with higher loads. This type of curve was always obtained with ice surfaces cooler than -1° C. Curve *b* shows a typical result for ice at -27° C. The general relation is the same but the friction is higher, $\mu_k = 0{\cdot}064$. If the ice was at 0° C, however, and the surfaces were allowed to run in the same track for some time, a different behaviour was observed (curve *c*). Under these circumstances the coefficient of friction μ_k increased at heavy loads and with the time of running. An examination of the surfaces showed that a thick film of water had formed on them. If this thick film of water was wiped off the lower surface with cotton-wool or was frozen with a block of carbon dioxide, the friction immediately fell again. If water was then added to the surface the friction again rose. The addition of a small quantity of water to ice at 0° C, for example, raised the friction from $\mu_k = 0{\cdot}024$ to $\mu_k = 0{\cdot}075$. When this water was removed by freezing, the friction immediately fell to its initial value. This shows that the presence of a *thick* layer of water increases the friction between the rapidly moving surfaces. This thick layer can be formed by prolonged running on ice which is very nearly at 0° C. In order to prevent disturbances due to this effect measurements were made with short runs.

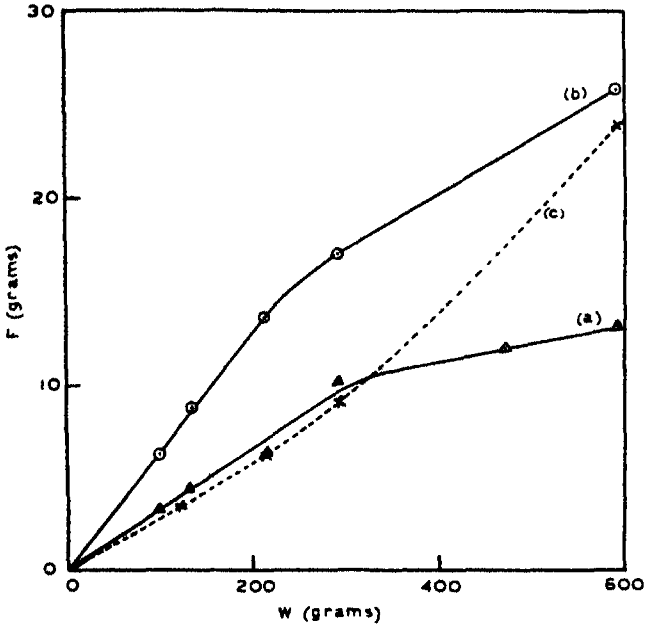

FIG. 2. The relation between the frictional force (F) and the load (W) for ice sliding on ice. Curve (a) mean surface temperature $-3{\cdot}3°$ C; curve (b) mean surface temperature $-27{\cdot}5°$; curve (c) mean surface temperature 0°; long runs with the surfaces wet.

The influence of the area of contact on the friction.

The apparent area of contact was varied by changing the size of the top surface. It was not easy to carry out the experiments under identical conditions, but the results of a number of experiments are shown in Table I. The sliding speed in each case was 400 cm./sec., and the range of loads was from 0 to 300 g. The apparent area of contact varied from 0·02 to 3·1 cm.^{2}.

Owing to the difficulty of carrying out these experiments under exactly comparable conditions, the results must necessarily be only approximate. It will be seen, however, that although the apparent area of contact was altered by a factor of 150, the coefficient of friction showed little change; this has also been observed with other solids (Beare and Bowden 1935).

If the ice was near 0° C and the upper surface was curved, prolonged running again caused an obvious melting or wearing away, so that a flat was worn on it and the area was increased to a large value. This had little effect on μ_k provided that a thick film of water was not allowed to form on the surface. If this thick film did form the friction again rose to a high value.

TABLE I

Exp. no.	Apparent area of contact cm.^{2}	Mean temperature ° C	μ_k
1	0·6	−1·4	0·019
	2·3	−2·0	0·019
2	0·6	−3·0	0·017
	2·5	−3·0	0·019
3	0·02	−1 to −10	0·016
	3·1	−3·0	0·021

The influence of temperature on the friction.

If the low friction on ice is due to the formation of a thin water film, we should expect the friction to be a function of the temperature. The film would be more difficult to form at low temperatures and the friction should be higher. This is true whether its mechanism of formation is by pressure melting or by frictional heating. Experiments were carried out to investigate this point.

Both the ice surfaces could be cooled with liquid air or with ether and carbon dioxide. In practice, the surfaces were cooled to a low temperature and the friction measured at different intervals of time as the surfaces warmed up. The surface temperature of the ice was measured by pressing a special thermojunction of small heat capacity against the stationary surfaces, and the temperatures recorded are the mean of the temperatures taken before and after the friction measurements. The results for different loads are shown in fig. 3. The sliding speed in each case was 400 cm./sec. The friction at each temperature was measured with a variety of different surfaces and areas of contact. The values showed some variation and each curve is the average of a large number of determinations. It will be seen that in each case the kinetic friction increases as the temperature falls. Fig. 3, for a load of 130 g., for example, shows that the friction at −140° C may be some five or six times greater than it is at 0° C. The value of the coefficient of friction ($\mu_k = 0{\cdot}11$) at these low temperatures is of the same order of magnitude as that observed on other crystalline solids. Hutchison

(1938 unpublished) has shown that the friction on calcite is $\mu_k = ca.\ 0{\cdot}2$. In all three curves the effect of temperature on friction is much greater from 0 to $-40°$ C than over the range -40 to $-140°$ C. The effect of temperature is much greater on ice than it is on metals. Over the first part of the curve the average decrease in the friction of ice for a 10° rise in temperature was about 30 %. In the case of metals the decrease in the friction for a 10° rise was only about 0·05 %.

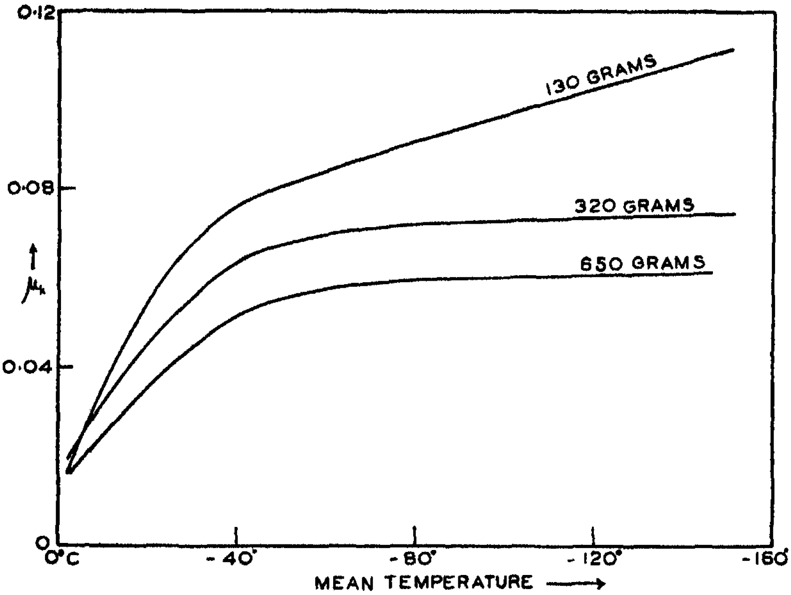

FIG. 3. The influence of temperature on the kinetic friction between ice surfaces.

Static and kinetic friction and the influence of speed.

The value of μ_s, the static friction, depended on the time for which the surfaces were allowed to remain in contact. This was particularly true for temperatures close to the melting-point. If the surfaces were allowed to stand in contact for some minutes at temperatures near 0° C, they became frozen together, and the force required to start motion was very great indeed. At temperatures well below the melting-point, this effect was not so marked. Although the values of the static friction were not very reproducible and showed some variation at different points, it was possible to obtain some idea of its general behaviour. The relation between the load and the frictional force was similar to that observed for kinetic friction (fig. 2). The F/W curve was at first linear showing that μ_s was independent of the load, but at heavier loads the curve became concave to the load axis, showing that μ_s becomes less at heavier loads.

The effect of temperature on μ_s is shown in Table II.

TABLE II

Temperature, ° C ...	0	−12	−71	−82	−110
μ_s	0·05–0·15	0·3	0·5	0·5	0·5

Provided the ice was not actually melting the static friction was always much higher than the kinetic friction, and was of the same order of magnitude as that observed on other solids. At −12° C, μ_s has the value 0·3 as compared with $\mu_k = 0{\cdot}03$ under the same conditions. The results show that the static friction decreases as the temperature approaches the melting-point. At, or very close to 0° C, the results were very variable. If the ice was actually melting, so that a film of water was present, the force required to start the motion was very small indeed ($\mu_s = 0{\cdot}02$). If, however, local freezing could occur, the static friction became too great for the apparatus to measure.

When the surfaces were set in motion the friction fell to the characteristic kinetic value, and this value was not greatly influenced by the speed of sliding until the speed became low. At very low speeds the coefficient of friction increased. An analysis of the sliding friction showed that, even at high speeds, μ_k was not constant but was fluctuating rapidly. It was clear that the surfaces were not sliding continuously, but were moving by a process of "stick and slip", and the general behaviour was very similar to that observed for metal surfaces (Bowden and Leben 1939). At temperatures near 0° C and at low speeds these fluctuations became very great indeed, and it was evident that an intermittent freezing together and breaking away was occurring.

If the pressure melting view is correct, there is no particular reason why the static friction should be so much higher than the kinetic friction. A water film should be present at the points of contact even though the surfaces are stationary. If, however, the water is melted by frictional heating we should expect the static friction to be very much higher than the kinetic friction. The results support the frictional heating mechanism. At first sight it might be thought that the kinetic friction should be very dependent upon velocity, and should decrease as the velocity increases since the rate of heat evolution and of melting should be greater. This is true for the slider but is not true for the lower surface. The slider is continuously moving forward on to a surface of fresh ice and the amount of heat evolved per square centimetre of this surface is independent of the speed of sliding.

The friction of other solids on ice. The influence of thermal conductivity

Experiments were carried out to study the friction of other solid surfaces sliding on ice. It was of particular interest to determine the influence that the thermal conductivity of the ski would have on the friction at low temperatures. If sufficient pressure is applied to the ice to lower the melting-point to the actual temperature of the ice, it is, of course, capable of melting. An appreciable quantity cannot melt, however, unless heat is supplied from some source at a temperature higher than the pressure melting-point equilibrium. Both the heat capacity of the ice and its thermal conductivity are small and this heat can most readily be supplied from some outside source. If the temperature of the atmosphere is higher than either of the ice surfaces, it could be supplied by conduction from the air. Under these conditions we should expect that the friction of a good thermal conductor would be less than that of a bad one. The friction of a brass ski on cold ice should be *less* than that of an ebonite one.

If, however, the lubricating film is formed by frictional heating, the converse will be true. The frictional heat is liberated at the interface between the sliding surfaces, and if the ski is a good thermal conductor, it will be carried away rapidly and less will be available for surface melting. (See Bowden and Ridler (1936) for an experimental proof of this.) On this view the friction of a brass ski on cold ice should be *greater* than that of an ebonite one. Experiments were made to test these hypotheses, using solid brass and ebonite ski, 1·5 cm. long, 0·5 cm. wide and 0·5 cm. high. The results are shown in fig. 4. The sliding speed was again 400 cm./sec., the load was 130 g., and the temperature of the ice varied from 0 to −70° C. The values again showed some variation and each curve is the average of a number of determinations. The friction of ice on ice is added for comparison.

At temperatures near 0° C the frictions of both ski were the same. At lower temperatures, however, the results showed that the friction of the brass was considerably greater than that of the ebonite. The lower the temperature the more pronounced this difference usually became. A similar effect was observed for higher loads (up to 600 g.). At the higher loads μ_k was lower for both substances than at lower loads as in the case of ice surfaces, but the two curves again diverged and at low temperatures the friction of the brass was again greater than that of the ebonite.

Some further experiments were carried out with a hollow ski so constructed that its effective thermal conductivity could be altered while the actual sliding surface was always of the same material. A hollow frame of ebonite was made in the shape of a ski and the bottom was covered with a thin copper sheet. If the air on top of this sheet were displaced by filling the ski with mercury, the thermal conductivity and heat capacity would be considerably increased. The results in Table III show that the coefficient of friction of this ski on cold ice was increased by a factor of 1·3–1·7 when the mercury was added.

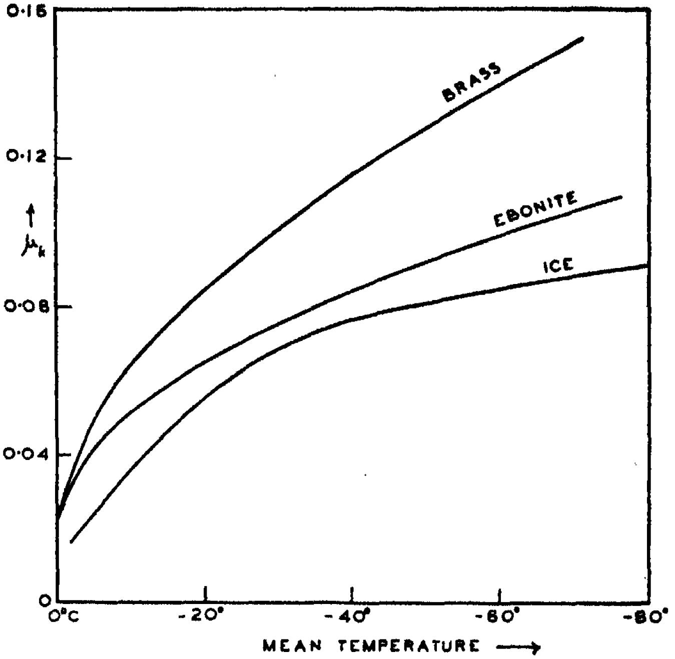

FIG. 4. The influence of temperature on the friction of brass, ebonite and ice sliding on ice.

TABLE III

Metal	μ_k (no mercury)	μ_k (mercury on ski)	μ_k Hg/μ_k
Copper	0·022	0·031	1·4
	0·027	0·034	1·3
	0·032	0·043	1·3
	0·032	0·054	1·7
Constantan	0·021	0·020	1·0

The thermal conductivity of constantan (0·054) is considerably less than that of copper (0·92), and when the copper was replaced by constantan it will be seen that the addition of mercury had little effect.

These results provide strong evidence for the view that frictional heating plays a large part in the formation of the lubricant water film.

Some measurements were also made with solid brass and ebonite ski heated to 10° C and placed on ice at 0° C. The values of the kinetic friction (sliding speed 400 cm./sec.) are shown in Table IV.

TABLE IV

	Load 200 g.	Load 1000 g.
Brass ski	0·010	0·005
Ebonite ski	0·025	0·010

In this case the heat for surface melting can be supplied by the ski itself since this is above 0° C. It will be seen that the good thermal conductor, brass in this case, now gives the *lower* friction. Under these conditions, when the temperature of the ski is above 0° C, the static friction is also very low, *ca.* $\mu_s = 0{\cdot}005$.

The friction of hickory ski and the influence of wax.

A small hickory ski, length 4 cm., width 1·3 cm., and thickness 0·2 cm., was made and the lower surface rubbed smooth on fine emery paper. The general behaviour of this ski was similar to that of the other substances, except that μ_k was considerably higher at all temperatures. The ski was then waxed with a thin layer of Sohm's Red Gleitwax, and its friction again measured. The effect of wax on the friction of a small brass ski was also studied, and the results are shown in Table V.

TABLE V

	Load 200 g.	
Nature of ski surface	Temp. − 3° C	Temp. − 7° C
Unwaxed hickory	0·08	—
Waxed hickory	0·03	0·04
Unwaxed brass	0·030	0·05
Waxed brass	0·025	0·045

The results show that the friction of a hickory surface is reduced to about half its value by a layer of wax. The friction of brass at temperatures near the melting-point is already low so that the addition of wax has comparatively little effect. At these temperatures there is little to choose between brass and waxed hickory as sliding surfaces, but at lower temperatures when the friction of brass becomes high it is probable that the waxed hickory would be considerably better as a low friction ski.

The electrical conductivity of the surfaces during sliding.

If a water film is formed during sliding, we might expect that the electrical conductivity of the surface would change. Two small copper electrodes were set into the bottom of the ebonite ski, and the surface was ground flat and polished. The near edges of the electrodes were separated by a distance of 0·2 cm.

The turntable was cooled down to a low temperature and water containing 0·5 % potassium chloride was poured on to it. This immediately froze to a thin film of ice and the freezing was so rapid that little separation of the salt could occur. The ski was then placed on the stationary surface and a load applied. When the surfaces were cold, the conductivity was less than 5×10^{-7} mho. The surfaces were then set in motion and the surfaces allowed to warm up. The friction gradually fell as the temperature rose, and the value of the friction indicated that surface melting was occurring. The electrical conductivity at first showed little change and the results suggest that the melting was taking place only locally at the isolated points of contact. In the neighbourhood of the melting-point, however, there was a sudden rise in the conductivity to about 5×10^{-5} mho, showing that the water film had become continuous between the two electrodes. This film was still invisible, and under these conditions the friction had the low value of $\mu_k = ca.\ 0{\cdot}03$.

If we consider the composition of the remelted liquid to be the same as that of the original solution—a drastic assumption—we may make an approximate estimate of the thickness of the film. The specific conductivity of 0·5 % potassium chloride at 0° C is 0·005 mho/cm. The dimensions of the film are $0{\cdot}2 \times 0{\cdot}3 \times d$ cm. where d is the thickness. Since the observed conductivity was 5×10^{-5} mho, the thickness d of the liquid film is equal to *ca.* 7×10^{-3} cm. This is a reasonable order of magnitude.

Friction on snow surfaces

Experiments with the model ski.

Experiments were also carried out on snow surfaces. The snow used was finely crystalline snow which had fallen two days previously outside the laboratory. It was placed on the turntable and pressed down with a cold glass plate. It was not possible to run the turntable at high speed under such conditions because the snow was flung off. The experiments on sliding friction were then made at a sliding speed of about 10 cm./sec. The small ski of brass, ebonite, and hickory were used.

The general behaviour was very similar to that observed on ice, except that the friction was always higher. For example, the friction of waxed hickory on snow was $\mu_k = 0{\cdot}09$ as compared with $\mu_k = 0{\cdot}04$ for ice at the same temperature. This higher friction is almost certainly due to the extra mechanical work of displacing and compressing the snow. The friction was again independent of the load, provided this was not too great. At heavy loads the F/W curve became concave to the W axis, as before, showing that the coefficient of friction decreased under these conditions. The effect of velocity was not investigated in detail because of the difficulty of rotating the surfaces at high speeds. There was evidence, however, that the friction decreased considerably at high speeds. The friction was again dependent on the surface temperature of the snow and increased as the temperature fell. Table VI shows some typical results for waxed hickory at different temperatures.

TABLE VI

Temperature, ° C ...	0	−3	*ca.* −10	−40
μ_k	0·04	0·09	0·18	0·4

It will be seen that the friction becomes very high at low temperatures. On the other hand, if the snow was very wet so that the ski was sliding on "slush", then the friction observed, $\mu_k = 0{\cdot}14$, was higher than that on "dry" snow at 0° C. This is similar to the results obtained on wet ice. It is in agreement with the practical experience that ski run comparatively slowly on very wet snow.

Experiments with real ski.

A pair of hickory ski were waxed with Sohm's Red Gleitwax and lashed together. The load was applied to the centre of the ski by adding rocks of known weight. The experiments were carried out on a level plateau outside the cold laboratory. The snow, which was about two days old, was finely crystalline, and was similar to the snow used in the earlier laboratory experiments. The experimental work was conducted between 10 a.m. and 12 noon, and the sun was obscured by a slight mist. The snow was at 0° C, and towards the end of the experiments some surface melting had occurred.

The force required to pull the ski along was measured with a spring balance. The ski were slid in their own tracks, so that the force of cutting their initial track was not included in the friction. In order to eliminate any errors due to the tracks not being level, the ski were reversed after each measurement, and the values of the friction given are the mean of these two measurements. Both the static and the kinetic friction were measured, and the results are shown in fig. 5 for a range of loads. The sliding speed for the kinetic friction was about 10 cm./sec.

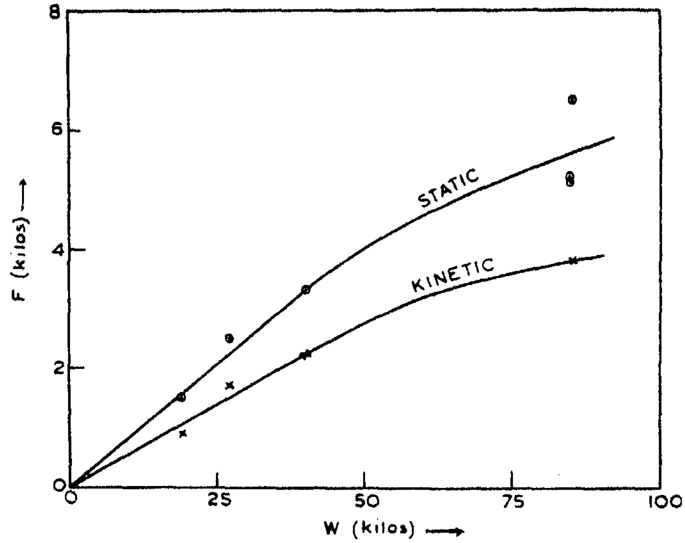

Fig. 5. The F/W relation for real ski on snow.

It will again be seen that Amonton's law is approximately true for both static and kinetic friction. The value of the static friction, $\mu_s = 0{\cdot}08$, was higher than that of the kinetic friction, $\mu_k = 0{\cdot}06$. Both the static and kinetic friction were lower than for the model ski on snow in the laboratory. We should anticipate such a result, since the mechanical effect of displacing and packing the snow is relatively greater for the small ski.

After the ski had slid over the track many times and some slight surface melting had occurred, the kinetic friction fell to a lower value, $\mu_k = 0{\cdot}04$. The static friction under these conditions was also less, and did not differ greatly from the kinetic, $\mu_s = 0{\cdot}045$.

Discussion

These experiments show that, although the static friction on ice at a few degrees below its melting-point may be of the same order of magnitude as that observed on other solids ($\mu_s = 0{\cdot}3$ to $0{\cdot}5$), the kinetic friction is very much lower ($\mu_k = 0{\cdot}02$ to $0{\cdot}03$). This is even lower than the frictions observed between metals lubricated under boundary conditions.

The kinetic friction increases as the ice is cooled down, and on very cold ice at −140° C, it rises to values as high as $\mu_k = 0{\cdot}12$. At any one temperature the kinetic friction shows approximate agreement with the same general laws observed with other solids. The coefficient of kinetic friction μ_k is nearly independent of the apparent area of contact, it is nearly independent of the load provided that this is not too heavy, and it is not greatly influenced by the speed of sliding provided this speed is not too slow.

The experiments suggest that the low kinetic friction of ice is due to surface melting. Measurements of the electrical conductivity of cold ice surfaces show that the melting occurs only locally at the points of contact, and the water film is not continuous. When the temperature is at, or is very close to 0° C, however, the electrical conductivity of the moving surfaces may rise to a high value showing that the water film becomes continuous.

It has often been suggested that the melting is caused by pressure melting. Calculations show however that at low temperatures this is unlikely, even when allowance is made for the difference between the real and apparent areas of contact. On the other hand, some elementary calculations of the amount of frictional heat liberated suggest that this may cause local melting at the points of sliding contact. The experimental results, particularly those showing the influence of thermal conductivity on friction, indicate that this latter view is correct. The results suggest that, although pressure melting may play some part, the low friction observed for rapidly moving solids on ice is due in a large measure to local melting by frictional heating.

The results on snow are very similar to those on ice, except that the friction under any given set of conditions is greater. This is due mainly to the extra work of displacing and compressing the snow.

The observations have an interesting bearing on sledging and ski-ing. No quantitative measurements of the friction of sledges seem to have been published, but there is general agreement that the friction increases at low temperatures. Many arctic explorers, Wright (1924, p. 44), J. M. Scott (1933, p. 273), Cherry-Garrard (1922, pp. 456–7), have recorded that at very low temperatures, −30 to −40° C, the friction between the snow and the runners became so great that the sensation was that of pulling a sledge over sand. Wright, summarizing the conclusions of the Scott Polar Expedition of 1911–13 says:

"Quite apart from any question of the hardness of the snow, however, the surface temperature has an important influence. Our opinion was that the friction decreased steadily as the temperature rose above zero Fahrenheit (– 18° C), the presence of brilliant sunlight having an effect, which was more than a psychological one, on the speed of advance. With air temperatures above freezing point, however, there was some danger that snow would melt in contact with the runners, and subsequently freeze in lumps to increase the friction notably. Below zero Fahrenheit (– 18° C) the friction seemed to increase progressively as the temperature fell, as if a greater and greater proportion of the friction were due to relative movement between the snow grains and less to sliding friction between the runner and snow." This steady increase in friction as the temperature of the ice or snow falls is clearly shown in fig. 3. The effect is less marked at very low temperatures, and it is probable that below – 40° C very little surface melting occurs under these conditions.

The influence of the thermal conductivity of the sliding body on the friction, shown in fig. 4, is also borne out by practical experience. It will be seen from this figure and from Table III that at low temperatures the friction of a good thermal conductor is considerably greater than that of a poor one. Nansen (1898, pp. 445–6) compared two sledges, one having nickel plated runners and the other maple runners. The temperature was low, the exact value is not given but the mean temperature during that month was – 36·8° C (– 34·2° F). He found that the friction of the metal was higher, "the difference was so great that it was at least half as hard again to draw a sledge on the nickel runners as on the tarred maple runners".

The thermal conductivity is also important in ski-ing. Nowadays most ski are fitted with brass or steel edges, although sometimes vulcanite or composition edges are used. The friction measurements show that the latter will be faster at low temperatures. If metal must be used, one of low thermal conductivity such as German silver or constantan should be better.

Waxing may reduce the friction of a hickory surface very considerably, and it is probable that the main effect is due to the substitution of a hydrophobic surface for a hydrophilic surface. It is clear that, in addition to this, a very important property of a wax is its ability to adhere to the wood at the local points of rubbing contact. Since the friction of the bare hickory is very high the local removal of wax from the small points of the surface irregularities may cause a comparatively large increase in the friction. The ability of the wax to flow over the surface and to repair the local damage may also be an important factor. In practice waxes differing very widely in physical and chemical properties are used under different snow conditions. No systematic investigation of the friction and behaviour of different waxes has so far been made.

This work was carried out on the glaciological expedition to the Jungfraujoch in 1938 organized and led by Mr Gerald Seligman, and the authors would like to express their great indebtedness to him. They wish to express their appreciation to Professor von Muralt and the Council of the Jungfraujoch Research Station for their hospitality and for laboratory facilities, and to Herr Liechti, Chairman of the Jungfraubahn, for assistance and many kindnesses.

They also wish to thank the Royal Society and the Ski Club of Great Britain for grants for apparatus, and the Trustees of the Ramsay Memorial Fund for a Fellowship (T.P.H.).

SUMMARY

Experimental studies of the friction on ice surfaces have shown that the low frictions observed at temperatures near the melting-point were due to lubrication by a thin water film at the points of contact between the sliding surfaces. The coefficient of kinetic friction was found to be independent of the load, apparent area of contact, and speed of sliding over a certain range. When the temperature of the ice was decreased, the friction rose markedly as the water film became more difficult to form. Using ski of various materials, it was observed that the friction depended very largely on the thermal conductivity of the ski. This result suggested that frictional heating played a large part in melting a water film during sliding; it had been previously considered that pressure melting was alone responsible for the formation of this water film.

Experiments with miniature and real ski on snow surfaces showed that the same general laws were obeyed as on ice surfaces. The higher frictions obtained on snow were attributed to the extra work done in displacing and compressing the snow crystals.

REFERENCES

Beare, W. G. and Bowden, F. P. 1935 *Phil. Trans.* A, **234**, 329–54.
Bowden, F. P. and Hughes, T. P. 1937 *Proc. Roy. Soc.* A, **160**, 575–87.
Bowden, F. P. and Leben, L. 1939 *Proc. Roy. Soc.* A, **169**, 371–91.
Bowden, F. P. and Ridler, K. E. W. 1936 *Proc. Roy. Soc.* A, **154**, 640–56.
Bowden, F. P. and Tabor, D. 1939 *Proc. Roy. Soc.* A, **169**, 391–413.
Cherry-Garrard, A. 1922 *The worst journey in the world*, **2**. London: Constable and Co.
Holm, R. 1929 *Wiss. Veröff. Siemens-Konz.* **7** (2), 217–71.
Jeffreys, H. 1935 *Phil. Mag.* **19**, 840–6.

Johnston, J. 1912 *J. Amer. Chem. Soc.* **34**, 788–802.

Nansen, F. 1898 *Farthest north*, **1**. London: George Newnes.

Poynting, J. H. 1881 *Phil. Mag.* (5), **12**, 32–48.

Reynolds, O. 1901 *Papers on mechanical and physical subjects*, **2**. Camb. Univ. Press.

Scott, J. M. 1933 *The land that God gave Cain.* London: Chatto and Windus.

Wright, C. S. 1924 From *Miscellaneous data* (Scott Polar Expedition of 1911–1913), compiled by Colonel H. G. Lyons. London: Harrison and Sons.

The action of ultra-violet radiation on barium and strontium azides

By W. E. Garner, F.R.S. and J. Maggs

(*Received* 22 *May* 1939)

[Plate 15]

The alkaline earth azides decompose at appreciable rates at temperatures above 100° C, and the reactions which occur are of the accelerating type increasing in speed as the 6th–8th power of the time, there being a marked induction period during which the reaction occurs at a negligible rate (Harvey 1933; Marke 1937; Maggs 1939). The decomposition is accelerated and the length of the induction period shortened when the solid is acted upon by β-rays at room temperature before the heat treatment (Garner and Moon 1933; Maggs 1939). It was, therefore, possible that ultra-violet light would cause an acceleration of these reactions in a similar manner. Müller and Brous (1933) have shown that sodium azide is decomposed by ultra-violet light at a rate which is proportional to the intensity and that the threshold wave-length for the decomposition is around 405 mμ. In the present investigation it is shown that barium and strontium azides are decomposed by ultra-violet light at room temperature and that the thermal decomposition of these substances is accelerated by pre-treatment with this radiation.

Experimental

The azides were prepared by suspending hydroxides of A.R. quality in water and passing hydrazoic acid through the suspension, by the method described in previous papers. The barium azide was obtained as the monohydrate in flat needles, which lost water over anhydrous calcium chloride. The strontium azide was obtained in crystalline aggregates and could not be prepared in the form of single crystals. The strontium azide was employed mainly in the ground state

Apparatus

This was similar in construction to that employed by Harvey (1933). It was, however, made entirely out of pyrex and silica so that it could be readily torched to remove adsorbed gases. The reaction was followed by measurement of the nitrogen evolved on a McLeod gauge. The reaction vessel was separated from the gauge and vacuum pumps by a liquid-air trap to prevent mercury reaching the crystalline azide. Several types of reaction vessel were used, of which the final form is described below. This consisted of a pyrex tube (fig. 1) mounted with a winch *A* at the top, by which a silica bucket containing the azide could be raised or lowered into the heated part of the reaction vessel. The middle portion of the vessel, *D*, was encased in a steam-jacketed electric furnace and was maintained at constant temperatures ranging between 100 and 130° C. The lower part of the reaction vessel, *C*, was closed at the bottom with a silica cell which possessed a plane window, and could be detached at will from the main part of the reaction vessel at a ground joint. At the beginning of the experiment, the azide was placed in a silica bucket and suspended from the winch so that it rested on the plane window at the bottom of the cell. It was then illuminated at a temperature determined by the water circulating through *F* (fig. 2), and after illumination rapidly raised to the furnace level and the rate of reaction followed on the gauge. *E* was a Compur camera shutter having a range of speeds from 1 to $\frac{1}{250}$ sec., and *D*, *C* and *B* were filters used for separating out various wave-lengths of a mercury arc spectrum. *A* was a quartz mercury arc, the Hanovia S 500, running off 210 constant voltage supply and generating 175 μW/cm.^{2} at 40 in. distance (from 3200 A downwards). It was necessary to run the arc for 15 min. before it reached a constant intensity, and therefore to screen the substance by a shutter during this preliminary period.

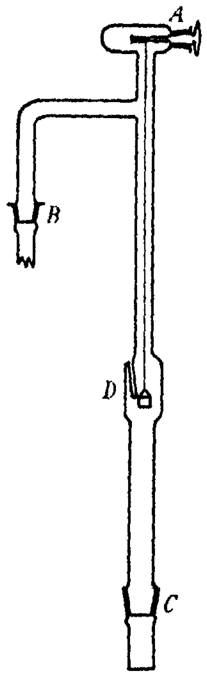

FIG. 1

For dividing the ultra-violet spectrum into various wave-lengths, a series of filters described by Bowen (1935) was used. The $Ni_2(SO_4)_3$-$CO_2(SO_4)_3$ filter was placed in the silica flask *B*, chlorine gas placed in the silica cell *C*, and various other solutions in *D*.

Absorption spectra

Attempts were made to measure the threshold for absorption for crystals of barium azide and strontium azide. Since the crystals are opaque, the reflected light from the powdered crystals was studied, but no success was obtained by the methods employed. It was therefore decided to study the absorption spectrum of potassium azide, which could be obtained in transparent crystals of fairly uniform thickness. A crystal of about 0·5 mm. thickness was mounted on a Hartmann diaphragm (three-aperture wedge) by means of soft red wax. Photographs were taken through the crystal of the spectrum of a 15,000 V iron tungsten arc.

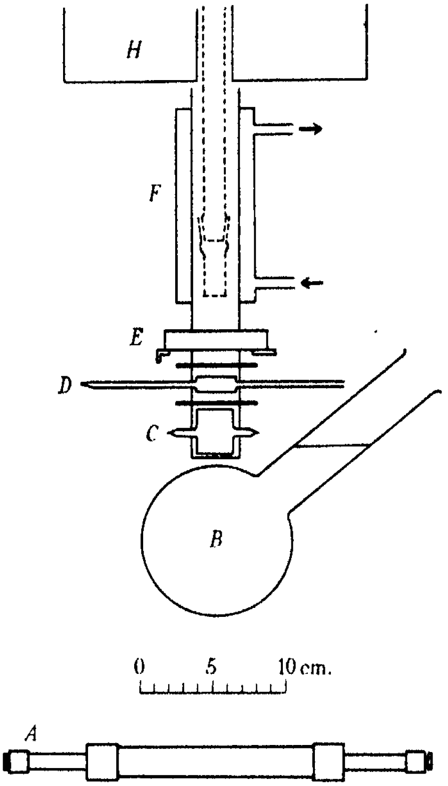

FIG. 2

Exposures of 10, 20, 80, 160 and 320 sec. were given, and comparison spectra of the arc (1 sec. exposure) were made before and after the above series. From the spectrograph it was seen that there was a very strong absorption band commencing at 2600 A and continuing into the far ultraviolet.

Some measurements were also made of the extinction coefficients of aqueous solutions of strontium azide, 0·65 N, and also diluted 10, 100, 1000 and 3000 times respectively. The results are given in fig. 3, which shows that there is an absorption edge in the neighbourhood of 2700 A. The question arises as to the nature of the particles which are responsible

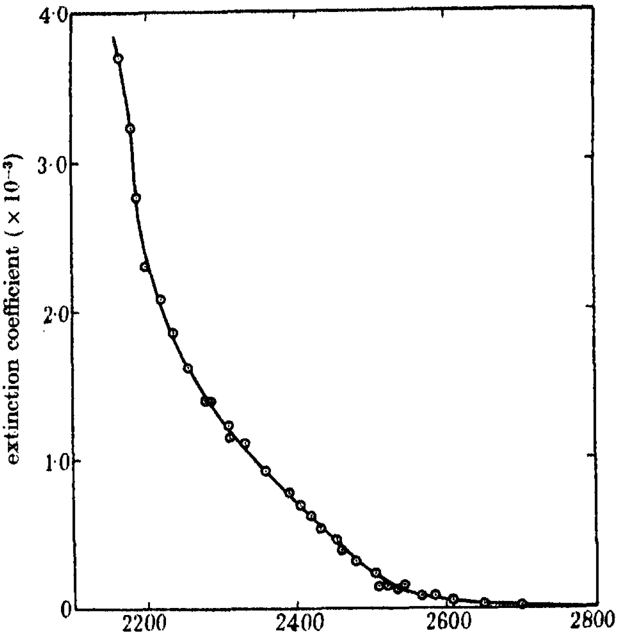
4·0
3·0
2·0
1·0
0
extinction coefficient (× 10⁻³)
2200
2400
2600
2800
wave-length (A)

FIG. 3

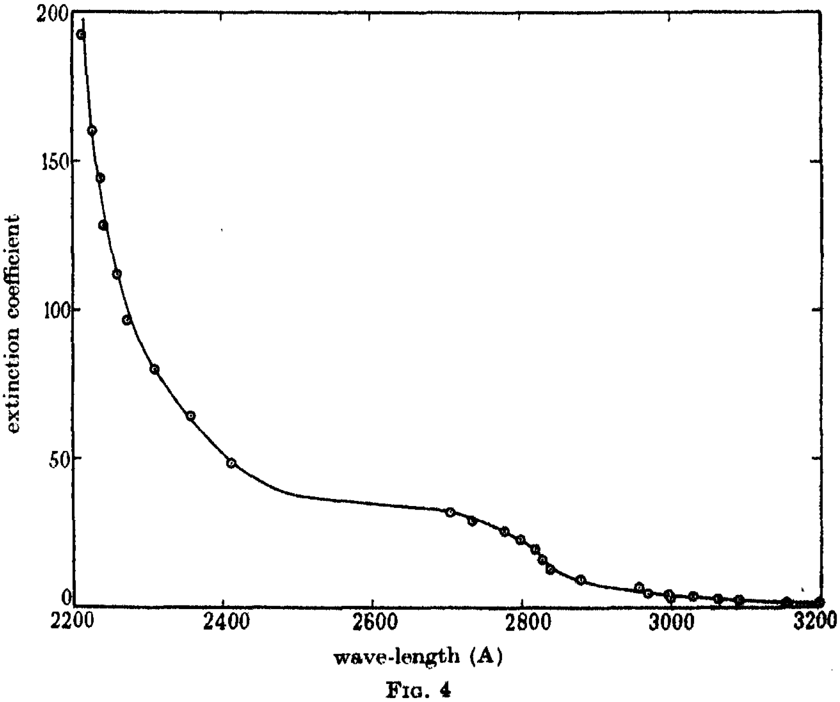
200
150
100
50
0
extinction coefficient
2200
2400
2600
2800
3000
3200
wave-length (A)

FIG. 4

for the absorption. It is probable that the absorption is due to the N_3 ions, and in order to test if this were the case, the absorption spectra of aqueous solutions of hydrazoic acid were also measured. The graph, extinction coefficient against wave-length, is shown in fig. 4. The extinction coefficients are much smaller in this case, especially for the shorter wave-lengths, as would be expected if the absorption were due to the N_3 ions, since the dissociation constant of HN_3 is only $1{\cdot}2 \times 10^{-5}$ at 20° C, whereas that of strontium azide must be very much larger. There is, however, a marked band in the HN_3 spectrum at 2700 A, which is absent in that of SrN_6. This band is possibly due to unionized N_3, especially since a band in the same region is claimed for the azido group in azido compounds by Kuhn (1929, 1930).

It has been shown, therefore, that absorption first becomes appreciable in solutions containing the N_3^- ion at 2700 A, and in a solid containing this ion at 2600 A. There is, however, no very sharp absorption edge in either case.

Photochemical reaction

A series of experiments was carried out to determine the threshold of the light necessary to produce an acceleration of the thermal decomposition. A thin, slightly compressed layer of ground strontium azide was placed in a silica bucket and illuminated by the arrangement shown in fig. 2. The thermal decompositions were carried out at 101·3° C, and at this temperature the induction period without pre-illumination is 120 ± 3 min., the induction period being arbitrarily taken as that required to give a nitrogen pressure of 10^{-4} cm.

A series of experiments is shown in fig. 5, where $\log p$ is plotted against t. The curves are not all on the same time scale, it having been necessary to shift 1, 2, 3 and 4 along the time axis. The amount of shift can be found from the induction periods given below. A typical experiment without illumination is shown in curve 1. In this case the induction period was 117 min. The form of the curve which is obtained when the heating is carried out with the powder in a silica bucket is very different from that when a crystal is heated in a platinum bucket, as was done in the earlier investigations. In the latter case, a good straight line is obtained between $p = 10^{-4}$ and 10^{-3} cm., but for experiments in the silica bucket, the $\log p$-t plot is always curved as in fig. 5. It is found that this curve is closely given by the relationship $\log dp/dt = n \log p + \text{const.}$, where n varies between 0·7 and 1·0, according to circumstances. The presence of small amounts of nitrogen initially has no effect on the form of the curve, so that the curvature at low pressures is not due to the absorption of nitrogen. This curvature is possibly due to the slow escape of nitrogen from the crystal in the early stages of the reaction.

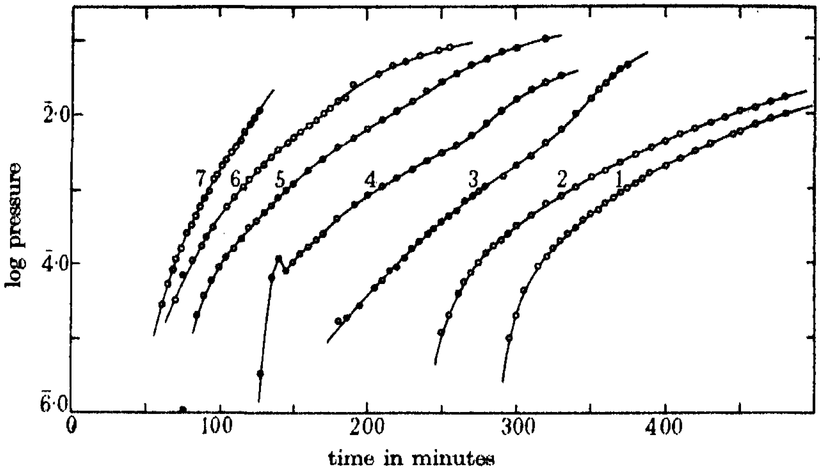

FIG. 5

The powder was pre-illuminated for 60 sec. with light at a number of wave-lengths, the lamp being placed 28 cm. from the crystals. The results are plotted in fig. 5 and summarized in Table I.

TABLE I

Wave-length A	Induction period	Remarks
1 Nil	117	—
2 3340–3030	124	Curve very similar to 1
3 3340–2650	120	Bump at 5×10^{-3} cm. Hg
4 2820–2650	100	Bump at 5×10^{-3} cm. Hg
5 2660–2480	102	Bump at 5×10^{-3} cm. Hg
6 2820–2480	82	—
7 3340–2480	70	—

The bumps seen on the curves for 3, 4 and 5 were never observed for decompositions carried out without pretreatment with ultra-violet light. Their form was not, however, strictly reproducible. They are most probably due to bursts of nuclei produced by ultra-violet light which, at particular pressures, become of sufficient importance to affect the *p-t* curves. The initial rise on 4 is an irreproducible effect, the nature of which has not been traced with certainty.

No effect of ultra-violet with wave-length greater than 3030 A has been observed. Radiation between 3030 and 2650 A does not affect the induction period appreciably but causes a bump at 5×10^{-3} cm. A progressively greater effect is found as the wave-length decreases. It is clear, therefore, that the threshold for photochemical action corresponds approximately with those for the ultra-violet absorption edge of the N_3^- in solution and in the solid state.

The experiments 1, 5, 6 and 7 are plotted as $\log p$ against $\log t$ in fig. 6; 2, 3 and 4 lie too close to 1 to be plotted. It will be seen that the form of the curve is not much affected by the illumination, the main effect being a shift along the time axis. There is, however, a gradual change in the power relationship as the induction period is shortened, viz. from 6 to 8 over the range of $\log p$, $\bar{4}$–$\bar{3}$.

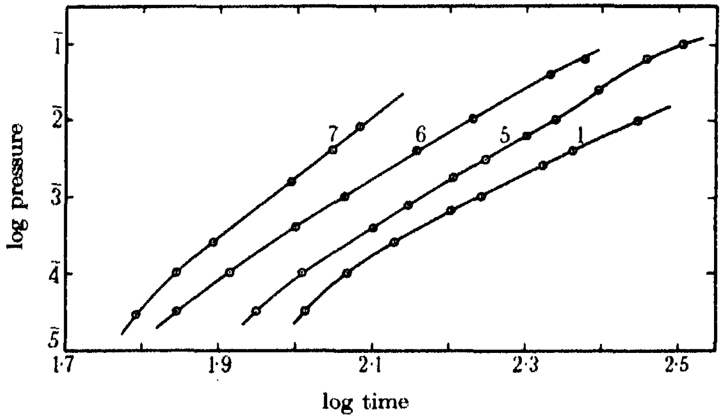

Fig. 6

Effect of pre-illumination with ultra-violet light on the length of induction period

Experiments were carried out on the effect of variations in the time of illumination at room temperature, τ, on the length of induction period, t_i, for strontium azide in the powder form, and on barium azide in the crystalline and powder form. The induction period was taken as the time required to reach a pressure of 10^{-4} cm. The results are summarized in Table II. 5–10 mg. of azide were employed.

A few measurements were carried out with the strontium azide powder maintained at 40° C during illumination, but these gave values of t_i agreeing with the results in Table II. It was also shown that there was no appreciable decay of the effect of the illumination after standing for 48 hr.

TABLE II

2360–2820 A on strontium azide	102° C	τ sec.	0	0·25	1·0	4·0	18	60	66	180			
		t_i min.	102	80	73	58	51	45	47	42			
Full arc on strontium azide	102° C	τ sec.	0	0·1	0·2	1·0	5·0	15	60	240	960	3600	
		t_i min.		90	87	73	59	51	40	31	19	8	
Full arc on powdered BaN_6	110° C	τ sec.	0	0·04	0·2	1	5	15	60	240	1680		
		t_i min.		98	85	67	58	50	33	23	10		
Full arc on crystal of BaN_6	110° C	τ sec.	0	0·04	0·2	0·5	1·0	5	15	60	120	240	480
		t_i min.	145	115	101	76	67	59	49	46	37	24	7

It should be noted that the results for powdered strontium and barium azides under the action of the full arc give very good straight lines when log τ is plotted against t_i.

A few results have been obtained by Mr D. K. Peacock on the effect of pre-illumination with ultra-violet light on crystals of barium azide. The crystals were heated to 115° C in an apparatus similar to that described in the following paper by Dr A. Wischin, and the induction period measured by noting the time of the appearance of nuclei and these are recorded below.

Table III

Full arc on crystal of BaN_6	τ min.	0	0·5	1	1·5	2	2·5	3	4
	t_i min.	59	45	40·5	39	35·5	30·5	26	24·5

The character of the nuclei changed at about 1·5 min. illumination, individual nuclei being observed up to this time, but afterwards all that was observed was a black mist that suddenly made its appearance.

Effect of variation in the intensity of ultra-violet light
(by Mr D. K. Peacock)

The radiation was passed through a diaphragm and a shutter placed close to the lamp and the distance of the lamp from the crystal varied. The pre-illumination given was in all cases 1 min. The length of the induction period before the appearance of nuclei at first decreases as the intensity increases, reaches a minimum, and then increases. The results given below are each the mean of three experiments, the intensities being given in arbitrary units.

TABLE IV

I	0	0·8	0·95	1·18	1·40	1·65	11·1
t_i	58	48	40	35	29	35	48

The intensity in the experiments given in Table III is 0·95 on this basis.

There is thus a phenomenon which is analogous to that of solarization which occurs with the photographic plate on prolonged exposures to light.

The decomposition of crystals of barium azide at room temperature under prolonged exposure to ultra-violet light (full arc)

In Exp. 211 (fig. 7) the crystal used weighed 6·1 mg. and was 3·3 mm. long and 0·6 mm. wide. There was an induction period of 25 min. before the pressure of nitrogen became measurable, and then the rate of evolution of gas became linear, reaching 2×10^{-4} cm. Hg after 180 min. A repetition of this run showed an induction period of 35 min. (Exp. 220). The occurrence of an induction period is of interest, since it shows that the main photochemical reaction is occurring at the surface of nuclei which are formed only slowly by the action of light. When the nuclei have been produced in sufficient numbers, the reaction becomes stabilized at a steady rate.

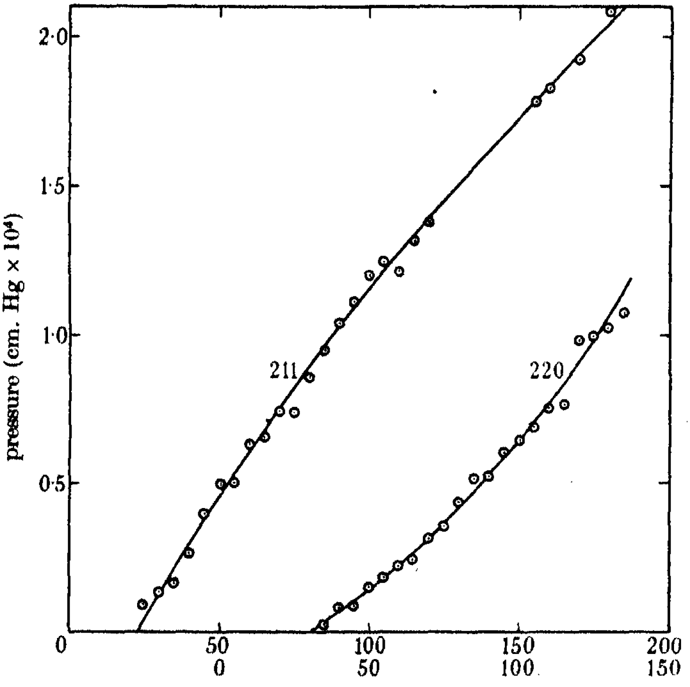

FIG. 7

Microphotographs

An investigation was commenced into the parts played by the numbers of the barium nuclei and their rates of growth on the rate of liberation of nitrogen during the decomposition. Crystals of barium azide were mounted in a silica vessel with a plane silica window and heated by an electric furnace to 110° C approx. The apparatus will not be described in detail, since it was a preliminary form of that described by Dr A. Wischin in the following paper. The results on the rates of growth were of a preliminary character only, but it was established that they increased in size at a linear rate. Photographs were taken on a Zeiss film camera (major 44) of the nuclei as they developed, and in fig. 8 (Plate 15) are shown typical photographs of crystals with no pre-illumination, $\frac{1}{10}$ and 1 sec. illumination with the lamp at 28 cm. from the crystal. It is clear from these photographs that there is an enormous increase in the numbers of nuclei after the treatment with ultra-violet light.

Effect of an electric field on the thermal decomposition of barium azide

These experiments were carried out by Mr S. A. Perry. A crystal was mounted between two polished silver plates and held in position by the pressure of a spring. It was heated in a vacuum with and without a field across the plates. log p changed linearly with the time in all of the experiments. These are summarized below.

	Induction period min.	Slope
No field	132	0·028
500 V/cm.	135	0·026
1250 V/cm.	125	0·028

There is no material effect on the rate of reaction as a result of applying the field. Experiments carried out in which 1250 V/cm. was applied to a crystal which was undergoing decomposition, showed that there was no appreciable change in the rate of decomposition due to the application of the field.

Discussion

The experiments carried out on the photodecomposition of azides are of a preliminary character, being devised with a view to making a broad survey of the field. Some of the sections will require further investigation

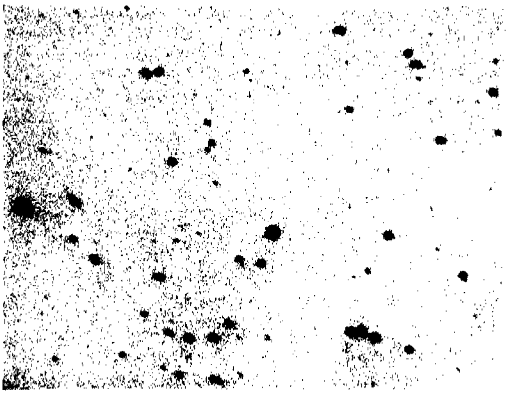

FIG. 8 (*a*). No illumination—after 90 mins. (× 120)

FIG. 8 (*b*). $\frac{1}{10}$ sec. illumination—after 42 mins. (× 120)

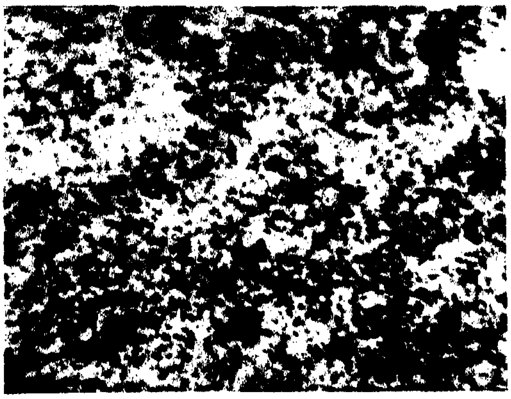

FIG. 8 (*c*). 1 sec. illumination—after 32 mins. (× 120)

(*Facing p.* 308)

before the details of the reaction kinetics can be worked out. Sufficient has been done, however, to make it possible to establish the general features of the processes that occur. An understanding of the results obtained with ultra-violet light is only possible when the nature of the thermal decomposition is understood. An investigation on the nature of the thermal decomposition has been completed by Dr Wischin, and it will be relevant to this discussion to quote briefly the results obtained.

In the early stages of the thermal decomposition of the alkaline earth azides, nuclei are formed which, over the range at which measurements are possible, increase in size at a linear rate. This means that the volume of the nuclei grows as the cube of the time. Also, it was shown that the numbers of nuclei increase at a rate which varies as the cube of the time. It can readily be deduced from these relationships that the rate of reaction should increase as the 6th power of the time, and this is approximately what is found, although when the reaction is followed by pressure measurements, sometimes higher powers—up to the 8th—are observed. This discrepancy may be due to a variety of causes which are referred to in Dr Wischin's paper.

The fact that the rate of formation of nuclei obeys the square law is an indication that this process is bimolecular. Professor Mott has suggested to us that nuclei are formed as a result of a slow surface decomposition of azide ions. This decomposition sets free barium metal atoms, which diffuse over the internal surfaces or through the lattice, and when two of these atoms meet, a nucleus is found.

The rate of the interface reaction between metal and azide is very much greater than that of the decomposition of azide on the crystal surface, and the activation energy for the interface reaction is much smaller than that for the initial surface reaction. Therefore once nuclei are formed, the reaction occurs to a preponderating extent at the metal-azide interface.

The effects of ultra-violet light on the induction period

It has been shown that the principal effect of ultra-violet light on the pressure-time curves is to cause a shortening of the time which elapses before there is any measurable decomposition, i.e. there is a shift of the p-t curves to shorter times. The slope of the $\log p$-$\log t$ curves, however, increases from 6 to 8 and this may be of some significance. Since in the purely thermal process, two barium atoms are required to form a nucleus, the above effect on the slopes may mean that in the photo accelerated process, the number of barium atoms required to form a nucleus is increased to 3 or 4.

A confirmation of this view is obtained when the effects of pre-illumination on the length of the induction period are studied. If the sole effect of ultra-violet light be to increase the number of centres at which nuclei can be formed, then the number of nuclei formed during the initial period of the thermal treatment will vary as t^n, where $n-1$ is the number of barium atoms required to form a nucleus. Let P, the predisposition to nuclei formation, be proportional to the time of illumination, τ, then it can be shown that at the end of the induction period, const. $\tau t_i^{n+3} = p = 10^{-4}$ cm. Therefore $\tau = \text{const.}/t_i^{n+3}$. In fig. 9 is shown a plot of $\log \tau$ against $\log t_i$ for powdered strontium and barium azides. The initial slope of these curves ranges from 8 to 9, and therefore $n-1$ is 4–5, in fair agreement with the number of barium atoms required to form a nucleus, which has been deduced from the pressure-time curves. There is, however, a departure from this relationship for times of illumination greater than 15 sec. when

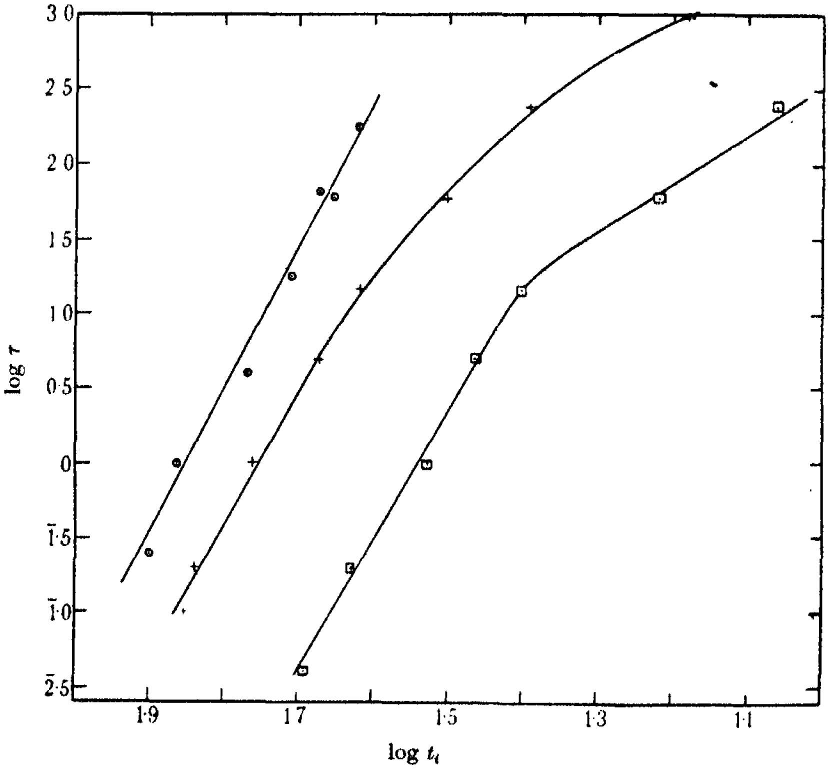

Fig. 9. ⊙ strontium azide, 2360–2820 A; + strontium azide, full arc; ☐ barium azide, full arc.

the full arc is used, but not for illumination of light of wave-lengths longer than 2360 A. It thus appears that there is an additional effect of ultra-violet light where the wave-length exceeds 2360 A.

Crystalline barium azide (fig. 10) also gives curves with similar slopes, although the individual values obtained for the induction periods are more erratic than for powders. The change of slope occurs for somewhat greater periods of illumination than for powders, viz. 1–1½ min. In fig. 10 are also shown the results of Mr Peacock for an examination of barium azide crystals where the induction periods are measured by visual examination of the appearance of the nuclei. The change of slope in this case occurs at an illumination of 1 min.

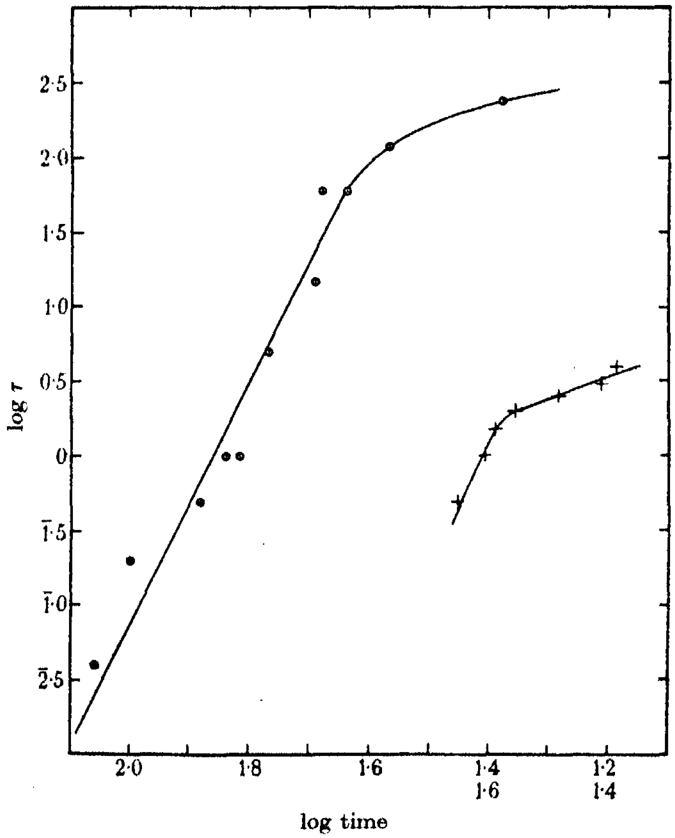

FIG. 10. ⊙ BaN_6 crystals at 110° C; + BaN_6 crystals at 115° C.

The results obtained above for illuminations less than 0·25–1·5 min. seem to require that but few nuclei are formed during the period of illumination and that the majority of the nuclei are formed subsequently during the thermal treatment. A latent image is produced which is developable by thermal treatment into nuclei. For illuminations longer than 1 min., a departure from $\tau = k/t_i^3$ occurs which may be due to the formation of nuclei by the light. Assuming that this is the case, and that the nuclei are very small and all approximately of the same size, n may be taken as constant during the thermal treatment and τ should vary as the reciprocal of t_i^3. Actually, the slope measured is less than 3, which is probably due to the growth made by the nuclei under the action of the light. The view that nuclei are formed during prolonged illumination with ultra-violet light is supported by the fact that it is in this region that solarization is observed and also by the results shown in fig. 7. The departure from the normal relationship, however, occurs only with short ultra-violet and therefore appears to be an effect independent of that occurring in the early stages of the illumination and not derived from it. These nuclei, or the centres from which the nuclei grow, are produced in very large numbers by the action of the full arc, as can be shown by visual examination of the crystal during the thermal development. It is found that there is a very marked increase in the numbers of the nuclei after the point of departure from the t_i^3 relationship. After this stage the nuclei are no longer observed individually but as a black mist suddenly appearing in patches over the crystal. It is possible that they are formed not on the surface but in the body of the lattice by short ultra-violet and at first grow more slowly than those formed on the surface. However, on account of their large numbers, they are visible in mass earlier than the surface nuclei when the times of illumination exceed 1 min.

The effect of ultra-violet light at room temperature

The results shown in fig. 7 of the liberation of nitrogen under the action of ultra-violet light at room temperature prove that there is no measurable gas pressure until after 25–35 min. By this time presumably the numbers of nuclei which have been formed are sufficiently large for the bulk of the electrons liberated by the ultra-violet light to attach themselves to the nuclei. Consequently, the rate of evolution of nitrogen becomes proportional to the ultra-violet light absorbed and an approximately linear rate is observed.

Activation energies

Although the activation energy for the thermal process after treatment with ultra-violet light has not been measured, it has been shown by one of us (Maggs 1939) that the activation energies calculated from the log p-t

curves are the same within experimental error both for the purely thermal process and for that accelerated by β-rays. These calculated activation energies are composed in a complex fashion of the activation energies of both nuclear growth and nuclei formation, and hence it would appear that the thermal processes occurring both with and without pre-illumination are of an essentially similar character. Although the treatment with β-rays may not necessarily produce the same effects as ultra-violet light, the above may be taken as a guide, that the nature of the mechanisms occurring during the heating of azides is probably not markedly affected by pre-illumination with ultra-violet light.

A possible theoretical explanation of the above facts is that the nuclei are formed at holes in the lattice in positions normally occupied by N_3 ions. It is assumed that these holes are present on the surfaces of the grains of untreated crystals, but they are also produced by ultra-violet light which causes the decomposition of N_3 ions. In order to account for the diverse effects of ultra-violet light, it is necessary to assume that there are at least two types of centres produced, one on the surface and the other in the interior of the grains. For the nuclei initiated thermally, the nuclei formation will be brought about by the diffusion of barium atoms to these holes, there being required on an average two barium atoms per hole. In the case of the photochemically initiated nuclei, the surface cavities may require 3–4 barium atoms to form a nucleus, as is indicated by the fact that $p = kt^8$ and $\tau = k/t_i^8$. The nuclei formed at centres in the interior of the grains appear in larger numbers, but grow more slowly than the nuclei initiated on surfaces. Their formation appears to be limited to wavelengths < 2360 A. As a consequence of the occurrence of two nuclear types in the pre-illuminated crystals, the curves in figs. 9 and 10 show a marked change of slope at the larger illuminations, due to the reaction in the interior of the grains overtaking that of the superficial reaction. This all occurs within the induction period of the curve fig. 7, which shows the rate of liberation of nitrogen by ultra-violet light at room temperature.

We wish to express our thanks to Professor Mott for suggestions in the theoretical part of the paper and to Imperial Chemical Industries, Ltd., and to the Colston Research Society for grants for the purchase of apparatus.

SUMMARY

1. The threshold for the absorption of ultra-violet light by N_3^- ions in solution and in the solid state is 2600–2700 A and that for the photochemical reaction is in the same region.

2. Pre-illumination with ultra-violet light at room temperature shortens the induction period of the thermal process for BaN_6 and for short times of illumination $\tau = k/t_i^8$, where t_i is the length of the induction period.

3. Prolonged illumination with light of wave-length shorter than 2360 A produced nuclei of metallic barium at room temperatures.

4. Solarization effects are observed in the region where nuclei are produced by the action of ultra-violet light.

5. The thermal decomposition of BaN_6 is unaffected by a field of 1250 V/cm.

6. The general features of the reaction kinetics of the photochemical reaction are discussed.

REFERENCES

Bowen, E. J. 1935 *J. Chem. Soc.* p. 78.
Garner, W. E. and Moon, C. H. 1933 *J. Chem. Soc.* p. 1398.
Harvey, F. E. 1933 *Trans. Faraday Soc.* **29**, 653.
Kuhn, W. 1929 *Z. phys. Chem.* B, **4**, 26.
— 1930 *Z. phys. Chem.* B, **8**, 284.
Maggs, J. 1939 *Trans. Faraday Soc.* **35**, 433.
Marke, D. J. B. 1937 *Trans. Faraday Soc.* **33**, 770.
Müller, R. H. and Brous, G. C. 1933 *J. Chem. Phys.* **1**, 482.

The thermal decomposition of crystals of barium azide

BY A. WISCHIN, PH.D.

(*Communicated by W. E. Garner, F.R.S.—Received* 22 *May* 1939)

INTRODUCTION

In solid reactions of the type $A_{\text{solid}} = B_{\text{solid}} + C_{\text{gas}}$ the reactions are sometimes autocatalytic, being accelerated by the solid product. The solid product may be disseminated throughout the crystal in a diffuse manner, as has been shown by the microscopical examination of partially decomposed crystals of mercury fulminate (Garner and Hailes 1933) or potassium azide (Garner and Marke 1936), or may be aggregated into visible nuclei as in the case of alkaline earth (Harvey 1933; Marke 1937; Maggs 1939) or lead azides (Garner and Gomm 1931).

In previous investigations an induction period has been found during which the evolution of gas is negligible, which is followed by an accelerating rate of development of pressure. For a certain period of the reaction the relationship of pressure and time is that of an exponential type which in a number of cases takes the simple form, $\log p = kt + \text{const}$. This expression is obeyed over the early part of the reaction for single crystals of mercury fulminate (Garner and Hailes 1933), barium azide (Harvey 1933), and lead styphnate (Hailes 1933). It also holds for silver oxalate (Macdonald 1936*a*, *b*) in a finely crystalline form and for ground mercury fulminate. Attempts have been made to account for the exponential relationship in terms of the spread of reaction chains throughout the crystal, but there are certain difficulties in the way of the application of the chain theory, especially when nuclei are formed. There are, besides, cases where this simple expression does not fit the experimental results, notably that of ground calcium (Marke 1937) and barium (Harvey 1933) azides.

In the case of BaN_6, which has been investigated in this work, nuclei are formed. Therefore the rate of development of pressure is determined by the rate of increase in numbers of the nuclei and by the rate at which these nuclei grow. The dependence of size as well as numbers of nuclei upon the time has been investigated for a range of temperatures.

There have been few measurements of the rate of nuclei formation in physical and chemical changes occurring in the solid state. In a few cases the numbers of nuclei increase linearly with time, as for $CuSO_4.5H_2O$ (Bright and Garner 1934) and chrom alum (Cooper and Garner 1936), but for $NiSO_4.7H_2O$ (Garner and Southon 1935) the numbers increase as the square of the time. Kornfeld (1935) and Kornfeld and Pawlow (1937) have found for the recrystallization of stretched aluminium wire that the numbers increase at a rate which varies between the first and the second power of the time. As far as the rate of growth is concerned, the nuclei in hydrate reactions, when above a certain size, increase in diameter linearly with time. If it be assumed for the decomposition of barium azide that the rate of progression of the interface is linear and the numbers of nuclei increase linearly with time, the pressure should obey the relationship, $p = p_0 lkt^4$, where l is the number of nuclei formed in unit time and k is the rate of advancement of the interface expressed in appropriate units. Harvey (1933) has found that for barium azide p varies as the 7th–10th power, and Maggs (1939) that it varies as the 6th–8th power of the time. It is clear, therefore, that there is some inaccuracy in the above assumptions, and one of the objects of this investigation was to clear up the discrepancy.

EXPERIMENTAL

Material and apparatus. Barium azide was prepared from hydrazoic acid and barium hydroxide as described previously (*loc. cit.*). A concentrated solution of BaN_6 was placed in a desiccator over calcium chloride until it began to crystallize. Crystals of good shape were picked out and carefully dried and dehydrated in an evacuated desiccator over calcium chloride for 24 hr. The crystals, which were at first translucent, turned white, losing their water of crystallization. The average weight of the crystals was 2–4 mg. The length was on an average 3–4 mm., the breadth 1–2 mm., the depth 0·5–1 mm. A few crystals were of twice or three times that size. A specimen of barium azide obtained from the General Electric Company was recrystallized and the crystals were of the same shape and size as the others. The experiments so far have shown no material differences between the crystals of the G.E.C. and those prepared in our laboratory.

The decomposition of the BaN_6 crystals took place in an evacuated silica reaction vessel (see fig. 1). The pressure of the nitrogen was measured by a MacLeod gauge, calibrated for the pressure range, 10^{-5} cm. Hg to 10^{-2} cm. Hg. The reaction vessel was heated by an electric furnace and the temperature of the crystals was measured by a Pt-PtRh thermocouple.

The first form of the apparatus was designed by Maggs. A few alterations had to be made in this in order that there should be better control of the temperature of the crystal. The carrier for the crystals was altered in such a way that the junction of the thermocouple was situated inside the copper disk (see fig. 1, *A*) on which the platinum carrier for the crystal was soldered. The wires of the thermocouple were insulated by means of glass

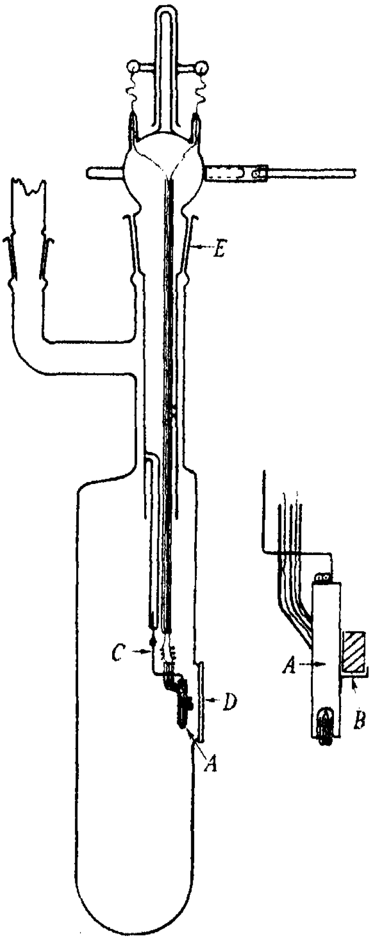

FIG. 1

tubing. The carrier (B) was made of platinum foil and the crystal was held in position by bending the edges of the foil over the edges of the crystal. In order to put the crystal into the right alignment for photography, the copper disk was brought into different positions by bending the copper wire (C). As the temperature near the window (D) is lower than at the back of the reaction vessel, it was essential that the crystal occupy the former position in as short a time as possible. This was achieved by turning the carrier by means of the ground joint (E). As the wires of the thermocouple were sealed into the glass supporting the carrier and were led through glass tubing to the ice junctions, the turning of the carrier would have necessitated the turning of the ice junction. This was obviated by the arrangement at the top of the carrier (see fig. 1). During the experiment the ground joint was water-cooled.

The crystal was illuminated by a pointolite lamp when a photograph was to be taken, and to protect the crystal from heat-rays, a water cell was interposed. To keep the temperature constant, the whole reaction vessel was put into a box, so that draughts could be kept out, and this box was opened only during the time when a photograph was taken. With this arrangement the temperature was constant to within 1-2° C.

Procedure. After weighing and measuring the crystal, it was fixed on the carrier and brought into the right position as described above. Then the air was pumped out from the reaction vessel for 18 hr. with an oil pump and mercury pump. After checking the vacuum in the reaction vessel, the heating was turned on, and during the heating the crystal was turned away from the window. It took about 10 min. to attain the required temperature. The temperature was carefully watched (galvanometer) and the electric current regulated by means of two rheostats. When the first nuclei became visible, photographs were taken at fixed time intervals and at the same times the pressure was measured. The magnification was 36. The experiments were followed until the surface of the crystal was covered with nuclei. After developing the film, the nuclei were measured and counted. A print of one film is shown in fig. 2. As the crystal was already in the reaction vessel when the heating was started, the moment when the crystal had attained the required temperature could not be determined exactly. Therefore an error is involved in the determination of the time of initiation of the reaction, which became more marked at high temperatures when the time of reaction is short. The experiments were carried out for three temperatures, 100, 115 and 123·5° C.

Rate of growth. The radius of the nuclei increases linearly with time,

$$r = k_1 t. \tag{1}$$

In fig. 3, the rate of growth for the three different temperatures is shown. The mean value of the diameter of ten nuclei was taken and the probable error of the mean diameter is 2–4 %. When the nuclei first appear, they are much fainter than later on. Therefore the early measurements of nuclei diameter are not very accurate and they were usually neglected. Towards the end of the experiment, when the nuclei are relatively large, a spot of

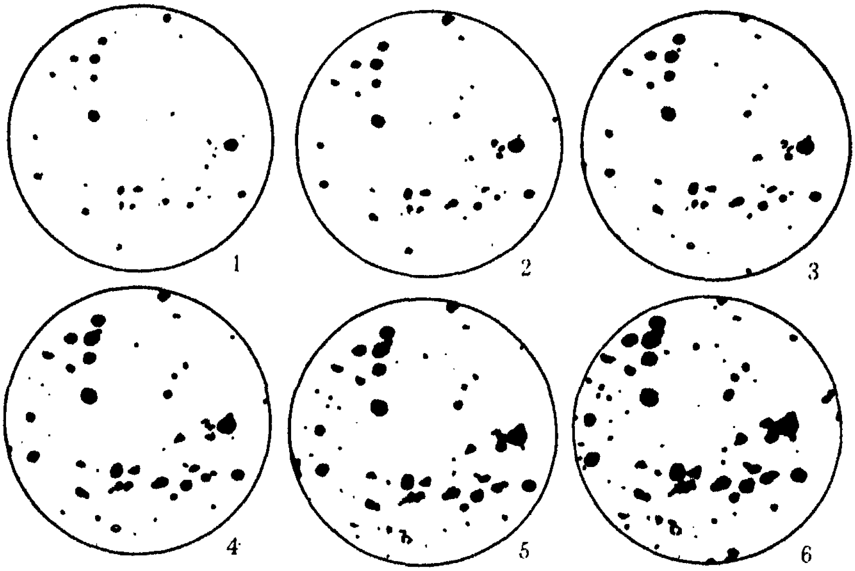

FIG. 2. Temp.: 115° C. Time: no. 1 taken after 142 min., the following at 10 min. intervals. Magnification: 120.

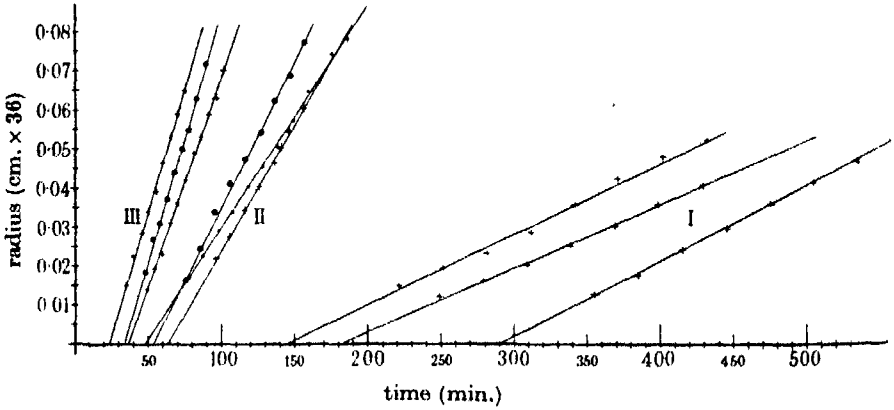

FIG. 3. I: 100° C. II: 115° C. III: 123·5° C.

reflected light appears very often in the middle of the nucleus, which seems to indicate that the nuclei are growing out from the surface. In Table I the rates of growth for the three temperatures are tabulated.

TABLE I

No. of exp.	Temperature °C	$\frac{dr}{dt} \times 7{\cdot}2 . 10^3$ cm./min.	Average
1*T*	100	0·033	0·036
2*T*		0·036	
3*T*		0·038	
8	115	0·120	0·1275
11		0·150	
12		0·110	
13		0·115	
1*t*	123·5	0·225	0·239
2*t*		0·250	
3*t*		0·244	

As has been mentioned in the introduction, it was assumed that there is an induction period before the reaction starts, because the evolution of nitrogen is delayed. This delay seems in part at least to be due to the difficulty with which nitrogen escapes from the crystal. This is shown by the fact that when the radius of the largest nuclei on a film is plotted against time and extrapolated to $r = 0$, the time at which these nuclei start to grow is seen to be very close to that of the time of the commencement of the heating.

The increase of numbers of nuclei. The numbers were also counted on the film. The first very small numbers were neglected, because of their inaccuracy. As has previously been said, the small nuclei are very faint, partly because of the reflection of light from the white crystal surface into the camera, so that nuclei which could be seen through the microscope could not be seen on the film.

It was found that the numbers increase as the third power of the time,

$$N = k_2 t^3. \tag{2}$$

In fig. 4, $\log N$ is plotted against $\log (t - \tau)$, τ being the time that a nucleus needs to become visible, which can be easily computed from the plot of r against t (fig. 3). The slopes of the $\log N = k \log t + \text{const.}$ vary between 2·5 and 3·5. That k_2 is not always exactly 3 is probably due to the uncertainty in the values of t, which has been mentioned previously. If we plot the numbers against $(t - \tau)^3$, we get straight lines through the origin for the experiments at 100° C, where the inaccuracy in the time is insignificant, because of the long duration of the reaction. At higher temperatures, however, the $N-(t-\tau)^3$ lines are not straight and do not go through the origin.

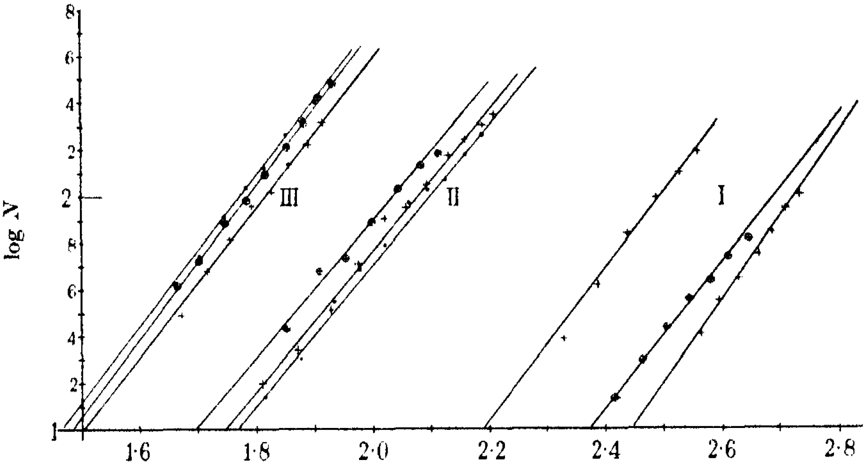

FIG. 4. I: 100° C. II: 115° C. III: 123·5° C.

The pressure of the nitrogen increases with the 6th to 8th power of the time, $p=k_3t^{(6-8)}$. At the beginning certain irregularities sometimes occurred, but they may be due to the MacLeod gauge not being accurate enough for the low-pressure measurements. In fig. 5, the log of the pressure is plotted against the log of the time. These pressure curves are not reproducible to a great extent, especially at the lower temperatures. This is due to the fact that the formation of nuclei is a structure sensitive property. The temperature coefficient k_3 computed from the intercept on the Y-axis is therefore very inaccurate. To decrease the error, the intercept on the Y-axis has been computed from the distance between the lines at a value of log p equal to -5, taking a mean slope and a mean distance for every series of experiments for every temperature:

$$\log p = 6{\cdot}8 \log t - 24{\cdot}98, \quad 110^\circ\ \mathrm{C},$$

$$\log p = 7{\cdot}9 \log t - 20{\cdot}9, \quad 115^\circ\ \mathrm{C},$$

$$\log p = 8{\cdot}2 \log t - 19{\cdot}22, \quad 123{\cdot}5^\circ\ \mathrm{C}.$$

(As already mentioned above, for a certain part of the reaction the pressure increases exponentially with time.)

Activation energies. The activation energy for the radial rate of growth of nuclei is 23·5 kcal.,

$$r = k_1 t, \tag{1}$$

$$\log k_1 = -0{\cdot}516 \times 10^4 \frac{1}{T} + 8{\cdot}5 \tag{3}$$

(fig. 6, *A*), *dr*/*dt* being expressed in cm./min.

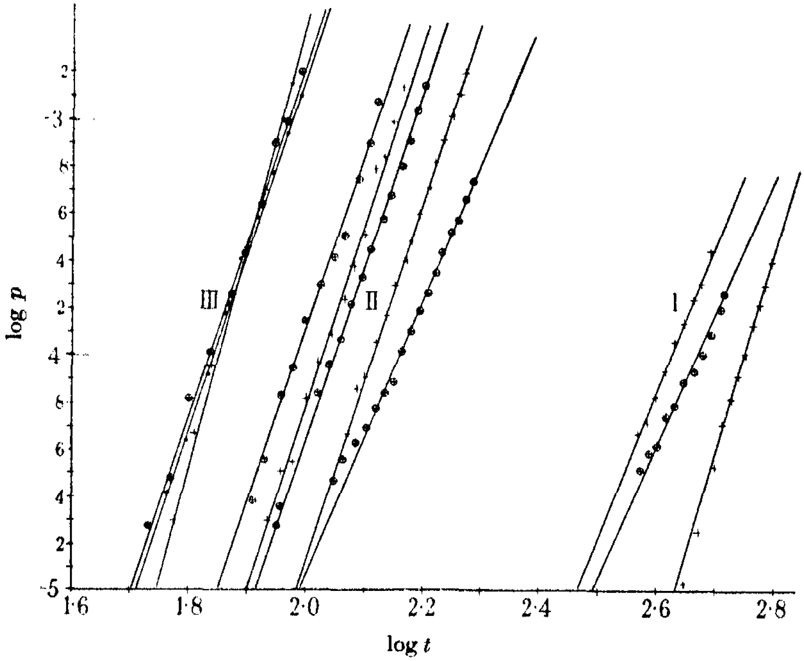

FIG. 5. I: 100° C. II: 115° C. III: 123·5° C.

The activation energy for the formation of nuclei is 74 kcal.,

$$\left.\begin{aligned}\log N &= a \log t - \log k_2,\\ \log k_2 &= -1{\cdot}43 \times 10^4 \frac{1}{T} + 32{\cdot}44\end{aligned}\right\} \tag{4}$$

(fig. 6, *B*), the time being expressed in minutes.

The activation energy for the pressure is 166 kcal.,

$$\left.\begin{aligned}\log p &= b \log t - \log k_3,\\ \log k_3 &= -3{\cdot}61 \times 10^4 \frac{1}{T} + 71{\cdot}64\end{aligned}\right\} \tag{5}$$

(fig. 6, *C*). $\log k_2$ and $\log k_3$ are calculated as described above.

It will be noted, however, from fig. 6, that whereas there is a good straight line for the rates of growth, this is not the case for rates of formation of nuclei or the development of pressure. It is a possibility that the activation energy in the last two cases decreases with increase in temperature.

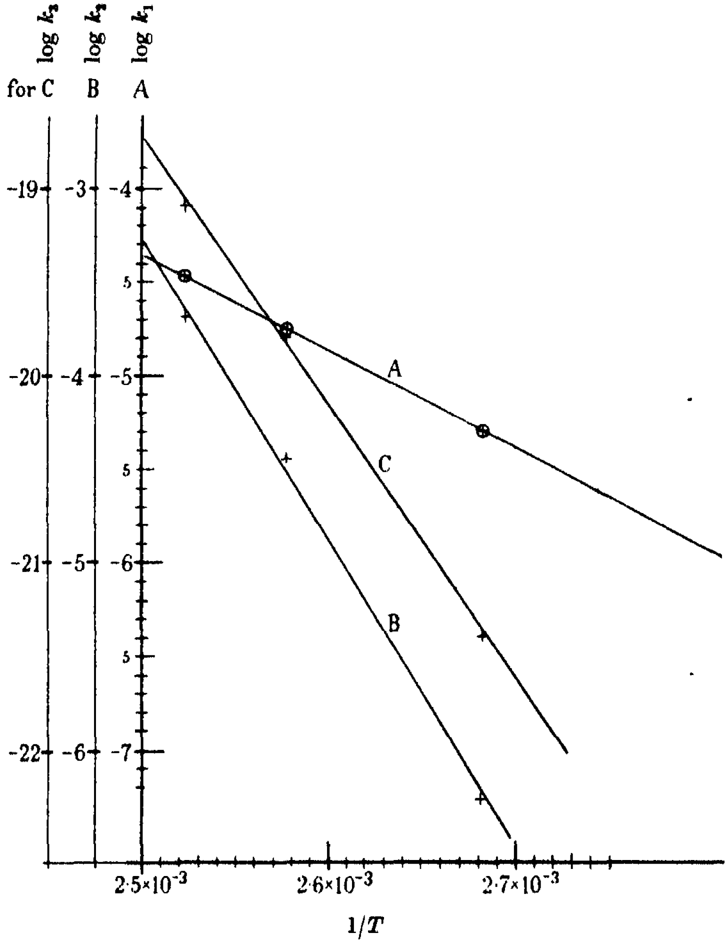

Fig. 6

The activation energy was calculated by Harvey (1933) from the slopes of the log p-t curves and a value of 21 kcal. was found. This is in good agreement with the value given above, but the agreement is probably fortuitous since into the activation energy as calculated by Harvey there enters the activation energy of both nuclei growth and nuclei formation (see Mott 1939, the paper following this).

DISCUSSION

From equation (3), it will be seen that the rate of progression of the barium-barium azide interface at infinite temperature is 3×10^8 cm./min. Taking the distance between the planes of azide ions found by Hendricks and Pauling (1925) for potassium azide, this rate corresponds with 10^{14} layers of azide ions per sec. This represents a high frequency of activation. Similar values have been found previously for the decomposition of lead azide (Garner and Gomm 1931) and potassium azide (Garner and Marke 1936), copper sulphate pentahydrate (Topley 1932) and silver carbonate (Spencer and Topley 1929). Since the latter two decompositions are endothermic, it would appear that the high frequencies are not due to chain reactions.

Since the radii of the nuclei increase linearly with the time, and the numbers of the nuclei increase as the 3rd power of the time, it can be readily shown that the pressure should increase as the 6th power of the time. Thus $p = \text{const.}\, t^x$, where x should be 6 or at the most 6·5. It has been found experimentally at 100, 115 and 123·5° C that x is 6·8, 7·9 and 8·2 respectively. There is a discrepancy of about one unit. This could be explained if the numbers increased as the 4th power of the time, which seems unlikely from the experimental evidence of the counts on the surface. It should, however, be borne in mind (*a*) that counts have been made only on the external surface and that nuclei are formed also within the pseudomorph, (*b*) that the form of the p-t curves is influenced by the nature of the support and nothing is known of the rate of increase of nuclei on the surface in contact with the support.

A reaction occurring at a rate which increases as the 6th power of the time must show an apparent induction period. The induction periods met with in the case of the alkaline azides are to be ascribed to the fact that the numbers of nuclei increase as the 3rd power and that the volume of each nucleus increases also as the 3rd power of the time. In the case of mercury fulminate, there is a still more marked induction period, the pressure increasing as the 20th–24th power of the time. If nuclei are formed in this case, which is by no means certain, it would be expected that the numbers of nuclei increase as the 20th power of the time.

The rate of formation of nuclei is a bimolecular process. Professor Mott has suggested as an explanation of this, that there is an evaporation of nitrogen from the surface of the crystal which is constant at constant temperature, and that, as a result of this evaporation, barium atoms are left on the surface in number proportional to the time. These barium atoms are mobile and when two atoms meet a nucleus is formed. This would account for the rate of production of nuclei increasing as the square of the time. Although there is no experimental evidence of the occurrence of surface evaporation in the case of barium azide, there is ample evidence that it occurs in potassium and sodium azides and mercury fulminate during the induction period. There is thus no difficulty in the way of the assumption of surface evaporation for barium azide also.

On the basis of the above theory, the activation energy for the unit process occurring on the surface of crystals of barium azide is 37 kcal. This is of the same order as the activation energies of the interface reactions in PbN_6, 38 kcal.; NaN_3, 34 kcal.; and KN_6, 36 kcal. This may, however, be a coincidence. The values are, however, very different from that of the interface reaction of BaN_6 which is 23·5 kcal. The low values for the interface reactions of the alkaline earth azides are no doubt responsible for the low temperatures at which they decompose. The alkaline earth azides decompose at temperatures 200° C lower than the other azides so far investigated.

SUMMARY

The nuclei formed in the decomposition of barium azide increase in radius at a linear rate and increase in number as the 3rd power of the time.

The activation energy for nuclear growth has been shown to be 23·5 kcal., and that for nuclei formation 74 kcal. approximately. The frequency of activation in the case of nuclei growth is 10^{14}.

The author wishes to express her thanks to Imperial Chemical Industries, Ltd., and to the Colston Research Society for grants for the purchase of apparatus, and to Professor W. E. Garner, F.R.S., for his constant interest and advice.

REFERENCES

Bright N. F. H. and Garner, W. E. 1934 *J. Chem. Soc.* p. 1872.
Cooper, J. A. and Garner, W. E. 1936 *Trans. Faraday Soc.* **32**, 1739.
Garner, W. E. and Gomm, A. S. 1931 *J. Chem. Soc.* p. 2123.
Garner, W. E. and Hailes, H. R. 1933 *Proc. Roy. Soc.* A, **139**, 576.
Garner, W. E. and Marke, D. J. B. 1936 *J. Chem. Soc.* p. 657.
Garner, W. E. and Southon, W. R. 1935 *J. Chem. Soc.* p. 1705.
Hailes, H. R. 1933 *Trans. Faraday Soc.* **29**, 544.
Harvey, F. E. 1933 *Trans. Faraday Soc.* **29**, 653.
Hendricks and Pauling 1925 *J. Amer. Chem. Soc.* **47**, 2904.

Kornfeld, M. 1935 *Phys. Z. Sowjet.* **7**, 432.
Kornfeld, M. and Pawlow, W. 1937 *Phys. Z. Sowjet.* **12**, 301.
Macdonald, J. Y. 1936*a* *J. Chem. Soc.* p. 832.
— 1936*b* *J. Chem. Soc.* p. 839.
Maggs, J. 1939 *Trans. Faraday Soc.* **35**, 433.
Marke, D. J. B. 1937 *Trans. Faraday Soc.* **33**, 770.
Mott, N. F. 1939 *Proc. Roy. Soc.* A, **172**, 325.
Spencer, W. D. and Topley, B. 1929 *J. Chem. Soc.* p. 2633.
Topley, B. 1932 *Proc. Roy. Soc.* A, **136**, 413.

On the decomposition of metallic azides

By N. F. Mott, F.R.S.
H. H. Wills Physical Laboratory, University of Bristol

(*Received* 22 *May* 1939)

The purpose of this paper is to attempt a theoretical explanation of some of the phenomena observed during the decomposition of metallic azides by heat or by irradiation with ultra-violet or β-rays, and in particular of the new results on barium azide $Ba(N_3)_2$ obtained in the two preceding papers (Garner and Maggs 1939; Wischin 1939).

This salt is stable at room temperature in the absence of radiation. If heated to a temperature of the order of 100° C, it decomposes slowly, nitrogen being given off. A similar effect may be obtained at room temperature through prolonged irradiation with ultra-violet light. In both cases metallic nuclei are formed on the surface of the crystals, and also inside it (at internal cracks?).

We shall consider first some of the phenomena observed on heating. The number N of nuclei formed on a given surface of a crystal after heating for a time t is (Wischin 1939) given approximately by the law

$$N = At^3. \tag{1}$$

Formula (1) is satisfied best for the lower temperatures at which decomposition is observed; for higher temperatures a rather higher exponent than 3 fits the facts better.

The constant A is "structure-sensitive"; in other words it varies from one crystal to another. Also rows of nuclei are observed, probably along cracks, showing that there exist on the crystal surface favoured places where a nucleus can form easily.

The rate of growth of each nucleus is given by

$$\frac{dr}{dt} = B, \tag{2}$$

where r is its radius and B a constant at a given temperature for all nuclei. Thus at time t

$$r = B(t-t_0), \tag{3}$$

where t_0 is the time at which the nucleus was formed.

The pressure p of nitrogen after a time t is observed to be given by

$$p = Ct^x, \tag{4}$$

where the value of x lies between 6 and 8.

Before discussing the experimental material any further we shall prove that (4) with $x = 6$ follows from (1) and (2), if we make the assumption that the amount of nitrogen given off is proportional to the amount of metal formed in the nuclei. At time t the volume of the metal present in the nuclei is

$$\int_0^t \frac{4\pi}{3}\{B(t-t_0)\}^3 \frac{dN(t_0)}{dt_0}\,dt_0,$$

which is equal to $\frac{1}{15}\pi A B^3 t^6.$

Thus $x = 6$ and

$$C = \tfrac{1}{15}\pi A B^3. \tag{5}$$

The fact that the observed values of x are rather greater than 6 may mean that during the initial stages of nuclear growth the nitrogen escapes from the crystal with a certain time lag.

Wischin (1939) has measured the variation with temperature of the constants A, B, C. They may be expressed*

$$A = A_0 e^{-a/RT}, \quad B = B_0 e^{-b/RT}, \quad C = C_0 e^{-c/RT},$$

where (in kcal.) $a \sim 74, \quad b \sim 23{\cdot}5, \quad c \sim 166.$

---

* The activation energy for the reaction has usually been obtained by plotting $\log p$ against t, drawing a straight line through the points, and expressing the slope in the form

$$\alpha = \frac{d(\log p)}{dt} = \text{const. } e^{-E/kT}.$$

If we fit a curve of the type $p = p_0 e^{\alpha t}$ to the curve $p = Ct^6$ at a given value p' of the pressure by means of the equations

$$p_0 e^{\alpha t} = Ct^6, \quad p_0 \alpha e^{\alpha t} = 6Ct^5,$$

we obtain $\alpha = 6/t = 6(C/p')^{\frac{1}{6}}.$

It follows that the conventional activation energy is $\frac{1}{6}$ of C, namely, 23 kcal. This is very close to the experimental values for the alkaline earth azides.

According to formula (5), we should have

$$c = a + 3b = 144 \text{ kcal.}$$

Some discrepancy with the observed value is not surprising, since x does not have the theoretical value 6.

The constant B_0 is found by Wischin to have the value

$$B_0 \sim 10^7 \text{ cm./sec.}$$

for all nuclei observed.

We turn now to the effect of prolonged irradiation on barium azide crystals. At room temperature this produces metallic nuclei with the liberation of nitrogen. Under constant intensity of irradiation the nitrogen pressure increases linearly with the time after an initial induction period (Garner and Maggs 1939).

Irradiation at room temperature within the induction period has a marked effect on the subsequent thermal decomposition of the crystal. After a very short illumination the subsequent liberation of nitrogen on heating follows the same law, $p = Ct^x$ with $x \sim 6-8$, as before, but with a very much larger value of C. Also a much larger number of nuclei are observed after a given time of heating. A reasonable explanation is that both the rate of production of nuclei, and their rate of growth, follow the same law as before, but that A (formula (1)) is increased by the illumination. In other words, the number of sensitive spots where a nucleus can form is increased by the illumination. A hypothesis as to how this happens will be proposed below.

After a more prolonged illumination, the value of x becomes smaller, approaching the value 3. This must obviously be due to the formation of nuclei by the light; since the volume of each nucleus increases at t^3 during heating, the pressure will also increase as t^3 if a large number of nuclei are already present.

The formation and growth of nuclei in irradiated barium azide with the liberation of nitrogen appears very similar to the photochemical reduction of silver halides with the liberation of halogen; in both cases the metal is found in the form of nuclei. For the latter case a theory has been given by Gurney and Mott (1938), and *as regards the rate of growth of nuclei when they are once formed*, we believe that exactly the same theory can be applied to barium azide. We assume, then

(1) That $Ba(N_3)_2$ is an ionic conductor at room temperature, a certain small proportion of metal ions in a crystal in thermal equilibrium being in interstitial positions and therefore mobile. The N_3^- ions are assumed not to be mobile.

(2) That under ultra-violet irradiation barium azide should show photoconductivity; electrons are ejected from the azide ions into the conduction band of the crystal. The positive holes left in the full band corresponding to the N_3 ions are mobile and eventually diffuse to the surface. When the "holes" reach the surface the N_3 radicals can escape, and break up to form molecular nitrogen.

(3) An electron in the conduction band will wander around until it finds a speck of metallic barium; it will then be trapped by the speck.

(4) The resulting electric field round the speck will attract the interstitial metal ions; the speck will therefore grow by a process of electrolysis.

Such a mechanism gives a quantity of reaction products proportional to the radiation absorbed, as observed for long periods of irradiation.

As regards the induction period, however, we have to consider under what conditions nuclei can be formed in the first place. The clearest evidence about nuclear formation in azides comes from their behaviour under heat treatment, and we shall now consider this.

A number of polar salts and oxides, when heated in vacuum, lose atoms of the electronegative constituent, the excess metal going into solid solution in the body of the crystal. Zinc oxide is a case in point. On heating it oxygen is driven off, the excess zinc remaining as interstitial atoms, which at high temperatures dissociate into *interstitial* zinc ions which diffuse into the crystal and electrons in the conduction band. The chief observable effect of the excess zinc is to increase the conductivity by a very large factor (cf. von Baumbach and Wagner 1933).

It seems probable that something of this sort happens in barium azide; when it is heated nitrogen is driven off from the surface, and excess metal atoms go into solid solution. Since these will dissociate, the first effect of heating will be to increase the concentration of interstitial ions already present (which must already be quite high, because the azide is, according to our hypothesis, an ionic conductor even at room temperature), and also to add free electrons, of which there are initially none. We suggest that these electrons are responsible for the formation of nuclei, in a way to be discussed below.

If our hypothesis is correct, there should be, as well as the emission of nitrogen which is catalysed by the presence of nuclei and which gives a pressure increasing as the sixth to the eighth power of the time, a slow uncatalysed emission at a constant rate; we expect an emission following the law

$$p = \text{const.}\, t + Ct^6.$$

Actually a slow emission of this type, followed by an accelerated reaction, is observed for KN_3 (Garner and Marke 1936) and is illustrated in fig. 1; for BaN_6 the slow emission must be too slow to be observed.

During the slow emission of nitrogen, we may assume that the number n of electrons per unit volume in the crystal increases linearly with the time. In a crystal of volume V and surface area S, we may therefore write

$$\frac{dn}{dt} = \frac{SQ}{V}, \tag{6}$$

where Q is a constant at a given temperature. It is reasonable to suppose that Q varies with the temperature according to the law

$$Q = Q_0 e^{-q/RT}. \tag{7}$$

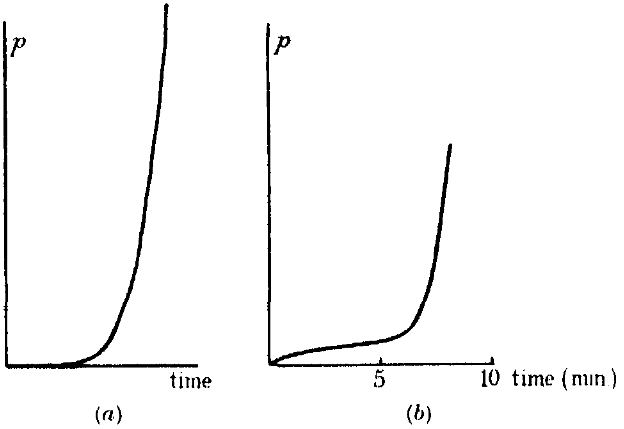

FIG. 1. Pressure-time curves for barium azides. (a) $p = t^6$ (BaN_6 at 100° C); (b) type observed for KN_3 at 300° C.

We do not know anything of the mechanism of the escape of nitrogen; perhaps q represents the work required to remove an electron into the conduction band from a *surface* ion.

Integrating (6) we obtain

$$n = \frac{SQ}{V} t.$$

Now we have in the crystal a large number of interstitial metal ions, and a few electrons. The state of affairs is very like that in a halide grain of a photographic emulsion. In emulsions the sensitivity is enormously increased if on its surface the grain has specks of silver sulphide (sensitivity specks). The function of the sensitivity specks is, according to Gurney and Mott (1938), to catch an electron, so that it stays in one place for a time so long that interstitial metal ions can be attracted to it.

Since in azide crystals the formation of nuclei is structure sensitive, it is probable that the existence of an electron trap on the surface makes possible the formation of a nucleus there. These traps* may be points where a negative ion is missing from the surface layer. This would account for the increase in A (formula (1)) produced by previous illumination for a short period, since an effect of illumination would be to drive off a few N_3 ions from the surface.

In photographic emulsions the developed density depends not only on the product It (I = intensity of light, t = time of exposure), but on I and t separately. For given It, the density drops off as I is decreased. This can be explained as follows (Webb and Evans 1938; Gurney and Mott (1938)). When an electron is captured by a sensitivity speck, an ion is attracted and moves up to the speck. The very small "nucleus" thus formed cannot keep the electron indefinitely; after a certain time it will escape, and the ion will thus be able to escape too, unless another electron comes along first, in which case the nucleus will have a chance to build itself up to a size so large that it will be stable.

Exactly the same thing may be expected to happen in azides. The probability per unit time that an electron is trapped at a given sensitive point is proportional to n. The probability that a second electron comes along before the first escapes is also proportional to n. If σ electrons are necessary to form a stable nucleus, the probability that a nucleus is formed in a given time interval is proportional to n^σ. Thus if N is the number of nuclei at time t

$$\frac{dN}{dt} = \left(\frac{SQt}{V}\right)^\sigma \times \text{const.},$$

or, on integrating,

$$N = \left(\frac{SQ}{V}\right)^\sigma \frac{t^{\sigma+1}}{\sigma+1} \times \text{const.} \tag{8}$$

We have seen that for barium azide at 100° C, N is proportional to t^3, so that we may deduce that $\sigma = 2$. It follows that a nucleus with two electrons and thus one interstitial barium ion is stable, or can catalyse the thermal decomposition. At higher temperatures, since N varies as a rather higher power of t, a rather larger nucleus must be required.

Formula (8) gives for the constant A in formula (1)

$$A = (SQ/V)^\sigma.$$

---

* The "F-centres" in alkali-halides are supposed to be electrons trapped at points where the negative ion is missing and we know (Pohl 1937) that F-centres can trap another electron.

We thus expect a larger A (shorter induction period) for powders, in which the area of surface is large. This seems to be in agreement with some results of Garner and Hailes (1933) on mercury fulminate.

With $\sigma = 2$, we see that $q = \frac{1}{2}a$. Thus the activation energy* to free a N_3 radical is 37 kcal.

We turn now to the induction period observed during prolonged illumination. The linear rate of growth under illumination after a certain time has elapsed suggests that, if sufficient nuclei are present, *all* the electrons liberated by the light are trapped by nuclei, and that there is no recombination. If however no nuclei are present (as at the beginning of the experiment) two things can happen. The electron can recombine with the positive hole, or the hole will first get to the surface, so that nitrogen is liberated. If we neglect the second process, illumination with intensity I will give a *constant* density of electrons n_0 per cm.^{3}, with

$$n_0 \text{ proportional to } \sqrt{I}.$$

We have already suggested that the radiation increases the number of places on the surface where a nucleus can form. Thus we may set the number of places proportional to It, so that the rate of formation of nuclei, dN/dt, is

$$\begin{aligned} \frac{dN}{dt} &= Itn_0^2 \times \text{const.} \\ &= I^2t \times \text{const.} \end{aligned}$$

Thus
$$N = (It)^2 \times \text{const.}$$

Thus the number of nuclei increases as the square of the exposure It; the rate of liberation of nitrogen should initially be proportional to Nn_0, because, while the number of nuclei is small, the chance of an electron being captured by a nucleus and not wasted by recombination is proportional to Nn_0. Thus the pressure of nitrogen should increase initially as $t^3I^{\frac{5}{2}}$.

We now turn to the law governing the rate of growth of nuclei when the salt is heated in the absence of radiation. The presence of nuclei increases enormously the rate of liberation of nitrogen; as already emphasized, the steady emission from the surface before nuclear formation is, in barium azide, too small to be observed. In potassium azide the rate of emission measured *in vacuo*, so that the nuclei evaporate at once, is several thousand times less than in potassium vapour. We see then that the contact between metal and azide accelerates or catalyses the reaction. It is unlikely, however, that the reaction takes place only at the interface, because then nitrogen atoms or molecules would be liberated in the middle of the material, at the interface, and it is difficult to see how they could escape.

---

* This may be activation energy to free a pair of adjacent radicals, to form three N_2 molecules.

In the theory which we shall propose the nitrogen is actually liberated at the surface of the azide crystals, some way from the nuclei just as in the photochemical reaction.

We have to remember that the salt contains plenty of interstitial and hence mobile metal ions, which can flock together to build up the nuclei; the difficulty is to provide the electrons. We know from the photochemical evidence that, once the electrons are provided, the nuclei will grow.

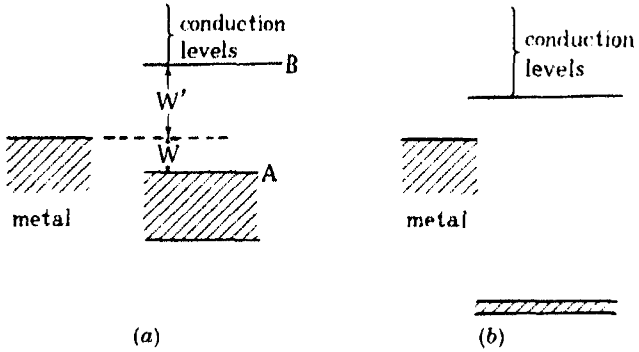

FIG. 2. Energy levels in polar salts in contact with metal; (*a*) barium azide and barium; (*b*) sodium chloride and sodium.

Fig. 2 shows the energy levels for any insulator; for an azide the full band gives the energy levels of electrons of the azide ions. We show also the energy levels for the metal. Illumination with ultra-violet raises electrons from the full band into the conduction band, which requires an energy of several electron volts; the electrons subsequently find their way to the metal. It will however obviously require less energy to raise an electron from the full band directly into the metal. We mark this energy by W in fig. 2, and suppose that W is to be identified with the activation energy for nuclear growth, $b = 23{\cdot}5$ kcal.

Our picture of nuclear growth is thus the following: every now and then an azide ion adjacent to the metallic nucleus receives enough energy from heat motion to lose an electron to the metal, thus forming an azide radical. The radical, being in the middle of the material, cannot break up; however, almost immediately an adjacent ion will hand over its electron to it; the "positive hole" so formed will diffuse away from the nucleus, and eventually reach the surface. The radical formed at the surface can, as we have seen, escape and break up. This may be quite a slow process; we have no direct evidence about the rate. The metallic nucleus which has received an electron will grow in the way already described, by attracting interstitial positive ions.

The rate of nuclear growth may be estimated as follows: the emission of "positive holes" from the metal into the salt ought to be given by just the same formula as the thermionic emission of electrons from a metal into a vacuum. Thus the emission per unit area, in number of electrons per second, should be

$$Ke^{-W/kT}$$

with (Fowler 1936) $K \sim 10^{26}$ cm.^{2} sec.$^{-1}$ at 400° K. Thus if Ω is the atomic volume of barium metal, we should have

$$\frac{dr}{dt} = K\Omega e^{-W/kT} \qquad K\Omega \sim 10^4 \text{ cm./sec.}$$

The value of $K\Omega$ is some 100–1000 smaller than that observed. This may be due to a temperature variation of W due to thermal expansion. If W is of the form

$$W = W_0(1+\alpha T),$$

$K\Omega$ will have to be increased by a factor

$$e^{W_0\alpha/R} = e^{12,000\alpha}.$$

If this is to be 1000, we must have

$$\alpha \sim 5 \times 10^{-4} \text{ degree}^{-1}.$$

This is perhaps surprisingly large—we should expect a value of the order of the thermal expansion coefficient, say, 10^{-4} degree^{-1}.

Since barium azide crystals do not absorb light of visible wave-lengths, it follows that the energy interval AB in fig. 2 must be of the order 3 eV or more. Since $W \sim 1$ eV, it follows that the energy W' (fig. 2) required to bring an electron from the metal into the empty conduction band is more than 2 eV, and hence greater than W. We contrast the state of affairs in NaCl, where the energy interval separating the two bands ~ 10 eV, but W' is much less, about 1·7 V (Mott 1938).

Since, in BaN_6, W' is so large, and assuming that the work required to bring a positive ion from barium metal into an interstitial position in the crystal is positive, we may deduce that the solubility of barium in the azide is negligible. It is possible that in other salts this is not the case. If the solubility were not vanishingly small, no nucleus could form until, owing to the slow escape of nitrogen from the surface, the solution became supersaturated. In that case there would be a true induction period, with formation of metal and activated emission of nitrogen starting after a definite time. It is possible that this may be the case for mercury fulminate. Since both W and W' would have to be of the order 1 to 1·5 eV, and since the crystal would absorb light of a frequency given by $h\nu = W + W'$, such a crystal could not have its absorption bands far in the ultra-violet.

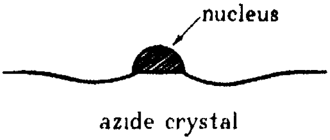

FIG. 3. Suggested form of the surface round a nucleus.

Finally we must emphasize that, according to our theory, metallic nuclei due to heating or to irradiation are formed by diffusion of interstitial metal ions through the crystal, the nitrogen escaping from the surrounding free surface of the crystal. There is thus no escape of atoms or heavy ions from the metal salt interface; no azide is removed to make room for the nucleus. It follows that if a nucleus were formed inside a crystal, the surroundings would be subject to an enormous strain. We think that nuclei are probably formed only at surfaces, and at the surfaces of internal cracks, and that they grow outwards, the escape of nitrogen from the surrounding surface giving to the surface a form such as that shown in fig. 3. Wischin (1939) has in fact observed that the nuclei appear to protrude from the surface.

The author has pleasure in expressing his thanks to Professor Garner for many discussions about the experimental material.

SUMMARY

A theoretical discussion of the decomposition of metallic azides, based on the Wagner-Schottky theory of ionic conductivity and the electron theory of solids. The main points discussed are: the formation of metallic nuclei and the nature of the induction period; the way in which the presence of nuclei catalyses the reaction; the action of ultra-violet light. The similarity between the decomposition of azides and the photochemical reduction of silver halides is pointed out.

REFERENCES

Fowler 1936 *Statistical mechanics*, p. 352.
Garner and Hailes 1933 *Proc. Roy. Soc.* A, **139**, 576.
Garner and Maggs 1939 *Proc. Roy. Soc.* A, **172**, 299.

Garner and Marke 1936 *J. Chem. Soc.* p. 1398.
Gurney and Mott 1938 *Proc. Roy. Soc.* A, **164**, 151.
Mott 1938 *Trans. Faraday Soc.* **334**, 500.
Pohl 1937 *Proc. Phys. Soc.* **49** (extra part), 1.
von Baumbach and Wagner 1933 *Z. phys. Chem.* **22**, 199.
Webb and Evans 1938 *J. Opt. Soc. Amer.* **7**, 249.
Wischin 1939 *Proc. Roy. Soc.* A, **172**, 314.

A crystallographic investigation of glacier structure and the mechanism of glacier flow*

BY M. F. PERUTZ, *Cavendish Laboratory, Cambridge*
AND GERALD SELIGMAN

(*Communicated by Sir William Bragg, P.R.S.—Received* 15 *March* 1939—*Revised* 21 *April* 1939)

[Plates 16–19]

1. INTRODUCTION

(*a*) *The transition of firn into glacier ice; glacier structure*

Glaciers are divided into two main parts: the accumulation area, firn region or *névé* where the annual accumulation in the form of snow exceeds the loss by melting, evaporation and wind erosion, and the ablation area or glacier tongue. The dividing line between the two regions is called the Firn Line. Granular, compacted snow called firn covers the accumulation area. Its crystals are rarely larger than 2 mm. in diameter and are mixed with a considerable volume of air, so that the specific gravity is much lower than that of ice. The surface of the tongue consists of blue or glassy ice, more or less covered with rock debris; here the diameter of the ice crystals varies between 1 and 10 cm. or even more; the specific gravity of the ice is never far below 0·90. In summer the tongue has a bluish or grey appearance, while the firn region retains its white or whitish hue.

Previous research.

The attention of glaciologists has largely been confined to the ablation areas since they are more easily accessible. Only recently have any attempts been made to investigate the economy of the firn region and to measure such features as the increase of specific gravity and grain size with the depth, the temperature distribution, the accumulation of snow in the winter and the production of melt water during the summer (Streiff-Becker 1936, 1938; Ahlmann 1935–6). These experiments constitute a valuable first step towards the understanding of glacier structure but fall short of providing a complete solution of the problem of the transition of firn into ice. For instance, temperatures and specific gravities have never been determined to a depth sufficient to reach the lowest layers of the firn; again, measurements have only been carried out at one or two points on each glacier. Furthermore, insufficient attention has been paid to the microscopic changes which accompany the transition, such as variations in the size and shape of the crystals and of the air spaces between them. It was always expected that if sufficient depth were reached the firn would become ice, but this depth had to be calculated by extrapolation of the specific gravity curves (Sorge 1935), an unreliable proceeding since there was always the possibility that the transition might not be continuous. Indeed, there had been indications that the dividing line which separates the firn from the ice at the surface with considerable abruptness extended upwards far into the firn area underneath the surface and that the transition along this plane was equally abrupt. In order to test this possibility it would, of course, be necessary to measure the distribution of specific gravity with depth at a series of points at different altitudes and levels between the source of the glacier and the firn line. No such measurements, however, have been made.

---

* Publication No. 1 of the Jungfraujoch Research Party, 1938.

Finally, it need scarcely be emphasized that any mechanism which consists largely of an increase of the average volume of the single ice crystal cannot be understood without following the changes in the crystals themselves. Such an examination has never been carried out in any detail.

(*b*) *Stratification bands*

Two varieties of stratification bands have been observed in the *névé* area. First the annual or dirt bands which consist of a deposit of fine rock dust spread over the glacier by the wind. They form in the late summer when the mountains are comparatively bare of snow. They are very convenient for estimating the age of any stratum of firn (fig. 1, Plate 16). The ice bands which represent the second variety are thin strata of clear ice extending over considerable areas through the *névé* (fig. 2, Plate 16). A formation resembling the ice bands also exists in the glacier tongue, where bands of clear, air-free ice alternate with thicker bands of ice containing air bubbles. These are called blue bands (fig. 11, Plate 19). The origin of the ice bands and the question of their continuity with the blue bands have been the subjects of much discussion.

(c) *Glacier flow*

The maximum velocities of the larger Alpine glaciers vary between 80 and 150 m. a year. Several glaciers, notably the Rhône Glacier and the Hintereisferner, have been accurately measured for long periods, and a large amount of reliable data relating to their movements has been collected. These observations have established that the flow of glaciers resembles that of highly viscous fluids, that is to say they flow faster at the centre than at the sides and faster at the surface than in the interior. This is known as differential movement. While the rate of differential movement has been measured in several glaciers, its internal mechanism has been, and still is, one of the most controversial subjects in glaciology. Two opponent and apparently irreconcilable views are prevalent throughout the literature. While one school of thought (Philipp 1920; Chamberlin 1928) maintains that the differential movement proceeds through the spasmodic motion of rigid masses over large thrust planes (laminar motion*), the other believes that glaciers are plastic and move through non-laminar and continuous deformation (Hess 1933; von Engeln 1934). The first group regards all stratification bands as remnants of former thrust planes, whereas the other adheres to the view that they are of entirely sedimentary origin. Amongst the second group, opinions diverge again as to the mechanism of plastic deformation; some workers assume crystal growth by molecular exchange across the crystal boundaries and glide along the basal planes of the crystals to be the essential factors, while others attribute more importance to the motion of the crystals past one another. (For more detailed accounts of the different views see Visser (1938) or von Engeln (1934).)

In most cases the experimental material offered in support of these theories is very incomplete and far from convincing: first, because detailed and precise strain measurements were not taken; second, because no attempt was made to study the crystal texture of glacier ice; and third, because investigators approached the glaciers from their tongues and made their way upwards, commencing as it were at the end of the process of glacier formation. To us the most promising approach to the problem appeared to be a thorough investigation of a glacier from its origin down to the snout, in this way tracing the phenomena in their correct sequence. We proposed to apply the standard methods of optical crystallography in conjunction with direct measurements of the differential movement and observations of the origin of the banding.

---

* Throughout this paper the terms laminar and non-laminar motion are meant to describe macroscopic phenomena only. While laminar motion implies the existence of large-scale thrust planes, the term non-laminar motion is merely applied to cases where such thrust planes are absent, but does not preclude the occurrence of local thrusts on a small scale or glide within the single crystals.

We hoped to overcome the technical difficulties which had hitherto proved an obstacle to a research of this nature by using the scientific station on the Jungfraujoch as our base of operations. Being situated at the source of the Great Aletsch Glacier, the largest ice stream in the Alps, this station offers ideal facilities for work on glaciological problems.

(*d*) *Programme of research*

It was decided to undertake a programme of research of which the following were the principal items:

(1) The measurement of temperature distribution to the lowest possible depth in the *névé* area.

(2) The tracing of the transition of firn into glacier ice by determining the distribution of specific gravity with depth at a series of points between the firn line and the source of the glacier.

(3) The carrying out of various experiments to decide the relative importance of melting and compression (settling) in the development of glacier ice.

(4) The study of glacier structure and the mechanism of glacier flow by extensive crystallographic observations.

(5) An investigation of the origin of the ice and blue bands and their possible relationship to the mechanism of flow.

Only items (4) and (5) will be dealt with in this paper; the researches on the other problems will be described elsewhere in separate publications (T. P. Hughes, M. F. Perutz and G. Seligman (1939), T. P. Hughes and G. Seligman (1939)).

2. INSTRUMENTS AND METHODS

Collection of samples

The samples for the crystallographic examinations were taken either from the walls of crevasses or from ice grottoes and pits which were dug in the glacier.

The deepest of the crevasses found on the Mönch- and Jungfrau firn reached 28 m., the rest seldom exceeded 20 m. Rope ladders were used for descending into them and served as a support to the operator when cutting samples from the walls. Generally, a layer about 40 cm. thick had to be removed from the surface of the wall before a sample could be taken, since conditions on exposed surfaces are generally disturbed by weathering. A square block was then hewn out and its orientation in the glacier marked with a saw cut. The sample was immediately placed in a Dewar flask cooled with solid CO_2 and was carried up to the Jungfraujoch on the same day. A chamber excavated in the stationary ice on the Jungfraujoch itself served as a cold laboratory maintaining a fairly constant temperature of $-4°$ C throughout the summer.

Cutting the sections

In the laboratory one portion of the sample was used for the determination of specific gravity, the other was cut down to a cube of about 1·5 cm. and cooled to the temperature of solid CO_2. One face of the cube was then ground flat on glass paper and polishing paper. The cube was then allowed to reach room temperature, after which it was melted on to a microscope slide. The slide was clamped on to the stage of a section cutting machine.* This machine was devised to cut thin sections of ice by means of a mechanically driven fret-saw (for description see Bader 1939). The thickness of the sections could be varied between 0·2 and 5 mm. During the cutting the ice block had to be cooled by solid CO_2. The finished section was again ground flat and polished to remove any saw marks, and finally a cover-slip was melted on to it. Sections so made can be kept indefinitely if the space between the slide and the edge of the cover-slip is filled with vaseline to prevent evaporation.

The largest section the machine would cut was 4 $cm.^2$, so that if the crystals were very large too few of them appeared in the section to give a proper impression of the general texture of the sample. Therefore it was found necessary to prepare sections by hand when the individual crystals measured more than 5 mm. across. In that case the section had to be ground on glass paper. Sections about 5 cm. square and 1 mm. thick were fashioned in this manner, but the process proved to be very laborious because the samples had to be cooled for half an hour after grinding for only 1 min. Besides this thermal tensions in the ice often produced cracks which caused the section to break up.

---

* This machine was lent to the party by the courtesy of the Swiss Snow and Avalanche Commission in Davos.

Crystallographic examination

The general texture of the sections was examined under a polarising enlarging apparatus specially constructed to obtain a large field of view. The apparatus consisted of a mirror, two Polaroid plates, 5 cm. in diameter, a copper stage which could be cooled, an enlarging lens and camera. All components slid on a common rail and could be removed separately. The apparatus was used mainly for photographing the thin sections in polarized light.

A polarizing microscope fitted with a mechanical stage was employed for the determination of the crystal orientation. Generally between 50 and 100 crystals were examined in each section. In order to avoid arbitrary selection either the axial position of all the crystals in the section or in one part of the section were determined. The path difference was measured with a Berek compensator; the inclination of the hexagonal axis was found by means of a chart relating the double refraction with the axial inclination of ice. The absolute position of the axis was determined conoscopically.

The accuracy of the optical method proved satisfactory in sections which were thicker than 0·3 mm. Any axial inclinations of over 5° from the vertical could be determined with the compensator; if the angle was less it was estimated by conoscopic examination. The thickness of a section was measured either by focusing first on its lower and then on its upper surface, or, more accurately, by comparison between the optic image and the compensator reading in the following manner: the thin sections generally contained crystals with their hexagonal axes parallel to the plane of the section; these could be recognised by their optic image and their thickness calculated from the compensator reading and the known double refraction of ice. The axial positions of the crystals in each section were plotted on a stereographic projection.*

3. THE FIRN REGION

(*a*) *The transition of firn into glacier ice; firnification*

Firn forms from fallen snow during the spring and summer mainly by the process of melting and refreezing and that of settling.† Its consistency is quite different from that of powdery fresh or old winter snow. The single crystals are several times larger and are normally compacted into a mass which becomes loosened when the sun shines, only to freeze again at night. Since the whole winter accumulation of snow on Alpine glaciers is turned into firn during the summer the latter represents a most important intermediate stage in the transformation of snow into ice.

---

* The method of cutting thin sections and a modification of the optical method were used by the Swiss Avalanche Commission for investigating the properties of snow and are described in detail by H. Bader (1939).

† The relative influence of settling and melting is described elsewhere by Hughes, another member of our party and one of the authors (G. S.) (Hughes and Seligman 1939).

The properties of newly fallen snow and the changes which it undergoes under different weather conditions had been the theme of investigations by one of the authors and by the Swiss Snow and Avalanche Commission (Seligman 1936; Bader 1939; Haefeli 1939) and lay outside the scope of our experiments which were primarily concerned with the transition of firn into glacier ice.

Definitions of firn and ice.

Based on our measurements of specific gravities and our observation of the characteristics of firn and glacier ice we define the former as an aggregate of ice crystals penetrated by intercommunicating air spaces and glacier ice as an aggregate of ice crystals without intercommunicating air spaces. This means that firn is to a greater or smaller extent porous and ice nonporous. As a rule the critical density at which intercommunicating air ceased to exist was found to vary between 0·82 and 0·84.

Structure of firn and ice.

The first two samples for crystallographic examination were taken from the surface of the glacier immediately above and below the firn line. Figs. 3 and 4 (Plate 17) show photomicrographs between crossed nicols of the thin sections cut from these samples. The fundamentally different character of firn and ice is evident from these pictures. In contrast to the small regular grains and the multitude of air spaces, most of them intercommunicating in the firn, the ice shows large irregular crystals with relatively few small air bubbles all well separated from each other.

Orientation of crystals in firn and ice.

A stereogram (diagram 1) illustrates the results of the crystallographic analysis of the firn section. Each circle in the stereogram represents the projection of the hexagonal axis of one crystal in the section. The equatorial plane of the stereogram is parallel to the surface of the glacier. Therefore all axes which are normal to the glacier surface have their projection at the centre of the stereogram. The angles enclosed by the axes and the normal to the surface correspond in the stereogram to the distances of the projections from the centre, all axes in positions parallel to the surface having their projections on the circumference of the circle. It is seen at once from the stereogram that the distribution of axial positions in the firn is not a random one. A large percentage of the projections is grouped round the centre, corresponding to crystal axes normal to the glacier surface. It was soon realised that this effect was not a local one confined to the neighbourhood of the firn line, but that samples of firn from all parts of the glacier showed similar orientation. To explain this phenomenon several possibilities had to be taken into consideration:

(1) The process of grinding and cutting of the sections might have caused a reorientation of the crystals.

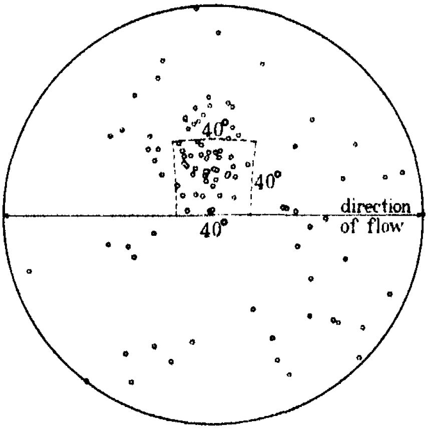

Diagram 1. Stereogram of firn taken from immediately above the firn line on the Mönchfirn. Each circle represents the projection of the hexagonal axis of one crystal in the section. The equatorial plane of the stereogram should be parallel to the surface of the glacier; the shift of the peak from the centre is due to an inaccuracy in the cutting of the section. 100 crystals. (See also fig. 3, Plate 17.)

(2) A proportion of the flakes of falling snow consists of plates and flat dendrites. These might have settled with their flat faces parallel to the surface, such orientation being preserved in the firn.

(3) The differential movement of the glacier might have favoured the growth of crystals in certain orientations.

(4) It has been commonly observed that ice crystals solidify with their main axes parallel to the direction of the temperature gradient. The crystals of pond ice provide the best example, but there are several others, for instance the crystal axes in icicles are vertical at first but, as the icicle grows in thickness and freezing proceeds from the sides, the axes of the new crystals assume horizontal positions pointing towards the direction of maximum temperature gradient. The crystals grown from water vapour,

such as crevasse hoar or depth hoar, invariably develop in similar orientation.

(1) We were able to prove conclusively that the preparation of the thin section had no influence on the orientation of the crystals. These maintained their orientation at whichever angle to the glacier surface the section was cut.

(2) The only direct test concerning the second assumption would have been, of course, a crystallographic examination of fallen snow. Neither Bader nor one of the present writers (M. F. P.) has succeeded, however, in securing a section of this loose, fluffy material. It can, however, be inferred from other evidence that the initial orientation of fallen snow cannot be of great importance. Only a relatively small proportion of it consists of plates and of these many are broken by the wind; therefore the number settling on their flat sides would be comparatively small. Moreover, the conditions of turbulence accompanying most snowfalls at high altitudes should in themselves preclude any settling of the grains other than in haphazard orientation. Again, old firn generally showed more orientation than new, while the opposite effect would have been expected if the orientation had had its origin in newly fallen snow.

(3) If differential movement had been the cause of the orientation the crystals should have been orientated at random where differential movement was absent. A sample of firn was therefore taken from 100 cm. below the surface of a flat snowfield close to the Jungfraujoch where the differential, and in fact all, movement was either completely absent or negligibly small. Here the crystals in the firn as well as in the ice underneath showed the same orientation as everywhere else in the glacier.

(4) Consequently we may argue that the orientation of the crystals in the firn is dependent on the direction of the temperature gradient and this theory has been confirmed by many of our subsequent observations. The phenomenon appears to be of universal importance in the recrystallisation of ice and can be explained as follows: Tammann and Dreyer (1929) observed the changes which occur in a thin section of ice prepared by rolling snow in a small rolling mill and found that it was not the relative size which determined the growth of some crystals at the expense of others, but their relative orientation. They showed that the crystals incorporated new basal planes faster than prismatic or pyramidal planes and that in consequence the former grew at the expense of the prismatic and pyramidal planes of neighbouring crystals. They attributed the migration of molecules from one lattice to another to the closer packing of atoms in the basal planes. It is obvious that under the conditions of recrystallization prevalent

in snow and firn the direction of fastest growth, which Tammann and Dreyer found to coincide with the hexagonal axis, must also lie parallel to the temperature gradient. Accordingly, the perfection of the orientation in firn depends mainly on the number of times recrystallisation by sublimation or by melting and refreezing has been repeated. The orientation is destroyed by the differential movement of the glacier, as described below, and therefore best developed in flat stationary firn fields.

Our next step was to examine conditions in the interior of the glacier. The best results were obtained from a crevasse at an altitude of 3330 m. which had a depth of 28 m. Three samples were taken: one at 8 m. below the surface (age 2 years, specific gravity 0·63), another at 14 m. (age 3 years, specific gravity 0·72) and the third at 23 m. (age 6 years, specific gravity 0·80). No photomicrograph of the first sample is shown because a typical example of firn near the surface has already been given (fig. 3, Plate 17). The photographs of the other two samples illustrate the metamorphoses of the firn (figs. 5, 6, Plate 17). It can be seen that little alteration in the size and shape of the crystals has taken place, while the air spaces have undergone important changes. At 14 m. they are intercommunicating channels offering little resistance to the percolation of melt water through the firn. At 23 m. they have decreased in number and are now well separated from each other; water can no longer flow through them—in other words the firn has turned into glacier ice. Diagrams 2–4

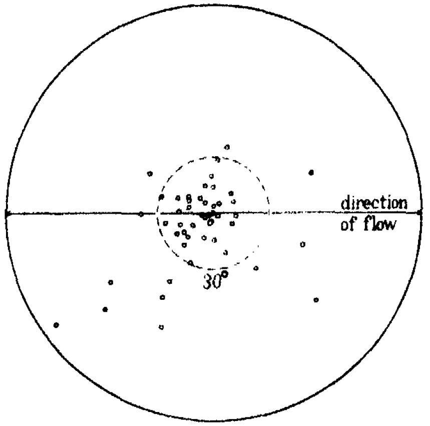

Diagram 2. Firn from a crevasse in the Mönchfirn. Altitude 3330 m., depth 8 m., specific gravity 0·63, age 2 years. Equatorial plane parallel to the glacier surface. 50 crystals.

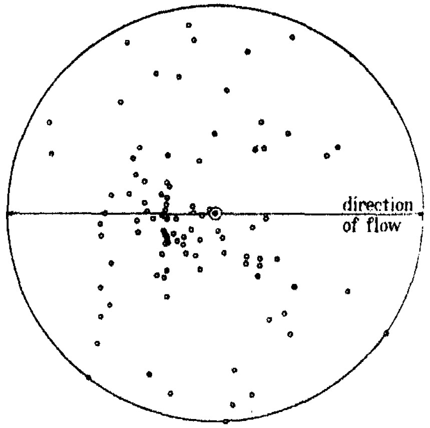

Diagram 3. Firn from the same crevasse. Depth 14 m., specific gravity 0·72, age 3 years. Equatorial plane parallel to the glacier surface. 100 crystals. (See also fig. 5, Plate 17.)

show the stereograms prepared from the sections of these samples. At 8 m. the crystals are orientated similarly to those in the firn near the firn line on the glacier surface. At 14 m. a certain amount of scattering from the vertical position is noticeable. At 23 m. the aspect has changed entirely. Only a few clusters of crystals have retained their axial positions near the vertical line, while the others are scattered over almost all possible angles.

This transition from order to disorder with increasing depth was also observed in other crevasses at lower altitudes. They were not as deep as the first one, but owing to the smaller surplus of accumulation of snow the annual layers lay closer together, so that the ages of the samples were approximately similar to those taken from the first crevasse. Conditions, however, were never as simple again, as the ice in all the other crevasses had already passed through crevassed areas where disturbances had altered the original orientation of the strata. Under these circumstances it was, of course, difficult to decide whether or not any catastrophic events such as the bending or breaking of large masses had altered the crystal orientation. The first crevasse, on the other hand, was one of the uppermost on the glacier, and it could easily be seen from its position that none of the firn or ice in it could have passed through any previous crevassed areas.

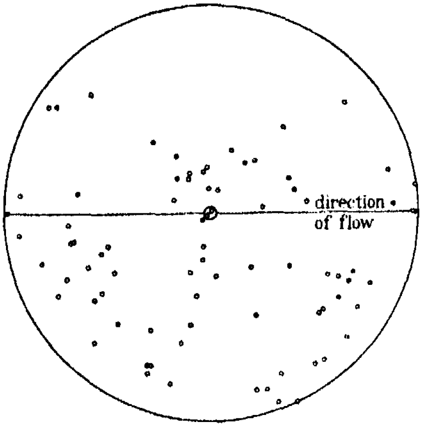

DIAGRAM 4. Ice from the same crevasse. Depth 23 m., specific gravity 0·80, age 6 years. Equatorial plane parallel to the glacier surface. 79 crystals. (See also fig. 6, Plate 17.)

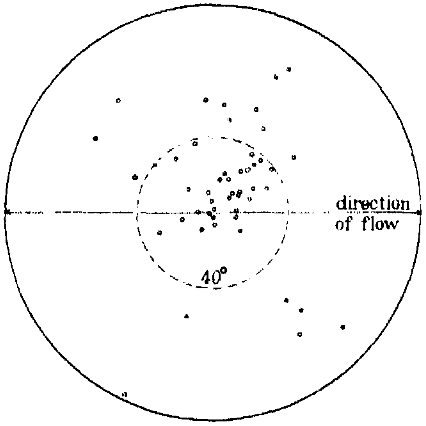

DIAGRAM 5. Ice-band from the same crevasse. Depth 22·8 m., specific gravity 0·9, age 6 years. Equatorial plane parallel to the plane of the ice-band. 50 crystals.

Liquid film of brine.

Von Engeln suggested that glaciers owe their plasticity to relative movements of the crystals which are facilitated by the presence of a liquid film of brine at the crystal boundaries (von Engeln 1934). It was therefore desirable to test whether such a film could be detected. No impurities could, however, be discovered by the method used by Tammann who observed a residue of NaCl crystals after a thin section of ice had evaporated from a slide (Tammann and Dreyer 1929). Later Hughes made an experiment to see whether ice from 23 m. depth (altitude 3330 m.) contained impurities in sufficient quantity to cause a depression of the melting point detectable by a Beckmann thermometer. Two consecutive experiments, one of them carried out with ice from an annual band, yielded negative results, although the method allowed for the detection of 0·004 % NaCl and 0·008 % NH_4NO_3 respectively.

(*b*) *The structure and origin of the ice bands and their relationship to differential movement in the glacier*

Structure of ice bands.

The cross-section of an ice band in its earliest stage is shown in fig. 7 (Plate 17) which represents a vertical section cut through a crust about 2 mm. thick embedded in firn. The crystals of the crust are larger and enclose fewer air spaces than those of the firn. The crystal texture of ice bands was found to be identical with that of pond ice, the vertical orientation of the hexagonal axes prevalent in the firn being very strongly accentuated in the bands. In contrast to the firn the orientation of the crystals in the ice bands does not depend upon the depth, as is shown by the following experiment: a sample of an ice band was taken from a depth of 23 m., 20 cm. away from that of the ice of diagram 4. A thin section was cut parallel to the surface of the band. The stereogram (diagram 5) illustrates well the difference between its structure and that of the ordinary ice next to it (diagram 4). The crystals have largely retained the original orientation of the axes perpendicular to the surface of the band.

As the structure of the ice bands conformed with that of pond ice it was easy to suppose that they had originated in a stratum of water in the firn. This was confirmed by the following facts: it was often observed that ice bands started to grow in very large numbers on the walls of pits dug in the glacier. These bands did not extend for more than 30 cm. inwards and when removed during warm summer weather with positive day air temperatures revealed behind them a layer of firn soaked with water. The layers lay deep enough below the surface to be outside the range of diurnal temperature variations and had frozen when the existence of the pit enabled the low night temperatures to reach them. The bands apparently develop at levels where melt water is either held up by a crust or by a particularly fine grained layer of firn of high capillarity. They freeze into bands of clear ice when a wave of low temperature from the surface reaches them.

Possible causes of ice bands.

The origin of the bands has persistently been connected with differential movement in the glacier stream. This is supposed to proceed by a series of slips in certain selected planes and to be the source of melt water produced by frictional heat. The water in its turn is believed to act as lubricant as long as the movement lasts and to freeze as soon as it stops, thereby forming an ice band in the former slip plane (Philipp 1920). It was therefore decided to investigate whether any such slip planes could be detected and, if so, whether they would give rise to the development of ice bands. Finally, it had to be considered whether the total differential movement was sufficient to produce the quantity of frictional heat necessary for the melting.

Differential movement in the Sphinx Crevasse.

A device for measuring the differential movement was constructed in a crevasse (which we called the Sphinx Crevasse) near the source of the Mönchfirn at an altitude of 3475 m.

A large vertical groove was cut into the lower wall of the crevasse to a depth of 8 m. Bridging the top of the crevasse a long pole was firmly fixed in a horizontal position and a plumb-line suspended from it down the vertical wall of the groove. A number of wooden pegs were driven into the wall down the line allowing the distance of the line relative to each peg to be measured with an accuracy of ± 1·0 mm. Notwithstanding the destruction of our apparatus by an avalanche shortly after the experiment had come into operation, we had fortunately by that time ascertained that the differential movement was of the order of magnitude of 1 mm. per 1 m. depth per day, showing that firn travelled one millimetre faster at the surface than a metre below, and so on. The inclination of the slope was 35° and the total movement at the surface of the glacier at this point was about 5 cm. per day.

Differential movement in No. 2 auxiliary pit on the Mönchfirn.[*]

A similar arrangement was set up in a large pit which had been dug on the Mönchfirn at an altitude of 3460 m. and which was called the No. 2 auxiliary pit. The wooden pegs were here replaced by a vertical line of pins which offered two distinct advantages (fig. 8, Plate 18). First, readings could be taken more accurately and second, the pins could be placed so close together as to allow for the detection of small irregularities in the movement. The pin line was 221 cm. long and the pins were pushed in up to their heads about 1 cm. apart. The average differential movement in 39 days was found to be 0·35 mm. per 1 m. depth per day (± 0·02 mm.). The inclination of the glacier was 8° and the total movement at the surface about 7 cm. per day.

Owing to the known existence of differential movement, it might have been expected that the line of pins would have canted, at the same time preserving its linear arrangement. Quite a different result presented itself. Within two days distinct irregularities in the line could be seen. Some pins were moving faster than their neighbours (see fig. 8). As they were firmly imprisoned in the firn this can only have meant that certain units of firn were moving faster than others. As soon as this was noticed a second plumb-line of pins and then a third and a fourth were stuck in at equal levels at intervals of about 5 cm. If movement by layers were taking place, these auxiliary lines would show pin movements corresponding to those in the main line. Examination of fig. 9 (Plate 18) shows that this is not the case.

Later a network of pins consisting of both horizontal and vertical lines was added. This showed that only large scale distortions were shared by more than one or two vertical lines of pins and no common trend in the displacement of pins at equal levels could be detected.

It was also noticed that pins, which had originally been driven straight into the wall, later protruded from it at different angles. Only pins which had been stuck into ice bands retained their true horizontal position. Figs. 8 and 9 show the network and part of the lines of pins early on in the experiment and near its close.

It can therefore be asserted that no slip by layers in the upper portions of the *névé* is observable. The implications of this experiment in connexion with the mechanism of flow will be discussed below.

---

[*] This experiment is described in greater detail elsewhere (Hughes, Perutz and Seligman 1939).

Heat produced by the differential movement.

Even if the outcome of these experiments indicates that there is no relation between the formation of bands and the differential movement it may be useful to calculate whether the mechanism suggested by Philipp would be physically possible. Let us suppose that an ice band of 5 mm. thickness develops 100 cm. below the glacier surface in firn of specific gravity 0·55, then 0·19 c.c. of water will be needed to fill the air spaces in ½ c.c. of this firn. The heat required for melting a corresponding quantity of ice will be 15 cal., provided the temperature of the firn is at the melting point. It might be assumed as an idealized case that the total potential energy which the firn loses in travelling down the glacier is converted into frictional heat and liberated in an imaginary slip plane. Then the work (A) done by a column of firn 100 cm. high and 1 cm. square, moving at the rate of v cm. per year over a slope inclined at $\alpha°$, is given by the equation

$$A = 0{\cdot}55\,.\,100vg\sin\alpha.$$

Taking the slopes near the Sphinx Crevasse and the pit as bases for the calculations, the annual production of heat is 0·67 and 0·23 cal. respectively. This means that it would take 11 and 33 years respectively to melt the quantity of water necessary for the formation of an ice band of the thickness of 5 mm. It should be added that ice bands were more frequent in No. 2 auxiliary pit than in the Sphinx Crevasse although the differential movement was faster in the latter.

These considerations leave little doubt that the ice bands are of purely sedimentary origin.

(*c*) *Mechanism of flow in the névé region*

The experiments described in the foregoing pages proved that no laminar motion over large scale thrust planes takes place. The differential motion was found to be of the nature of a non-laminar deformation. In considering the internal mechanism of this deformation the following facts have to be taken into account:

(1) The small difference between the average sizes of the single crystals in firn of medium and very low depth, as illustrated by the photomicrographs. This suggests that no recrystallization by the formation of new crystal nuclei or growth of one portion of the crystals at the expense of their neighbours takes place after the crystals have passed the initial stages of firnification and that the actual age of the crystals in any given sample is not much less than the age of the sample as indicated by the number of annual bands which separate it from the surface.

(2) The change in crystal texture with increasing depth shown by the stereograms. As we have seen, the initial orientation of the crystal axes perpendicular to the glacier surface gradually gives way to a random distribution, whereas the orientation of the crystals in the ice bands remains unchanged. It was concluded from these results that in the firn where the crystals are in relatively loose contact owing to the large amount of enclosed air, single crystals or clusters of single crystals can turn round, move independently and thereby alter their relative orientation. In the ice bands, on the other hand, the crystals preserve their orientation because independent movements are prevented by their dense packing.

(3) The displacement of the pins from the vertical line in the experiment on the Mönchfirn confirmed this view. There can be no doubt that the pins were displaced and tilted by genuine movements of the crystals around them and not by melting or other disturbances caused by the pins themselves. Hence the small and irregular shifts of the pins must have been due to the haphazard motion of small units in a large mass which is subjected to strain.

The mechanism of settling—the sinking together of the firn under its own weight—appears to be intimately connected with that of the differential movement, as the continuous rearrangement of the small units must also cause them to become more closely compacted.

4. THE ICE REGION

(a) *Experiments*

Crystal orientation of ice under stress.

(i) *Grotto in ice apron.* We found a good example of non-laminar distortion in an old ice grotto which communicated with our cold laboratory. Both the grotto and our laboratory had been excavated in an apron of glassy ice frozen to the steep rock ridge above the bergschrund at the source of the Great Aletsch Glacier. The grotto had been built as an attraction for tourists in 1917 and had been out of use for some years. Its air temperature was −4° C. The roof of the grotto was supported by two large columns which, according to the guide who had excavated them, had been hewn out of the ice vertically and had become deformed by the creep of the ice until they had reached the shape shown in fig. 10 (Plate 19). Diagram 6 illustrates the position of one of the columns in relation to the slope and the direction of creep of the ice apron. The rate of deformation of the column was measured for two months with a simple compression meter, one end of which rested against the rock bed underneath the grotto and the other against the top of the column. Under the assumption that the rate of movement remains uniform throughout the year, it was calculated to be 6·3 cm. per annum. In the diagram, the x- and y-axes are parallel to the surface of the ice apron, the former being parallel and the latter normal to the direction of flow. The z-axis is perpendicular to the surface of the ice apron.

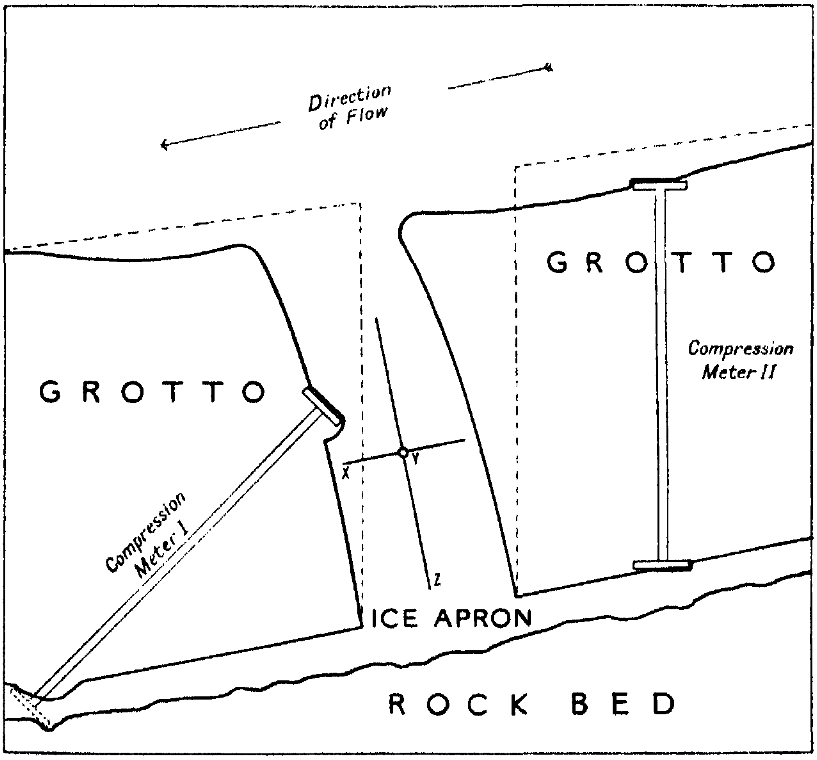

Diagram 6. Distortion of column in ice grotto. The dotted lines represent the positions of the column and the roof after the grotto had been excavated in 1917. The lines drawn in full show the column and roof as in 1938. Distance from floor to roof approximately 2 m.

Several thin sections were cut from the ice in this column. It was found that most of the crystals examined were orientated with their main axes parallel to the z-axis. The others showed deviations up to 30° from this position. These deviations, however, were strictly limited to the yz-plane. Thus the basal planes of the crystals all lay parallel to the direction of flow (x-axis), but not to the surface of the ice apron (xy-plane). The results obtained from this locality have not been tabulated in a stereogram since each section contained but a few crystals and was cut from a different part of the column.

The next step was to ascertain whether the orientation of the crystals in the columns had originally developed on the surface of the ice apron and had remained unchanged ever since or whether it was due to the effect of strain on an aggregate of crystals of a different or even random orientation. Therefore a sample of ice was cut from the surface of the steep slope above the grotto where the ice of the columns must have originated. A stereogram (diagram 7) shows that the crystals were largely orientated at random, the usual orientation of the axes parallel to the direction of the temperature gradient being absent, apparently owing to the steepness of the slope and its exposure to violent winds which disturb normal conditions of crystal growth. Therefore the orientation in the columns must have developed in the interior of this small body of ice under the influence of strain. The process must have taken place at temperatures below freezing-point, since, according to measurements carried out in August, the temperature in the interior of this ice apron was negative from the surface downwards.

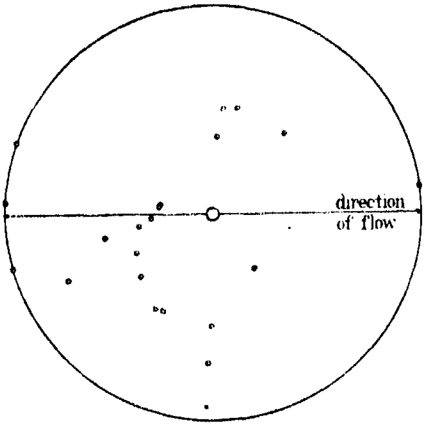

Diagram 7. Ice from the surface of the slope above the cold laboratory on the Jungfraujoch. Equatorial plane parallel to the glacier surface. Section ground by hand. 21 crystals.

(ii) *Grotto in glacier ice.* The second experiment was carried out in an ice grotto in the Eigergletscher at an altitude of 2300 m., where the temperature of the ice was, of course, at the melting-point. Here a device for measuring the differential movement similar to that in the pit on the Mönchfirn was set up. As pins did not remain fixed in the ice, screws were used instead (fig. 11, Plate 19). A diagrammatic representation of the displacement of the screws from the plumb line after 14 days is given in diagram 8. It is seen that the upper screws (1–21) remained stationary, that a maximum displacement of 3·5 mm. occurred between screws 21 and 22 and that below screw 22 the displacement was proceeding fairly uniformly at the average rate of 0·78 mm. per metre per day. A peculiar blue band crossed the line of screws at screw 22; it can be seen in the photograph; it enclosed an angle of about 20° with the other blue bands which were parallel to each other. It was also noticed that all the air bubbles in the walls of the grotto had the shape of flat ellipsoids whose equatorial plane was parallel to the plane of the slanting blue band. Above the band a crack about 1 mm. wide was to be seen which, on closer inspection, was found to consist of very large air bubbles separated from each other and squeezed flatter than the bubbles elsewhere. The crystals in the band were rather larger than those in the adjacent ice.

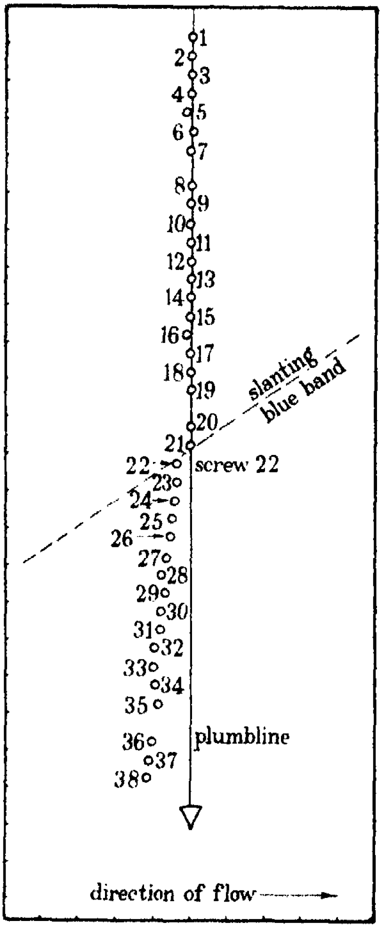

Diagram 8. Displacement of the screws from the plumb line after fourteen days. Horizontal scale: 1 division = 1 cm. Vertical scale: 1 division = 5 cm.

It was evident from the displacement of the screws and the flattened air bubbles that the latter and single band were parallel to a plane of shear. The ice above screw 22 was being carried bodily over the band, which acted as a thrust plane, and was exercising a drag on the ice below, which yielded by plastic non-laminar deformation. Since the air bubbles were mostly intracrystalline, their flattening into ellipsoids also implied that deformation of the single crystals had taken place. The system of parallel blue bands seen in the photograph probably represents the original sedimentary stratification of the ice, while the single band which crosses them appears to be of tectonic origin.* The large size of the single crystals, the concentration of air bubbles above the band and the displacement of the screws point to the conclusion that this single band owes its development to an increased rate of crystal growth caused by shear in a certain layer. During the process the air bubbles contained in it must have been pushed out and concentrated above the band.

---

* Bands of sedimentary origin can never cross each other since they all develop parallel to the glacier surface.

A thin section of ice from the band was cut by hand. The crystals were abnormally large in the plane of the band and five out of the six crystals contained in the section had their basal planes parallel or nearly parallel to the plane of the band. Unfortunately time did not permit the cutting of any more sections from this interesting locality.

Common orientation of the crystals was also found in various other places on glacier tongues. No special significance could, however, be assigned to any of these results as the local strains were not known and the causes of the orientation could not be ascertained. It was not possible to investigate conditions in the ablation area as thoroughly as those in the firn region because the experiments in the latter had occupied most of the four months during which this research had to be carried out and each measurement of the differential movement took several weeks before definite results could be obtained.

(*b*) *Mechanism of flow in the ice region and the origin of the bands*

Conclusions.

The mechanism of flow in the ablation area is different from that in the firn region. In the latter non-laminar flow alone was found to be of importance, while in the ice area laminar and non-laminar flow appear to occur side by side.

The mechanism of non-laminar motion also undergoes substantial changes as the haphazard motion of single crystals or clusters of crystals can no longer function owing to the dense packing and the complex shape of the crystals. In explaining the mechanism of non-laminar motion in the ice region, the following facts have to be taken into account:

(1) The random crystal orientation which characterizes the deepest layers of firn is again transformed into an orderly arrangement. In one case (grotto in ice apron) the main axes lay in a plane perpendicular to the direction of flow. In glacier tongues it was ascertained that the crystals undergo plastic deformation and that there exists a general tendency for them to lie with their basal planes parallel to planes of shear.

(2) No evidence of mechanical twinning or the formation of new crystal nuclei could be found.

(3) The average size of the single crystal increases with the length of the glacier. In Alpine glaciers crystals may reach diameters up to 10 cm., while from Greenland glaciers single crystals as large as melons have been reported.

(4) Bader (1939), in a preliminary study of the mechanical properties of ice, found that in a block of ice of random crystal orientation which was being subjected to shear, the majority of the crystals became orientated with their hexagonal axes parallel to a plane which was parallel to the direction and normal to the plane of shear. The process, carried out in the neighbourhood of – 5° C, was accompanied or followed by an increase in the average size of the single crystals. No formation of new crystal nuclei or twinning was observed, but merely growth of some crystals in favoured orientations at the expense of their neighbours.

These facts show that the effect of the differential flow on glacier ice is to some extent analogous to the influence of rolling on a multicrystalline sheet of a metal of hexagonal symmetry. In magnesium, for instance, cold rolling produces a reorientation of the axes relative to the crystal boundaries which is caused by glide along the basal planes and results in an orientation of the basal planes parallel to the plane of the sheet (Schmidt and Wassermann 1930). If the rolled sheet is heated to a high temperature for a short period, recrystallisation sets in, i.e. new crystal nuclei form in regions of high internal stress and grow at the expense of existing ones. If the heating is sufficiently prolonged, a process of crystal growth occurs which generally results in an increase of the average size of the single crystals.

The orientation of the ice crystals under conditions of strain mentioned in points 1 and 4 is in good agreement with the phenomena observed in cold worked metals and it is therefore reasonable to suppose that the reorientation of the ice crystals is due to a mechanism similar to that occurring in metals. The absence of mechanical twinning, in particular, suggests the analogy with magnesium. A discrepancy, which we have so far been unable to explain, is presented by the orientation of the crystals in the ice column in the grotto. While in this grotto the crystal axes all lay in the plane *normal to the direction of deformation* (xz-plane), the axes in Bader and Haefeli's experiment and in rolled sheets magnesium lie in a plane which is normal to the plane of shear (viz. of the sheet) and *parallel to the direction of deformation*. It may be possible, however, that a more precise knowledge of the strain in the column would have furnished us with an explanation of this result.

It is also difficult to account for the growth of crystals in glacier tongues to sizes which are unusually large as compared with those observed in deformed metals and rocks and, on the other hand, for the absence of recrystallization by the formation of new crystal nuclei as exemplified by the complete absence of crystals under 5 mm. in diameter. As a working hypothesis it may be suggested that differences in the energy content of neighbouring crystals are responsible for the growth. It would appear that crystals whose orientation allows them to yield to shearing forces by glide along the basal planes are subjected to a relatively smaller stress than other crystals in a different orientation which cannot yield. The former would thus possess less free energy than the latter and therefore would have a tendency to grow at the latter's expense by the transfer of molecules across the crystal boundaries. In considering the absence of recrystallization on the other hand, it must be borne in mind that the temperature of the whole of the ice region is always at the pressure melting point and that high local stresses, which at lower temperatures might favour the formation of new crystal nuclei, would here cause melting to take place instead.

Blue bands.

The problem of laminar motion is intimately connected with that of the blue bands and the question of their continuity with the ice bands in the firn region. We distinguished three types of blue bands in the glacier tongue: first, those which are of sedimentary origin and represent the survivors of the ice bands in the *névé* area; second, those which are the traces of closed cracks and crevasses; and third, those which develop in the ice and are caused by shear in thrust planes. There can be no doubt that the ice bands from the *névé* region survive for a considerable period in all parts of the glacier tongue and are continuous with at least part of the blue bands. Observers such as H. F. Reid (1903) followed the stratification bands in the firn right down to the ends of glaciers in the Alps. We noted that the appearance and frequency of ice bands in the lower parts of crevasses of the firn region differ in no respect from those of the blue bands in the tongue.

The second variety of blue band can be of no particular importance in the mechanism of flow, since cracks and crevasses rarely reach far below the surface and their traces soon disappear owing to ablation. An example of the third variety was seen in the ice grotto on the Eigergletscher. It did not seem probable, however, that this band could have developed from a crack in which the ice crystals had become crushed and mixed with water, a mechanism which Philipp imagines to take place (1920). It appeared rather as though abnormal strain had accelerated recrystallization in a certain layer and caused reorientation of the crystals and removal of the air bubbles. The differential motion in the thrust plane itself must have been more in the nature of creep accompanied by crystal growth and deformation than of spasmodic motion such as that described by Chamberlin.*

The work of the Jungfraujoch Research Party was largely financed by the grant of a Leverhulme Fellowship to one of the authors (G. S.) and by grants from the Ski Club of Great Britain, the Royal Geographical Society and the Alpine Ski Club. To these bodies we extend our grateful thanks.

Our thanks also are due to Herr Liechti, Chairman of the Jungfrau Railway and to Professor A. von Muralt, Director of the Jungfraujoch Scientific Station, for the facilities they provided and the many kindnesses which they showed us. We also desire to express our gratitude to Professor C. E. Tilley, F.R.S., for the loan of a polarizing microscope from the Department of Mineralogy in Cambridge, to the Swiss Snow and Avalanche Commission for the section cutting machine which they kindly put at our disposal and to Dr H. Bader, Professor J. D. Bernal, F.R.S., and Dr F. P. Bowden for their advice and collaboration in planning this research. We are also greatly indebted to Dr H. Bader and Dr R. Haefeli for the hospitality and helpful instruction given us during visits to the Snow and Avalanche Research Station on the Weissfluhjoch, Davos.

5. SUMMARY

The mechanism of glacier flow and the transformation of firn into glacier ice were investigated on the Great Aletsch Glacier and in neighbouring regions. Samples of firn or ice were taken from the walls of crevasses and from grottoes and pits dug in the glaciers. Thin sections were cut from these samples and examined by the standard methods of optical crystallography and a study made of the size, shape and orientation of the crystals and the distribution of air spaces between them. The following results were obtained:

(1) During the transition of firn into glacier ice the air spaces, forming a system of intercommunicating capillaries in the firn, become reduced in number and separated from each other by compression and by the growth of the crystals. This growth is primarily effected by the refreezing of melt water retained in the capillaries.

---

* We carried out no detailed examination of the extensive vertical or nearly vertical bands such as are to be found in the Lower Grindelwald Glacier and are therefore not certain to which of the three categories they belong.

(2) A large percentage of the firn crystals near the surface of the *névé* lie with their hexagonal axes at right angles to the surface of the glacier. This orientation appears to be part of a general rule whereby recrystallization of snow by melting and refreezing or by sublimation involves a reorientation of the crystals with their axes parallel to the direction of the temperature gradient.

(3) In the course of 6–8 years the initial orientation of the crystals near the surface gives way to a random distribution. The change seems to be due to the haphazard motion of single crystals or clusters of single crystals which constitute independently moving units in the mechanism of flow in the *névé* area. They are the bearers of the "differential movement" which measurements showed to be irregular on a small scale but uniform and continuous when regarded as a whole. Large thrust planes are absent in the *névé*.

(4) Stratification bands in the *névé* form by the freezing of wet strata of firn and have no connexion with any irregularities in the differential movement. The orientation of their crystals is similar to that of pond ice. The blue bands in the glacier tongue are divided into three categories: first, those which are old ice bands originally present in the *névé*; second, remnants of former fissures and crevasses; and third, those which represent thrust planes and are caused by laminar motion of large strata of ice.

(5) Examples both of non-laminar and of laminar motion were observed in the glacier tongue. In places where the ice was subjected to shear the crystals were orientated with their basal planes parallel to the direction of shear. A mechanism of plastic deformation is proposed which accounts for these findings and is based on the growth, deformation and reorientation of the crystals.

References

Ahlmann, H. W. and Sverdrup, H. U. 1935–6 Results of the Norwegian-Swedish Spitsbergen Expedition. *Geogr. Ann.*

Bader, H. 1939 Der Schnee und seine Metamorphose. *Beitr. Geol. Schweiz*, ser. *Hydrol.*, pt 3. Bern.

Chamberlin, R. T. 1928 *J. Geol.* **36**, 1.

von Engeln, O. D. 1934 *Science*, **80**, 401.

Haefeli, R. 1939 Schneemechanik mit Hinweisen auf die Erdbaumechanik. *Beitr. Geol. Schweiz*, ser. *Hydrol.*, pt 3. Bern.

Hamberg, A. 1932 *Naturw. Untersuch. Sarekgeb.* **1**, pt 3, 69.

Hess, H. 1933 Das Eis der Erde. *Handb. Geophysik*, **8**.

Hughes, T. P., Perutz, M. F. and Seligman, G. 1939 (in the Press).

Hughes, T. P. and Seligman, G. 1939 *Mon. Not. R. astr. Soc. geophys.* Suppl. (in the Press).

Philipp, H. 1920 *N. Jb. Min. Geol. Paläont.* supp. vol. **43**, 439.

Reid, H. F. 1903 *Int. geol. Congr.* (9, Vienna), *C.R.*
Schmidt, E. and Wassermann, G. 1930 *Metallwirtschaft*, **9**, 698.
Seligman, G. 1936 *Snow structure and ski fields*. Macmillan.
Sorge, E. 1935 *Wiss. Ergebn. dtsch. Grönl. Exped.*
Streiff-Becker, R. 1936 *Z. Gletscherk.* **24**, 31.
— 1938 *Z. Gletscherk.* **26**, 1.
Tammann, G. and Dreyer, K. L. 1929 *Z. anorg. Chem.* **182**, 289.
Visser, P. C. 1938 *Wiss. Ergebn. Holl. Exped. Karakorum*. Leyden.

DESCRIPTION OF PLATES 16–19

Plate 16

FIG. 1. Annual bands in a crevasse on the Mönchfirn. The distances between successive bands vary between 3 and 4 m. Ice bands are not visible owing to the weathering of the surface by the sun. On the left-hand wall all bands are covered by a thin layer of fresh snow.

FIG. 2. Ice bands in a crevasse on the Mönchfirn. The thickness of the larger bands is about 5 cm.

Plate 17

FIG. 3. Thin section of firn between crossed nicols. The sample was taken from immediately above the firn line on the Aletsch Glacier. Sp. gr. ~ 0·50. The scale is marked by the fret-saw blade at the bottom of the photograph. The distance between two successive teeth corresponds to 0·9 mm. (For stereogram see diagram 1, p. 342.)

FIG. 4. Section of ice taken from below the firn line.

FIG. 5. Firn from a crevasse in the Mönchfirn. Altitude 3330 m., depth 14 m., sp. gr. 0·72, age 3 years. (For stereogram see diagram 3, p. 344.)

FIG. 6. Ice from the same crevasse. Depth 23 m., sp. gr. 0·80, age 6 years. (For stereogram see diagram 4, p. 345.)

FIG. 7. Vertical section of thin crust embedded in early firn. Altitude 3400 m., depth 1 m.

Plate 18

FIG. 8. Plumb lines and pins in No. 2 Auxiliary Pit on the Mönchfirn on 9 August. The row of pins on the left had been constructed on 22 July with the pins accurately in line. The rectangular network of pins in the centre is seen immediately after its construction. The auxiliary pin rows above and below the network were made on 2 August. The pins are approximately 1 cm. apart.

FIG. 9. The same on 22 August. It is seen that the network of pins has become distorted and that the displacements of the pins in the row on the left and the two auxiliary rows have increased considerably. An increase in the thickness of the large ice band can also be noticed, as the lowest horizontal pin row of the network, which is well clear of the ice band in the picture on the left, is now enclosed by the band. The direction of the glacier flow is from right to left.

Plate 19

FIG. 10. Ice column in the grotto on the Jungfraujoch. Height approximately 2 m. Direction of flow from right to left. The hanging thermometer shows the vertical.

FIG. 11. The row of screws and the slanting blue band in the ice grotto on the Eigergletscher. The bands corresponding to the sedimentary stratification are visible in the lower part of the picture. The distances between successive screws vary between 2 and 3 cm. Direction of flow from left to right.

A theory of electric polarization, electro-optical Kerr effect and electric saturation in liquids and solutions

By A. PIEKARA, PH.D.

Lecturer in Experimental Physics, Jagiellonian University, Cracow;
Physical Laboratory, Prince Sułkowski Lyceum, Rydzyna (Poland)

(*Communicated by R. H. Fowler, F.R.S.—Received* 28 *March* 1939)

1. INTRODUCTION

I recently published some papers (Piekara 1937*a*, 1938) concerning the theory of dielectric polarization in polar liquids and their solutions in non-polar solvents. I have assumed the existence of two kinds of intermolecular coupling forces. The coupling forces of the first kind are due to the directional field produced by the surrounding molecules (ordered as in a crystal lattice) of potential energy $-W_1 \cos\theta_1$; θ_1 is the angular displacement of the dipole axis from the momentary axis of equilibrium, which can take all possible directions in space. This idea has been derived from R. H. Fowler (1935) and P. Debye (1935*a*), who developed with the help of this conception a theory of dielectric polarization. In order to obtain a satisfactory agreement with experiments on liquids, it proved, however, necessary to assume still a second kind of coupling forces. Simultaneously it has been shown, that these latter play a more important role than the first ones. The coupling forces of the second kind are due not to aggregates of well-ordered molecules, but to the next molecule, which happens to be in the neighbourhood of the molecule just considered. As a matter of fact there are several such molecules in the vicinity, the action of which should be taken into account. Let us, however, consider only one such molecule, which is quite satisfactory as a first approximation when molecular dipoles tend

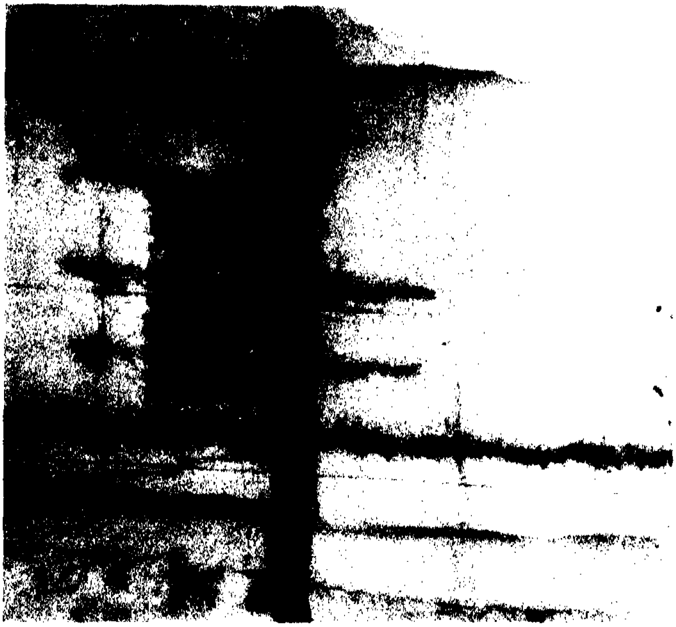

FIG. 9

FIG. 8

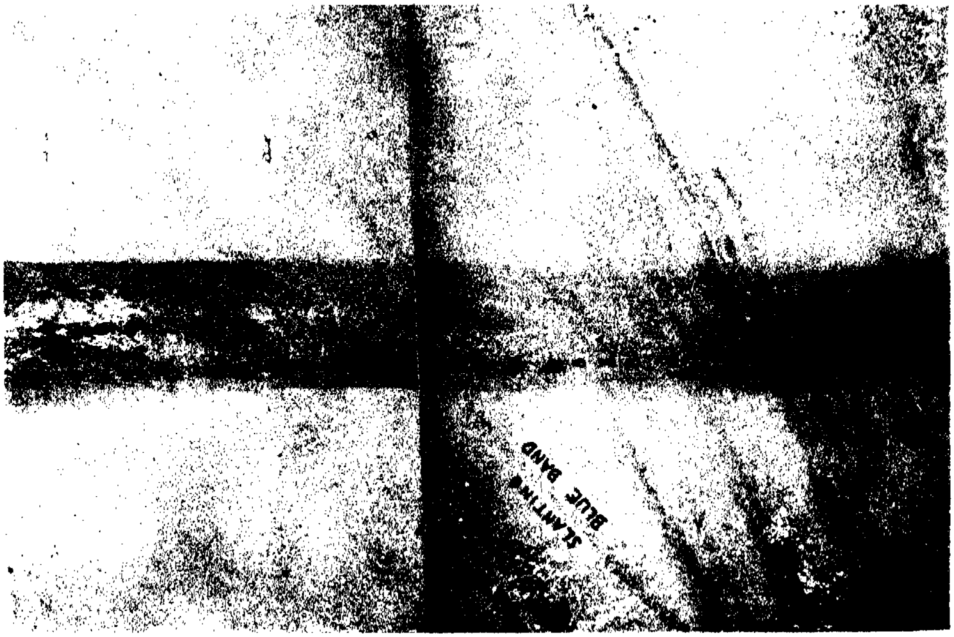

Fig. 11

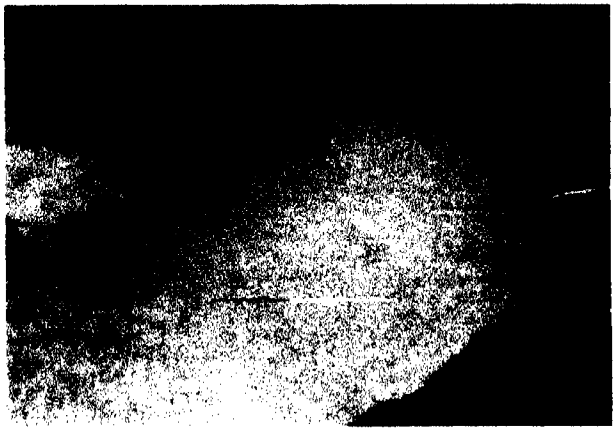

Fig. 10

to antiparallel orientation. This is the case of liquids in which the dielectric polarization depends on the concentration as in the case of nitrobenzene. Polar molecules, when oriented antiparallel, form transitory aggregates, whose field, being similar to that of a quadrupole, has a short range. In the opposite case, when the molecules tend to a parallel orientation, and the field of the aggregate has a rather long range, like the field of a dipole, it would be necessary to allow for other surrounding molecules. We shall therefore consider only molecules of the kind of nitrobenzene. The potential energy of the coupling of the second kind is to a first approximation $-W_2 \cos\theta_2$, where, as in our case when molecules tend to antiparallel orientation, $180° - \theta_2$ is the angle between the dipole axes of the molecule in question and its antiparallel neighbour. This conception is not synonymous with the existence of association between the molecules, which implies the existence of stoichiometrically defined aggregates besides single molecules. On the contrary, according to this conception all molecules are more or less subject to coupling forces, and W_2 is only a certain statistical mean value of the mutual energy for different distances of two neighbouring molecules.

A first attempt at such a theory has been recently developed in which the coupling of the first kind only was taken into account in the first approximation; an exact calculation involved unsurmountable difficulties, and a second approximation yielded extremely complicated formulae, without much improving the accuracy of the result. I owe to Professor R. H. Fowler a suggestion, according to which I could avoid the difficulties mentioned above. The theory offered in this paper leads in the special case of small values of W_1 to the formulae obtained in my preceding papers. In order to avoid burdening the argument, the necessary mathematical proofs are relegated to an appendix.

2. GENERAL FORMULAE

Upon the molecule, whose dipole axis has the orientation OM (fig. 1), acts (1) the coupling field vector of the first kind, W_1/μ, in the direction OA_1, and (2) the coupling field vector of the second kind, W_2/μ, in the direction OA_2. The angle between these vectors is Λ. The molecule is therefore at a given instant under the influence of the resultant intermolecular field vector, W/μ, acting along the axis OA, where

$$W = (W_1^2 + W_2^2 + 2W_1 W_2 \cos\Lambda)^{\frac{1}{2}}.$$

Moreover, the external electric field F acts also on the molecules. The axes OA_1, OA_2, OA and the dipole moment axis OM are at a given instant inclined to the field vector F at the angles Ω_1, Ω_2, Ω and θ respectively. The total potential energy of the molecule is

$$U = -W_1 \cos\theta_1 - W_2 \cos\theta_2 - \mu F \cos\theta = -W\cos\theta' - \mu F\cos\theta, \qquad (1)$$

where θ' is the angle AOM.

Let us denote by the symbol ϕ any function, connected with the molecule, being itself a function of the angles between its moment axis and the previously mentioned forces and of the angles determining the orientation of these forces in space. Let us assume at first that the direction of the axes OA_1, OA_2 and F in space is a fixed one, and that only the moment axis OM may take up different orientations. The statistical mean of the function ϕ, which will be denoted in what follows by $\mathbf{M}(\phi)$, is in this case represented by the well-known formula

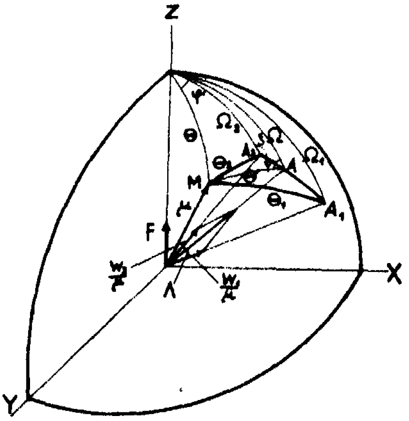

FIG. 1

$$\mathbf{M}(\phi) = \frac{\overline{\phi e^{-U/kT}}}{\overline{e^{-U/kT}}}, \qquad (2)$$

where in the Boltzmann distribution factor $e^{-U/kT}$ the kinetic energies of rotation and vibration are omitted; the single bar denotes the usual geometrical average, i.e. an average over all directions of the moment axis, ascribing equal weights to all directions. We introduce the following notation:

$$x = \mu F/kT, \qquad (3)$$

$$y_1 = W_1/kT, \qquad (4)$$

$$y_2 = W_2/kT, \qquad (5)$$

and

$$Y = W/kT = (y_1^2 + y_2^2 + 2y_1 y_2 \cos\Lambda)^{\frac{1}{2}}. \qquad (6)$$

Moreover, we let $\mathbf{M}^0(\phi)$ denote the statistical mean of ϕ in the absence of any external field,

$$\mathbf{M}^0(\phi) = \frac{\overline{\phi\, e^{Y\cos\theta'}}}{\overline{e^{Y\cos\theta'}}}. \tag{7}$$

In this case the statistical mean in the presence of the external field may be expressed by expanding the expression (2) in the following series:

$$\begin{aligned}\mathbf{M}(\phi) &= \mathbf{M}^0(\phi) + x\,[\mathbf{M}^0(\phi\cos\theta) - \mathbf{M}^0(\phi)\,\mathbf{M}^0(\cos\theta)] + \\ &\quad + \tfrac{1}{2}x^2\,[\mathbf{M}^0(\phi\cos^2\theta) - \mathbf{M}^0(\phi)\,\mathbf{M}^0(\cos^2\theta) - \\ &\quad - 2\,\mathbf{M}^0(\phi\cos\theta)\,\mathbf{M}^0(\cos\theta) + 2\,\mathbf{M}^0(\phi)\,\{\mathbf{M}^0(\cos\theta)\}^2] + \ldots \text{ etc.}\end{aligned} \tag{8}$$

The values of $\mathbf{M}^0(\phi)$ and the other terms depend, of course, on the directions of the axes OA_1 and OA_2 in space. If, keeping the position of the axis OA_2 fixed, we let the axis OA_1 assume all possible directions, then we may calculate new mean values, which will be denoted in what follows by a bar, $\overline{\mathbf{M}^0(\phi)}$, and so forth. We calculate therefore

$$\begin{aligned}\overline{\mathbf{M}(\phi)} &= \overline{\mathbf{M}^0(\phi)} + x\,[\overline{\mathbf{M}^0(\phi\cos\theta)} - \overline{\mathbf{M}^0(\phi)}\,\overline{\mathbf{M}^0(\cos\theta)}] + \\ &\quad + \tfrac{1}{2}x^2\,[\overline{\mathbf{M}^0(\phi\cos^2\theta)} - \overline{\mathbf{M}^0(\phi)}\,\overline{\mathbf{M}^0(\cos^2\theta)} - \\ &\quad - 2\,\overline{\mathbf{M}^0(\phi\cos\theta)\,\mathbf{M}^0(\cos\theta)} + 2\,\overline{\mathbf{M}^0(\phi)}\,\overline{\{\mathbf{M}^0(\cos\theta)\}^2}] + \ldots.\end{aligned} \tag{9}$$

This expression is a function only of the angle Ω_2 and of x, y_1 and y_2. Finally, we must take into account the fact that the axis OA_2, being actually the moment axis of a molecule similar to the molecule under consideration (OM), may assume in space different directions, which are now, of course, not equally likely *a priori*. When, as we assume, the molecules tend to antiparallel positions, then the axes $\overrightarrow{OM}$ and $\overrightarrow{A_2O}$ have in space an identical distribution. This distribution is, however, perturbed by the interaction of the molecules upon each other. We shall obtain, as a result, a "statistical perturbed average", which may be designated by an asterisk: $\overline{\mathbf{M}(\phi)}^*$. The manner of calculation of this average will be examined further. $\cos\theta$ will play the role of ϕ in the calculation of dielectric polarization, whilst $\cos^2\theta$ plays the same role in the Kerr effect.

3. ELECTRIC POLARIZATION

The molecular polarization, ${}_{\text{gas}}P$, of free molecules (in the gaseous state) may be calculated from the well-known formula

$${}_{\text{gas}}P = \frac{4\pi}{3}N\frac{\partial}{\partial F}\mathbf{M}(m_F),$$

where $\mathbf{M}(m_F)$ is the statistical average of the moment component of the molecule in the direction of the external field. If we consider only the part of the polarization arising from the dipoles (${}_{\text{gas}}P^{\text{dip}}$), then

$$\mathbf{M}(m_F) = \mu\,\mathbf{M}(\cos\theta)$$

and

$${}_{\text{gas}}P^{\text{dip}} = \frac{4\pi}{3} N\mu \frac{\partial}{\partial F}\mathbf{M}(\cos\theta). \tag{10}$$

Omitting the effect of electric saturation, we obtain, for free molecules:

$$\mathbf{M}(\cos\theta) = \tfrac{1}{3}x,$$

and

$${}_{\text{gas}}P^{\text{dip}} = \frac{4\pi}{9}\frac{N\mu^2}{kT}. \tag{10a}$$

On the other hand, the molecular polarization P^{dip} of pure polar liquids and their solutions must be calculated by the formula

$$P^{\text{dip}} = \frac{4\pi}{3} N\mu \frac{\partial}{\partial F}\overline{\mathbf{M}(\cos\theta)}^{*}. \tag{10b}$$

Now in this case we calculate $\overline{\mathbf{M}(\cos\theta)}^{*}$ from the series (8) by taking into account only the first two terms of the development (i.e. by neglecting the saturation effect)

$$\mathbf{M}(\cos\theta) = \mathbf{M}^0(\cos\theta) + x\left[\mathbf{M}^0(\cos^2\theta) - \{\mathbf{M}^0(\cos\theta)\}^2\right].$$

Since

$$\cos\theta = \cos\theta'\cos\Omega + \sin\theta'\sin\Omega\cos\phi,$$

$$\mathbf{M}^0(\cos\theta') = L(Y)$$

and

$$\mathbf{M}^0(\cos^2\theta') = 1 - 2\frac{L(Y)}{Y}$$

(L being Langevin's function); therefore

$$\mathbf{M}(\cos\theta) = L(Y)\cos\Omega + x\left[\frac{L(Y)}{Y}(1 - 3\cos^2\Omega) + \{1 - L^2(Y)\}\cos^2\Omega\right]. \tag{11}$$

In order to calculate $\overline{\mathbf{M}(\cos\theta)}$, we shall not apply the integration over all directions of the axis OA_1, because it offers too grave mathematical difficulties. We shall rather perform the calculation in a manner similar to that used by Fowler in his above-mentioned paper. Let us consider all the transitory aggregates (pairs) of molecules, whose one partner has its dipole axis oriented at the given instant inside a small solid angle $d\omega$ with the axis OA_2. The axis OA_1 may assume all possible directions. We may therefore admit, with a certain approximation, that the axes OA_1 of one-sixth of the whole number of pairs assume directions approximately parallel to OA_2 ($\Lambda = 0$), that the axes of another one-sixth assume antiparallel directions

($A = 180°$), and lastly that the axes of the remaining two-thirds assume directions approximately perpendicular to OA_2 ($A = 90°$), all these latter directions being equally possible, since the external field has no influence upon the direction of the axis OA_1. It follows from the proper spherical triangle in fig. 1 that

$$\cos\Omega = \frac{1}{Y}\left[(y_2 + y_1\cos A)\cos\Omega_2 + y_1\sin A\sin\Omega_2\cos\xi\right].$$

We obtain, by calculating in the above manner,

$$\begin{aligned}\overline{\mathbf{M}(\cos\theta)} = {} & \left[\frac{1}{6}L(y_1+y_2) - \frac{1}{6}L(y_1-y_2) + \frac{2}{3}\frac{y_2}{\sqrt{(y_1^2+y_2^2)}}L\{\sqrt{(y_1^2+y_2^2)}\}\right]\cos\Omega_2 + \\ & + x\left\{\frac{1}{6}\frac{L(y_1+y_2)}{y_1+y_2}(1-3\cos^2\Omega_2) + \frac{1}{6}\left[1-L^2(y_1+y_2)\right]\cos^2\Omega_2 + \right. \\ & + \frac{1}{6}\frac{L(y_1-y_2)}{y_1-y_2}(1-3\cos^2\Omega_2) + \frac{1}{6}\left[1-L^2(y_1-y_2)\right]\cos^2\Omega_2 + \\ & + \frac{2}{3}\frac{L\{\sqrt{(y_1^2+y_2^2)}\}}{\sqrt{(y_1^2+y_2^2)}}\left[1 - 3\frac{\frac{1}{2}y_1^2 + (y_2^2 - \frac{1}{2}y_1^2)\cos^2\Omega_2}{y_1^2+y_2^2}\right] + \\ & \left. + \frac{2}{3}\left[1 - L^2\{\sqrt{(y_1^2+y_2^2)}\}\right]\frac{\frac{1}{2}y_1^2 + (y_2^2 - \frac{1}{2}y_1^2)\cos^2\Omega_2}{y_1^2+y_2^2}\right\}. \end{aligned} \tag{12}$$

The statistical perturbed average of $\cos\theta$ may be calculated, by putting $\overline{\mathbf{M}(\cos\theta)}^*$ instead of $\overline{\mathbf{M}(\cos\theta)}$ and $\overline{\mathbf{M}(\cos\Omega_2)}^*$ instead of $\cos\Omega_2$, while, according to what has been said at the end of § 2,

$$\overline{\mathbf{M}(\cos\theta)}^* = -\overline{\mathbf{M}(\cos\Omega_2)}^*. \tag{13}$$

Similarly we replace $\cos^2\Omega_2$ by $\overline{\mathbf{M}(\cos^2\Omega_2)}^*$. This last value will be strictly calculated in the next paragraph. Meanwhile, since $\overline{\mathbf{M}(\cos\theta)}^*$ will be determined with the omission of higher powers of x, it suffices to put the first approximation

$$\overline{\mathbf{M}(\cos^2\Omega_2)}^* = \tfrac{1}{3}. \tag{14}$$

This is a correct value, since, when there is no coupling, we have

$$\mathbf{M}(\cos^2\Omega_2) = 1 - 2\frac{L(x)}{x} = \tfrac{1}{3} + \tfrac{2}{45}x^2 - \ldots,$$

and when coupling appears it can change only the second term (see the next paragraph). On the other hand, the first term must remain unchanged, because for $x = 0$ (the absence of an external field) the distribution of the directions of the axes OM and A_2O must be wholly disorderly, since there is no privileged direction. By applying the conditions expressed in (13) and (14) to (12), we obtain

$$\overline{\mathbf{M}(\cos\theta)}^{*} = \tfrac{1}{3}xR, \tag{15}$$

where

$$R = \frac{1-\frac{1}{6}\left[L^2(y_1+y_2)+L^2(y_1-y_2)+4L^2\{\sqrt{(y_1^2+y_2^2)}\}\right]}{1+\frac{1}{6}\left[L(y_1+y_2)-L(y_1-y_2)+4\frac{y_2}{\sqrt{(y_1^2+y_2^2)}}L\{\sqrt{(y_1^2+y_2^2)}\}\right]}. \tag{16}$$

R is a "reducing factor", which can be determined experimentally with the help of the formula

$$P^{\text{dip}} = {}_{\text{gas}}P^{\text{dip}}R. \tag{17}$$

This latter follows from comparing (10*a*), (10*b*) and (15). When there exist no coupling forces of the first kind ($y_1 = 0$), formula (16) changes into

$$R = 1 - L(y_2). \tag{18}$$

Developing the numerator and the denominator of (16) in a series of powers of y_1 and neglecting the terms containing higher powers than the second, we obtain my former formula, derived in my last paper, for the case in which there exists coupling of the second kind and feeble coupling of the first kind (Piekara 1937*a*, formula 22*a*; Piekara 1938, formula 1). Formula (16) is, as a matter of fact, also approximate, because in calculating (12) instead of integrating we have applied an approximate method, but it has the advantage over my former formula, that it yields exact results also for the opposite case of a strong coupling of the first kind and a weak one of the second kind, not yielded by the former formula. In particular we obtain from it for $y_2 = 0$ the formula derived by Fowler and Debye:

$$R = 1 - L^2(y_1) = 2\frac{\coth y_1}{y_1} - \frac{1}{y_1^2} - \frac{1}{\sinh^2 y_1}. \tag{19}$$

In order to apply formula (16) to solutions of polar liquids in non-polar solvents, we assume that y_1 and y_2 are proportional to the number of molecules per c.c., since W_1 and W_2 are proportional to $1/r^3$, where r is the distance between the dipoles. Besides this coupling of the polar molecules of the solute there still exists a comparatively weak coupling between the dissolved molecules and those of the solvent. We may allow for this last coupling by assuming that it is proportional to the number of the molecules of the solvent per c.c. We have, therefore,

$$y_1 = A_1cd + B_1(1-c)\,d, \tag{20a}$$

$$y_2 = A_2cd, \tag{20b}$$

where c denotes the concentration by weight of the solution, and d its density. A_1 and B_1 are coefficients responsible for the coupling of the first kind, B_1 denoting in particular the coupling with the solvent, and A_2 the coupling of the second kind. We have calculated R, assuming either $A_1 = 4{\cdot}3$, $B_1 = 1{\cdot}5$ and $A_2 = 6{\cdot}2$, or $A_1 = 1$, $B_1 = 1{\cdot}5$ and $A_2 = 8$. The corresponding values of R are plotted against concentration in fig. 2. In this figure the curve for the first set of constants A_1, B_1 and A_2 is designated by R^{I}_p and the curve for the second set of constants by R^{II}_p. The circles denote the experimental values of R for solutions of nitrobenzene in hexane

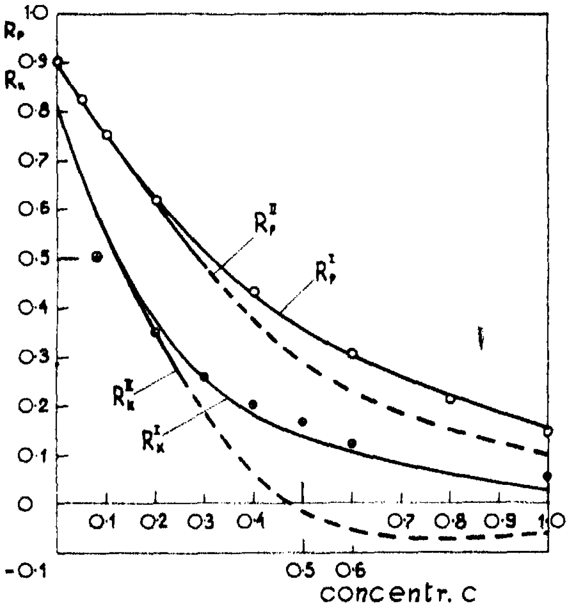

FIG. 2

(Piekara 1937*a*). The first graph (R^{I}_p) shows a very good agreement with experiment for all concentrations between 0 and 1, while the second one (R^{II}_p) does this only in the case of diluted solutions (concentrations between 0 and 0·2).

The diagrams of the function $R = f(y_1)$ for different values of y_2 are represented in fig. 3. The corresponding values of y_2 are marked over each graph. This permits us to observe an interesting role of the coupling forces of the first kind. Namely, when the coupling of the second kind is weak (small values of y_2), the coupling of the first kind diminishes the value of R, and consequently the electric polarization, acting jointly with the coupling of the second kind. When, on the other hand, the coupling of the second kind is strong (large values of y_2), the coupling forces of the first kind act in the opposite sense: they increase R, and therefore also the polarization, impairing the coupling of the second kind. This happens for instance in the case of solutions of fatty acids in hexane or other non-polar solvents. The polarization of these solutions rises with growing concentration instead of diminishing (Piekara and Piekara 1934). A quantitative comparison cannot be made, unless we know the dependence of y_2 on the concentration. The simplest assumption, that y_2 is constant, which would denote the existence of a true association into double molecules, independent from the concentration, is not sufficient. The experiments show rather that y_2 diminishes with rising concentration (dissociation).

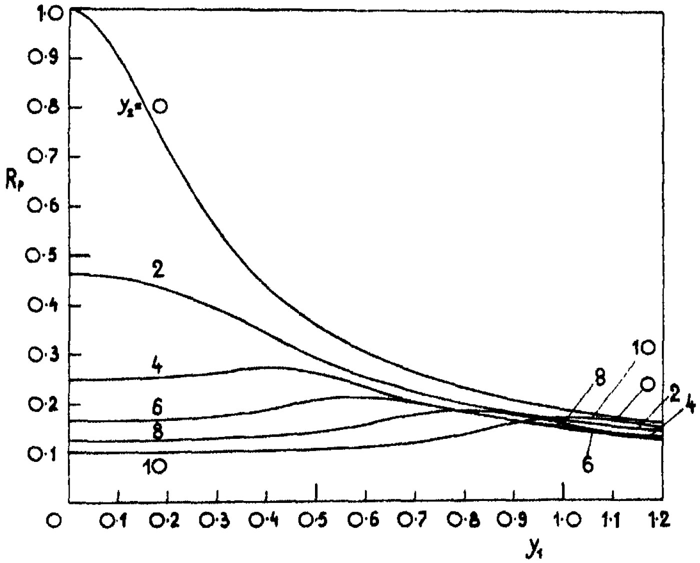

FIG. 3

4. ELECTRO-OPTICAL KERR EFFECT

Let us denote by x, y, z a co-ordinate system connected with the molecule and by X, Y, Z another co-ordinate system fixed in space. The electrical vector F of the external field may act in the direction of the Z-axis and the electric vector of the light-wave E' may act either in the direction of the Z- or the X-axes. These latter axes make with the co-ordinate axes x, y, z the following angles:

	x	y	z
$Z(F)$	α_1	α_2	α_3
X	α_1'	α_2'	α_3'

The moment of the molecule may lie in the direction of the z-axis; then $\alpha_3 = \theta$. Let us introduce an angle ϕ' between the planes zOZ and XOZ and another angle ψ determining the rotation of the molecule around its moment axis (z-axis). Thus the cosines of the angles of the above table turn into

$$\left.\begin{aligned}
\cos\alpha_1 &= -\sin\theta\cos\psi,\\
\cos\alpha_2 &= \sin\theta\sin\psi,\\
\cos\alpha_3 &= \cos\theta,\\
\cos\alpha_1' &= \cos\theta\cos\phi'\cos\psi-\sin\phi'\sin\psi,\\
\cos\alpha_2' &= -\cos\theta\cos\phi'\sin\psi-\sin\phi'\cos\psi,\\
\cos\alpha_3' &= \sin\theta\cos\phi'.
\end{aligned}\right\} \tag{21}$$

When E' lies in the direction of F, it induces in the molecule an electric moment whose component along F is

$$m_F = \gamma_F E',$$

where

$$\begin{aligned}
\gamma_F = {} & b_1\cos^2\alpha_1+b_2\cos^2\alpha_2+b_3\cos^2\alpha_3+2b_{12}\cos\alpha_1\cos\alpha_2+\\
& +2b_{23}\cos\alpha_2\cos\alpha_3+2b_{13}\cos\alpha_1\cos\alpha_3.
\end{aligned} \tag{22}$$

Here $b_1, b_2, \ldots$ denote, as customary, the tensor components of the optical molecular polarizability. Similarly, when E' is perpendicular to F (i.e. E' oscillates along X), it induces in the molecule a moment, whose component in this direction is

$$m_X = \gamma_X E',$$

where

$$\begin{aligned}
\gamma_X = {} & b_1\cos^2\alpha_1'+b_2\cos^2\alpha_2'+b_3\cos^2\alpha_3'+2b_{12}\cos\alpha_1'\cos\alpha_2'+\\
& +2b_{23}\cos\alpha_2'\cos\alpha_3'+2b_{13}\cos\alpha_1'\cos\alpha_3'.
\end{aligned} \tag{23}$$

On account of the strong directional action, exerted by the field F upon the dipoles, let us neglect that part of the saturation which comes from the electrical anisotropy of molecules. This assumption limits the applicability of this theory to those polar substances which show in the Kerr effect an anisotropic term feeble in comparison with the dipole term. There are many such substances: nitrobenzene, acetone, alkyl halogenides, etc. Hence we may calculate, after the introduction of expressions (21) into (22) and (23), the averages for all rotational situations around the dipole axis, by evaluating the integrals $\frac{1}{2\pi}\int_0^{2\pi}\gamma_F\,d\psi$ and $\frac{1}{2\pi}\int_0^{2\pi}\gamma_X\,d\psi$. It must be mentioned, moreover, that all directions of the dipole OM around the Z-axis,

$\theta, \theta', \Omega, \ldots$ etc. being constant, are equally possible. Therefore we can calculate the averages for different values of the azimuth ϕ', by taking integrals $\frac{1}{2\pi}\int_0^{2\pi} \gamma_F \, d\phi'$ and $\frac{1}{2\pi}\int_0^{2\pi} \gamma_X \, d\phi'$. Thus we obtain

$$\gamma_F = \tfrac{1}{2}(b_1+b_2)(1-\cos^2\theta) + b_3 \cos^2\theta, \tag{24}$$

$$\gamma_X = \tfrac{1}{4}(b_1+b_2)(1+\cos^2\theta) + \tfrac{1}{2}b_3(1-\cos^2\theta). \tag{25}$$

Now the evaluating of the statistical perturbed averages of the polarizability γ_F and γ_X reduces itself to calculating only $\overline{\mathbf{M}(\cos^2\theta)}^{*}$:

$$\overline{\mathbf{M}(\gamma_F)}^{*} = \tfrac{1}{2}(b_1+b_2)\{1-\overline{\mathbf{M}(\cos^2\theta)}^{*}\} + b_3 \overline{\mathbf{M}(\cos^2\theta)}^{*}, \tag{26}$$

$$\overline{\mathbf{M}(\gamma_X)}^{*} = \tfrac{1}{4}(b_1+b_2)\{1+\overline{\mathbf{M}(\cos^2\theta)}^{*}\} + \tfrac{1}{2}b_3\{1-\overline{\mathbf{M}(\cos^2\theta)}^{*}\}. \tag{27}$$

In order to calculate $\overline{\mathbf{M}(\cos^2\theta)}^{*}$ with an accuracy including x^2, we must first evaluate $\overline{\mathbf{M}(\cos^3\theta)}^{*}$ with an accuracy including x^1 and $\overline{\mathbf{M}(\cos^4\theta)}^{*}$ with an accuracy including only x^0. We calculate these expressions with the help of formula (9), putting $\phi = \cos^3\theta$ or $\phi = \cos^4\theta$ and using the method applied already to formula (12). In analogy to (13) we write the generalized condition

$$\overline{\mathbf{M}(\cos^{2n}\theta)}^{*} = \overline{\mathbf{M}(\cos^{2n}\Omega_2)}^{*} \tag{28}$$

and

$$\overline{\mathbf{M}(\cos^{2n-1}\theta)}^{*} = -\overline{\mathbf{M}(\cos^{2n-1}\Omega_2)}^{*} \tag{29}$$

and we obtain as the result

$$\overline{\mathbf{M}(\cos^4\theta)}^{*} = \tfrac{1}{5}, \tag{30}$$

$$\overline{\mathbf{M}(\cos^3\theta)}^{*} = \tfrac{1}{5}xR, \tag{31}$$

R being determined by formula (16). Thus, profiting from the two last results, we obtain

$$\overline{\mathbf{M}(\cos^2\theta)}^{*} = \tfrac{1}{3} + \tfrac{2}{45}xR_K, \tag{32}$$

where R_K is a new reducing factor expressed by the formula

$$R_K = \frac{\left[\begin{array}{l}\mathscr{R}(y_1+y_2)+\mathscr{R}(y_1-y_2)+4\mathscr{R}\{\sqrt{(y_1^2+y_2^2)}\}- \\ \qquad -2R\left[\dfrac{L^2(y_1+y_2)}{y_1+y_2}-\dfrac{L^2(y_1-y_2)}{y_1-y_2}+4\dfrac{y_2}{\sqrt{(y_1^2+y_2^2)}}\dfrac{L^2\{\sqrt{(y_1^2+y_2^2)}\}}{\sqrt{(y_1^2+y_2^2)}}\right]\end{array}\right]}{2\dfrac{y_1^2}{y_1^2+y_2^2}+\dfrac{L(y_1+y_2)}{y_1+y_2}+\dfrac{L(y_1-y_2)}{y_1-y_2}+4\dfrac{y_2^2-\frac{1}{2}y_1^2}{y_1^2+y_2^2}\dfrac{L\{\sqrt{(y_1^2+y_2^2)}\}}{\sqrt{(y_1^2+y_2^2)}}}. \tag{33}$$

$\mathscr{R}$ has the form

$$\mathscr{R}(y) = \frac{L(y)}{y}\left[2-3\frac{L(y)}{y}-2L^2(y)\right]. \tag{34}$$

When there exists only coupling of the first kind ($y_1 > 0, y_2 = 0$), R becomes identical with the reducing factor of Debye (cf. Friedrich 1937)

$$R_K = 3\mathscr{R}(y_1). \tag{35}$$

Combining (32) with (26) and (27) we get

$$\overline{\mathbf{M}(\gamma_F)}^* = \tfrac{1}{3}(b_1+b_2+b_3) + F^2 \frac{\mu^2}{45k^2T^2}(2b_3-b_1-b_2)\,R_K, \tag{36}$$

$$\overline{\mathbf{M}(\gamma_X)}^* = \tfrac{1}{3}(b_1+b_2+b_3) - \tfrac{1}{2}F^2 \frac{\mu^2}{45k^2T^2}(2b_3-b_1-b_2)\,R_K. \tag{37}$$

Hence we see that the dipole term, denoted in the Kerr effect, as usual, by θ_2, which for $\mu_1 = \mu_2 = 0$ and $\mu_3 = \mu$ is equal to $\frac{\mu^2}{45k^2T^2}(2b_3-b_1-b_2)$, is now reduced in proportion to $R_K : 1$. Also the "molecular Kerr constant" K_0^m is reduced in the same proportion. For gases it is

$$K_0^m = \frac{2\pi}{9}N(\theta_1+\theta_2).$$

For liquids and solutions, on the other hand, it turns (on account of neglecting the term of anisotropy θ_1) into

$$K^m = K_0^m R_K. \tag{38}$$

This expression allows one to determine experimentally the value of R_K for the mixtures of nitrobenzene and hexane, referred to in the foregoing paragraph. These values may be compared with those computed from formula (33). It is characteristic that formula (33) does not contain any new constant, since the constants A_1, B_1 and A_2, involved in y_1 and y_2, are already determined from the corresponding polarization-concentration curve.

The comparison of the values of R_K calculated and measured is shown on fig. 2. The curves on this figure are theoretical curves calculated from formula (33) for different concentrations, while the circles on this same figure represent experimental values of R_K, as obtained by L. Kozłowski[†] for solutions

---

[†] In order to calculate $(R_K)_{obs} = K^m/K_0^m$, I applied the following values of K^m, privately communicated to me by Dr L. Kozłowski (some of these results have been published in 1938):

$c =$	0·08	0·20	0·30	0·40	0·50	0·60
$K^m \times 10^{12} =$	645	448	334	261	214	158

I accepted for K_0^m at 25° the value 1280×10^{-12} according to the value of Friedrich (1937) 1304×10^{-12} for 23°. The value of $(R_K)_{obs}$ for pure nitrobenzene ($c = 1$) has been derived from Friedrich for 23°.

of nitrobenzene in hexane at 25° and for $\lambda = 578\,\mathrm{m}\mu$. The coincidence between theory and experiment, when the first triplet of constants is used (viz. $A_1 = 4{\cdot}3$, $B_1 = 1{\cdot}5$ and $A_2 = 6{\cdot}2$, graph R_K^{I}), *for a formula, which does not contain any new constant*, is rather satisfactory. It is interesting, that for the second triplet of constants (viz. $A_1 = 1$, $B_1 = 1{\cdot}5$ and $A_2 = 8$, graph R_K^{II}) the theory predicts, for sufficiently large concentrations, negative values of R_K. This result will not be so stupefying, if we take into account that, in this theory, the deformation of molecules due to intermolecular forces is disregarded. This deformation, changing the orientation of the dipole moment relatively to the ellipsoid of polarizability, may produce a very significant influence on the Kerr effect. It may even cause a change of sign of the Kerr constant, in the case when the dipole axis becomes nearly perpendicular to the axis of the greatest optical polarizability of the molecule. It seems probable that this effect of "intermolecular field deformation" may in many liquids compensate the change of sign due to the coupling of the second kind.

5. ELECTRIC SATURATION EFFECT

In order to evaluate the saturation effect in electric polarization, let us calculate $\overline{\mathbf{M}(\cos\theta)}^{*}$ with a greater accuracy than in § 3, namely including also the terms containing x^3. Taking into account in the expression (8) also the fourth term of the development, we obtain with $\phi = \cos\theta$

$$\begin{aligned}\mathbf{M}(\cos\theta) = {} & \mathbf{M}^0(\cos\theta) + x\left[\mathbf{M}^0(\cos^2\theta) - \{\mathbf{M}^0(\cos\theta)\}^2\right] + \\ & + \tfrac{1}{2}x^2\left[\mathbf{M}^0(\cos^3\theta) - 3\,\mathbf{M}^0(\cos\theta)\,\mathbf{M}^0(\cos^2\theta) + 2\{\mathbf{M}^0(\cos\theta)\}^3\right] + \\ & + \tfrac{1}{6}x^3\left[\mathbf{M}^0(\cos^4\theta) - 4\,\mathbf{M}^0(\cos\theta)\,\mathbf{M}^0(\cos^3\theta) - 3\{\mathbf{M}^0(\cos^2\theta)\}^2 + \right. \\ & \left. + 12\,\mathbf{M}^0(\cos^2\theta)\{\mathbf{M}^0(\cos\theta)\}^2 - 6\{\mathbf{M}^0(\cos\theta)\}^4\right]. \qquad (39)\end{aligned}$$

$\mathbf{M}(\cos\theta)$ and $\mathbf{M}(\overline{\cos\theta})$ will be calculated in a manner similar to that used in expressions (11) and (12). With the help of the conditions expressed in (28) and (29) and applying for $\cos\Omega_2$ the expressions (30), (31) and (32), we evaluate $\overline{\mathbf{M}(\cos\theta)}^{*}$:

$$\overline{\mathbf{M}(\cos\theta)}^{*} = \tfrac{1}{3}xR - \tfrac{1}{45}x^3R_S, \qquad (40)$$

where R_S is a reducing factor responsible for the diminution of the electric saturation effect in a liquid as compared to the same effect in the gaseous state (i.e. calculated after Debye's former theory). It amounts to

$$R_S = \frac{\begin{bmatrix} \frac{1}{6}R^*(y_1+y_2)+\frac{1}{6}R^*(y_1-y_2)+\frac{2}{3}R^*\{\sqrt{(y_1^2+y_2^2)}\} - \\ -2R_K\left[\frac{1}{6}S(y_1+y_2)+\frac{1}{6}S(y_1-y_2)+\frac{2}{3}\{(y_2^2-\frac{1}{2}y_1^2)/(y_1^2+y_2^2)\}\,S\{\sqrt{(y_1^2+y_2^2)}\}\right] - \\ -9R\left[\frac{1}{6}s(y_1+y_2)-\frac{1}{6}s(y_1-y_2)+\frac{2}{3}\,\{y_2/\sqrt{(y_1^2+y_2^2)}\}\,s\{\sqrt{(y_1^2+y_2^2)}\}\right]\end{bmatrix}}{1+\frac{1}{6}L(y_1+y_2)-\frac{1}{6}L(y_1-y_2)+\frac{2}{3}\{y_2/\sqrt{(y_1^2+y_2^2)}\}\,L\{\sqrt{(y_1^2+y_2^2)}\}}. \tag{41}$$

R and R_K denote here the reducing factors respectively of the electric polarization and of the Kerr effect. Both are determined by formulae (16) and (33). R^* is Debye's function† represented by the formula

$$R^*(y) = 3\left\{1-4L^2(y)+3L^4(y)+4\frac{L(y)}{y}[2L^2(y)-1]+6\frac{L^2(y)}{y^2}\right] \tag{42}$$

and
$$S(y) = Q(y)-\frac{L(y)}{y}, \tag{43a}$$

$$s(y) = Q(y)\,L(y), \tag{43b}$$

where Q is Fowler's function†

$$Q(y) = 1-2\frac{L(y)}{y}-L^2(y) = \frac{1}{y^2}-\frac{1}{\sinh^2 y}. \tag{43c}$$

On the other hand, relying upon the relation

$$\overline{\mathbf{M}(\overline{\cos\theta})}^* = \frac{\overline{\mathbf{M}(m_F)}^*}{\mu},$$

where $\overline{\mathbf{M}(m_F)}^*$ in the presence of coupling forces has the same significance as $\mathbf{M}(m_F)$ in paragraph 3 without them, we obtain in the well-known manner the formula

$$\Delta\epsilon = -12\pi n\left(\frac{\epsilon+2}{3}\right)^4\frac{\mu^4}{45k^3T^3}E^2R_S. \tag{44}$$

Here n denotes the number of molecules per c.c., ϵ the dielectric constant of the liquid and $\Delta\epsilon$ its change under the influence of an electric field E, in e.s. units. This formula enables us to make an experimental determination of the reducting factor R_S of the electric saturation.

It is interesting that, according to experiments of the author and B. Piekara (1936) performed with nitrobenzene purified and dried in the best possible manner, $\Delta\epsilon$ is *positive*. This is the so-called "inverse saturation effect". In other words, R_S is *negative* when the liquid is quite dry. The cleanest nitrobenzene, which has been applied by the authors, shows relatively very large effects: $\Delta\epsilon = +2{\cdot}4\times10^{-3}$ at $E = 35{,}000$ volts/cm., that leads to $R_S = -5\times10^{-4}$. On the other hand, we obtain for solutions of nitrobenzene in non-polar solvents normal negative effects, i.e. for R_S positive values, but only when the concentration of nitrobenzene is less than *ca.* 90%.

---

† Cf. Appendix VII, where the numerical values of the functions L, Q, R^* and $\mathcal{R}$ for different values of the argument are gathered in a table.

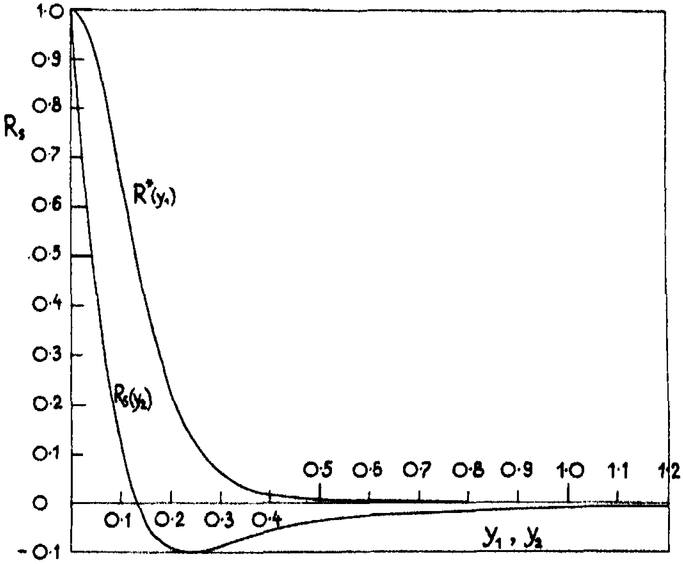

FIG. 4

If we put in the formula (41) $y_2 = 0$, i.e. if we neglect the coupling of the second kind, we get

$$R_S(y_1) = R^*(y_1), \tag{45}$$

i.e. the former formula of Debye (1935 *b*). The function $R_S(y_1)$ is represented by the graph on fig. 4. We see that R^* never turns negative, and therefore this theory cannot explain the inverse saturation effect. On the other hand, if we take the opposite extreme case, i.e. when there exists only coupling of the second kind, then, by putting $y_1 = 0$ into formula (41), we obtain

$$R_S(y_2) = 6\frac{L(y_2)}{y_2} - [1+5L(y_2)]\,[1-L(y_2)]. \tag{46}$$

The function $R_S(y_2)$ is represented by the second graph on fig. 4. We see from this graph that, for $y_2 > ca.\ 1{\cdot}33$, $R_S(y_2)$ becomes negative, which explains the appearance of the inverse saturation effect.† The mechanism of the origin of this effect may be described as follows. The molecules associate by pairs of a transitory character, more or less strongly coupled. The external field tends to orient both the partners of such a pair parallel to F. As a result of this action the angle between the axes of the partners of the pair changes by a very small amount, which yields statistically a slight increase of the resulting moment of such transitory pairs. Hence appears the inverse effect of the saturation, which may easily surpass the ordinary Langevin-Debye negative effect of the saturation.

The quantitative application of formula (41) to polar liquids is for the present of little importance, on account of the small accuracy of experiments performed as yet, especially with conducting liquids. On the other hand, there exists the deformation of the molecules under the action of the external electric field (deformation of second order), which has a strong influence upon the electric saturation effect, as has been shown by the author both theoretically (Piekara 1937*a*) and experimentally (Piekara and Piekara 1937). This deformation should be taken into account besides the coupling of both kinds. This "external field deformation of the second order" should not be confused with the "intermolecular field deformation" mentioned in § 4 of this paper. This latter may induce a change of situation of the molecular moment relatively to the axes of its ellipsoid of polarizability. This deformation effect may have a very strong influence on the electro-optical Kerr effect, but, on the other hand, it seems to have no significant influence on the electric saturation effect, in which the dipole moment and not the ellipsoid of polarizability play the chief role.

Recently Onsager (1936) has developed a theory of dielectric polarization in liquids, which has attained some success (see also Van Vleck 1937 and Falkenhagen 1938). On the other hand, its application to polar liquids and especially to their solutions in non-polar solvents offers some discrepancies with the experiment (Zakrzewski and Piekara 1939). It should be added here that this theory, considering the molecular interaction as owing to the continuous medium, cannot, however, account for the existence of the inverse saturation effect.

Lastly it may be mentioned that the coupling of the second kind has proved to be also responsible for the magnitude of the magnetic birefrin gence in polar liquids and for its variation with temperature (Piekara 1939). These effects cannot be explained either by the coupling of the first kind or by Onsager's theory.

---

† For this second extreme case the author has already previously calculated R_S, taking into account R_K only approximately (cf. A. Piekara 1937*b*, formula (4)). Notwithstanding this simplification, the course of R_S in dependence from y_2, as shown by formula (4) in the mentioned note, differs but very little from the course of R_S, as shown by formula (46).

The author wishes to express his thanks to Professor R. H. Fowler for his valuable suggestion concerning this work and for his kind interest in it.

MATHEMATICAL APPENDIX

I. *Calculation of some averages of the form of* M⁰(cosⁿ θ′)

According to formula (7) we have without external field

$$\mathrm{M}^0(\cos^n\theta') = \frac{\int_0^\pi \cos^n\theta' \, e^{Y\cos\theta'} 2\pi \sin\theta' \, d\theta'}{\int_0^\pi e^{Y\cos\theta'} 2\pi \sin\theta' \, d\theta'}. \tag{a}$$

Or, putting $\cos\theta' = x$, we calculate

$$\mathrm{M}^0(\cos^n\theta') = \frac{\int_{-1}^{1} x^n e^{Yx} dx}{\int_{-1}^{1} e^{Yx} dx} = \frac{e^Y + (-1)^{n-1} e^{-Y} - n\int_{-1}^{1} x^{n-1} e^{Yx} dx}{e^Y - e^{-Y}}.$$

For $n = 1$ we obtain

$$\mathrm{M}^0(\cos\theta') = \frac{e^Y + e^{-Y}}{e^Y - e^{-Y}} - \frac{1}{Y} = \coth Y - \frac{1}{Y} = L(Y),$$

i.e. the well-known Langevin function L. Denoting, for brevity,

$$\mathrm{M}^0(\cos^n\theta') = L_n, \tag{b}$$

we find

$$\left.\begin{aligned} L_0 &= 1, \\ L_1 &= L, \\ L_2 &= 1 - 2\frac{L}{Y}, \\ L_3 &= L - 2\frac{1}{Y} + 6\frac{L}{Y^2}, \\ L_4 &= 1 - 4\frac{L}{Y} + 8\frac{1}{Y^2} - 24\frac{L}{Y^3}, \text{ etc.} \end{aligned}\right\} \tag{c}$$

II. *Calculation of some averages of the form of* $\mathbf{M}^0(\cos^n\theta)$

For $\phi = \cos^n\theta$ formula (7) becomes

$$\mathbf{M}^0(\cos^n\theta) = \frac{\int_0^{\pi}\int_0^{2\pi}\cos^n\theta\, e^{Y\cos\theta'}\sin\theta'\,d\phi\,d\theta'}{\int_0^{\pi}\int_0^{2\pi} e^{Y\cos\theta'}\sin\theta'\,d\phi\,d\theta'}. \qquad (d)$$

Since $$\cos\theta = \cos\theta'\cos\Omega + \sin\theta'\sin\Omega\cos\phi$$

and taking into account that

$$\int_0^{2\pi}\cos^{2n+1}\phi\,d\phi = 0,\quad \int_0^{2\pi}\cos^2\phi\,d\phi = \pi,\quad \int_0^{2\pi}\cos^4\phi\,d\phi = \tfrac{3}{4}\pi,\quad \text{etc.},$$

we can write, using (*a*) and (*b*),

$$\mathbf{M}^0(\cos^n\theta) = L_n\cos^n\Omega + \frac{1}{2}\frac{n(n-1)}{2!}(L_{n-2}-L_n)\cos^{n-2}\Omega\sin^2\Omega +$$
$$+\frac{3}{8}\frac{n(n-1)(n-2)(n-3)}{4!}(L_{n-4}-2L_{n-2}+L_n)\cos^{n-4}\Omega\sin^4\Omega+\dots. \qquad (e)$$

Thus, using (*c*), we obtain for $n = 1, 2, 3$ and 4

$$\left.\begin{aligned}
\mathbf{M}^0(\cos\theta) &= L\cos\Omega,\\
\mathbf{M}^0(\cos^2\theta) &= \left(1-3\frac{L}{Y}\right)\cos^2\Omega+\frac{L}{Y},\\
\mathbf{M}^0(\cos^3\theta) &= \left(L-5\frac{1}{Y}+15\frac{L}{Y^2}\right)\cos^3\Omega+3\frac{1}{Y}\left(1-3\frac{L}{Y}\right)\cos\Omega,\\
\mathbf{M}^0(\cos^4\theta) &= \left(1-10\frac{L}{Y}+35\frac{1}{Y^2}-105\frac{L}{Y^3}\right)\cos^4\Omega+\\
&\quad +6\frac{1}{Y}\left(L-5\frac{1}{Y}+15\frac{L}{Y^2}\right)\cos^2\Omega+3\frac{1}{Y^2}\left(1-3\frac{L}{Y}\right).
\end{aligned}\right\} \qquad (f)$$

III. *The manner of calculation of averages* $\overline{\mathbf{M}^0(\cos^n\theta)}$ *and* $\overline{\mathbf{M}(\cos^n\theta)}$

Denoting (see fig. 1) the angle AOA_2 by ψ, we can write

$$\cos\Omega = \cos\psi\cos\Omega_2 + \sin\psi\sin\Omega_2\cos\xi.$$

On the other hand

$$\cos\psi = \frac{W_2+W_1\cos A}{W} = \frac{y_2+y_1\cos A}{Y}$$

and $$\sin\psi = \frac{W_1\sin A}{W} = \frac{y_1\sin A}{Y}.$$

Thus $\cos\Omega$ becomes

$$\cos\Omega = \frac{1}{Y}[(y_2+y_1\cos A)\cos\Omega_2+y_1\sin A\sin\Omega_2\cos\xi]. \tag{g}$$

To calculate $\overline{\mathbf{M}^0(\cos\theta)}$, $\overline{\mathbf{M}^0(\cos^2\theta)}$, etc., we assume that for one-sixth of pairs of molecules, $A = 0$; for one-sixth, $A = 180°$; and for two-thirds, $A = 90°$. In these three cases we have, according to (6) and (g),

$$\left.\begin{aligned} &(1)\ A = 0 \text{ (fraction } \tfrac{1}{6}\text{)}: Y = y_1+y_2,\ \cos\Omega = \cos\Omega_2;\\ &(2)\ A = 180° \text{ (fraction } \tfrac{1}{6}\text{)}: Y = y_2-y_1,\ \cos\Omega = \cos\Omega_2;\\ &(3)\ A = 90° \text{ (fraction } \tfrac{2}{3}\text{)}: Y = \sqrt{(y_1^2+y_2^2)},\\ &\qquad\qquad \cos\Omega = \frac{1}{\sqrt{(y_1^2+y_2^2)}}(y_2\cos\Omega_2+y_1\sin\Omega_2\cos\xi). \end{aligned}\right\} \tag{h}$$

In this last case all directions perpendicular to OA_2 are equally possible, so that the mean value of $\cos\Omega$, which we denote by $\overline{\cos\Omega}'$ (the dash serves for distinction from the geometrical average over the sphere), may be obtained by calculating the integral $\frac{1}{2\pi}\int_0^{2\pi}\cos\Omega\,d\xi$. In similar manner we obtain the mean values of higher powers of $\cos\Omega$. It follows that

$$\left.\begin{aligned} \overline{\cos\Omega}' &= \frac{y_2}{(y_1^2+y_2^2)^{\frac{1}{2}}}\cos\Omega_2,\\ \overline{\cos^2\Omega}' &= \frac{1}{y_1^2+y_2^2}(y_2^2\cos^2\Omega_2+\tfrac{1}{2}y_1^2\sin^2\Omega_2),\\ \overline{\cos^3\Omega}' &= \frac{y_2}{(y_1^2+y_2^2)^{\frac{3}{2}}}(y_2^2\cos^3\Omega_2+\tfrac{3}{2}y_1^2\cos\Omega_2\sin^2\Omega_2),\\ \overline{\cos^4\Omega}' &= \frac{1}{(y_1^2+y_2^2)^2}(y_2^4\cos^4\Omega_2+3y_2^2y_1^2\cos^2\Omega_2\sin^2\Omega_2+\tfrac{3}{8}y_1^4\sin^4\Omega_2). \end{aligned}\right\} \tag{i}$$

Applying the rule expressed by (h) to (f) and taking into account (i), we can calculate $\overline{\mathbf{M}^0(\cos^n\theta)}$. We obtain, for example,

$$\overline{\mathbf{M}^0(\cos\theta)} = \left[\frac{1}{6}L(y_1+y_2)-\frac{1}{6}L(y_1-y_2)+\frac{2}{3}\frac{y_2}{\sqrt{(y_1^2+y_2^2)}}L\{\sqrt{(y_1^2+y_2^2)}\}\right]\cos\Omega_2, \tag{j}$$

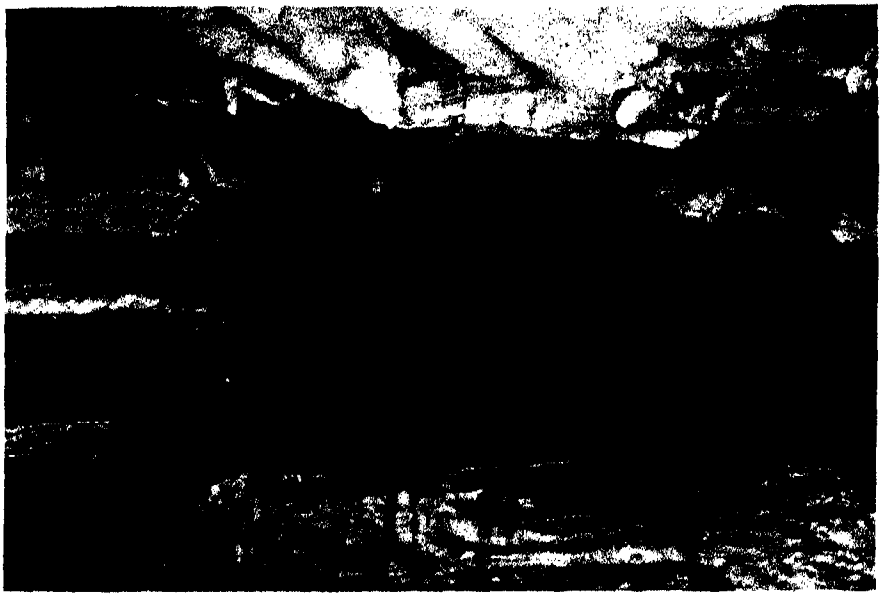

FIG. 2

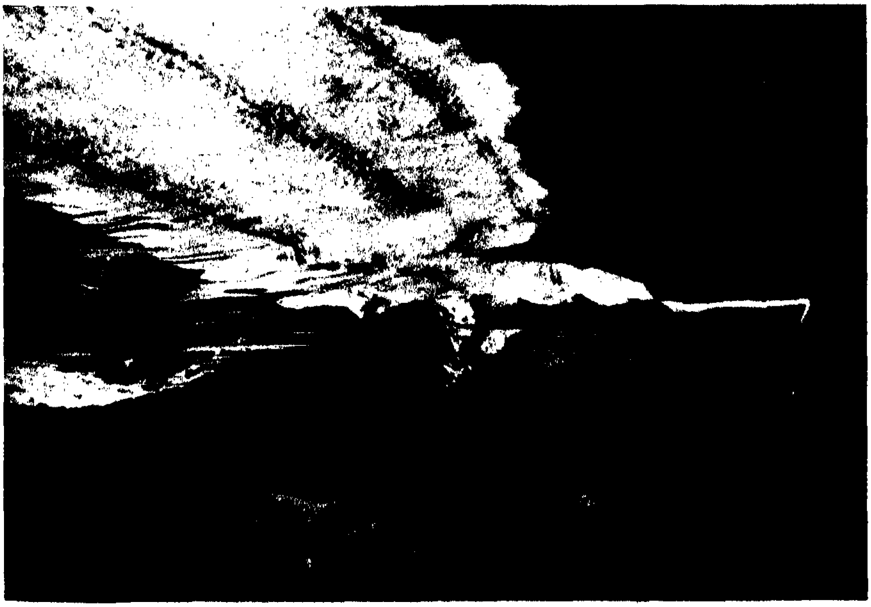

FIG. 1

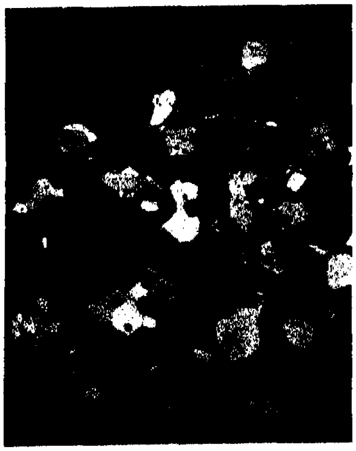

FIG. 3

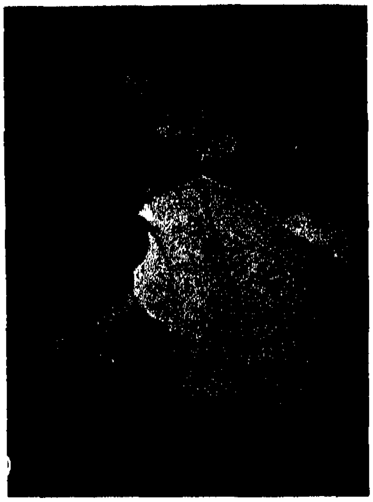

FIG. 4

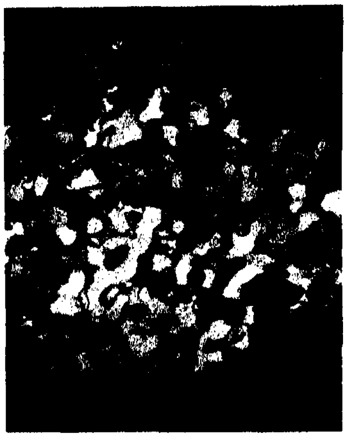

FIG. 5

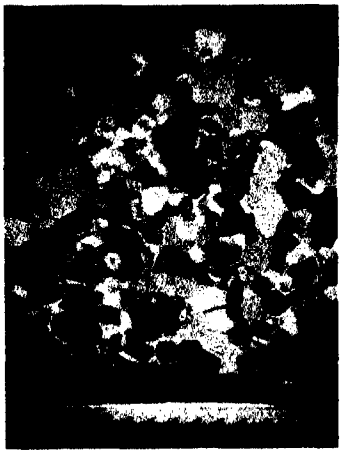

FIG. 6

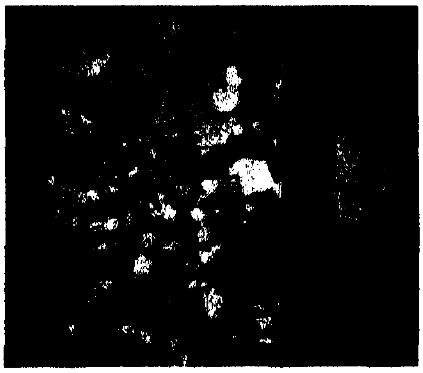

FIG. 7

$$\overline{\mathbf{M}^0(\cos^2\theta)} = \frac{1}{6}\left\{\left[1-3\frac{L(y_1+y_2)}{y_1+y_2}\right]\cos^2\Omega_2+\frac{L(y_1+y_2)}{y_1+y_2}\right\}+$$
$$+\frac{1}{6}\left\{\left[1-3\frac{L(y_1-y_2)}{y_1-y_2}\right]\cos^2\Omega_2+\frac{L(y_1-y_2)}{y_1-y_2}\right\}+$$
$$+\frac{2}{3}\left\{\left[1-3\frac{L\{\sqrt{(y_1^2+y_2^2)}\}}{\sqrt{(y_1^2+y_2^2)}}\right]\frac{(y_2^2-\frac{1}{2}y_1^2)\cos^2\Omega_2+\frac{1}{2}y_1^2}{y_1^2+y_2^2}+\frac{L\{\sqrt{(y_1^2+y_2^2)}\}}{\sqrt{(y_1^2+y_2^2)}}\right\} \qquad (j')$$

and so forth. Putting these expressions in formula (9) with $\phi = \cos^n\theta$, we calculate the averages of the form of $\overline{\mathbf{M}(\cos^n\theta)}$. In this manner, for $n = 1$ and without higher powers of x than the first, the expression (12) for $\overline{\mathbf{M}(\cos\theta)}$ is deduced.

IV. *Derivation of perturbed averages* $\overline{\mathbf{M}(\cos^n\theta)}^*$ *in zero and in first approximation*

Neglecting higher powers of x than 1, we can write, according to (9),

$$\overline{\mathbf{M}(\cos^n\theta)} = \overline{\mathbf{M}^0(\cos^n\theta)} + x\,[\overline{\mathbf{M}^0(\cos^{n+1}\theta)} - \overline{\mathbf{M}^0(\cos^n\theta)\,\mathbf{M}^0(\cos\theta)}], \qquad (k)$$

where the bar denotes the operation expressed by (h) and (i). Thus $\overline{\mathbf{M}(\cos^n\theta)}$ depends only on $\cos^m\Omega_2$. Since the spacial distribution of axes $\overrightarrow{OM}$ and $\overrightarrow{A_2O}$ is identical, we put instead of $\overline{\mathbf{M}(\cos^n\theta)}$ and $\cos^m\Omega_2$ the averages, which we denote respectively by $\overline{\mathbf{M}(\cos^n\theta)}^*$ and $\overline{\mathbf{M}(\cos^m\Omega_2)}^*$ and which we call "perturbed statistical averages". The equal powers of these averages, when even, are identical by pairs, and, when odd, are of opposite signs, as shown by conditions (28) and (29). Writing

$$\overline{\mathbf{M}(\cos^n\theta)}^* = \overline{\mathbf{M}^0(\cos^n\theta)}^* + x\,[\overline{\mathbf{M}^0(\cos^{n+1}\theta)}^* - \overline{\mathbf{M}^0(\cos^n\theta)\,\mathbf{M}^0(\cos\theta)}^*], \qquad (l)$$

we denote that the above described new operation is to be performed upon all terms of this expression.

At first we see that the zero approximation for $n = 2$ is

$$\overline{\mathbf{M}(\cos^2\theta)}^* = \overline{\mathbf{M}^0(\cos^2\theta)}^*.$$

Using (j') and condition (28), we find

$$\overline{\mathbf{M}(\cos^2\theta)}^* = \overline{\mathbf{M}(\cos^2\Omega_2)}^* = \tfrac{1}{3}, \qquad (m)$$

i.e. the value identical with the simple geometrical average $\overline{\cos^2\theta}$. Evidently, it was to be expected, because in the absence of an external field all directions of the dipole axes are equally possible. Therefore we can also write

$$\overline{\mathbf{M}(\cos^4\theta)}^{*} = \overline{\mathbf{M}^0(\cos^4\theta)}^{*} = \overline{\cos^4\theta} = \overline{\mathbf{M}(\cos^4\Omega_2)}^{*} = \tfrac{1}{5}. \qquad (n)$$

Using (m) and the condition (29) or (13), and performing the operation denoted by the asterisk upon the expression (12), we obtain the first approximation of $\overline{\mathbf{M}(\cos\theta)}^{*}$ in the form

$$\overline{\mathbf{M}(\cos\theta)}^{*} = -\overline{\mathbf{M}(\cos\Omega_2)}^{*} = \tfrac{1}{3}xR, \qquad (o)$$

where R, the reducing factor of electric polarization, is given by formula (16).

In a similar way we calculate $\overline{\mathbf{M}(\cos^3\theta)}^{*}$. According to (l) we have

$$\overline{\mathbf{M}(\cos^3\theta)}^{*} = \overline{\mathbf{M}^0(\cos^3\theta)}^{*} + x\left[\overline{\mathbf{M}^0(\cos^4\theta)}^{*} - \overline{\mathbf{M}^0(\cos^3\theta)\,\mathbf{M}^0(\cos\theta)}^{*}\right].$$

Performing successively the operations denoted by bars and by asterisks upon three terms of the right side of the above expression and using (m), (n), (o) and (29), we find

$$\overline{\mathbf{M}(\cos^3\theta)}^{*} = -\overline{\mathbf{M}(\cos^3\Omega_2)}^{*} = \tfrac{1}{5}xR, \qquad (p)$$

with the same R as given by (16).

V. *Deduction of the formula for the reducing factor R_K for the molecular Kerr constant*

For this purpose it is necessary to calculate $\overline{\mathbf{M}(\cos^2\theta)}^{*}$ in the second approximation, i.e. by neglecting higher powers of x than 2. According to (9) and to the rule of averaging with perturbation, we have

$$\begin{aligned}\overline{\mathbf{M}(\cos^2\theta)}^{*} = {} & \overline{\mathbf{M}^0(\cos^2\theta)}^{*} + x\left[\overline{\mathbf{M}^0(\cos^3\theta)}^{*} - \overline{\mathbf{M}^0(\cos^2\theta)\,\mathbf{M}^0(\cos\theta)}^{*}\right] + \\ & + \tfrac{1}{2}x^2\left[\overline{\mathbf{M}^0(\cos^4\theta)}^{*} - \overline{\{\mathbf{M}^0(\cos^2\theta)\}^2}^{*} - 2\,\overline{\mathbf{M}^0(\cos^3\theta)\,\mathbf{M}^0(\cos\theta)}^{*} + \right. \\ & \left. + 2\,\overline{\mathbf{M}^0(\cos^2\theta)\{\mathbf{M}^0(\cos\theta)\}^2}^{*}\right]. \qquad (r)\end{aligned}$$

Anticipating the form of this expression, we may accept a form, containing only the even powers of x (like the usual statistical average:

$$\mathbf{M}(\cos^2\theta) = \tfrac{1}{3} + \tfrac{2}{45}x^2 - \ldots),$$

since the change of sign before x (i.e. the change of direction of the external field) cannot yield any change in the mean value of $\cos^2\theta$. Thus we can write

$$\overline{\mathbf{M}(\cos^2\theta)}^{*} = \overline{\mathbf{M}(\cos^2\Omega_2)}^{*} = \tfrac{1}{3} + \tfrac{2}{45}x^2R_K - \ldots, \qquad (s)$$

where R_K is to be calculated. For this purpose we must calculate all terms on the right hand of (r): the first—with an accuracy including x^2, the second and the third—with an accuracy including x^1, and the rest—by omitting even x^1. Thus, putting (s) in (j'), we find

$$\overline{\mathbf{M}^0(\cos^2\theta)}^{\,*} = \tfrac{1}{3} + \tfrac{2}{45}x^2 R_K \left[1 - \frac{y_1^2}{y_1^2+y_2^2} - \frac{1}{2}\frac{L(y_1+y_2)}{y_1+y_2} - \frac{1}{2}\frac{L(y_1-y_2)}{y_1-y_2} - 2\frac{L\{\sqrt{(y_1^2+y_2^2)}\}}{\sqrt{(y_1^2+y_2^2)}}\frac{y_2^2-\frac{1}{2}y_1^2}{y_1^2+y_2^2}\right]. \qquad (t)$$

In such a way, using expressions (f), (h), (i) and approximations (m), (n), (o), (p), sufficiently accurate in this case, we obtain the other terms of (r). By equating the left side of (r) with (s), we calculate R_K and so we find the formula (33).

Calculating expressions as (t) and others, we put in (j') or in similar expressions $\overline{\mathbf{M}(\cos^n \Omega_2)}^{\,*}$ instead of $\cos^n \Omega_2$. In the cases (1) and (2) (i.e. when $\Lambda = 0$, or 180°, see (h)) we may write, since $\cos\Omega_2$ is identical with $\cos\Omega$,

$$\overline{\mathbf{M}(\cos^n \Omega)}^{\,*} = \overline{\mathbf{M}(\cos^n \Omega_2)}^{\,*},$$

or

$$\overline{\mathbf{M}(\cos \Omega)}^{\,*} = -\tfrac{1}{3}xR, \qquad (u)$$

$$\left.\begin{aligned} \overline{\mathbf{M}(\cos^2 \Omega)}^{\,*} &= \tfrac{1}{3} + \tfrac{2}{45}x^2 R_K, \\ \overline{\mathbf{M}(\cos^3 \Omega)}^{\,*} &= -\tfrac{1}{5}xR, \\ \overline{\mathbf{M}(\cos^4 \Omega)}^{\,*} &= \tfrac{1}{5}. \end{aligned}\right\} \qquad (u')$$

In the case (3) ($\Lambda = 90°$), on the other hand, these equalities do not hold. There appear, instead of them, the formulae resulting from (i) and (n), (o), (p), (s). It is convenient, in such calculations, to express these averages in a final form. Thus, in the case $\Lambda = 90°$, we have

$$\overline{\mathbf{M}(\overline{\cos \Omega'})}^{\,*} = -\frac{1}{3}\frac{y_2}{\sqrt{(y_1^2+y_2^2)}}xR, \qquad (v)$$

$$\left.\begin{aligned} \overline{\mathbf{M}(\overline{\cos^2 \Omega'})}^{\,*} &= \frac{1}{3} + \frac{2}{45}\frac{y_2^2-\frac{1}{2}y_1^2}{y_1^2+y_2^2}x^2 R_K, \\ \overline{\mathbf{M}(\overline{\cos^3 \Omega'})}^{\,*} &= -\frac{1}{5}\frac{y_2}{\sqrt{(y_1^2+y_2^2)}}xR, \\ \overline{\mathbf{M}(\overline{\cos^4 \Omega'})}^{\,*} &= \tfrac{1}{5}. \end{aligned}\right\} \qquad (v')$$

VI. *Deduction of the formula for reducing factor R_S for electric saturation effect*

According to the formula (39), we write a similar expression for $\overline{\mathbf{M}(\cos\theta)}^{*}$. The calculation of the right-hand terms, which have a general form of $\overline{\mathbf{M}^0(\cos^n\theta)\,\mathbf{M}^0(\cos^m\theta)}^{*}$, is rather long, but does not offer any special difficulties. Using the expressions (f) and applying the rule expressed by (h), together with the first expression of (i), and together with (u') and (v'), we calculate $\overline{\mathbf{M}(\cos\theta)}^{*}$ with an accuracy including x^3. Thus we find

$$\begin{aligned}\overline{\mathbf{M}(\cos\theta)}^{*} = {} & \left[\frac{1}{6}L(y_1+y_2)-\frac{1}{6}L(y_1-y_2)+\frac{2}{3}\frac{y_2}{\sqrt{(y_1^2+y_2^2)}}L\{\sqrt{(y_1^2+y_2^2)}\}\right]\overline{\mathbf{M}(\cos\Omega_2)}^{*}+ \\ & +\tfrac{1}{3}x\left[1-\tfrac{1}{6}L^2(y_1+y_2)-\tfrac{1}{6}L^2(y_1-y_2)-\tfrac{2}{3}L^2\{\sqrt{(y_1^2+y_2^2)}\}\right]+ \\ & +\frac{1}{45}x^3\left\{R_K\left[\frac{2y_2^2}{y_1^2+y_2^2}-\frac{L(y_1+y_2)}{y_1+y_2}-\frac{L(y_1-y_2)}{y_1-y_2}-\right.\right. \\ & -4\frac{y_2^2-\frac{1}{2}y_1^2}{y_1^2+y_2^2}\frac{L\{\sqrt{(y_1^2+y_2^2)}\}}{\sqrt{(y_1^2+y_2^2)}}-\frac{1}{3}L^2(y_1+y_2)-\frac{1}{3}L^2(y_1-y_2)- \\ & \left.-\frac{4}{3}\frac{y_2^2-\frac{1}{2}y_1^2}{y_1^2+y_2^2}L^2\{\sqrt{(y_1^2+y_2^2)}\}\right]+9R\left[\frac{1}{6}L(y_1+y_2)\,Q(y_1+y_2)-\right. \\ & \left.-\frac{1}{6}L(y_1-y_2)\,Q(y_1-y_2)+\frac{2}{3}\frac{y_2}{\sqrt{(y_1^2+y_2^2)}}L\{\sqrt{(y_1^2+y_2^2)}\}\,Q\{\sqrt{(y_1^2+y_2^2)}\}\right]- \\ & \left.-\tfrac{1}{6}R^*(y_1+y_2)-\tfrac{1}{6}R^*(y_1-y_2)-\tfrac{2}{3}R^*\{\sqrt{(y_1^2+y_2^2)}\}\right\}, \qquad (w)\end{aligned}$$

where Q and R^* are given by formulae (43c) and (42). Putting

$$\overline{\mathbf{M}(\cos\theta)}^{*} = -\overline{\mathbf{M}(\cos\Omega_2)}^{*},$$

we obtain the expression (40) with R_S, given by formula (41).

VII. *Evaluation of some hyperbolic function of one variable*

The reducing factors R, R_K and R_S, obtained in this theory, are generally dependent upon two variables: y_1 and y_2. Since in the formulae determining these factors appear some characteristic functions of one variable y ($y = y_1+y_2$, or $y = y_1-y_2$, or $y = \sqrt{(y_1^2+y_2^2)}$), it is convenient to evaluate these functions for a number of values of the parameter y. This has been performed for the functions of Langevin (L), Fowler (Q) and Debye (R^* and $\mathscr{R}$). The corresponding values are collected in the table. They serve for drawing the graphs, from which the values for other y's may be interpolated and used to calculate any required values.

TABLE. SOME NUMERICAL VALUES OF HYPERBOLIC FUNCTIONS L, Q, R^* AND $\mathscr{R}$

y	$L(y)$	$Q(y)$	$R^*(y)$	$\mathscr{R}(y)$
0	0	0·3333	1	0·3333
0·1	0·0333	0·3326	0·996	0·3326
0·2	0·0665	0·331	0·982	0·3304
0·3	0·0994	0·328	0·961	0·3268
0·5	0·1639	0·318	0·902	0·3154
0·8	0·2560	0·295	0·759	0·2909
1·0	0·3130	0·276	0·655	0·2708
1·3	0·3913	0·245	0·4989	0·2380
1·5	0·4381	0·224	0·4041	0·2161
2·0	0·5373	0·174	0·2230	0·1656
2·5	0·6136	0·1327	0·1150	0·1253
3·0	0·6716	0·1012	0·0575	0·0955
4·0	0·7507	0·0610	0·0168	0·0581
5·0	0·8001	0·0398	0·0054	0·03833
6·0	0·8333	0·0277	0·0023	0·02702
8·0	0·8750	0·0156	0·00073	0·01539
10·0	0·9000	0·0100	0·00030	0·00990
12·0	0·9167	0·00694	0·00014	0·00688

REFERENCES

Debye, P. 1935 *a* *Phys. Z.* **36**, 100.
— 1935 *b* *Phys. Z.* **36**, 193.
Falkenhagen, H. 1938 *Phys. Z.* **39**, 806.
Fowler, R. H. 1935 *Proc. Roy. Soc.* A, **149**, 1.
Friedrich, H. 1937 *Phys. Z.* **38**, 318.
Kozłowski, L. 1938 *Math.-phys. Abh. Warschau*, **46**, 31.
Onsager, L. 1936 *J. Amer. Chem. Soc.* **58**, 1486.
Piekara, A. 1937 *a* *Act. phys. polon.* **6**, 130, 150.
— 1937 *b* *C.R. Acad. Sci., Paris*, **204**, 1106
— 1938 *Z. Phys.* **108**, 395.
— 1939 *C.R. Acad. Sci., Paris*, **208**, 990, 1150.
Piekara, A. and Piekara, B. 1934 *C.R. Acad. Sci., Paris*, **198**, 1018.
— — 1936 *C.R. Acad. Sci., Paris*, **203**, 852.
— — 1937 *Phys. Z.* **38**, 671.
Van Vleck, J. H. 1937 *J. Chem. Phys.* **5**, 320.
Zakrzewski, K. and Piekara, A. 1939 *Bull. Acad. Pol. Sci., Cracow*, A (in the press).

Classical theory of mesons

By H. J. Bhabha
Gonville and Caius College, Cambridge

(*Communicated by P. A. M. Dirac, F.R.S.—Received* 11 *April* 1939—
Revised 29 *June* 1939)

The quantum theory of the meson (Kemmer 1938; Fröhlich, Heitler and Kemmer 1938; Bhabha 1938; Yukawa, Sakata and Taketani 1938; Stueckelberg 1938), in spite of its great similarity to the quantum theory of radiation, differs from it in certain important respects. The total Hamiltonian for the system of protons or neutrons and mesons contains terms in the interaction energy of mesons with the heavy particles which increase with increasing energy of the mesons. This has brought physicists to the prevalent view that for high energies this theory leads to large probabilities for multiple processes, and to explosions of the type first investigated by Heisenberg (1936). Indeed, the possibility of such processes has recently caused Heisenberg (1938) to take the position that they set a limit to the applicability of quantum mechanics. Connected with the same behaviour of the interaction is the fact that many effects, such for example as the perturbation of the self-energy of a proton calculated to the second order in the interaction, diverge more acutely than in ordinary radiation theory, and this has led Heitler (1938) and others to doubt the correctness of the fundamental equations even for mesons of energy comparable with their rest mass.

All the above views are in essence based on the results of second-order perturbation calculations. There is, however, another approach to the problem. Using the commutation rules for the observables and the well-known equations of motion of quantum mechanics, we can derive exactly from the same Hamiltonian on the one hand the Dirac equation for the proton or neutron under the influence of a given meson field, and on the other hand the equations of the meson field influenced by the presence of neutrons. (For brevity we shall henceforth only speak of neutrons, whereas our remarks will apply equally well to protons, since the two are on the same footing as far as this theory is concerned.) Treating the Hamiltonian "classically", that is, treating all the observables occurring in it as commuting variables, we can as usual again derive the same two sets of equations. In this paper, as a first step in the problem, we shall deal with classical equations, since it is possible either to solve them exactly, or at least to give approximate solutions the errors of which can be strictly estimated.

Now meson theory differs from ordinary radiation theory in three particulars. First, the mesons have a finite rest mass μ. Secondly, they have a direct interaction with the spin of the neutron characterized by the constant g_2, besides the constant g_1 which corresponds to the charge in electromagnetic theory. Thirdly, the meson field itself may carry electromagnetic charge. It should be noticed at once that g_2 is of the dimensions of a length times charge, so that the meson theory introduces *two independent* lengths which may be defined by $\chi = \hbar/\mu$ and g_2/g_1, and although with the experimental values of the constants these are of the same order of magnitude, theoretically the two must not be confused as there is no connexion between them yet. As has already been mentioned the quantized meson theory seems to lead to results different in many essentials from those of radiation theory, and in order to determine to what extent this is due to each of the three differences mentioned above, we shall deal as a first step with a theory which differs from radiation theory in only one particular. In this paper we shall investigate the classical behaviour of an *uncharged* meson field with a characteristic length χ connected with the rest mass μ, while the constant g_2 will be put equal to zero. In the course of the paper the result will be established that *the finite rest mass of the meson introduces no essential difference in the behaviour of mesons at high energies* and hence that the fundamental length required by Heisenberg cannot be identified with χ. *The type of explosions investigated by Heisenberg, if they exist, cannot therefore be connected with the rest mass of the meson but would be due either to the interaction constant g_2 or to the fact that the meson field carries electric charge.*

We shall assume that the equations for the meson field influenced by the presence of neutrons are exact. On the other hand, we should not expect the Dirac equation describing the motion of the neutron under the influence of the meson field to be exact, since this neglects what is the equivalent of radiation damping on the neutron. We shall therefore derive new classical equations for a point neutron from the consideration that energy and momentum must be conserved. In this way we shall arrive at a self-consistent mathematical scheme which is entirely free from any difficulties about infinite self-energies. This scheme is a generalization of the scheme already obtained by Dirac (1938) for the classical behaviour of electrons and radiation, and goes over continuously into it as the mass of the meson tends to zero.

By using these equations we shall calculate the scattering of mesons by neutrons and obtain a formula which is a generalization of the Thomson formula as modified by Dirac. It will appear that as far as the classical theory is concerned, we can at any stage in the calculations put $\chi = 0$ and make a transition to electromagnetic theory without getting any infinities or inconsistencies. For mesons the classical theory is also of practical interest. The treatment of a field classically instead of quantum-mechanically is equivalent to a neglect of the momentum properties of the individual light quanta. We may therefore expect the classical theory to give correct results for all processes where the momenta of individual mesons is small compared with the rest mass of neutrons. This covers the whole field of nuclear phenomena and an important part of cosmic-ray phenomena. The classical theory will give correct results for mesons of a few hundred million volts, and will even give the correct order of magnitude for mesons of 10^9 eV.

THE MESON FIELD OF NEUTRONS

We shall use tensor notation throughout, and for the purpose of raising and lowering suffixes use the fundamental tensor $g_{\mu\nu}$ defined by $g_{00} = 1$, $g_{11} = g_{22} = g_{33} = -1$ with all the other components vanishing. The velocity of light will be put equal to unity. We shall further use the notation of writing u for $+(u_\mu u^\mu)^{\frac{1}{2}}$, where u_μ is any vector. We assume that the meson field is described by potentials U_μ and field strengths $G_{\mu\nu}$ which satisfy the equations

$$\left.\begin{aligned} G_{\mu\nu} - 4\pi S_{\mu\nu} &= -\left(\frac{\partial}{\partial x^\mu} U_\nu - \frac{\partial}{\partial x^\nu} U_\mu\right), \\ \chi^2 U_\nu - 4\pi R_\nu &= \frac{\partial}{\partial x_\mu} G_{\mu\nu}, \end{aligned}\right\} \tag{1}$$

where $\chi = \mu/\hbar$, μ being the rest mass of the meson. In classical theory neither μ nor $\hbar$ will appear explicitly, but only through the constant χ which is now a fundamental constant belonging to the field. The limit $\mu = 0$ corresponds to the limit $\chi = 0$, and in this case the equations (1) become the Maxwell equations. Since we are dealing with neutral mesons, we may take all the quantities in (1) to be real. R_ν is a four vector describing the effect of the neutron "charge" on the field, and $S_{\mu\nu}$ is an antisymmetrical tensor describing the effect of the neutron dipole moment. From the second of equations (1) it follows that

$$\chi^2 \frac{\partial}{\partial x_\nu} U_\nu = \frac{\partial}{\partial x_\nu} R_\nu. \tag{2}$$

A proton remains a proton and a neutron a neutron when a neutral meson is absorbed or emitted. We may further assume for the purpose of this paper that the emission of no charged mesons takes place. The right-hand side of

(2) then vanishes, and hence also the left-hand side. It then follows from the equations (1) that

$$\frac{\partial}{\partial x_\mu}\frac{\partial}{\partial x^\mu}U_\nu + \chi^2 U_\nu = 4\pi R_\nu + 4\pi\frac{\partial}{\partial x_\mu}S_{\mu\nu}. \tag{3}$$

It is shown in the appendix that the solution of (3) can be given with the help of a Green's function in the form

$$U_\nu(x_\rho) = \iiint\int_{-\infty}^{\infty} dx'_\rho\, G(x_\rho, x'_\rho)\left\{R_\nu(x'_\rho) + \frac{\partial}{\partial x'_\mu}S_{\mu\nu}(x'_\rho)\right\}, \tag{4}$$

where x'_ρ stands for the four variables x'_0, x'_1, x'_2, x'_3. The Green's function for this problem is

$$G(x_\rho, x'_\rho) = \left.\begin{pmatrix} 2\delta(u^2) - \dfrac{\chi}{u}J_1(\chi u) \\ 0 \\ 0 \end{pmatrix}\quad \begin{array}{r} u_0 > u_r \\ |u_0| < u_r \\ u_0 < -u_r \end{array}\right\} \tag{5a}$$

or

$$G(x_\rho, x'_\rho) = \left.\begin{pmatrix} 0 \\ 0 \\ 2\delta(u^2) - \dfrac{\chi}{u}J_1(\chi u) \end{pmatrix}\quad \begin{array}{r} u_0 > u_r \\ |u_0| < u_r \\ u_0 < -u_r \end{array}\right\} \tag{5b}$$

where we have written $u_\rho = x_\rho - x'_\rho$, and $u_r = \sum\limits_1^3 (-u_k u^k)^{\frac{1}{2}}$. Here J_1 is the Bessel function of order 1. We shall frequently have to make use of the following properties of Bessel's functions:

$$s^{-n}J_{n+1}(s) = -\frac{d}{ds}\{s^{-n}J_n(s)\}, \tag{6a}$$

$$\operatorname*{Lt}_{s\to 0}\frac{1}{s^n}J_n(s) = \frac{1}{2^n n!}. \tag{6b}$$

We notice that the Green's function only has a singularity in the form of a δ-function, the second part dependent on χ only contributing a plain discontinuity on the light cone. This part tends to zero as $\chi \to 0$. This is the basis of all the results which will follow below, and shows at once that the worst singularities in the meson field are identical with those of the electromagnetic field, the additional singularities being of lesser order.

In the classical theory we must treat the neutron as a point with a dipole attached to it moving along a classical world line which we assume to be given. We denote its co-ordinates by z_μ which are functions of τ, the proper time along the world line from some arbitrary point on it. Consistently with the quantum-mechanical expression for R_ν as a charge-current density, we now assume

$$R_\nu = g_1 \int_{-\infty}^{\infty} d\tau\, v_\nu(\tau)\, \delta(x_0 - z_0)\, \delta(x_1 - z_1)\, \delta(x_2 - z_2)\, \delta(x_3 - z_3), \tag{7}$$

where v_ν is the velocity $\dot{z}_\nu$. We shall denote a differentiation with respect to the proper time by a dot. g_1 is a constant playing the part of a charge. Similarly we may write for $S_{\mu\nu}$

$$S_{\mu\nu} = g_2 \int_{-\infty}^{\infty} d\tau\, S'_{\mu\nu}(\tau)\, \delta(x_0 - z_0)\, \delta(x_1 - z_1)\, \delta(x_2 - z_2)\, \delta(x_3 - z_3), \tag{8}$$

the $S'_{\mu\nu}$ being a function of τ satisfying the relation $S'^2 =$ constant along the world line. g_2 is another constant. The $S_{\mu\nu}$ term can be treated exactly like the R_ν term, but on account of the very much greater complication which it introduces, we shall omit it from this paper in order not to confuse the issue. Since g_2 does not occur any further, we shall simply write g instead of g_1.

Introducing (7) into (4) and using (5a)

$$U_\nu^{\text{ret}}(x_\rho) = g\frac{v_\nu}{\kappa} - g\chi \int_{-\infty}^{\tau_0} d\tau \frac{v_\nu}{s} J_1(\chi s), \tag{9}$$

where

$$\left.\begin{aligned} s_\mu &= x_\mu - z_\mu(\tau), \\ \kappa &= s_\mu v^\mu, \end{aligned}\right\} \tag{10}$$

and τ_0 is the proper time of the "retarded" point, i.e. the point on the world line such that $s_\mu s^\mu = 0$ and $s_0 > 0$. We at once make the convention that whenever any quantity dependent on τ does not occur inside an integral with respect to τ then it is to be taken at the retarded point $\tau = \tau_0$. Thus the first term on the right-hand side of (9) is $v_\nu(\tau_0)\,[\{x_\mu - z_\mu(\tau_0)\}\, v^\mu(\tau_0)]^{-1}$. This is the expression corresponding to the retarded potentials. There is a similar solution given by (5b), which gives one the advanced potentials. In this paper we shall only consider retarded potentials since the theory is quite symmetrical in retarded and advanced potentials.

From the first of equations (1) it then follows, using the rules that are given in the appendix for differentiating with respect to x_μ, that

$$G_{\mu\nu}^{\text{ret}} = G_{\mu\nu}^{0} + G_{\mu\nu}^{\chi}, \tag{11}$$

where

$$G_{\mu\nu}^{0} = -g\left\{\frac{s_\mu v_\nu - s_\nu v_\mu}{\kappa^3}(1-\kappa') + \frac{s_\mu \dot{v}_\nu - s_\nu \dot{v}_\mu}{\kappa^2}\right\}, \tag{12}$$

with $\kappa' = s_\mu \dot{v}^\mu$, and

$$G_{\mu\nu}^{\chi} = g\frac{\chi^2}{2}\frac{s_\mu v_\nu - s_\nu v_\mu}{\kappa} - g\chi^2 \int_{-\infty}^{\tau_0} d\tau \frac{s_\mu v_\nu - s_\nu v_\mu}{s^2} J_2(\chi s). \tag{13}$$

The first term of $G^{\chi}_{\mu\nu}$ is singular on the world line, since its value at any point on it is not unique, but depends on the direction from which the point is approached. Both $G^{\chi}_{\mu\nu}$ and the part dependent on χ in U^{ret}_{ν} of (9) are, however, quite finite at all points of space including the world line of the neutron, and tend continuously to zero as $\chi \to 0$. The only infinities in the retarded field are therefore contained in $G^{0}_{\mu\nu}$ which is just the Maxwell field for a moving-point charge. The expressions ($5a$, b) and (11) show explicitly that the singularities in the meson field are no more acute than in ordinary Maxwell theory, and further, that the limit to the case $\chi = 0$ can be made continuously.

The energy-momentum tensor $T_{\mu\nu}$ corresponding to the equations (1) in a region not occupied by a neutron is (see for example Proca 1936)

$$4\pi T_{\mu\nu} = G_{\mu\sigma} G^{\sigma}{}_{\nu} + \tfrac{1}{4} g_{\mu\nu} G_{\sigma\rho} G^{\sigma\rho} + \chi^2 U_{\mu} U_{\nu} - \frac{\chi^2}{2} g_{\mu\nu} U_{\rho} U^{\rho}. \tag{14}$$

In the absence of neutrons, the solution of (1) can be written in the form of plane waves

$$U_{\mu} = \alpha_{\mu} \cos(w_{\nu} x^{\nu}), \tag{15}$$

where the direction of polarization α_{μ} and the direction of propagation ω_{ν} satisfy the relations which follow from (2) and (3)

$$\left.\begin{aligned} \alpha_{\mu}\omega^{\mu} &= 0, \\ \omega_{\mu}\omega^{\mu} &= \chi^2. \end{aligned}\right\} \tag{16}$$

The energy momentum tensor for this solution, using (14), is, on the average,

$$-\frac{1}{8\pi} \omega_{\mu} \omega_{\nu} \alpha^2. \tag{17}$$

We notice that since α_{μ} is perpendicular to the time-like vector ω_{μ}, α^2 is negative.

THE CLASSICAL EQUATIONS OF MOTION OF A NEUTRON

We have now to find the classical equations of motion of a neutron to take the place of the Dirac equation of the quantized theory, and we further wish to take account not only of the effect of an external meson field on the neutron, but also of the reaction of the neutron's own radiated meson field. The easiest way to do this is, following Dirac, to consider the world line of the neutron as given and to enclose it by a narrow tube, the radius of which will in the end be made to tend to zero. We now derive the equations of motion from the condition that the flow of energy and momentum out of a portion of the tube in the presence of an external field as calculated by using (14) shall only depend on the conditions at the two ends of the tube, that is, that it shall be a perfect differential. We shall thus have conservation of energy and momentum, and the reaction of the radiated meson field will be included in the equations.

It can be shown easily that our results will not depend on the actual shape of the world tube. It is convenient to take the world tube defined by

$$\kappa \equiv s_\mu v^\mu = \epsilon, \tag{18}$$

where ϵ is some constant which in the end will be made to tend to zero. s_μ, in accordance with (10), is the distance from a point x_μ on the world tube to the retarded point $z_\mu(\tau_0)$, so that $s^2 = 0$. If we fix our attention on any point on the world line in the Lorentz frame in which the electron is instantaneously at rest, then a sphere about this point of radius ϵ taken at a time ϵ later is a section of this world tube.

It is shown in the appendix that the flow of energy and momentum out of that portion of the world tube with ends defined by the proper times τ_1 and τ_2 is

$$\int_{\tau_1}^{\tau_2} d\tau \left[g^2 \left(\frac{1}{2} \frac{\dot{v}_\mu}{\epsilon} - \tfrac{2}{3} v_\mu \dot{v}^2 \right) + g(\tilde{G}^\chi_{\mu\sigma} + G^{\text{in}}_{\mu\sigma})\, v^\sigma \right], \tag{19}$$

where terms which vanish with ϵ are omitted. $G^{\text{in}}_{\mu\nu}$ is the incoming external field, defined, following Dirac, as the actual field $G^{\text{act}}_{\mu\nu}$ at the point minus the retarded field $G^{\text{ret}}_{\mu\nu}$ given by (11),

$$G^{\text{in}}_{\mu\nu} = G^{\text{act}}_{\mu\nu} - G^{\text{ret}}_{\mu\nu}. \tag{20}$$

$\tilde{G}^\chi_{\mu\nu}$ is the second term in (13) of $G^\chi_{\mu\nu}$,

$$\tilde{G}^\chi_{\mu\nu} = -g\chi^2 \int_{-\infty}^{\tau_0} d\tau \, \frac{s_\mu v_\nu - s_\nu v_\mu}{s^2} J_2(\chi s). \tag{21}$$

The first term of $G^\chi_{\mu\nu}$ in (13) is not single valued on the world line. Its value averaged over all directions of approach to a point on the world line is, however, zero. We may alternatively look on $\tilde{G}^\chi_{\mu\nu}$ as the value of $G^\chi_{\mu\nu}$ at any point averaged over a small region of space surrounding that point. $\tilde{G}^\chi_{\mu\nu}$ will then be identical with $G^\chi_{\mu\nu}$ everywhere except on the world line, where it will reduce to (21). In expression (20), the values of $G^{\text{in}}_{\mu\nu}$ and $\tilde{G}^\chi_{\mu\nu}$ are taken for any value of τ at the point on the world line corresponding to it.

In accordance with what we have said at the beginning of this section, the integrand of (19) must be a perfect differential, since it must only depend on conditions at the two ends of the tube. We must then have

$$g^2\left(\frac{1}{2}\frac{\dot{v}_\mu}{\epsilon}-\tfrac{2}{3}v_\mu\dot{v}^2\right)+g(\tilde{G}^\chi_{\mu\sigma}+G^{\text{in}}_{\mu\sigma})\,v^\sigma=\dot{B}_\mu, \tag{22}$$

where $\dot{B}_\mu$ is some tensor. Multiplying (22) by v_μ we see that $\dot{B}_\mu$ must satisfy

$$\dot{B}_\mu v^\mu=-\tfrac{2}{3}g^2\dot{v}^2. \tag{23}$$

Here we have made use of two of the relations

$$\left.\begin{aligned} v^2&=1,\\ v_\mu\dot{v}^\mu&=0,\\ v_\mu\ddot{v}^\mu+\dot{v}^2&=0.\end{aligned}\right\} \tag{24}$$

Therefore $\dot{B}_\mu$ must be of the form

$$\dot{B}_\mu=\dot{B}'_\mu+\tfrac{2}{3}g^2\ddot{v}_\mu,$$

where $\dot{B}'_\mu v^\mu=0$. The simplest assumption for B'_μ is to put it equal to a constant times v_μ. Writing the constant in the form $(1/2\epsilon-M)$, we finally get for the equations of motion

$$M\dot{v}_\mu-\tfrac{2}{3}g^2\ddot{v}_\mu-\tfrac{2}{3}g^2v_\mu\dot{v}^2+g(\tilde{G}^\chi_{\mu\sigma}+G^{\text{in}}_{\mu\sigma})\,v^\sigma=0. \tag{25}$$

Dividing by $\tfrac{2}{3}g^2$ and introducing (21), we may write them in the form

$$a\dot{v}_\mu-\ddot{v}_\mu-v_\mu\dot{v}^2-\tfrac{3}{2}\chi^2v^\sigma\int_{-\infty}^{\tau}d\tau'\,\frac{s_\mu v_\sigma(\tau')-s_\sigma v_\mu(\tau')}{s^2}\,J_2(\chi s)=-\frac{3}{2g}G^{\text{in}}_{\mu\sigma}v^\sigma, \tag{26}$$

where we have written a for $3M/2g^2$. Explicitly, $s_\mu=z_\mu(\tau)-z_\mu(\tau')$. These are the fundamental equations of motion of a neutron in a meson field. They have a very similar form to the equations recently given by Dirac (1938) for the classical motion of an electron in an electromagnetic field. The only difference is the appearance of the term $\tilde{G}^\chi_{\mu\nu}$. It shows that the motion of the neutron at a time τ is influenced in principle by the whole previous history of the neutron. In practice, however, the integral (21) converges fairly rapidly, and only the behaviour at times not very much earlier than $1/\chi$ will be of importance. This is what we should expect, since meson waves are propagated with all velocities less than that of light so that a neutron may be influenced at a time τ by a disturbance it has emitted at an earlier instant. We notice again that the equations go over quite continuously as $\chi\to 0$ into the equation given by Dirac. We shall return to this point later.

The equations (26) with no ingoing field, that is with the right-hand side equal to zero, have solutions of two types, as in the case of the equations found by Dirac. We can see at once that v_μ constant is a solution, for the integral vanishes from antisymmetry since in this case s_μ is proportional to v_μ, and the other three terms also vanish. The second type consists of solutions in which the neutron by itself works up an acceleration at an ever-increasing rate. We shall not consider these in detail. The corresponding solutions when $\chi = 0$ have been given by Dirac. It is enough to say that following Dirac we must postulate here also that only those solutions occur in nature for which the velocity does not tend to infinity as time progresses. Boundary conditions restricting the allowed solutions to those which do not tend to infinity at large distances are common in physics. We have here for the first time a boundary condition in the time co-ordinate, restricting the allowed solutions to those where the velocity does not become infinite in the infinitely distant future.

ENERGY OF THE FIELD ASSOCIATED WITH A NEUTRON

Pryce (1938) has shown that it is possible to alter the definition of the electromagnetic energy-momentum tensor when a charge is present, so that the total energy associated with a point charge is finite. It is possible to do the same for the meson field. Since we have already shown that the singularities in the meson field are identical with those of the electromagnetic field, the additional terms being finite, it follows that we can at once take over the tensor which has to be subtracted from (14). The new definition of the energy-momentum tensor $T'_{\mu\nu}$ for the meson-field energy is then

$$T'_{\mu\nu} = T_{\mu\nu} - \frac{\partial}{\partial x_\sigma}\kappa_{\sigma\mu\nu}, \tag{27}$$

where the tensor $\kappa_{\sigma\mu\nu}$ is the one given in the paper of Pryce.

We now wish to calculate the meson-field energy associated with a neutron at rest. Instead of starting from $T'_{\mu\nu}$ it is more convenient to do it by a different way. For a neutron at rest at the origin

$$U_0 = g\frac{e^{-\chi r}}{r}; \quad U_1 = U_2 = U_3 = 0 \quad \left(r^2 = \sum_1^3 x_k^2\right).$$

In this case, using (14) and (1),

$$4\pi T_{00} = \tfrac{1}{2}\sum_{k=1}^{3}\left(\frac{\partial}{\partial x_k}U_0\right)^2 + \tfrac{1}{2}\chi^2 U_0^2.$$

We surround the neutron by a small sphere of radius ϵ. The meson-field energy outside this sphere given by (14) is

$$\int T_{00}\, d\text{ vol.} = \frac{1}{8\pi}\int\left\{\sum_{1}^{3}\left(\frac{\partial}{\partial x_k}U_0\right)^2+\chi^2U_0^2\right\}d\text{ vol.}$$

$$= \frac{1}{8\pi}\int\left\{\sum_{k=1}^{3}\frac{\partial}{\partial x_k}\left(U_0\frac{\partial}{\partial x_k}U_0\right)-\sum_{1}^{3}U_0\frac{\partial^2}{\partial x_k^2}U_0+\chi^2U_0\right\}d\text{ vol.}$$

The last two terms cancel each other in free space by (3), and the first term can be transformed to an integral over the surface of the sphere

$$-\frac{1}{8\pi}\int\left(U_0\frac{\partial}{\partial r}U_0\right)dS = \frac{g^2}{2}\left[\frac{1}{\epsilon}+\chi\right]e^{-2\chi\epsilon} \doteqdot \frac{g^2}{2}\left\{\frac{1}{\epsilon}-\chi+O(\epsilon)\right\}.$$

If $\chi = 0$ this is just the electromagnetic energy of a point charge. The subtracting of the tensor $\kappa_{\sigma\mu\nu}$ has just the effect of cancelling this term, since Pryce has shown that the electromagnetic energy of a point charge is zero with a new definition of the type (27). Hence the meson-field energy of a point neutron consistent with the equations (26) as defined by the tensor (27) is just $-\frac{1}{2}g^2\chi$. The mass of the neutron which plays a part in nuclear phenomena is not the real mass M but an effective mass M' connected with M by

$$M' = M - \tfrac{1}{2}g^2\chi. \tag{28}$$

We shall come across this point again later. For the scattering of mesons, however, and for all processes where frequencies comparable with χ are involved, it is the real mass M that matters. Using the actual values of M, g and χ, we find that M' differs from M by about ten million volts, or roughly 1 %.

SCATTERING OF MESONS BY NEUTRONS

We now consider the solutions of (26) where the external force on the neutron has the nature of a harmonic oscillation along the x-axis. In other words, we put

$$\left.\begin{aligned} G^{\text{in}}_{10} &= \gamma\cos\omega_0 t, \\ G^{\text{in}}_{20} &= G^{\text{in}}_{30} = 0, \end{aligned}\right\} \tag{29}$$

where we have written t instead of z_0 to conform to the more usual notation. We shall solve these equations for the case where γ is small, so that the velocity of the neutron is always small. We choose our co-ordinates so that the neutron executes oscillations about the origin along the x-axis. We write the solution in the form

$$z_1 = \frac{\beta}{\omega_0}\sin(\omega_0 t+\delta); \quad z_2 = z_3 = 0, \tag{30}$$

where δ is a phase and β an amplitude, which have to be determined. We shall assume that $\beta \ll 1$, so that higher powers of β can be neglected. We have

$$\frac{dz_1}{dt} = \beta\cos(\omega_0 t+\delta),$$

and hence to the first order

$$\left.\begin{aligned} v_1 &= \frac{dz_1}{dt}\left\{1-\left(\frac{dz_1}{dt}\right)^2\right\}^{-1} \fallingdotseq \beta\cos(\omega_0 t+\delta), \\ v_0 &= \left\{1-\left(\frac{dz_1}{dt}\right)^2\right\}^{-1} \fallingdotseq 1. \end{aligned}\right\} \tag{31}$$

The right-hand side of (26) has then only one term, namely,

$$-\frac{3}{2g}\gamma\cos\omega_0 t. \tag{32}$$

To this approximation we may replace $d\tau$ by dt. Hence, in the integral in (26),

$$s_0 = z_0(\tau)-z_0(\tau') \fallingdotseq t-t',$$

$$s_1 = z_1(\tau)-z_1(\tau') = \frac{\beta}{\omega_0}\{\sin(\omega_0 t+\delta)-\sin(\omega_0 t'+\delta)\},$$

and $$s = \sqrt{(s_0^2-s_1^2)} \fallingdotseq t-t'.$$

The integral on the left-hand side of (26) then becomes

$$\int_0^\infty ds\,\frac{J_2(\chi s)}{s^2}\left[\frac{\beta}{\omega_0}\sin(\omega_0 t+\delta)-\frac{\beta}{\omega_0}\sin(\omega_0 t'+\delta)-s\beta\cos(\omega_0 t'+\delta)\right]$$

$$= \frac{\beta\chi}{\omega_0}A\sin(\omega_0 t+\delta)-\frac{\beta\chi}{\omega_0}\frac{1}{2i}[e^{i(\omega_0 t+\delta)}B-\text{conj. complex}]$$

$$-\frac{\beta}{2}[e^{i(\omega_0 t+\delta)}C+\text{conj. complex}].$$

Here

$$A = \int_0^\infty ds \frac{J_2(s)}{s^2} = \tfrac{1}{3},$$

$$B = \int_0^\infty ds \frac{J_2(s)}{s^2} e^{-i\nu s} = \begin{cases} \tfrac{1}{3}[(1-\nu^2)^{\frac{3}{2}} + i\nu^3 - \tfrac{3}{2}i\nu] & 0 < \nu \equiv \omega_0/\chi < 1, \\ \tfrac{1}{3}[-i(\nu^2-1)^{\frac{3}{2}} + i\nu^3 - \tfrac{3}{2}i\nu] & \nu > 1, \end{cases}$$

$$C = \int_0^\infty ds \frac{J_2(s)}{s} e^{-i\nu s} = \begin{cases} \tfrac{1}{2} - \nu^2 - i\nu\sqrt{(1-\nu^2)} & 0 < \nu < 1, \\ \tfrac{1}{2} - \nu^2 + \nu\sqrt{(\nu^2-1)} & \nu > 1, \end{cases}$$

with ν standing for ω_0/χ. The term containing the integral on the left-hand side of (26) can then be written

$$\beta\omega_0^2 P \sin(\omega_0 t + \delta) + \beta\omega_0^2 Q \cos(\omega_0 t + \delta), \tag{33}$$

with

$$\left.\begin{aligned} P &= \begin{cases} \dfrac{1}{2\nu^3} - \dfrac{1}{2}\dfrac{\sqrt{(1-\nu^2)}}{\nu^3} - \dfrac{\sqrt{(1-\nu^2)}}{\nu} & 0 < \nu < 1, \\ \dfrac{1}{2\nu^3} & \nu > 1, \end{cases} \\ Q &= \begin{cases} 1 & 0 < \nu < 1, \\ 1 - \dfrac{1}{2}\dfrac{\sqrt{(\nu^2-1)}}{\nu^3} - \dfrac{\sqrt{(\nu^2-1)}}{\nu} & \nu > 1. \end{cases} \end{aligned}\right\} \tag{34}$$

Introducing (29), (30) and (33) into (26), we get

$$-\beta a\omega_0 \sin(\omega_0 t + \delta) + \beta\omega_0^2 \cos(\omega_0 t + \delta) - \beta\omega_0^2 P \sin(\omega_0 t + \delta) - \beta\omega_0^2 Q \cos(\omega_0 t + \delta) = -\frac{3}{2}\frac{\gamma}{g}\cos\omega_0 t.$$

From this we obtain at once

$$\beta = \frac{3}{2}\frac{\gamma}{g\omega_0[(a+\omega_0 P)^2 + \omega_0^2(Q-1)^2]^{\frac{1}{2}}}, \tag{35}$$

$$\cos\delta = \frac{\omega_0(Q-1)}{[(a+\omega_0 P)^2 + \omega_0^2(Q-1)^2]^{\frac{1}{2}}}. \tag{36}$$

Now it is shown in the appendix that the field at a very distant point with the co-ordinates X, Y, Z, T produced by a neutron executing the motion (30) is given by

$$\left.\begin{aligned} U_1 &= \begin{cases} \dfrac{g\beta}{R}\, e^{-R\sqrt{(\chi^2-\omega_0^2)}} \cos(\omega_0 T+\delta) & \dfrac{\omega_0}{\chi} \equiv \nu < 1, \\ \dfrac{g\beta}{R} \cos\{\omega_0 T - R\sqrt{(\omega_0^2-\chi^2)}+\delta\} & \nu > 1, \end{cases} \\ U_0 &= \begin{cases} \dfrac{g\beta X}{R^2} \dfrac{\sqrt{(\chi^2-\omega_0^2)}}{\omega_0}\, e^{-R\sqrt{(\chi^2-\omega_0^2)}} \sin(\omega_0 T+\delta) & \nu < 1, \\ \dfrac{g\beta X}{R^2} \dfrac{\sqrt{(\omega_0^2-\chi^2)}}{\omega_0} \cos\{\omega_0 T - R\sqrt{(\omega_0^2-\chi^2)}+\delta\} & \nu > 1. \end{cases} \end{aligned}\right\} \tag{37}$$

These naturally satisfy (2) and (3) for empty space.

When $\nu < 1$, i.e. if $\omega_0 < \chi$, the field falls off exponentially at large distances, and no energy is radiated by the neutron. It is interesting to note that in this case the whole field moves in phase with the neutron. We should therefore expect an extra mass due to the meson field to be added to the real mass M. This is in fact so. By (34)

$$Q - 1 = 0, \tag{38}$$

so that the amplitude of the oscillations in (35) is determined by $(a+\omega_0 P)$. For the case of very slow oscillations, $\omega_0 \ll \chi$, we find using (34) that the effective mass is

$$\tfrac{2}{3}g^2(a+\omega_0 P) \doteqdot M - \tfrac{1}{2}g^2\chi; \tag{39}$$

this agrees with what we found in the previous section.

The work done by the external force on the neutron in a cycle is by (29) and (31)

$$-g\int G_{10}^{\text{in}} v_1\, dt = -\tfrac{1}{2}g\gamma\beta\cos\delta.$$

This vanishes by (36) and (38) when $\omega_0 < \chi$, consistently with the result already mentioned, that no radiation takes place. It is thus possible even in the classical meson theory for a neutron to vibrate with frequency less than χ without radiating any energy. This is in contrast with the usual radiation theory.

We now consider the more interesting case $\omega_0 > \chi$. The field given by (37) for $\nu > 1$ has the character of a plane wave at large distances. It can at once be split into transverse and longitudinal waves, the amplitudes of the two parts being given by

$$\left.\begin{aligned} &\alpha_0^{\text{tr}} = \alpha_2^{\text{tr}} = \alpha_3^{\text{tr}} = 0; \quad \alpha_1^{\text{tr}} = \frac{g\beta}{R}\sqrt{\left(1-\frac{X^2}{R^2}\right)}; \\ &\alpha_0^{\text{long}} = \frac{g\beta X}{R^2}\frac{\sqrt{(\omega_0^2-\chi^2)}}{\omega_0}; \quad \alpha_1^{\text{long}} = \frac{g\beta X}{R^2}; \quad \alpha_2^{\text{long}} = \alpha_3^{\text{long}} = 0. \end{aligned}\right\} \tag{40}$$

Using the expression (17) for the energy-momentum tensor of a plane wave we find that the energy crossing unit area per unit time in the direction R is for transverse waves

$$\frac{1}{8\pi}\frac{g^2\beta^2}{R^2}\left(1-\frac{X^2}{R^2}\right), \tag{41a}$$

and for longitudinal waves $$\frac{1}{8\pi}\frac{g^2\beta^2X^2}{R^4}\frac{\chi^2}{\omega_0^2}. \tag{41b}$$

Thus, calling θ the angle between the direction R in which the meson radiation is observed and the x-axis, i.e. the direction of oscillation of the neutron, we find that the energy of the transverse waves has a distribution proportional to $\sin^2\theta$, while that of the longitudinal waves is $\cos^2\theta$, as we should expect. The total energy radiated in transverse waves is proportional to $\frac{1}{3}g^2\beta^2$, and in longitudinal waves $\frac{1}{6}g^2\beta^2\chi^2/\omega_0^2$. Thus, for low frequencies $\omega_0\sim\chi$, twice the energy is radiated in transverse as in longitudinal waves, whereas for higher frequencies, progressively less is radiated in longitudinal waves.

To find the scattering of meson waves by neutrons we have only to suppose that the external field (29) is due to a plane wave. If this wave is transverse, then it must travel perpendicular to the x-axis, and hence have a potential in essence of the form

$$U_0=U_2=U_3=0;\quad U_1=\frac{\gamma}{\omega_0}\sin\{\omega_0t-y\sqrt{(\omega_0^2-\chi^2)}\}.$$

By (17), the energy flow associated with this is $\gamma^2/8\pi\omega_0$. If the original plane wave is longitudinal, then it must travel along the x-axis and be described by the potential

$$U_0=\frac{\sqrt{(\omega_0^2-\chi^2)}}{\chi^2}\gamma\sin\{\omega_0t-x\sqrt{(\omega_0^2-\chi^2)}\},$$

$$U_1=\frac{\omega_0}{\chi^2}\gamma\sin\{\omega_0t-x\sqrt{(\omega_0^2-\chi^2)}\},$$

$$U_2=U_3=0.$$

The energy flow associated with this is $\gamma^2\omega_0/8\pi\chi^2$. Dividing the total radiated energy $\frac{1}{3}g^2\beta^2(1+\frac{1}{2}\chi^2/\omega_0^2)$ by the inflowing energy, and using (35) and (34), we finally obtain for the effective "cross-section" for the scattering of transverse meson waves

$$6\pi\left(1+\frac{1}{2}\frac{\chi^2}{\omega_0^2}\right)\frac{1}{\left(a+\frac{1}{2}\frac{\chi^3}{\omega_0^2}\right)^2+\left(\omega_0^2-\frac{3}{4}\frac{\chi^4}{\omega_0^2}-\frac{1}{4}\frac{\chi^6}{\omega_0^4}\right)}, \tag{42}$$

and of longitudinal meson waves

$$6\pi\frac{\chi^2}{\omega_0^2}\left(1+\frac{1}{2}\frac{\chi^2}{\omega_0^2}\right)\frac{1}{\left(a+\frac{1}{2}\frac{\chi^3}{\omega_0^2}\right)^2+\left(\omega_0^2-\frac{3}{4}\frac{\omega_0^4}{\chi^2}-\frac{1}{4}\frac{\omega_0^6}{\chi^4}\right)}. \tag{43}$$

If we let $\chi \to 0$, the first just becomes $6\pi(a^2+\omega_0^2)^{-1}$ which is the generalization of the Thomson formula recently given by Dirac. On the other hand, the scattering cross-section of the longitudinal waves goes to zero as $\chi \to 0$ as we should expect. The relation of this theory to the quantum-mechanical cross-sections will be discussed below.

The sufficient condition for the correctness of the above cross-sections is that the maximum velocity acquired by the neutron shall always be small compared with unity, i.e. that $\beta \ll 1$. For longitudinal mesons the field varies in the direction of motion of the neutron, so that we have further to consider the approximation made in taking the field acting on the neutron as the field at the origin. This approximation will be a good one if the amplitude of the neutron β/ω_0 is small compared with the wave-length $(\omega_0^2-\chi^2)^{-\frac{1}{2}}$, in other words if $\beta \ll 1$.

The cross-section (42) in common with the corresponding cross-section given by Dirac has a very interesting property. For $\omega_0 \gg a \equiv 3M/2g^2$ it becomes proportional to ω_0^{-2}, since then a may be neglected. In other words, for extremely high frequencies the scattering ceases to depend either on the mass M or the change g of the neutron. It is clear that a behaviour of this sort cannot be approximated to by a series in ascending powers of g^2.

The above cross-sections neglect the effect of the spin $S_{\mu\nu}$ of the neutron, which was put equal to zero at the beginning. Its effect will be treated later. The effect of the spin term is to alter the angular distribution of the emitted mesons, but not to change the relative order of magnitude of the transverse and longitudinal cross-sections.

As we have already stated in the introduction, by treating a field classically instead of by quantum mechanics we neglect the momentum properties of the individual field quanta. Classical formulae will therefore be correct for those processes where the momenta of the field quanta concerned may be neglected. For the scattering that we have calculated above, this will be so if the momentum of a meson is small compared to M, the neutron mass. Hence the formulae (42) and (43) may be taken at once to describe the scattering of mesons by neutrons up to meson energies $\hbar\omega_0$ small compared to 10^9 eV. They will still give the correct order of magnitude for energies of 10^9 eV. They may be taken to supersede completely the formulae previously given by Heitler (1938) and myself, from which they differ by an order of magnitude. Our theory shows that the scattering of mesons is a small effect, the cross-section being of the order $8\pi g^4/3M^2 \sim 10^{-28}$ cm.^{2}, though scattering may be through large angles when it takes place.

The expressions (42) and (43) show another curious effect. Mesons of the same energies will have a very different scattering, dependent on their polarization. The scattering of longitudinally polarized mesons is less than that of transversely polarized ones by a factor χ^2/ω_0^2. When scattering does take place, however, the scattered mesons will be transversely polarized in most cases, so that their chance of being scattered again will be much greater.

RELATION TO THE QUANTIZED MESON FIELD THEORY

We now wish to compare the results we have obtained above with those derivable from the quantized theory of uncharged and charged mesons. In the notation of a previous paper (Bhabha 1938) the interaction energy of neutral mesons with a neutron can be written in momentum space in the form

$$I_0 = \sum_p \frac{1}{\sqrt{V\sqrt{(2E)}}}\Big[-ig_1\Big\{\sum_{r=1,2}\alpha_{rp}(\overline{a_{rp}}-b_{rp})-\frac{p}{\mu}(\overline{a_{3p}}+b_{3p}) + \alpha_{3p}\frac{E}{\mu}(\overline{a_{3p}}-b_{3p})\Big\}\tau_3\exp\Big\{-\frac{i}{\hbar}(p, X)\Big\}+\text{conj. complex}\Big]. \quad (44)$$

This only differs from the corresponding expression (58*a*) in the above paper for charged mesons in having the isotopic operator τ_3 instead of τ_{NP} and τ_{PN}. For brevity we have omitted the g_2 term. The interaction (44) contains the mass of the meson μ, and has terms which increase proportionally to the momentum or energy of the meson. According to the prevalent view an interaction of this sort should lead for high energies to multiple processes and explosions of Heisenberg's type. This is however not so. The scattering of *neutral* mesons by neutrons calculated quantum-mechanically by Booth and Wilson* leads to a result which for meson energies small compared with the rest mass of the *neutron* agrees with the above cross-sections (42) and (43), if we neglect there the effects of damping, that is all the terms in square brackets except a. For higher energies the cross-sections *decrease* with increasing energy. This clearly demonstrates that interaction terms which increase with increasing energy of the particles, as in (44), are *not* sufficient to produce Heisenberg explosions. It becomes clear from our classical calculations and the above quantum-mechanical result that the mass of the meson has nothing whatsoever to do with the fundamental length required by Heisenberg for the occurrence of explosions. It does not yet follow that no explosions involving neutral mesons will occur, for as we have pointed out in the introduction, the existence of the g_2 term introduces another length in the interaction independent of μ, and we have not yet shown that this will not lead to explosions.

---

* Dr Heitler has also calculated this result in the non-relativistic case.

One can also see that the mass of the meson will not lead to the occurrence of Heisenberg explosions by the general argument given by me in a previous note (1939). For according to the prevalent view the critical energy $\hbar\chi$ above which multiple processes become important is smaller the smaller χ. In the limiting form of our theory $\chi = 0$, which constitutes electrodynamics, all energies are therefore above the critical energy (which in this case is zero), and hence if this argument were correct, we would always expect explosions to occur. The well-known results of electrodynamics show that this argument is wrong, and that in the actual meson theory for energies large compared with χ we should expect the theory to behave progressively more like electrodynamics. This expectation is also confirmed by our treatment of the classical meson theory, which shows that for high frequencies $\omega_0 \gg \chi$ all processes approximate with increasing closeness to those on the classical Maxwell theory.

It is not possible to use the same argument for a charged meson field, for a limit to the case $\mu = 0$ is not then possible. This is due to the physically evident reason that a field with $\mu = 0$ must propagate itself with the velocity of light, and if such a field carried electric charge, the electromagnetic fields concerned would become infinite. In other words, a charge-bearing field cannot exist without having a fundamental length χ or a mass μ associated with it.

This is also put into evidence by the scattering of charged mesons by neutrons calculated in an earlier paper. In the non-relativistic case, with $g_2 = 0$, this cross-section may be written for longitudinal mesons in the form

$$\text{const.}\frac{g^4}{\mu^2}\frac{(\omega_0^2-\chi^2)^2}{\omega_0^2\chi^2}, \tag{45}$$

and is zero for transverse mesons, as has also been shown by Heitler (1938). (45) does not contain M but μ in the denominator. It is therefore much larger than (42) and (43), and goes to infinity as $\mu \to 0$. This behaviour is directly connected with the charge of the meson, for whereas on the present theory a positive meson may only be absorbed by a neutron and emitted by a proton, a neutral meson may be absorbed or emitted by either a neutron or a proton. There are thus twice as many intermediate states leading to the scattering of neutral mesons as of charged mesons, and these largely compensate each other, reducing the cross-section (45) to magnitudes of the order of (42) and (43).* Since however the *interaction* of charged mesons with neutrons and protons has no correspondence with any classical theory, I do not think it is yet possible to say to what extent this part of the theory is correct. The cross-section (45) is in any case too large to be reconciled with experiment.

The fundamental equations (26) have only two constants of the dimensions of a reciprocal length in them. Using the value of g given by $g^2/\hbar c \fallingdotseq \frac{1}{6}$, their magnitudes are

$$\left.\begin{aligned} a = \frac{3M}{2g^2} &\fallingdotseq 3\times 10^{14}\,\text{cm.}^{-1}, \\ \chi &\fallingdotseq 5\times 10^{12}\,\text{cm.}^{-1}. \end{aligned}\right\} \tag{46}$$

We see that with the actual magnitudes of the constants as they occur in nature

$$a \gg \chi.$$

Electromagnetic theory is the particular limit where $\chi = 0$. *Hence we should not expect the meson theory to differ much from electromagnetic theory for frequencies* $\omega_0 \gg \chi$. *Characteristic differences will become marked only for frequencies* $\omega_0 \lesssim \chi$. This is all borne out by our previous calculations and is contrary to the prevalent view. The formulae (42) and (43) show that the effects of the reaction of the emitted meson field on the motion of neutrons becomes important when $\omega_0 \gtrsim a$. Its effect is small for $\omega_0 \ll a$, for its neglect is equivalent to the neglect of all the terms in the square brackets in (42) and (43) except a. The energies concerned are very large, being

$$\hbar\omega_0 \gtrsim \hbar a \sim 10\,M \sim 10^{10}\,\text{eV}.$$

Since the quantized theory of the neutral meson field neglects this reaction, we have good reason for believing that it will be correct to a good approximation up to this energy, and only go wrong above it.

APPENDIX

To solve the equation (3) we first solve the equation

$$\left(\frac{\partial}{\partial x_\mu}\frac{\partial}{\partial x^\mu} + \chi^2\right) G = \delta(x_0 - x_0')\,\delta(x_1 - x_1')\,\delta(x_2 - x_2')\,\delta(x_3 - x_3'). \tag{47}$$

---

* I am indebted to Professor Pauli for drawing my attention to this point in a letter.

The solution of this can be written in the form of a quadruple integral with respect to four variables p_0, p_1, p_2, p_3, and for brevity we shall write all formulae as if these constituted the components of a four-vector:

$$G(x_\rho, x'_\rho) = -\frac{1}{(2\pi)^4}\iiiint_{-\infty}^{\infty} dp_0\,dp_1\,dp_2\,dp_3\,\frac{e^{ip_\mu(x^\mu - x'^\mu)}}{p_\mu p^\mu - \chi^2}. \tag{48}$$

The denominator in (48) has two roots given by

$$p_0 = \pm\sqrt{(p^2+\chi^2)},$$

where $p = \sum_1^3 p_k^2$. We write $u_\mu = x_\mu - x'_\mu$ for brevity. In order that the solution shall not tend to infinity for small u, we choose the path of the p_0 integration to go from $-\infty$ to $+\infty$ and pass in the complex plane below both the singularities $\pm\sqrt{(p^2+\chi^2)}$, or above both of them. The p_1, p_2 and p_3 integrations go along the real axis from $-\infty$ to $+\infty$. In order to see that (48) is a solution, introduce it into the left-hand side of (47) and interchange the orders of integration and differentiation We get at once

$$\frac{1}{(2\pi)^4}\iiiint_{-\infty}^{\infty} dp_0\,dp_1\,dp_2\,dp_3\,e^{ip_\mu(x^\mu - x'^\mu)} = \delta(x_\rho - x'_\rho),$$

which proves the result. G is the Green's function of this equation.

To evaluate G, we first introduce polar co-ordinates for p_k and carry out the angular integrations.

$$G = \frac{1}{(2\pi)^3}\frac{1}{u_r}\frac{\partial}{\partial u_r}\iint_0^\infty dp\,dp_0\,\frac{e^{ip_0u_0 + ipu_r}}{p_0^2 - p^2 - \chi^2}.$$

Now carrying out the p_0 integration, we are left with the residues at the two poles $\pm\sqrt{(p^2+\chi^2)}$,

$$G = \frac{i}{(2\pi)^2}\frac{\partial}{u_r\partial u_r}\left[\int_0^\infty dp\,\frac{e^{iu_0\sqrt{(p^2+\chi^2)} + iu_rp}}{\sqrt{(p^2+\chi^2)}} - \text{conj. complex}\right],$$

which, writing $p = \chi\sinh q$, becomes

$$-\frac{1}{(2\pi)^2}\frac{\partial}{u_r\partial u_r}\int_{-\infty}^{\infty} dq\,\sin\{\chi\sqrt{(u_0^2 - u_r^2)}\cosh q\} \quad \text{if } u_0 > |u_r|.$$

If $|u_0| < |u_r|$, we get $\sinh q$ instead of $\cosh q$, and the integral vanishes. For $u_0 > |u_r|$ the integral is just equal to $\pi J_0\{\chi\sqrt{(u_0^2 - u_r^2)}\}$.

If $u_0 < 0$, the path of the p_0 integration in (48) can be deformed into an infinite semicircle below the real axis with centre at the origin, and hence G vanishes. We thus arrive at the result

$$G(x_\rho, x'_\mu) = -\frac{1}{4\pi}\frac{\partial}{u_r\partial u_r}F, \tag{48a}$$

with

$$F = \begin{pmatrix} J_0\{\chi\sqrt{(u_0^2-u_r^2)}\} \\ 0 \\ 0 \end{pmatrix} \begin{matrix} u_0 > u_r \\ |u_0| < u_r \\ u_0 < -u_r. \end{matrix} \tag{48b}$$

If we choose the path of the p_0 integration in (48) to run *above* both the singularities $\pm\sqrt{(p^2+\chi^2)}$, we obtain the Green's function (48a) with F given by

$$F = \begin{pmatrix} 0 \\ 0 \\ J_0\{\chi\sqrt{(u_0^2-u_r^2)}\} \end{pmatrix} \begin{matrix} u_0 > u_r \\ |u_0| < u_r \\ u_0 < -u_r. \end{matrix} \tag{48c}$$

The differentiation with respect to u_r give the δ-functions at $u_0 = u_r$ due to the discontinuities in F. Our final result can then be put in the form given in the text.

In differentiating U_ν with respect to the co-ordinates, we notice the following points.

$$s_\mu = x_\mu - z_\mu(\tau).$$

Hence, when s_μ occurs inside an integral,

$$\frac{\partial s_\mu(\tau)}{\partial x_\nu} = \delta^\nu_\mu \tag{49}$$

and

$$\frac{\partial s(\tau)}{\partial x_\nu} = \frac{s^\nu}{s}.$$

When it occurs outside an integral

$$\frac{\partial s_\mu(\tau_0)}{\partial x_\nu} = \delta^\nu_\mu - v_\mu(\tau_0)\frac{\partial \tau_0}{\partial x_\nu}.$$

Since

$$s_\mu(\tau_0)\,s^\mu(\tau_0) = 0,$$

$$s^\mu(\tau_0)\frac{\partial s_\mu(\tau_0)}{\partial x_\nu} = 0.$$

Hence

$$\frac{\partial \tau_0}{\partial x_\nu} = \frac{s^\nu}{\kappa}, \tag{50}$$

where

$$\kappa \equiv s_\mu v^\mu.$$

Similarly
$$\frac{\partial v_\mu(\tau_0)}{\partial x_\nu} = \dot{v}_\mu \frac{\partial \tau_0}{\partial x_\nu} = \frac{\dot{v}_\mu s^\nu}{\kappa},$$
$$\frac{\partial \kappa(\tau_0)}{\partial x_\nu} = v^\nu - \frac{s^\nu}{\kappa}(1-\kappa'),$$
with
$$\kappa' = s_\mu \dot{v}^\mu.$$

In differentiating the integral in (9) it should be remembered that we get a contribution from the change in s_μ according to (49), the limits being kept fixed, and a contribution due to the change of the upper limit τ_0 according to (50).

We now calculate the flow of energy and momentum out of the world tube. This is given by
$$-\int T_{\mu\nu} dS^\nu,$$
where dS^ν are the components of an element of the three-dimensional surface of the world tube. The world tube is determined by
$$\left.\begin{aligned} s_\mu s^\mu &= 0. \\ \kappa = s_\mu v^\mu &= \epsilon. \end{aligned}\right\} \qquad (51)$$

Hence, for variations dx_μ on the surface,
$$\left.\begin{aligned} s^\mu dx_\mu &= s^\mu v_\mu d\tau = \epsilon\, d\tau, \\ v^\mu dx_\mu &= (1-\kappa')\, d\tau. \end{aligned}\right\} \qquad (52)$$

Multiplying the first equation by $(1-\kappa')$ and the second by ϵ and subtracting
$$\{s^\mu(1-\kappa') - v^\mu \epsilon\}\, dx_\mu = 0.$$

Hence, $s_\mu(1-\kappa') - v_\mu \epsilon$ is the normal to the world tube. Its absolute length is $\epsilon\sqrt{(1-2\kappa')}$. The normalized normal is therefore
$$N_\mu = \frac{s_\mu(1-\kappa') - v_\mu \epsilon}{\epsilon\sqrt{(1-2\kappa')}}. \qquad (53)$$

The surface of the world tube at any point can be determined by three vectors $\epsilon^{(1)}$, $\epsilon^{(2)}$ and $\epsilon^{(3)}$. Two, say $\epsilon^{(1)}$ and $\epsilon^{(2)}$, can be taken as pure space vectors lying in the surface of the two-dimensional sphere in the rest system, i.e. the system in which the retarded point is instantaneously at rest. The space components of $\epsilon^{(3)}$ are then along the normal to the sphere, i.e. proportional to s_k. The time component is determined by (52). In the rest system v_μ has the components (1, 0, 0, 0) and therefore $s_0 = \epsilon$. Hence
$$\epsilon_0^{(3)} = (1-\kappa')\, d\tau.$$

It is also normal to N_μ, so that

$$-s^0\kappa'(1-\kappa')\,d\tau + s^k(1-\kappa')\,\epsilon^{(3)}_k = 0,$$

i.e.

$$\epsilon^{(3)}_k = -\frac{s_k}{\epsilon}\kappa' d\tau.$$

The length of $\epsilon^{(3)}$ is $\sqrt{(1-2\kappa')}\,d\tau$. Thus an element of volume corresponding to a displacement $d\tau$ of the retarded point is

$$dS = \sqrt{(1-2\kappa')}\,d\tau\,d\sigma,$$

where $d\sigma$ is an element of the surface of the sphere round the retarded point. It finally follows that

$$dS^\nu = N^\nu dS = \{s_\mu(1-\kappa') - v_\mu\epsilon\}\,\epsilon\,d\tau\,d\omega, \tag{54}$$

$d\omega$ being an element of solid angle in the rest system.

From (12) and (13), on the world tube

$$-\frac{1}{g}G^0_{\mu\nu} = \frac{s_\mu v_\nu - s_\nu v_\mu}{\epsilon^3}, + \frac{s_\mu \dot{v}_\nu - s_\nu \dot{v}_\mu}{\epsilon^2} - \frac{s_\mu v_\nu - s_\nu v_\mu}{\epsilon^3}\kappa' \tag{55}$$

and

$$-\frac{1}{g}G^\chi_{\mu\nu} = -\frac{\chi^2}{2}\frac{s_\mu v_\nu - s_\nu v_\mu}{\epsilon} + \chi^2\int_{-\infty}^{\tau_0} d\tau \frac{s_\mu v_\nu - s_\nu v_\mu}{s^2} J_2(\chi s), \tag{56}$$

where we have separated terms of different order in ϵ by a comma. The first term in (55) is of the order ϵ^{-2}, the other two being of order ϵ^{-1}. $G^\chi_{\mu\nu}$ is of order 1. dS^ν is of order ϵ^2. The energy tensor (14) may be written

$$T_{\mu\nu} = T^0_{\mu\nu} + T^{\text{mix}}_{\mu\nu} + T^{\text{in}}_{\mu\nu},$$

where $T^0_{\mu\nu}$ is the tensor which only consists of $G^0_{\mu\nu}$ and U^0_ν. Since $G^\chi_{\mu\nu}$ is of order 1, it may be treated together with $G^{\text{in}}_{\mu\nu}$. $T^{\text{in}}_{\mu\nu}$ when integrated over the tube is of order ϵ^2 and may be neglected. In $T^{\text{mix}}_{\mu\nu}$, we need only consider the first term of order ϵ^{-2} in (55), and neglect the κ' term in (54), since these give contributions of higher order.

Now from (55) and (54)

$$-\frac{1}{g}G^0_{\mu\nu}dS^\nu = \{v_\mu(1-\kappa') + \epsilon\dot{v}_\mu\}\,d\omega\,d\tau. \tag{57}$$

Therefore

$$\frac{1}{g^2}G^0_{\mu\sigma}G^{0\sigma}{}_\nu dS^\nu = \left[\frac{s_\mu - \epsilon v_\mu}{\epsilon^3},\ -2\frac{s_\mu - \epsilon v_\mu}{\epsilon^3}\kappa' - \frac{v_\mu}{\epsilon^2}\kappa' - \frac{\dot{v}_\mu}{\epsilon},\ +\frac{s_\mu}{\epsilon^3}\kappa'^2 + \frac{s_\mu \dot{v}^2}{\epsilon}\right]d\omega\,d\tau,$$

$$\frac{1}{g^2}G_{\sigma\rho}G^{\sigma\rho} = -\frac{2}{\epsilon^4}.$$

For the purposes of integration we note the following formulae, which can be derived easily in the rest system, and then written at once in tensor form. A_μ is any tensor not a function of position on the sphere:

$$\left.\begin{aligned}
&\frac{1}{4\pi}\int(s_\mu-\epsilon v_\mu)\,d\omega = 0,\\
&\frac{1}{4\pi}\int s_\mu A^\mu d\omega \doteq A_0 = v_\mu A^\mu,\\
&\frac{1}{4\pi}\int s_\mu s_\nu A^\nu d\omega = \begin{cases} v_\nu A^\nu & \text{for} \quad \mu=0,\\ -\tfrac{1}{3}A_k & \text{for} \quad \mu = k\end{cases}\\
&\qquad\qquad\qquad\quad = -\tfrac{1}{3}A_\mu+\tfrac{4}{3}v_\mu v_\nu A^\nu.
\end{aligned}\right\} \tag{58}$$

With the help of these

$$-\frac{1}{4\pi}\int\{G^0_{\mu\sigma}G^{0\sigma}{}_\nu+\tfrac{1}{4}g_{\mu\nu}G^0_{\rho\sigma}G^{0\rho\sigma}\}\,dS^\nu = g^2\left[\frac{1}{2}\frac{\dot{v}_\mu}{\epsilon}-\tfrac{2}{3}v_\mu\dot{v}^2\right]d\tau. \tag{59}$$

In calculating the flow due to $T^{\text{mix}}_{\mu\nu}$ we notice that the first term in (56) will contribute nothing. For this could only give a contribution when multiplied by the first term of (55). But the first term of (55) when multiplied by itself should have given a contribution of order ϵ^{-2} to (59). (59) shows that this term vanishes. Since the first term in (56) is just $-\chi^2\epsilon^2/2$ times the first term of (55), it will give no contribution to the energy flow. The second term in (56) is continuous everywhere and hence may be just considered as a part of $G^{\text{in}}_{\mu\nu}$. For brevity we will not write it explicitly in the calculations and add it in the final formula. Using (54), (55) and (57)

$$\begin{aligned}
&-\frac{1}{4\pi}\int\{G^0_{\mu\sigma}G^{\text{in}\,\sigma}{}_\nu+G^{\text{in}}_{\mu\sigma}G^{0\,\sigma}{}_\nu\}\,dS^\nu\\
&\quad = g\int\frac{s_\mu v_\sigma-s_\sigma v_\mu}{\epsilon^2}\,G^{\text{in}\,\sigma}{}_\nu(s_\nu-v_\nu\epsilon)\,d\omega\,d\tau+g\int G^{\text{in}}_{\mu\sigma}v^\sigma d\omega\,d\tau\\
&\quad = g[-\tfrac{1}{3}v_\sigma\,G^{\text{in}\,\sigma}{}_\mu+G^{\text{in}}_{\mu\sigma}v^\sigma]\,d\tau\\
&\quad = \tfrac{4}{3}g\,G^{\text{in}}_{\mu\sigma}v^\sigma d\tau
\end{aligned} \tag{60}$$

Next,

$$\begin{aligned}
&-\frac{1}{4\pi}\int\tfrac{1}{2}g_{\mu\nu}\{G^0_{\rho\sigma}\,G^{\text{in}\rho\sigma}\}\,dS^\nu\\
&\qquad = \frac{g}{8\pi}\int\frac{s_\rho v_\sigma-s_\sigma v_\rho}{\epsilon^2}\,G^{\text{in}\rho\sigma}(s_\mu-\epsilon v_\mu)\,d\omega\,d\tau\\
&\qquad = -\tfrac{1}{3}g\,G^{\text{in}}_{\mu\sigma}v^\sigma d\tau.
\end{aligned} \tag{61}$$

We have still to consider the U_μ terms in (26). The first term of (9) is of the order ϵ^{-1}, so that only the product of this term with itself will make a contribution to the energy flow:

$$-\frac{\chi^2}{4\pi}\int U_\mu U_\nu dS^\nu = -g^2\frac{\chi^2}{4\pi}\int\frac{v_\mu v_\nu}{\epsilon}(s^\nu - v^\nu\epsilon)\,d\omega\,d\tau = 0,$$

$$\frac{\chi^2}{4\pi}\int\tfrac{1}{2}g_{\mu\nu}U_\rho U^\rho dS^\nu = g^2\frac{\chi^2}{8\pi}\int\frac{s_\mu-\epsilon v_\mu}{\epsilon}\,d\omega\,d\tau = 0.$$

Adding (59), (60) and (61), we finally find for the energy flow out of a length $d\tau$ of the tube

$$\left[g^2\left(\frac{1}{2}\frac{\dot{v}_\mu}{\epsilon}-\tfrac{2}{3}v_\mu\dot{v}^2\right)+g(\tilde{G}^{\chi}_{\mu\sigma}+G^{\text{in}}_{\mu\sigma})\,v^\sigma\right]d\tau,$$

which is the result quoted in (19).

We now derive the expressions for the potentials U_μ at a large distance R due to a neutron oscillating according to

$$z_1 = \frac{\beta}{\omega_0}\sin\omega_0 t;\quad z_2 = z_3 = 0.$$

For this purpose it is convenient to write the expression (9) for the potential U_ν by partial integration in the form

$$U_\nu = g\int_{-\infty}^{\tau_0} d\tau\, J_0(\chi s)\frac{d}{d\tau}\left(\frac{v_\nu}{\kappa}\right). \tag{62}$$

To the first order in β $\quad s^2 \risingdotseq (T-t)^2-R^2,$

$$\kappa \risingdotseq (T-t)-X\beta\cos\omega_0 t,$$

Therefore $\quad \dfrac{d}{d\tau}\left(\dfrac{v_1}{\kappa}\right) \risingdotseq -\dfrac{\beta\omega_0\sin\omega_0 t}{T-t}+O\left(\dfrac{1}{(T-t)^2}\right)+O(\beta^2),$

$$\frac{d}{d\tau}\left(\frac{v_0}{\kappa}\right) = -\frac{\beta\omega_0 X\sin w_0 t}{(T-t)^2}.$$

Hence from (62), neglecting higher orders,

$$U_1 = g\int_0^\infty ds\,\frac{s}{(s^2+R^2)^{\frac{1}{2}}}J_0(\chi s)\left\{-\frac{\beta\omega_0\sin\omega_0 t}{(s^2+R^2)^{\frac{1}{2}}}\right\}$$

$$= -g\frac{\beta\omega_0}{2i}[e^{i\omega_0 T}I-\text{conj. complex}],$$

where $\quad I = \displaystyle\int_0^\infty ds\,\frac{s}{s^2+R^2}J_0(\chi s)\,e^{-i\omega_0\sqrt{(s^2+R^2)}}$

$$= \int_{i\omega_0}^{\infty+i\omega_0} d\omega_0\int_0^\infty ds\,\frac{s}{\sqrt{(s^2+R^2)}}J_0(\chi s)\,e^{-\omega_0\sqrt{(s^2+R^2)}}.$$

Now by a well-known theorem of Bessel functions (see Watson)

$$\int_0^\infty ds \frac{s}{\sqrt{(s^2+R^2)}} J_0(\chi s)\, e^{-\omega_0\sqrt{(s^2+R^2)}} = \frac{e^{-R\sqrt{(\chi^2+\omega_0^2)}}}{\sqrt{(\chi^2+\omega_0^2)}}.$$

Therefore

$$I = \int_{i\omega_0}^{\infty+i\omega_0} d\omega_0 \frac{e^{-R\sqrt{(\chi^2+\omega_0^2)}}}{\sqrt{(\chi^2+\omega_0^2)}} = \begin{cases} \dfrac{e^{-R\sqrt{(\chi^2-\omega_0^2)}}}{i\omega_0 R} & \text{for } |\omega_0|<\chi, \\ \dfrac{e^{-iR\sqrt{(\omega_0^2-\chi^2)}}}{i\omega_0 R} & \text{for } |\omega_0|>\chi, \end{cases}$$

neglecting higher powers in $1/R$.

Hence, at large distances

$$U_1 = \begin{cases} \dfrac{g\beta}{R} e^{-R\sqrt{(\chi^2-\omega_0^2)}} \cos(\omega_0 T) & |\omega_0|<\chi, \\ \dfrac{g\beta}{R} \cos\{\omega_0 T - R\sqrt{(\omega_0^2-\chi^2)}\} & |\omega_0|>\chi, \end{cases}$$

which is the result quoted in the text.

We similarly find

$$U_0 = g\int_0^\infty ds \frac{s}{(s^2+R^2)^{\frac{1}{2}}} J_0(\chi s) \left\{ -\frac{\beta\omega_0 X \sin\omega_0 t}{s^2+R^2} \right\}.$$

Here we have to integrate twice with respect to ω_0. After some easy analysis we get the result quoted in the text in (37).

SUMMARY

The vector equations for the meson field and their associated energy tensor are taken as exact, and the meson-field quantities are taken as commuting classical variables. A self-consistent classical scheme is developed for treating the meson-field and point neutrons (or protons) moving along classical world lines. The scheme takes account of the reaction of the emitted meson field on the motion of the neutron. The mass of the neutron (or proton) which occurs in nuclear phenomena is shown not to be the real mass but less than it by about ten million volts. For high-energy phenomena the real mass counts. Formulae are given for the scattering of mesons by neutrons which are valid to energies comparable with the mass of the neutron, and supersede the previous formulae. These show that for the same high energies, longitudinally polarized mesons are scattered much less than transversely polarized mesons, giving them much greater penetrating power. It is shown that classically the reaction of the emitted radiation is not important till energies of ten times the neutron mass and hence that the quantized neutral

meson theory which neglects this is valid up to about these energies. It is proved that the rest mass of the meson is not connected with Heisenberg explosions, but that if these exist, they must be due either to the spin interaction g_2 or to the fact that the meson field is electrically charged.

REFERENCES

Bhabha 1938 *Proc. Roy. Soc.* A, **166**, 501–28.
— 1939 *Nature, Lond.*, **143**, 276.
Dirac 1938 *Proc. Roy. Soc.* A, **167**, 148–69.
Fröhlich, Heitler and Kemmer 1938 *Proc. Roy. Soc.* A, **166**, 154–77.
Heisenberg 1936 *Z. Phys.* **101**, 533–40.
—— 1938 *Z. Phys.* **110**, 251–66.
Heitler 1938 *Proc. Roy. Soc.* A, **166**, 529–43.
Kemmer 1938 *Proc. Roy. Soc.* A, **166**, 127–53.
—— 1938 *Proc. Camb. Phil. Soc.* **34**, 354–64.
Proca 1936 *J. Phys. Radium*, **7**, 347–53.
Pryce 1938 *Proc. Roy. Soc.* A, **168**, 389–401.
Stueckelberg 1938 *Helv. phys. Acta*, **11**, 299–328.
Yukawa, Sakata and Taketani 1938 *Proc. Phys. Math. Soc. Japan*, **20**, 319–40.

Distribution of charge and potential in an electrolyte bounded by two plane infinite parallel plates

By A. J. Corkill, B.Sc. and L. Rosenhead, Ph.D., D.Sc.
University of Liverpool

(*Communicated by W. C. M. Lewis, F.R.S.—Received* 28 *April* 1939)

1. Introduction

The density of electricity, ρ, in a positively charged binary electrolyte associated with the distribution of ions in it is connected with the electrostatic potential, ψ, by the equations

$$\nabla^2\psi = -4\pi\rho/D, \tag{1·1}$$

$$\rho = \nu FC[\exp(-\nu F\psi/RT) - \exp(\nu F\psi/RT)]. \tag{1·2}$$

(See § 2 for the meaning of the various symbols.)

If the electrolyte is contained between two plane infinite parallel plates which cut the x-axis at right angles at the points $x = 0$ and $x = l$, the equation (1·1) assumes the form

$$\frac{d^2\psi}{dx^2} = -\frac{4\pi\rho}{D}, \tag{1·1a}$$

while equation (1·2) remains unchanged.

The basis of the following theory is due to Gouy (1910), and the above equations can be found, with a somewhat different notation, in a paper due to Chapman (1913). Gouy calculated the distribution of charge in a semi-infinite electrolyte bounded by a plane plate. Rosenhead and Miller (1937) applied his results to the case of an electrolyte between two plane plates by assuming that the charges associated with the two plates could be superposed. This assumption can only be justified when $\nu F\psi/RT$ is so small that powers of it higher than the second can be neglected so that the differential equation for ψ, and hence that for ρ, becomes linear. In this paper an exact solution of the problem of the distribution of charge between two plane plates is obtained.

The following investigation is also of interest from a different point of view and has some practical application as follows. Certain colloid oxides, such as, for example, Fe_2O_3 and WO_3, show a tendency to separate out in horizontal layers at the bottom of the vessels which contain them (Zocher

1925). In order to explain the characteristics of this phenomenon certain assumptions were made (Bergmann, Löw-Beer and Zocher 1938) and reference was also made to the distribution of charge in the electrolyte between the layers so formed. The mathematical theory of the "Zocher Stratification", as originally stated, is approximate, and as the quantities under consideration are very small, the approximations made mask a number of interesting features. In particular the evaluation of the force between the plates is open to criticism. Mr Bikerman proposes to develop an alternative theory for the evaluation of this force. In this theory a number of points arose which are dealt with in §§ 7, 8, 9, 10 of this paper. Mr Bikerman proposes to apply these results to his theory in the near future.

A summary of the results obtained can be found in § 12. Tables of numerical values can be found in §§ 4, 6, 8.

During the work a number of points arose for the elucidation of which we are greatly indebted to Mr J. J. Bikerman of the Department of Colloid Science, Cambridge.

2. List of symbols

x	the distance from the plate $x = 0$;
l	the distance between the plates;
ψ	the electrostatic potential;
$-\psi_0$	the potential at $x = 0$;
$-\psi_1$	the potential at $x = \frac{1}{2}l$;
ζ	the electrokinetic potential difference (in § 11 this is identified with $-(\psi_0 - \psi_1)$);
Q	the total charge in a column of electrolyte of unit section between $x = 0$ and $x = l$;
ρ	the volume density of charge in the electrolyte;
σ	the surface density of charge on the plates;
N	the ratio of the concentration of positive ions at any point in the field to that in the undisturbed field $[= \exp(-\nu F\psi/RT)]$;
N_0	the concentration ratio at $x = 0$;
N_1	the concentration ratio at $x = \frac{1}{2}l$;
ν	the valency of the electrolyte (which is assumed to be binary);
F	Faraday's constant, equal to 96,494 coulombs, $= 2{\cdot}89 \times 10^{14}$ e.s.u.;
C	the concentration of the electrolyte between the plates;
R	Boltzmann's constant, equal to $8{\cdot}32 \times 10^7$ ergs per degree;
T	the absolute temperature;
D	the dielectric constant of the solution;

W the electrostatic energy in a column of electrolyte of unit cross section between $x = 0$ and $x = l$;

S the weight per unit area of the plates less the hydrostatic upthrust per unit area;

$\alpha = 2\nu F(2\pi C/DRT)^{\frac{1}{2}}$; $\beta = \nu F/2RT$; $k = e^{-2\beta\psi_1}$;

$z = e^{\beta(\psi+\psi_1)}$; $a = \sin^{-1} e^{\beta(\psi_1-\psi_0)}$; $k'^2 = 1-k^2$;

$A = \dfrac{e^{\beta\psi_0}+1}{e^{\beta\psi_0}-1}$; $\Delta = \sqrt{(1-k^2\sin^2\phi)}$; $\Delta_a = \sqrt{(1-k^2\sin^2 a)}$.

3. EXACT FORMULA FOR THE DISTRIBUTION OF POTENTIAL

We assume that the electrolyte has a positive body charge, that is $\rho > 0$, and hence, from (1·2), that ψ is everywhere negative. By symmetry the system is symmetrical about the middle of the channel, that is

$$\psi(x) = \psi(l-x).$$

The surface density of electrification on the plates is σ, where

$$\begin{aligned}\sigma &= -\frac{D}{4\pi}\frac{d\psi}{dx} \text{ at } x = 0\\ &= +\frac{D}{4\pi}\frac{d\psi}{dx} \text{ at } x = l.\end{aligned}$$

The total charge, per unit area of cross section, in a column of electrolyte between $x = 0$ and $x = l$ is

$$\begin{aligned}Q &= \int_0^l \rho\, dx\\ &= \nu FC\int_0^l (e^{-2\beta\psi} - e^{2\beta\psi})\, dx\\ &= 2\nu FC\int_0^{\frac{1}{2}l} (e^{-2\beta\psi} - e^{2\beta\psi})\, dx.\end{aligned}$$

Since all the tubes of force originating in the fluid must end on the plates, the following relation must be true identically,

$$Q + 2\sigma = 0,$$

that is $$\left(\frac{d\psi}{dx}\right)_{x=0} = \frac{4\pi\nu FC}{D}\int_0^{\frac{1}{2}l} (e^{-2\beta\psi} - e^{2\beta\psi})\, dx.$$

The validity of this identity can be checked from the relations which will be obtained subsequently. We see however that $(d\psi/dx)_{x=0}$ must be positive and hence that ψ must increase as x increases from 0 to $\frac{1}{2}l$. Let $-\psi_0$ be the value of ψ at $x = 0$, and $-\psi_1$ its value at $x = \frac{1}{2}l$.

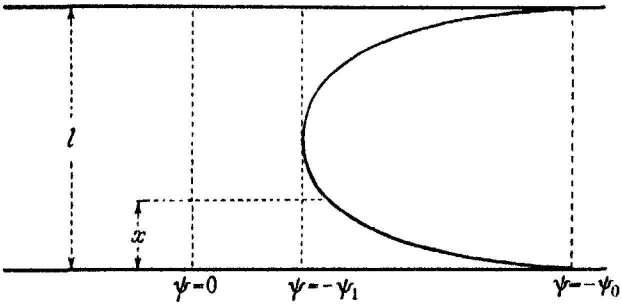

FIG. 1

If ρ is eliminated between (1·1 *a*) and (1·2), we get

$$\frac{d^2\psi}{dx^2} = -\frac{4\pi\nu FC}{D}[e^{-2\beta\psi} - e^{2\beta\psi}], \tag{3·1}$$

which can be integrated immediately to

$$\left(\frac{d\psi}{dx}\right)^2 = \frac{8\pi CRT}{D}[e^{-2\beta\psi} + e^{2\beta\psi} - B], \tag{3·2}$$

where B is a constant of integration. If $d\psi/dx = 0$ at $x = \frac{1}{2}l$, where $\psi = -\psi_1$, we have

$$B = e^{2\beta\psi_1} + e^{-2\beta\psi_1}. \tag{3·3}$$

Since N, the ratio of concentration of positive ions at any point in the field to that outside the field (where $\psi = 0$), is equal to $e^{-2\beta\psi}$, we see that

$$B = N_1 + N_1^{-1},$$

where N_1 is the concentration ratio at $x = \frac{1}{2}l$. If in equation (3·2) we put

$$\left.\begin{aligned} k &= e^{-2\beta\psi_1} = N_1^{-1} \leqslant 1, \\ z &= e^{\beta(\psi+\psi_1)} = k^{-\frac{1}{2}}e^{\beta\psi} = (N_1/N)^{\frac{1}{2}} \leqslant 1, \end{aligned}\right\} \tag{3·4}$$

it becomes

$$\left(\frac{dz}{dx}\right)^2 = \tfrac{1}{4}\alpha^2 k^{-1}(1-z^2)(1-k^2z^2), \tag{3·5}$$

where $\alpha^2 = 8\pi\nu^2F^2C/DRT$.

Hence

$$\frac{dz}{dx} = \tfrac{1}{2}\alpha k^{-\frac{1}{2}}(1-z^2)^{\frac{1}{2}}(1-k^2z^2)^{\frac{1}{2}}, \tag{3·6}$$

in the range $0 \leqslant x \leqslant \frac{1}{2}l$, in which range $(N_1/N_0)^{\frac{1}{2}} \leqslant z \leqslant 1$. On integration this becomes

$$F[k, \sin^{-1} e^{\beta(\psi+\psi_1)}] - F[k, \sin^{-1} e^{\beta(\psi_1-\psi_0)}] = \tfrac{1}{2}k^{-\frac{1}{2}}x, \tag{3·7}$$

where

$$F(k, \phi) = \int_0^{\phi} \frac{d\phi}{(1-k^2\sin^2\phi)^{\frac{1}{2}}}.$$

Both the elliptic integrals in (3·7) are positive and less than, or equal to, K, the complete elliptic integral of the first kind.

Near the plate $x = 0$, the potential is given by

$$\psi = -\psi_0 + x\left(\frac{d\psi}{dx}\right)_{x=0},$$

neglecting terms in $x^2, x^3, \ldots$.

That is

$$\psi = -\psi_0 - \frac{4\pi\sigma}{D}x.$$

Tables of values of σ for different values of ψ_0 and l may be found in § 6.

4. THE "PERIOD EQUATION"

Since $\psi = -\psi_1$, when $x = \frac{1}{2}l$ equation (3·7) gives

$$\begin{aligned} \tfrac{1}{4}k^{-\frac{1}{2}}\alpha l &= F[k, \sin^{-1}(1)] - F[k, \sin^{-1} e^{\beta(\psi_1-\psi_0)}] \\ &= K - F[k, \sin^{-1} e^{\beta(\psi_1-\psi_0)}], \end{aligned} \tag{4·1}$$

from which it can be deduced that $Kk^{\frac{1}{2}} > \frac{1}{4}\alpha l$. Writing $a = \sin^{-1} e^{\beta(\psi_1-\psi_0)}$ and $\Delta = \surd(1-k^2\sin^2\phi)$, this becomes

$$\tfrac{1}{4}k^{-\frac{1}{2}}\alpha l = \int_a^{\frac{1}{2}\pi} \frac{d\phi}{\Delta}. \tag{4·2}$$

Equation (4·2) connects up ψ_0, ψ_1 and l. We shall call it the "period equation". The results of the numerical solution of the period equation are shown in Table I.

In fig. 2 the relation between ψ_0, ψ_1 and l is exhibited graphically. From the curves it appears that, for any given value of αl, ψ_1 increases with ψ_0, but tends to a finite limit as ψ_0 tends to infinity. The limiting value of ψ_1 is a function of l. It is zero when l is infinite, and as l tends to zero $\int_a^{\frac{1}{2}\pi} \frac{d\phi}{\Delta}$ tends to zero. That is, a tends to $\frac{1}{2}\pi$, or ψ_1 tends to ψ_0.

TABLE I. NUMERICAL VALUES OF ψ_0, ψ_1 AND l

ψ_0 (volts)	ψ_1 (volts)					
	$\alpha l \to 0$	$\alpha l = 4$	$\alpha l = 8$	$\alpha l = 12$	$\alpha l = 16$	$\alpha l > 16$
0·000		0·0000	0·0000	0·0000	0·0000	0·0000
0·010		0·0028	0·0004	0·0000	0·0000	⋮
0·020		0·0052	0·0007	0·0001	0·0000	⋮
0·030		0·0077	0·0010	0·0001	0·0000	⋮
0·040		0·0100	0·0014	0·0002	0·0000	⋮
0·050		0·0122	0·0017	0·0002	0·0000	⋮
0·060		0·0142	0·0020	0·0002	0·0000	⋮
0·070		0·0157	0·0022	0·0003	0·0000	⋮
0·080		0·0171	0·0024	0·0003	0·0000	⋮
0·090		0·0183	0·0026	0·0003	0·0000	⋮
0·100		0·0194	0·0028	0·0004	0·0000	⋮
0·110		0·0202	0·0030	0·0004	0·0000	⋮
0·120	$\psi_1 \to \psi_0$ for all values of ψ_0	0·0210	0·0031	0·0004	0·0000	⋮
0·130		0·0216	0·0032	0·0004	0·0000	⋮
0·140		0·0222	0·0033	0·0004	0·0000	⋮
0·150		0·0226	0·0033	0·0005	0·0001	⋮
0·160		0·0230	0·0034	⋮	⋮	⋮
0·170		0·0233	0·0034	⋮	⋮	⋮
0·180		0·0236	0·0035	⋮	⋮	⋮
0·190		0·0238	0·0035	⋮	⋮	⋮
0·200		0·0239	0·0035	⋮	⋮	⋮
0·210		0·0241	0·0035	⋮	⋮	⋮
0·220		0·0242	0·0036	⋮	⋮	⋮
0·230		0·0243	0·0036	⋮	⋮	⋮
0·240		0·0244	0·0036	⋮	⋮	⋮
0·250		0·0245	0·0036	⋮	⋮	⋮
0·260		0·0245	0·0036	⋮	⋮	⋮
0·270		0·0246	0·0037	⋮	⋮	⋮
0·280		0·0246	⋮	⋮	⋮	⋮
0·290		0·0246	⋮	⋮	⋮	⋮
0·300		0·0247	⋮	⋮	⋮	⋮
⋮		⋮	⋮	⋮	⋮	⋮
∞		0·0247	0·0037	0·0005	0·0001	0·0000

5. DISTRIBUTION OF POTENTIAL ($\alpha l > 20$)

We have shown that $Kk^{\frac{1}{2}} > \frac{1}{2}\alpha l$, so that if $\alpha l > 20$ it can be seen from tables that the limits between which k must lie are given by the relation

$$1 \geqslant k \geqslant 0{\cdot}9996,$$

and hence, from (3·4), that $2\beta\psi_1$ is very small. The modulus of the elliptic functions is therefore approximately equal to 1.

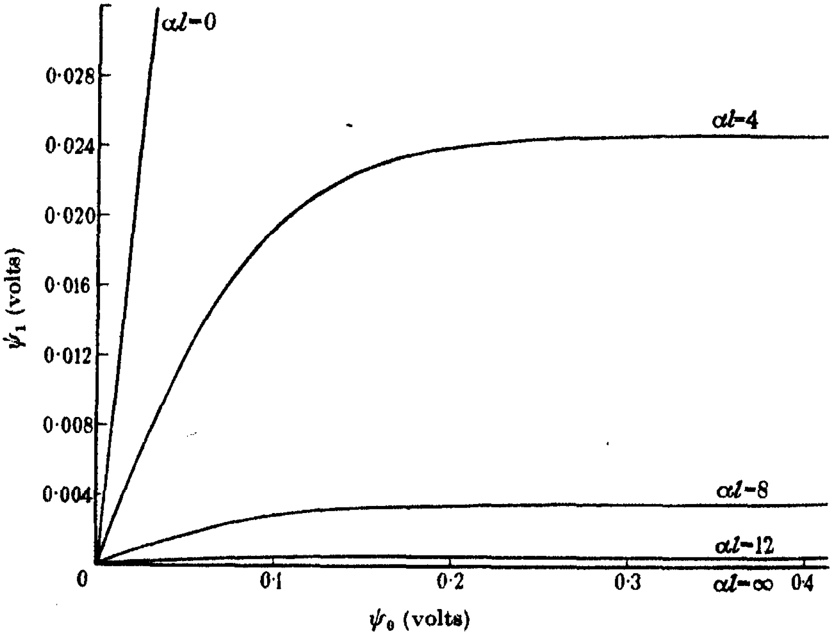

FIG. 2

If $k = 1$ exactly, then $K = \infty$. Further, $\psi_1 = 0$, from (3·4), and $l = \infty$, from (4·1), so that $k = 1$ corresponds to the case discussed by Gouy in which the electrolyte is bounded by one infinite plate. Equation (3·7) becomes

$$\tfrac{1}{2}\log\frac{1+e^{\beta\psi}}{1-e^{\beta\psi}}-\tfrac{1}{2}\log\frac{1+e^{-\beta\psi_0}}{1-e^{-\beta\psi_0}} = \tfrac{1}{2}\alpha x,$$

$$\left.\begin{aligned} &\text{that is} && e^{\beta\psi} = \frac{Ae^{\alpha x}-1}{Ae^{\alpha x}+1},\\ &\text{and hence} && N = e^{-2\beta\psi} = \left(\frac{Ae^{\alpha x}+1}{Ae^{\alpha x}-1}\right)^2,\\ &\text{and} && \rho = \nu FC(N-N^{-1}) = 8\nu FC\frac{Ae^{\alpha x}(A^2e^{2\alpha x}+1)}{(A^2e^{2\alpha x}-1)^2},\end{aligned}\right\} \qquad (5{\cdot}1)$$

which agree with the expressions found by Gouy. The equations were first published in this form by Bikerman (1933).

When k is approximately equal to 1 and u is small, the expression $\operatorname{sn} u$ can be replaced by

$$(1+\tfrac{1}{4}k'^2)\tanh(1-\tfrac{1}{4}k'^2)\,u, \tag{5·2}$$

where $k'^2 = 1-k^2$ (Tannery and Molk).

In the case under consideration $k'^2 = 1-e^{-4\beta\psi_1} = 4\beta\psi_1$, approximately, which is less than or equal to 0·0008. Hence ψ_1 is less than $3·1 \times 10^{-8}$ e.s.u., that is $9·3 \times 10^{-6}$ V.

Applying (5·2) to (4·1), we get

$$\tfrac{1}{4}(1+\tfrac{1}{4}k'^2)\,\alpha l = \tfrac{1}{2}(1+\tfrac{1}{4}k'^2)\log(16/k'^2) - \tfrac{1}{2}(1+\tfrac{1}{4}k'^2)\log\frac{1+e^{-\beta\psi_0}}{1-e^{-\beta\psi_0}},$$

that is

$$\log A = \log(16/k'^2) - \tfrac{1}{2}\alpha l,$$

or

$$\begin{aligned} k'^2 &= 16A^{-1}e^{-\frac{1}{2}\alpha l} \\ &= 4\beta\psi_1. \end{aligned} \tag{5·3}$$

We therefore see that ψ_1 is zero only if $l = \infty$.

Applying (5·2) to (3·7) we obtain expressions identical with those given in (5·1) and we see, as was to be expected, that the distribution of potential in the neighbourhood of any one plate is unaffected by the presence of the second plate. The exact solution (3·7) does not reduce to the approximate solution (5·1) when x approaches $\tfrac{1}{2}l$, for then the argument of the inverse elliptic functions approaches the value 1. Combining (3·7) with (4·1) however, we obtain

$$F[k, \sin^{-1} e^{\beta(\psi+\psi_1)}] = K + \tfrac{1}{2}k^{-\frac{1}{2}}\alpha(x-\tfrac{1}{2}l),$$

and hence

$$e^{\beta(\psi+\psi_1)} = \frac{\operatorname{cn}[\tfrac{1}{2}k^{-\frac{1}{2}}\alpha(x-\tfrac{1}{2}l)]}{\operatorname{dn}[\tfrac{1}{2}k^{-\frac{1}{2}}\alpha(x-\tfrac{1}{2}l)]}. \tag{5·4}$$

In the centre of the channel where $(x-\tfrac{1}{2}l)$ is small this equation can be replaced by the approximate relation

$$k^{-\frac{1}{2}}e^{\beta\psi} = \frac{1-\tfrac{1}{4}k'^2\sinh^2\tfrac{1}{2}\alpha(x-\tfrac{1}{2}l)}{1+\tfrac{1}{4}k'^2\sinh^2\tfrac{1}{2}\alpha(x-\tfrac{1}{2}l)},$$

which reduces to

$$\psi = -\psi_1\cosh\alpha(x-\tfrac{1}{2}l). \tag{5·5}$$

When $0 < \alpha l < 20$ the potential rises monotonically from $x = 0$ to $x = \tfrac{1}{2}l$ and then decreases monotonically to $x = l$, the system being symmetrical with respect to $x = \tfrac{1}{2}l$.

6. THE ELECTROSTATIC FORCE BETWEEN THE PLATES AND THE DIFFUSE IONIC LAYERS

The electrostatic force per unit area exerted on the plates by the ions tending to neutralize their charges is equal to $2\pi\sigma^2/D$. Now

$$\sigma = -\frac{D}{4\pi}\left(\frac{d\psi}{dx}\right)_{x=0},$$

and

$$\left(\frac{d\psi}{dx}\right)^2_{x=0} = \frac{8\pi CRT}{D}(e^{2\beta\psi_0}+e^{-2\beta\psi_0}-e^{2\beta\psi_1}-e^{-2\beta\psi_1})$$

$$= \frac{8\pi CRT}{Dk}\cot^2 a(1-k^2\sin^2 a).$$

Hence the electrostatic force per unit area between the plates and the ions is an attraction of amount,

$$2CRT(\cosh 2\beta\psi_0 - \cosh 2\beta\psi_1) = \frac{1}{k}CRT\cot^2 a(1-k^2\sin^2 a).$$

The surface density of charge, σ, on the plates is given by

$$\sigma = -\sqrt{\frac{DCRT}{\pi}}(\cosh 2\beta\psi_0 - \cosh 2\beta\psi_1). \tag{6·1}$$

As $l \to 0$, however, $\int_a^{\frac{1}{2}\pi}\frac{d\phi}{\Delta} \to 0$. That is $a \to \frac{1}{2}\pi$ and $\sigma \to 0$. As $l \to \infty$, $\psi_1 \to 0$ and

$$\sigma \to -\left(\frac{2DCRT}{\pi}\right)^{\frac{1}{2}}\sinh\beta\psi_0.$$

Numerical values of $-\sigma/\sqrt{CD}$ and αl are given in Table II. In order to obtain a representative case T was assumed to be equal to 290° A, and ν, the valency of the binary electrolyte, equal to 1.

The force $2\pi\sigma^2/D$ does not affect the distance between the plates. The force tending to separate the plates is $-\partial W/\partial l$, where W is the electrostatic energy in a column of electrolyte of unit cross section between $x = 0$ and $x = l$. The theory associated with this will be published later by Mr Bikerman.

7. EXACT FORMULA FOR THE ELECTROSTATIC ENERGY

According to the general formula the electrostatic energy in a column of electrolyte of unit cross section, between $x = 0$ and $x = l$, is

$$W = \frac{D}{8\pi}\int_{x=0}^{x=l}\left(\frac{d\psi}{dx}\right)^2 dx = \frac{D}{4\pi}\int_{\psi=-\psi_0}^{\psi=-\psi_1}\frac{d\psi}{dx}\,d\psi. \tag{7·1}$$

TABLE II. NUMERICAL VALUES OF $\sigma/\sqrt{(CD)}$, ψ_0, AND αl (TEMP. = 17° C)

ψ_0 (volts)	$-\sigma/\sqrt{(CD)}$ (e.s.u.)			
	$\alpha l \to 0$	$\alpha l = 4$	$\alpha l = 8$	$\alpha l \geqslant 12$
0·00		0·000	0·000	0·000
0·01		$2{\cdot}366 \times 10^4$	$2{\cdot}462 \times 10^4$	$2{\cdot}464 \times 10^4$
0·02		$4{\cdot}854 \times 10^4$	$5{\cdot}021 \times 10^4$	$5{\cdot}024 \times 10^4$
0·03		$7{\cdot}554 \times 10^4$	$7{\cdot}784 \times 10^4$	$7{\cdot}788 \times 10^4$
0·04		$1{\cdot}057 \times 10^5$	$1{\cdot}084 \times 10^5$	$1{\cdot}085 \times 10^5$
0·05		$1{\cdot}402 \times 10^5$	$1{\cdot}433 \times 10^5$	$1{\cdot}434 \times 10^5$
0·06		$1{\cdot}804 \times 10^5$	$1{\cdot}838 \times 10^5$	$1{\cdot}838 \times 10^5$
0·07		$2{\cdot}282 \times 10^5$	$2{\cdot}315 \times 10^5$	$2{\cdot}315 \times 10^5$
0·08		$2{\cdot}849 \times 10^5$	$2{\cdot}880 \times 10^5$	$2{\cdot}881 \times 10^5$
0·09		$3{\cdot}541 \times 10^5$	$3{\cdot}570 \times 10^5$	$3{\cdot}571 \times 10^5$
0·10		$4{\cdot}353 \times 10^5$	$4{\cdot}379 \times 10^5$	$4{\cdot}380 \times 10^5$
0·11		$5{\cdot}360 \times 10^5$	$5{\cdot}383 \times 10^5$	$5{\cdot}384 \times 10^5$
0·12		$6{\cdot}550 \times 10^5$	$6{\cdot}571 \times 10^5$	$6{\cdot}571 \times 10^5$
0·13		$8{\cdot}031 \times 10^5$	$8{\cdot}049 \times 10^5$	$8{\cdot}049 \times 10^5$
0·14		$9{\cdot}785 \times 10^5$	$9{\cdot}801 \times 10^5$	$9{\cdot}801 \times 10^5$
0·15		$1{\cdot}197 \times 10^6$	$1{\cdot}199 \times 10^6$	$1{\cdot}199 \times 10^6$
0·16		$1{\cdot}457 \times 10^6$	$1{\cdot}458 \times 10^6$	$1{\cdot}458 \times 10^6$
0·17		$1{\cdot}781 \times 10^6$	$1{\cdot}782 \times 10^6$	$1{\cdot}782 \times 10^6$
0·18	$\sigma/\sqrt{(CD)} \to 0$	$2{\cdot}165 \times 10^6$	$2{\cdot}166 \times 10^6$	$2{\cdot}166 \times 10^6$
0·19	for	$2{\cdot}646 \times 10^6$	$2{\cdot}647 \times 10^6$	$2{\cdot}647 \times 10^6$
0·20	all	$3{\cdot}217 \times 10^6$	$3{\cdot}217 \times 10^6$	$3{\cdot}217 \times 10^6$
0·21	values	$3{\cdot}929 \times 10^6$	$3{\cdot}930 \times 10^6$	$3{\cdot}930 \times 10^6$
0·22	of	$4{\cdot}780 \times 10^6$	$4{\cdot}781 \times 10^6$	$4{\cdot}781 \times 10^6$
0·23	ψ_0	$5{\cdot}834 \times 10^6$	$5{\cdot}834 \times 10^6$	$5{\cdot}834 \times 10^6$
0·24		$7{\cdot}090 \times 10^6$	$7{\cdot}091 \times 10^6$	$7{\cdot}091 \times 10^6$
0·25		$8{\cdot}661 \times 10^6$	$8{\cdot}661 \times 10^6$	$8{\cdot}661 \times 10^6$
0·26		$1{\cdot}068 \times 10^7$	$1{\cdot}068 \times 10^7$	$1{\cdot}068 \times 10^7$
0·27		$1{\cdot}305 \times 10^7$	$1{\cdot}305 \times 10^7$	$1{\cdot}305 \times 10^7$
0·28		$1{\cdot}594 \times 10^7$	$1{\cdot}594 \times 10^7$	$1{\cdot}594 \times 10^7$
0·29		$1{\cdot}947 \times 10^7$	$1{\cdot}947 \times 10^7$	$1{\cdot}947 \times 10^7$
0·30		$2{\cdot}308 \times 10^7$	$2{\cdot}308 \times 10^7$	$2{\cdot}308 \times 10^7$
0·31		$2{\cdot}904 \times 10^7$	$2{\cdot}905 \times 10^7$	$2{\cdot}905 \times 10^7$
0·32		$3{\cdot}375 \times 10^7$	$3{\cdot}375 \times 10^7$	$3{\cdot}375 \times 10^7$
0·33		$4{\cdot}122 \times 10^7$	$4{\cdot}122 \times 10^7$	$4{\cdot}122 \times 10^7$
0·34		$5{\cdot}034 \times 10^7$	$5{\cdot}034 \times 10^7$	$5{\cdot}034 \times 10^7$
0·35		$6{\cdot}149 \times 10^7$	$6{\cdot}149 \times 10^7$	$6{\cdot}149 \times 10^7$

Let $k^{-\frac{1}{2}} e^{\beta\psi} = \sin\phi$, so that $\beta\, d\psi = \cot\phi\, d\phi$. From (3·2)

$$\left(\frac{d\psi}{dx}\right)^2 = \frac{8\pi CRT}{D}\left[\frac{1}{k\sin^2\phi} + k\sin^2\phi - \frac{1}{k} - k\right],$$

and hence

$$\frac{d\psi}{dx} = \sqrt{\left(\frac{8\pi CRT}{D}\right)}\, k^{-\frac{1}{2}} \Delta \cot\phi,$$

in the range $0 \leqslant x \leqslant \frac{1}{2}l$, in which range $-\psi_0 \leqslant \psi \leqslant -\psi_1$. Thus

$$W = \left(\frac{4CRT}{\alpha k^{\frac{1}{2}}}\right) \int_a^{\frac{1}{2}\pi} \Delta \cot^2\phi \, d\phi,$$

where $$a = \sin^{-1} e^{\beta(\psi_1 - \psi_0)}.$$
Hence

$$\begin{aligned} \frac{\alpha k^{\frac{1}{2}}}{4CRT} W &= \int_a^{\frac{1}{2}\pi} \Delta \cos\phi \frac{\cos\phi}{\sin^2\phi} d\phi \\ &= \Big[-\Delta \cot\phi\Big]_a^{\frac{1}{2}\pi} + \int_a^{\frac{1}{2}\pi} \operatorname{cosec}\phi\left(-\Delta \sin\phi - \frac{k^2 \sin\phi \cos^2\phi}{\Delta}\right) d\phi \\ &= \cot a \Delta_a - 2\int_a^{\frac{1}{2}\pi} \Delta \, d\phi + (1-k^2)\int_a^{\frac{1}{2}\pi} \frac{d\phi}{\Delta} \\ &= \cot a \Delta_a - 2\int_a^{\frac{1}{2}\pi} \Delta \, d\phi + \tfrac{1}{4}\alpha l \, k^{-\frac{1}{2}}(1-k^2), \end{aligned}$$

from (4·2), where $\Delta_a = \sqrt{(1 - k^2 \sin^2 a)}$. That is,

$$\frac{\alpha}{4CRT} W = \tfrac{1}{4}(k^{-1} - k)\,\alpha l - k^{-\frac{1}{2}}\left[2\int_a^{\frac{1}{2}\pi} \Delta \, d\phi - \cot a \Delta_a\right]. \tag{7·2}$$

Either (7·1) or (7·2) may be used to obtain expressions for dW/dl. From (7·1)

$$\begin{aligned} \frac{dW}{dl} &= \frac{D}{8\pi}\frac{d}{dl}\left[\int_{x=0}^{x=l} \left(\frac{d\psi}{dx}\right)^2 dx\right] \\ &= \frac{D}{8\pi}\left[\left(\frac{d\psi}{dx}\right)^2_{x=l} + \int_0^l \frac{d}{dl}\left(\frac{d\psi}{dx}\right)^2 dx\right] \\ &= \frac{2\pi\sigma^2}{D} + 2CRT\int_0^l \frac{d}{dl}(\cosh 2\beta\psi - \cosh 2\beta\psi_1)\, dx. \end{aligned} \tag{7·3}$$

The expressions for dW/dl contained in the following sections have been derived from (7·2) on the assumption that

(i) $(\psi_0 - \psi_1)$ is independent of l,

(ii) ψ_0 is independent of l,

(iii) σ is independent of l.

8. EXACT FORMULA FOR dW/dl, ON THE ASSUMPTION THAT $(\psi_0-\psi_1)$ IS INDEPENDENT OF l

Differentiating (7·2) with respect to k we obtain

$$\begin{aligned}\frac{\alpha}{4CRT}\frac{dW}{dk} &= \tfrac{1}{4}(k^{-1}-k)\,\alpha\frac{dl}{dk}+\tfrac{1}{4}\alpha l\left(-\frac{1}{k^2}-1\right)\\ &\quad -k^{-\frac{1}{2}}\left[\frac{2}{k}\left(\int_a^{\frac{1}{2}\pi}\Delta\,d\phi-\int_a^{\frac{1}{2}\pi}\frac{d\phi}{\Delta}\right)+\frac{k\cot a\sin^2 a}{\Delta_a}\right]\\ &\quad +\tfrac{1}{2}k^{-\frac{3}{2}}\left[2\int_a^{\frac{1}{2}\pi}\Delta\,d\phi-\cot a\Delta_a\right]\\ &= \tfrac{1}{4}(k^{-1}-k)\,\alpha\frac{dl}{dk}+\tfrac{1}{4}\alpha lk^{-2}k'^2-k^{-\frac{1}{2}}\int_a^{\frac{1}{2}\pi}\Delta\,d\phi-\tfrac{1}{2}k^{-\frac{3}{2}}\cot a\,\frac{1+k^2\sin^2 a}{\Delta_a}.\end{aligned}\tag{8·1}$$

Further $$\tfrac{1}{4}\alpha l = k^{\frac{1}{2}}\int_a^{\frac{1}{2}\pi}\frac{d\phi}{\Delta}.$$

Hence $$\tfrac{1}{4}\alpha\frac{dl}{dk} = k^{\frac{1}{2}}\int_a^{\frac{1}{2}\pi}\frac{k\sin^2\phi}{\Delta^3}\,d\phi+\tfrac{1}{2}k^{-\frac{1}{2}}\int_a^{\frac{1}{2}\pi}\frac{d\phi}{\Delta},$$

which, after some manipulation, becomes

$$\tfrac{1}{4}\alpha\frac{dl}{dk} = \frac{1}{kk'^2}\left[k^{\frac{1}{2}}\int_a^{\frac{1}{2}\pi}\Delta\,d\phi-\tfrac{1}{8}\alpha lk'^2+\frac{k^{\frac{3}{2}}\sin a\cos a}{\Delta_a}\right].\tag{8·2}$$

Combining (8·1) and (8·2) we obtain

$$\frac{1}{CRT}\frac{dW}{dl} = \frac{\alpha}{4CRT}\frac{dW}{dk}\bigg/\tfrac{1}{4}\alpha\frac{dl}{dk}$$

$$= \frac{\left[\begin{aligned}&k^{-2}\left[k^{\frac{1}{2}}\int_a^{\frac{1}{2}\pi}\Delta\,d\phi-\tfrac{1}{8}\alpha lk'^2+\frac{k^{\frac{3}{2}}\sin a\cos a}{\Delta_a}\right]\\ &\qquad +\tfrac{1}{4}\alpha lk^{-2}k'^2-k^{-\frac{1}{2}}\int_a^{\frac{1}{2}\pi}\Delta\,d\phi-\tfrac{1}{2}k^{-\frac{3}{2}}\cot a\,\frac{1+k^2\sin^2 a}{\Delta_a}\end{aligned}\right]}{\dfrac{1}{kk'^2}\left[k^{\frac{1}{2}}\int_a^{\frac{1}{2}\pi}\Delta\,d\phi-\tfrac{1}{8}\alpha lk'^2+\dfrac{k^{\frac{3}{2}}\sin a\cos a}{\Delta_a}\right]},$$

the numerator of which can be simplified to $\tfrac{1}{8}\alpha lk'^2k^{-2}-\tfrac{1}{2}k^{-\frac{3}{2}}\cot a\Delta_a$.

Finally $$\frac{dW}{dl} = \frac{CRT\lambda_1(\lambda_2-\lambda_3)}{\lambda_4-\lambda_2+\lambda_5},\tag{8·3}$$

where
$$\lambda_1 = \frac{1}{k} - k,$$
$$\lambda_2 = \tfrac{1}{8}\alpha l k'^2,$$
$$\lambda_3 = \tfrac{1}{2}k^{\frac{1}{2}} \cot a \Delta_a,$$
$$\lambda_4 = k^{\frac{1}{2}} \int_a^{\frac{1}{2}\pi} \Delta \, d\phi,$$
$$\lambda_5 = k^{\frac{3}{2}} \sin a \cos a / \Delta_a.$$

The expression for dW/dl was put into the form (8·3) in order to facilitate numerical computation.

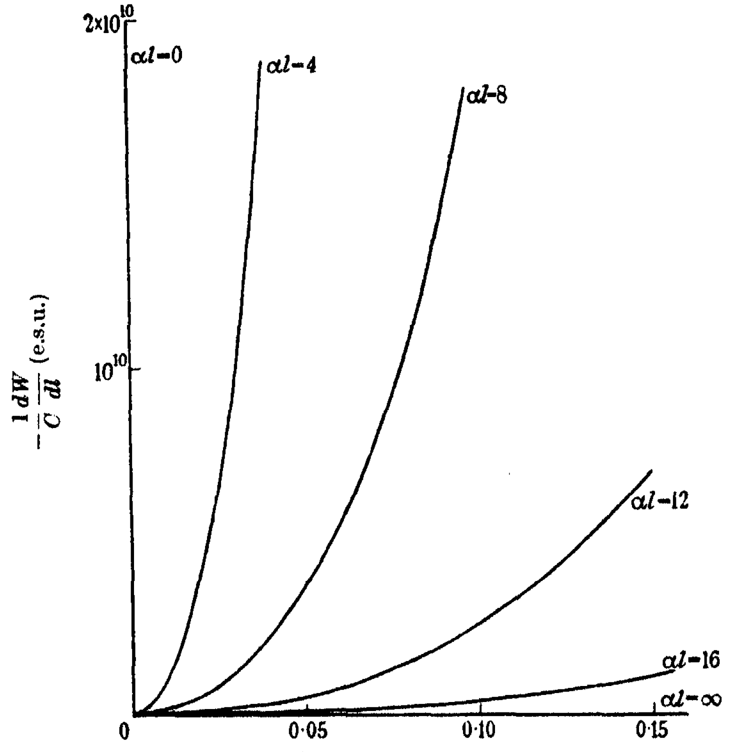

FIG. 3

Numerical values of $-\frac{1}{C}\frac{dW}{dl}$ are given in Table III. In order to obtain a representative case T was assumed to be equal to 290° A and ν equal to 1. Fig. 3 shows the relationship between $-\frac{1}{C}\frac{dW}{dl}$ and $(\psi_0 - \psi_1)$ in graphical form. As l tends to zero, ψ_1 tends to ψ_0. The limiting curve for $\alpha l = 0$

therefore coincides with the line $(\psi_0-\psi_1)=0$. When l is infinite, dW/dl is zero, and the curve $\alpha l=\infty$ coincides with the line $dW/dl=0$.

TABLE III. NUMERICAL VALUES OF $\left(-\frac{1}{C}\frac{dW}{dl}\right)$, $(\psi_0-\psi_1)$ AND l

(TEMP. = 17° C)

$\psi_0-\psi_1$ (volts)	$\left(-\frac{1}{C}\frac{dW}{dl}\right)$ (e.s.u.)				
	$\alpha l=4$	$\alpha l=8$	$\alpha l=12$	$\alpha l=16$	$\alpha l\to\infty$
0·0000	0·000	0·000	0·000	0·0000	
0·0003	$7\cdot616\times10^{5}$	...	...	...	
0·0008	...	...	$1\cdot080\times10^{5}$	...	
0·0011	$1\cdot227\times10^{7}$	...	...	...	
0·0024	$6\cdot213\times10^{7}$	...	...	...	
0·0025	...	$8\cdot492\times10^{6}$	...	...	
0·0031	...	...	$1\cdot765\times10^{6}$	...	
0·0045	$2\cdot432\times10^{8}$	...	...	...	
0·0058	...	...	...	$8\cdot210\times10^{5}$	
0·0069	$5\cdot065\times10^{8}$	...	...	...	$-\frac{1}{C}\frac{dW}{dl}\to0$ for all values of $(\psi_0-\psi_1)$
0·0070	...	...	$8\cdot968\times10^{6}$	...	
0·0102	$1\cdot102\times10^{9}$	$1\cdot409\times10^{8}$	...	...	
0·0124	...	...	$2\cdot872\times10^{7}$	...	
0·0142	$2\cdot187\times10^{9}$	...	...	...	
0·0175	...	$4\cdot075\times10^{8}$	...	...	
0·0194	$4\cdot107\times10^{9}$	...	...	...	
0·0196	...	...	$7\cdot178\times10^{7}$	...	
0·0234	...	...	...	$1\cdot404\times10^{7}$	
0·0235	...	$7\cdot455\times10^{8}$	...	...	
0·0268	$7\cdot899\times10^{9}$	...	...	...	
0·0346	$1\cdot396\times10^{10}$	...	...	...	
0·0349	...	$1\cdot692\times10^{9}$	...	...	
0·0469	$2\cdot732\times10^{10}$	...	...	...	
0·0544	...	...	$6\cdot031\times10^{8}$	...	
0·0560	...	$4\cdot704\times10^{9}$	...	...	
0·0571	...	...	...	$9\cdot116\times10^{7}$	
0·0667	$6\cdot201\times10^{10}$	...	...	...	
0·0708	...	$8\cdot096\times10^{9}$	...	...	
0·0820	...	$1\cdot137\times10^{10}$	...	...	
0·0875	$1\cdot215\times10^{11}$	...	...	...	
0·0914	...	$1\cdot522\times10^{10}$	...	...	
0·1034	...	...	$2\cdot793\times10^{9}$	...	
0·1056	...	$2\cdot232\times10^{10}$	...	...	
0·1114	$2\cdot333\times10^{11}$	...	...	...	
0·1250	...	$3\cdot619\times10^{10}$	...	...	
0·1316	$3\cdot800\times10^{11}$	...	...	...	
0·1537	...	...	...	$1\cdot226\times10^{9}$	
0·1562	...	$7\cdot380\times10^{10}$	...	...	
0·1673	$8\cdot482\times10^{11}$	...	...	...	
0·2490	...	$1\cdot642\times10^{11}$	...	...	

The curves show that for "reasonably large" values of $(\psi_0-\psi_1)$ the value of dW/dl is always negative. The sign of dW/dl when $(\psi_0-\psi_1)$ is small needs more careful attention. The following brief investigation, however, shows that even in this region dW/dl is always negative.

When $(\psi_0-\psi_1)$ is very small, k is very nearly equal to 1 and a is nearly equal to $\frac{1}{2}\pi$. Put $(\psi_0-\psi_1)=\epsilon$ and $a=(\frac{1}{2}\pi-\eta)$, where ϵ and η are very small quantities. Since $\sin a = e^{\beta(\psi_1-\psi_0)}$, we have, as a first approximation,

$$1-\tfrac{1}{2}\eta^2 = 1-\beta\epsilon,$$

that is $$\eta=\sqrt{(2\beta\epsilon)};\quad a=\tfrac{1}{2}\pi-\sqrt{(2\beta\epsilon)}.$$

With these values

$$\tfrac{1}{4}\alpha l k^{-\frac{1}{2}} = \int_a^{\frac{1}{2}\pi}\frac{d\phi}{\Delta} = \int_{\frac{1}{2}\pi-\eta}^{\frac{1}{2}\pi}\frac{d\phi}{\sqrt{(1-k^2\sin^2\phi)}} \approx \eta\frac{1}{\sqrt{(1-k^2)}} = \frac{\sqrt{(2\beta\epsilon)}}{k'},$$

that is $$\lambda_2=\tfrac{1}{8}\alpha l k'^2 = \tfrac{1}{2}k^{\frac{1}{2}}k'\sqrt{(2\beta\epsilon)}.$$

Further $$\lambda_3=\tfrac{1}{2}k^{\frac{1}{2}}\cot a\Delta_a = \frac{\frac{1}{2}k^{\frac{1}{2}}\sqrt{(2\beta\epsilon k'^2)}}{1-\beta\epsilon} = \frac{\frac{1}{2}k^{\frac{1}{2}}k'\sqrt{(2\beta\epsilon)}}{1-\beta\epsilon}.$$

Hence $$\frac{dW}{dl}=0 \quad\text{when}\quad \tfrac{1}{2}k^{\frac{1}{2}}k'\sqrt{(2\beta\epsilon)} = \frac{\frac{1}{2}k^{\frac{1}{2}}k'\sqrt{(2\beta\epsilon)}}{1-\beta\epsilon},$$

that is, when $$\epsilon=0,\ \text{or}\ 1-\beta\epsilon=1.$$

dW/dl is therefore negative when $(\psi_0-\psi_1)$ is very small.

9. EXACT FORMULA FOR dW/dl, ON THE ASSUMPTION THAT ψ_0 IS INDEPENDENT OF l

Differentiating (7·2) with respect to k, we obtain

$$\begin{aligned}\frac{\alpha}{4CRT}\frac{dW}{dk} &= \tfrac{1}{4}(k^{-1}-k)\,\alpha\frac{dl}{dk}-\tfrac{1}{4}(1+k^{-2})\,\alpha l+\tfrac{1}{2}k^{-\frac{3}{2}}\left[2\int_a^{\frac{1}{2}\pi}\Delta\,d\phi-\cot a\Delta_a\right]\\ &\quad -k^{-\frac{1}{2}}\left[2\left(-\Delta_a\frac{da}{dk}+k^{-1}\int_a^{\frac{1}{2}\pi}\Delta\,d\phi-k^{-1}\int_a^{\frac{1}{2}\pi}\frac{d\phi}{\Delta}\right)\right.\\ &\quad \left.-\frac{-2\cot a\operatorname{cosec}^2 a\dfrac{da}{dk}-2k\cos^2 a+2k^2\cos a\sin a\dfrac{da}{dk}}{2\cot a\Delta_a}\right],\end{aligned}$$

which, on substituting $(-\tan a/2k)$ for da/dk, simplifies to

$$\frac{\alpha}{4CRT}\frac{dW}{dk} = \tfrac{1}{4}(k^{-1}-k)\,\alpha\frac{dl}{dk} - \tfrac{1}{4}(1-k^{-2})\,\alpha l$$

$$-k^{-\frac{1}{2}}\int_a^{\frac{1}{2}\pi}\Delta d\phi - \tfrac{1}{2}k^{-\frac{1}{2}}\tan a\,\frac{1+k^2\cos 2a}{\Delta_a}. \tag{9·1}$$

Further $$\tfrac{1}{4}\alpha l k^{-\frac{1}{2}} = \int_a^{\frac{1}{2}\pi}\frac{d\phi}{\Delta},$$

and hence

$$\tfrac{1}{4}\alpha l(-\tfrac{1}{2}k^{-\frac{3}{2}}) + \tfrac{1}{4}\alpha\frac{dl}{dk}k^{-\frac{1}{2}} = -\frac{1}{\Delta_a}\frac{da}{dk} + \frac{1}{kk'^2}\int_a^{\frac{1}{2}\pi}\Delta\,d\phi - \frac{1}{k}\int_a^{\frac{1}{2}\pi}\frac{d\phi}{\Delta} + \frac{k\sin a\cos a}{k'^2\Delta_a},$$

that is $$\tfrac{1}{4}\alpha k^{-\frac{1}{2}}\frac{dl}{dk} = \frac{\tan a}{2k\Delta_a} + \frac{1}{kk'^2}\int_a^{\frac{1}{2}\pi}\Delta\,d\phi + \frac{k\sin a\cos a}{k'^2\Delta_a} - \tfrac{1}{8}\alpha l k^{-\frac{3}{2}},$$

or $$\alpha\frac{dl}{dk} = \frac{2(k'^2\tan a + k^2\sin 2a)}{k^{\frac{1}{2}}k'^2\Delta_a} + \frac{4}{k^{\frac{1}{2}}k'^2}\int_a^{\frac{1}{2}\pi}\Delta\,d\phi - \tfrac{1}{2}\alpha l k^{-1}. \tag{9·2}$$

Combining (9·1) and (9·2) and simplifying, the expression for dW/dk reduces to

$$\frac{\alpha}{4CRT}\frac{dW}{dk} = \tfrac{1}{2}\alpha l\left(\frac{k'}{k}\right)^2. \tag{9·3}$$

Combining (9·2) and (9·3), we have

$$\frac{1}{CRT}\frac{dW}{dl} = \frac{\alpha}{CRT}\frac{dW}{dk}\Big/\alpha\frac{dl}{dk}$$

$$= \frac{\tfrac{1}{8}\alpha l k^{-1}k'^2}{\tfrac{1}{2}k^{\frac{1}{2}}\tan a\,\dfrac{1+k^2\cos 2a}{\Delta_a} + k^{\frac{1}{2}}\displaystyle\int_a^{\frac{1}{2}\pi}\Delta\,d\phi - \tfrac{1}{8}\alpha l k'^2},$$

or $$\frac{dW}{dl} = \frac{CRT\lambda_1\lambda_2}{\lambda_4-\lambda_2+\lambda_6}, \tag{9·4}$$

where $$\lambda_1 = \left(\frac{1}{k}-k\right),$$

$$\lambda_2 = \tfrac{1}{8}\alpha l k'^2,$$

$$\lambda_4 = k^{\frac{1}{2}}\int_a^{\frac{1}{2}\pi}\Delta\,d\phi,$$

$$\lambda_6 = \tfrac{1}{2}k^{\frac{1}{2}}\tan a\,(1+k^2\cos 2a)/\Delta_a.$$

Consideration of fig. 2 shows that if ψ_0 remains fixed ψ_1 diminishes as l increases. That is to say dl/dk is always positive. Moreover, by (9·3) dW/dk is always positive, and hence dW/dl is always positive.

Let us now consider limiting values of dW/dl, that is when αl is very small and when αl is very large. When αl is very small ψ_0 is very nearly equal to ψ_1 and a is approximately $\frac{1}{2}\pi$. Writing $a = (\frac{1}{2}\pi - \eta)$, where η is very small, the formula for dW/dl becomes, on simplification,

$$\frac{dW}{dl} = \text{constant} \times \eta^2,$$

which tends to zero as αl tends to zero. When αl is very large k tends to 1 and

$$\tfrac{1}{4}\alpha l k^{-\frac{1}{2}} k'^2 \to \int_a^{\frac{1}{2}\pi} \frac{1-k^2}{\sqrt{(1-k^2\sin^2\phi)}}\,d\phi$$

$$\leqslant \int_a^{\frac{1}{2}\pi} \sqrt{(1-k^2)}\,d\phi$$

$$\to 0 \text{ as } k \to 1.$$

Hence dW/dl tends to zero as αl tends to infinity.

On account of these two properties it is clear that, for a fixed value of ψ_0, dW/dl increases from zero to some maximum value and then decreases back to zero as αl ranges from zero to infinity. Therefore when αl is comparatively large dW/dl diminishes as αl increases. Such a state of affairs cannot possibly account for the observed phenomenon. Experiment shows that as the colloid substance separates out into layers, the distance between the layers diminishes as the number of layers, counting from the top, increases. With special reference to fig. 4 this means that $l_1 > l_2 > l_3 \ldots$, where l_1 is the distance between the first and second layers, l_2 the distance between the second and third layers, etc. Consideration of the statical equilibrium of the nth layer shows that $A_n = A_{n-1} - S$, where A_n is the electrostatic force of attraction between the nth and $(n+1)$th layers and the layer corresponding to $n = 0$ is at infinity. It can be seen quite easily that $A_n = A_0 - nS$. This means that the electrostatic force of attraction diminishes as l diminishes. This is true for all values of l, particularly at the top of the system where l is comparatively large. This experimental fact shows that the assumption, made at the beginning of this section, that ψ_0 is independent of l is invalid.

Alternatively the fact that the assumption that ψ_0 is independent of l leads to $A_0 = 0$ is sufficient to show that the assumption is invalid, for the top layer cannot be in equilibrium.

10. Exact formula for dW/dl, on the assumption that σ is independent of l

We have
$$\frac{\alpha}{4CRT}W = \tfrac{1}{4}(k^{-1}-k)\,\alpha l - k^{-\frac{1}{2}}\left(2\int_a^{\frac{1}{2}\pi}\Delta\,d\phi - \cot a\Delta_a\right), \tag{10·1}$$
$$\left(\frac{2\pi}{DCRT}\right)^{\frac{1}{2}}\sigma = -k^{-\frac{1}{2}}\cot a\Delta_a, \tag{10·2}$$
$$0 = \int_a^{\frac{1}{2}\pi}\frac{d\phi}{\Delta} - \tfrac{1}{4}k^{-\frac{1}{2}}\alpha l \equiv h(\psi_0, \psi_1, l), \text{ say.} \tag{10·3}$$

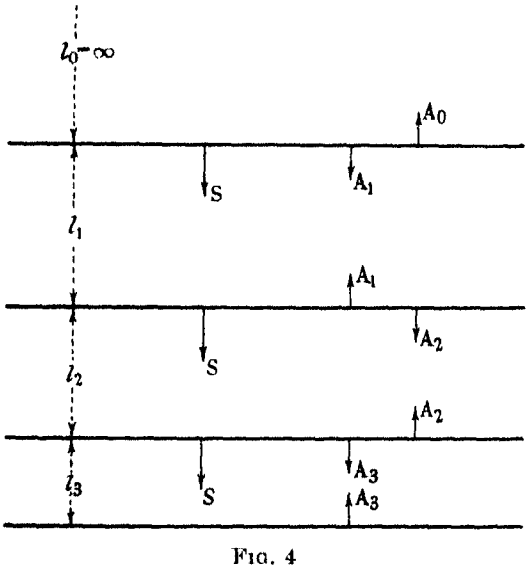

FIG. 4

Now
$$\left.\begin{aligned} dW &= \frac{\partial W}{\partial \psi_0}d\psi_0 + \frac{\partial W}{\partial \psi_1}d\psi_1 + \frac{\partial W}{\partial l}dl,\\ 0 &= \frac{\partial \sigma}{\partial \psi_0}d\psi_0 + \frac{\partial \sigma}{\partial \psi_1}d\psi_1 + \frac{\partial \sigma}{\partial l}dl,\\ 0 &= \frac{\partial h}{\partial \psi_0}d\psi_0 + \frac{\partial h}{\partial \psi_1}d\psi_1 + \frac{\partial h}{\partial l}dl, \end{aligned}\right\} \tag{10·4}$$
where
$$\frac{\alpha}{4CRT}\frac{\partial W}{\partial \psi_0} = \beta k^{-\frac{1}{2}}\left(\frac{\cot a}{\Delta_a} - \tan a\Delta_a\right),$$
$$\frac{\alpha}{4CRT}\frac{\partial W}{\partial \psi_1} = \tfrac{1}{2}\alpha l\beta(k-k^{-1}) + 2\beta k^{-\frac{1}{2}}\int_a^{\frac{1}{2}\pi}\Delta\,d\phi + \beta k^{-\frac{1}{2}}k'^2\tan a/\Delta_a,$$

$$\frac{\alpha}{4CRT}\frac{\partial W}{\partial l} = \tfrac{1}{4}\alpha(k^{-1}-k),$$

$$\left(\frac{2\pi}{DCRT}\right)^{\frac{1}{2}}\frac{\partial\sigma}{\partial\psi_0} = -\beta k^{-\frac{1}{2}}\left(\frac{\cot a}{\Delta_a}+\tan a\Delta_a\right),$$

$$\left(\frac{2\pi}{DCRT}\right)^{\frac{1}{2}}\frac{\partial\sigma}{\partial\psi_1} = \beta k^{-\frac{1}{2}}\left(\frac{k^2\sin a\cos a}{\Delta_a}+\tan a\Delta_a\right),$$

$$\frac{\partial\sigma}{\partial l} = 0,$$

$$\frac{\partial h}{\partial\psi_0} = \frac{\beta\tan a}{\Delta_a},$$

$$\frac{\partial h}{\partial\psi_1} = \tfrac{1}{4}\alpha l\beta k^{-\frac{1}{2}} - \frac{2\beta}{k'^2}\int_a^{\frac{1}{2}\pi}\Delta\,d\phi - \frac{\beta}{k'^2\Delta_a}(2k^2\sin a\cos a + k'^2\tan a),$$

$$\frac{\partial h}{\partial l} = -\tfrac{1}{4}\alpha k^{-\frac{1}{2}}.$$

Substituting these values in (10·4) we obtain, on simplification,

$$\frac{1}{CRT}\frac{dW}{dl} \doteq \frac{k'^2\dfrac{1+k^2\sin^2 a}{\Delta_a} - 4k^2\sin^2 a - \tfrac{1}{4}\alpha lk^{-\frac{1}{2}}k'^2\left(\dfrac{\cot a}{\Delta_a}+\tan a\Delta_a\right)}{\left(\tfrac{1}{4}\alpha lk^{-\frac{1}{2}} - \dfrac{2}{k'^2}\displaystyle\int_a^{\frac{1}{2}\pi}\Delta\,d\phi\right)\left(\dfrac{\cot a}{\Delta_a}+\tan a\Delta_a\right) - \dfrac{1+k^2\cos^2 a + k^4\sin^2 a\cos 2a}{k'^2\Delta_a}}. \tag{10·5}$$

When αl is very small this reduces to

$$\frac{1}{CRT}\frac{dW}{dl} = \frac{k'(1-k')}{2-k'},$$

and as αl tends to infinity, $\dfrac{1}{CRT}\dfrac{dW}{dl} \to 0.$

The curves obtained by plotting $\dfrac{1}{CRT}\dfrac{dW}{dl}$ against ψ_0 when $\alpha l = 0$ and when $\alpha l = \infty$ are shown in fig. 5 and rough numerical calculations lead to the conclusion that the curves corresponding to intermediate values of αl lie between these two limiting curves. dW/dl is, therefore, always positive and the electrostatic force between the plates one of attraction.

To each pair of values of αl and ψ_0 there is a single value of σ, and if αl is fixed σ increases numerically from zero to infinity with ψ_0. To each point on an (αl) curve there is a corresponding value of σ, and if the points representing the same value of σ are joined we obtain a series of curves along each of which σ is constant. These are the dotted lines in fig. 5. Each (σ) curve cuts each (αl) curve in one and only one point.

It is clear from the form of the curves that, for a fixed value of σ, dW/dl increases from zero to some maximum value and then decreases back to zero as αl falls from infinity to zero. When αl is large, or only moderately large, therefore, dW/dl increases as αl diminishes and since this result is contrary to observed fact it follows that the original assumption, namely that σ is independent of l, is invalid. This can be seen more concretely from a consideration of the equilibrium of the top layer (see fig. 4). The force A_0 corresponding to $\alpha l = \infty$ is zero, and hence the top layer is not in equilibrium.

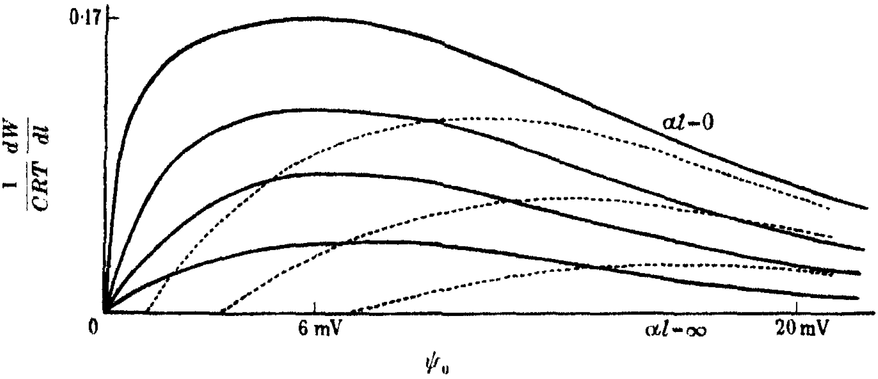

Fig. 5

11. Comparison with experiment

Experimental results are contained in the paper by Bergmann *et al.* (1938, Table I, p. 309). The authors experimented with NaCl, $NaNO_3$, KCl, KNO_3, KOH and HCl and observed the value of l experimentally when the number of layers above the point of observation lay between 100 and 1000. The conclusion they arrived at was that the electrokinetic potential difference, ζ, which we here identify with $-(\psi_0 - \psi_1)$ was approximately 88 mV, and that σ was approximately 10^3 e.s.u. Table IV is a composite one containing some of the experimental results of Bergmann *et al.* and theoretical numerical values deduced from the present investigation.

The fact that a range of values of ζ is given in Table IV should not be taken to imply that ζ varies with the number of layers above the point of observation. On account of the fact that the column headed "αl" gives only an average value valid for the range in which the number of overhanging layers lies between 100 and 1000, it is impossible to specify ζ more closely than is done in Table IV. The column headed ζ (100 layers) gives the value of ζ if the number of overhanging layers had been exactly 100 and that headed ζ (1000 layers) gives the value if the number had been exactly 1000.

It is interesting to note that σ is not more than about 360 e.s.u., while for small concentrations σ can be as low as 10 e.s.u. In the paper by Bergmann, Löw-Beer and Zocher σ was deduced to be about 1000 e.s.u.

The assumptions made in this investigation lead to values of ζ which are rather low.

TABLE IV. RANGE OF VALUES OF THE ELECTROKINETIC POTENTIAL DIFFERENCE CONSISTENT WITH EXPERIMENTAL RESULTS, DEDUCED FROM THE ASSUMPTION $\zeta = -(\psi_0 - \psi_1)$

C per unit volume	l (average value) (experimental) (cm.)	αl (average value) (experimental)	$\frac{1}{C}\times$ force per unit area on layer, in dynes per sq. cm.		ζ mV	
			100 layers	1000 layers	100 layers	1000 layers
$1{\cdot}5\times10^{-8}$	$5{\cdot}4\times10^{-5}$	6·9	$4{\cdot}0\times10^{7}$	$4{\cdot}0\times10^{8}$	5	10
$4{\cdot}0\times10^{-8}$	$4{\cdot}5\times10^{-5}$	9·3	$1{\cdot}5\times10^{7}$	$1{\cdot}5\times10^{8}$	5	11
$6{\cdot}0\times10^{-8}$	$4{\cdot}2\times10^{-5}$	10·7	$1{\cdot}0\times10^{7}$	$1{\cdot}0\times10^{8}$	6	19
$9{\cdot}0\times10^{-8}$	$3{\cdot}8\times10^{-5}$	11·8	$6{\cdot}7\times10^{6}$	$6{\cdot}7\times10^{7}$	6	20
$16{\cdot}0\times10^{-8}$	$3{\cdot}3\times10^{-5}$	13·7	$3{\cdot}7\times10^{6}$	$3{\cdot}7\times10^{7}$	7	20
$25{\cdot}0\times10^{-8}$	$2{\cdot}8\times10^{-5}$	14·5	$2{\cdot}4\times10^{6}$	$2{\cdot}4\times10^{7}$	7	20
$36{\cdot}0\times10^{-8}$	$2{\cdot}4\times10^{-5}$	14·9	$1{\cdot}7\times10^{6}$	$1{\cdot}7\times10^{7}$	7	20
$49{\cdot}0\times10^{-8}$	$2{\cdot}2\times10^{-5}$	16·0	$1{\cdot}2\times10^{6}$	$1{\cdot}2\times10^{7}$	8	20
$64{\cdot}0\times10^{-8}$	$2{\cdot}1\times10^{-5}$	17·4	$9{\cdot}4\times10^{5}$	$9{\cdot}4\times10^{6}$	8	22

12. SUMMARY OF THE PRINCIPAL RESULTS

1. The potential ψ at distance x from a plate is given by

$$F[k, \sin^{-1} e^{\beta(\psi+\psi_1)}] - F[k, \sin^{-1} e^{\beta(\psi_1-\psi_0)}] = \tfrac{1}{2}k^{-\frac{1}{2}}\, x.$$

ψ increases monotonically from $x = 0$ to $x = \frac{1}{2}l$ and then decreases monotonically to $x = l$, the system being symmetrical with respect to $x = \frac{1}{2}l$. If $\alpha l > 20$,

$$\psi = \frac{1}{\beta}\log_e \frac{Ae^{\alpha x}-1}{Ae^{\alpha x}+1}.$$

2. The surface density of charge, σ, on the plates is given by

$$\sigma = -\sqrt{\left[\frac{DCRT}{\pi}(\cosh 2\beta\psi_0 - \cosh 2\beta\psi_1)\right]}.$$

As $l \to 0$, $\sigma \to 0$; and as $l \to \infty$, $\sigma \to -\left(\frac{2DCRT}{\pi}\right)^{\frac{1}{2}} \sinh \beta\psi_0$.

3. ψ_0, ψ_1 and l are connected by the equation

$$\tfrac{1}{4}k^{-\frac{1}{2}}\alpha l = \int_a^{\frac{1}{2}\pi} \frac{d\phi}{\Delta}.$$

For any given value of αl, ψ_1 increases with ψ_0 and tends to a finite limit as ψ_0 tends to infinity. The limiting value of ψ_1 is a function of l, being zero when l is infinite. As l tends to zero, ψ_1 tends to ψ_0.

4. The consequences of the following assumptions are investigated.

(i) $(\psi_0 - \psi_1)$ is independent of l. This produces a repulsion between the layers. A consequence of this assumption, which is in agreement with the experimental facts, is that the distance between consecutive layers diminishes as the number of layers above the point of observation is increased. The range of values of the electrokinetic potential difference, which is identified with $-(\psi_0 - \psi_1)$, consistent with experimental results is 5–22 mV.

(ii) ψ_0 is independent of l. This produces an attraction between the layers which cannot account for observed phenomena.

(iii) σ is independent of l. This also produces an attraction between the layers which cannot account for observed phenomena.

REFERENCES

Bergmann, Löw-Beer and Zocher 1938 *Z. phys. Chem.* **181**, 301.
Bikerman 1933 *Z. phys. Chem.* **163**, 378.
Chapman 1913 *Phil. Mag.* (6), **25**, 475.
Gouy 1910 *J. Phys. Radium* (4), **9**, 457.
Rosenhead and Miller 1937 *Proc. Roy. Soc.* A, **163**, 298.
Tannery and Molk *Functions Elliptiques*, **4**, 127 (1898 edition).
Zocher 1925 *Z. anorg. Chem.* **147**, 91.

The absorption spectrum of nitrosyl chloride

By C. F. Goodeve and S. Katz

The Sir William Ramsay and Ralph Forster Laboratories, University College, London

(*Communicated by S. Sugden, F.R.S.—Received* 28 *April* 1939)

Although the photodecomposition of nitrosyl chloride has often been quoted as a typical photochemical reaction, there is considerable disagreement in the literature with regard to its exact mechanism. Early workers (Kiss 1923; Bowen and Sharpe 1925) found a quantum efficiency, γ, of 0·5 for the visual region, while Kistiakowsky (1930) found a value of 2.

Quanta of wave-lengths shorter than 7600 A have sufficient energy to dissociate NOCl. Kistiakowsky, however, found fine structure in the spectrum as far down as 4100 A and suggested therefore that the reaction occurred as a result of a collision between a photochemically activated molecule and a normal molecule. On the other hand, Allmand (1931) pointed out that the fact that γ was not reduced (Kistiakowsky 1930) either by sevenfold dilution with nitrogen or reduction in pressure by a factor of nine, indicated a primary dissociation mechanism. He suggested the possibility of this occurring without the disappearance of rotational fine structure.

Recently, Winn (1939) has found photochemical decomposition of NOCl to occur with a quantum efficiency of 2 down to extremely low pressures.

The existence of rotational fine structure associated with primary dissociation still awaits clarification. The authors have therefore reinvestigated the absorption spectrum of nitrosyl chloride in the visible and ultraviolet regions, and have measured the extinction coefficients over a wide range. Manganini (1889) was the first to study this spectrum but made only qualitative measurements. Leermakers and Ramsperger (1932), incidental to another problem, measured the extinction coefficient of NOCl over a small part of the visible region, but made no mention of fine structure.

The molecular structure of NOCl has been investigated recently by both infra-red and electron diffraction methods (Bailey and Cassie 1934; Ketelaar and Palmer 1937; Fox and Martin 1938). The molecule is apparently triangular, the only non-linear completely asymmetrical triatomic molecule reported in the literature.* The other nitrosyl halides are presumably similar. The characteristics of the vibrations of such a molecule still await complete solution.

EXPERIMENTAL

NOCl is normally in equilibrium with traces of NO and Cl_2 at ordinary temperatures. It is therefore very important that all traces of oxygen be eliminated to prevent the formation of NO_2 which possesses a high extinction coefficient. Special precautions were taken to avoid this possibility.

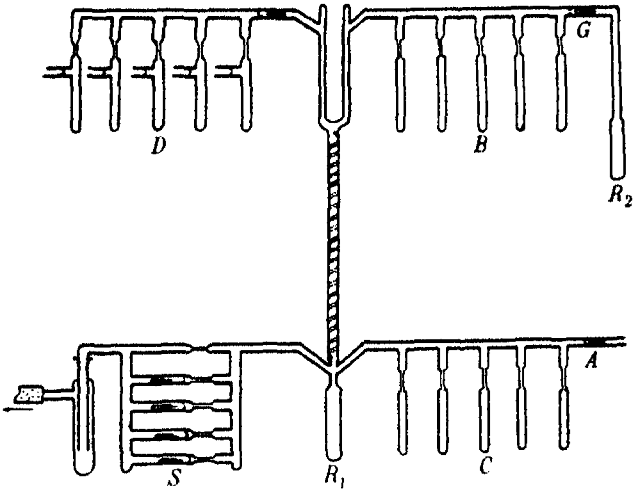

FIG. 1. The arrangement for purification of NOCl.

NOCl was prepared by the method of Scott and Johnson (1929). The apparatus was all of glass, and was thoroughly flushed with purified nitrogen before the beginning of the actual preparation. Nitrosyl sulphuric acid was prepared by passing sulphur dioxide into fuming nitric acid. The nitrosyl chloride was then formed by the addition of hydrogen chloride gas.

Purification was effected in an all glass fractionating system (see fig. 1). The system was flushed thoroughly with nitrogen, then evacuated and sealed off. The NOCl was admitted from the reaction vessel by breaking the septum A, and was collected in the reservoir R_1 below the column; the connecting tube was then sealed off. The column was warmed to room temperature at the bottom, and cooled to about −50° C at the top. A small fraction was removed by cooling one of the bulbs at *B* to −75° C, and was discarded after sealing off. The bulk of the NOCl was then distilled into the reservoir R_2, which was closed by manipulating the internal ground joint *G* with a magnet, and the residual fraction was removed by distillation into *C*. The bulk was returned to R_1 and the distillation repeated. Between successive distillations the NOCl was cooled to −75° C, one of the bank of septa was opened and the system pumped down and again sealed off. After six such fractionations and out-gassings, the remainder of the NOCl was transferred to the receiving bulbs *D*, which were then sealed off. These bulbs had septum-sealed side arms to permit the transfer of the NOCl without atmospheric contamination.

---

* DOH and DSH are possible exceptions to this. In the case of the former, however, the dimensions appear to be the same as those for H_2O (Barker and Sleator 1935). The structure of DSH (Nielsen and Nielsen 1937) has not been finally settled but it too appears to be symmetrical.

NOCl reacts with tap grease and mercury, and therefore taps and mercury cut-offs and manometers were excluded from the optical part of the apparatus. In this, the quartz absorption cells were attached to one side of a quartz Bodenstein spiral manometer *M* and through a graded seal to a glass reservoir. The other side of the gauge was connected to a mercury manometer. A bulb *D* was attached by its septum-sealed side arm to the reservoir, and its contents transferred by evacuating, breaking the septum and distilling.

Pressures were adjusted in the absorption cell by cooling the reservoir to the appropriate temperature. The indicator on the gauge was observed through a telescope, and pressures were read on the manometer, using the gauge as a null instrument.

OPTICAL MEASUREMENTS

The molecular extinction coefficient, ϵ, and the absolute extinction coefficient, α, are defined by

$$\epsilon = \log_{10}\frac{I_0}{I_t}\frac{1}{cl} \quad \text{and} \quad \alpha = \log_e\frac{I_0}{I_t}\frac{1}{nl},$$

where I_0 and I_t are the intensities of the incident and transmitted beams, l is the length of the absorbing column in cm., c the concentration of vapour in g.-mol. per litre, and n the number of molecules per c.c.

To obtain as wide a range of extinction coefficients as possible, several optical systems were used, as shown in Table I. All measurements were made photographically, the intensity of the transmitted light being compared with that of light of the same initial intensity reduced to a known fraction by some standard device.

In the first and fourth systems, comparison spectra taken through the empty tube were placed adjacent to the absorption spectra. In the former, a nitrogen atmosphere was used in the spectrograph to eliminate oxygen bands around 2000 A. Match points, i.e. points of equal blackening on the photographic plate, were determined visually. In several difficult cases, notably with the E 1 and V 2 spectrographs, matchings were decided by superimposing microphotometer tracings of the absorption spectrum on tracings of the reference spectrum. The frequencies of the maxima of the bands in the visible were obtained to an accuracy of 10 cm.$^{-1}$ by means of microphotometer tracings.

TABLE I

	Light source	Absorbing column cm.	Range of pressures cm. Hg	Range of frequencies cm.$^{-1}$	Method of photometry	Spectrograph
I.	Hydrogen discharge tube	0·1	(3·85)	54000 to 47600	Single cell, different exposures	Hilger E 370
II.	Tungsten iron spark	1 and 4	5–65	44000 to 22000	Spekker, divided beam photometer (Twyman 1931)	Hilger E 3
III.	500 c.p. pointolite	4, 10, and 16	89–119	25000 to 15000	Judd Lewis (1921) photometer	Hilger V 2
IV.	500 c.p. pointolite	138	10–40	20000 to 12500	Single cell, different exposures	Hilger E 1

The extinction coefficients in the visible were also measured at 233° K using the arrangement described in IV, Table I. The tube was placed in a metal trough filled with alcohol. Solid carbon dioxide was added at intervals to maintain the tube at approximately the desired temperature.

For observations at 457·4° K, a cell system was used with an outer jacket filled with the vapour from boiling aniline, and with evacuated end cells to prevent heat loss at the windows of the main cell. The comparison beam of the photometer passed through an empty cell. The optical system was otherwise identical with III, Table I, with the absorbing column 10 cm. long.

RESULTS

In fig. 2 the logarithms of the extinction coefficients at 293° K are shown plotted against the frequencies in wave numbers. Within the range of pressures indicated in Table I, Beer's law was found to be obeyed at all frequencies. The positions and values of the maxima are indicated in Table II.

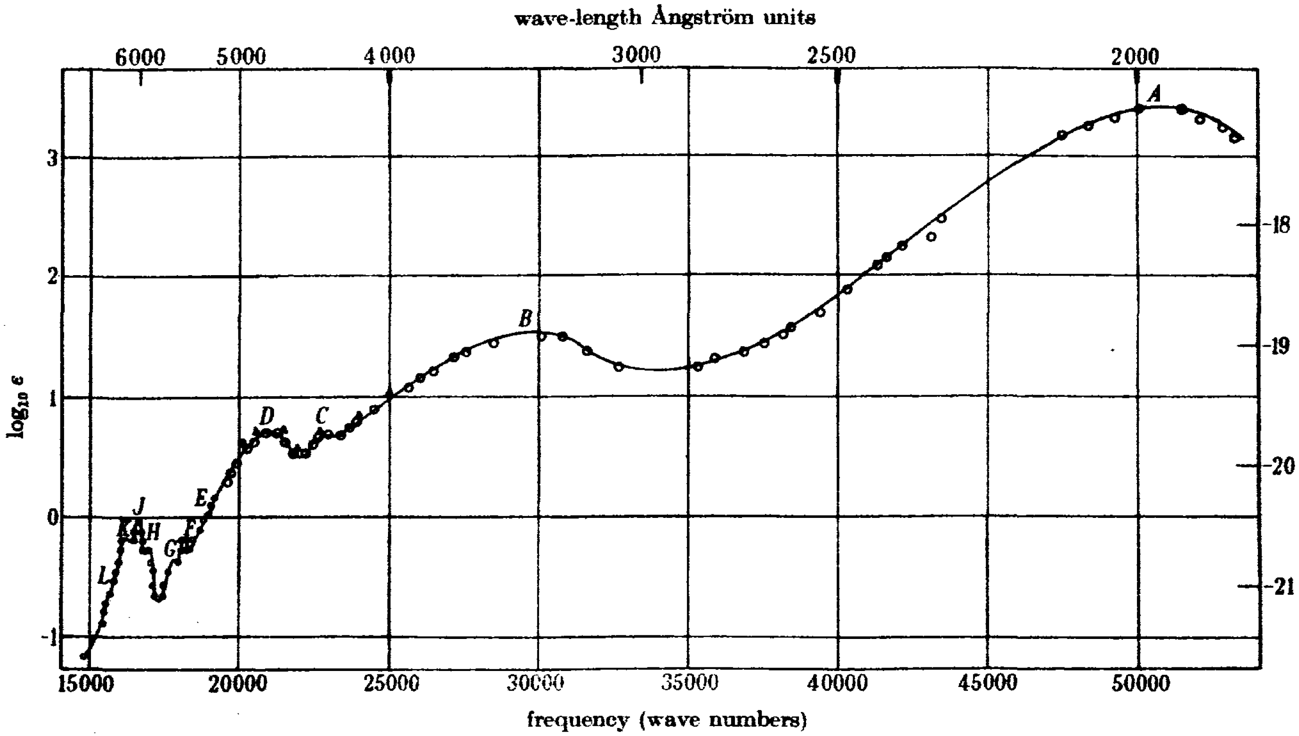

FIG. 2. The extinction coefficient curve of NOCl vapour at room temperature, showing the eleven bands. (▲ = results of Leermakers and Ramsperger.)

TABLE II

	Wave-length A	Wave number cm.$^{-1}$	Extinction coefficient at room temperature ϵ	Extinction coefficient at room temperature α
A	1970	50800	2550	$9{\cdot}69 \times 10^{-18}$
B	3350	29900	32·5	$1{\cdot}23 \times 10^{-19}$
C	4400	22720	5·0	$1{\cdot}91 \times 10^{-20}$
D	4750	21050	5·3	$2{\cdot}02 \times 10^{-20}$
E	5385	18570	(0·73)	$2{\cdot}79 \times 10^{-20}$
F	5495	18200	0·65	$2{\cdot}49 \times 10^{-21}$
G	5612	17820	0·37	$1{\cdot}41 \times 10^{-21}$
H	5879	17010	0·53	$2{\cdot}01 \times 10^{-21}$
J	6017	16620	0·94	$3{\cdot}59 \times 10^{-21}$
K	6158	16240	0·69	$2{\cdot}64 \times 10^{-21}$
L	6431	15550 ± 40	(0·17)	$6{\cdot}38 \times 10^{-22}$

(The values in brackets are rather inaccurate.)

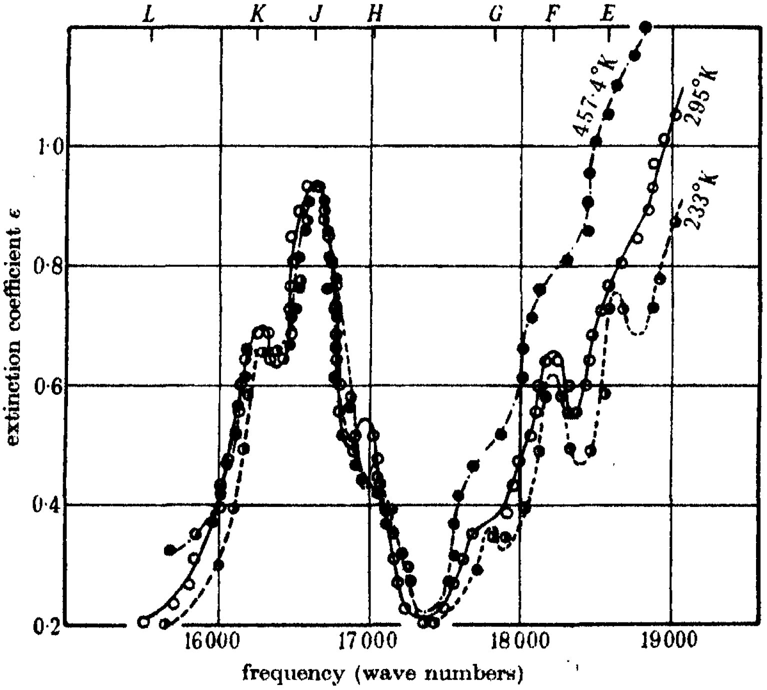

FIG. 3. Showing the effect of temperature on the green and yellow band system G.

The six maxima E to K are shown in fig. 3. They appear on the spectrum as two sets of diffuse bands, each consisting of a central band with a weaker band on either side. Between the sets is a region of low absorption. Band L gives rise only to an inflexion in the curve rather than to a definite maximum. No further absorption was found up to 8000 A. In all parts of the spectrum the absorption was continuous and showed no suggestion of fine structure even with the highest dispersion and resolution used (experimentally determined as 15 A/mm. and 5500 respectively).

The fine structure found by Kistiakowsky (1930) consisted of lines separated by as much as 5 A. The discrepancy between our observations and his may have been due to insufficient precautions to avoid traces of NO_2 in the samples which he used. The extinction coefficients of the peaks of the NO_2 bands are 100–500 times those of NOCl in the visible, and 0·3 % of NO_2 would have been sufficient to account for Kistiakowsky's observations. The other characteristics of the absorption found by him are in qualitative agreement with those described here.

The effect of temperature on the absorption in the visible region is shown in fig. 3. At the highest temperature considered here, 457·4° K, it becomes necessary to take into account the dissociation,

$$2NOCl \rightleftharpoons 2NO + Cl_2.$$

The equilibrium at this temperature was observed to be established in a few minutes, in agreement with the reaction velocities determined by Waddington and Tolman (1935). At this temperature, the equilibrium constant is 0·17 cm. mercury (Dixon 1931). The total pressure of 144·2 cm. used corresponds therefore to 119 cm. of NOCl.

Fortunately, over the region studied NO is transparent and the extinction coefficient of Cl_2 very low (Halban and Siedentopf 1922). Corrections for these were therefore unnecessary.

The effect of temperature is principally to broaden the bands with the result that, for example, band J partially obscures bands H and K. For the three bands, E, F and G, this broadening is accompanied by a general rise in absorption, which is probably due to an increase in the lower part of the D band as the temperature is raised. Such an effect of temperature is common to bands of continuous absorption (Fink and Goodeve 1937). Leermakers and Ramsperger (1932) found an increase in extinction coefficient with temperature for the region 22,000–24,500 cm.$^{-1}$, i.e. in the lower part of band B.

DISCUSSION

The interpretation of the spectrum of nitrosyl chloride requires a consideration of the possible dissociation products. Bailey and Cassie (1934) have calculated the heat of the reaction

$$NOCl \rightarrow NO(^2\Pi) + Cl(^2P_{\frac{3}{2}}) \qquad (I)$$

to be 38 kcal. (13,300 cm.$^{-1}$), and estimated that of the reaction

$$\mathrm{NOCl} \rightarrow \mathrm{NCl} + \mathrm{O} \qquad \text{(II)}$$

to be 125 kcal. (44,000 cm.$^{-1}$). The energy states of the chlorine atom are well known and except for the metastable state $^2P_{\frac{1}{2}}$ (2·5 kcal. above the ground-level $^2P_{\frac{3}{2}}$) there is no excited state below the ^2S (205 kcal.) (Kiess and de Bruin 1929). According to Jevons (1932, p. 288) the first excited state of NO, the $^2\Sigma^+$, lies 125 kcal. (44,000 cm.$^{-1}$) above the $^2\Pi$.

It is seen from these data that reaction I is possible over the whole of the spectrum investigated, but excited states of the products are excluded. Reaction II is possible for band A only.

Bands A, B and D are of the shape associated with transitions to electronic levels in which there is a repulsive force between some parts of the molecule; the potential energy-distance curve has no minimum. As the N-O distance in the product (1·146 A (Jevons 1932)) is almost exactly equal to the N-O distance in NOCl (1·14 A (Ketelaar and Palmer 1937)), the NOCl molecule can, for dissociations of type I, be considered to a good approximation as a diatomic molecule, (NO)-Cl. Furthermore, Bailey and Cassie (1934) have interpreted the infra-red spectrum on the basis that the fundamental frequency 633 cm.$^{-1}$ corresponds to a vibration along the (NO)-Cl axis. Small sections of the potential energy curves corresponding to bands A, B and D have been calculated by the method used by Goodeve and Taylor (1935) using this frequency and a reduced mass of $2{\cdot}68 \times 10^{-23}$ g. These sections of the potential energy curves are plotted in fig. 4, and it is seen that their extrapolation to a dissociation level corresponding to

$$\mathrm{NO}(^2\Pi) + \mathrm{Cl}(^2P)$$

is a very reasonable one in view of the usual shapes of these curves (Fink and Goodeve 1937; Porret and Goodeve 1938). The values of the slopes of these curves for the region of the maximum of absorption (and therefore for a separation r''_e, see fig. 4) are as follows:

Band	A	B	D
Slope, cm.$^{-1}$/A	$-7{\cdot}7 \times 10^4$	$-7{\cdot}7 \times 10^4$	$-2{\cdot}35 \times 10^4$

Similar, but more approximate calculations, have been made assuming that band A leads to dissociation into O + NCl (reaction II). It was not found possible, however, to extrapolate the calculated section of the potential energy curve to the energy level of these products without introducing either a minimum at an unusually large separation or a discontinuity in curvature. The available evidence therefore is in favour of primary photodissociation for the three bands A, B and D, the products being normal NO and Cl.

While the bands A, B and D can be attributed to transitions to three separate electron excited states the set of seven bands E to L in the visible are too narrow to be interpreted in this way and more probably arise from transitions to separate vibration levels in *one* electronic state. The existence of vibration means that the potential energy curve shows a minimum and that the excited molecule is stable even if for only a very short time. The

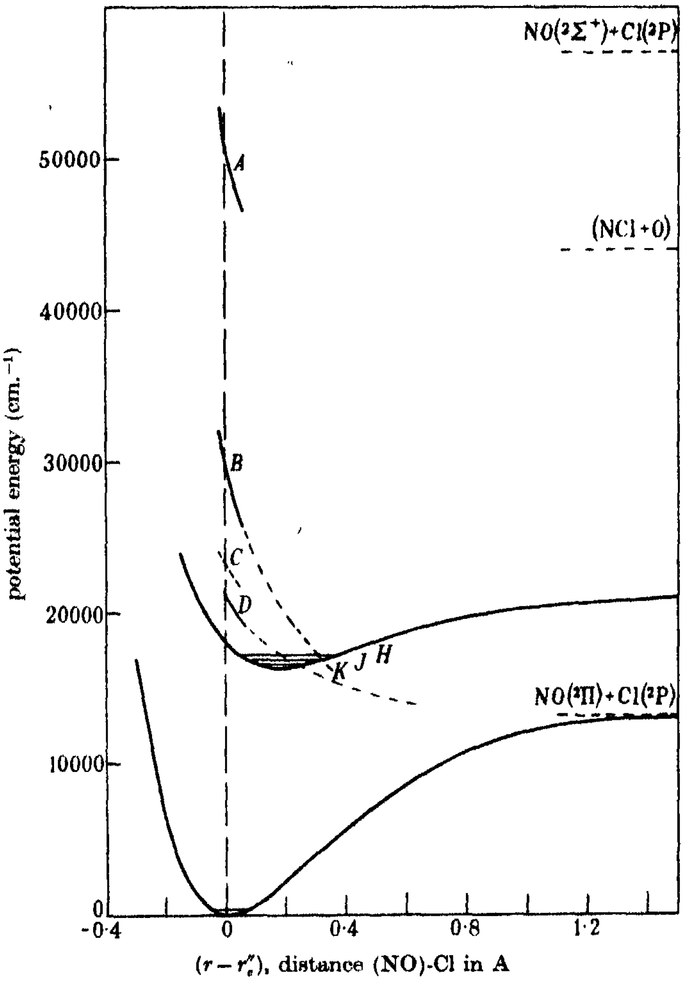

Fig. 4. *The energy of the various excited states of the NOCl molecule as a function of the (NO)-Cl distance.*

extinction coefficients of these bands are abnormally low, indicating that the transition is partially "prohibited" (i.e. it may involve a change of electron spin).

The continuous nature of these bands may be attributed to predissociation in the usual way—the potential energy curve cutting a curve of the repulsion type. As is seen from fig. 3, each band is approximately symmetrical, that is there is no suggestion of a band head. In this way the spectrum differs from the predissociation spectra of other tri- or even tetra-atomic molecules such as SO_2, NO_2, ClO_2, NH_3, SO_3, CH_2O etc. (Bailey and Cassie (1934) found for NOCl that "none of the infra-red bands showed any of the characteristics of normal resolution such as was obtained in COS, or in the even heavier molecule, Cl_2O"). Symmetrical bands are however found with some more complex molecules such as CH_3ONO (Thompson and Purkis 1936), CH_2N_2 (Kirkbride and Norrish 1933). The question arises, Do these bands of NOCl mean that primary photochemical decomposition takes place, or is it merely that with such an asymmetric molecule the multiplicity of rotation levels due to perturbations makes resolution impossible? From the dimensions given by Ketelaar and Palmer (1937) the principal moment of inertia is $1{\cdot}55 \times 10^{-38}$ g.cm.^{2} which would give a rotation level separation of $1{\cdot}1$ cm.$^{-1}$. This separation is unresolvable on the instrument used (capable of resolving 3 cm.$^{-1}$) and when the other rotations are considered together with their perturbations the probability of achieving resolution with any instrument seems remote. In other words for molecules of this or higher degree of complexity, spectroscopic evidence is as yet of little value in deciding whether or not predissociation (dissociation in 10^{-12} to 10^{-13} sec.) occurs. On the other hand, calculations of the upper potential energy curve for this band system indicate that an intersection of this curve with one of a repulsion type does take place as shown in fig. 4. On the whole it can be said that two of the conditions for predissociation are fulfilled—unresolved bands and intersection of potential energy curves.

An assignment of vibration quantum numbers is suggested by the following arguments. Bailey and Cassie found three fundamental frequencies, 1832, 923, 633 cm.$^{-1}$ respectively. From the Boltzmann distribution we find that, at the highest temperatures used here, the number of molecules having one quantum of vibration even in the lowest of these fundamentals is small and we can therefore assume that the bands E to K arise from molecules in the zero levels. This conclusion is further substantiated by the fact that the intensities of the bands are practically independent of temperature (the change in extinction coefficient for the bands

E, F and G has been attributed above to an increase in the lower part of band D). The six bands therefore represent six vibration levels in the excited state and it may be seen from the plate that they divide themselves into two sets which are very similar in appearance. These sets are separated by 1580 cm.$^{-1}$, while the bands in each set are separated by 380 cm.$^{-1}$. Bailey and Cassie have assigned the fundamental frequency, 1832 cm.$^{-1}$, of the ground state, to a vibration, (ω_1), involving mainly a movement between the oxygen and nitrogen atoms, an assignment which is in harmony with the strength of this link and the frequency of the molecule NO, 1883 cm.$^{-1}$ (Snow, Rawlins and Rideal 1929). It seems reasonable therefore to assign the frequency 1580 cm.$^{-1}$ to the same vibration in the excited state.

A close examination of the microphotometer tracings disclosed the fact that for band J the slope of the extinction coefficient curve on the red side is about three-fifths of that on the blue side; in other words the band degrades towards the red. It appears that this would also be true for the other bands if it were possible to separate them completely from their neighbours. Degradation towards the red implies that the nuclear separation is greater in the excited than in the ground state (see Jevons 1932, p. 68). An increase in separation is invariably accompanied by a decrease in the fundamental frequency, and we therefore expect to find in the excited state a frequency less than 633 cm.$^{-1}$, associated with the (NO)-Cl vibration. It is suggested that this frequency is the 380 cm.$^{-1}$ found as an interval in the bands E to K. The tentative assignment is shown in Table III.

TABLE III

	$\omega''_1 = 1832$	$\omega''_2 = 633$	$\omega'_1 = 1580$	$\omega'_3 = 380$	Frequency of	
Band	v''_1	v''_2	v'_1	v'_3	Band	Interval
E	0	0	1	2	18570	> 370
F	0	0	1	1	18200	> 380
G	0	0	1	0	17820	
					1580	
H	0	0	0	2	17010	> 390
J	0	0	0	1	16620	> 380
K	0	0	0	0	16240	> 690 ± 40
L	0	1	0	0	origin 15550 (± 40)	

The assignment of band L depends upon the validity of the other assignments but is in agreement with its low extinction coefficient and its interval from band K.

This assignment makes possible a rough calculation of the upper potential energy curves corresponding to these bands as shown for bands H, J and K in fig. 4. The displacement of the minimum from that of the ground state, $r'_e - r''_e$, has been calculated by means of Badger's Rule (1935) written in the form

$$r'_e - r''_e = C^{ik}\left(\frac{1}{\sqrt[3]{k'}} - \frac{1}{\sqrt[3]{k''}}\right),$$

where C^{ik} is a constant given by Badger's table and equal to 0·535 and k' and k'' the force constants of the excited and ground states respectively. It may be seen from the figure that this potential energy curve of the NOCl molecule cannot arise from unexcited NO and Cl. On the other hand if it should arise from states involving excitation to any known level of either of these products, one would expect, from the resultant high heat of formation, very strong binding and an increase rather than a decrease in the fundamental frequency. Reversing the argument, as the dissociation energy of a bond is generally proportional to the force constant and thus to the square of the frequency (see for example Fox and Martin 1938), we can deduce that the heat of dissociation of NOCl in its excited state is of the order of magnitude of 13,800 cal. (4850 cm.$^{-1}$). This must mean that there exists a hitherto unknown excited state for either the NO molecule or the Cl atom. As the analysis of the spectrum of Cl appears to be complete, it seems likely that the unknown level belongs to NO and lies at a frequency of about 8000 cm.$^{-1}$. (The lowest level of NO, a $^4\Pi$ level, has not been observed but Mulliken (1932) predicted that it lies at about 35,000 cm.$^{-1}$.) The potential energy curve for bands E, F and G is identical to that shown except that it is displaced upwards by a distance 1580 cm.$^{-1}$.

The intensities of the bands F and J are greater than the others of each trio, and from the assignment in Table III it follows that transitions $v''_3 = 0 \rightarrow v'_3 = 1$ are the most probable. This is in qualitative agreement with what is to be expected from an application of the Franck-Condon Principle to the curves in fig. 4. It is not, however, to be expected that Badger's Rule should give an accurate value of r'_e.

Band C is separated from band D by 1670 cm.$^{-1}$, an interval which may well be the frequency of the N-O vibration for the excited state corresponding to the D band. Hence absorption of light in band C probably leads to dissociation into Cl plus NO with one quantum of vibration. Transitions to higher vibration levels would be masked by band B. Bands A and B might also be double but each part would be too broad for isolation to be possible. Band A may arise from the new excited state of NO predicted as a result of the analysis of the bands E to L.

The authors are indebted to Dr C. L. Child for his assistance. One of them (S. K.) wishes to express his thanks to the Royal Society of Canada for a Fellowship under which this work was carried out.

SUMMARY

The extinction coefficient curve of nitrosyl chloride has been measured in the visible and ultra-violet and eleven bands have been observed. Four of these in the ultra-violet and blue have been attributed to transitions to upper potential energy curves of the repulsion type. The remaining bands in the green and yellow are of the type found for transitions to vibration levels in a stable or partly stable excited state. This excited state appears to arise from a hitherto unknown level of the NO molecule. These latter bands showed no fine structure and were nearly symmetrical. A tentative assignment which is in accordance with all the observations, including studies of the effect of temperature, has been put forward.

REFERENCES

Allmand, A. J. 1931 *Chem. Soc. Discussions*, p. 34.
Badger, R. M. 1935 *J. Chem. Phys.* **3**, 710.
Bailey, C. R. and Cassie, A. B. D. 1934 *Proc. Roy. Soc.* A, **145**, 336.
Barker, E. F. and Sleator, W. W. 1935 *J. Chem. Phys.* **3**, 660.
Bowen, E. J. and Sharpe, J. F. 1925 *J. Chem. Soc.* **127**, 1026.
Dixon, J. K. 1931 *Z. phys. Chem.*, Bodenstein Festband, p. 679.
Fink, P. and Goodeve, C. F. 1937 *Proc. Roy. Soc.* A, **163**, 592.
Fox, J. J. and Martin, A. E. 1938 *J. Chem. Soc.* p. 2106.
Goodeve, C. F. and Taylor, A. W. C. 1935 *Proc. Roy. Soc.* A, **152**, 221.
Halban, H. von and Siedentopf, K. 1922 *Z. phys. Chem.* **103**, 71.
Jevons, W. 1932 *Report on band spectra of diatomic molecules.* Camb. Univ. Press.
Judd Lewis, S. 1921 *J. R. Soc. Arts*, **69**, 799.
Ketelaar, J. A. A. and Palmer, K. F. 1937 *J. Amer. Chem. Soc.* **59**, 2629.
Kiess, C. C. and de Bruin, T. L. 1929 *Bur. Stand. J. Res., Wash.* **2**, 1117.
Kirkbride, P. W. and Norrish, R. G. W. 1933 *J. Chem. Soc.* p. 119.
Kiss, A. 1923 *Rec. Trav. chim. Pays-Bas*, **42**, 665.
Kistiakowsky, G. B. 1930 *J. Amer. Chem. Soc.* **52**, 102.
Leermakers, J. A. and Ramsperger, H. C. 1932 *J. Amer. Chem. Soc.* **54**, 1837.
Manganini, G. 1889 *Z. phys. Chem.* **4**, 427.
Mulliken, R. S. 1932 *Rev. Mod. Phys.* **4**, 51.
Nielsen, A. H. and Nielsen, H. H. 1937 *J. Chem. Phys.* **5**, 277.
Porret, D. and Goodeve, C. F. 1938 *Proc. Roy. Soc.* A, **165**, 31.
Scott, A. F. and Johnson, C. R. 1929 *J. Phys. Chem.* **33**, 1975.
Snow, C. P., Rawlins, F. I. G. and Rideal, E. K. 1929 *Proc. Roy. Soc.* A, **124**, 453.
Thompson, H. W. and Purkis, C. H. 1936 *Trans. Faraday Soc.* **32**, 674.
Twyman, F. 1931 *Trans. Opt. Soc.* **33**, 9.
Waddington, G. and Tolman, R. C. 1935 *J. Amer. Chem. Soc.* **57**, 689.
Winn, A. G. 1939 (unpublished results).

The photosynthesis of carbohydrates from hydrated carbon dioxide

By E. C. C. Baly, F.R.S.

(*Received* 12 *May* 1939)

INTRODUCTION. THE EARLIER EXPERIMENTS

In a previous communication (1927) it was shown that when suspensions of nickel or cobalt carbonate in water, saturated with carbon dioxide, were irradiated with white light organic compounds were photosynthesized. These compounds gave the Molisch and Rubner reactions, reduced Benedict's solution and gave a solid osazone, and hence it was concluded that they were carbohydrates.

The two carbonates used in this investigation were specimens of 1 kg. each which for many years had been kept in the museum of the Liverpool University Chemical Department.

EVIDENCE OF PHOTOSYNTHESIS OBTAINED WITH HYDRATED NICKEL CARBONATE PREPARED BY THE ELECTROLYTIC METHOD

In a further communication (1929) a method was described of preparing nickel carbonate by the electrolysis in a glass cell of a solution of carbon dioxide in conductivity water with electrodes of pure nickel.

The powder was activated by spreading 50 g. in a thin layer over a glass plate with an area of about 5 sq. ft. On this glass plate was placed a light wooden frame about 2 in. deep, and a second glass plate rested thereon to protect the hydrated carbonate from dust. The powder was then irradiated for 18 hr. on both sides by three 100 W lamps placed above and below the apparatus. Immediately after this treatment the powder was suspended in 1400 ml. of conductivity water in a rectangular glass cell and irradiated on each side by a 100 W lamp for 2 hr., carbon dioxide being passed through the suspension.

More than 1000 g. of the hydrated nickel carbonate were thus prepared; no variation whatever was found in its properties, and convincing evidence was obtained that carbohydrates of the nature of reducing sugars were photosynthesized by this method.

FAILURE TO REPEAT THE RESULTS

Several attempts were made to repeat this work by other investigators, notably by Bell (1931), and in no case was any evidence of photosynthesis obtained. These consistently negative results necessitated a re-examination of the above method at Liverpool, and despite many trials complete failure to repeat the original results was experienced. It was, however, noted that the hydrated nickel carbonate prepared by the electrolytic method in this second investigation was very different in its properties from that prepared in 1929. Whereas the first product was granular, becoming friable on drying, and contained no alkali, the second product was flocculent and on drying formed hard masses which were very difficult to pulverize and contained adsorbed alkali.

These negative results were at the time both disappointing and incomprehensible. A possible explanation of the successful results obtained in 1929 and the subsequent failures is that by chance the electrolytic cell used in the first investigation was made of a glass having an unusually small solubility in water. This cell was unfortunately broken, and in the second investigation the electrolytic cell used was made of a glass having the usual solubility.

It may be noted that alkali adsorbed on nickel carbonate cannot be removed by washing with distilled water. In order to test the material for the presence of alkali it is necessary to heat it at 250° in a porcelain dish with constant stirring until the evolution of carbon dioxide and water vapour has ceased. The black product readily yields previously adsorbed alkali on treatment with distilled water.

In view of the contradictory results obtained by myself and other investigators, it was obviously necessary to determine whether nickel carbonate capable of promoting photosynthesis could be prepared by precipitation methods. A long investigation was carried out in which the concentrations of the two reactants, nickel nitrate and potassium hydrogen carbonate, and the temperature were varied, but no satisfactory method was found. Many hundred preparations were made and each of these was proved to be photosynthetically inactive and to contain considerable amounts of adsorbed alkali.

THE USE OF THORIUM OXIDE AS PROMOTER

In view of the probability that in the cases in which satisfactory evidence of photosynthesis was obtained the nickel carbonate acted as a photocatalyst, it was decided to examine the effect of the addition of small quantities of thorium oxide which is known to act as a promoter when present in certain heterogeneous catalysts. Preparations were made of nickel carbonate containing various amounts of thorium oxide. The surface potential of each of these preparations was determined by the method of cataphoresis and it was found that the surface potential was a periodic function of the thorium oxide content. It was also found that maximum values of the surface potential were obtained when the molecular ratio of thorium was $1ThO_2 : 24 \times 3, 5, 7$, etc., NiO.

EVIDENCE OF PHOTOSYNTHESIS WITH NICKEL CARBONATE CONTAINING THORIUM OXIDE

Now it had previously been found that the surface potential of the nickel carbonate prepared by the electrolytic method in 1929 was considerably smaller than that of the preparations which were made by the same method in the second investigation and found to give no evidence of photosynthesis. This fact suggested the possibility that the photosynthetic activity of nickel carbonate may be in some way connected with its surface potential. It was decided, therefore, to determine whether the presence of thorium oxide in the molecular ratio of $1ThO_2 : 24NiO$ would render nickel carbonate photosynthetically active. Preparations of this material were made and after being ground to a fine powder were pre-irradiated in the manner described above and then immediately irradiated in suspension in water saturated with carbon dioxide. Some evidence was obtained of the photosynthesis of organic matter and this was encouraging in view of the failures which had been experienced.

THE PREPARATION OF A LAYER OF NICKEL OXIDE, CONTAINING THORIUM OXIDE, ADSORBED ON KIESELGUHR

As the result of a protracted investigation it was found that a photosynthetically active material can be obtained by the adsorption of nickel oxide, containing thorium oxide in the molecular ratio of $1ThO_2 : 24NiO$, on pure kieselguhr. It had been found by Mr W. P. Pepper in my laboratories that the hydrous oxides of aluminium, thorium, nickel and cobalt are readily adsorbed on kieselguhr. As was stated by us in 1935, the adsorption of alumina is restricted to a unimolecular layer and it was later found that the same is true of thorium oxide. With nickel and cobalt oxides a trimolecular layer is adsorbed, and in the case of nickel many difficulties had to be overcome before a satisfactory product was obtained.

The method which was finally adopted for coating the kieselguhr with NiO containing ThO_2 in the molecular ratio of $1ThO_2 : 24NiO$ may be given in exact detail. It is important at the outset to note that the quantities given refer only to the "Superfloss" brand of kieselguhr supplied by the Johns-Manville Company, and that the details of the method must be rigidly adhered to in order to obtain successful results.

The kieselguhr when purchased contained a small quantity of clay and organic matter which was removed by the following treatment. About 5 kg. of the kieselguhr were heated in a large enamelled iron basin with 15 l. of 4 N hydrochloric acid for about 5 hr. The mixture was kept in gentle ebullition and frequently stirred. During this treatment small quantities of a dark oily material separated and floated on the surface and this was removed as far as possible by means of filter paper. Fresh acid was added from time to time in order to make good the loss by evaporation. When the separation of the oily material had ceased, the mixture was filtered, about one-third at a time, by suction on a large Buchner funnel and washed on the funnel with water until the filtrate was colourless.

It is essential here to draw attention to the remarkable power of the kieselguhr to retain water. Even when no further water can be removed by suction from the bed of the kieselguhr on the funnel, the material still contains enough water to cause it to flow when removed from the funnel. It is necessary to disconnect the filter flask from the suction pump and gently to tap the bed of kieselguhr all over its surface with a large flat glass stopper. This causes the kieselguhr particles to form a more compact mass with the result that the whole becomes semifluid. The separated water is then removed by suction and the process repeated until no more water can be extracted.

The kieselguhr was then again extracted in quantities of about 300 g. at a time with boiling 4 N HCl, this process being repeated until the acid extract gave no reaction for ferric iron with ammonium thiocyanate. Usually two such extractions were found to be sufficient. The kieselguhr was then washed until it was completely free from acid, the following treatment being found to be necessary. The kieselguhr after being washed on the funnel with 5 l. of distilled water was divided into two approximately equal portions. One portion at a time was completely disintegrated by vigorous stirring in 7 l. of distilled water, and steam at 15 lb. pressure was blown in until the mixture boiled, after which the suspension was immediately filtered. This treatment was repeated until the filtrate was neutral to B.D.H. indicator and when this end had been achieved the kieselguhr was dried at 125°.

It must be remembered that kieselguhr consists of particles of different sizes with widely different sedimentation rates. In order to maintain homogeneity, therefore, it is essential that the sedimentation of any suspension be prevented and especially is this necessary with hot suspensions. In the washing process described above, the suspension after being brought to boiling point was continuously stirred and transferred to the Buchner funnel by means of a ladle.

Despite the foregoing treatment, the kieselguhr was found still to contain a small quantity of organic matter and this was removed by heating the finely disintegrated material at 600° in a current of air. This disintegration presented a problem of some difficulty. When small lumps of the material were crushed to powder by means of a spatula on a sheet of glazed paper, small laminae were formed which could not be disintegrated and these reduced the effective surface area of the kieselguhr. This difficulty was overcome by gently shaking small lumps of the kieselguhr in a tin-plate tube 30 in. long and 3 in. wide, which was provided with a tightly fitting lid at each end.

The finely disintegrated material was heated in a transparent vitreosil tube which was 4 ft. long and 3 in. wide. A glass-wool plug was placed at a distance of 1 ft. from one end of this tube and sufficient of the disintegrated kieselguhr was run into the tube to form a loosely packed column 16 in. long, and then a second glass-wool plug was placed at a distance of 2 ft. from the first plug. It was found undesirable that the kieselguhr, when distributed evenly between the two plugs, should fill more than two-thirds of the diameter of the vitreosil tube. The central portion of the tube containing the kieselguhr was heated at 600° for 8 hr. in an electric resistance furnace, a current of dry filtered air being passed continuously through it. At frequent intervals the tube was slowly rotated through several complete revolutions. The purified kieselguhr was proved to be free from organic matter, firstly by the fact that no volatile matter was obtained when it was heated at 600° under a pressure of 0·0004 mm., and secondly, by the fact that no carbon dioxide was obtained when it was heated in a current of CO_2-free air.

The method of coating the kieselguhr is based on certain facts which were established during the investigation. In the first place it is not possible to suspend the kieselguhr in a solution of nickel nitrate containing the requisite amount of thorium nitrate, because at the great dilution necessary the latter salt is almost completely hydrolysed with the result that the ThO_2 is at once adsorbed by the kieselguhr. It is, therefore, necessary to add a very dilute solution of the requisite amounts of potassium bicarbonate and thorium nitrate to a boiling suspension of the kieselguhr in a very dilute nickel nitrate solution and to maintain the concentration of nickel in that solution constant. In the second place it was found that the alkaline thorium solutions are stable, provided that they are freshly prepared from a concentrated solution of thorium nitrate, containing free nitric acid, and that the surface of the containing vessels has been cleaned with strong nitric acid and washed free from acid with distilled water.

A concentrated solution of thorium nitrate was prepared by dissolving the commercially pure salt in water, adding 20 ml. of concentrated nitric acid and then sufficient water to make the volume up to 250 ml. This solution on analysis was found to be 0·40834 M with respect to Th ions and 2·9091 N with respect to H ions. This procedure was rendered necessary by the uncertainty as to the composition of the commercially pure salt.

An exactly 0·1 M solution of pure nickel nitrate and an exactly 0·2 M solution of Merck's pure crystallized potassium bicarbonate were also prepared. It is essential that the alkali solution be stored in a quartz flask, because it was proved that when the solution was allowed to remain in contact with any glass surface sufficient silica was soon dissolved to render the adsorbed layer of nickel and thorium oxides useless.

Two solutions were prepared, each by diluting 14·00 ml. of the 0·1 M nickel nitrate to 2000 ml. Exactly 10 g. of the purified kieselguhr were deflocculated in 100 ml. of one of these solutions by means of a serrated disk electrically driven at 1500 rev./min. The kieselguhr suspension was transferred to a 4 l. enamelled iron saucepan which rested on a powerful gas ring burner and the remaining 1900 ml. of the nickel solution were added. An electrically driven stirrer was then placed in position so that its blades almost touched the bottom and one side of the saucepan, this position being adopted in order to guard against the formation of a central vortex in the solution. The blades of the stirrer were 1¼ in. long and the speed was 240 rev./min., the direction of rotation being such as to drive the suspension downwards.

Two 250 ml. burettes of the design shown in fig. 1 were placed in position so that the ends of their capillary delivery tubes were just above the blades of the stirrer, one on each side of its central axis. The object of the bulb and jet immediately below the stopcock of each burette was to enable the rate of flow of the contents to be observed and controlled. The stirrer was then started and the kieselguhr suspension in the nickel nitrate solution was heated and boiled vigorously for 10 min. in order completely to de-aerate it.

During these proceedings 0·07143 ml. of the thorium nitrate solution was measured out as accurately as possible by means of a micro-burette and diluted with water up to 500 ml., and 8·04 ml. of the 0·2 N potassium bicarbonate solution were also diluted to 500 ml. and these two solutions were mixed. This mixed solution contained one-half of the total amounts of thorium nitrate and potassium bicarbonate required. One of the two burettes was filled with this alkaline thorium solution and the other was filled with the second dilute nickel nitrate solution. These two solutions were added to the vigorously boiling suspension of kieselguhr at the same rate of 4 drops a second from the jets just below the stopcocks of the burettes. It was of course necessary from time to time to add boiling water in order to maintain the volume of the suspension approximately constant. This water had previously been boiled for some time in pyrex flasks in order completely to de-aerate it. Shortly before the first half of the alkaline thorium solution had been added to the boiling suspension, the second half was prepared as above and added to that remaining in the burette.

When the whole of the alkaline thorium and nickel solutions had been added, an operation which took about 3 hr., the suspension was boiled for a further 15 min. The coated kieselguhr was then collected on a 4 in. Buchner funnel and washed with 1 l. of distilled water. During the washing the coated kieselguhr tended to turn grey-black on the surface and this phenomenon proved to be of great indicative value, since the darkening was very pronounced with preparations which gave evidence of photosynthesis when subsequently irradiated. The washed product was immediately transferred to an electrically heated oven and allowed to dry overnight at 60°.

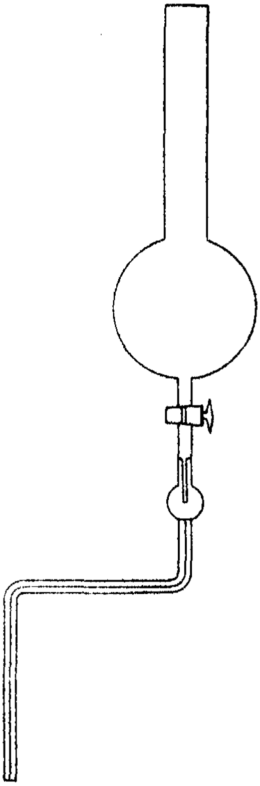

FIG. 1

Before the method of irradiating these preparations is described two points of interest may be mentioned. In the first place it was found that no evidence of photosynthesis was obtained with any of the preparations which were brought out of the drying oven into daylight and this was proved to be due to poisoning of the surface as will subsequently be explained. In the second place the total quantity of nickel and thorium adsorbed on a given weight of kieselguhr was known and the amount of adsorbed water was determined by the following method. A weighed quantity of the coated kieselguhr, after drying at 120° under reduced pressure, at which temperature hydrated nickel carbonate is stable, was heated under reduced pressure at 250–300° and the water evolved was collected in a weighed tube containing phosphoric oxide. The weight of water collected was equivalent to one-third of the nickel present expressed as NiO. It would seem that the only possible explanation of this is that the substance adsorbed by the kieselguhr is NiO containing ThO_2 in the molecular ratio of $1ThO_2 : 24NiO$ and that this adsorbate after drying at 120° is coated with a unimolecular layer of water.

THE IRRADIATION OF THE SUPPORTED NiO CONTAINING ThO_2

The irradiation of the kieselguhr preparations was carried out as follows. About 1400 ml. of a saturated solution of carbon dioxide in de-aerated distilled water were prepared in the glass irradiation vessel, the approximate dimensions of which were 8·5 × 5·5 × 2 in., and this was taken into the dark room. The coated kieselguhr was removed from the oven and added to the solution in complete darkness. Since the NiO and ThO_2 surface became immediately coated with adsorbed hydrated carbon dioxide in the presence of excess of solution, the suspension then could be brought into the light without danger of poisoning. The suspension, after being dispersed by an electrically driven stirrer, was irradiated for 2 hr. by two 250 W lamps, one being placed at a distance of 20 in. from each side of the vessel. The vessel rested on an electrically heated mat and the temperature was maintained at 28–30°, it having been proved (1929) that the rate of photosynthesis increases up to 31° and rapidly decreases when the temperature exceeds 31°. During the irradiation the suspension was stirred at intervals and after 2 hr. it was filtered and the filtrate examined immediately.

THE EVIDENCE OF PHOTOSYNTHESIS

First of all the presence of Ni ions was tested for with dimethylglyoxime and in general the amount present was less than the limit of this test. This test is important because it was found that when a visible precipitate of nickeldimethylglyoxime was formed the coated kieselguhr was not satisfactory.

When a small quantity of the filtrate was acidified with hydrochloric acid, no evidence of the hydrolysis of the product of photosynthesis could be obtained. When, however, a small quantity of the filtrate was saturated with sulphur dioxide and allowed to remain for 10 min., a definite Molisch reaction was obtained indicating the formation of a carbohydrate. As will subsequently be shown the concentration of this product was very small and it is probable that the failure to obtain any evidence of hydrolysis by hydrochloric acid was due to oxidation of the product of hydrolysis by dissolved oxygen. This oxidation would be prevented when sulphur dioxide is used, since the dissolved oxygen reacts at once to give sulphuric acid. The presence of dissolved oxygen was proved by the immediate formation of sulphuric acid when the solution was treated with sulphur dioxide.

If the filtrate from the irradiation were allowed to remain for 2 hr. at room temperature or if it were heated at 60°, it no longer gave the Molisch reaction after saturation with sulphur dioxide. This interesting fact was conclusively established by a great number of observations and it definitely proves that the first product of photosynthesis is an unstable substance which changes into a second substance, this change being slow at room temperature and more rapid at higher temperatures.

In the first series of irradiations of 10 g. of the supported NiO containing ThO_2 the filtrate was concentrated in a pyrex flask under reduced pressure on a steam bath, and when the volume had been reduced to about one-third a small quantity of a finely divided white solid began to separate. After further concentration this solid substance was collected on a Gooch crucible and dried at 60°. The dry substance had a greenish tinge owing to the presence of a trace of nickel and was proved to contain organic matter by the fact that it rapidly charred when treated with warm concentrated sulphuric acid.

As the result of the irradiation of several lots of 10 g. of the supported NiO containing ThO_2, about 0·03 g. of this product was collected. It was apparently unaffected by acid and a micro-combustion gave only minute quantities of water and carbon dioxide. It consisted of a white substance, part of which was organic, contaminated with traces of nickel. In view of the fact that in the leaves of the dicotyledonous plants "temporary" starch is formed as the result of photosynthesis, it occurred to me that the white organic product of photosynthesis obtained by the irradiation of the supported NiO containing ThO_2 might be a type of starch.

In order to test this a portion of the greenish-white solid was suspended in very dilute acid, a little pure taka-diastase was added and the mixture allowed to remain for 2 hr. at 37°. After filtration, the mixture was boiled with Fehling solution and reduction took place, a small quantity of cuprous oxide being obtained. A blank experiment was then carried out in which a solution of the taka-diastase of the same concentration was boiled with Fehling solution and in this case no reduction was obtained. This hydrolysis of the second complex carbohydrate to a reducing sugar by means of taka-diastase was confirmed several times.

Now the one observation which was difficult to understand was the failure to oxidize more than a very small fraction of the complex product of photosynthesis when the greenish-white solid was submitted to micro-combustion. A further quantity of 10 g. of the coated kieselguhr was irradiated and the filtrate was concentrated in a pyrex flask under reduced pressure on a steam bath until the greenish white solid commenced to separate. At this stage the liquid was tested with B.D.H. indicator and found to be alkaline. It was proved by experiment that this alkalinity was sufficient to dissolve a little silica from the walls of the pyrex flask and that this hydrated silica was brought down with the greenish white solid and prevented it from being more than superficially oxidized during micro-combustion. It thus became evident that the method of concentrating the filtrate from the irradiations had to be modified.

SECOND SERIES OF IRRADIATIONS OF THE SUPPORTED NiO CONTAINING ThO_2 AND EVIDENCE OF PHOTOSYNTHESIS

A second series of irradiations of 10 g. of the supported NiO containing ThO_2 was then carried out and in each case the filtrate, after the dimethylglyoxime test had established the presence of only minute quantities of nickel, was made neutral or only just acid by means of very dilute hydrochloric acid. Owing to the fact that the solution was itself acid, due to the dissolved carbon dioxide, its neutralization necessitated great care. The neutral or very slightly acid solution was evaporated to dryness in a pyrex flask under reduced pressure on a steam bath. No solid matter separated during the concentration and there was finally left a thin film of a colloidal substance which had a yellow tinge owing to the presence of traces of anhydrous nickel chloride. This film was dissolved in a little water and transferred together with the washings of the pyrex flask to a 50 ml. flask. After the addition of 2 ml. of acetate buffer solution and 2 ml. of taka-diastase solution, water was added to make the total volume up to 50 ml. The flask was then allowed to remain for 2 hr. in an oven at 37°, after which the solution was boiled under standard conditions (1906) with 50 ml. of Fehling solution. Reduction took place and 0·007 g. of cuprous oxide was obtained.

This result was confirmed many times, but it was remarkable that the amount of cuprous oxide obtained did not appreciably vary. Increasing the time of irradiation had no effect, the amount of cuprous oxide obtained remaining practically constant at 0·007 g. It became evident, therefore, that the amount of photosynthesized starch in solution in no case exceeded a definite concentration and that this concentration must be limited by some unknown factor coming into play.

IRRADIATION OF A STATIONARY LAYER OF THE SUPPORTED NiO CONTAINING ThO$_2$

In order to investigate this phenomenon a stationary layer of about 30 g. of the coated kieselguhr was irradiated in a large flat photographic dish whilst a slow stream of water, saturated with carbon dioxide, flowed over it. The apparatus used is shown in fig. 2. The irradiation dish *A* rested on a levelling table not shown in the diagram and placed near

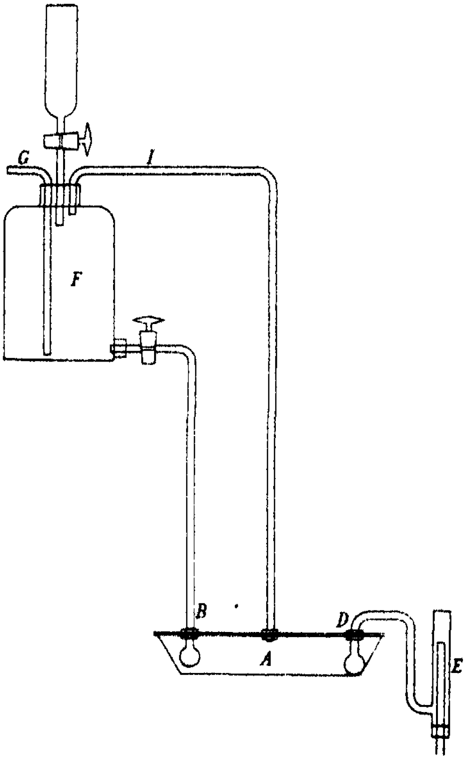

FIG. 2

a large window. The dish was covered by a plate-glass lid in which had been drilled three holes in a straight line, one in the centre and one near each end. In each of these holes was fixed by means of a rubber cork a short length of glass tubing. The tube *B* was sealed at its lower end to the centre of a glass tube ¾ in. in diameter, closed at each end. This glass tube extended the whole width of the dish and was provided with a series of small jets along its left-hand side in the diagram. The tube *D* was also sealed to the centre of a ¾ in. tube, sealed at each end, which extended the whole width of the dish and was provided with a series of small holes along its left-hand side. The plate-glass lid with its attachments could, therefore, be removed and replaced whenever it was necessary. *E* was a constant level apparatus which was later joined by means of rubber tubing to the tube *D*.

F was a 10 l. aspirator bottle which rested on a shelf 4 ft. above the dish. In the neck of the aspirator was fitted a rubber cork through which passed three glass tubes. The tube *G* was attached to a cylinder containing liquid carbon dioxide guaranteed to have been prepared from limestone. The central tube with its funnel and stopcock enabled the aspirator to be filled with liquid, whilst the tube *I* served to conduct the carbon dioxide into the porcelain dish.

The aspirator bottle *F* having been filled with distilled water saturated with carbon dioxide, a suspension of 30 g. of the supported NiO containing ThO_2 in 1500 ml. of water saturated with carbon dioxide was prepared as described above and poured into the dish. The plate-glass lid was then placed in position and the three connexions as shown in the diagram were made by short lengths of rubber tubing. The plate-glass lid was then covered by black velvet and the whole was allowed to remain for 3 hr. in order that the coated kieselguhr might settle out and form a compact layer.

Owing to the presence of very fine particles the supernatant liquid in the dish remained cloudy for a very long period and it was necessary to remove this. The stopcock of the aspirator was opened, when the water saturated with carbon dioxide was forced out through the jets on the tube attached to *B*. The jets of solution impinged on the side wall of the dish with the result that a slow and evenly distributed stream of water flowed over the layer of the supported oxides, the rate of flow being 1 l. in about 13 min. It was of course necessary to fill the aspirator at intervals with water which had been saturated with carbon dioxide from a second cylinder of the liquid gas. During this operation the overflow from the constant level apparatus *E* was allowed to run to waste.

When the overflow from the dish had become perfectly clear and free from suspended particles, the aspirator was filled with water saturated with carbon dioxide, the black velvet covering was removed from the plate-glass lid and the overflow was collected in a flask and returned to the aspirator.

EVIDENCE OF POISONING OF THE SUPPORTED NiO CONTAINING ThO_2

Almost immediately after the irradiation was commenced, evidence was obtained of the formation of the first product of photosynthesis which gives the Molisch reaction after it has been hydrolysed by sulphurous acid. The concentration of this product in the solution steadily increased during the first few hours of the irradiation and then quite suddenly the concentration began rapidly to decrease until no evidence whatever of the presence of this first product or of the starch could be obtained.

In view of the fact that the first product of photosynthesis slowly changes at room temperature to the second product, the only possible explanation of these observations would seem to be that the second product is adsorbed on the NiO and ThO_2 surface, the surface thereby becoming completely poisoned. This explanation was supported by the fact that when the irradiated powder was treated with the minimum volume of 3 N NCl, the filtrate gave a very definite Molisch reaction. This observation was confirmed several times.

This poisoning of the NiO and ThO_2 surface is quite in accord with the observation, previously recorded, that the preparations of kieselguhr coated with NiO *containing* ThO_2 *become poisoned if they are brought out of the drying oven into daylight.* It is known that when in the oven they are coated with an adsorbed layer of hydrated carbon dioxide which is only desorbed at 250–300°. In the absence of liquid water this adsorbed layer appears to be changed at once by the action of light into an adsorbed layer of the second product of photosynthesis.

The evidence obtained of the poisoning of the NiO and ThO_2 surface by the product of its irradiation indicates that, in order to obtain a reasonable quantity of the starch, it would be necessary to irradiate a stationary layer of the supported NiO containing ThO_2 with a continuous flow over it of a freshly prepared saturated solution of carbon dioxide. This would involve the use of 35–40 l. of this solution a day and, since no apparatus was at that time available for the rapid concentration of such large volumes of liquid, it was not found possible to carry out this method before my retirement from Liverpool.

PREPARATION OF UNSUPPORTED NiO CONTAINING ThO_2

Confirmation of the photosynthesis of the starch compound was later obtained by the irradiation of unsupported nickel and thorium oxides in the molecular ratio of $1ThO_2 : 24NiO$. The mixed oxides were prepared from the hydrated carbonate precipitated by the gradual addition of rather less than the equivalent quantity of potassium hydrogen carbonate in M/0·25 solution, to a solution which was M/5 with respect to nickel nitrate and M/120 with respect to thorium nitrate, the method being devised by my son Mr E. J. Baly and Mr J. W. Ireland.

When the potassium hydrogen carbonate solution is added to the solution of the two nitrates the first reaction which takes place is the neutralization of the free nitric acid produced by the hydrolysis of the thorium nitrate. Owing to the small concentration, no hydrated thorium oxide separates when the solution is completely neutralized. After this neutralization the following reaction takes place on the further addition of the potassium hydrogen carbonate solution,

$$Ni(NO_3)_2 + 2KHCO_3 = Ni(HCO_3)_2 + 2KNO_3,$$

and this proceeds until the solution becomes saturated with respect to nickel bicarbonate. On the further addition of the $KHCO_3$ solution hydrated nickel carbonate containing ThO_2 separates with the evolution of carbon dioxide.

Two gram-molecular weights or 581·6 g. of pure nickel nitrate crystals were dissolved in 4 l. of distilled water. To the filtered solution was added a volume of thorium nitrate solution containing one-twelfth of a gram-molecular weight or 22·010 g. of ThO_2 and the mixture was diluted to 10 l. 400 g. of Merck's pure potassium bicarbonate crystals were dissolved in distilled water and the solution, after filtration, was diluted to 10 l. The alkaline solution was added from burettes to the nickel and thorium solution which was vigorously stirred by means of two serrated disks electrically driven at 1500 rev./min.

The precipitated material was collected on a large Buchner funnel, washed with distilled water and then disintegrated by vigorous stirring in 9 l. of cold distilled water. After filtration the product was again disintegrated in distilled water and again collected on a Buchner funnel. Finally the product was disintegrated in 6 l. of distilled water, and steam at 15 lb. pressure was passed in until the suspension boiled and then the product was collected and dried at 100°. It is to be noted that during the treatment with steam some carbon dioxide was evolved and the colour of the product changed from pale green to a pure emerald green.

The steam at 15 lb. pressure was that used for the laboratory supply of distilled water. The steam was supplied at 40 lb. pressure from boilers through over 100 yd. of pipes and the pressure was adjusted to 15 lb. by reducing valves. Distilled water raised to 100° by passing in the steam and then cooled contained no organic matter soluble in ether.

The reasons for the adoption of the above method of precipitation may be explained. In the first place 400 g. of $KHCO_3$ were used in place of the theoretical quantity of 433·81 g. because it was believed that the danger of the presence of adsorbed alkali would be minimized by the presence of excess of nickel nitrate. As previously stated all the photosynthetically inactive preparations of hydrated nickel carbonate made by the electrolytic method were found to contain adsorbed alkali. In the second place it was found essential that the precipitation of the hydrated nickel carbonate containing thorium oxide be carried out at room temperature. Owing to the solubility of nickel bicarbonate and to some loss due to dissolution during the first washings of the precipitated material the yield of the final product was only about 70 % of that calculated.

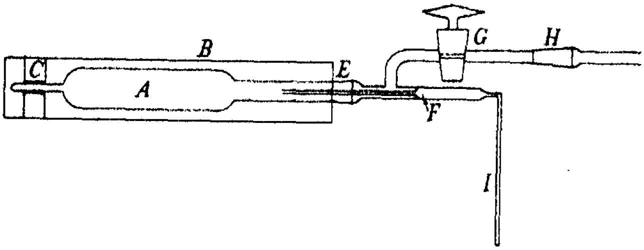

FIG. 3

It was shown in a previous communication (1936) that when hydrated nickel carbonate is heated in air it is converted into crystal units of NiO which are superficially coated with Ni_2O_3. Furthermore, it was found that if the carbonate is heated under as low a pressure as possible and air is admitted after cooling to room temperature the NiO turns black owing to the formation of the superficial layer of Ni_2O_3. It was necessary, therefore, in order to prepare a product uncontaminated with Ni_2O_3, to heat the hydrated nickel carbonate containing thorium oxide under as low a pressure as possible and, after cooling to room temperature, to admit water saturated with carbon dioxide.

About 100 g. of the hydrated carbonate containing ThO_2 were heated in the apparatus shown in fig. 3. The vessel *A* was made of transparent fused quartz and was supported inside the vitreosil tube *B* of an electric resistance furnace at one end by the vitreosil reel *C* and by glass wool packing at the other end. The central portion of the vessel *A* was 15 in. long and 3 in. wide, whilst the narrow portion was 1¼ in. wide. At the end of this narrow portion was an accurately ground quartz to glass joint *E*, and at *F* a long thin-walled capillary tube was internally sealed which projected well into the quartz vessel. The tube *F* was drawn out as shown to a fine capillary *I* which was bent at a right angle and sealed at the end. Connexion with a Hyvac pump was made through the stopcock *G* and the ground glass joint *H*. The temperature inside the resistance furnace was measured by a thermo-junction and galvanometer.

Owing to the fact that the adsorbed water is desorbed very rapidly when the hydrated carbonate is first heated, the following procedure was adopted. A glass tube containing anhydrous calcium chloride was sealed to the plug of the ground glass joint *H* and connexion was made to the Hyvac pump through a second glass tube containing phosphoric oxide. The quartz vessel and the connecting tubes were first evacuated to the lowest pressure attainable and then the temperature of the quartz vessel was slowly raised to 250°. Some liquid water soon condensed in the tubes connecting the quartz vessel with the tube containing calcium chloride and when this had been completely evaporated the stopcock *G* was closed and a tube containing phosphoric oxide was substituted for the tube containing calcium chloride. The two tubes containing phosphoric oxide were then completely evacuated, after which the stopcock *G* was again opened.

The temperature was then raised to 300° at which it was maintained constant and the evacuation continued until the pressure measured by means of a McLeod gauge was reduced to 0·001 mm. This operation lasted 6 hr., after which the stopcock *G* was closed, the heating was discontinued and the whole apparatus allowed to remain overnight. On the following morning the ground glass joint *H* was opened and the quartz vessel with its attachments removed from the resistance furnace. The tip of the capillary tube *I* was then broken off under the surface of water which had been charged with carbon dioxide in a sparklet apparatus, this solution being delivered directly on to the mixed oxides which were at once coated with adsorbed layers of hydrated carbon dioxide and thereby protected from atmospheric oxidation. The ground-glass plug was then removed from the joint *E* and after the lubricant had been carefully removed the suspension was transferred to the rectangular porcelain dish shown in fig. 2.

IRRADIATION OF UNSUPPORTED NiO CONTAINING ThO_2

The irradiation of the NiO containing ThO_2 was carried out exactly as described above for the supported oxides, except that it was continued for 3½ days, the dish being covered by a velvet cloth during the night. The solution, which had a volume of 12 l. and was almost saturated with respect to nickel bicarbonate, was concentrated under reduced pressure on steam baths. The hydrated nickel carbonate which separated was removed from time to time until there began to separate the same white substance as was obtained previously by the irradiation of the supported NiO containing ThO_2. As the result of further concentration the white substance increased in amount until quite suddenly it turned brown and acquired a gummy consistency. At this stage it was found that the solution had a strong alkaline reaction and there can be no doubt that the gummy product, which had a characteristic organic odour, was produced by the action of the alkali on the white product of photosynthesis.

It was evident from this result that the NiO containing ThO_2 was contaminated with alkali which, although it did not inhibit photosynthesis, was considerably in excess of that present in the filtrates from the irradiation of NiO and ThO_2 adsorbed on kieselguhr. When the unsupported NiO containing ThO_2 is irradiated, the amount of alkali which passes into solution must be proportional to the total amount of $Ni(HCO_3)_2$ which dissolves. In the irradiation described above the 12 l. of water used became almost saturated with the bicarbonate and hence the total amount of alkali present in the solution would be reduced to one-twelfth if only 1 l. of water were used. The advantage of this would outweigh the possible decrease in the amount of the product of photosynthesis.

The use of a relatively small volume of water precludes the use of the apparatus shown in fig. 2, and hence suspensions of 20 g. of NiO containing ThO_2 in 1400 ml. of water saturated with CO_2 were prepared by the method already described. These suspensions were irradiated in the rectangular glass cell for 2 hr. The oxides were maintained in suspension by an electrically driven stirrer and CO_2 was passed in during the whole period.

METHOD OF TREATMENT OF THE FILTRATE FROM THE IRRADIATION OF UNSUPPORTED NiO CONTAINING ThO_2

The treatment of the filtrate from an irradiation required careful consideration. The method adopted in the case of the filtrates from the irradiation of supported NiO containing ThO_2 was to neutralize them by the careful addition of very dilute hydrochloric acid and then to evaporate them to dryness under reduced pressure, the residue being dissolved in water and treated with diastase. These filtrates contained only minute quantities of nickel, whilst those from the irradiation of the unsupported oxides were saturated with respect to nickel bicarbonate.

The immediate neutralization of the filtrates in the latter case, with the attendant formation of $NiCl_2$, raised the question as to whether the activity of taka-diastase is affected by the presence of Ni ions. A carefully controlled series of experiments with boiled starch solution proved that the activity of the diastase is appreciably decreased when the concentration of Ni ions exceeds 0·006 M, that is to say when 50 ml. of the starch, acetate buffer and diastase solution contain more nickel than corresponds to 0·028 g. of $Ni(OH)_2$. It followed from this that if the activity of the diastase were not to be affected, it would be necessary to continue the concentration of the filtrate from an irradiation until sufficient of the hydrated nickel oxide had separated to reduce the total amount in solution to 0·028 g.

Now evidence has already been given that the white product of photosynthesis forms insoluble complexes with the very small amount of $Ni(OH)_2$ which separates when the filtrates from the irradiation of the supported NiO containing ThO_2 are concentrated. There can be little doubt, therefore, that some of this white product must be brought down with the large amount of $Ni(OH)_2$ which separates when the filtrate from the irradiation of the unsupported oxides is concentrated under reduced pressure. It follows from this that the amount of the white product left in solution after the filtrate has been so far concentrated that the total amount of $Ni(OH)_2$ in solution has been reduced to 0·028 g. may be considerably smaller than that originally photosynthesized.

It appeared to be necessary, therefore, in treating the filtrate from the irradiation of the unsupported NiO containing ThO_2 to adopt a method which lay between the two extremes, namely, (1) immediate neutralization by means of acid, and (2) concentration under reduced pressure until the total Ni content is reduced to 0·028 g. expressed as $Ni(OH)_2$. The method adopted was to concentrate the filtrate under reduced pressure until the rate of separation of the $Ni(OH)_2$ began rapidly to decrease. The solution, after filtration, was then exactly neutralized by dilute hydrochloric acid and evaporated to dryness. The residue was dissolved in water and treated with taka-diastase by the method already described.

EVIDENCE OF PHOTOSYNTHESIS WITH UNSUPPORTED NiO CONTAINING ThO_2

Several irradiations of the unsupported NiO containing ThO_2 were carried out and in each case evidence was obtained of a reducing sugar being formed by the action of taka-diastase. The amount of cuprous oxide formed on boiling with Fehling solution varied from 0·008 to 0·005 g., but as already explained these amounts in all probability do not represent the total amount of photosynthesized material. These observations, therefore, confirmed those obtained by the irradiation of NiO containing ThO_2 adsorbed on kieselguhr.

FURTHER EVIDENCE OF PHOTOSYNTHESIS WITH UNSUPPORTED NiO CONTAINING ThO_2

In the previous communication (1927) evidence was given that hydrated nickel carbonate on irradiation turns dark on the surface owing to the formation of Ni_2O_3 and that this superficial layer of Ni_2O_3 reverts to NiO in the presence of hydrated carbon dioxide. As was shown in 1936, hydrated nickel carbonate when heated in air until all the carbon dioxide and water has been driven off gives crystal units of NiO which are superficially coated with Ni_2O_3. It occurred to me, therefore, that a photosynthetically active product might be obtained by heating in air the hydrated nickel carbonate containing ThO_2 until it is completely decomposed. 25 g. of this material were heated in a porcelain dish at 250° with constant stirring until the evolution of gaseous products had ceased. The black residue was then irradiated for 2 hr. in suspension in water saturated with carbon dioxide. The filtrate was treated in exactly the same way as was described above in the irradiation of unsupported NiO containing ThO_2. The same result was observed, about 0·006 g. of cuprous oxide being obtained when the product of hydrolysis of the photosynthesized starch by taka-diastase was boiled with Fehling solution. This result, which was obtained eight times, affords additional confirmation of the results obtained by the irradiation of NiO containing ThO_2 adsorbed on kieselguhr.

In spite of the confirmation thus obtained of the photosynthesis of a carbohydrate by the irradiation of unsupported NiO containing ThO_2 in the presence of hydrated carbon dioxide, it may be pointed out that the difficulties associated with the use of this material are sufficiently great to render the method unsatisfactory. There is no question but that the use of NiO containing ThO_2 adsorbed on kieselguhr is preferable for two reasons. In the first place the amount of adsorbed alkali is minimized and in the second place this photocatalyst alone gives evidence of the photosynthesis of the unstable product which changes to the starch.

THE ESSENTIAL IMPORTANCE OF THE PRESENCE OF ThO_2 IN THE NiO

It must be emphasized in conclusion that in all the preparations of nickel oxide described in this communication, whether adsorbed on kieselguhr or unsupported, the presence of thorium oxide in the molecular ratio of $1ThO_2 : 24NiO$ was found to be essential. Many preparations of NiO were made which contained no ThO_2 and these were irradiated, the procedure being identical with that described above. In no case was any evidence of photosynthesis obtained. The function of the thorium oxide and the mechanism of the photosynthetic process will be described in a subsequent communication.

I have to record my grateful thanks to many who have rendered valuable help in this investigation and in particular to Messrs E. J. Baly, J. W. Ireland, L. B. Morgan, W. P. Pepper and C. E. Vernon. I also thank Messrs Parke, Davis and Co. for their gift of pure taka-diastase. To the late Sir Robert Mond I owe a very deep debt, since it was due to his most generous financial assistance that this investigation has been carried out. My grateful thanks are also due to my friend Sir Robert Robertson for his kindly criticism and advice.

SUMMARY AND CONCLUSIONS

It may be claimed that the results of the foregoing investigations indicate:

(1) That when a surface of NiO which contains ThO_2 in the molecular ratio of $1ThO_2 : 24NiO$, preferably adsorbed on kieselguhr, is irradiated in the presence of hydrated carbon dioxide an organic compound is photosynthesized.

(2) That the first product of photosynthesis, which gives the Molisch reaction after hydrolysis, is unstable and changes slowly at room temperature and rapidly at 60° to a stable compound.

(3) That this stable compound, which is colourless, can be hydrolysed by taka-diastase to a reducing sugar and is probably, therefore, a type of starch.

(4) That the first product of photosynthesis is the parent of the starch, the existence of which has not hitherto been recognized.

REFERENCES

Baly and Davies 1927 *Proc. Roy. Soc.* A, **116**, 219.
Baly and Hood 1929 *Proc. Roy. Soc.* A, **122**, 393.
Baly and Pepper 1935 *Nature, Lond.*, **136**, 28.
— — 1936 *Trans. Faraday Soc.* **32**, 375.
Bell 1931 *Trans. Faraday Soc.* **27**, 771.
Munson and Walker 1906 *J. Amer. Chem. Soc.* **28**, 663.

On fluctuations in electromagnetic radiation

(A CORRECTION)

BY M. BORN, F.R.S. AND K. FUCHS, *Edinburgh*

(*Received* 6 *June* 1939)

Dr M. Fierz (Zürich) has kindly drawn our attention to a mistake in our paper on fluctuations in electromagnetic radiation (1939), which influences appreciably the final result. In the first equation on p. 257, the indices α, β should be interchanged. This equation should be replaced by

$$[\mathbf{k}_\lambda \wedge \mathbf{e}_\lambda^\alpha][\mathbf{k}_\mu \wedge \mathbf{e}_\mu^\beta] = \frac{\omega_\lambda \omega_\mu}{c^2}\{(\mathbf{s}_\lambda \cdot \mathbf{s}_\mu)(\mathbf{e}_\lambda^\alpha \cdot \mathbf{e}_\mu^\beta) - (\mathbf{e}_\lambda^\alpha \cdot \mathbf{s}_\mu)(\mathbf{e}_\mu^\beta \cdot \mathbf{s}_\lambda)\},$$

where $\mathbf{s}_\lambda$ is a unit vector in the direction of $\mathbf{k}_\lambda$.

Instead of (3·9) we obtain for the energy density

$$u = \frac{1}{L^3}\sum_{\lambda,\mu}\sum_{\alpha,\beta} F_{\lambda\mu}^{\alpha\beta}\omega_\lambda\omega_\mu\{(q_\lambda^\alpha q_\mu^{\beta\dagger} + q_\mu^{\beta\dagger} q_\lambda^\alpha)\, e^{i(\mathbf{k}_\lambda - \mathbf{k}_\mu \cdot \mathbf{r})} - q_\lambda^\alpha q_\mu^\beta\, e^{i(\mathbf{k}_\lambda + \mathbf{k}_\mu \cdot \mathbf{r})} - q_\lambda^{\alpha\dagger} q_\mu^{\beta\dagger}\, e^{-i(\mathbf{k}_\lambda + \mathbf{k}_\mu \cdot \mathbf{r})}\}, \quad (3{\cdot}9)$$

with $$F_{\lambda\mu}^{\alpha\beta} = F_{\mu\lambda}^{\beta\alpha} = \tfrac{1}{2}[(\mathbf{e}_\lambda^\alpha \cdot \mathbf{e}_\mu^\beta)\{1 + (\mathbf{s}_\lambda \cdot \mathbf{s}_\mu)\} - (\mathbf{e}_\lambda^\alpha \cdot \mathbf{s}_\mu)(\mathbf{e}_\mu^\beta \cdot \mathbf{s}_\lambda)].$$

In the following equations $(\mathbf{e}_\lambda^\alpha \cdot \mathbf{e}_\mu^\alpha)$ should be replaced by $F_{\lambda\mu}^{\alpha\beta}$ and the summation $\sum_\alpha$ be split in two $\sum_{\alpha,\beta}$, accompanied by a corresponding splitting of the products $q_\lambda^\alpha q_\mu^{\alpha\dagger}$, etc. into $q_\lambda^\alpha q_\mu^{\beta\dagger}$.

The essential difference to the original calculation comes from the average over all directions of polarization. Instead of (4·10) we obtain

$$\overline{(F_{\lambda\mu}^{\alpha\beta})^2} = \tfrac{1}{8}(1 + \cos\vartheta_{\lambda\mu})^2,$$

so that in (4·12) and (5·9) $1+\cos^2\vartheta_{\lambda\mu}$ is to be replaced by $\frac{1}{2}(1+\cos\vartheta_{\lambda\mu})^2$. Equation (5·9) now reads

$$\left.\begin{aligned}\overline{\Delta U_1^2} &= \frac{1}{8}\left(\frac{l}{2\pi}\right)^6 \sum_{\alpha,\beta}\iint(1+\cos\vartheta_{\lambda\mu})^2\hbar^2\omega_\lambda\omega_\mu(\bar{n}_\lambda^\alpha+1)\bar{n}_\mu^\beta f^2(\mathbf{k}_\lambda-\mathbf{k}_\mu)\,d\mathbf{k}_\lambda\,d\mathbf{k}_\mu,\\ \overline{\Delta U_2^2} &= \frac{1}{16}\left(\frac{l}{2\pi}\right)^6 \sum_{\alpha,\beta}\iint(1+\cos\vartheta_{\lambda\mu})^2\hbar^2\omega_\lambda\omega_\mu\{(\bar{n}_\lambda^\alpha+1)(\bar{n}_\mu^\beta+1)+\bar{n}_\lambda^\alpha\bar{n}_\mu^\beta\}\\ &\qquad\qquad f^2(\mathbf{k}_\lambda+\mathbf{k}_\mu)\,d\mathbf{k}_\lambda\,d\mathbf{k}_\mu.\end{aligned}\right\} \tag{5·9}$$

Applying the formula (5·10) we find that $\overline{\Delta U_2^2}$ vanishes, since the integrand is zero for $\mathbf{k}_\lambda = -\mathbf{k}_\mu$ (i.e. $\cos\vartheta_{\lambda\mu} = -1$). Instead of (5·11) we obtain

$$\overline{\Delta U_1^2} = \overline{\Delta U_2^2} = \frac{1}{2}\left(\frac{l}{2\pi}\right)^3 \sum_{\alpha,\beta}\int\hbar^2\omega_\lambda^2(\bar{n}_\lambda^\alpha+1)\bar{n}_\lambda^\beta\,d\mathbf{k}_\lambda. \tag{5·11}$$

Comparing this expression with (5·14) we see that for isotropic radiation $(\bar{n}_\lambda^\alpha = \bar{n}_\lambda^\beta)$ they are identical if we replace

$$(\bar{n}_\lambda^\alpha+\tfrac{1}{2})^2 \quad\text{by}\quad \bar{n}_\lambda^\alpha(\bar{n}_\lambda^\alpha+1).$$

The result is that in the final formula (5·19) the term which was interpreted as the fluctuation of the zero energy drops out. We obtain the previously accepted formula

$$\overline{\Delta U_\nu^2} = \frac{\bar{E}_\nu^2}{vz_\nu}+h\nu\bar{E}_\nu. \tag{5·19}$$

It therefore turns out that the interference calculation for a partial system leads to the same result as the thermodynamical treatment of a closed system. The latter comes to rest in its lowest quantum state; in the partial system the zero waves continue to run from one partial volume to the other, but—at least if we take the partial volume sufficiently large—there is no fluctuation of energy.

Our mathematical objections against the critical paper of Heisenberg (1931) have to be withdrawn.

REFERENCES

Born, M. and Fuchs, K. 1939 *Proc. Roy. Soc.* A, **170**, 252.
Heisenberg, W. 1931 *Ber. sächs. Ges. (Akad.) Wiss.*, Math.-Phys. Klasse, p. 3.

The properties of flow of liquid He II

BY J. F. ALLEN AND A. D. MISENER

(*Communicated by J. D. Cockcroft, F.R.S.—Received* 29 *March* 1939)

INTRODUCTION

The problem of the viscosity of liquid He II has been the subject of several recent investigations. In their experiments, Misener, Burton and others at Toronto (1935*a*, *b*) and later MacWood (1938) at Leiden used the methods of oscillating cylinder and disk respectively. Kapitza (1938) employed radial flow between parallel plates, and Giauque, Stout and Barieau (1938), Burton (1938), and the present authors (1938*a*, *b*) have used the method of flow through capillaries. There has been wide disagreement among the investigators with regard to the magnitude of the viscosity, and the determination of the value by the different investigators varies from an upper limit of 5×10^{-9} c.g.s. units, as found by Kapitza (1938), to a value of 10^{-5} c.g.s. units, as observed by Burton (1938). In addition to this the present authors reported (1938*a*) that, at least for long, narrow capillaries, the flow of liquid He II appeared to be non-classical in that the velocity of flow bore a relation to the pressure, which corresponded neither to laminar nor turbulent conditions.

Flow is classically defined as laminar when the average velocity over the cross-section of the tube is directly proportional to the hydrostatic pressure which produces the flow. At sufficiently high velocity, the flow ceases to be laminar; it becomes turbulent and the velocity is then proportional to the square root of the pressure. It was observed that for He II in long, narrow capillaries the velocity became almost independent of pressure and the suggestion was advanced that this might be attributed to slip on the walls of the capillary.

The present research was undertaken in the hope that a comprehensive investigation of the flow through capillaries of various diameters and lengths might throw more light on the nature of the phenomenon. Data has been secured over the temperature range from the λ-point (2·186° K) down to 1·15° K. The present paper also includes measurements of the flow of He II through tightly packed powder.

APPARATUS AND METHOD FOR FLOW EXPERIMENTS

The apparatus and the experimental method employed were essentially the same for all of the flow measurements. A glass capillary was connected at one end to a cylindrical glass reservoir of such a diameter that the flow caused the liquid level in it to change at a rate convenient for measurement. The other end of the capillary was free and opened into the bath of liquid helium. The top of the reservoir was usually left open, but the opening was constricted to a diameter of from 0·5 to 1 mm., depending on the size of the reservoir. The purpose of the constriction was to reduce as far as possible any transfer of the liquid to the reservoir by means of mobile surface films passing over the rim of the reservoir. Daunt and Mendelssohn (1938) have found that the films of He II form to a thickness of the order of 10^{-6} cm. which does not appear to change much with temperature, and have a flow velocity of roughly 18 cm./sec. at 1·2° K. A striking property of the films is that the rate of transfer of liquid in them is independent of the hydrostatic pressure or length of path of the film. Hereafter, in this paper, we shall refer to the mobile films forming *above* the liquid surface as supra-surface films.

By constricting the opening at the top of the reservoir, we have restricted the transfer by supra-surface films to less than 5×10^{-5} cm.^{3}/sec.

Most of the reservoirs were afterwards tested with the capillaries closed off, to measure the actual amount of liquid transferred by the films. The proportion thus transferred was generally less than 1 %, although in the case of the finest glass capillaries it did amount to 7 or 8 %.

During the experiments the reservoir was always partially immersed in the bath. The flow was initiated by raising or lowering the reservoir and capillary, thereby separating the reservoir and bath levels. The rate of change of both reservoir and bath levels was then observed with a cathetometer. The latter was provided with a graduated eyepiece scale, and the times at which the levels passed successive divisions were recorded. The rate of change of bath level was always much slower because of its greater cross-section.

When long capillaries were used they were coiled horizontally to fit the flask containing the liquid helium bath. The diameter of the coils was usually 4 or 5 cm., i.e. approximately one hundred times the diameter of the capillary, which could, therefore, be considered as essentially straight.

With very fine capillaries, the volume of liquid flowing into the reservoir per second through a single capillary would not be large compared with that transported into the reservoir by the surface films or lost by evaporation. This difficulty was overcome by the following method:

A large number of stainless steel wires (diameter 0·0061 cm.) was bound together with all the wires as nearly parallel as possible. The bundle was slipped into a thick-walled nickel-silver tube which was then drawn through a succession of steel dies of decreasing diameter. This process, carried beyond the point where the wires were close packed inside the tube, produced a deformation. The deformation (toward a hexagonal cross-section of the individual wires) decreased the size of the interstices between the wires, and by continuing the process, channels of any desired size between the wires could be obtained. The channels are naturally very far from circular in cross-section, and the type of flow observed in them might be expected to be slightly different from that in channels of circular cross-section. Glass reservoirs were attached to the wire-filled tubes by means of short platinum tubes.

Steady vapour pressures and hence constant temperatures were maintained by means of a manually adjusted needle valve and a differential oil manometer in the helium pumping line. It was found to be essential to keep the temperature drift below 10^{-3} degree/min. during measurements, particularly when they were carried out close to the λ-point.

The maximum hydrostatic pressure used in the flow measurements was 15 mm. of liquid helium, and the cathetometer magnification was adjusted so that the 15 mm. height occupied the whole field of view of the eyepiece.

RESULTS OF FLOW THROUGH CAPILLARIES

To determine the effect of change in radius, the flow was observed through single capillaries each 20 cm. in length, with radii $4\cdot38 \times 10^{-2}$, $1\cdot53 \times 10^{-2}$, $5\cdot0 \times 10^{-3}$ and $1\cdot62 \times 10^{-3}$ cm. For still smaller channels, three metal tubes were packed with wires as described above. The mean channel width in each of the three tubes was $3\cdot9 \times 10^{-4}$, $7\cdot9 \times 10^{-5}$ and $1\cdot2 \times 10^{-5}$ cm. respectively. Throughout the diagrams in the paper the radii of the single capillaries are plotted in conjunction with the mean channel widths and not half-widths of the wire-filled tubes. It will be shown that the flow through wire-filled tubes corresponds more closely to flow between parallel plates than to flow through cylindrical channels, so that the difference between mean channel width and half the mean channel width becomes of little importance. The wire-filled tubes will be fully discussed later.

Investigation of the effect of change in length of capillary was confined to one capillary size, namely, $1\cdot53 \times 10^{-2}$ cm. radius. The lengths used were 40, 20, 10 and 4·75 cm., and 1 mm. In all cases the change in reservoir level was plotted against the time. The slope of the graph at any point could then be transformed into the volume per second or the average velocity, v, of the liquid passing through the capillary. At the same point the difference between reservoir and bath levels gave the pressure head, p, corresponding

TABLE I

Capillary length 20 cm.

Radius ... $r = 4{\cdot}38 \times 10^{-2}$ cm.		$r = 1{\cdot}53 \times 10^{-2}$ cm.		$r = 5{\cdot}0 \times 10^{-3}$ cm.	
T° K	Slope	T° K	Slope	T° K	Slope
2·163	0·80	2·162	0·73	2·160	0·50
2·103	0·68	2·102	0·64	2·105	0·44
2·006	0·63	1·996	0·59	2·002	0·39
1·751	0·57	1·751	0·53	1·15	0·30
1·191	0·54	1·191	0·47		

Radius ... $r = 1{\cdot}62 \times 10^{-3}$ cm.		$d = 3{\cdot}9 \times 10^{-4}$ cm.		$d = 1{\cdot}2 \times 10^{-5}$ cm.	
T° K	Slope	T° K	Slope	T° K	Slope
2·165	0·22	2·160	0·12	2·170	0·04
2·096	0·16	2·102	0·11	2·00	0·0
1·985	0·14	2·005	0·10	1·15	0·0
1·749	0·13	1·750	0·10		
1·335	0·12	1·150	0·10		

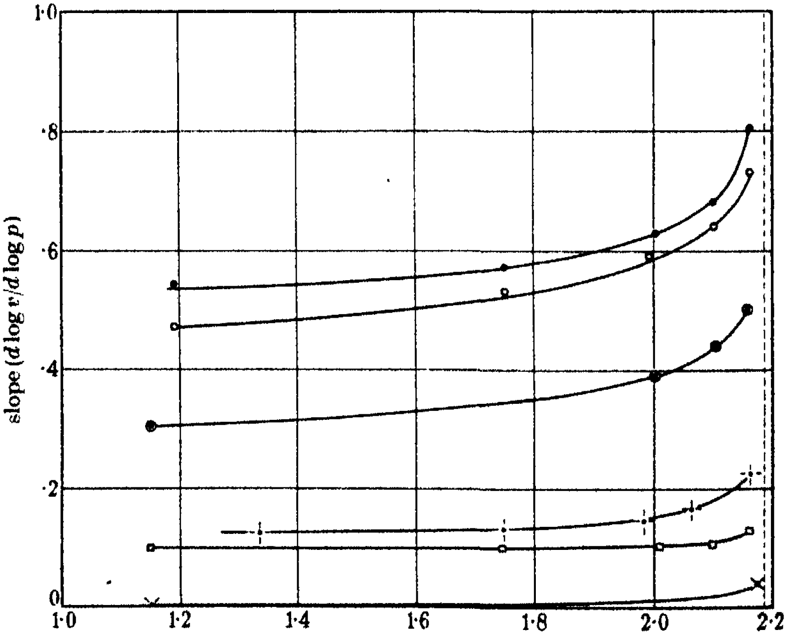

FIG. 1. The temperature variation of the relation between velocity and pressure for flow through capillaries of different size but constant length.

● $r = 4{\cdot}38 \times 10^{-2}$ cm.	+ $r = 1{\cdot}62 \times 10^{-3}$ cm.
○ $r = 1{\cdot}53 \times 10^{-2}$ cm.	☐ $d = 3{\cdot}9 \times 10^{-4}$ cm.
⊙ $r = 5{\cdot}0 \times 10^{-3}$ cm.	× $d = 1{\cdot}2 \times 10^{-5}$ cm.

to the velocity so determined. From each graph a velocity-pressure table was constructed which was plotted logarithmically. The resulting logarithmic curves were always straight lines within the limits of accuracy and within the limits of pressure used, i.e. from 160 dynes/cm.^{2} to 5 dynes/cm.^{2}. The slope ($d \log v/d \log p$) of the lines on the logarithmic graph then represents the index of p in the velocity-pressure relation. According to classical theory the slope or the index is unity for pure laminar flow, and is $\frac{1}{2}$ for pure turbulent flow.

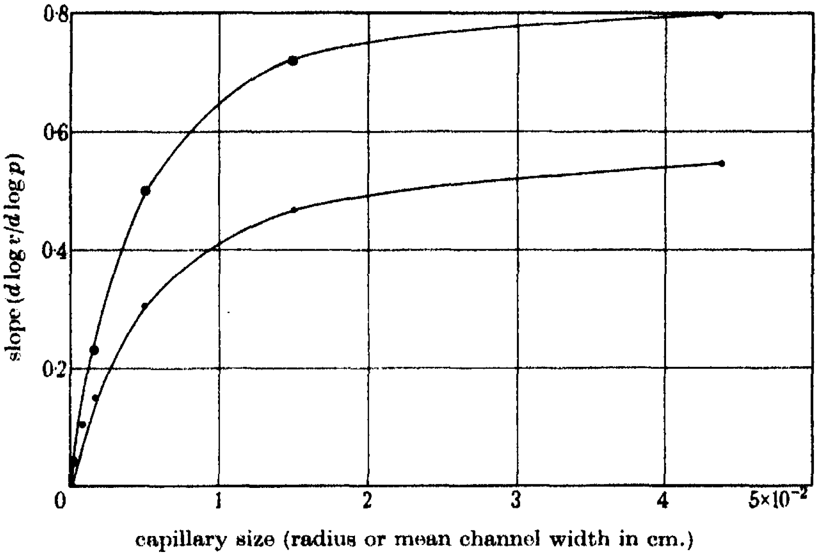

FIG. 2. The variation with channel size of the relation between velocity and pressure for flow through capillaries at two temperatures.
⊙ $T = 2{\cdot}160°$ K. ○ $T = 1{\cdot}20°$ K.

The data giving the slope as a function of the capillary size (radius or mean channel width) and as a function of the temperature for capillaries of constant length is given in Table I and shown in figs. 1 and 2. Fig. 1 contains a family of curves each giving the variation with temperature of the slope of the $\log v$, $\log p$ relation for a particular capillary size. It is quite evident that the type of flow with which we are concerned is of a complex character and that He II cannot be treated as a normal viscous fluid. Fig. 1 shows two important features. First, the slope tends to approach unity for all capillary sizes as the temperature approaches the λ-point (the dotted ordinate, 2·186° K). Secondly, over the whole temperature range investigated, except very close to the λ-point, the slope approaches zero as the size of the capillary becomes very small. With the finest capillary, at all temperatures below 1·75° K the slope was zero within the limits of experimental error. This means that, within the observed pressure range from 160 to zero dynes/cm.^{2}, the velocity of flow was completely independent of the pressure. That the pressure-independent velocity extended all the way to zero pressure at the lowest bath temperature is shown in fig. 8. As the reservoir and bath levels came together it was found that the reservoir level maintained its motion past the position of equilibrium and oscillated slowly about it for several minutes.

For temperatures between 1·75° K and the λ-point, however, in the three wire-filled tubes, the low value of the slope, $d \log v / d \log p$, was not

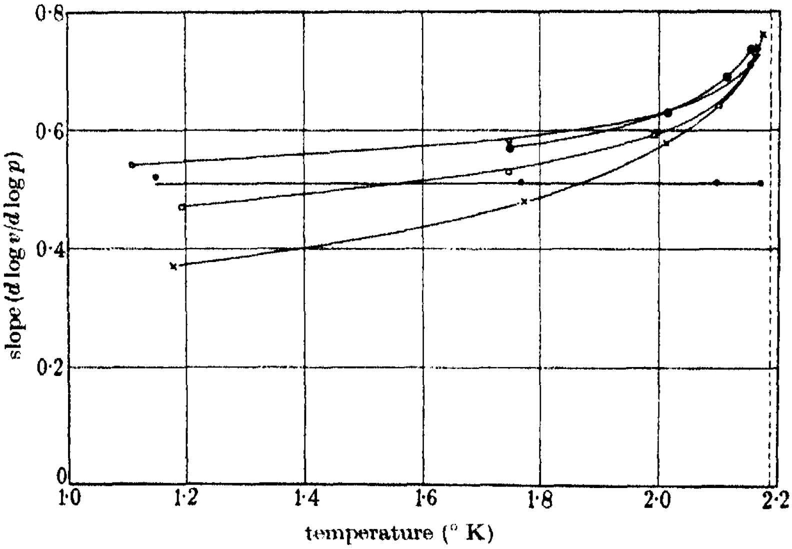

Fig. 3. The temperature variation of the relation between velocity and pressure for flow through capillaries of constant radius ($r = 1·53 \times 10^{-2}$ cm.), but different length.

● l = 1 mm. ☐ l = 20 cm.
○ l = 4·75 cm. × l = 40 cm.
⊙ l = 10·0 cm.

TABLE II

Capillary radius $1·53 \times 10^{-2}$ cm.

Length... 40 cm.		10 cm.		4·75 cm.		1 mm.	
T° K	Slope	T° K	Slope	T° K	Slope	T° K	Slope
2·173	0·76	2·156	0·73	2·156	0·71	2·160	0·51
2·163	0·74	2·116	0·69	1·746	0·58	2·096	0·52
2·016	0·58	2·014	0·63	1·112	0·54	1·780	0·52
1·774	0·48	1·750	0·57	0·0	0·0	1·150	0·53
1·179	0·37						

maintained down to zero pressure. Instead, as is shown in fig. 9, for pressures smaller than 20–40 dynes/cm.^{2}, the velocity lost its pressure-independence and varied linearly with the pressure. The latter phenomenon and the level oscillation will be discussed more fully in the section on wire-filled tubes.

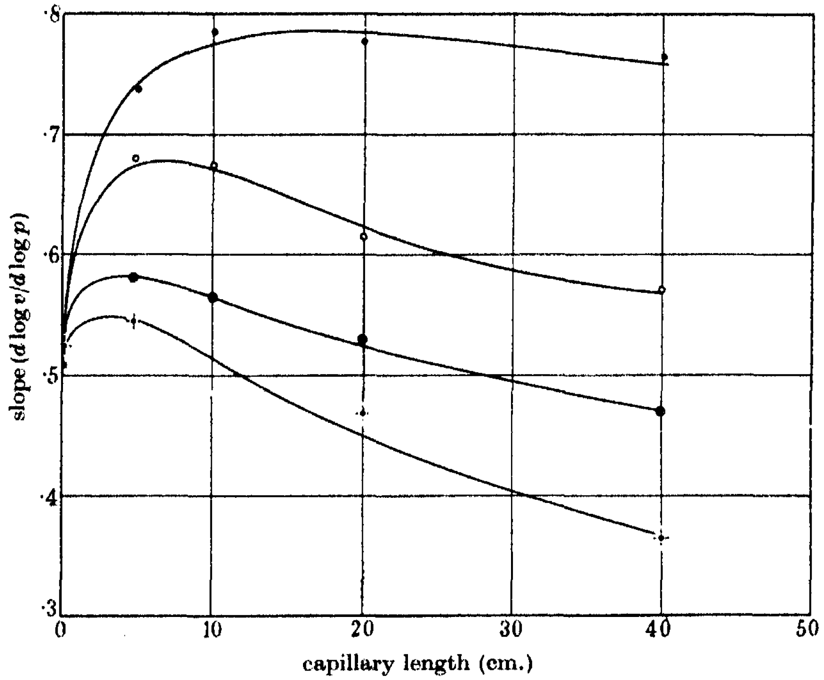

FIG. 4. The variation with length of the relation between velocity and pressure for capillary flow at different temperatures.

● $T = 2{\cdot}175°$ K. ⊙ $T = 1{\cdot}750°$ K.
○ $T = 2{\cdot}00°$ K. + $T = 1{\cdot}20°$ K.

The fact that the slope approaches zero for a large range of temperatures as the size of the capillary diminishes is demonstrated more strikingly in fig. 2, which shows the variation of slope with capillary size at two different temperatures near the extremes of the available He II range. From the rate of increase of slope with increasing capillary size it is apparent that the production of purely laminar flow in He II would involve apparatus of considerable magnitude.

Table II and figs. 3 and 4 contain the data concerning the flow as a function of length and of temperature for capillaries of constant radius. Here two features are to be noted. First, for long capillaries, as in the case of variation of radius, the slope tends to approach unity as the temperature approaches the λ-point. Secondly, the slope approaches a temperature-independent value of 0·5 as the length approaches zero, which is to be expected according to classical hydrodynamics.

When we examine the variation of velocity with the length and radius of the capillary, we are confronted with further unusual phenomena. Fig. 5,

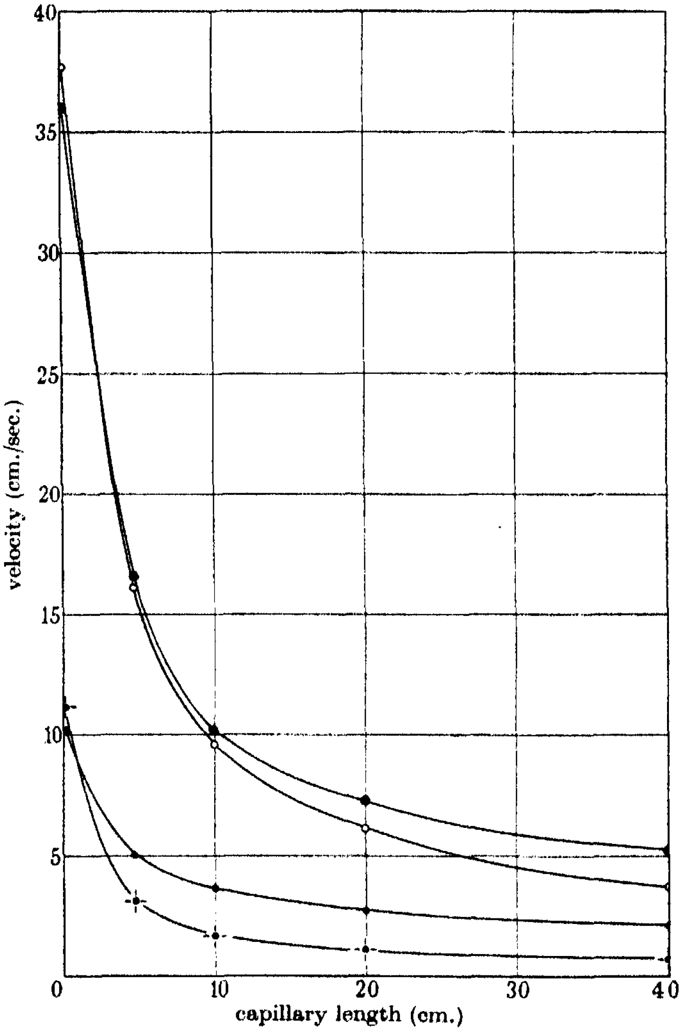

FIG. 5. The variation of velocity with length for capillary flow at different constant temperatures and pressures.

+ $T = 2{\cdot}160°$ K, $p = 15$ dynes/cm.^{2}. ○ $T = 2{\cdot}160°$ K, $p = 160$ dynes/cm.^{2}.
● $T = 1{\cdot}20°$ K, $p = 15$ dynes/cm.^{2}. ⊙ $T = 1{\cdot}20°$ K, $p = 160$ dynes/cm.^{2}.

drawn from Table III, gives the average velocity of flow over the cross-section of the capillary as a function of the length for two constant pressure heads, and at two different temperatures. With increasing length, and particularly at low pressures, the velocity tends to approach a value which is independent of length. A normal viscous liquid, under conditions of laminar flow, should show a velocity that varies inversely with the length, if the length be sufficiently great to eliminate end effects. An important point is that the velocity increases with decreasing temperature in long capillaries, whilst the reverse is true in very short capillaries.

TABLE III

Capillary radius $1{\cdot}53 \times 10^{-2}$ cm.

	Length ...	40 cm.	20 cm.	10 cm.	4·75 cm.	1 mm.
	$T°$ K	v cm./sec.	v	v	v	v
$p = 15$ dynes/cm.^{2}	1·20	2·0	2·8	3·65	4·8	10·2
	2·160	0·46	1·1	1·70	3·0	11·2
$p = 160$ dynes/cm.^{2}	1·20	5·2	7·3	10·1	16·5	35·9
	2·160	3·6	6·0	9·5	16·0	37·7

TABLE IV

Capillary length 20 cm.

Radius (cm.) ...	... ...	$4{\cdot}38 \times 10^{-2}$	$1{\cdot}53 \times 10^{-2}$	$5{\cdot}0 \times 10^{-3}$	$1{\cdot}62 \times 10^{-3}$
	$T°$ K	v	v	v	v
$p = 15$ dynes/cm.^{2}	1·20	3·5	2·8	2·9	3·1
	2·160	2·5	1·1	0·42	0·46
$p = 160$ dynes/cm.^{2}	1·20	12·2	7·3	5·7	4·7
	2·160	16·1	6·0	1·4	0·75

Average width of channel (cm.) ...		$3{\cdot}9 \times 10^{-4}$	$7{\cdot}9 \times 10^{-5}$	$1{\cdot}2 \times 10^{-5}$
	$T°$ K	v	v	v
$p = 15$ dynes/cm.^{2}	1·20	2·8	7·1	12·9
	2·160	0·50	0·235	1·0
$p = 160$ dynes/cm.^{2}	1·20	4·1	8·0	12·9
	2·160	0·70	1·0	1·25

Fig. 6, constructed from data in Table IV, shows the variation of velocity with capillary radius at two constant temperatures and two constant pressures. For very small channel widths, the velocity of flow, instead of approaching zero as it would in a normal liquid, appears to increase. The increase is quite marked in the case of the narrowest channel, $d = 1{\cdot}2 \times 10^{-5}$ cm., at the lowest bath temperature, 1·15° K. Also in capillaries larger than 5×10^{-3} cm. radius and at low pressures, the velocity is almost independent of the radius. For a normal viscous fluid, the velocity should vary as the square of the radius.

Two other features in fig. 6 are noteworthy. First, under constant pressure the rate of increase of velocity with decreasing temperature becomes greater as the radius of the capillary diminishes. Secondly, at sufficiently high pressures in larger capillaries the velocity decreases with decreasing temperature.

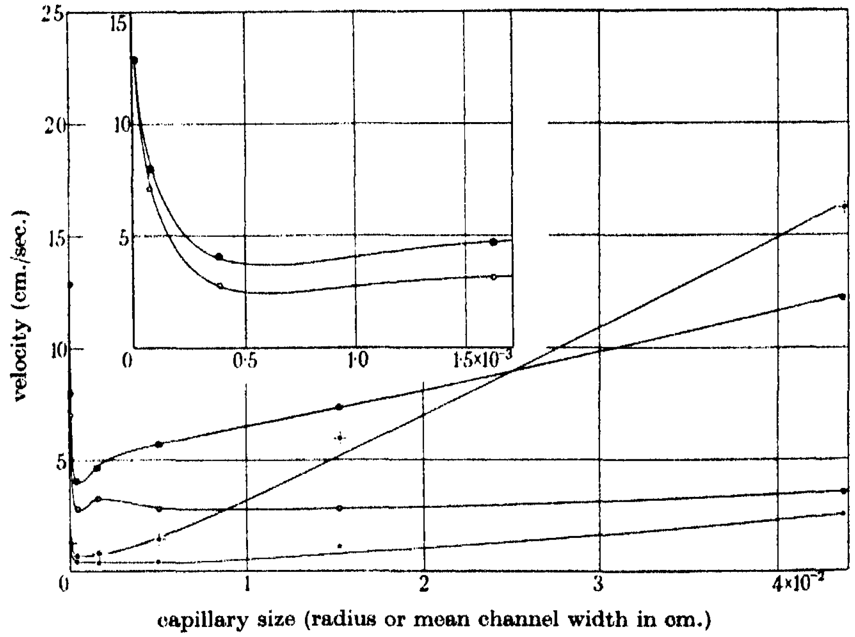

Fig. 6. The variation with capillary size of the velocity at different temperatures and pressures.

● $T = 2{\cdot}160^\circ$ K, $p = 15$ dynes/cm.^{2}. + $T = 2{\cdot}160^\circ$ K, $p = 160$ dynes/cm.^{2}.
○ $T = 1{\cdot}20^\circ$ K, $p = 15$ dynes/cm.^{2}. ⊙ $T = 1{\cdot}20^\circ$ K, $p = 160$ dynes/cm.^{2}.

Fig. 7, drawn from Table V, gives the variation of velocity with temperature for different capillary radii. The velocity values are those which correspond to a pressure head of 160 dynes/cm.^{2}. The figure shows again the decrease in velocity with decreasing temperature in the largest capillary, although under a smaller pressure head the large capillary, in common with the others, would show higher velocities at lower temperatures. It is most important to note that as the capillary radius gets very small, the velocity-temperature curve shows a more and more marked resemblance to that observed by Daunt and Mendelssohn (1938) for the flow of supra-surface films of He II.

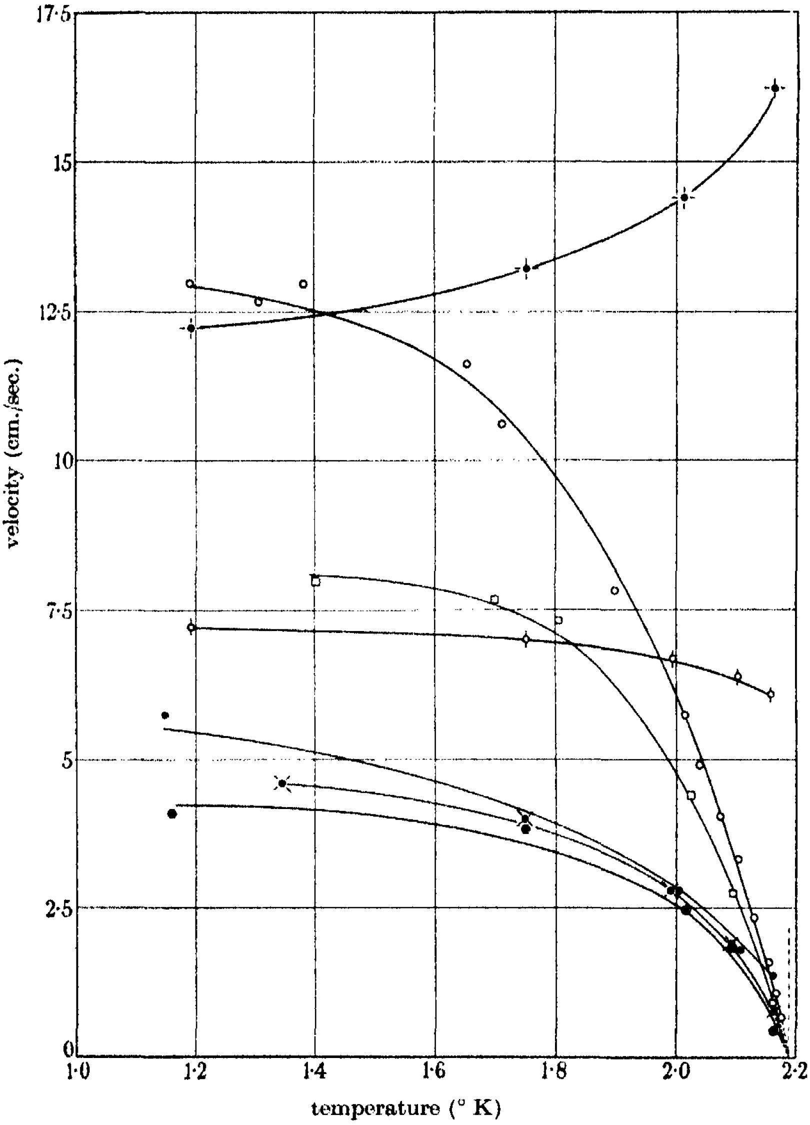

FIG. 7. The variation of velocity with temperature for flow in capillaries of different size at a pressure head of 160 dynes/cm.^{2}.

+ $r = 4{\cdot}38 \times 10^{-2}$ cm.
ϕ $r = 1{\cdot}53 \times 10^{-2}$ cm.
● $r = 5{\cdot}0 \times 10^{-3}$ cm.
× $r = 1{\cdot}62 \times 10^{-3}$ cm.

⊙ $d = 3{\cdot}9 \times 10^{-4}$ cm.
□ $d = 7{\cdot}9 \times 10^{-5}$ cm.
○ $d = 1{\cdot}2 \times 10^{-5}$ cm.

Table V

$p = 160$ dynes/cm.^{2}. Capillary length 20 cm.

Radius (cm.) ... $4·38 \times 10^{-2}$		$1·53 \times 10^{-2}$		5×10^{-3}	
T° K	v cm./sec.	T° K	v	T° K	v
2·163	16·2	2·162	6·1	2·160	1·35
2·006	14·4	2·102	6·35	2·105	1·8
1·751	13·2	1·996	6·7	2·002	2·8
1·191	12·2	1·751	7·0	1·15	5·75
		1·191	7·20		

$r = 1·62 \times 10^{-3}$ cm.		$d = 3·9 \times 10^{-4}$ cm.		$d = 7·9 \times 10^{-5}$ cm.		$d = 1·2 \times 10^{-5}$ cm.	
T° K	v	T° K	v	T° K	v	T° K	v
2·165	0·75	2·162	0·70	2·162	0·85	2·173	0·73
2·096	1·95	2·092	1·85	2·095	3·0	2·165	1·07
1·985	2·80	2·015	2·45	2·020	4·7	2·153	1·62
1·749	4·0	1·749	3·85	1·805	7·4	2·130	2·36
1·335	4·6	1·161	4·05	1·709	7·7	2·102	3·3
				1·400	8·0	2·070	4·55
						2·035	4·95
						1·900	7·8
						1·650	11·6
						1·38	12·9
						1·31	12·6
						1·20	12·9

Flow through tubes filled with wires

The three wire-filled tubes, whose velocity-temperature curves bear such a close resemblance to that for mobile surface films, can now be considered in more detail. The size and nature of the channels through these tubes have been determined by two methods and are given in Table VI, which also contains comparative data for supra-surface films from measurements made by Daunt and Mendelssohn. First, by means of the passage of helium gas at high pressure and at room temperature, the effective total open cross-section, S_p, was found using the Poiseuille formula for the flow of a compressible fluid, and considering the flow to take place in the channels between the close-packed wires. If the number of wires is n, the number of channels will be approximately $2n$. Since the method assumes a circular cross-section for the flow channel, the effective cross-section so calculated for the wire-filled tubes will represent too small an area. The relation between surface and area will also not be correct.

We have been able to determine the total open cross-section of tubes A and C by another method. In both tubes at the lowest bath temperature

(1·15° K), oscillation of the reservoir level about its equilibrium position with the bath level was observed. This was most pronounced for tube *C*, and is shown in fig. 8. The curve represents the relation between the position of the reservoir level and the time. In this diagram the bath level has been kept at a fixed point in the eyepiece scale for convenience of observation.

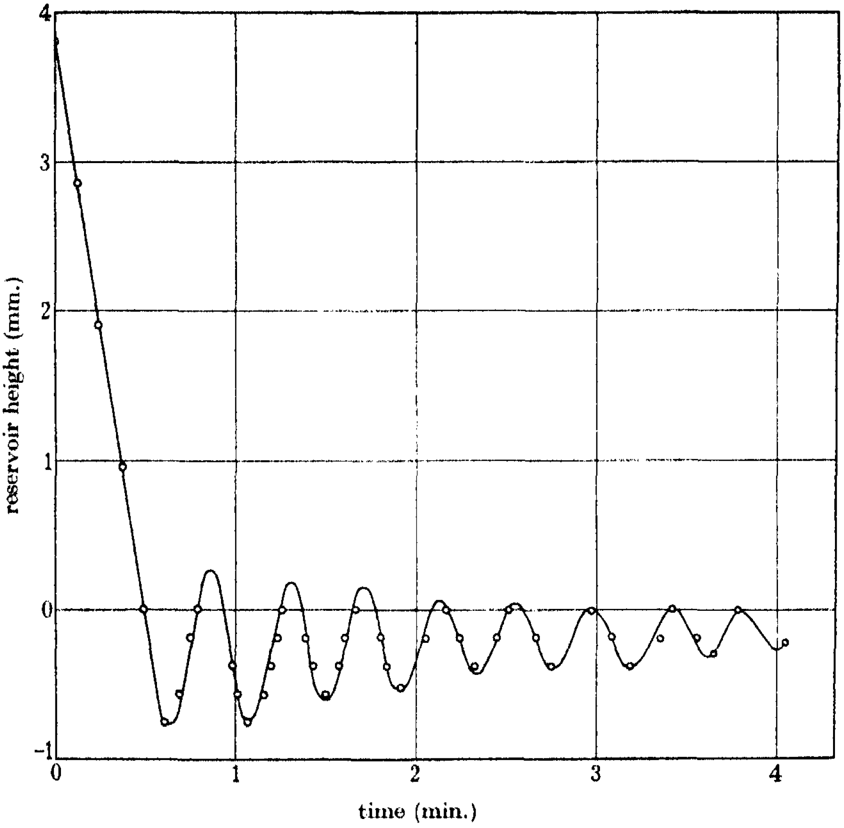

FIG. 8. The oscillation of reservoir level in the wire-filled tube *C*, at $T = 1{\cdot}20°$ K.

From the time and height of reservoir level at which the observation commenced, the level fell at a constant rate until it had passed the bath level. The reservoir level then oscillated slowly about the bath level. The oscillations were recorded for several minutes until the view was obscured by moisture condensing on the flask.

It would appear that the oscillations must be caused by the inertia of the liquid in the capillary. If so, then the open cross-section, S_0, of the capillary can be found from the relation

$$\tau = 2\pi \sqrt{\left(\frac{Al}{S_0 g}\right)},$$

where A is the cross-section of the reservoir attached to the capillary, and l is the length of the capillary, and τ is the periodic time of the oscillation. For tube C, $A = 1{\cdot}25 \times 10^{-4}$ cm.^{2}, $l = 15{\cdot}8$ cm., and the observed τ was approximately 25 sec. Inserting these values, we observed a value for S_0, which is larger than S_p by a factor of 3·8. This seemed to indicate that the flow might correspond more closely to that between parallel plates, rather than through separate circular channels. The total open cross-section was accordingly calculated using a suitable formula for flow between parallel plates and employing the data used in calculating S_p. The cross-section calculated in this way was 30 % higher than S_0. The wire-filled tubes appear, therefore, to provide a network of channels having approximately parallel sides. This has been further borne out by an examination of wires taken from the tube after drawing down. The wires appeared hexagonal in shape with well-defined edges. It is apparent that He II flows in these very narrow channels with a very slight retardation.

In order to test the validity of the application of the oscillation equation, two reservoirs differing in size by a factor of 6·3 were attached to tube A. The two values of S_0, obtained from the two values of τ observed, differed by approximately 12 %. The average of the two values for S_0 is given in Table VI. It is seen from the table that for tube A, S_0 is the same as S_p, which might be expected since the drawing down of tube A was not carried past that required for close packing of the undistorted wires.

No oscillation data was available for tube B, but since its Poiseuille cross-section, S_p, fell midway between those of tubes A and C, S_0 was estimated to be twice as large as S_p.

We have assumed in the calculations that the total circumference of all the wires in each of the tubes is in contact with liquid helium. Then the average width of the channel, d, was determined by dividing S_0 by half the total circumference of wires. Table VI helps to show the similarity between the flow in tube C and transfer by means of supra-surface films.

An interesting feature of the flow through wire-filled tubes, as has been mentioned earlier, is that in each of them above 1·75° K, the slope, $d \log v / d \log p$, did not maintain its very low value down to zero pressure. Instead, as is seen from fig. 9, for pressure below 30 or 40 dynes/cm.^{2}, the slope increased to unity. If the flow, however, was treated as viscous in

TABLE VI

	Tube *A*	Tube *B*	Tube *C*	Supra-surface films
Length (cm.)	15	14·2	15·8	—
No. of wires	890	990	2000	—
Total circumference of wires in the tube after drawing (cm.)	15·5	16·5	21	—
S_p (cm.^{2})	$2·9 \times 10^{-3}$	$3·2 \times 10^{-4}$	$3·3 \times 10^{-5}$	—
S_0 (cm.^{2})	$2·9 \times 10^{-3}$	$\sim 6·4 \times 10^{-4}$	$1·25 \times 10^{-4}$	—
Average width of channel, *d* (cm.)	$3·9 \times 10^{-4}$	$\sim 7·9 \times 10^{-5}$	$1·2 \times 10^{-5}$	$\sim 4 \times 10^{-6}$
Vol./sec. at 1·2° K and under 160 dynes/cm.^{2} (cm.^{3}/sec.)	$1·2 \times 10^{-2}$	$\sim 5·1 \times 10^{-3}$	$1·6 \times 10^{-3}$	—
Vol./sec./cm. width of surface at 1·2° K and under 160 dynes/cm.^{2}	$8·3 \times 10^{-4}$	$\sim 3·1 \times 10^{-4}$	$7·7 \times 10^{-5}$	8×10^{-5}
Velocity at 1·2° K and under 160 dynes/cm.^{2} (cm./sec.)	4·1	$\sim 8·0$	12·9	18

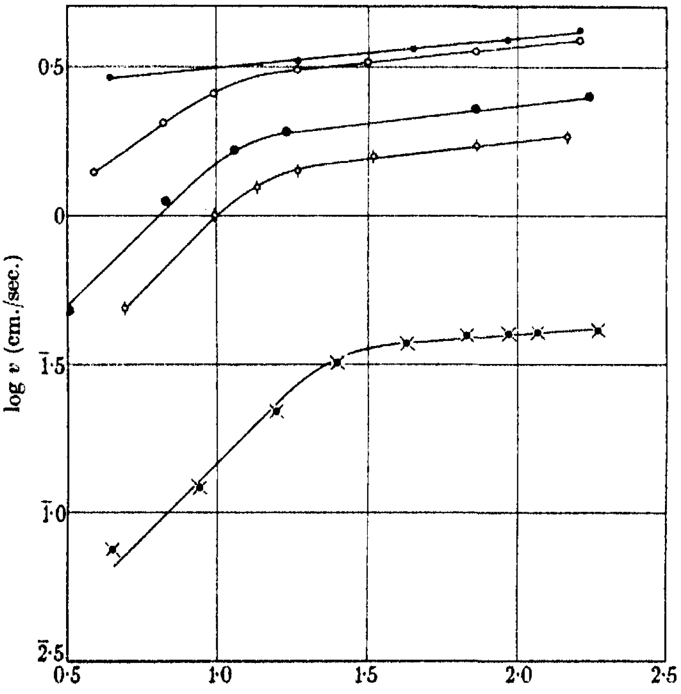

FIG. 9. The relation between velocity and pressure in the wire-filled tube *A* at different temperatures.

● $T = 1·164°$ K. ⊙ $T = 2·017°$ K. ⨯ $T = 2·162°$ K.
○ $T = 1·748°$ K. ⦶ $T = 2·092°$ K.

this pressure region, the viscosity so calculated was found not only to decrease very rapidly with decreasing temperature, but also to decrease with the size of the channels. Thus the viscosity determined from flow through tube *A* varied from 5×10^{-7} c.g.s. units near the λ-point to 1×10^{-8} c.g.s units at 1·75° K, while that determined from tube *C* varied over a corresponding temperature range from 1×10^{-8} c.g.s units to 1×10^{-10} c.g.s. units. It is doubtful, therefore, whether any significance can be attached to a determination of the viscosity in this way.

It is obvious that viscosity can have little to do with the damping of the oscillation shown in fig. 8. The decrement must arise partly from the transfer of kinetic energy at the ends of the tube and probably partly from thermal effects associated with the flow, which are to be discussed in a later paper. If, however, we treat the damping as though it were due to viscosity, we arrive at the very minute figure of 5×10^{-11} c.g.s. units for the flow of liquid through tube *C* at 1·2° K.

FLOW OF He II THROUGH POWDER

During the course of the experiments on the flow through very fine capillaries, measurements were made on the flow through a tube packed with fine powder. The tube had a bore of 3 mm. and a wall thickness of 3 mm. A length of 10 cm. was tightly packed with jewellers' rouge. The process of packing consisted in pouring in successive small quantities of the rouge and tamping it down each time with a steel rod. Before the powder-filled tube was inserted in the cryostat, helium gas at high pressure was forced through it, both to remove the air from the interstices in the powder and to provide data for the determination of the viscosity of He II by the comparison method using D'Arcy's Law:

$$\eta_L = \eta_G \frac{q_G p_L}{q_L p_G},$$

where η is the viscosity, q is the quantity of liquid/sec. and p is the hydrostatic pressure. The subscript L refers to He II, and the subscript G refers to helium gas at room temperature.

The flow was measured by the same method as was used for flow through capillaries. Fig. 10 gives the volume of liquid per second passing through the powder as a function of the temperature for a constant pressure of 100 dynes. The similarity of the curve to that for flow through a very fine capillary (fig. 7) is quite marked. At the temperature 2·177° K, the vol./sec. was proportional to the pressure for small pressures as is seen from fig. 11. At higher pressures it became proportional to the square root of the pressure. At all other temperatures below the λ-point, the vol./sec. was proportional to the square root of the pressure for all pressures. From a comparison with the passage of helium gas at high pressures and at room temperature, the coefficient of "viscosity" at 2·177° K was calculated to be 1×10^{-8} c.g.s. units.

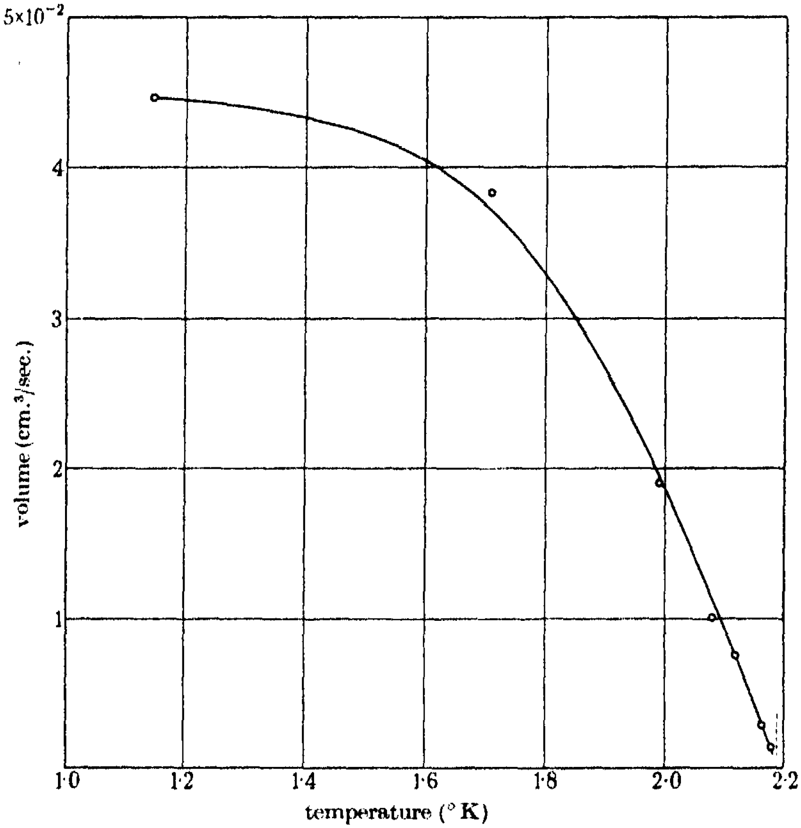

FIG. 10. The variation with temperature of the rate of flow through tightly packed jewellers' rouge under a pressure of 100 dynes/cm.².

The thirty-fold increase in the velocity of flow from 2·177 to 1·145° K shows that the "viscosity" must drop to the order of 10^{-10} c.g.s. units at 1·145° K. It seems unlikely that the powder contracted away from the walls as the glass tube was cooled to helium temperature, since then one might have expected the flow to be less dependent on pressure. Also, the flow of He I through the powder was not detectable.

For laminar flow through very fine powder, Reynold's number should be unity. The observed laminar flow per second was of the order 10^{-3} cm.^{3}/sec. The velocity down the tube was therefore 10^{-2} cm./sec. whilst the average particle size was 10^{-5} cm. diameter. Thus Reynolds' number, $R = r\rho v/\eta$, where r is the particle radius, ρ the density of He II, and v the velocity, is of the order unity for the viscosity of 1×10^{-8} c.g.s. units at 2·177° K. The rapid increase of v with decreasing temperature would quickly put the Reynolds' number up sufficiently to give turbulent flow, which is observed for all temperatures below 2·177° K.

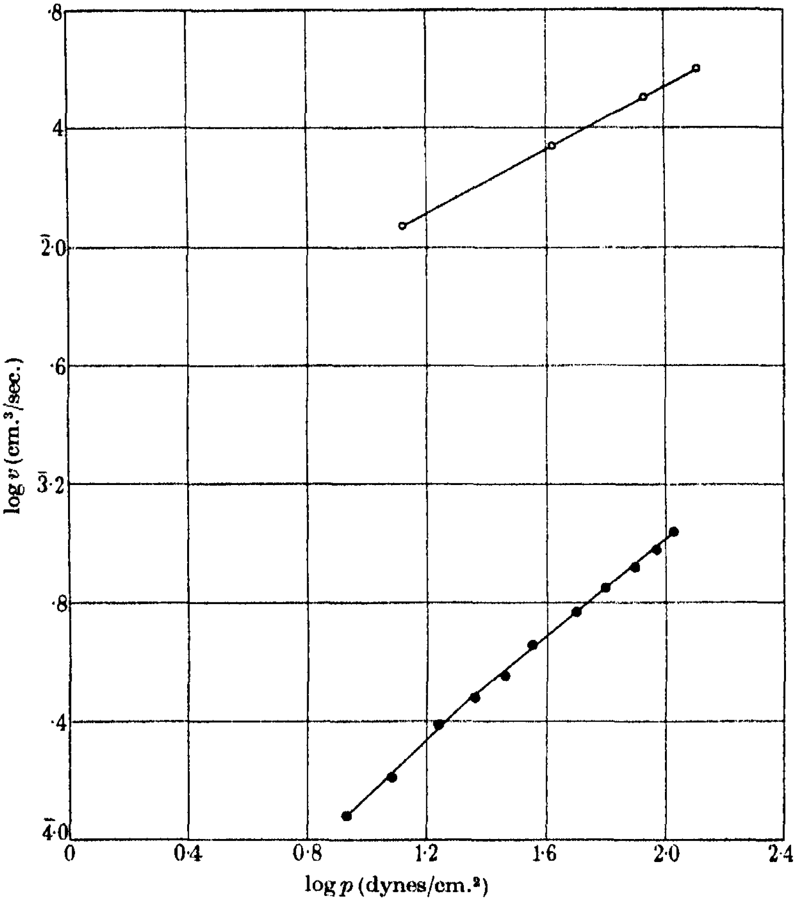

Fig. 11. The velocity-pressure relation for flow through rouge at different temperatures.
⊙ $T = 2{\cdot}177°$ K. ○ $T = 1{\cdot}145°$ K.

The "viscosity" determined by means of the flow through very fine powder is roughly the same as that observed in tube C. The average size of the interstices between the powder particles could not be greater than 10^{-6} cm. which is even smaller than the average width of channel in tube C. Although the type of flow through powder appears to represent a true viscosity, the interpretation of the phenomena of the flow through powder and through the wire-filled tubes still remains obscure.

DISCUSSION

It is obvious that the flow through large single capillaries bears little direct relation to a viscosity as low as 10^{-8} to 10^{-10} c.g.s. units. We must, therefore, look further for an explanation of the observed flow phenomena in larger channels.

The general features of the flow of He II, and particularly the minima observed in the curves in fig. 6, seem to indicate that a certain part of the liquid can flow most easily along the walls of the capillary, and that the velocity is, therefore, higher along the walls than it is in the centre of the channel. That there is a part of the flow proportional to the amount of surface present is shown in fig. 12. There the vol./sec./cm. width of surface is plotted against the radius or the average width of channel. Since the curve does not approach zero for $r = 0$, except at temperatures very close to the λ-point, the intercept on $r = 0$ must represent the liquid transported along the surface of the channel.

From fig. 12 it is evident that, especially at low temperatures and low pressures, the function vol./sec./cm. of surface varies almost linearly with the radius. A large part of the flow, therefore, must be proportional to the area of cross-section of the channel. This is clearly seen from fig. 6, where the velocity (vol./sec./πr^2) is almost independent of the radius for low pressures. Since the amount of liquid actually transported along the surface is small, it is the flow proportional to the cross-section which carries the bulk of the liquid in all sizes of capillary. This may be the reason for the wide variety of values for the viscosity which have been found by previous investigators. Eliminating the surface and cross-section parts of the flow, the remainder was found to vary as a higher power of the radius.

This portion of the flow does not vary exactly as r^4, which would represent a pure viscous term. Nor has any simple empirical formula been found which gives the flow as the sum of surface, cross-section and viscous terms.

It is impossible to give a complete picture of the flow of He II through capillaries from the above data. It is evident, however, that the data cannot be explained by a viscous liquid which slips along the boundary. Such a picture could not give rise to the minima observed in the velocity-radius curves. It must be concluded, that there is a flow of liquid along the boundary of the channel which bears a close resemblance to transfer by supra-surface films. The liquid in the interior is apparently influenced both by the walls of the channel and by the surface flow, since at low pressures the velocity of flow becomes independent of the radius, which indicates that the liquid is dragged along with the surface layer but at a much lower velocity.

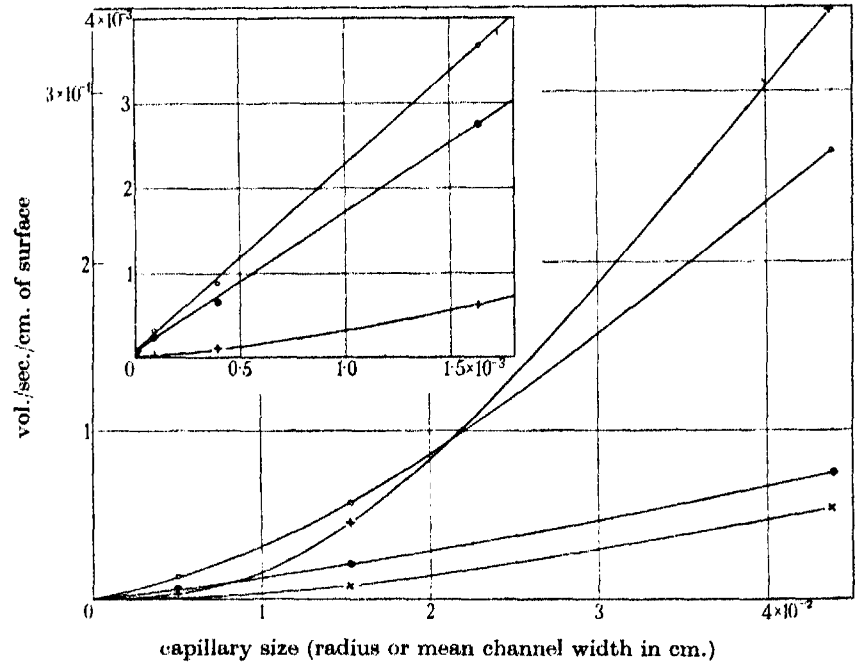

FIG. 12. *The flow as a function of the amount of surface present* in the capillary, for capillaries of different size.

× $T = 2{\cdot}160°$ K, $p = 15$ dynes.
+ $T = 2{\cdot}160°$ K, $p = 160$ dynes.
⊙ $T = 1{\cdot}20°$ K, $p = 15$ dynes.
○ $T = 1{\cdot}20°$ K, $p = 160$ dynes.

It is open to question whether or not the surface layer forms a continuous, coherent film over the whole surface, because the lower velocity in the centre of the channel can only arise from interaction with the walls. If the surface layer were continuous to a depth comparable with that of supra-surface films, i.e. 4×10^{-6} cm., it would be difficult to see how interaction with the walls could occur.

Since the present investigation was concerned with channels no narrower than $1 \cdot 2 \times 10^{-5}$ cm., it is impossible to say how the velocity varies as the channels approach atomic dimensions. It has been observed above, however, that for channels $1 \cdot 2 \times 10^{-5}$ cm. in width, i.e. roughly twice the thickness of supra-surface films, the average velocity in the channels is only two-thirds that for supra-surface films. There is thus an indication of a velocity gradient in the surface layer itself, but further research will be necessary before the nature of the boundary conditions for the flow of He II is completely understood.

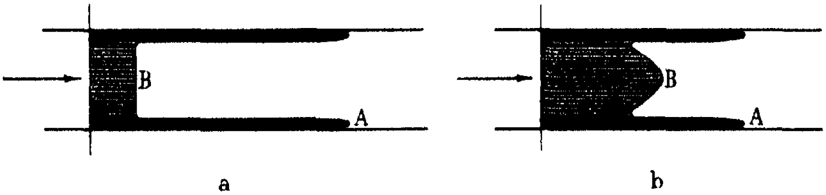

FIG. 13. Probable appearance of the variation of velocity across the diameter of a capillary, (*a*) at low pressure, (*b*) at higher pressure. *A* represents the sub-surface film, whilst *B* represents the bulk liquid in the centre of the capillary.

We might depict the flow of He II in capillaries as in fig. 13. The flow for pressures approaching zero is shown (*a*), where the velocity in the interior of the liquid is independent of the radius. In (*b*), for flow at higher pressures, the viscosity of the liquid would play a greater part and the velocity would show a dependence on both radius and pressure.

An idea of the magnitude and the temperature variation of the viscosity of the liquid when not associated with a boundary can be gained from a consideration of the flow through the largest capillary. The slope $(d \log v / d \log p)$ near the λ-point is 0·8, which is a sufficiently close approximation to the laminar condition of slope unity to justify a calculation of the viscosity from Poiseuille's formula. The value of the coefficient of viscosity so calculated is 8×10^{-5} c.g.s. units which must be, under the circumstances, a lower limit. At 2·3° K in He I, η has been found to be $2 \cdot 7 \times 10^{-4}$ c.g.s. units by Wilhelm, Misener and Clarke (1935*a*). It is conceivable, therefore, that there is no discontinuity of viscosity between He I and He II at the λ-point. This is further borne out by Burton (1938), who found no difference in the rate of flow as the λ-point was passed, for flow through a capillary 0·3 mm. diameter and 3 cm. in length. The temperature variation of viscosity of He II can also be estimated. Since the velocity in the largest tubes decreased with decreasing temperature, the viscosity must, therefore, increase with decreasing temperature. Furthermore, the increase of viscosity must be even greater than is indicated by the observed change of velocity, since the influence of the surface layer would tend to increase the velocity at lower temperatures. Such a temperature variation of the coefficient of viscosity would also explain the temperature variation of velocity in the shortest capillary (Table III), where the influence of the surface layer would be small. One might expect, therefore, the viscosity of He II to increase by a factor of two or three between the λ-point and 1·15° K. Since the velocity of flow both of the surface layer and of the liquid in the largest capillary tend to approach a constant value below 1·5° K, it must be inferred that the viscosity attains a more or less constant value at that temperature. Such great similarity has been observed between the flow in the narrowest channels and in supra-surface films, that it might be assumed that the two phenomena are really the same. The mobile surface layer inside the liquid might therefore be called a subsurface film.

The phenomenon of pressure independent flow in surface films has not so far received an adequate explanation. The velocity of transfer also appears to be independent of the nature of the surface and of the length of path as well, both from our experiments and from those of Daunt and Mendelssohn (1939*a*). The velocity appears to be characteristic for any given temperature of He II. Under certain conditions, however, the rate of pressure independent flow can be affected. If the flow is from a very narrow reservoir and the amount of surface on which the flow takes place is very great, the transfer velocity is reduced; that is, the transfer velocity is dependent on the surface area of the liquid in the reservoir. The reduction in velocity under these circumstances appears to be caused by a restriction on the rate of escape of heat generated by the flow. The magnitude of the reduction varies greatly with temperature, it is small at 1·2° K but rises at higher temperatures and becomes indefinitely large at the λ-point. Such effects have been observed both in the wire-filled tubes and in an experiment where the transfer by supra-surface films was greatly increased by hanging a large bundle of very fine wires over the rim of a reservoir. In the latter case the reduction in velocity caused by a ten-fold reduction in the reservoir cross-section was as much as a factor of six at a temperature near the λ-point. A detailed description of these experiments will be given in a later paper together with a description of other experiments carried out to investigate thermal effects* associated with the flow of He II.

---

* Daunt and Mendelssohn (1939*b*) have recently observed the inverse process of the "fountain effect" (Allen and Jones 1938). They have observed the production of a temperature difference between the ends of a channel through which He II is flowing.

The effect on the velocity of flow in narrow channels due to the dimensions of the reservoir probably accounts for the second minimum in the velocity radius curves found at $r = 5 \times 10^{-4}$ cm. and shown in fig. 6. Recent measurements on tube A showed that an increase by a factor of six in the cross-section of the reservoir produced an increase of approximately 15 % in the velocity of flow through the tube at 1·2° K. By using sufficiently large reservoirs on the wire-filled tubes, therefore, the second minimum in the velocity-radius curves might be made to disappear.

The errors involved in the flow measurements are rather great. The large rate of evaporation of the helium bath (approximately 1 cm.^{3}/min.), which has not been corrected for, produced an error probably as high as 5 or 10 % for some of the intermediate sizes of capillary, particularly when the bath temperature was near the λ-point. Unsteadiness of the bath temperature also undoubtedly produced a certain amount of error. The effect of the dimensions of the reservoir on the rate of flow in the wire-filled tubes adds a further uncertainty to the measurements. It is difficult, in view of the many variables involved, to see how any method for the determination of the viscosity of He II could give an absolute value to within 50 %.

The observations and deductions given above, however, might help to explain the variation in the determinations of the coefficient of viscosity which have been made by different methods. Our results are in general agreement with those of Burton at temperatures close to the λ-point. The turbulent flow and the low viscosity (less than 5×10^{-9} c.g.s. units) observed by Kapitza (1938) might be explained as partly due to end-effect, since the radial flow channel which he used was only 1 cm. in length, and partly due to the subsurface film. The oscillating disk method of MacWood (1938) might be expected to be influenced both by the subsurface film and the bulk liquid, which would explain the intermediate range for 3×10^{-5} c.g.s. units near the λ-point to 2×10^{-6} c.g.s. units at 1·2° K, which he observed. The recent flow measurements on He II by Giauque *et al.* (1939), which gave values for the viscosity between those of Kapitza and MacWood, are more difficult to assess as the method that was employed involved the simultaneous flow of both He II and vapour in the measuring channel.

The authors desire to express their thanks to Dr J. D. Cockcroft and to Dr H. Jones for many helpful discussions during the course of the research and to Dr J. Reekie for his kind assistance in taking measurements during the latter part of the research. The authors' thanks are also due to the Royal Commission for the Exhibition of 1851, who have made this work possible for one of us (A. D. M.).

SUMMARY

By measuring the flow through capillaries and through fine powder, the hydrodynamic properties of liquid He II have been investigated. Capillary channels varying from 1 mm. to 1×10^{-5} cm. in diameter were used. The flow through capillaries was found to bear no relationship to ordinary laminar or turbulent flow, although the latter conditions were approached for large capillaries at temperatures close to the λ-point. The effect upon the flow of length of channel was investigated with capillaries varying in length from 40 cm. to 1 mm. Classical hydrodynamic flow was observed only in the shortest capillary which corresponded essentially to an orifice. The flow through powder (tightly packed jewellers' rouge) gave results which could be interpreted according to classical hydrodynamics over the whole experimental temperature range in He II, from the λ-point down to 1·15° K.

The main features of the flow of He II may be summarized as follows:

(1) The dependence of the velocity of flow on pressure became less
  (*a*) as the radius of the capillary was reduced, or
  (*b*) as the capillary was lengthened, or
  (*c*) as the temperature was lowered.

(2) In the largest capillaries at a temperature close to the λ-point, an approximation to laminar conditions of flow was observed.

(3) In all capillaries at low pressures, the velocity increased with decreasing temperature, but the reverse held at higher pressures in large capillaries.

(4) At all temperatures there was a minimum in the relation between the radius of the channel and the velocity at constant pressure. For channels smaller than 5×10^{-4} cm. in width, the velocity increased rapidly with decreasing channel size.

(5) At pressures above 50 dynes/cm.^{2} in the narrowest channels, the velocity was completely independent of pressure at all temperatures. The curve between the pressure-independent velocity and the temperature bears a strong resemblance both in magnitude and shape to that for mobile surface films of He II above the hydrostatic surface of the liquid.

(6) In channels less than 10^{-3} cm. in width, at temperatures close to the λ-point, and at low pressures, the flow became laminar with evidence of an exceedingly small viscosity.

(7) For flow through tightly packed fine powder, the observed viscosity appeared equal in magnitude and temperature variation to that observed in the narrowest smooth channels.

The results have been interpreted in terms of two types of flow occurring together in the liquid; one, a surface flow along the walls of the capillary, in which the velocity is independent of the pressure. The other, predominant in large capillaries, has a viscosity of the order of 10^{-4} c.g.s. units which increases with decreasing temperature, and has a value just below the λ-point probably not much different from that of He I.

REFERENCES

Allen, J. F. and Jones, H. 1938 *Nature, Lond.*, **141**, 243.
Allen, J. F. and Misener, A. D. 1938*a* *Nature, Lond.*, **141**, 75.
— — 1938*b* *Nature, Lond.*, **142**, 643.
Burton, E. F. 1935*b* *Nature, Lond.*, **135**, 265.
— 1938 *Nature, Lond.*, **142**, 72.
Daunt, J. G. and Mendelssohn, K. 1938 *Nature, Lond.*, **141**, 911.
— — 1939*a* *Proc. Roy. Soc.* A, **170**, 423.
— — 1939*b* *Nature, Lond.*, **143**, 719.
Giauque, W. F., Stout, J. W. and Barieau, R. E. 1938 *Phys. Rev.* **54**, 146.
— — — 1939 *J. Amer. Chem. Soc.* **61**, 654.
Kapitza, P. 1938 *Nature, Lond.*, **141**, 74.
MacWood, G. E. 1938 *Physica*, **5**, 737.
Wilhelm, J. O., Misener, A. D. and Clarke, A. R. 1935*a* *Proc. Roy. Soc.* A, **151**, 342.

Luminescence of mercury vapour along an α-ray pencil, and transfer of nitrogen excitation to mercury

By A. Luyckx*

(*Communicated by Lord Rayleigh, F.R.S.—Received* 3 *April* 1939)

[Plates 20, 21]

When α-rays from a small glass bulb with thin walls containing radon irradiate a gas, there is no observable increase of the faint luminescence emitted by the radon bulb in vacuum. This glow is only visible in a dark room; and the bulb contours can be clearly seen by direct observation or on the photographic plate. In special conditions a mixture of nitrogen and mercury vapour irradiated by α-rays emits a relatively intense green glow, which completely masks the contours of the bulb and can be easily photographed and even studied spectrographically. In this paper I describe the phenomena observed and try to show the analogy of the glow with the "wing effect" of Lord Rayleigh (1929–1934) in the fluorescence of optically excited mercury.

Mercury vapour luminescence at room temperature

A horizontal pyrex tube of diameter 2 cm. and length 30 cm. contains at one end iron oxide, Fe_3O_4, at the other end a radon bulb and a drop of mercury. A good vacuum is made in this tube. During the pumping, the iron oxide is warmed to a red heat; precautions are taken to keep the radon bulb end cool. After 2 hr. pumping some 50 cm. of nitrogen are introduced into this tube. The tube is closed by a stopcock and detached. It is inclined and tapped till the rays reach the iron oxide. After some time the green glow appears, sufficiently intense to be seen when the tube is protected against direct light.

Fig. 1 (Plate 20) shows two bulbs of radon placed in a pyrex tube. No volume luminosity is visible, though the contours of the bulbs can be seen. The presence of air has quenched the glow. The time of exposure was 27 hr.

Fig. 2 (Plate 20) shows the luminescence phenomenon under consideration. The only difference between figs. 1 and 2 is that in the latter the nitrogen is pure. One cannot even guess where the bulbs are. In the absence of

---

* Associé du Fonds National Belge de la Recherche Scientifique.

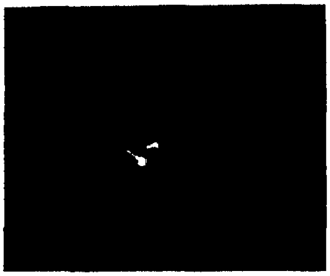

Fig. 1. With Fe_3O_4 and air.

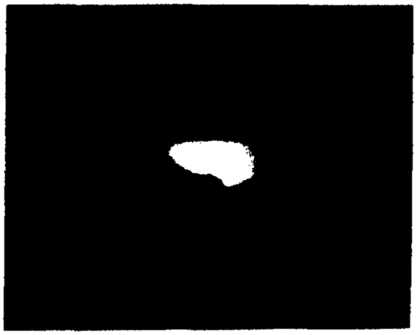

Fig. 2. With Fe_3O_4 and N_2.

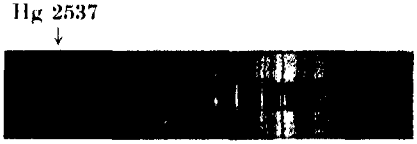

Fig. 3. Spectrum I, without oxide, $N_2 + \alpha$ part.

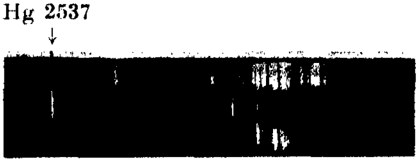

Fig. 4. Spectrum II, with oxide.

Fig. 5. Spectrum III.

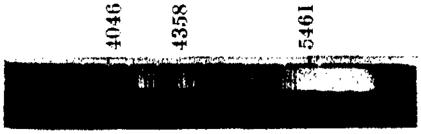

Fig. 6. Spectrum IV, with oxide and N_2 visible.

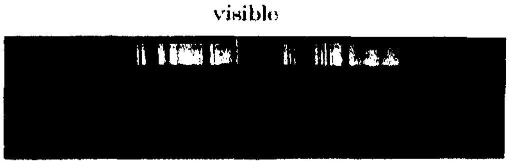

Fig. 7. Spectrum V, without oxide, with N_2.

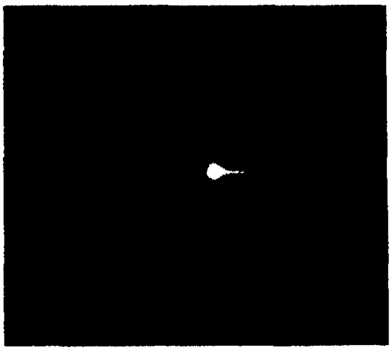

Fig. 9

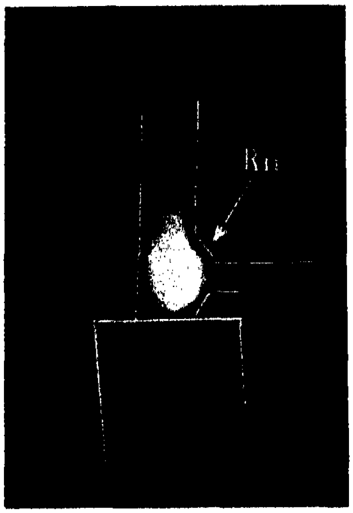

Fig. 10

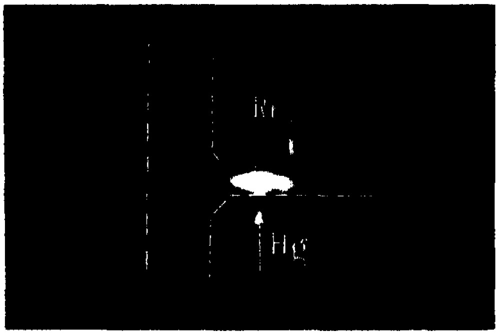

Fig. 11

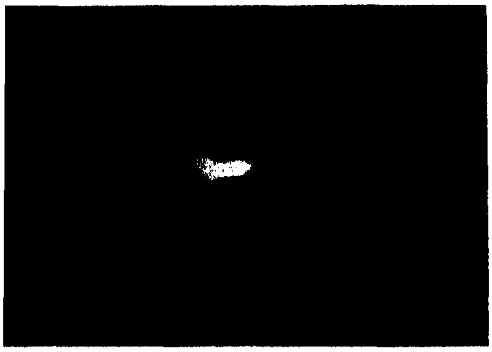

Fig. 12

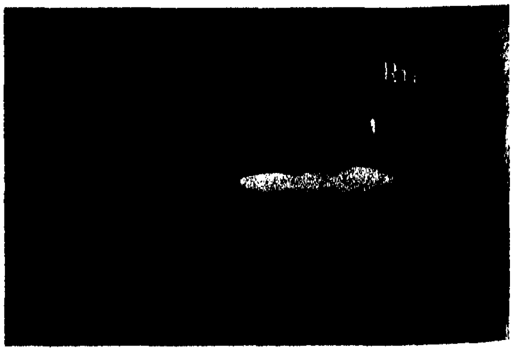

Fig. 13

nitrogen or iron oxide no glow could be seen and fig. 1 was obtained. The quantity of radon in the bulbs was generally about 50 millicuries, but the glow is visible even with bulbs of less than 3 millicuries. The luminosity appears only in the regions irradiated by α-rays and when the iron oxide is reached by the α-rays. The walls of the radon bulb are thin enough to allow the α-particles transmitted to have a range of about 3 cm. in nitrogen at atmospheric pressure. Increase of pressure intensifies the glow but contracts the luminescent region owing to the diminished range of the α-rays. The glow becomes brighter by increasing the temperature. I shall not here discuss the mechanism by which the iron oxide promotes the production of the luminescence but I shall assume provisionally that it produces in the tube a supersaturated mercury vapour.

EMISSION SPECTRUM EXCITED BY α-RAYS

The first two spectra show that the green glow was accompanied by an increase in intensity of the resonance line 2537 A. Tests made by varying the time of exposure showed that this line was about 30 times more intense in presence of iron oxide. The spectrum in fig. 3 (Plate 20), which shows the nitrogen bands, was described elsewhere (Luyckx 1937) and was taken with α-ray irradiation in the absence of iron oxide. No glow was visible. The exposure time was 22 hr. The spectrum of fig. 4 (Plate 20) was taken when the green glow was emitted. The 2537 A line is much more intense. The time exposure was 11 hr., and the bulb was three days older than for fig. 3. In a spectrogram not given here the resonance line is about twice as intense after 70 min. exposure, when the green glow is emitted, as after 16 hr. of exposure when the glow is absent. For the spectrum in fig. 5 (Plate 20) a Hilger spectrograph was used to compare the resonance line excited by α-rays with the same line excited by a mercury lamp.

The visible mercury triplet 5461, 4358, 4046 and a continuum having a maximum at about 4800 appear only when the luminescence is emitted (see fig. 6, Plate 20). These lines and continuum are absent in the spectrum *V* shown in fig. 7 (Plate 20) which was taken when iron oxide was not present; no glow was visible.

α-RAY EXCITED LUMINESCENCE IN DISTILLING MERCURY

The presence of iron oxide introduces a complication, which we were able to avoid after many attempts, in the following conditions.

The radon bulb (fig. 8) may be placed in different positions in b', b'' or b''' by means of an electromagnet. Mercury is warmed in A. The apparatus is of pyrex and warmed during the pumping. When a good vacuum is obtained stopcock R is turned. No glow can be seen, the contours of the bulb remain clear even when the oven F is red hot and the whole apparatus warmed with a flame (fig. 9, Plate 21).

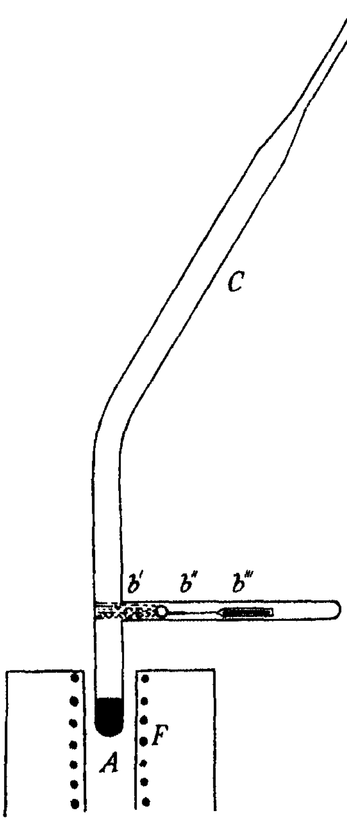

FIG. 8. Apparatus.

The green luminescence of mercury appears only when nitrogen is introduced into the tube. With 2 mm. of nitrogen the glow appears, it increases, and becomes very intense with some centimetres of nitrogen (see fig. 10, Plate 21); $p(N_2) = 10$ mm., exposure $t = 15$ min. The radon bulb is placed in the distilling stream. In fig. 11 (Plate 21) the bulb is in b' and is indicated by the arrow Rn; $p(N_2) = 30$ mm., $t = 20$ min. The most brilliant region is not that immediately surrounding the bulb. The lateral tube being cooler than the central tube, mercury vapour condenses in the entrance of this lateral tube and it is the irradiation by the α-rays of this region which is the most brilliant. In fig. 12 (Plate 21), the bulb is in b'', $p(N_2) = 20$ mm., $t = 12$ min. In fig. 13 (Plate 21), the bulb is in b'''; $p(N_2) = 10$ mm., $t = 120$ min. The luminescence of the α-ray pencil is visible in figs. 11 and 13 (Plate 21).

Spectroscopic observation shows the lines 5461 and 4358 and between them a brilliant green continuum having a maximum at about 4800 A. The apparatus not being in silica, the research of the 3300 band or the other series was not possible.

THE "WING EFFECT" OF LORD RAYLEIGH AND THE α-RAY EXCITED LUMINESCENCE

R. W. Wood (1936) found that the emission of the ultra-violet resonance light of mercury vapour was accompanied by a green light when nitrogen at a pressure of 2 mm. was introduced in the resonance tube. Phillips (1913) excited distilling mercury by the resonance line 2537 and observed a green fluorescence carried by the moving stream. Lord Rayleigh (1929, etc.) distinguished the "core effect" resonance excited by the core of the 2537 line and the "wing effect" fluorescence excited by a hot mercury lamp or an iron arc. From the comparison of their three principal characters we shall try to show the similitudes of the phenomena that we observed with fluorescence excited by ultra-violet lines, especially with the "wing effect", and deduce some information as to the mechanism of its excitation.

(i) *Spectra.* The fluorescence spectra consist principally of a continuum having a maximum at 4850 A, a continuum having a maximum at 3300 A; the visible triplet 5461, 4358 and 4046, the 2537 A, the "wing" and "core" series. In the emission spectra of mercury vapour excited by α-rays we find:

In the 4850 A (or 4880 A) continuum, emitted at room temperature in presence of iron oxide (fig. 6, Plate 20) or in boiling mercury, the triplet 5461, 4358, 4046 and the resonance line 2537 A.

The 3300 A continuum is much less intense in the "wing effect" spectrum without superheating. In our case we did not find this continuum nor the Rayleigh and Woods series which need probably a stronger emanation bulb and longer exposure.

(ii) *Survivance of luminescence to hydrogen action.* It is known that this gas quenches the resonance phenomena excited by the resonance line 2537.

P. Pringsheim and A. Terenin (1928), exciting mercury vapour with a hot mercury lamp or an aluminium spark, found that complete extinction occurred with a pressure of 10^{-4} mm. of hydrogen. Lord Rayleigh confirmed this quenching effect of hydrogen but only for the "core effect". He found that the "wing effect" survives very large additions of hydrogen.

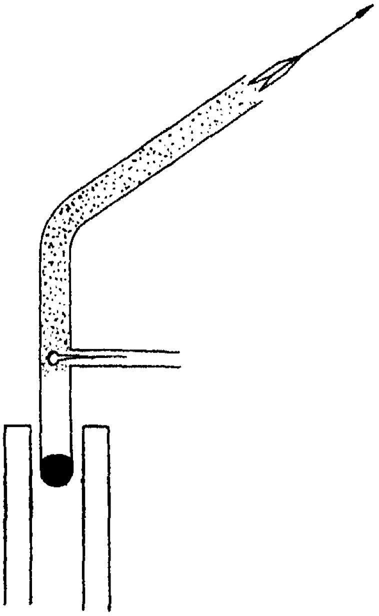

Fig. 14

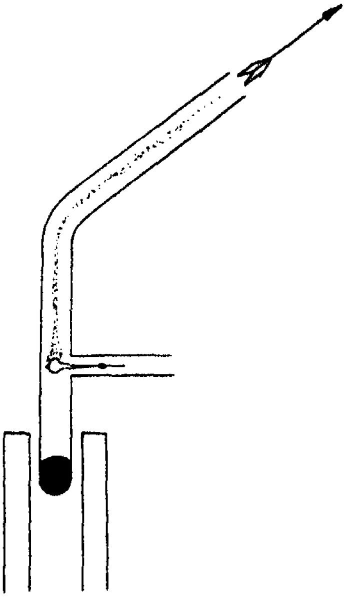

Fig. 15

We found also that the green luminescence excited by α-rays is not quenched by large quantities of hydrogen, while traces of air quenched the glow. This was investigated in the distilling apparatus of fig. 8. Hydrogen has only a diluting effect not comparable to the poisoning effect of air. At room temperatures in presence of iron oxide the glow is very brilliant even when radon and iron oxide are mixed with 20 cm. of hydrogen and 20 cm. of nitrogen. It was in an experiment of this kind that the glow was first observed in the neighbourhood of the magnetic oxide. On shaking, the luminosity spread throughout the whole tube and became brighter.

(iii) *Persistence of the luminescence.* In figs. 11 and 13 (Plate 21) the limits of the α-ray pencil are well marked; it is not easy to guess the direction of the distilling stream, in an atmosphere of nitrogen at constant pressure of about 20 cm. Let us consider the experiment relative to the bulb placed in the axis of the distilling stream (fig. 14). If the stopcock *R* is opened the luminescent region surrounding the bulb moves upwards and is still visible more than 15 cm. after the bending of the tube, which stops every α-ray.

Sometimes with lower pressures of nitrogen, instead of a moving luminescent column a thin luminous streamlet rises from the bulb as shown in fig. 15 and follows the axis of the tube in *C*. At room temperature and in presence of iron oxide, at a pressure of 40 cm. the absence of an after-glow was proved by the following method. A system of metallic screens are fixed as shown in fig. 16 by the wires *f*. In a dark room the α-ray pencils which pass between the screens are easily visible when nitrogen is present and iron oxide spread over the screens. Delicate taps on the apparatus make the screens vibrate and the α-ray pencils oscillate. If there was an appreciable after-glow of $\frac{1}{2}$ sec. duration, the oscillation of the α-pencils would have as a consequence to broaden them and to contract the dark intervals *i*. The limits of the pencils would no longer be clear when the screens are vibrating. This preliminary experiment showed that no after-glow of the order of $\frac{1}{2}$ sec. was visible. The limits of the pencils remained always clear.

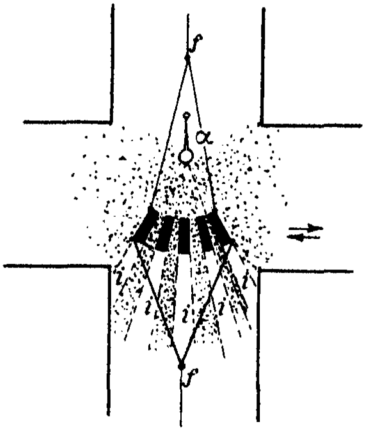

FIG. 16

Is it the nitrogen or the mercury which carries the energy in the persistent phenomena previously described? To answer this question the following experiment was made, fig. 17. Mercury distilling in the lateral tube *D* is irradiated by α-rays in *A*. The pressure of nitrogen is of a few centimetres. We expected that the glow would begin in *A* and spread towards *X* owing to diffusion of the nitrogen activated in *A*. In fact the glow *X* was seen but between *A* and *X* there was a dark space which complicated the interpretation. By interposing a screen *E* of aluminium or lead as shown in fig. 17 the intensity of this glow increased about tenfold. The experiment was reproducible, nothing else being changed. When distillation occurs at a lower temperature the luminescence *X* disappears; with the interposition of the aluminium screen, the luminescence *X* appears again. This green glow is less intense than the *A* luminescence excited by direct α-ray bombardment. An exposure of 15 min. gave nothing on the plate. This phenomenon is probably due to secondary γ-rays.

Other experiments were made to decide whether it is nitrogen or mercury which carries the excitation, but no positive result was found.

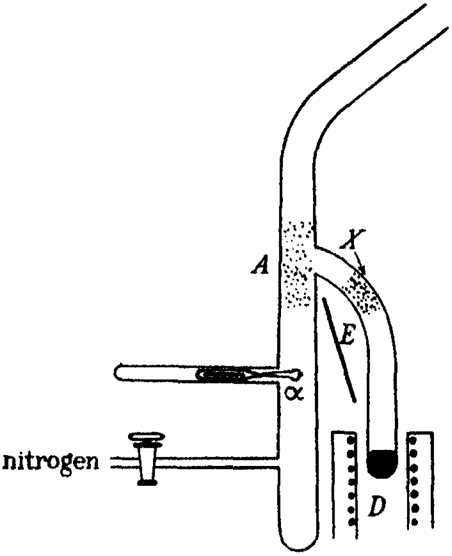

FIG. 17

DISCUSSION. LUMINESCENCE OF DIATOMIC MERCURY

I have shown that optically excited mercury fluorescence phenomena and α-ray excited luminescence present incontestable similarities. The primary process of excitation is however essentially different in these two cases.

When fluorescence is excited by the core of the resonance line, the mercury atom absorbs the radiant energy and the electron is carried from the inner or $6\,^1S_0$ orbit to the $6\,^3P_1$ orbit. The resonance radiation results from the return of the electron to the inner orbit.

It is also by an atomic mechanism that an explanation was found for the fact that in the triplet (5461, 4358, 4046) the relative intensities of the lines increase from 4 : 2 : 1 to 128 : 32 : 4 by the addition of a few millimetres of nitrogen. This increase of intensity is due to collisions of excited mercury with nitrogen molecules which bring about a transfer of $6\,^3P_1$ atoms to the metastable state $6\,^3P_0$ of longer life and greater chance to absorb the 4046 line. In these collisions nitrogen molecules gain 0·2 V of vibrational energy.

Lord Rayleigh proved by direct experiments the presence of metastable atoms $6\,^3P_2$ and $6\,^3P_0$ in the persistent luminosity of the "core effect". In the "wing effect", the primary process consists in absorption of light by diatomic molecules (Rayleigh, *loc. cit.*; Mrozowski 1934, 1937). This interpretation is based principally on the following facts.

(1) "Wing effect" fluorescence is not quenched by hydrogen and it is known that very minute additions of hydrogen destroy excited mercury atoms in the $6\,^3P_1$ or metastable state (Cario and Franck 1922, 1926; Meyer 1926; Pringsheim and Terenin 1928).

(2) Application of the direct method for the detection of metastable atoms or $6\,^3P_1$ atoms gave negative results.

Under the α-ray bombardment the green luminescence appears in an atmosphere of 20 cm. of nitrogen mixed with mercury vapour, while in the absence of nitrogen at the same temperature or at higher temperatures no glow can be seen. The mercury vapour absorbs in these conditions a notable part of the α-particle energy without producing the luminous phenomenon.

We therefore conclude that the mercury luminescence results from the transfer to mercury vapour of the nitrogen excitation by the α-rays. To explain the appearance of the visible triplet (5461, 4358, 4046) one cannot think of a mechanism analogous to the one already mentioned about fluorescence. Such a process involves only mercury atoms and nitrogen molecules. This assumption cannot be admitted, since the indifference of the luminescence to hydrogen action excludes a participation of the atoms in the mechanism of production of the glow.

The nitrogen molecules excited by the α-rays transfer their excitation to diatomic molecules responsible for emission of the 4850 A continuum.

It is known that nitrogen excited by an electrical discharge can carry this activation several metres away by a moving nitrogen stream. The nitrogen can thus be considered as the energy carrier responsible for the persistence phenomena which have been described; α-particles have energy enough to activate nitrogen. No direct proof was however found to confirm this point of view. Similar persistence phenomena have been described by Lord Rayleigh in mercury fluorescence where a direct optical activation of nitrogen was impossible.

Indifference of the luminescence to hydrogen action indicates that only small concentrations, if any, of metastable atoms can be expected to be found in the glow carried away with the moving stream. This could be controlled by the application of Lord Rayleigh's direct method. Complete absence of atoms in the excited state cannot however be deduced from the present experiments; new experimental photometric data would be necessary to distinguish between the dilution effect of hydrogen and a small possible quenching effect. The only indication that a small part of the glow may be due to excited mercury atoms is the presence of the visible triplet in the spectrum of the glow. This triplet is present in all the "core effect" spectra and absent in the "wing effect" glow in which it appears only by superheating.

No definitive mechanism was found to explain how the iron oxide at room temperature promotes the appearance of the mercury luminescence. We think at the present time that the presence of iron oxide is favourable to formation of a mercury explosive nitride. This nitride subsequently is locally decomposed by α-rays and liberates a notable quantity of mercury vapour which condenses in fine droplets floating in the neighbourhood of the bombarded oxide. By illuminating in a quartz tube such a region emitting the green glow, with a hot mercury lamp, a yellow light appeared. We shall give elsewhere the details of experiments which have been made in this direction. Let us mention here that the formation of iron and mercury nitrides was revealed chemically and that a very intense glow was found when previous nitrification by active nitrogen of the iron oxide occurred. In this first work the luminescence observed at room temperatures and in distilling mercury were considered provisionally as the same phenomenon.

I wish to express my thanks to Professor W. Mund who gave me a laboratory and facilities to make these experiments and Professor M. de Hemptinne who lent me quartz lenses.

SUMMARY

It is shown that mercury vapour luminescence phenomena, similar to the optically excited fluorescence phenomena, can be excited by α-rays excitation in presence of nitrogen.

The green luminescence renders visible an α-ray pencil by light emission; this new method is quite different from the well-known expansion method of C. T. R. Wilson. However in this case no individual track was seen.

The emission spectrum of this luminescence consists of a visible mercury triplet (5461, 4358, 4046), a continuum having a maximum near 4850 A and the resonance line 2537 A.

Persistent phenomena were observed. The spectra and persistent phenomena are similar to the fluorescent phenomena.

No luminescence can be seen in the absence of nitrogen. In a primary process the α-rays excite nitrogen molecules which transfer their energy to mercury by collisions of the second kind.

The green luminescence is extinguished by small quantities of air, while hydrogen has no quenching effect.

This survivance of the glow to the addition of large quantities of hydrogen brought us to assume that this luminescence is a sort of "wing effect" due to the transfer to diatomic mercury molecules of the energy of the nitrogen molecules excited by α-rays.

REFERENCES

Cario and Frank 1922 *Z. Phys.* **11**, 161.
— — 1926 *Z. Phys.* **37**, 61.
Luyckx 1937 *Nature, Lond.*, **139**, 672.
Meyer 1926 *Z. Phys.* **37**, 639.
Mrozowski 1934 *Z. Phys.* **87**, 340.
— 1937 *Z. Phys.* **106**, 458.
Phillips 1913 *Proc. Roy. Soc.* A, **89**, 39.
Pringsheim and Terenin 1928 *Z. Phys.* **47**, 330.
Rayleigh 1929 *Proc. Roy. Soc.* A, **122**, 22.
— 1931 *Proc. Roy. Soc.* A, **125**, 650.
— 1932*a* *Proc. Roy. Soc.* A, **135**, 617.
— 1932*b* *Proc. Roy. Soc.* A, **137**, 110.
— 1933 *Proc. Roy. Soc.* A, **139**, 507.
— 1934 *Proc. Roy. Soc.* A, **143**, 280.
Wood 1936 *Physical optics.*

Dielectric loss due to polar molecules in solid paraffin wax

By D. R. Pelmore

(*Communicated by E. V. Appleton, F.R.S.—Received* 27 *April* 1939)

Introduction

According to most theories of dielectric loss the maximum rate of change of dielectric constant and the maximum value of the specific energy loss per unit volume occur at an angular frequency ω ($= 2\pi\nu$) which is the inverse of a quantity τ known as the relaxation time of the dielectric.

The relaxation time is the time required for the polarization of the dielectric to revert to $1/\epsilon$ of its value after the removal of the applied electric field: and this is a quantity which can be determined experimentally.

According to Debye's theory of polar molecules, part of the dielectric polarization is due to the orientation of the dipoles in line with the applied field and the relaxation time is related closely to the time taken for the molecules to revert to their random positions after removal of the field.

On the assumption that Stokes' law is applicable to the polar molecules, it can be shown that

$$\tau = \frac{4\pi\eta a^3}{kT}, \tag{1}$$

where a = molecular radius, η = coefficient of viscosity, k = Boltzmann's constant.

Thus from the experimentally determined values of τ at any temperature we can obtain values for the molecular radii of the rotating molecules in terms of the viscosity. The method has in fact been used for the estimation of molecular weights of substances in solution: thus Bridgeman (1938) finds that the molecular weights of zein, gliadin, haemoglobin, etc., deduced from dielectric measurements on the solutions in benzene, are in agreement with the values obtained from other methods.

Debye's theory was based on assumptions which are really valid only for gases and dilute solutions of polar substances in non-polar solvents, but the work of recent experimenters has shown that the theory is also able to explain the observed dielectric properties of many solids.

Thus Jackson (1935*b*) showed that the dielectric relaxation time of a chlorinated diphenyl was proportional to the macroscopic viscosity over a wide range of temperature and that a change of state from a brittle glass to a mobile liquid did not alter the form of the curves of the dielectric loss as a function of temperature. Jackson (1935*a*) also found that the behaviour of cetyl palmitate (spermaceti) mixed with solid paraffin wax could be accounted for on the assumption that the power loss was due to the rotation of the polar molecules (or part of them) and that the system had the characteristics of a polar liquid. These experiments are still less amenable to interpretation by Debye's analysis, because the paraffin and the ester molecules consist of long, rigid chains of carbon atoms, and it is not permissible to liken such to a sphere. Jackson suggested that the polar group might possibly be capable of rotation in the ester chain and that a rotation of this group did not involve a rigid body rotation of the whole ester molecule. According to this supposition he deduced from Debye's equation (equation 1) that the *internal viscosity* of solid paraffin wax was of the same order as the viscosity of castor oil.

Jackson's experiments were extended by Sillars (1938) who studied the behaviour of a solution consisting of 5% of various normal esters dissolved in the same wax which Jackson had used. Sillars' experiments showed that the relaxation time in this wax depended enormously on the chain length of the ester, thus showing that Jackson's suggestion of free rotation of the polar group was untenable: for if this group could rotate without carrying the whole molecular chain with it, then the length of the chain would have no effect on the relaxation time. Sillars also showed that the relaxation time appropriate to a given chain length did not depend on the position of the polar group in the chain: thus the relaxation time of butyl palmitate was the same as that of ethyl stearate, despite the movement of the polar group from a position in the first at 1/5th of the chain length to 1/10th in the second. The relaxation time increases as the length of the ester chain is increased, but becomes substantially constant when the ester is longer than the paraffin molecule.

This paper describes experiments which are a logical extension of Sillars' work. In the main, it examines how the relaxation time is affected by altering the chain length of the wax in which a given ester is dissolved: in contrast to Sillars who changed the length of the esters dissolved in a given wax.

METHODS AND APPARATUS

The loss angle of a condenser containing the material under test was measured at various temperatures and frequencies: the loss angle of the material was then deduced after subtracting the previously determined loss angle inherent to the circuit, when the condenser did not contain the test specimen. The condenser was identical in size and construction with that used by Sillars, and has been described already (Sillars 1938). At radio frequencies the loss angle of the circuit was determined from the resonance curve obtained by varying a small calibrated condenser connected in parallel with the main condenser. (In Sillars' measurements, the resonance curve was obtained by varying the frequency, the parameters of the test circuit being invariable.)

The loss angle of the material is given by

$$\tan\delta = F = \frac{\Delta C_1 - \Delta C_2}{2C}\,\frac{C}{C - C_S} = \frac{\Delta C_1 - \Delta C_2}{2(C - C_S)},$$

where C = capacity of test condenser as measured by substitution,

C_S = stray capacities in test condenser and leads (i.e. that part of C *which is not due to the solid dielectric),*

ΔC_1 = width of resonance curve at $1/\sqrt{2}$ of its maximum height,

ΔC_2 = the same width when the test condenser contains only air.

The value of C_S/C was less than 10 %.

Experience shows that repeated heating and cooling sometimes alter the capacitance by a detectable amount, indicating that the effective value of C_S has increased slightly. For this reason equation (3) must tend to yield a value for F which is less than it ought to be: Sillars suggests (Sillars 1938, p. 69) that uncertainty from this cause may be as much as -7 %.

A Schering type bridge with Wagner earth was used to measure the loss angle at frequencies up to 25 kc./sec. The methods of preventing condensation and leakage have been described already by Sillars.

Results and discussion

These experiments extend Jackson's work on mixtures of spermaceti with a paraffin wax. For this purpose a number of waxes with different setting point were procured and in all cases the form of the curve relating loss angle and temperature was similar to that found by Jackson, and is described approximately by Debye's equation

$$\tan\delta = \frac{\epsilon_0 - \epsilon_\infty}{\sqrt{(\epsilon_0\epsilon_\infty)}}\,\frac{A\omega\tau}{A^2 + \omega^2\tau^2}, \tag{4}$$

where ϵ_0 is the dielectric constant for static fields,

ϵ_∞ is the dielectric constant for high-frequency fields,

ω is the angular frequency of the alternating field,

τ is the relaxation time of the polar molecules at the relevant temperature.

$$A = \sqrt{\left(\frac{\epsilon_0}{\epsilon_\infty}\right)\left(\frac{\epsilon_\infty + 2}{\epsilon_0 + 2}\right)} \doteqdot 1.$$

It follows from (4) that tan δ is a maximum when $\omega\tau = A$, and in practice the value of A differs very little from unity. When $\omega\tau \ll 1$, the permanent dipoles can rotate freely without appreciable dissipation of energy: when $\omega\tau \gg 1$, the rotation is negligible and hence again the energy loss is very small. In general tan δ is measured as a function of temperature for some constant value of ω. At low temperatures the viscous restraint on the polar molecules is very great, thus making the relaxation time very long: hence $\omega\tau > 1$. At high temperatures this restraint becomes small, and hence $\omega\tau < 1$. It is only for a narrow range of temperature that $1/\tau$ is comparable with ω and within which appreciable power loss takes place.

tan δ has been measured as a function of temperature for several different constant frequencies. Jackson made these measurements on a 57–60° C setting point wax and showed that if a wax of slightly different setting point was used then the curves of tan δ were shifted along the temperature axis by about the same amount as the change in setting point.

In order to obtain more information about the dependence of relaxation time on the nature of the paraffin wax medium, it was thought desirable to use waxes with a wide range of setting point. The writer wishes to take this opportunity of thanking the Burmah Oil Company for presenting the waxes and to members of their Research Department for discussing the problem with him and for supplying the following information about the samples chosen:

(1) Fraction (1) from "Match Wax", s.p. 35·5° C.
(2) Fraction (6) from "Match Wax", s.p. 40·2° C.
(3) Fraction (2) from 130/135° F grade, s.p. 50·0° C.
(4) Fraction (5) from 130/135° F grade, s.p. 55° C.
(5) Fraction (2) from 145/150° F grade, s.p. 59·3° C.

The above samples were obtained by fractional distillation under reduced pressure of the specified commercial grades. They probably consist of mixtures of straight chain normal paraffins, together with some oily impurity.

All these fractions were recrystallized twice from benzene, which removes the oily impurities: in some cases the setting point was slightly higher after recrystallization. Care was taken to remove the last traces of the solvent by passing carbon dioxide for many hours through the molten wax. (*Note*: It is important to avoid heating the wax in the presence of air, because the oxidation products have a deleterious effect on the dielectric properties—see Jackson 1935*a*, p. 201.)

(6) Residue from 125/130° F grade, s.p. 64·3° C.

(7) Residue from 145/150° F grade, s.p. 70·1° C.

Samples (6) and (7) are believed to contain substantial proportions of "iso" (branched chain) paraffins.

(8) Wax from "slop wax distillate", s.p. 70·3° C.

This is believed to consist of normal paraffins and required no further purification.

(9) "Sucker rod wax" no. 2, s.p. 94·4° C.

This wax is the highest setting point paraffin procurable from petroleum. It is not quite pure and probably contains a small amount of oil: further purification, however, is troublesome, because of its small solubility in all ordinary solvents.

In order to obtain a wax having a melting point much lower than can be obtained from petroleum, the writer prepared the synthetic hydrocarbon

(10) *Hexadecane*, m.p. 15·5° C. Made from cetyl alcohol by converting to the iodide and reducing this by means of zinc dust and acetic acid: the product was fractionated under reduced pressure.

The dielectric loss inherent in the hexadecane was measured in the temperature range to be used subsequently in experiments on mixtures of esters with it: it was found that tan δ was too small to measure at room temperature but increased to 0·3 % at $-60°$ C (compare with Jackson's experience, *loc. cit.*, of 0·005 % for 57–60° C wax). This residual loss is probably due to impurities: it is, however, small compared with the maximum values of tan δ (2·1 %) which occur when the wax contains 5 % of spermacete or of ethyl stearate. The value of tan δ appropriate to these two esters was deemed to be the measured value less that found for the hexadecane at the relevant temperature.

Two further synthetic paraffins were kindly made by Mr E. L. Simons:

(11) *Octadecane*, $C_{18}H_{38}$, m.p. 27–28° C. From octadecyl alcohol by the same method as (10).

(12) *Docosane*, $C_{22}H_{46}$, m.p. 44° C. From erucic acid. The ethyl ester was reduced to ethyl behenate with hydrogen using a palladium catalyst and this was then reduced by the Bouveault Blanc method to the alcohol $C_{22}H_{45}OH$, which was then converted to the paraffin as before.

The effect of temperature on the relaxation time of spermaceti in all these waxes can be presented conveniently by plotting log $1/f$ against T_m, where T_m is the temperature at which tan δ is a maximum for frequency f. It will be remembered that at this maximum $\omega\tau = 1$, and hence that

$$\log 1/f = \log 2\pi\tau.$$

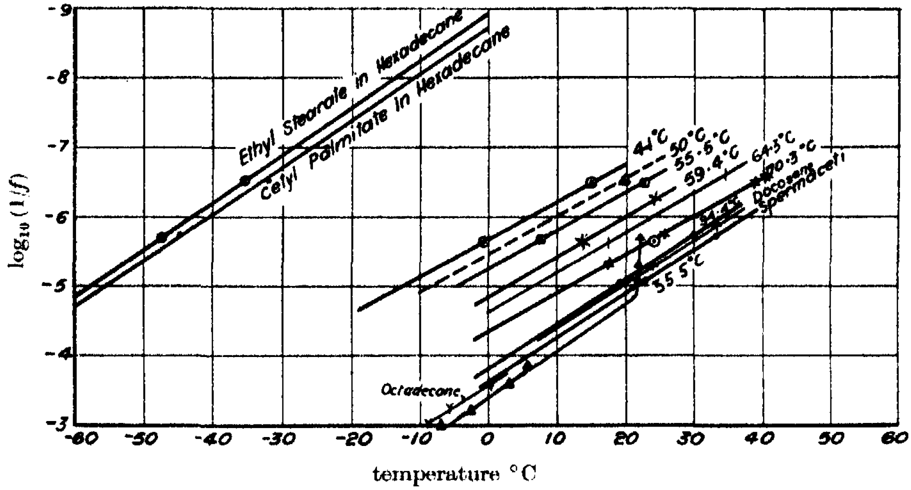

FIG. 1. The temperatures in the figure denote the setting points of the waxes. A different sign is used to denote the points for each wax.

Both Jackson and Sillars found that the relation between log $1/f$ and T_m was linear over a wide range.

This representation for the waxes (1)–(12) is used in fig. 1. Doubtless it will be noticed that each line in fig. 1 is determined from a few points only: since, however, these lines are all sensibly parallel and moreover parallel to those obtained by Sillars (1938, fig. 6) for various esters in a 57–60° C wax, there seemed no doubt that the linear relationship between log $1/f$ and T_m was fulfilled.

The data summarized in fig. 1 enable us to connect T_m (at any constant frequency) and also f_m (at any constant temperature) with the setting point of the wax: this is done in figs. 2 and 3 for $f = 10^5$ cycles/sec. and 0° C respectively. (*Note*: The point in each graph which lies far off the curves refers to a second peak which occurs in the wax of setting point 41° C—see figs. 6 and 8.)

It is interesting to compare these curves with the results of Sillars for a series of esters of different chain length in a wax of setting point 57–60° C. He considered that the ester rotated as a whole about its long axis and found that the relaxation time depended mainly on its chain length and not on the position of the polar group: he plotted T_m as a function of the number of carbon atoms in the ester chain. It is therefore interesting to try to relate the relaxation time of spermaceti with the mean chain length of the wax medium.

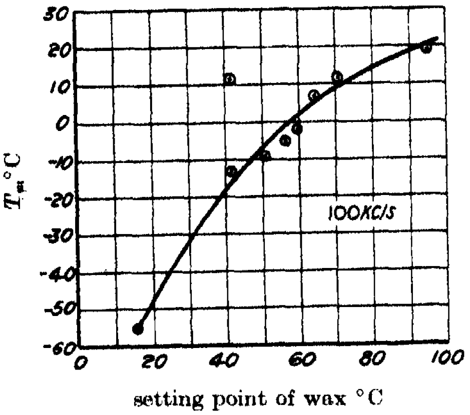

FIG. 2. Spermaceti in paraffin wax. Temperature for maximum tan δ (T_m) and setting point of wax.

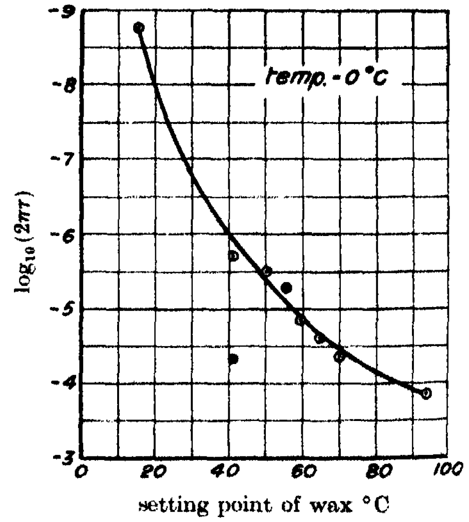

FIG. 3. Spermaceti in paraffin wax. $\log_{10} 2\pi\tau$ and setting point of wax.

As stated previously, there is reason to believe that the waxes 1–5, 8 and 9 consisted mainly of mixtures of normal paraffins. The waxes gave sharp X-ray powder photographs which showed that the principal chain length was approximately that of the pure paraffin having the same setting point. Accordingly, in figs. 4 and 5, T_m and log $2\pi\tau$ respectively are plotted against the number of carbon atoms inferred from the setting point. (The values were read from a curve connecting melting point and number of carbon atoms) (Moullin 1938).

Spermaceti consists mainly of cetyl palmitate ($C_{15}H_{31}COOC_{16}H_{33}$), together with esters of comparable chain length and a small proportion of other high aliphatic compounds. Having regard to Sillars' demonstration that the relaxation time is insensitive to the length of the ester chain provided this exceeds about 30 carbon atoms, it is considered justifiable, for our purpose, to regard spermaceti as though it were homogeneous and of chain length 33 (that is, 32 carbon atoms plus one unit for the oxygen link in the ester group).

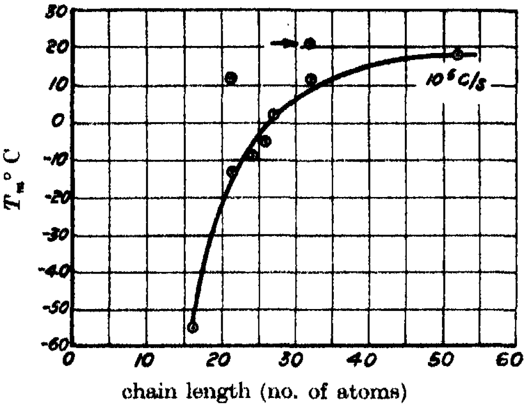

FIG. 4. Spermaceti in paraffin wax. Temperature for maximum tan δ (T_m) and chain length of wax. The point marked thus → refers to spermaceti by itself.

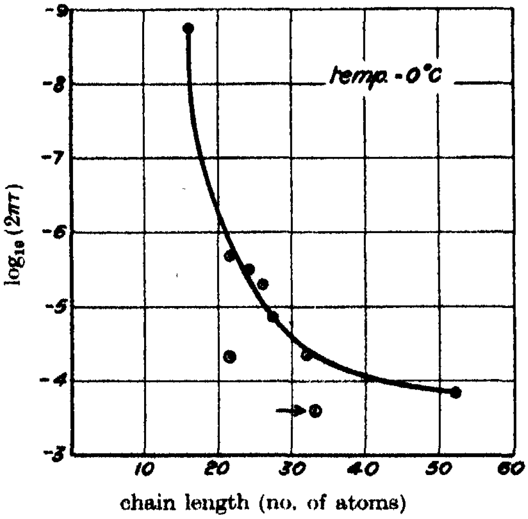

FIG. 5. Spermaceti in paraffin wax. $\log_{10} 2\pi\tau$ and chain length of wax.

We must now attempt to interpret the information contained in figs. 1–5, and in particular that the curves in figs. 2–5 all flatten out for the higher paraffins, whereas the relaxation time in the lower paraffins is sensitive to the setting point, a behaviour which has an exact parallel in the dependence of the relaxation time of a series of esters in a particular paraffin wax (Sillars 1938).

According to Debye's theory of dilute solutions of polar molecules in a non-polar liquid solvent, the relaxation time is given by equation (1), namely,

$$\tau = \frac{4\pi\eta a^3}{kT}. \qquad (1\ bis)$$

In our experiments, as with those of Jackson and of Sillars, it is not possible to assign a value to η: however, the value of ηa^3 deduced from (1) is grotesquely small (even if a^3 is taken as 100 A^3, the volume of HCO_2CH_3, Jackson found that the value deduced for η was of the same order as that of castor oil). It is clear that the Debye theory combined with the strict application of Stokes' law cannot be used directly.

It is clear from the work of Müller and others that in certain circumstances long-chain molecules in the solid state are able to rotate about their long axes. Sillars considers that such rotation might be the cause of power loss in these substances, and the present experiments tend to support this view.

The restriction of this rotation may be of various kinds. Where X-ray examination discloses molecular rotation, the rotation does not occur until the temperature reaches a definite transition point which in general is near the melting point of the solid. Below this transition point the molecules are able to vibrate about one or other of two equivalent equilibrium positions, separated by a potential barrier: the difficulty of surmounting this barrier increases with the length of the molecule. If our systems of esters and paraffins consist of true solid solutions and the ester takes its place in the paraffin lattice, it is possible that the ease of rotation is governed by the length of the ester molecule provided this is less than the length of the wax and is governed by the length of the wax molecule when this is less than the ester. This supposition is supported by consideration of figs. 4 and 5 and also by Sillars' results: this explanation, however, is not necessarily fundamental and moreover it seems unlikely that these systems are true solid solutions.

It is important to know the precise environment of the ester molecules. Jackson assumed that spermaceti formed a solid solution with the wax, because of the similarity in structure. Some subsequent experimental evidence, however, seems to contradict this hypothesis.

The relation between concentration and freezing point was found for spermaceti, butyl stearate and octadecyl palmitate in paraffin wax: the molecular concentrations were plotted against the freezing point and it was found that the points for all three substances lay on the same straight line for concentrations up to 50 %. The molecular weights calculated from the gradient of this line and the cryoscopic constant of the wax (deduced from the latent heat) were found to be in good agreement with the known values. This is taken as evidence that the systems are eutectics although the complete freezing point curves for the binary mixtures show only a slight indication of a eutectic point.

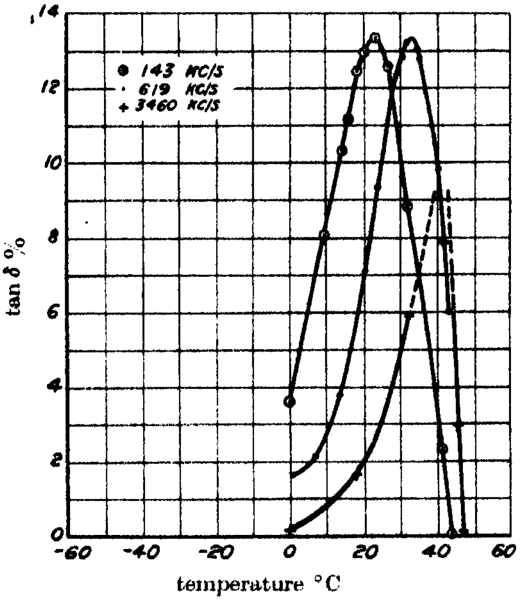

Fig. 6. Spermaceti, m.p. 47° C.

If the mixtures consist of simple solid suspensions then we should expect the effect of the wax would be small and that the relaxation times would differ little from those obtaining in undiluted spermaceti. The dielectric loss characteristics of spermaceti itself were measured and the results are shown in fig. 6. Reference to this will show that the absorption curves are similar to those obtained by Jackson for 5 % of spermaceti in paraffin wax: moreover the magnitude of the absorption shows there is no great departure from the linear relation between concentration and absorption (Jackson 1935*a*, fig. 5). Fig. 1 includes a line for undiluted spermaceti and thus indicates the manner in which the wax matrix modifies the relaxation time. It will be noticed that the absorption curve relevant to a frequency of 3460 kc./sec. in fig. 6 is not symmetrical and that tan δ falls rapidly when the temperature is but a few degrees below the setting point.

These curves for spermaceti in *sucker-rod wax* (s.p. 94° C) are also abnormal in this respect and are therefore shown in fig. 7. It is significant that the temperature at which tan δ falls rapidly to zero is the same in both figures in spite of the high setting point in the latter case; this suggests that the spermaceti is present as a suspension in the sucker-rod wax and not in true solution.

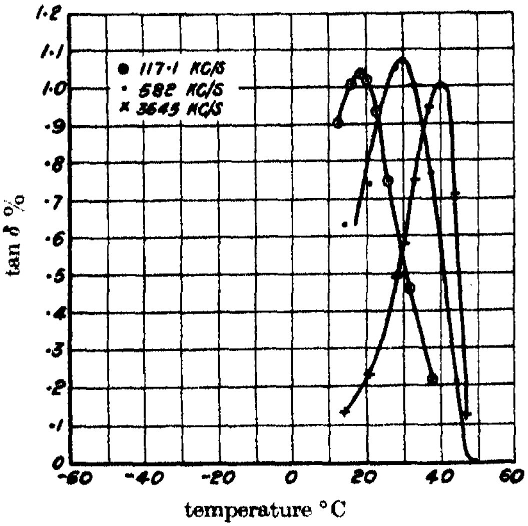

FIG. 7. 8·28 % spermaceti in sucker rod wax, s.p. 94° C.

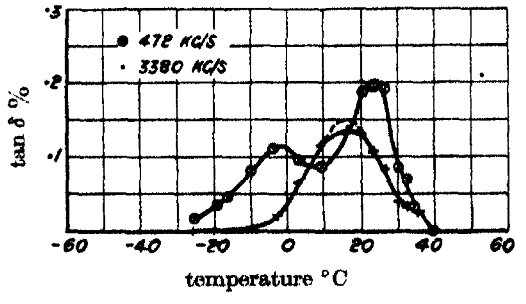

FIG. 8. 4·68 % spermaceti in paraffin wax, s.p. 41° C.

An abnormal absorption curve is shown in fig. 8 and relates to the behaviour of spermaceti in a wax of setting point 41° C: here the curve has two maxima disclosing two possible relaxation times, which probably correspond to two different environments of the polar molecules. (*Note*: Compare Sillars' experience of two relaxation times for an impure sample of butyl stearate—see Sillars 1938, figs. 4, 5 and 8.) It can be seen from fig. 2 that the lower value of T_m is the one appropriate to a setting point of 41° C, whereas the higher value of T_m is appropriate to a setting point of 70° C.

The behaviour of spermaceti in the wax of s.p. 35·5° C was normal in respect of the shape of the absorption curves but the relaxation times (fig. 1) are longer than in any other waxes and even longer than for spermaceti itself. When the temperature reaches 22° C the relaxation time changes very rapidly with temperature, although the mixture is still solid, a behaviour which seems to be entirely analogous with the observation in a number of aliphatic compounds in which molecular rotation suddenly becomes possible at temperatures a little below the m.p. (for example, see Müller 1937).

The behaviour in the synthetic paraffins octadecane (m.p. 27° C) and docosane (m.p. 44° C) was similar to that in the natural wax of s.p. 35·5° C: it can be seen from fig. 1 that the relaxation times in these paraffins are not greatly different from those in the spermaceti alone.

The absorption curves for the mixture with docosane show a sharp cut off at about 36° C corresponding closely with the transition point of the wax.

The mixtures with the wax samples (6) and (7), which are believed to contain *iso*paraffins, gave normal absorption curves and the relaxation times correspond closely with the setting points. Thus the line marked 64·3° C in fig. 1 is due to sample (6) and the point marked * on the line marked 70·3° C is due to sample (7) which also sets at 70° C but is believed to contain branched chains: the extent of chain branching in these waxes is not known, and it is not possible to infer the principal chain length from the setting point.

All the mixtures not specifically mentioned gave absorption curves exactly similar to those found by Jackson and the points in fig. 1 give the regions of temperature and frequency for which the loss angle is a maximum.

It has been suggested earlier that the dielectric relaxation times of paraffin wax media might depend upon the chain length of the polar and non-polar molecules, whichever is the shorter. Against this hypothesis it has been pointed out that the paraffin wax ester systems appear to be simple solid suspensions and not true solid solutions. That the points for spermaceti itself in figs. 4–5 do not lie on the curves drawn through the other points shows that the chain length is certainly not the only factor: in spermaceti itself the relaxation time is longer than in the wax-ester systems at the same temperature, showing that there is more resistance to molecular rotation.

The points relating to mixtures of spermaceti with octadecane, docosane and the natural wax of s.p. 35·5° C have not been included in figs. 2–5 because it is clear from fig. 1 that these mixtures behaved very differently to all others. Fig. 1 may be interpreted as showing that in general there are two possibilities for the relaxation time in a wax-spermaceti system: either it will be substantially independent of the wax and the same as in undiluted spermaceti or else it will have a value given by curves 2–5.

The samples of octadecane and docosane were made in the expectation of obtaining relaxation times intermediate between those of spermaceti in hexadecane and those in the wax of s.p. 41° C: as can be seen from figs. 1–5, this expectation was not fulfilled.

A further attempt to bridge the gap between hexadecane and the wax of s.p. 41° C was made by mixing spermaceti with a mixture of hexadecane and docosane (50 % of each) (s.p. of mixture, 32° C). In this mixture of spermaceti with two synthetic paraffins there were two relaxation times corresponding exactly with those in the same paraffins separately.

Some recent experiments of Müller (1938) show that an increase of external pressure not only raises the melting point of long-chain ketones but also raises the transition point above which molecular rotation can take place. It is possible that the increase of relaxation time with increasing setting point of the wax is due to the increased hardness of the latter, which increases the relaxation time in the particles of spermaceti in the same way as the external pressure would increase the difficulty of molecular rotation.

The chain-length theory has, however, been taken as a working hypothesis and used to suggest further experiments.

Comparison of the behaviour of ethyl stearate with spermaceti in hexadecane

If the chain length of the ester is without effect on the relaxation time, provided that it is longer than the chain length of the molecules of the paraffin matrix then ethyl stearate ($C_{17}H_{35}CO_2C_2H_5$) and cetyl palmitate ($C_{15}H_{31}CO_2C_{16}H_{33}$) should have the same relaxation time in hexadecane. Experiment showed that this expectation was substantially fulfilled, as may be seen by reference to fig. 1.

It is interesting to contrast this result with those of Sillars for the same two esters in a paraffin wax medium of setting point 57–60° C (chain length about 26 carbon atoms):

	Temp. for max. loss at 1 mc./sec.		Relaxation time in sec. at −20° C	
Ester	Paraffin wax, 57–60°	Hexadecane	Paraffin wax	Hexadecane
Cetyl palmitate	13·5	−40·5° C	$1{\cdot}56 \times 10^{-5}$	$6{\cdot}34 \times 10^{-9}$
Ethyl stearate	−31	−43·2° C	$3{\cdot}19 \times 10^{-8}$	4×10^{-9}

It was found, however, that the absorption in hexadecane was greater than in the harder wax media, being about twice as much for ethyl stearate and about four times as much for cetyl palmitate: it is hoped that this phenomenon will be discussed in a later paper.

Experiments with esters which contain two polar groups

Experiments have also been made with two esters of dibasic acids in a paraffin wax of setting point 57–60° C: the esters chosen were dioctyl sebacate,

$$C_8H_{17}OOC(CH_2)_8COOC_8H_{17}$$

and dioctyl azelate,

$$C_8H_{17}OOC(CH_2)_7COOC_8H_{17}.$$

The second ester (3·373 % concentration) gave a maximum $\tan\delta$ of 0·33 %, whereas with the first ester (2·4 % concentration) no loss in excess of $\tan\delta = 0{\cdot}025\ \%$ was detected in the temperature range -25 to $+60°$ C, and frequency range 224 to 3400 kc./sec. For the second ester $T_m = -10°$ C for $f = 224$ kc./sec. and $T_m = -2°$ C for $f = 507$ kc./sec. If these values are compared with the corresponding relaxation times obtained by Sillars for single esters, it will be seen they are sensibly the same as for a single ester of the same total length of chain, suggesting once more that the chain length is a predominant factor.

The sebacate and the azelate differ only in the number of carbon atoms separating the polar groups (the number being 8 and 7 respectively). If the zigzag chain of carbon atoms is straight and rigid in the solid state then it follows that the sense of the components of the dipole moments resolved perpendicular to the long axis are opposite in the sebacate and like in the azelate. Hence these experiments support the view that absorption of power is due to molecules of ester which rotate as a rigid whole (compare Wyman 1938) about their long axes, the magnitude of the absorption depending on the component of the dipole moment perpendicular to the long axis.

A further conclusion may be drawn which may prove to have considerable industrial significance. The results obtained clearly suggest that in seeking new low-loss dielectrics among natural or synthetic materials which contain compounds whose molecules are in the form of chains containing polar groups, the best results will be achieved if those molecules contain an even number of polar groups so arranged that one half of the dipole components transverse to the chain have opposite sense to the remaining half.

The experimental work was carried out in the Engineering Laboratory, Oxford, under the direction of Mr E. B. Moullin. The author is indebted to Mr Moullin for help with the electrical side of the work and criticism of the manuscript; to Dr J. C. Smith for continual help and invaluable advice with the chemical side of the work; to the Department of Scientific and Industrial Research for a grant which enabled the research to be performed.

SUMMARY

This paper describes an extension of the work of Jackson and Sillars who investigated the causes of dielectric loss in systems consisting of paraffin wax and an aliphatic ester.

It confirms their conclusions that the loss in these systems is due to the rotation of the polar molecules and can be interpreted in terms of the Debye theory.

The effect of different paraffin waxes has been studied and a suggestion is made that the dielectric relaxation time of these systems depends mainly upon the lengths of the carbon chains of the molecules of the shorter component, a conclusion borne out very strongly by the comparison of the behaviour of ethyl stearate and spermaceti in hexadecane as compared with their behaviour in a natural wax whose mean chain length was approximately 26.

Finally experiments were made with esters containing two ester groups in each molecule and in agreement with expectations it was found that the dielectric loss was positive or negligible according to the relative sense of the two polar groups: when these were arranged so that the dipole components transverse to the chain had opposite sense, no dielectric loss was observed. On the other hand, when the dipole components had the same sense the dielectric loss had a maximum value (at any given temperature) for a particular frequency and the relaxation time corresponded closely with that anticipated from the chain length.

This appears to confirm the conclusion that the loss is due to the rigid rotation of the carbon chains about their long axes, and also to indicate that chain compounds containing polar groups should be most effective as components of low-loss dielectrics prepared for practical use, when the molecules contain an even number of polar groups so arranged that one-half of the dipole components transverse to the chain have opposite sense to the remaining half.

REFERENCES

Bridgeman 1938 *J. Amer. Chem. Soc.* **60**, 530.
Jackson 1935*a* *Proc. Roy. Soc.* A, **150**, 197.
— 1935*b* *Proc. Roy. Soc.* A, **153**, 158.
Moullin 1938 *Proc. Camb. Phil. Soc.* **34**, 459.
Müller 1937 *Proc. Roy. Soc.* A, **158**, 403.
— 1938 *Proc. Roy. Soc.* A, **166**, 316.
Sillars 1938 *Proc. Roy. Soc.* A, **169**, 66.
Wyman 1938 *J. Amer. Chem. Soc.* **60**, 328.

Absorption of penetrating cosmic ray particles in gold

BY J. G. WILSON, PH.D.

(*Communicated by P. M. S. Blackett, F.R.S.—Received* 15 *May* 1939)

1. INTRODUCTION

A considerable amount of experimental data on the energy loss of cosmic-ray particles in metal plates is now available. Much of this, however, represents work carried out before the separate nature of the hard and soft components was fully understood, so that in many cases unsuitable conditions make the interpretation of the results difficult. The soft component is known to consist of electrons, and these predominate in the cosmic-ray energy spectrum for energies less than 2×10^8 e-volts. It has been verified for these electrons that the energy loss by ionization (Corson and Brode 1938) and by radiative collisions (Blackett 1938) is in close agreement with the theoretical predictions. At energies greater than 2×10^8 e-volts, very few electrons are found at sea level, and for all higher energies the majority of the particles are now considered to be mesotrons. These, together with an uncertain, but small, number of protons form the hard component of the cosmic rays.

Absorption measurements for the hard component are more difficult than for the electrons, since the particles are, in general, of higher energy and the loss of energy in an absorbing plate is very much smaller. The early observations (Blackett and Wilson 1937; Crussard and Leprince Ringuet 1937; Wilson 1938*a*) lead to the conclusion that at an electron energy

($E_e = 300H\rho$)* of about 5×10^8 e-volts, the total energy loss of penetrating particles was very small—of the same order as that due to ionization alone—but that at higher energies, $E_e \sim 1{\cdot}5 \times 10^9$ e-volts, a considerable additional energy loss took place, which did not appear to be attributable to the inclusion of electrons in the measurements (Wilson 1938*a*). With the comparatively thin absorbing plates used, however, it was not certain that all electrons had been excluded from these measurements.

Recently, measurements of the energy loss in 9 cm. of gold of those rays which penetrate a preliminary layer of 15 cm. of lead have been made by Ehrenfest (1938), who finds no appreciable energy loss beyond that due to ionization. Ehrenfest concludes that the comparatively large absorption mentioned above which is observed for $E_e \sim 1{\cdot}5 \times 10^9$ e-volts must be due to the inclusion of electrons. In the present series of measurements the absorbing layer is 2 cm. of gold. Although this thickness is much smaller than that used by Ehrenfest, it is sufficient to lead to a complete differentiation of behaviour between electrons and penetrating particles (§ 4).

Our new observations with gold are in general agreement with our earlier results with lead and copper. The energy loss at low energies has been accurately measured, and it now seems certain that for $E_e < 7 \times 10^8$ e-volts mesotrons suffer no other energy loss comparable with that due to ionization. At higher energies the additional energy loss is again found, but is now interpreted as due to the presence of a few absorbable particles which are probably protons; these are considered in detail in § 5, and it is the presence of these rays in our measurements, but not in those of Ehrenfest, which is probably responsible for the difference between the two sets of results.

2. EXPERIMENTAL DETAILS

The general considerations involved in cloud-chamber measurements of energy loss have already been discussed (Wilson 1938*a*), and the methods described in the previous work have been followed closely. The number of photographs taken is much larger, and although the number selected for measurement is also greater than before, a higher standard of photographic quality in the tracks to be measured has been reached. It is of interest that this more rigorous selection does not seem to have increased the accuracy of curvature measurement, showing that the factors which limit the accuracy of measurement probably still lie in the variable conditions in the expansion chamber. The estimates of the maximum detectable energy for the present series of measurements are: (i) from tracks in zero magnetic field, $1 \cdot 1 \times 10^{10}$ e-volts; (ii) from tracks in magnetic field ($E_e > 2 \times 10^9$ e-volts), $0 \cdot 9 \times 10^{10}$ e-volts.

---

* E_e is a convenient energy unit whenever the mass of the particles involved is not specified. For all particles, it approximates to the true energy when $\beta \rightarrow 1$ and it is directly proportional to the actual measured quantity ρ.

For particles of low energy the accuracy of measurement has been greatly increased by the use of a new optical curvature-compensating instrument, which has a range up to curvatures of 10 m.$^{-1}$. The limit below which the less accurate micrometer method is used is therefore reduced from $H\rho \sim 3 \times 10^6$ to $H\rho \sim 10^6$ G-cm.

3. THE ENERGY LOSS OF PENETRATING PARTICLES

The *mean* energy loss of all penetrating particles in 2 cm. gold is given in Table I in a form comparable with that used for measurements in lead and copper (Wilson 1938*a*). Here $R = \frac{2}{t}\frac{E_1 - E_2 - tE_i}{\bar{E}}$, while ϕ/ϕ_0 is the mean absorption cross-section for processes other than ionization as a fraction of the electron radiation cross-section.

TABLE I. MEAN ENERGY LOSS PENETRATING PARTICLES IN 2 CM. GOLD

Range of energies in $E_e = 300H\rho$ (e-volts)	No. of tracks	$\bar{R}$	ϕ/ϕ_0	Mean absolute energy loss in excess of minimum of ionization (in 10^6 e-volts)
$2 \times 10^8 - 4 \times 10^8$	19	0	0	0
$4 \times 10^8 - 7 \times 10^8$	30	$0 \cdot 007 \pm 0 \cdot 011$	$0 \cdot 004 \pm 0 \cdot 006$	8 ± 12
$7 \times 10^8 - 10^9$	16	$0 \cdot 092 \pm 0 \cdot 016$	$0 \cdot 053 \pm 0 \cdot 012$	156 ± 40
$10^9 - 1 \cdot 5 \times 10^9$	16	$0 \cdot 136 \pm 0 \cdot 027$	$0 \cdot 087 \pm 0 \cdot 018$	340 ± 70
$1 \cdot 5 \times 10^9 - 2 \times 10^9$	17	$-0 \cdot 055 \pm 0 \cdot 049$	$-0 \cdot 025 \pm 0 \cdot 023$	-160 ± 150

These results are compared with our earlier measurements in Table II and in fig. 1. In the table the mean measured *absolute* energy loss in excess of that due to ionization is given, while in the diagram the absorption cross-section is plotted. On either basis of comparison the agreement is satisfactory for $E_e < 1 \cdot 5 \times 10^9$ e-volts, but at higher energies the accuracy of measurement is certainly overestimated. The earlier values at low energies, where electrons were definitely present, are not included.

We therefore conclude that the measurements in gold are in agreement with our earlier observations, confirming the very low absorption at energies $E_e \sim 4 \times 10^8$ e-volts—which is now accurately measured—and also confirming the increased energy loss at higher energies $E_e \sim 10^9$ e-volts. It is not possible at present to decide whether the excess loss is best represented as an increased *rate* of absorption or as a *single absolute* extra energy loss.

In the new measurements no electrons are included, and it may be noted that in view of the rapid decrease of the known electron spectrum with energy, the low measured values of absorption for $E_e \sim 4 \times 10^8$ e-volts in our earlier results provide definite evidence against the presence of an appreciable number of electrons at this energy, and hence, since the electron spectrum is probably monotonic, at higher energies. Therefore we cannot consider our previous increased values of energy loss as due to electrons.

TABLE II. MEAN ABSOLUTE-ENERGY LOSS, IN EXCESS OF IONIZATION, OF PENETRATING PARTICLES IN METAL PLATES. IN 10^6 E-VOLTS

$(-(dE/dx)_{\text{ion}} = 13{\cdot}5 \times 10^6$ e-volts/cm. lead, see Table III.)

Energy range $E_e = 300H\rho$ e-volts	1 cm. lead	2 cm. copper	2 cm. gold	9 cm. gold (Ehrenfest)
$2 \times 10^8 - 4 \times 10^8$	—	—	0	~ 40
$4 \times 10^8 - 7 \times 10^8$	—	—	8 ± 12	
$7 \times 10^8 - 10^9$	145 ± 40	36 ± 45	156 ± 40	
$10^9 - 1{\cdot}5 \times 10^9$	380 ± 80	210 ± 60	340 ± 70	—
$1{\cdot}5 \times 10^9 - 2 \times 10^9$		460 ± 130	-160 ± 150	—

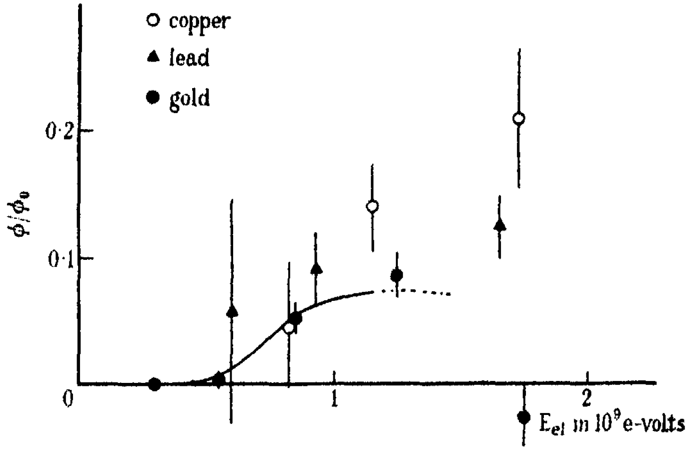

FIG. 1. Mean measured cross-section for all penetrating particles for absorption by processes other than ionization, expressed as fractions of the electron radiation cross-section.

The energy loss for particles of low energy, $E_e < 7 \times 10^8$ e-volts

In this energy range the ionization along proton tracks would be noticeably heavier than normal; no such tracks have been measured, and hence this group probably consists entirely of mesotrons. For the range $2 \times 10^8 < E_e < 4 \times 10^8$ e-volts, the measured energy loss in 2 cm. gold is $(41 \cdot 4 \pm 6 \cdot 9) \times 10^6$ e-volts and for $4 \times 10^8 < E_e < 7 \times 10^8$ the loss is $(49 \cdot 0 \pm 12 \cdot 5) \times 10^6$ e-volts. These values are compared in Table III with the theoretical energy loss due to ionization, using the values given by Bhabha (1938) for particles heavier than electrons. It is clear that no other energy loss at all comparable with that due to ionization takes place. For all these particles the spread of observed values is consistent with the errors of experiment as applied to a constant true energy loss, and the measurements may be regarded as a direct confirmation of the theoretical value of energy loss due to ionization by mesotrons. The value given by Ehrenfest as consistent with his results

$$(16 \times 10^6 \text{ e-volts/cm. Pb})$$

is rather larger than our measurement, but he records comparatively few particles in this energy range, and of these some reach such a low energy that their ionization must be appreciably above the minimum value.

TABLE III. ENERGY LOSS PER CM. LEAD DUE TO IONIZATION

	Energy of particles, $E_e = 300H\rho$	
	$2 \times 10^8 < E_e < 4 \times 10^8$ e-volts	$4 \times 10^8 < E_e < 7 \times 10^8$ e-volts
Bloch formula, electrons	$20 \cdot 5 \times 10^6$ e-volts	$22 \cdot 2 \times 10^6$ e-volts
Bloch formula, mesotrons ($\mu = 200m_0$)	$13 \cdot 2 \times 10^6$ e-volts	$14 \cdot 0 \times 10^6$ e-volts
Experimental value, mesotrons	$(12 \cdot 1 \pm 2 \cdot 0) \times 10^6$ e-volts	$(14 \cdot 3 \pm 3 \cdot 6) \times 10^6$ e-volts

Only two penetrating particles of very low energy, $H\rho < 7 \times 10^5$ G-cm., were observed, and both of these show the increased energy loss anticipated for mesotrons, although neither has reached so low an energy that the increase of ionization in the chamber is conspicuous.* The detailed measurements of these two tracks are given in Table IV, and in fig. 2 they are plotted upon a diagram giving the curvature change due to ionization in 2 cm. gold for particles of different masses. A track reported by Nishina, Takeuchi and Ichimiya (1937, 1939) is also included.

---

* The observed larger change of $H\rho$ at very low energies is due partly to the increased value of energy loss, and partly to the concurrent increase of $d(H\rho)/dE$. Hence the measured change of $H\rho$ increases more rapidly at low energies than does the number of ions formed on the tracks in the cloud chamber.

All three tracks are consistent with a mesotron mass of about $\mu = 200m_0$, an estimate which is necessarily rough and which may be too high on account

TABLE IV. ABSORPTION OF SINGLE PENETRATING PARTICLES OF LOW ENERGY

($H = 10{,}000$ G)

	$H\rho_1$	$H\rho_2$	$\overline{H\rho}$ G-cm. 10^{-5}	$\Delta H\rho$
(1)	7·7	4·2	6·5 ± 0·3	2·5 ± 0·5
(2)	5·5	2·9	4·2 ± 0·2	2·6 ± 0·3

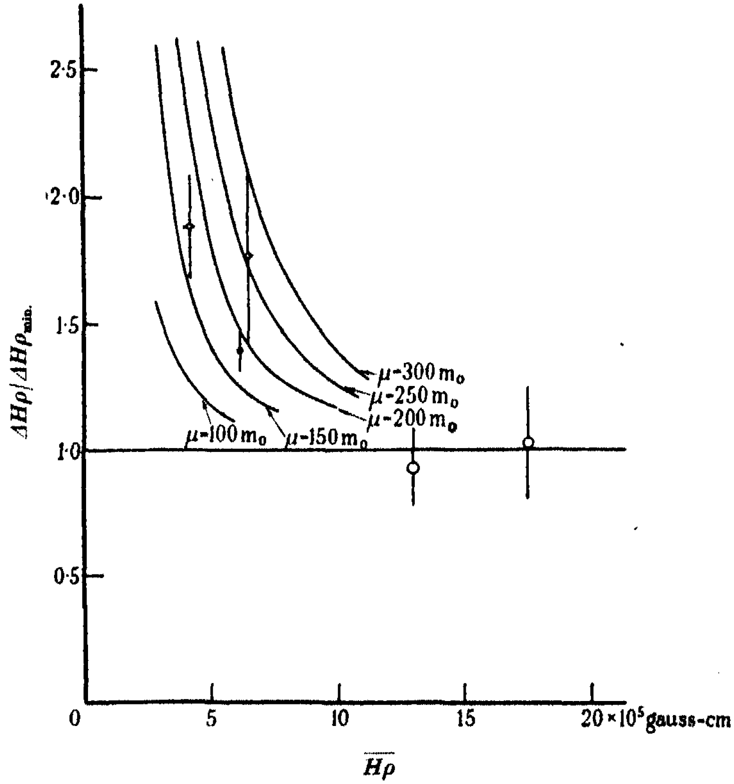

FIG. 2. The absorption of slow mesotrons. The curves show the theoretical ionization energy loss for various values of particle mass. o Single tracks on 2 cm. gold, showing probable error of $\overline{H\rho}$ and $\Delta H\rho$. O Mean values of $\Delta H\rho$ for groups of tracks in 2 cm. gold (Table III). ● Track in 3·5 cm. lead—Nishina, Takeuchi and Ichimiya (1937, 1939).

of the increased path travelled due to scattering. The track of lower energy ($H\rho = 4{\cdot}2 \times 10^5$ G-cm.) gives very much the more reliable single point, corresponding to the mass $\mu = (170 \pm 20)\, m_0$, in agreement with the value $\mu = (180 \pm 20)\, m_0$ given by Nishina. It is notable that for this track the curvature change is very sensitive to an *increase* of mass of the particle, and that the measurements cannot be reconciled with a mass as great as $\mu = 220 m_0$.

Distribution of energy loss at higher energies

The tracks of more energetic particles have been divided into three groups: (*a*) $5 \times 10^8 < E_e < 10^9$ e-volts; (*b*) $10^9 < E_e < 2 \times 10^9$ e-volts; (*c*) $E_e > 2 \times 10^9$ e-volts, containing respectively 46, 32, and 86 tracks. The observations on these tracks are given in fig. 3 in diagrams showing the distribution of

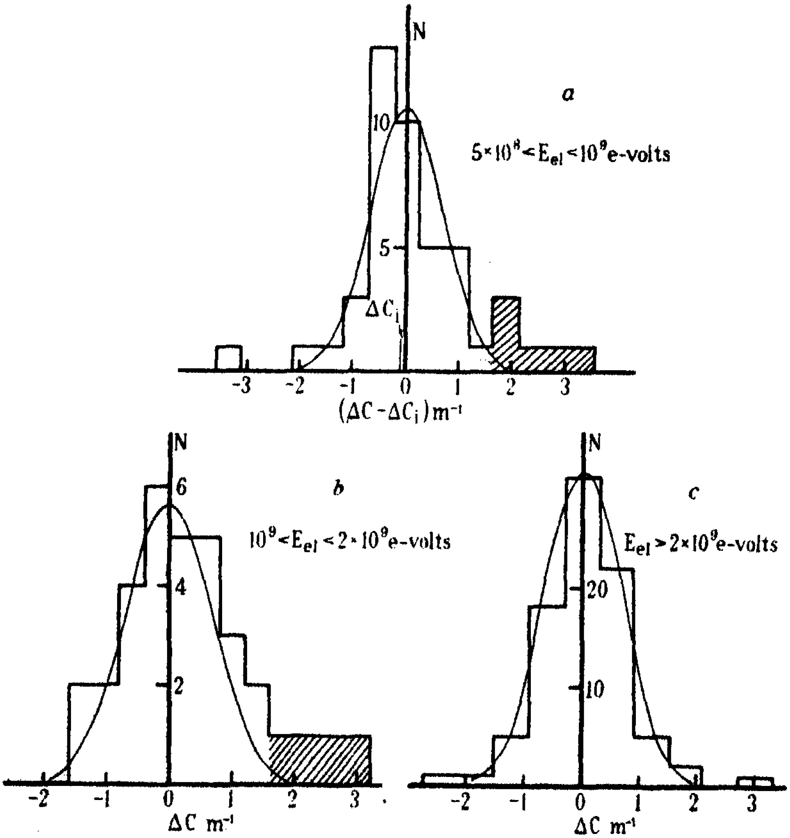

FIG. 3. Distribution of measured changes of curvature for penetrating tracks traversing 2 cm. gold. The numerical values of curvature refer to the photographic image and not to the actual track. Photographic magnification = 1/10th.

measured curvature change of the particle passing through the gold plate. In the first group (*a*), the curvature change due to normal ionization has already been subtracted from the measurements and the mean value of this correction is indicated. This correction is inappreciable for the groups of higher energy. The curvature changes in group (*c*) are assumed to be entirely due to errors of experiment, and so lead to the second value of the maximum detectable energy given in § 2. The Gaussian curve of these errors is included in all three diagrams. In figs. 3*a* and *b* can be seen a group of particles, shown shaded, whose measured energy loss is clearly greater than that corresponding to the error curve. Nine particles are included in this group —about 5% of all the penetrating particles—and it is the presence of this group which results in the mean energy loss being greater than that due to ionization (Tables I and II).

4. THE IDENTIFICATION OF ELECTRONS

The behaviour of electrons of various energies traversing 2 cm. gold is summarized in Table V, the figures of which are deduced from the results of Bhabha and Heitler (1937).

TABLE V. PASSAGE OF ELECTRONS THROUGH 2 CM. GOLD

($l = 8{\cdot}5 l_0$)

Incident energy of electron	4×10^8	10^9	2×10^9 e-volts
Probability that primary particle emerges with $E > 10^8$ e-volts	$\ll 0{\cdot}01$	$< 0{\cdot}01$	0·01
Probable number of secondaries with $E > 10^7$ e-volts	2	6	12
Probable number of secondaries with $E > 10^8$ e-volts	$\ll 0{\cdot}01$	$< 0{\cdot}1$	0·5

From these values it is apparent that for all energies of an incident electron the presence of a single particle below 2 cm. gold is improbable, and that when it does occur, the energy of the outgoing particle will be of the order of 10^7 e-volts. The probability that it will have an energy greater than 10^8 e-volts is always negligible, for the plate thickness is greater than that required for a small cascade shower to reach maximum intensity, so that an incident electron will appear, if at all, beneath the plate as a cascade shower in its later stages.

Accordingly, all particles which pass through the gold plate without the production of secondary particles and emerge with energy greater than 10^8 e-volts* are not normal electrons.

---

* For incident penetrating particles of energy lower than 4×10^8 e-volts an emergent energy less than 10^8 e-volts can give an equally valid criterion.

No such particles have been observed in *showers* incident upon the gold plate from above the apparatus, in agreement with the observation of Janossy (1938) that the number of penetrating particles in showers is very small.

The production of electron secondaries from penetrating particles by elastic collision, and in particular the cascades arising from these electrons, might occasionally lead to doubt as to the nature of the primary particles. In practice no cases have been observed in which there was any ambiguity.

5. Discussion of results

5·1. *Low energies,* $E_e < 7 \times 10^8$ *e-volts*

Our measurements for these energies, summarized in Tables III and IV, and those due to Ehrenfest (1938) indicate that at low energies mesotrons suffer no other energy loss in dense materials comparable in magnitude to that due to ionization. The spontaneous decay of mesotrons is only appreciable in a gaseous absorber.

It is therefore evident that interaction with nuclear particles plays very little part in the absorption of mesotrons at low energies, and that at these energies ($E_{\text{kin}} \sim$ a few multiples of μc^2), the theoretical cross-sections for various processes given by Heitler (1938) are greatly overestimated.

The complete absorption of mesotrons by the processes

$$Y^+ + N = P + h\nu \quad \text{and} \quad Y^- + P = N + h\nu \tag{1}$$

is of particular interest, since the reverse process, for which a similar cross-section may be anticipated, leads to the creation of mesotrons by radiation and so might be the origin of the hard component in the upper atmosphere. Heitler has considered (1) and the reverse processes

$$N + h\nu = P + Y^- \quad \text{and} \quad P + h\nu = N + Y^+ \tag{2}$$

from this point of view, and has given an estimate of the cross-section for both (1) and (2) which must occur if process (2) is to be an important factor in the birth of mesotrons. We distinguish between very low energies ($E_{\text{kin}} \lesssim \mu c^2$) where the theory may be valid and the higher energies for which a cross-section for (2) is *estimated* to give a reasonable mesotron production. Our experimental arrangement is not particularly suitable, nor have enough tracks been observed, to give a verification in the first case ($E_{\text{kin}} \lesssim \mu c^2$); but for particles of higher energy the data of Wilson (1938*b*) and others on electrons arising from penetrating particles is inconsistent with the cross-section suggested by Heitler (see § 5·2). It is therefore unlikely that the process (2) is important in the formation of the mesotron component near the top of the atmosphere.

The treatment given by Heitler also suggests that single scattering by the constituent nuclear particles will be very important at low energies ($E_{\mathrm{kin}} \sim \mu c^2$), the range determined by this process alone being of the order of 2–5 cm. lead. Measurements of scattering have been made for energies only very little higher than those for which the theory is developed. The scattering of a group of 31 mesotrons

$$0{\cdot}3 < H\rho < 1{\cdot}7 \times 10^6 \,\mathrm{G\text{-}cm.} \left(0{\cdot}4 < \frac{E_{\mathrm{kin}}}{\mu c^2} < 4{\cdot}1 \text{ for } \mu = 200m_0\right)$$

was examined; the mean multiple scattering for these particles was $(0{\cdot}51 \pm 0{\cdot}05)$ degrees $\times H\rho/10^6$, in agreement with our former results (Blackett and Wilson 1938), and also with the theoretical value 0·50 for scattering in the shielded atomic Coulomb field alone (Williams 1939). Thus for kinetic energies a little greater than the particle rest mass, no anomalies either of scattering or of energy loss are observed and it seems certain that the cross-section given by Heitler is not of the correct order of magnitude at these energies.

A more detailed account of measurements of mesotron scattering and of their bearing upon short range forces for the mesotron will be given elsewhere.

5·2. *Electron secondaries arising from penetrating particles*

The direct measurement of energy loss (Table III) gives experimental verification of the theory of ionization for mesotrons of moderate energy. There are, therefore, strong reasons for supposing that the theory will give correctly the equilibrium number of electrons accompanying a beam of penetrating particles, which have arisen by collisions. This number will include both electrons to which energy has been given in elastic collisions by the mesotrons, and also other electrons arising from these by cascade multiplication, the latter being associated near their origin to form a shower of electrons. The theory of production of this electron component has been given by Bhabha, (1938) and the experimental evidence (Wilson 1938*b*; Trumpy 1938; Hopkins, Nielsen and Nordheim 1939; Lovell 1939) shows that it does in fact account for all electrons associated with the penetrating component under dense matter. The measurements give no indication of any other process of electron production of comparable magnitude, and are directly opposed to the large cross-section for mesotron absorption given by Heitler (equation (1)). All the measurements referred to are of the equilibrium ratio of electrons to mesotrons under a layer of dense matter. In the atmosphere, when not under dense material, we expect in addition an electron component arising from the spontaneous decay of mesotrons.

5·3. *High energies*, $7 \times 10^8 < E_e < 2 \times 10^9$ *e-volts*

The measurements of particles in this energy range are given in Tables I and II, and indicate an excess energy loss which is in satisfactory agreement with our earlier measurements. There is an apparent discrepancy between these results and those of Ehrenfest which show no comparable excess energy loss over that due to ionization.

Ehrenfest, however, observed only particles which penetrated at least 30 cm. lead equivalent, while our experiments, although made under various conditions, never imposed a minimum range greater than 8 cm. lead. Hence although Ehrenfest would have observed with greater facility any large but rare energy loss of the predominant mesotrons, his arrangement would exclude a small entrant group of *more absorbable* particles. We therefore conclude that the excess energy loss must be attributed not to a rare process of the mesotrons, but to the presence of a few more absorbable particles, represented by the shaded parts of figs. 3*a* and *b*. Thus the absorption of mesotrons mainly by ionization, which is proved (§ 5·1) for low energies, probably extends to much higher energies.

The possibility that the measured curvature change for these particles arises from an undetected systematic error cannot be completely excluded, but this interpretation is difficult to reconcile with the general consistency of all the remaining measurements. All tracks showing large curvature change have been measured independently by two observers, and the measurements were in every case in agreement. Further experiments are certainly needed, however, to establish definitely the existence of the more absorbable particles.

Of the nine absorbable particles, which we now consider separately, eight are positive: the single negative particle lies close to the main mesotron distribution, and may well belong to it. One of the particles (positive, $E_e \sim 1{\cdot}9 \times 10^9$ e-volts) is observed to stop completely, and may represent a mesotron absorption process, as, for example, the production of an uncharged mesotron.

It seems most probable that the remaining seven positive particles of this group are protons, and they represent about 7% of the penetrating particles in the energy range in which they lie, in good agreement with existing estimates of the number of protons (Blackett 1938). But if this is so, in at least three cases the outgoing particle cannot still be a proton, for it shows normal ionization at an energy for which a proton would ionize heavily. Under these conditions, the observed change of curvature is not a measure of energy loss, and the numerical values are not of immediate interest.

We therefore consider the possible existence of a process by which a proton interacting with a nuclear field can produce a mesotron. If this is the correct interpretation, the cross-section for this process must be very large, as compared with very small cross-sections for the processes already considered (§ 5·1).

That the main production of mesotrons in the atmosphere arises from heavy particles has already been suggested by Johnson (1938, 1939), and support is afforded for this view by the doubt now thrown on the frequency of their production by photons (§§ 5·1, 5·2). The former process must clearly involve very rapid absorption of protons in the atmosphere, an absorption, in fact, comparable with that observed in gold. It is probable that the same process will be observable under cloud-chamber conditions at sea level, where, however, all the protons will presumably be of secondary origin.

It is unsatisfactory that, while a considerable momentum loss is in every case involved, no abnormality of scattering can be found for these tracks. Further and more accurate experiments are necessary to remove this apparent contradiction in the results. The direct distinction of fast protons and mesotrons, possible in principle by measurements of track ionization, is also of great importance if processes of this type do occur for protons of high energy.

6. THE ASSOCIATION OF PENETRATING PARTICLES

The presence of two penetrating particles in a single photograph may arise either from a real association of the particles, or else from the random entry of two unconnected particles in a certain short time interval. We estimate that tracks are visually contemporary, under the conditions of our observations, if they enter the chamber separated by less than 1/50th sec., while the mean time separation of penetrating particles entering the counter-controlled solid angle of the cloud chamber is 80 sec. Since only one of the particles need pass through the counter system, and the other may lie in a solid angle estimated as three or four times as large, random association should take place for about 1 in 1000 photographs. Actually of 900 photographs in this series, two show penetrating particles associated. One of these is certainly a random association; the other, which shows exceptional features, will be discussed elsewhere.

Our photographs, therefore, give no definite evidence for the association of penetrating particles at sea level.

I am indebted to Professor P. M. S. Blackett for the opportunity of using the large magnet, for his advice and for many discussions. My thanks are also due to Mr A. H. Chapman who took all the photographs.

SUMMARY

Absorption measurements of the penetrating component of the cosmic radiation have been made by cloud-chamber observations of the curvature change of tracks in a field of 10,000 G, using a gold absorber 2 cm. thick.

At low energies ($E_e < 7 \times 10^8$ e-volts) the measurements indicate an absorption due entirely to ionization; from a track of very low energy ($E_e < 2 \times 10^8$ e-volts) the increase of this absorption leads to an estimate of the mass of the mesotrons of $\mu = (170 \pm 20) m_0$. There is no indication of cross-sections for interaction of mesotrons with nuclear particles of comparable magnitude to that for absorption by ionization.

At higher energies ($E_e > 7 \times 10^8$ e-volts) a few particles were observed which appeared to undergo greater absorption, and these are shown to be in agreement with our previous measurements. Experiments due to Ehrenfest make it unlikely that these particles belong to the predominant group of mesotrons, and it is probable that they are protons. Since the particle emerging from the gold plate is, in some cases, definitely not a proton, this hypothesis suggests a strong absorption of protons with the production of mesotrons in 2 cm. gold. A similar process has been suggested by Johnson for the production of mesotrons in the upper atmosphere.

REFERENCES

Bhabha 1938 *Proc. Roy. Soc.* A, **166**, 501.
Bhabha and Heitler 1937 *Proc. Roy. Soc.* A, **159**, 432.
Blackett 1938 *Proc. Roy. Soc.* A, **165**, 11.
Blackett and Wilson 1937 *Proc. Roy. Soc.* A, **160**, 306.
— — 1938 *Proc. Roy. Soc.* A, **165**, 209.
Corson and Brode 1938 *Phys. Rev.* **53**, 773.
Crussard and Leprince Ringuet 1937 *C.R. Acad. Sci., Paris*, **204**, 243.
Ehrenfest 1938 *C.R. Acad. Sci., Paris*, **207**, 573.
Heitler 1938 *Proc. Roy. Soc.* A, **166**, 529.
Hopkins, Nielsen and Nordheim 1939 *Phys. Rev.* **55**, 233.
Janossy 1938 *Proc. Camb. Phil. Soc.* **34**, 614.
Johnson 1938 *Phys. Rev.* **54**, 385.
— 1939 *J. Franklin Inst.* **227**, 37.
Lovell 1939 *Proc. Roy. Soc.* A, **172**, 568.
Nishina, Takeuchi and Ichimiya 1937 *Phys. Rev.* **52**, 1198.
— — — 1939 *Phys. Rev.* **55**, 585.
Trumpy 1938 *Z. Phys.* **111**, 338.
Williams 1939 *Proc. Roy. Soc.* A, **169**, 531.
Wilson 1938*a* *Proc. Roy. Soc.* A, **166**, 482.
— 1938*b* *Nature, Lond.*, **142**, 73.

The electrical conductivity of thin films of mercury

By E. T. S. Appleyard* and J. R. Bristow
H. H. Wills Physical Laboratory, University of Bristol

(*Communicated by A. M. Tyndall, F.R.S.—Received* 25 *May* 1939)

1. Introduction

In the present paper an account is given of experimental measurements on the electrical conductivity of thin films of mercury prepared by evaporative deposition in a high vacuum according to the technique described in previous papers (Lovell 1936; Appleyard and Lovell 1937).

In a brief preliminary note (Appleyard 1937) we have pointed out that the results for mercury are very different from those for the alkali metals, and that in particular a considerable thickness of mercury must be deposited on the pyrex surface before conductivity begins. We have since confirmed and extended these observations, obtained accurate absolute values for the thickness of the films, investigated their stability, and made an extended study of their temperature coefficients after heat treatment. A comparison with the results of previous workers is given later.

2. Apparatus and measuring methods

The experimental tubes in essentials were similar to that described by Lovell and need not be described. Vacuum technique, and methods of distilling the pure metal were also similar, though, owing to the higher vapour pressure of mercury, we were able to use an oil-bath thermostat to fix the vapour pressure of the mercury in the oven.

The film was in the form of a strip deposited across current electrodes of colloidal graphite and platinum. In some of the experiments the potential leads were embedded in the edge of the graphite as in Lovell's tube (Lovell 1938), in others separate potential electrodes of colloidal graphite touched the edge of the strip.

A first approximation to the intensity of the atomic beam may be calculated by the use of the gas kinetic formula for effusion from a small aperture at low pressures. But some atoms are also scattered from the concave diaphragm through which the pinhole is pierced and a certain proportion of these will pass through the main slit system and contribute to the atomic beam. This extra contribution cannot easily be calculated and the beam must therefore be calibrated directly in some way. The ionization method used in the case of the alkali metals could not be applied to mercury because of its high ionization potential. We were therefore driven to use the method of direct weighing. A cooled gold plated silver sheet was placed in the path of the beam for a period of about 24 hr., and the deposit of mercury weighed upon a Sartorius microbalance sensitive to 10^{-6} g.

---

* I regret to record the death of Dr Appleyard since this paper was communicated. A. M. T.

From the mass deposited the rate of deposition at the surface could be calculated in A/min. We took careful precautions to make certain that all mercury atoms striking the plate arrived at all times from the direct beam, and also to ensure that leakage of atoms from the pinhole before the steel ball was actually raised could contribute only a negligible amount to the total mass deposited.

The results were consistent to about 3 % provided the vacuum in the experimental tube was adequate. The calibration showed that the true deposition rate could be obtained by multiplying the rate obtained from the effusion formula by a factor varying between 1·13 and 1·35 for different tubes, and that this factor (as might be expected) depended on the geometry of the slit system.

Resistances were measured with a Wheatstone Bridge or by potentiometric comparison. It was convenient to detect the onset of conductivity by means of a small potential applied to the film and a sensitive galvanometer in series. By means of a switching gear it was possible to pass rapidly from one method of measurement to another, so that the resistance could be followed at short intervals as the deposition proceeded.

3. RESULTS

We have already indicated the types of resistivity-thickness curves obtained for mercury on pyrex (Appleyard 1937). For completeness in fig. 1 *a*, *b* we show the more precise and consistent results obtained since that date. Ordinates are resistivities in ohm cm., abscissae are thicknesses obtained by direct calibration. Rates of deposition were between 6 and 9 A/min. and between these rates the curves obtained were practically identical. The curves show that at temperatures of 64° K or below the resistivity of the films rapidly approaches a constant value as the thickness increases once conductivity has begun. At a deposition temperature of 64° K this constant value does not much exceed that of the bulk metal at the same temperature; but at a deposition temperature of 20° K it is considerably in excess of that of the bulk metal at 20° K.

In contrast to the results for the alkali metals local baking of the condensing surface had no detectable effect on the results obtained.

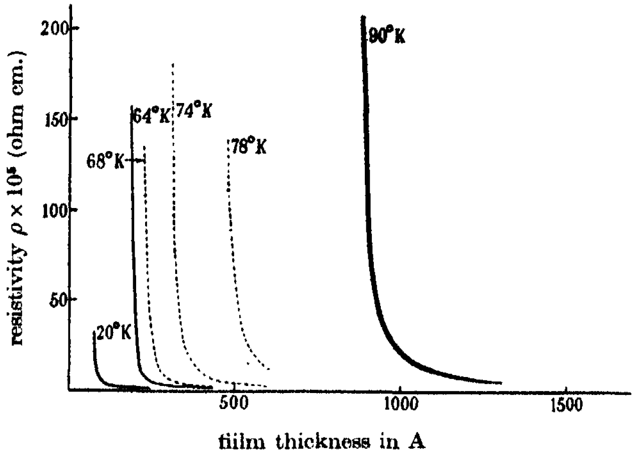

FIG. 1 *a*. Resistivity-thickness curves.

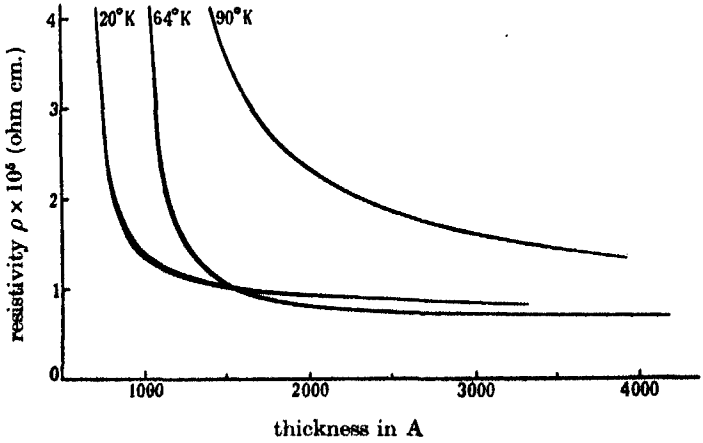

Fig. 1 *b*. Resistivity-thickness curves.

Variation in the vacuum conditions similarly had no effect over the range of pressure between 5×10^{-8} and 3×10^{-7} mm. Hg, though we made no extended investigation of the effect of residual gas since this had already been done very systematically by Johnson and Starkey (1935).

The results obtained with one and the same tube were very consistent. (The thickness of the curves for deposition temperatures of 20, 64 and

90° K is intended to indicate roughly the mean deviation from the mean in successive depositions.) Moreover, the resistivities obtained in these experiments all lie far below the values obtained for mercury films by previous workers (Braunbek 1930; Fukuroi 1936). Exact comparison is difficult, since the influence of deposition temperature on resistivity does not seem to have been previously investigated, but we may quote some representative results. Examination of fig. 1 shows that at all thicknesses a deposition temperature of 90° K gives films having the highest resistivity. At 4300 A, Braunbek quotes a resistivity of $4{\cdot}3 \times 10^{-5}$ ohm cm. for films deposited at liquid air temperatures, whereas our films had a resistivity of only $1{\cdot}3 \times 10^{-5}$ ohm cm. at this thickness. Similarly, Fukuroi (1936) apparently gives a specific resistance of about 10^{-3} ohm cm. at a thickness of 2000 A; our results give only about 2×10^{-5} ohm cm. at the same thickness.

We can only conclude that a somewhat more scrupulous vacuum technique and the absence of volatile impurities is probably responsible for the much lower results obtained by us.

The results for successive tubes agreed well in the region of high resistivities. Fresh deposition surfaces immediately sealed into the apparatus gave the same critical thickness at 64° K to within about 6 %. At thicknesses in the region of constant resistivity (fig. 1 *b*) we found small consistent deviations between results for successive tubes to which we shall refer later.

The graphite current leads had proved quite satisfactory in making contact with alkali metal films less than 1 molecular layer in thickness, so it seemed improbable that the phenomenon of delayed conductivity observed with all mercury films could be due to an effect of poor contact between the current leads and the film. Nevertheless, to test this point we used in one case current leads of chromium evaporated upon the pyrex surface. The same large critical thicknesses were reproduced at deposition temperatures of 64 and 90° K, and they agreed to within 10 % with those obtained using the standard electrodes. At deposition temperatures of 20° K the critical thicknesses obtained with the chromium electrodes were more capricious and on the whole smaller than those obtained using standard electrodes, but owing to the possibility of a permanent contamination of the surface during the preparation of the chromium electrodes, and to the tendency of the electrodes to break up on any rigorous heat treatment which made subsequent cleaning difficult, we are not inclined to attribute much significance to the deviations. We therefore conclude that the delayed conductivity is a property of the films themselves and is not caused by any effect at the electrodes.

The temperature coefficients of resistance of the films were all positive and reversible, provided the films were first annealed at the highest point of the temperature range within which it was desired to investigate the temperature coefficient. This was true for all temperatures of deposition in the range between 20 and 90° K and for all film thicknesses.

Fig. 2 *a* and *b* shows a family of resistivity-temperature curves after annealing at 90° K. Ordinates are resistivities in ohm cm., abscissae are temperatures in degrees absolute. In fig. 2 *b* electrode arrangements were similar to those used by Lovell (1938) in which the potential electrodes were embedded in the edge of the current leads, so that a small length (about 5 %) of the strip being measured overlay a surface of colloidal graphite. In fig. 2 *a* the potential electrodes were wedges of colloidal graphite which touched the edges of the film at points about 8 mm. apart. In these results therefore the section of film whose resistance is being measured lies entirely over a pyrex surface.

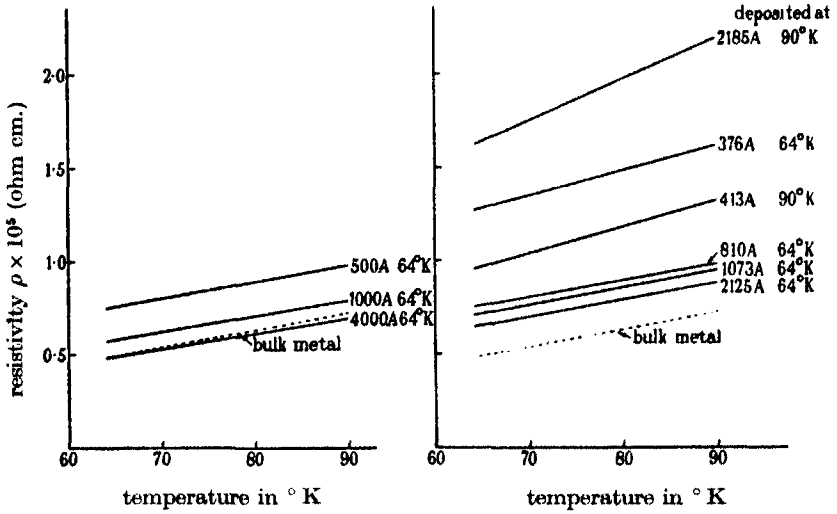

a *b*

Fig. 2 *a*, *b*. Resistivity-temperature curves.

For both series of results all films above 500 A in thickness deposited at 64 or 20·4° K and afterwards annealed to 90° K show resistivity-temperature curves which are very nearly parallel to that of the bulk metal. In fact, over the temperature range shown the difference of the film resistivities $\rho_{90}-\rho_{64}$ is on the average within 5 % of the value for the bulk metal as obtained by extrapolating Sckell's results (Sckell 1930) between the same temperature range, and this is within the limits of experimental error. (The values for the polycrystalline metal with random orientation have been calculated from the results for single crystals parallel and perpendicular to the axis.) The excess of resistance over that of the bulk metal for these films can then be regarded merely as an additional "residual resistance" which is dependent on thickness and also to some extent upon heat treatment. It was found that long annealing at 90° K produced a slow secular fall of residual resistance although most of the annealing was over in a few minutes. Comparison of fig. 2 *a* and *b* shows that on the whole the resistivities in fig. 2 *b* are somewhat higher than those in fig. 2 *a* at one and the same thickness. As we have mentioned above, the results for fig. 2 *b* differ from those for fig. 2 *a* only that for the former the resistances measured include those of a small section of film superposed upon a section of the graphite current electrodes. It follows that the sections of the film so superposed must have a higher strain resistance than those sections upon bare pyrex.

We have also previously referred to the small systematic variations of resistivity at large thicknesses which were observed between the results for successive tubes. This must be attributed to slight variations in the length of the film superposed upon the graphite, for from the method of preparation of the electrodes the disposition of the potential leads with respect to the graphite edges was not entirely reproducible. Thus the ends of the film lying over the graphite would add varying amounts of strain resistance to the measured resistivities.

In Table I some representative results are assembled in a different form. The columns show the total thickness of the film, the deposition temperature, the resistivity at the deposition temperature immediately after stopping deposition, and the resistivities at the highest and lowest points of the range over which the temperature coefficients were determined. Subscripts are temperatures in ° K.

For the films deposited at 64° K the resistivity measured at this temperature suffers an irreversible diminution on annealing at 90° K, obviously due to the lessening of the residual resistance.

The results for depositions at temperatures of 20·4° K are interesting, for they show that low deposition temperatures favour a high residual resistance. $\rho_{20\cdot4}-\rho_{14\cdot2}$ for these films is substantially the same as the corresponding value for the bulk metal. Hence although the resistivities of the film are far in excess of those of the bulk metal at the same temperature, this increase may justifiably be attributed to residual resistance. On annealing at 90° K the films lose most of this excess resistivity however

TABLE I

Series no.	Thickness A	Deposition temp. T °K	ρ_T	ρ_{90}	ρ_{64}	$\rho_{90}-\rho_{64}$	Remarks
1	1587	90	3·46	(3·46)	2·54	0·92	"Embedded electrodes", tube A_4
2	2180	90	2·18	(2·18)	1·62	0·56	,, ,,
3	4115	90	1·31	(1·31)	0·94	0·38	,, ,,
4	207	64	11·35	8·16	6·80	1·26	,, ,,
5	374	64	1·62	1·65	1·30	0·35	,, ,,
6	810	64	0·81	0·97	0·75	0·22	,, ,,
7	1071	64	0·76	0·94	0·70	0·24	,, ,,
8	2122	64	0·79	0·88	0·64	0·24	,, ,,
9	2981	64	0·67	0·88	0·64	0·24	,, ,,
10	772	20·4	0·94	0·89	0·67	0·22	,, ,,
11	776	20·4	0·93	0·89	0·68	0·21	,, ,,
12	1381	20·4	0·83	0·88	0·65	0·23	,, ,,
		Mean difference for films above 500 A				0·23	
		Sckell (1930) for bulk metal		0·72	0·48	0·24	
13	522	64	0·842	0·98	0·75	0·23	"Wedge electrodes", tube A_5
14	1083	64	0·58	0·79	0·57	0·22	,, ,,
15	4000	64	0·52	0·69	0·49	0·20	,, ,,
16	9120	64	0·51	0·73	0·50	0·23	,, ,,
17	1000	20·4	0·82	0·77	0·55	0·22	* See (17) below
		Mean for (13) to (17)				0·22	
			$\rho_{20\cdot4}$		$\rho_{14\cdot2}$	$\rho_{20\cdot4}-\rho_{14\cdot2}$	
17	1000	20·4	0·815		0·765	0·050	* Identical with film (17) above
18	733	20·4	0·93		0·885	0·045	"Embedded electrodes", tube A_4
	Sckell (1930) for bulk metal		0·135		0·08	0·055	

* Resistivities ρ are in ohm cm. × 10^5 and subscripts refer in all cases to temperatures in degrees absolute. ρ_T is the resistivity immediately after deposition stops at the temperature of deposition.

In the last two films mentioned, (17) and (18), the temperature coefficients between 20·4 and 14·2° K were determined without annealing, after deposition at 20·4° K.

and behave like a film of the same thickness deposited at 64° K. An example is indicated in the table.

The results are very similar to those of Suhrmann and Barth (1937) for copper films and to the results of Lovell (1938) for very thick deposits of the alkali metals.

4. DISCUSSION

In a previous paper (Appleyard 1937) one of us has put forward a picture which accounts for these results in broad outline, and which needs little modification to include the results on temperature coefficients quoted here. According to this model the mobility of the mercury atoms over the glass surface, even at the lowest temperatures of deposition, is so large that separate agglomerates are formed in the initial stages of deposition and only when they touch does conductivity begin. This is consistent with the very sudden increase in conductivity which occurs when the critical thickness is exceeded, and also with the observation that the critical thickness increases with the temperature of deposition (Appleyard 1937). In fig. 3*a* is represented a section of deposited film in which conductivity has just not yet begun; in fig. 3*b* deposition has continued until the initial roughness due to agglomeration has become but a small fraction of the total thickness. If the film in fig. 3*b* has the same crystal structure as the bulk metal its "nominal" resistivity should be the same as that of the bulk metal within the limits of error given by the ratio of the roughness to the average thickness, and these roughnesses at most should be of the order of the critical thickness.

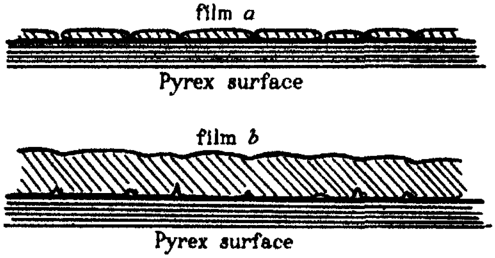

FIG. 3

This is what is actually found, except that as Table I shows there is a residual resistance dependent on thickness and on heat treatment, which also increases as the deposition temperature is lowered. In a previous communication (Appleyard 1937), it was suggested that the greater part of this residual resistance arose from the surfaces of misfit between the microcrystals composing the film. This apparently is also the view of Fukuroi (1937) though the changes of resistivity for his films, which were made of higher melting-point metals, were considerably greater. But we are now inclined to believe that the influence of the atomic forces at the pyrex substrate interface also plays a large part in distorting the mercury lattice and in thus introducing extra strain. (Fukuroi (1937) has also pointed out the influence of the substrate in affecting recrystallization.) The strain so introduced would extend upwards from the interface, gradually diminishing through the body of the film. This factor would account for the greater residual resistance in the case of the thinner films.

Whether the shortening of the effective mean free path of the electrons by collisions at the boundaries of the films (Lovell 1936) plays any part in accounting for the excess resistance of the films above the bulk metal cannot be definitely decided, since estimates of the mean free path are difficult for mercury, and the coherent films are so thick that the effect would not be very pronounced. Fuchs (1938) has indicated also that in the case of films of caesium a rather large fraction of the electrons must be specularly reflected and this factor would also tend to diminish any supplementary resistance from this cause. But to disentangle the excess from effects of strain and disintegration is difficult, and there seems no doubt that strain is the preponderating factor, since it can be affected by heat treatment. To summarize then, the thicker films we have been discussing so far can apparently for practical purposes be regarded as slices of the bulk metal having irregularities in thickness of the order of the critical thickness, and an excess resistance due to strain.

There is little to be said concerning the temperature coefficients of the films which are not coherent, e.g. Table I, films nos. 1, 2 and 3 deposited at 90° K, films nos. 4 and 5 (thin films) deposited at 64° K. The excess of resistance over the bulk metal is not entirely due to strain, but must be accounted for by geometrical disintegration, since the values of $\rho_{90} - \rho_{64}$ for these films are in excess of those for the bulk metal (Lovell 1938).

There is one other point to be mentioned. We believe that the simple agglomeration hypothesis is quite adequate to account for the large critical thicknesses at deposition temperatures above 64° K, as is shown by the visible roughness of the deposits at 90° K, and the observation that films not much in excess of the critical thickness are perfectly stable when retained at that temperature but show a "decay" of conductivity when raised to higher temperatures, which would be expected on an agglomeration hypothesis. But at deposition temperatures of 20·4° K or lower (in the following paper depositions carried out at 4·2° K are described) there still exists a critical thickness of about 15 atomic layers. It seems impossible that at these low temperatures the mobility of the mercury atoms can be sufficiently great to allow agglomeration.

It therefore seems possible that mercury deposited at very low temperatures may exist in a non-conducting modification in very thin films. Dr Skinner* of this laboratory has obtained indications that this may indeed be the case for thin films of beryllium by examining their soft X-ray emission bands.

We are indebted to Professor A. M. Tyndall for his constant interest in the work.

SUMMARY

The electrical resistance of mercury films deposited in very high vacua on surfaces cooled to various temperatures between 20·4 and 90° K has been investigated. The thickness of the films has been estimated by direct weighing to 3 %. The results indicate that the delayed appearance of conductivity as deposition proceeds is due to agglomeration of the mercury into solid droplets, and that the cause of the sudden onset of conductivity is the touching of these droplets. The temperature coefficients of resistance of these films are all positive and reversible after annealing at the highest point in the temperature range. From a study of these coefficients it is concluded that films above 500 A in thickness deposited at 64° K or lower can be regarded as coherent slices of metal, differing only from the bulk metal in being strained and in possessing a high residual resistance which can be modified by annealing treatment.

REFERENCES

Appleyard, E. T. S. 1937 *Proc. Phys. Soc.* **49** (extra part), 118.
Appleyard, E. T. S. and Lovell, A. C. B. 1937 *Proc. Roy. Soc.* A, **158**, 718.
Braunbek, W. 1930 *Z. Phys.* **59**, 191.
Fuchs, K. 1938 *Proc. Camb. Phil. Soc.* **34**, 100.
Fukuroi, T. 1936 *Honda Memorial Volume*, 80.
— 1937 *Sci. Pap. Inst. Phys. Chem. Res., Tokyo*, **32**, 196.
Johnson, M. C. and Starkey, T. V. 1935 *Proc. Roy. Soc.* A, **140**, 126.
Lovell, A. C. B. 1936 *Proc. Roy. Soc.* A, **157**, 311.
— 1938 *Proc. Roy. Soc.* A, **166**, 270.
Sokell, O. 1930 *Ann. Phys., Lpz.*, **6**, 932.
Suhrmann, R. and Barth, G. 1937 *Z. Phys.* **103**, 133.

---

* We are indebted to Dr H. W. B. Skinner for permission to mention this unpublished observation.

Superconductivity of thin films

I. Mercury

BY E. T. S. APPLEYARD,* J. R. BRISTOW,
H. LONDON AND A. D. MISENER
*H. H. Wills Physical Laboratory, University of Bristol and
Royal Society Mond Laboratory, Cambridge*

(*Communicated by A. M. Tyndall, F.R.S.—Received* 25 *May* 1939)

1. INTRODUCTION

This paper describes the results of measurements of the superconductive properties of thin films of mercury prepared according to the method described in a previous publication (Appleyard and Bristow 1939). Previous workers† on the superconductivity of thin films (Sizoo and Onnes 1925; Burton, Wilhelm and Misener 1934; Misener, Smith and Wilhelm 1935; Misener 1936; and Shalnikov 1938) have not been able to distinguish definitely between the effect of the finite size of their specimens (which is the feature primarily interesting from the theoretical point of view), and effects due to their uncertain structure which is often profoundly affected by the methods of preparation of the films. In particular they have not been able to show that the magnetic threshold value of their films approaches the value for the bulk metal when the thickness of the films is sufficiently increased except at very great thicknesses. Shalnikov (1938), for example, has performed a series of experiments on superconducting thin films of lead and tin. But his thickest films seem to have had a critical field 2–3 times in excess of the bulk metal, and his results seem not to have been very reproducible (Shoenberg 1938).

Pontius (1937) also obtained definite indications of a size effect with fine wires of very pure lead, but the difference in behaviour from that of the bulk metal was small. Results from wires are certainly reliable for the dimensions obtainable, but the difficulty of drawing a wire thinner than about 10^{-4} cm. sets a limit to the scope of the method.

On the other hand, by the method of evaporation (Appleyard and Bristow 1939) we succeeded in preparing films of a thickness of less than

---

* I regret to record the death of Dr Appleyard since this paper was communicated. A. M. T.

† Shoenberg (1938) provides a discussion of the significance of results arising from the investigation of superconducting bodies of small dimensions, to which we refer the reader.

10^{-5} cm. which seemed to have all the necessary characteristics for extending the experiments into the range of smaller thicknesses. Their properties are reproducible and differ only from those of the bulk metal in the following ways: (*a*) they may be disintegrated owing to initial agglomeration; (*b*) they may have a comparatively large residual resistance due to strain in the lattice. These factors can be controlled to some extent by varying the deposition temperature and by altering the degree of annealing respectively. Thus we have been able to show that the superconducting properties of the films are insensitive to variations in either of these factors; and that in consequence we may state with some assurance that the experimental results depend merely on the size of the films and are independent of their structure.

Our measurements show that the critical magnetic fields required to restore normal conductivity are larger for thin films than for the bulk metal, and this is in general agreement with Shalnikov's results. But the most important inference from the measurements is that the so-called depth of field penetration increases rapidly as the temperature of the specimen approaches the transition temperature (Appleyard, Bristow and London 1939).

2. APPARATUS

The experimental tubes and the vacuum technique used in these experiments were in most essentials identical with those described in the previous paper (Appleyard and Bristow 1939). The arrangement is shown in fig. 1 (see Lovell 1938) which is self-explanatory. For cooling the prepared film to superconducting temperatures, or for deposition at temperatures below 4·2° K, liquid helium had to be introduced into the internal pocket *J*.

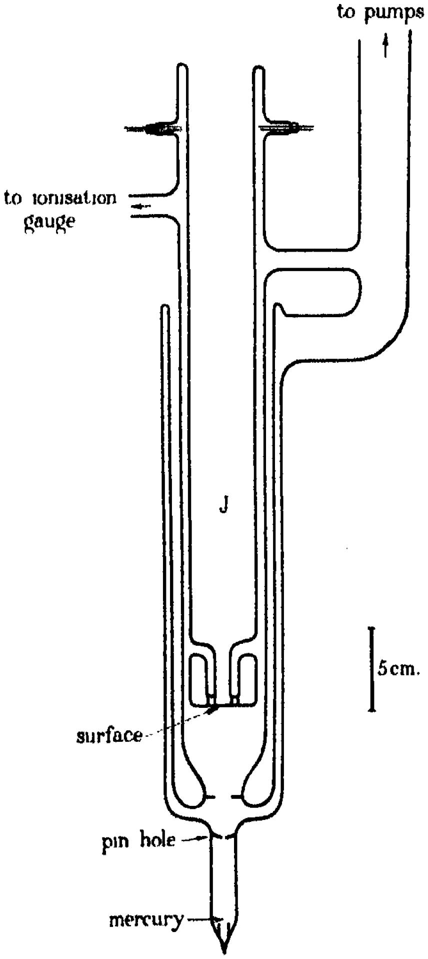

FIG. 1. The experimental tube.

To economize in liquid helium the liquid nitrogen jacket surrounding *J* was therefore made longer to minimize absorption of radiation. With these precautions a single filling of liquid helium lasted over 4 hr., which was long enough for the properties of the film to be fully investigated.

The pumping system was permanently attached to the experimental tube and was kept running throughout the experiments so that the films were surrounded by a good vacuum during their entire existence.

In these experiments films deposited on two forms of surface were employed. They are shown in detail below, fig. 2. One was identical with a type described in the previous paper (Appleyard and Bristow 1939), the film being deposited in the form of a strip. Electrical contact to the film was made by graphite current leads which overlapped the film. Potential leads also of graphite touched the sides of the film to enable accurate resistance measurements to be made (fig. 2*a*). The early investigations were made with this arrangement which for conciseness we shall refer to as the "strip tube".

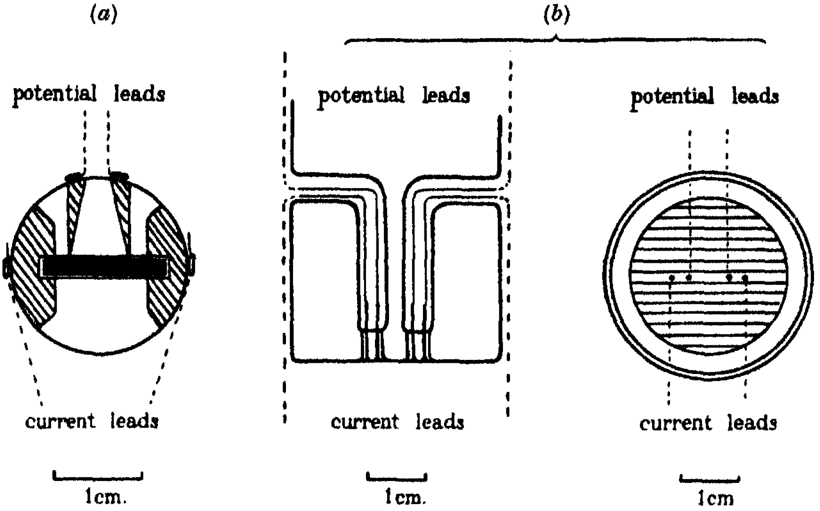

FIG. 2. The two types of depositing surface.

The other form of surface (fig. 2*b*) carried current and potential leads actually passing through the glass surface. The film was defined by a circular stop in this arrangement, and covered practically the whole lower surface of the pocket. This diminished effects due to the edges of the film, which were thinner than the film itself. We shall discuss these in detail later. This arrangement will be referred to in future as the "disk tube".

Resistances were measured with a Tinsley thermoelectric potentiometer. As far as possible the tube was designed to avoid thermal e.m.f.'s, but in spite of this the "disk" tube showed an internal thermal e.m.f. of several microvolts dependent on the level of the helium in *J*. An accurate correction could easily be applied for this since it changed only slowly with time; and except for the very lowest resistances no error is introduced on this account.

For the determination of the critical magnetic fields required to destroy supraconductivity in the films an electromagnet with a large gap giving a field up to 3500 G was available. If used consistently with an exciting current increased from zero it gave fields reproducible to 5 G or 2 % whichever is the greater. For fields less than 400 G Helmholtz coils were used, though in one or two cases the electromagnet was used for measurements in this region. Fields were determined with a calibrated fluxmeter.

The sequence of operations in preparing and examining a film was as follows: the film was deposited on a surface usually cooled to 64° K by means of oxygen boiling under reduced pressure. The deposition rate was about 9 A/min. After an appropriate thickness had been reached, deposition was stopped and the film was annealed at a temperature of 90° K (liquid oxygen at atmospheric pressure) or at 114° K (liquid methane at atmospheric pressure). Most of the liquefied gas in *J* was then removed with a swab of cotton and the whole apparatus was transported to the helium liquefier. Immediately before filling with liquid helium the last drops of methane or oxygen were swabbed out so as to leave a mere film of liquefied gas on the inner surface of *J*.

After filling with liquid helium the apparatus was removed from the liquefier, manometer and pumping connexions were made to the helium bath, and the resistance of the film was measured in its normally conducting state at a temperature of about 4·2° K as measured by the vapour pressure of the helium.

The transition to the superconducting state was now determined in zero magnetic field by measuring the resistance of the film as the pressure over the helium bath was diminished step by step. The transition was sharp except in the case of films deposited at 4·2° K and not afterwards annealed.

The tube was now introduced between the poles of the electromagnet so that the field was as nearly as possible parallel to the plane of the film, the helium bath was fixed at some definite temperature below the transition point, and the magnetic field was gradually increased until the resistance of the film began to return. In the case of the "disk tube" where the transitions were sharp we were able to adjust the surface accurately parallel to the magnetic field by increasing the field until about half the resistance had returned, and afterwards tilting the apparatus by means of set-screws until the restored resistance was a minimum. This adjustment was very critical, but once made it remained valid at all temperatures of the film. Experiment showed that in this particular position the restoration of resistance took place over the smallest range of magnetic field, and that also a maximum value was obtained for the critical field. From this we can infer that the method of levelling is satisfactory.

For the "strip tube" the transition region in the magnetic field was always extended, and the observations were merely made in a standard position set by eye as nearly as possible parallel to the field. Small variations of the order of 2° about the standard position altered the extent of the magnetic transition curves but made no difference to the general character of the phenomena. As this tube was used merely for exploratory work the conclusions of this paper are not affected by this uncertainty.

After adjustment and levelling as described, the temperature of the helium bath was held constant and the magnetic field increased step by step from zero to a sufficiently large value to restore the normal resistance completely. The observations were repeated at a series of lower temperatures. In work with the disk tube, to verify that the measuring current was small enough not to affect the results, it was usual to double the current at a temperature near the beginning and the end of an experimental series. If the transition curves so obtained were appreciably different from those obtained with the standard current, a lower standard value of the current was used and the previous results were rejected.

3. RESULTS

The early exploratory work with the strip tube proved at once that films between 500 and 10,000 A in thickness have a transition temperature in zero field the same as that of the bulk metal within about 0·03° C, provided the films were annealed at 90° K or more. We attributed the small difference between the accepted transition point for bulk mercury and the transition point experimentally obtained to stray radiation falling on the exterior surface of the cooled pocket (Appleyard and Misener 1938). Subsequent investigations with the disk tube have confirmed this point of view, and it has proved possible by carefully maintaining the level of the liquid nitrogen in the outer jacket to bring the values into even closer agreement. In most cases the correction to be added to the observed transition point in order to bring it into correspondence with the accepted value for the bulk metal amounts to less than 0·015° K, and there is no evidence of consistent variation of the transition point with thickness over the range from 250 to 10,000 A in the case of annealed films. This is in entire agreement with the results of Shalnikov for annealed films of lead and tin.

Deposition temperatures of 4·2° K were used in some cases, and the films were investigated without annealing. Unlike lead and tin films (Shalnikov 1938) mercury films in this case show a transition point displaced to *lower* temperatures; and the temperature range of the transition is much extended. (The latter point Shalnikov for technical reasons was unable to investigate.)

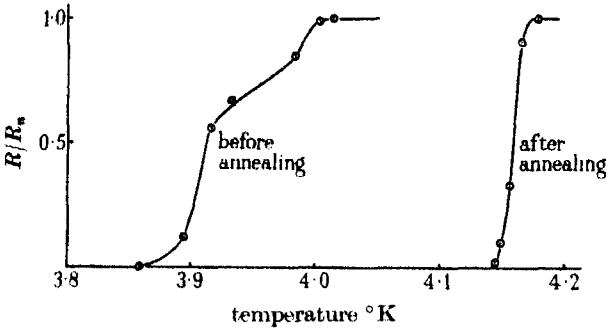

FIG. 3. Transition curves of 1187 A film (zero magnetic field). Deposition temperature 4·2° K.

Fig. 3 gives an example of the transition curves obtained before and after annealing for a 1187 A film deposited at 4·2° K. Films 302 and 600 A thick also show approximately the same depression of the transition point and rather irregular and extended transition curves.

Ordinates are values of R/R_n, where R is the resistance of the film at the temperature considered and R_n is the resistance when the film is conducting normally. The mean transition temperature is displaced from 4·159 to 3·933° K. Thus it appears that the highly strained, finely polycrystalline material produced by deposition at 4·2° K may be regarded, in some sense, as a different kind of superconducting metal from ordinary mercury and that the difference in properties may persist to very great thicknesses. There is no evidence of a variation of transition temperature with thickness for these films.

In the determination of the critical magnetic fields (as we have previously mentioned) the "strip" tube gave results which were not entirely satisfactory. The return to normal resistance took place as a rule over a large range of magnetic field. Also though the field at which resistance first began to return was fairly independent of all factors except the thickness, the range of the transition varied very much with such parameters as measuring current, degree of annealing and temperature of the film. The transition curves were also least steep for the thickest films, though we should expect that as these films most closely approximated to the bulk metal in all other properties they should show a sharp magnetic transition. It finally occurred to us that the whole of these confusing phenomena arose from an effect at the edges of the film.

Reference to fig. 2 *a* shows that surrounding the main body of the film there is a narrow strip (the "penumbra") in which the film thickness changes gradually to zero as we move outwards. The penumbra arises merely from the finite size of the pinhole, and from the geometry of the apparatus. Now it was known from our experiments that the critical field increased rapidly as the film examined diminished in thickness. Hence superconductivity may be destroyed in the thicker main body of the film, though the magnetic field is still not large enough to destroy it in the thinner edges. Thus, to a first approximation, the film will still show zero resistance until the magnetic field is sufficiently intense to force the region of normal conductivity into the thinner parts of the penumbra where the film is actually disintegrated.

In the penumbra, the transition from coherence to incoherence will be gradual, consequently the return to normal resistance will be extended. Also the current density in the penumbra will be very high so that the edge may pass into an intermediate state between normal and superconductivity, in which the resistance has intermediate values. This would account for the extended transition curve.

It was for these reasons that we adopted the electrode design of fig. 1*b*. It can be seen from the diagram that the measuring current can only get from one electrode to the other by passing through a considerable area of uniform film.

Measurements with this tube confirmed at once the above explanation of the extended transitions. Figs. 4 *a*, *b* show the type of transitions observed with the disk tube. Ordinates are R/R_n, abscissae are in gauss. Fig. 4*a* is for one of our thinner films (596 A), fig. 4*b* with a thicker film (2410 A). It can be seen that although there is still an extended range of transition for the 596 A films which we believe to be characteristic of very thin films, the 2410 A film gives extremely sharp transitions, quite different from those obtained with the "strip" tube.

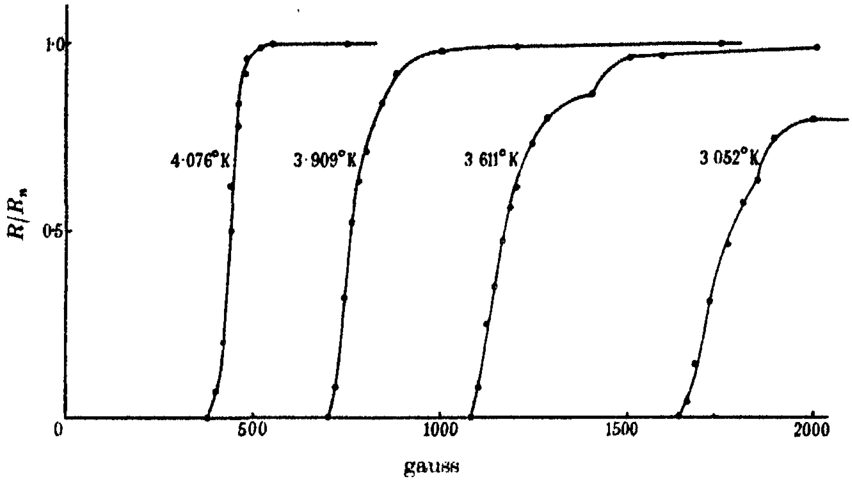

FIG. 4 *a*. Transition curves for film 596 A thick.

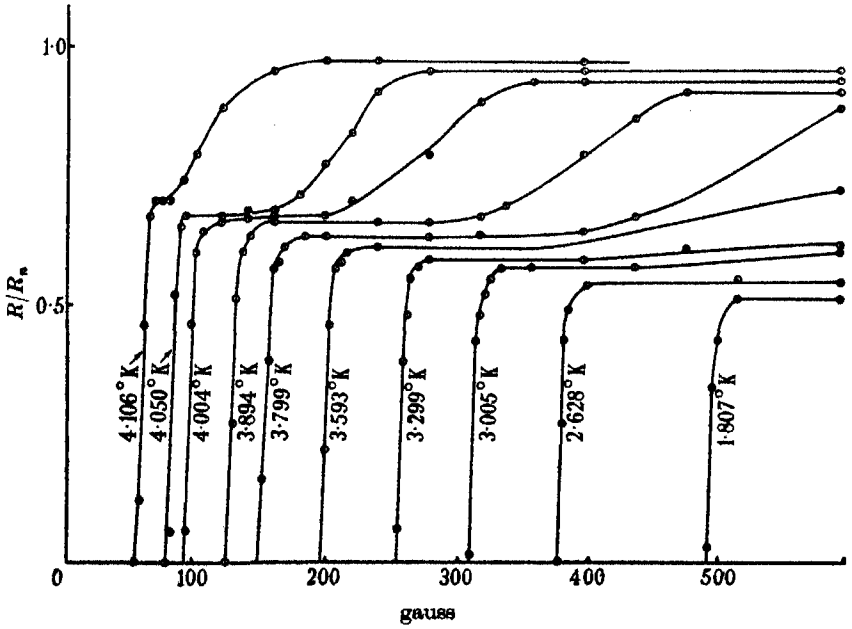

FIG. 4 *b*. Transition curves for film 2410 A thick.

The curious shape of the transition curves had already been predicted before any measurements were made with the "disk" tube. It will be seen from fig. 4*b* that as the field increases in the case of the 2410 A film the resistance returns sharply to about 0·70 of its normal value at these temperatures, remains constant for over a considerable range of field and then rises slowly to its normal value from the "plateau". The initial sharp rise is clearly due to the return of the body of the film to normal conduction. But at this field the penumbra (fig. 2*b*) still remains superconducting so that the disk is in effect surrounded by a perfectly conducting ring. A fraction of the measuring current will therefore pass from one electrode to the other by this path, which in the normal state is a path of very high resistance. The potential drop between the measuring electrodes will therefore be less than in the normal state, or the effective resistance will be diminished. This state will continue without much alteration until the

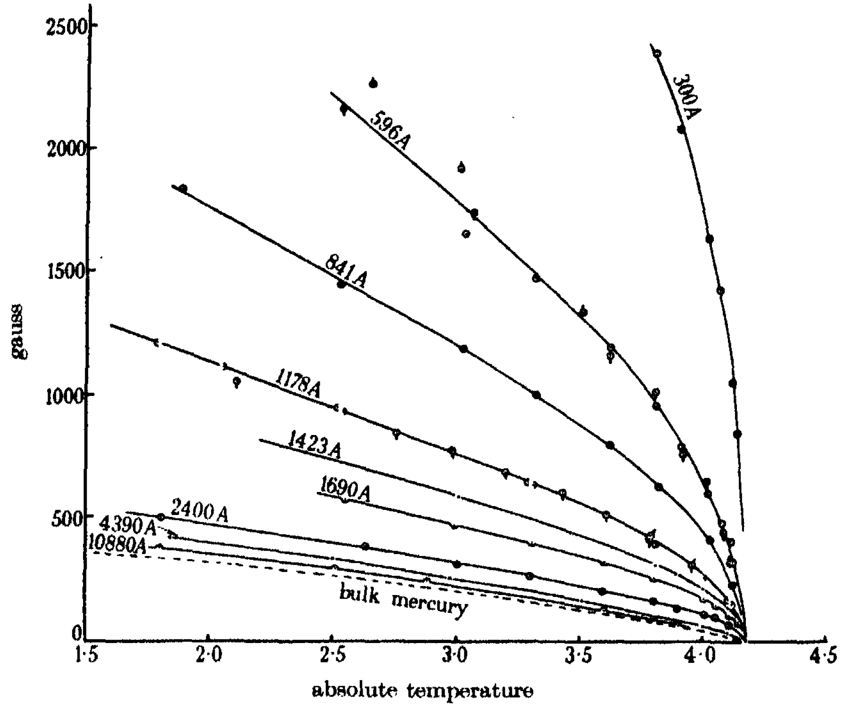

FIG. 5 *a*. Critical fields for mercury films. For film 1178 A thick.

⊙ Deposition temperature 64° K. Resistance at 4·2° K = $2·7 \times 10^{-2}\,\omega$
⊙ Deposition temperature 64° K. Resistance at 4·2° K = $2·0 \times 10^{-2}\,\omega$
⊙ Deposition temperature 4·2° K. Resistance at 4·2° K = $2·3 \times 10^{-2}\,\omega$
⊙ Deposition temperature 64° K. Resistance at 4·2° K = $3·5 \times 10^{-2}\,\omega$
⊙ Deposition temperature 64° K. Resistance at 4·2° K = $1·6 \times 10^{-2}\,\omega$

field is large enough to force out the superconducting ring into the cracked parts of the film, when normal conductivity will return.

All the experimental observations are in accordance with this picture. For very thin films where the coherent part of the penumbra extends outwards only a short way the plateau is only indicated, or non-existent. Thick films whose edges are coherent over a very large range of thickness show an extended plateau. Annealing, which is known to favour the disintegration of very thin films, also tends to shorten the plateau, and to make the subsequent rise to normal resistance much steeper, without affecting the initial rise from zero resistance appreciably. We are therefore justified in taking the initial steep rise of resistance as characteristic of the body of the film, and the magnetic field at half the height of the plateau as the critical field for that temperature.

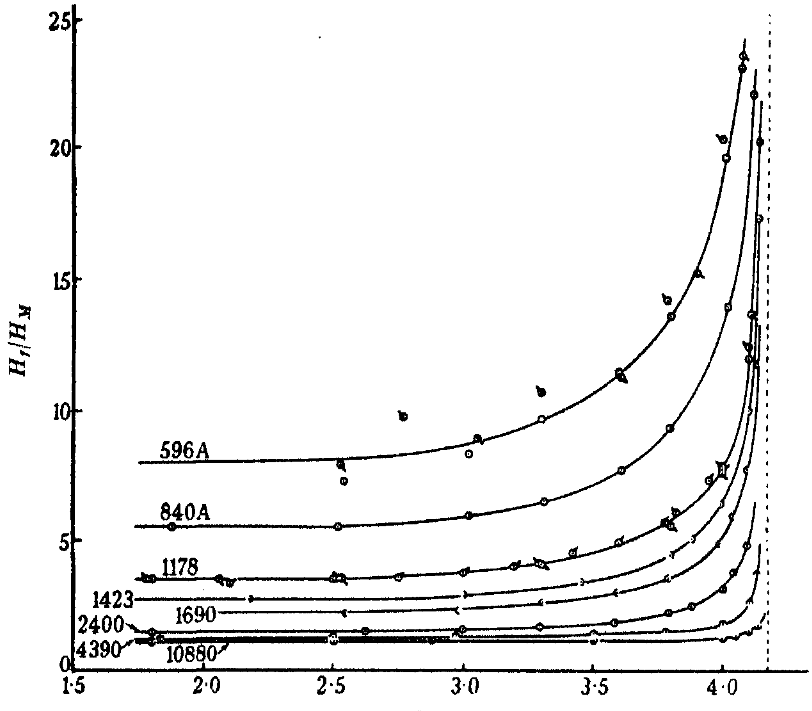

FIG. 5 *b*. Ratio of critical field of films to critical fields of bulk mercury at various temperatures.

Critical fields for films ranging between 300 and 10,000 A in thickness have been investigated. Curves showing the values of the critical field (H_f) in gauss against film temperature are shown for various films in fig. 5*a*.

For comparison, Misener's fields for specimens of bulk mercury are appended.* All film temperatures are corrected so as to bring the observed transition temperatures in zero field to the transition temperature for the bulk metal obtained by the extrapolation of Misener's smoothed results, viz. 4·167° K. The corrections were usually of the order of 0·01° K and can scarcely affect the results except at temperatures above 4·10° K. Temperatures are derived from helium vapour pressures by means of the Leyden (1937) formulae.

Two facts are immediately obvious from the curves. First, the critical fields at a given temperature increase very rapidly when the film thickness drops below 2400 A, which is in agreement with Shalnikov's previous qualitative observations (Shalnikov 1938). Secondly (what had not been observed before), the critical field-temperature curves for a given film are of an entirely different shape from those for the bulk metal. Fig. 5*b* shows the ratio of H_f/H_M for the series of films (H_f is critical field for the film, H_M that for the bulk metal at the same temperature). At low temperatures H_f/H_M is approximately constant and increases very slowly with temperature. Above 4° K, however, the field ratio rises very rapidly and shows every indication of approaching infinity at the transition point for all the films.†

To test whether the strain resistance or the disintegration of these films had any effect on the measurements of the critical fields we prepared five films 1178 A in thickness. One was deposited at 4·2° K and afterwards annealed at 90° K, the other four were deposited at the standard temperature of 64° K. Two of these were annealed for different periods at 90° K and two at 112° K for a few minutes. Reference to fig. 5*a* shows that all the experimental points for this thickness lie on a single curve. The investigations of the previous paper (Appleyard and Bristow 1939) indicate that these films may show inequalities in thickness comparable with the "critical thickness" which for the films deposited at 4·2° K is 80 A, for those deposited at 64° K is 180 A. Thus the critical fields are not sensitive to the geometrical roughness of these films.

The values of the critical fields are also insensitive to changes in the residual resistance as a result of varied annealing. It can be seen from fig. 5*a* that the measured resistance at 4·2° K (which at this temperature is almost entirely the result of strain) may change by a factor of 2·2 without producing any systematic change in the critical field at a given temperature.

---

* These agree with the values of Daunt and Mendelssohn (1937) to within 1 % and extend to somewhat higher temperatures.

† A slight indication of this rise of field ratio near the transition point may be obtained from the results on tin films published at Toronto (Misener *et al.* 1935).

Since geometrical disintegration and strain are the only properties in which our films differ from the bulk metal and since these factors have been shown to have little or no influence on the transition fields for the films (at least for those above 1200 A thick), we infer that the results obtained arise from a true size effect in superconductivity.

Hysteresis in the films was investigated in a few cases, though owing to the necessity for using iron in the magnetic circuit over most of the range of fields it was difficult to obtain precise results for the thinner films. We believe that for films less than 1700 A thick the difference in field between the ascending and descending portions of the loop did not much exceed 5 % of the critical field. In the range where air coils could be used in no case did the hysteresis exceed 10 %.

In almost all of these experiments the magnetic field was applied at right angles to the line joining the current electrodes. A few readings were taken with the field applied parallel to this line, but there was no definite evidence of a difference of more than 10 % in the values of the critical fields obtained in the two positions. Owing to the difficulties of levelling in the "parallel" position we are inclined to attribute the divergencies to experimental error.

4. DISCUSSION

When a superconducting body is placed in a magnetic field it is well known that the magnetic induction B inside the specimen rapidly falls to zero on crossing the boundary into the conductor. The depth of field penetration has been given theoretically (Becker, Heller and Sauter 1933; F. and H. London 1935) by the formula

$$\lambda = \left(\frac{mc^2}{4\pi ne^2}\right)^{\frac{1}{2}}, \tag{1}$$

where λ is the depth of penetration, n = the effective number of superconducting electrons per c.c. and e, m, c have their usual significance. On the assumption that the number of superconducting electrons is of the same order as the number of free electrons in the metal, this formula gives a depth of field penetration of about 2×10^{-6} cm. for mercury.

The most obvious way of investigating the penetration layer is through experiments on superconducting bodies, one of whose dimensions is comparable with the depth of field penetration. As has been pointed out by various authors, H. London (1935), v. Laue (1938), Pomerantchuk (1938), the finite penetration of the field leads to a modification of Gorter's thermodynamic relation between the magnetic threshold field and the difference in free energy of the superconducting and the normal states. This results in an increase in the magnetic threshold value for superconductors of small dimensions.

Since this modification of the theory depends on some assumptions which are rather uncertain, we begin with a purely dimensional argument which, when applied to our results, allows us to draw certain qualitative conclusions about the variation of field penetration with temperature. The rise of H_f/H_M at the transition temperature can only mean that the field penetration also must increase rapidly as the transition temperature is approached. The dimensional argument even allows us to calculate the way in which it varies with temperature.

Suppose $\lambda(T)$ is a parameter having the dimensions of a length, which defines the decrease of field inside a superconductor as we leave the boundary and which depends explicitly on the temperature alone for a given superconductor. It is a reasonable assumption that $\lambda(T)$ is independent of the film thickness. With this assumption we may write

$$\frac{H_f}{H_M} = f\left(\frac{d}{\lambda(T)}\right), \tag{2}$$

where f is some function, and d is the thickness of the film.

Equation (2) may be written in the form

$$\log_{10}\frac{H_f}{H_M} = g\{\log_{10} d - \log_{10}\lambda(T)\}, \tag{3}$$

where g is another function of d. This relationship is of the form

$$y = g(x - c),$$

where $$c = \log_{10}\lambda(T), \quad y = \log_{10}\frac{H_f}{H_M}, \quad \text{and} \quad x = \log_{10} d.$$

Thus if $\log_{10}\frac{H_f}{H_M}$ is plotted against $\log_{10} d$ at a series of different temperatures, we should obtain a family of curves displaced parallel to each other along the log d-axis; two curves for temperatures T_1 and T_2 being separated by a distance $\log_{10}\lambda(T_2) - \log_{10}\lambda(T_1)$. Fig. 6 shows the results of such a plot. The curves are all drawn identical in shape and fit the points adequately at all temperatures below 4·05° K where the results are more accurate. Three points for the very thick film diverge rather widely from their curves, but this discrepancy may be accounted for by the large percentage error in measuring the very small critical fields at these temperatures, for which our apparatus was not designed. From the displacement of the curves we may calculate $\lambda(T)/\lambda(2\cdot5)$ in an obvious way.

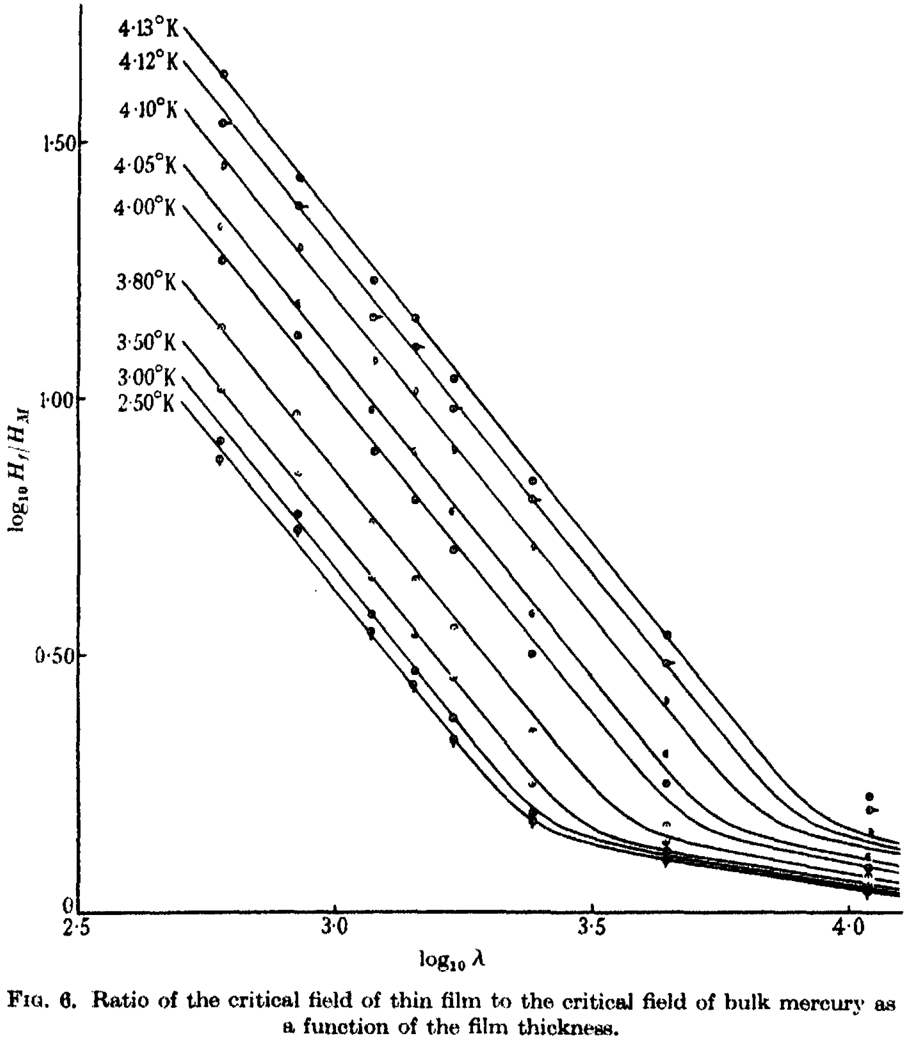

FIG. 6. Ratio of the critical field of thin film to the critical field of bulk mercury as a function of the film thickness.

The results are shown in fig. 7. Shoenberg (1939) measuring the magnetization of mercury colloids has confirmed this variation of field penetration in a very direct and independent way and his results are in substantial agreement with ours.

The actual algebraic form of $f(d/\lambda)$ in equation (2) can be derived only by making definite assumptions regarding the equilibrium between the normal and superconducting phases in a magnetic field. A simple derivation due to Pomerantchuk (1938) can be somewhat modified at the expense of generality by making definite assumptions as to the nature of the surface energy at the boundaries of the film as follows:

If a large superconductor is placed in a magnetic field H it behaves as a perfectly diamagnetic substance and the change in the total electromagnetic energy caused by the presence of unit volume of the superconductor is $H^2/8\pi$. The equilibrium equation between the normal and superconducting phases may then be written (where f_n and f_s are the free energies per unit volume of normal and superconducting states in the absence of a field)

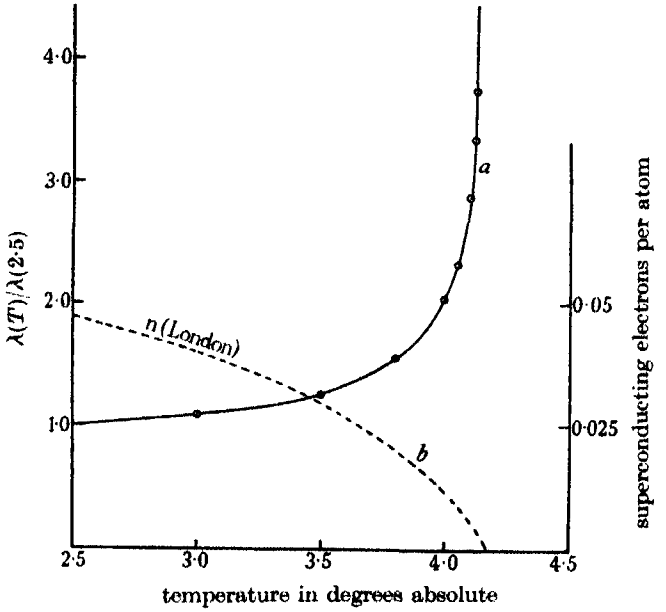

FIG. 7. Penetration of magnetic field into a superconductivity film. (*a*) Variation of depth of field penetration with temperature; (*b*) Variation of "effective" number of superconductivity electrons per atom with temperature.

$$f_n = f_s + \frac{H^2}{8\pi}. \tag{4}$$

If the superconducting body is a thin film, then the finite field penetration will make it an imperfectly diamagnetic substance. Its average magnetic energy per unit volume will therefore be $\eta H^2/8\pi$, where η is a factor less than unity which may be calculated by simple integration once a definite field distribution is assumed. Assuming, further, that $f_n - f_s$ is the same for the film as for the bulk metal the equilibrium equation for a thin film becomes

$$f_n - f_s = \frac{\eta H_f^2}{8\pi}, \tag{5}$$

or

$$\frac{H_f}{H_M} = \frac{1}{\eta^{\frac{1}{2}}}, \tag{6}$$

which is greater than unity, in accordance with experiment.

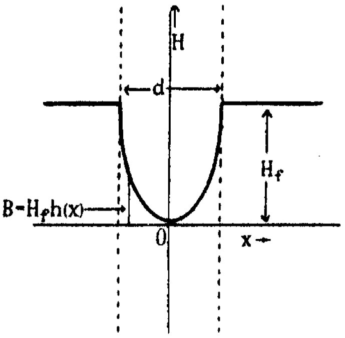

FIG. 8

To calculate η we proceed as follows: the magnetic induction inside the super-conductor must be of the form

$$B = H_f h(x),$$

where x denotes the distance measured from the middle, and $h(x)$ is a function such that

$$h(-d/2) = h(d/2) = 1$$

(cf. fig. 8).

The average magnetic energy per unit volume may easily be shown to be

$$\frac{1}{d}\int_{-d/2}^{+d/2} -\tfrac{1}{2} H_f I \, dx,$$

where $I = \frac{1}{4\pi}(B - H)$ is the intensity of magnetization at a point.

A simple calculation then gives for the average magnetic energy per unit volume the formula (5) with

$$\eta = 1 - \frac{2}{d}\int_0^{d/2} h(x)\, dx.$$

Now if d is large compared with the range in which $h(x)$ is appreciable, we may write

$$\int_0^{d/2} h(x)\, dx \approx \int_0^{\infty} h(x)\, dx.$$

The right-hand side of this equation is of the dimensions of a length and is a measure of the field penetration. We denote it by λ'. We may then write

$$\eta = 1 - \frac{2\lambda'}{d}$$

or (since $d \gg \lambda$), from (6)

$$\frac{H_f}{H_M} = 1 + \frac{\lambda'}{d}, \tag{7}$$

which is formally identical with the relation of Pomerantchuk.*

We may legitimately apply formula (7) only to our thickest film ($d = 10{,}880$ A). Calculation then gives $\lambda'_{2\cdot5} = 1\cdot2 \pm 0\cdot3 \times 10^{-5}$ cm.† (Actually (7) seems to be a good empirical formula even up to values of $H_f/H_M = 1\cdot5$, where it would not be expected to hold, and gives the same experimental value for $\lambda'_{2\cdot5}$.) This value may be used to fix absolute values of λ' at all temperatures using the ratios obtained dimensionally.

The order of magnitude of the field penetration so calculated is again confirmed by the direct investigations of Shoenberg (1939) (though owing to uncertainties in the size of his colloid particles exact comparison is difficult), and by the results of Pontius (1937) with lead wires.

To calculate H_f/H_M for thinner films we must make some assumption about the form of $h(x)$. If we assume the distribution resulting from the equations of F. and H. London, viz.

$$h(x) = \frac{\cosh x/\lambda}{\cosh d/2\lambda},$$

we obtain

$$\frac{H_f}{H_M} = \left(1 - \frac{2\lambda}{d}\tanh\frac{d}{2\lambda}\right)^{-\frac{1}{2}}. \tag{8}$$

The formula does not fit the experimental results very well. Values of λ (2·5) calculated from it for different films show systematic variations between $1\cdot3 \times 10^{-5}$ and $0\cdot80 \times 10^{-5}$ cm. in the range of thickness from 600 to 10,880 A. This discrepancy may indicate that the assumptions on which the derivation of equation (7) and subsequently equation (8) have been based are no longer applicable for very thin films.

To summarize the results of this discussion: We conclude from our experiments that the depth of field penetration rises rapidly as the tem-

---

* On the other hand a formula given by von Laue (1938) for large thicknesses becomes

$$\frac{H_f}{H_M} = 1 + 2e^{-d/\lambda}.$$

This converges towards unity as d increases much more rapidly than our experimental results indicate.

† The values of λ' so obtained depend very critically on the actual values of H_M assumed for bulk mercury. We have taken the values of Daunt and Mendelssohn (1937). But a 1 % error in either H_f or H_M leads to a 10 % error in the value of λ'. It is for this reason that we have increased the limits of error above those given in a previous note (Appleyard *et al.* 1939).

perature approaches the transition point, and that it probably becomes infinite there. We also conclude that even at temperatures as low as 2·5° K the field penetration is of the order of 10^{-5} cm. and not of 2×10^{-6} cm. as deduced from equation (1) if one assumes that all the conduction electrons are capable of carrying the superconducting currents. Alternatively, we may take the values for the field penetration and calculate from them the effective number of superconducting electrons per atom, using formula (1).

The dotted curve in fig. 7 shows values obtained at different temperatures. The number appears to be zero at the transition temperature and seems unlikely to exceed 0·05 electron per atom even at the lowest temperatures.

But it is clear that the effective number of free electrons calculated in this way depends upon numerous somewhat arbitrary assumptions, and the question of the equilibrium between electrons in the normal and in the superconducting states at different temperatures is still somewhat uncertain.

The cryogenic part of this work was carried out at the Royal Society Mond Laboratory at Cambridge with apparatus constructed and calibrated in Bristol at the Wills Laboratory. We are much indebted to Dr Cockcroft and Professor Tyndall of the respective laboratories for their generous provision of the necessary facilities.

We must also thank the various members of the two laboratories, in particular Dr Shoenberg, for valuable theoretical discussion and suggestions. One of us (J. R. B.) performed this work during the tenure of a grant from the Department of Scientific and Industrial Research.

SUMMARY

Mercury films prepared in high vacua have been examined in the superconducting state. The transition temperature from the normal to the superconducting state in films previously annealed at 90° K or more is very close to that of the bulk metal. On the other hand, films deposited at 4·2° K and not afterwards annealed show a displacement of the transition temperature downwards by about 0·2° K. In neither case is there evidence of any variation of transition temperature with the thickness of the films.

The critical longitudinal magnetic fields required to restore normal conductivity in the films at various temperatures have been determined.

If H_f is the critical magnetic field for a film at a definite temperature and H_M that for the bulk metal at the same temperature, it is found that at all temperatures H_f/H_M is larger than unity, and increases rapidly as the film

diminishes in thickness. For a film of a definite thickness H_f/H_M increases steeply as the transition temperature is approached. It is inferred from this result that the depth of field penetration likewise increases steeply as the transition temperature is approached.

REFERENCES

Appleyard, E. T. S. and Bristow, J. R. 1939 *Proc. Roy. Soc.* A, **172**, 530.
Appleyard, E. T. S., Bristow, J. R. and London, H. 1939 *Nature, Lond.*, **143**, 433.
Appleyard, E. T. S. and Misener, A. D. 1938 *Nature, Lond.*, **142**, 474.
Becker, R., Heller, G. and Sauter, F. 1933 *Z. Phys.* **85**, 772.
Burton, E. F., Wilhelm, J. O. and Misener, A. D. 1934 *Trans. Roy. Soc. Can.* **28**, III, 65.
Daunt, J. G. and Mendelssohn, K. 1937 *Proc. Roy. Soc.* A, **160**, 127.
Laue, von 1938 *Ann. Phys., Lpz.*, **32**, 71.
London, H. 1935 *Proc. Roy. Soc.* A, **152**, 651.
London, F. and H. 1935 *Proc. Roy. Soc.* A, **149**, 71.
Lovell, A. C. B. 1938 *Proc. Roy. Soc.* A, **166**, 271.
Misener, A. D. 1936 *Canad. J. Res.* **14**, 25.
Misener, A. D., Smith, H. G. and Wilhelm, J. O. 1935 *Trans. Roy. Soc. Can.* **29**, III, 13.
Pomerantchuk 1938 See Shoenberg (1938), p. 98.
Pontius, R. B. 1937 *Phil. Mag.* **24**, 787.
Shalnikov, A. 1938 *Nature, Lond.*, **142**, 74; see also Shoenberg (1938), p. 95.
Shoenberg, D. 1938 *Superconductivity*. Camb. Univ. Press.
— 1939 *Nature, Lond.*, **143**, 434.
Sizoo, G. J. and Onnes, H. K. 1925 *Commun. Phys. Lab. Univ. Leiden*, 180 (*a*).

The scattering of α-particles in helium

By S. Devons, M.A.

Senior Rouse Ball Student, Trinity College, Cambridge

(*Communicated by W. L. Bragg, F.R.S.—Received* 1 *June* 1939)

1. Introduction

In a previous paper (Devons 1939)* the author has discussed the possibility of observing resonance phenomena in the scattering of α-particles by light nuclei, and the experimental results given there show that in general resonances in scattering are observable for light nuclei of atomic number less than about 12 and for α-particle energies about equal to or greater than the potential barrier height.

In the case of the scattering by helium nuclei the classical coulomb scattering is very small, and therefore anomalies in the scattering due to excited states of Be^8, the compound nucleus formed by He^4 and an α-particle, should be comparatively easy to detect. In addition no disintegration is possible with α-particles of the energies used (less than 8·5 MeV), so that if the nucleus Be^8 is formed in an excited state it can only dissociate into two α-particles, and hence the width of any level of Be^8 excited by α-particle scattering in helium will be due practically entirely to elastic scattering. The investigation of the excited states of Be^8 by means of the scattering of α-particles by helium nuclei has a particular interest since the existence of a broad level of Be^8 with an excitation energy of about 3 MeV above the ground state, which is capable of splitting up into two α-particles, is postulated to account for the results of several disintegration experiments.

This evidence will be discussed in more detail later. The mass of Be^8 as deduced from disintegration data is about equal to that of two α-particles. This excited state of Be^8 should then, provided it does not possess an unusually large spin, give rise to an anomaly in the scattering in helium for α-particles of energies of about 6 MeV. (In the collision of an α-particle and a helium nucleus only one-half of the energy is available as excitation energy, the other half producing motion of the system as a whole.)

Certain peculiarities, both experimental and theoretical, in the investigation of the scattering in the present case, occur owing to the identity of the scattered particles and scattering nuclei. The angle of scattering in laboratory co-ordinates is one-half that in the centre of gravity co-ordinates and the α-particles scattered at large angles have considerably smaller energies than before scattering. It is not practicable to observe the scattering at angles greater than about 50°, but owing to the small atomic number of the scattering nucleus it should not be necessary to use larger scattering angles to observe phenomena in this case.

---

* Referred to subsequently as Paper I.

α-Particles possess no intrinsic spin and obey Einstein-Bose statistics. It follows then that the wave function describing the scattered α-particle and the scattered helium nucleus must be symmetrical in space co-ordinates alone. This means that in the expansion of the wave function in spherical harmonics no components of odd angular momenta, l, occur.

In addition only those α-particles with angular momentum, l quantum units, such that

$$l\lambda = r, \tag{1}$$

(where r is the radius of the nuclear forces and λ is the de Broglie wave-length of the α-particles) will be strongly affected by the nuclear forces. For r equal to about 4×10^{-13} cm. this means that for energies less than 8 MeV the only α-particles likely to be affected by nuclear forces are those having angular momentum $l = 0$ and $l = 2$ quantum units.

The scattering at an angle θ due to the nth angular momentum component contains the factor $P_n^2(\cos\theta)$, the angle θ being measured in a co-ordinate system moving with the centre of gravity of the system. $P_2 \cos(\theta)$ is equal to zero for θ equal to 54·4°. In the case of α-particles scattered by helium nuclei the angle of scattering in the centre of gravity co-ordinates is equal to twice that in the laboratory co-ordinates. If then the scattering is observed at 27° the only excitation states of Be^8 that will give rise to resonance scattering are those with spin momentum zero. For scattering at other angles states with spin momentum zero and two quantum units will be effective. The scattering has therefore been investigated carefully for two ranges of angles, the mean scattering angle in the two cases being 27° and 38·5°, so that it might be possible to ascertain the angular momentum of any state of Be^8 which might give rise to resonance scattering. The excitation level of Be^8 deduced from disintegration data must of course be "even" since it splits up into two normal α-particles.

Experiments on the scattering of α-particles in helium have already been carried out by a number of investigators: Rutherford and Chadwick (1927), Chadwick (1930), Wright (1932), and Mohr and Pringle (1937). Large anomalies in the scattering were observed by Rutherford and Chadwick for scattering angles greater than about 20°, but the scattering was only measured for a few α-particle energies and consequently no definite information regarding resonance phenomena can be obtained from their results. In the experiments of Chadwick and those of Mohr and Pringle the maximum energy of the α-particles used was only 4·5 MeV. The observations of Wright did not extend to angles greater than 27°, and in this case also the spacing of the observations with respect to energy in the region above 5 MeV was poor. A resonance at 6 MeV α-particle energy would not then have been observed in the above experiments, particularly if the level is a "D" level, i.e. has a spin momentum of two quantum units.

2. Experimental

For the observation of the scattering at small angles, the annular ionization chamber method described in Paper I does not offer any particular advantages, in fact in this case the resolution of the method is rather poor. The method used in the present investigation was the well-known annular ring method which has been used in all previous experiments. The construction of the apparatus is shown in fig. 1.

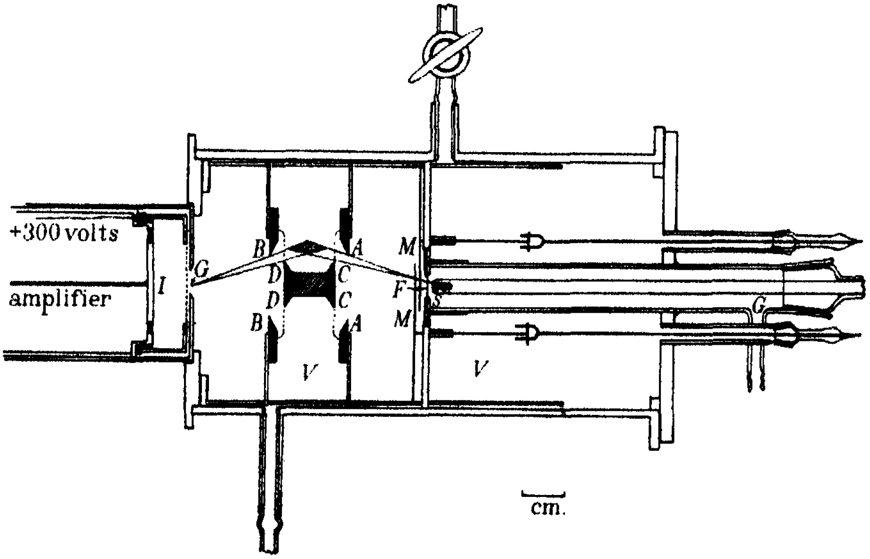

Fig. 1

The incident beam of particles from the source *S* was defined by the graphite stops *AA*, *CC*, and the scattered particles which were recorded were limited by the stops *BB*, *DD*. The effective scattering region (for point source and detector aperture) is shown shaded. The source *S*, an active deposit of Ra B + C, etc., was mounted in position by means of a ground glass joint in the tube *G*, the end of which was covered with a mica window of stopping power 0·7 cm. air equivalent. The window *F* and the tube *G* formed a gas tight system, so that new sources could be easily and quickly introduced without affecting the gas in the scattering chamber, *VV*. The energy of the α-particles at the scattering region could be altered by means of two rotating sets of four mica screens which could be adjusted from outside the scattering chamber. In this way the scattering could be measured for sixteen different energies in one experiment.

The scattered particles were recorded by means of the ionization chamber *I*, of depth 1·0 cm., the front high potential plate being in the form of a very fine grid. The aperture of the ionization chamber was 0·45 cm. in diameter. No window was placed over this opening in the ionization chamber in order not to absorb the scattered α-particles of low energy. It was found quite satisfactory to use the same gas in the ionization chamber and scattering chamber. The particles were counted by means of a linear amplifier and a single thyratron operating a mechanical meter, or in some cases, where larger counts were obtained, a hard valve scale of two counter (Lewis 1937) was used.

The presence of the strong source of γ-rays at *S* (the source strength varied between 30 and 100 millicuries) gave rise to a fairly large background in the amplifier, but for chamber voltages greater than about 500 V the impulses due to α-particles were about twice to three times the background height. The absence of serious straggling due to possible tarnishing of the source was tested by measuring the scattering in argon over the full range of energies investigated. This scattering was found to vary according to the classical coulomb law with energy, even for the smallest energies. The scattering in argon was also used to determine the ratio of the actual to classical scattering in the case of helium. The procedure in the present case was precisely the same as that described in Paper I.

The helium was purified by passage through a multiple U-tube containing activated carbon at liquid air temperature. The impurities in the argon were probably not greater than 2 %. Extraneous scattering due to the carbon screens was measured by filling the scattering chamber with hydrogen, since with the scattering angles and gas pressure used no α-particles scattered by hydrogen nuclei could reach the ionization chamber. Under these circumstances any α-particles scattered from the graphite stops would possess a comparatively large fraction of their original energy and could reach the ionization chamber. The bias on the counter was adjusted so as not to count recoil protons. The extraneous scattering was at most a few per cent of the total effect.

Using Ra B + C, etc. sources, it is only possible to investigate the energy region up to about 7·0 MeV. Sources of thorium active deposit up to 1 millicurie were available and for the scattering at 38·5° the effect produced using such a source was measurable, although of course with a low degree of accuracy. Experiments were, then, carried out with these sources in order to investigate the energy region 6–8·5 MeV. In order to increase the measured effect in this case, a rather low resolution was used, the apertures AA, DD being increased in size from 1·0 to 1·1 cm. diameter and the stops BB, CC reduced from 1·0 to 0·9 cm. A complication arises in this case owing to presence of two groups of α-particles from Th C and Th C′ of ranges 4·71 and 8·53 cm. respectively, the relative intensities of the two groups being 35 : 65. Since also a very wide range of angles is effective in the low resolution geometry of the experiments with thorium sources, all the scattered particles from Th C will not be recorded when the thicker mica screens are placed in front of the source. It was necessary, therefore, to measure with this particular geometrical arrangement the variation in the scattering for α-particle ranges up to 5·5 cm., using sources of Ra C′ α-particles. Since for a considerable energy region (i.e. up to the energies obtainable with Ra C′ α-particles) the ratio of the contributions from the Th C′ and Th C is then known, the effects of the two components can be separated in the energy region up to about 7·0 MeV. Further, knowing the complete variation of the effect due to the Th C α-particles, the effect of the Th C′ α-particles separately is at once obtained for the full range of energies up to 8·5 MeV.

3. RESULTS

The results obtained for the scattering of α-particles of Ra C′ at 27° and 38·5° are shown in figs. 2 and 3 respectively, where the ratio of the actual to classical-coulomb scattering, R, is plotted against energy, E, of the α-particles.

The measurements at 38·5° were carried out with three different sets of mica screens and with different mica windows in front of the source. The three sets of observations are shown by differently marked points in fig. 3.

In the case of Th C′ α-particles only the *variation* of the scattering with energy was observed. These observations were not of a very high statistical accuracy, and it was therefore sufficient to fit the results obtained with the thorium sources to the more accurate results obtained with Ra C′ in the

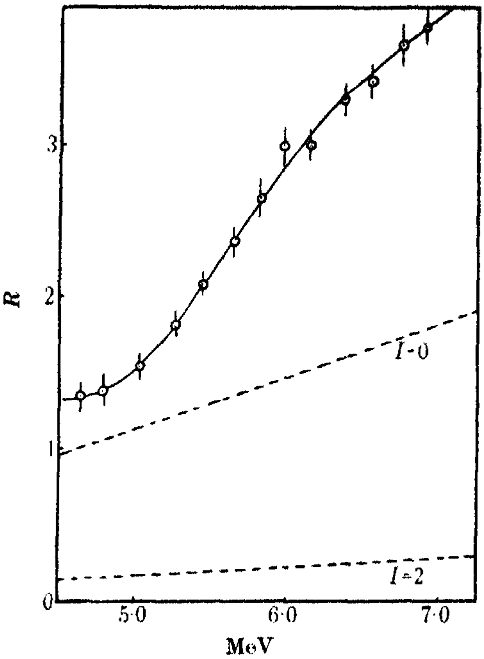

FIG. 2. Scattering of Ra C′ α-particles at 27°.

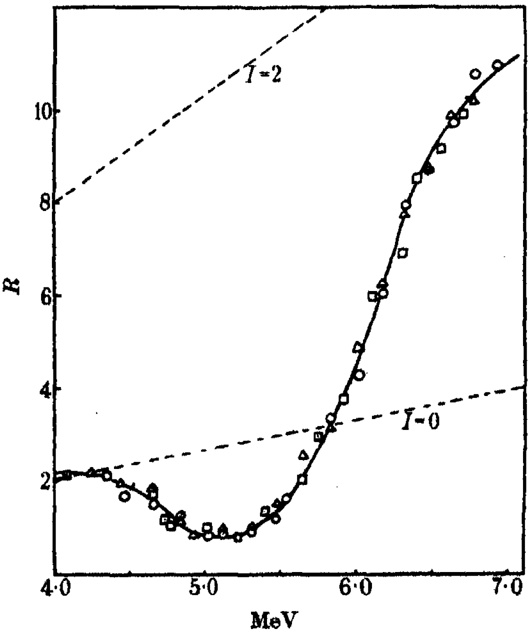

FIG. 3. Scattering of Ra C′ α-particles at 38·5°.

energy region 6–7 MeV. The results for Th C′ α-particles scattered at 38·5° are shown in fig. 4.

The range of angles in the experiments with Ra C′ α-particles was 6·5° for scattering at 27° and 12° for scattering at 38·5°. With the lower resolution arrangement used for Th C′ α-particles the range of angles was about 20°. The range of energies at the scattering region for a particular mica foil was, including straggling, about 0·2 MeV in the first two cases and 0·3 MeV in the third.

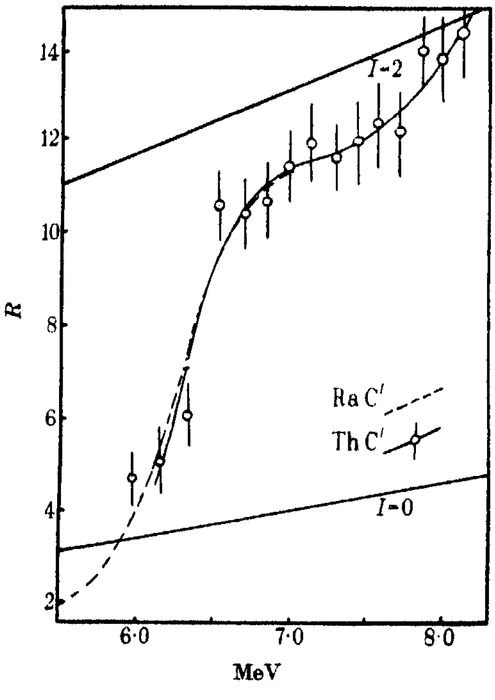

FIG. 4. Scattering of Th C′ α-particles at 38·5°.

4. DISCUSSION

The calculation of the maximum scattered anomalies due to resonance as used in Paper I (equation (4)) is complicated in the present case owing to the fact that the scattering nucleus and scattered particle are identical (Mott 1930). However, a rough value for the maximum contributions from resonance can be obtained by using the sum of two expressions, corresponding to scattering at θ and $\frac{1}{2}\pi-\theta$, since for each α-particle scattered at $\frac{1}{2}\pi-\theta$ a recoil helium nucleus is scattered at θ.

This gives for the approximate maximum resonance effects

$$R_{\max} = \frac{4(2I+1)^2}{e^4 z^2 Z^2} \left\{ \frac{P_I^2(\cos\theta) + P_I^2 \cos(\pi - \theta)}{\operatorname{cosec}^4 \frac{1}{2}\theta + \sec^4 \frac{1}{2}\theta} \right\} h^2 v^2 \tag{2}$$

(where I is the spin quantum number of the compound nucleus responsible for resonance) in place of equation (4) in Paper I, and the values from the above modified equation are shown by the straight lines in figs. 2–4, for values of I equal to zero and two respectively. It seems possible to account for the scattering anomalies at 27° by an interaction with the nuclear short range forces of the zero angular momentum component only. The anomalies at 38·5°, however, necessitate the introduction of the component with angular momentum two. The shape of the curve gives some indication that there is a broad resonance at an energy of about 6·6 MeV superposed on a general rise in the scattering ratio. This general increase is to be expected independently of resonance phenomena. (See discussion in Paper I.) This resonance would correspond to a broad excitation level of Be^8 at 3·3 MeV above the ground state, assuming the mass of normal Be^8 to be equal to that of two α-particles. The excited state would be an "even" D state, i.e. its spin momentum would be equal to two quantum units.

The difference in energy of the ground and excited states of Be^8 from disintegration data is not more than 3 MeV, so that a resonance in scattering at an α-particle energy greater than 6 MeV indicates that the mass of Be^8 in the ground state is greater than that of two α-particles.

The most definite information regarding this level of Be^8 from disintegration data is provided by the experiments of Dee and Gilbert (1936) and those of Oliphant, Kempton and Rutherford (1935), on the disintegration of boron of mass 11 by protons. In order to account for the distribution with energy of the α-particles produced it is necessary to assume that the products of the disintegration are either an α-particle and a Be^8 nucleus in the ground state (the homogeneous group of α-particles): or an α-particle and an excited Be^8 nucleus (with about 3 MeV excitation energy) which subsequently splits up into two short range α-particles (the continuous distribution). From the data of Oliphant, Kempton and Rutherford the excited level of Be^8 seems to have a width of about 0·5 MeV.

In the disintegration of boron of mass 10 by deuterons, there appears to be two groups of α-particles corresponding to the Be^8 produced being left in the normal state or in an excited state of about 3 MeV excitation energy (Cockcroft and Lewis 1936). The group of α-particles corresponding to Be^8 produced in the excited state is rather broad, indicating again that the level in Be^8 at about 3 MeV is a broad one. Feenberg and Wigner (1937) have shown theoretically that the first excited level of Be^8 should be an "even" D level at about 3 MeV. The large width of the level is due to the fact that it can break up easily into two α-particles.

There is no definite evidence in the γ-ray spectrum of Be^8 excited in the capture of protons by Li^7 of a transition to the level of Be^8 at 3 MeV. Such transitions would, however, be expected to occur since the ground state of Be^8 is probably an even S state and since transitions do occur to the ground state one would also expect transitions to the level at 3 MeV. However, the evidence is not conclusive as to whether transitions to this latter level do or do not occur.

I am indebted to Trinity College and the department of Scientific and Industrial Research for grants that have made this work possible, and to Professor Peierls and to Dr N. Feather for much helpful discussion.

SUMMARY

The scattering of α-particles in helium has been investigated for scattering angles of 27° and 38·5°, and for energies up to 8·5 MeV. It is found that the results are consistent with the existence of a broad level of Be^8 with spin two quantum units, and with an energy of about 3·3 MeV in excess of the ground state, which is assumed to possess a mass equal to that of two α-particles. The results for α-particle energies greater than 7·0 MeV are not very accurate owing to the low intensity of the sources of thorium active deposit available.

REFERENCES

Chadwick 1930 *Proc. Roy. Soc.* A, **128**, 114.
Cockcroft and Lewis 1936 *Proc. Roy. Soc.* A, **154**, 246.
Dee and Gilbert 1936 *Proc. Roy. Soc.* A, **154**, 278.
Devons 1939 *Proc. Roy. Soc.* A, **172**, 127.
Feenberg and Wigner 1937 *Phys. Rev.* **51**, 95.
Lewis 1937 *Proc. Camb. Phil. Soc.* **33**, 549.
Mohr and Pringle 1937 *Proc. Roy. Soc.* A, **160**, 190.
Mott 1930 *Proc. Roy. Soc.* A, **127**, 658.
Oliphant, Kempton and Rutherford 1935 *Proc. Roy. Soc.* A, **150**, 241.
Rutherford and Chadwick 1927 *Phil. Mag.* **4**, 605.
Wright 1932 *Proc. Roy. Soc.* A, **137**, 677.

Shower production by penetrating cosmic rays

BY A. C. B. LOVELL
Physical Laboratories, University of Manchester

(*Communicated by P. M. S. Blackett—Received* 12 *June* 1939)

[Plate 22]

1. INTRODUCTION

The transition curve, giving the cosmic-ray shower intensity under increasing thicknesses of lead, rises to a maximum at about 1·6 cm., falls fairly rapidly to 5 cm., and then falls off more slowly, maintaining a finite intensity at very great thicknesses. Further, the occurrence of showers deep underground has long been established (Follett and Crawshaw 1936; Ehmert 1937). The showers forming the initial part of the transition curve (up to about 5 cm. of lead) are adequately accounted for by cascade multiplication from incident electrons or photons (Bhabha and Heitler 1937). Some other mechanism, however, is required to explain the occurrence of showers under much greater thicknesses.

It is generally recognized that the showers forming the tail of the transition curve are associated with the penetrating component, and the theory developed by Bhabha (1938) suggests a probable mechanism, whereby a mesotron knocks-on an electron in a direct collision; the electron subsequently producing a shower through the normal cascade process. It has already been shown that the production of secondaries (small showers) by the penetrating component can be accurately explained by this knock-on mechanism (Wilson, J. G. 1938; Trumpy 1938; Hopkins, Nielsen and Nordheim 1939).

In the present investigation an automatic counter-controlled cloud chamber has been used to investigate the larger showers among those which form the tail of the transition curve. It has been found that the knock-on theory is capable of accounting for the showers observed. The probabilities for the existence of possible other processes of shower production under these conditions are also analysed.

2. EXPERIMENTAL ARRANGEMENT

The cloud chamber, which had a 1·8 cm. lead plate across its centre, was placed immediately under 10, 20 or 30 cm. of lead, and was operated by a coincidence of the four counters A, B, C, D, arranged either as in fig. 1*a* or 1*b*. The bias introduced by this counter system against showers containing only a few particles is desirable, both because of the technical disadvantage of handling large numbers of unwanted photographs, and the necessity for reducing the number of unrecorded showers, which occur when the chamber is inactive (about 2 min. after each expansion).

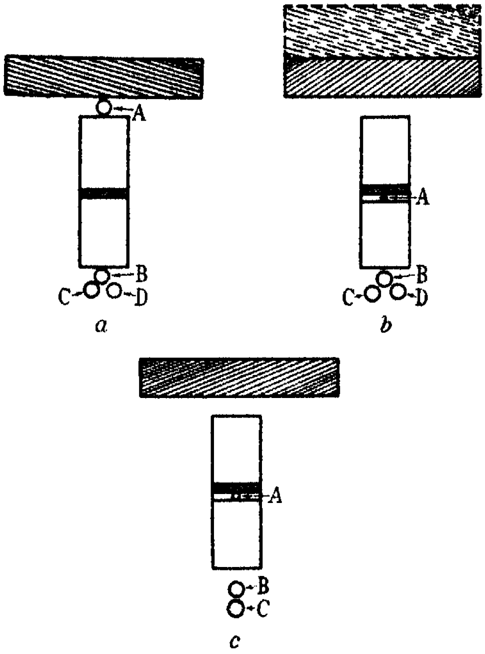

a *b* *c*

FIG. 1

TABLE I

Arrangement	Magnetic field G	Lead over chamber cm.	Number of photographs	Running time hr.	Information extracted
(*a*) Fig. 1*a*	750	10	1000	600	119 showers containing not less than 5 particles
(*b*) Fig. 1*b*	750	10, 20 or 30	1200	900	200 showers containing not less than 5 particles
(*c*) Fig. 1*c*	750	10	600	50	500 traversals of the chamber plate by single particles
(*d*) Various	750	< 10	3000	600	144 showers containing not less than 5 particles

The arrangement of fig. 1*c* has been used to photograph single particles (see § 9*c*). The runs made with these arrangements are given in Table I.

The data given by (*a*) is discussed in §§ 3–6; by (*b*) and (*c*) in § 9; and by (*a*)–(*d*) in § 8.

3. THE NUMBER OF PARTICLES IN THE SHOWERS

In estimating the number of particles in the showers, we confine our attention to particles with energies greater than the critical energy E_c, defined as the energy at which the mean energy loss by radiation equals that due to ionization ($E_c = 10^7$ eV for lead).

The number of particles with energies greater than E_c, appearing in the top half of the chamber, have been counted. The real number in the shower will be greater than this by a numerical factor depending on the relative size of the shower and the chamber. The number of particles above E_c in the showers are therefore somewhat greater than those given in Table II; but the calculated probabilities will not be appreciably affected.

4. REDUCTION OF OBSERVATIONS

For comparison with the theoretical probabilities it is convenient to calculate from the observations the probability $P(N)$ that a mesotron, passing through the lead, gives rise to an observed shower of N particles. That is, we require to find

$$P(N) = n/Q, \qquad (1)$$

where n = observed number of showers of N particles in time t, and Q = number of mesotrons passing through the lead in this time. Now Q depends on the geometrical arrangement of the apparatus and on the time of the experiment. We may write $Q = q\alpha t\delta$, where q = total vertical mesotron flux/unit time/unit area/unit solid angle, at sea-level, α = area of collection, t = time of experiment, and δ = solid angle for collection.

To find α and δ, the stereo-photographs have been reprojected to determine the points of origin of the showers in the lead above the chamber. About one-third of the showers, although originating in the lead, either entered the chamber obliquely, or did not have their axes placed centrally in the chamber. To include these in the statistics would introduce uncertainty in the solid angle for collection, and in the number of particles in the shower. Therefore a rigid selection of 32 showers has been made, emerging from an area in the lead situated directly above the illuminated portion of the chamber plate and about equal in area to it.

The vertical cosmic ray intensity at sea level is 0·80/sq. cm./min./unit solid angle (Street and Woodward 1934). The fraction of these which are penetrating is, according to Auger (1935), Blackett (1938) and others, about 80%. Thus $q = 0{\cdot}64$/sq. cm./min./unit solid angle.

In the experiment $\alpha = 96$ sq. cm., $\delta = 0{\cdot}10$, $t = 600$ hr.; therefore the number of mesotrons capable of producing the showers observed is $Q = q\alpha\delta t = 2{\cdot}2 \times 10^5$.

If we observe n showers of N particles during the experiment, the probability of such a shower being produced per mesotron is then

$$P(N) = \frac{n}{Q} = \frac{n}{2{\cdot}2} \times 10^{-5}. \tag{2}$$

In Table II we give the numbers of showers observed (n) of not less than N particles above the critical energy, and the probabilities calculated from (2).

TABLE II

N	n	$P(N)$	Theoretical value of $P(N)$ calculated from the knock-on theory
5	—	—	80×10^{-5}
10	18	$8{\cdot}2 \times 10^{-5}$	19×10^{-5}
20	7	$3{\cdot}2 \times 10^{-5}$	$3{\cdot}7 \times 10^{-5}$
30	4	$1{\cdot}82 \times 10^{-5}$	$1{\cdot}3 \times 10^{-5}$
40	1	$0{\cdot}45 \times 10^{-5}$	$0{\cdot}23 \times 10^{-5}$
50	1	$0{\cdot}41 \times 10^{-5}$	$0{\cdot}15 \times 10^{-5}$

5. THE KNOCK-ON THEORY OF SHOWER PRODUCTION

(a) *Probability of shower production*

The theory of the penetrating component given by Bhabha (1938) enables a calculation to be made of the probability that a mesotron knocks-on an electron in a direct collision, the electron subsequently producing a shower through the normal cascade process.

Bhabha has calculated the probabilities that mesotrons of energy E_0 emerge from a thick layer of lead accompanied by N electrons and positrons above the critical energy E_c. In this experiment we are concerned with particles of all energies incident on the lead, so that the probabilities for shower production by the knock-on process will depend on the incident energy spectrum of mesotrons.

If the number of mesotrons incident on the lead in the energy range E to $(E+dE)$ is $dn = S(E)\,dE$, then the probability for a shower of N

particles emerging from the lead above the critical energy, produced by the knock-on process, is

$$P(N) = \int_{E=0}^{E=\infty} \psi(E)\, S(E)\, dE, \tag{3}$$

where $\psi(E)$ is the probability that a mesotron of energy E_0 produces a shower below the lead of N particles above the critical energy. $\psi(E)$ is the expression calculated by Bhabha (equation 4·10, 1938).* From it we have calculated the values of ψ for different values of E_0, for $N = 5$ to 50 particles, assuming the mesotron mass $\mu = 200m$.

The probability $P(N)$ of equation (3) has been evaluated graphically, using the values of the energy spectrum given by Blackett (1937). $\psi(E)$ is not very sensitive to the value of μ. Thus the existence of a considerable number of protons in the incident beam will not affect the probabilities appreciably. These calculated probabilities are given in Table II for showers of 5–50 particles above the critical energy (10^7 eV).

(b) *Effect of the energy spectrum*

The combination of the observed incident energy spectrum of mesotrons, with the relation between E_0 and ψ, has important consequences. We consider the production of a shower of given size (N particles) by a mesotron of energy E_0. The maximum energy which a mesotron of mass μ can transfer to an electron of mass m in a free collision is (Bhabha 1938)

$$W_m = q_m E_0', \tag{4}$$

where

$$q_m = \frac{2m\mu(\gamma+1)}{m^2+\mu^2+2m\mu\gamma},$$

$$\gamma = E_0/\mu c^2,$$

and $E_0' = (E_0 - \mu c^2)$, the kinetic energy of the mesotron.

In this expression q_m approaches unity as γ increases. Thus the maximum energy which the mesotron can transfer to an electron, W_m, approaches E_0', as E_0' increases. Now $\psi(E)$ is zero for energies E_0' below a given value, and then increases rapidly with increasing E_0', until q_m approaches unity. In practice, however, this increase in the probability that a mesotron of energy E_0' produces a shower of N particles is more than counteracted by the fact that the number of incident mesotrons decreases rapidly with increasing energy. The combination of these two effects gives a probability curve with a pronounced peak at low energies.

---

* The equation (4·10) given by Bhabha contains two numerical errors. However, the numerical constant C in this equation is adjusted to bring the results of Table VI into accord with those of Table IV; thus the final results are not appreciably affected. As stated by Bhabha the probabilities given in his Table VI are roughly too large by a factor of 2. The value of C should be of the order of 1/4 and not 2.

We consider as an example the detailed predictions made by the knock-on theory, in the production of showers of $N = 5$ and $N = 50$ particles. In Table III we give the values of γ, q_m, W_m, and $\psi(E)$ for increasing values of E_0'.

TABLE III

E_0' eV	γ	q_m	W_m eV	$\psi(E)$ for $N = 5$	$\psi(E)$ for $N = 50$
5×10^8	6	$6\cdot6 \times 10^{-2}$	$3\cdot3 \times 10^7$	0	0
10^9	11	$1\cdot07 \times 10^{-1}$	$1\cdot07 \times 10^8$	0	0
5×10^9	51	0·34	$1\cdot7 \times 10^9$	$2\cdot2 \times 10^{-3}$	$6\cdot3 \times 10^{-7}$
10^{10}	100	0·505	$5\cdot05 \times 10^9$	$2\cdot5 \times 10^{-3}$	$1\cdot1 \times 10^{-5}$
10^{11}	1000	0·91	$9\cdot1 \times 10^{10}$	$3\cdot0 \times 10^{-3}$	$2\cdot9 \times 10^{-5}$
10^{12}	10,000	0·99	$9\cdot9 \times 10^{11}$	$3\cdot0 \times 10^{-3}$	$3\cdot1 \times 10^{-5}$

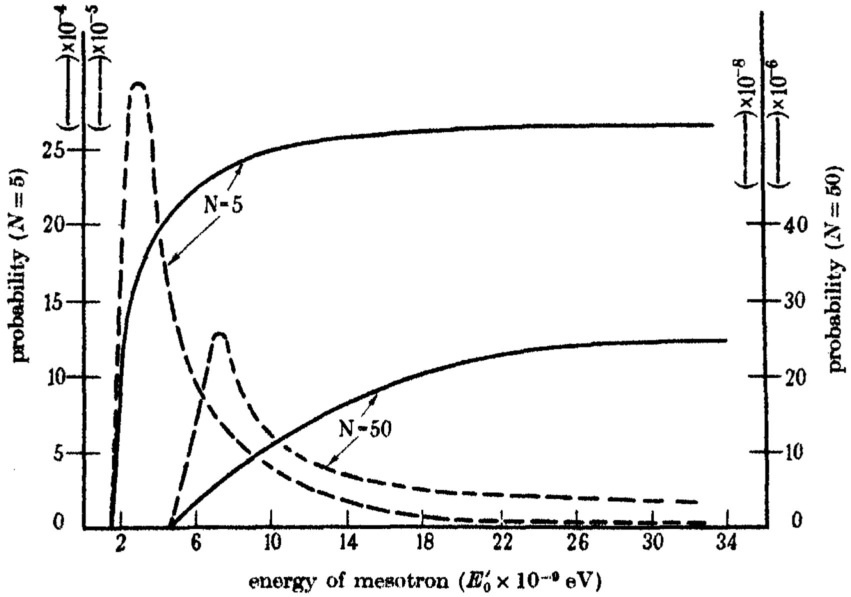

FIG. 2. (——) Theoretical probabilities for production of showers of $N = 5$ and $N = 50$ particles by the knock-on process, plotted against the energy of the mesotron. (– – –) Corresponding curves calculated for the observed energy spectrum.

The relation between $\psi(E)$ and E_0' is shown graphically by the full line curves in fig. 2, while the product of $\psi(E)$ by the incident energy spectrum is shown by the broken curves on the same diagram. These broken curves are the probability curves applicable to the observations.

The curve for $N = 5$ has a peak probability at about $E'_0 = 3 \times 10^9$ eV, that is, for a value of $q_m \simeq 0{\cdot}23$. The corresponding peak in the curve for $N = 50$ occurs at $7{\cdot}5 \times 10^9$ eV, for a value of $q_m \simeq 0{\cdot}43$. Thus for an increase in shower size of 10 times, the most probable energy for production increases only by a factor of 2·5. Hence it appears that almost all observed knock-on showers under lead are produced by mesotrons in a comparatively narrow energy range, and that showers of 50 particles or less are produced by mesotrons which transfer, on the average, not more than 1/2 of their energy to the knock-on electron. Thus we should expect the mesotron to appear in the shower photograph as a penetrating particle unless it is heavily scattered. The general complication of the shower photographs obtained here makes this observation difficult, but the mesotron can in fact be identified in about 25 % of the shower photographs.

(c) *The largest shower which can be produced by a given mesotron*

According to Bhabha and Heitler (1937), a shower of N positrons and electrons with energy over E_c can just be produced by an electron of energy E_n, where

$$N = 0{\cdot}124\left(\frac{E_n}{E_c}\right)^{0{\cdot}93}. \tag{5}$$

If the fluctuations of shower size are taken into account, however,

$$N = \frac{0{\cdot}124}{C}\left(\frac{E_n}{E_c}\right)^{0{\cdot}93},$$

where C is a numerical factor depending upon fluctuations. The value of C may be found by calculations similar to those made by Bhabha (1938), and assuming that fluctuations are of the form taken there (equation 4·4, 1938), we find its value to be approximately 1/4. Thus (5) becomes

$$N = 0{\cdot}5\left(\frac{E_n}{E_c}\right)^{0{\cdot}93}. \tag{6}$$

In considering showers produced by the knock-on process, E_n in this equation becomes W_m of equation (4), the maximum energy which the mesotron can transfer to an electron in collision. If $\mu = 200m$, then

$$q_m = \frac{\gamma}{\gamma + 100} \text{ provided } \gamma \gg 1 \text{ (i.e. } E'_0 > 5 \times 10^8 \text{ eV).}$$

Using (4) and (6) we obtain the kinetic energy of the mesotron E'_0 which can just produce a shower of N positrons and electrons:

$$N = 0{\cdot}5\left(\frac{\gamma E'_0}{E_c(\gamma + 100)}\right)^{0{\cdot}93}. \tag{7}$$

If $\gamma \gg 100$, i.e. for $E_0' \geqslant 10^{11}$ eV, this reduces to

$$N = 0{\cdot}5\left(\frac{E_0'}{E_c}\right)^{0{\cdot}93}. \tag{8}$$

Equations (7) and (8) thus give the largest cascade shower which can be produced by a mesotron of energy E_0', taking fluctuations into account.

(*d*) *The most probable energy for shower production*

The considerations of § 5*b* on the influence of the energy spectrum show that equations (7) and (8) are also a fair approximation to the energy of the mesotron which has the greatest probability of producing a shower of N particles. From fig. 2 we see that the most probable energy is about twice the minimum energy, so that, using (7), the most probable energy is given by

$$(E_0')_p = \frac{\gamma+100}{2\gamma} E_c (4N)^{1{\cdot}075}. \tag{9}$$

Neglecting fluctuations, the *minimum* energy required to produce the shower of N particles is from (5)

$$(E_0')_{\min} = \frac{\gamma+100}{\gamma} E_c (8N)^{1{\cdot}075}, \tag{10}$$

so that

$$\frac{(E_0')_p}{(E_0')_{\min}} = \frac{1}{2{\cdot}4}.$$

Thus, due to the influence of the energy spectrum, the most probable knock-on showers are produced as fluctuations. In the case of a shower of $N = 50$ particles, for example, equation (10) gives $(E_0')_{\min} = 1{\cdot}2 \times 10^{10}$ eV. From fig. 2 we conclude that, on the average, as many showers of this size are produced (through fluctuations) by mesotrons with energy below this value as are produced by mesotrons with energy greater than $(E_0')_{\min}$. With increasing shower-size the effect of fluctuations becomes more pronounced, since the energy spectrum falls off more rapidly at higher energies. Hence almost all showers of a hundred or more particles must be produced as fluctuations; a conclusion already reached by Montgomery and Montgomery (1938) for large cascade showers produced by an incident electron.

6. COMPARISON WITH EXPERIMENT

The theoretical and experimental probabilities may be compared in Table II, and in fig. 3, from which it is seen that the agreement is within the probable limits of the theory and experiment. The divergence for small showers is to be expected in view of the strong bias introduced by the counter system against recording them. But it has already been mentioned (§ 1) that the knock-on theory has been shown to account satisfactorily for the production of these small showers.*

Thus it appears that all the showers forming the tail of the transition curve in lead may be regarded as knock-on showers, and it does not seem necessary to assume any other process of appreciable cross-section. Several other processes have been suggested, however, and the evidence and probabilities for these processses will now be considered.

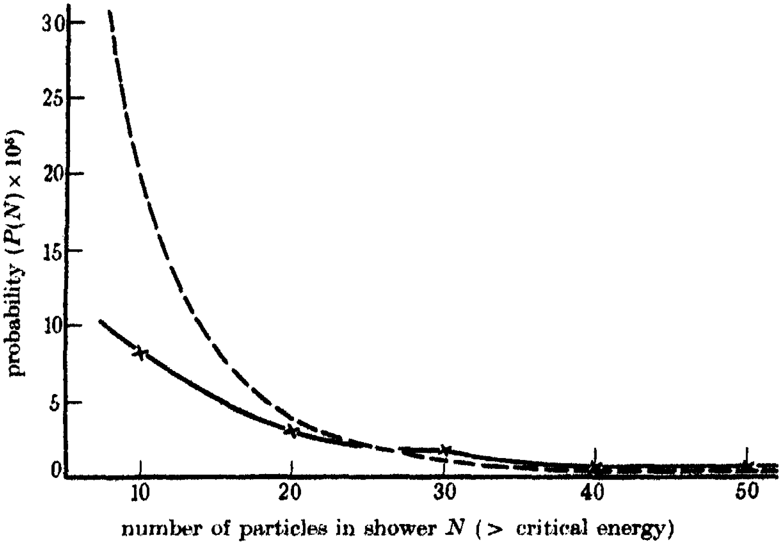

FIG. 3. Experimental and theoretical probabilities for production of knock-on showers by mesotrons. (– – – – –) theoretical; (— × — × —) experimental.

7. SHOWERS PRODUCED BY QUANTA

(a) *Collision radiation*

A mesotron may emit a photon when its motion changes in a nuclear field. The photon may then produce an ordinary cascade shower, and such a shower would be visually indistinguishable from those produced by a knock-on electron; thus the above experiments can give no direct information about the occurrence of this process.

---

* [*Note added in proof.*—The author is indebted to Dr Bhabha for information concerning recent modifications in the knock-on theory. These modifications raise the theoretical value of $P(N)$ for large showers but do not influence the existing values for small showers. The agreement with the experimental values is thus improved.]

Bhabha (1938) has shown, however, that the ratio of the chance of a mesotron emitting a quantum of energy greater than E_c, to the chance of its producing by collision an electron of energy greater than E_c, is of the order unity for $\mu = 10m$ and is small compared with unity for $\mu \gg 10m$.

Existing evidence indicates that μ is of the order of $170m$ and thus we expect a negligible contribution from this process to the observed showers.

(*b*) *Stoppage of mesotrons*

Heitler (1938) has considered processes in which a mesotron (Y) collides with a free neutron (N) or proton (P), its total energy being taken up by a light quantum:

$$Y^+ + N = P + h\nu,$$

$$Y^- + P = N + h\nu.$$

If these processes occur they should produce ordinary cascade showers, which would in general be visually indistinguishable from the knock-on showers. The cross-section for the processes is not accurately calculable, since the theory is not applicable for energies greater than μc^2. Two estimates have been made; by Heitler (1938), and by Massey and Corben (1939). The cross-section for the above processes, for a mesotron of 10^8 eV, lead to a probable path length of 2 m. and 30 m. of lead respectively, in the two estimates. But the experiments already considered have involved the traversal of 10 cm. of lead by $2 \cdot 2 \times 10^5$ mesotrons (§ 4); thus if the above processes occur for high energy mesotrons, with frequency comparable to that calculated for those of low energy, we should have observed between 1000 and 10,000 showers, whereas the number actually observed is about 50, all of which can be accounted for as knock-on showers. It is therefore clear that if such processes occur, their cross-section is of an order of magnitude lower than that of the present estimates for low energy mesotrons.

This result is of further interest since the inverse processes have been postulated by Heitler to explain the production of mesotrons in the high atmosphere. Considerable doubt must now be thrown on the occurrence of this process in view of the above conclusions.

8. NUCLEAR DISINTEGRATIONS

The occurrence of processes involving the ejection of protons is now well established. Many cases have been observed on photographic emulsions at high altitudes (Blau and Wambacher 1937; Wambacher 1938; Jdanoff

1939), while at sea level Fussell (1937) observed 3 in 900 showers, and several have been photographed by Blackett and Occhialini (1933) and by Brode and Starr (1938). Such cases have been considered by Heisenberg (1937), Williams (1938) and Heitler (1938) as cases of nuclear evaporation.

In the 5800 photographs under lead, referred to in Table I, we have observed in addition to 463 electronic showers of not less than 5 particles, 11 showers containing 1 proton, and two showers containing 2 protons. Reprojection of the photographs shows, however, that in all cases the path of the proton is widely separated from the shower origin. In addition there have been two cases of a definite nuclear disintegration occurring in the piston.

9. MULTIPLE PROCESSES

(a) *Introduction*

The production of showers of mesotrons by penetrating cosmic ray particles, in single multiple processes of the type

$$Y^{+}+N=P+Y^{+}+Y^{-}+\ldots, \tag{11}$$

have been suggested by Heitler (1938) and by Euler (1938). Also Kemmer (1938) and Arley and Heitler (1938) have pointed out that the existence of the neutral counterpart of the mesotron ("neutretto") is in conformity with contemporary theories of the nuclear forces; and that if it exists, it should be capable of giving rise to similar multiple processes:

$$Y^{0}+P=N+Y^{+}+Y^{-}+\ldots, \tag{12}$$

and of transforming itself into a mesotron during a collision with a proton or neutron:

$$\left.\begin{aligned} Y^{0}+N&=P+Y^{-},\\ Y^{0}+P&=N+Y^{+}.\end{aligned}\right\} \tag{13}$$

Such processes would give rise to showers, mainly of mesotrons, observable under dense materials; we have therefore made a direct search for processes of this type.

(b) *The search for showers*

If processes of the type (11) or (12) occurred in the lead over the chamber, they would appear as groups of particles traversing the 1·8 cm. lead plate across the chamber, without producing an appreciable number of secondaries. Apart from two very doubtful cases there are no showers of this type in 463 electronic showers. Though it must be pointed out that if only two or three penetrating particles are associated in a large electronic shower they would not be easily detected in these photographs, owing to the density of the tracks on the photographs.

A further experiment has been made in an endeavour to observe showers produced by non-ionizing particles other than photons. The experiment consisted of an attempt to photograph showers produced in a lead plate across the centre of the cloud chamber by non-ionizing particles. It was thus essential to photograph with all the counters below this plate. The normal arrangement with all the counters below the chamber gives an extremely poor yield of showers per photograph, due to the high rate of casual coincidences in the counter set, and to coincidences caused by bits of oblique showers originating in the magnet coils and surrounding metal. To obviate this, one counter was placed *inside* the cloud chamber (fig. 1*b*). This counter was contained in a thin-walled brass box, and the lead plate rested on top of this box. The experiment was carried out under a roof of lead from 10 to 30 cm. thick. The probability of a shower being produced in the lead plate by an energetic photon from the air was thus negligible.

The details of the run with this arrangement are given in Table I (*b*). Of the 200 showers obtained, 120 were clearly cases of cascade showers emerging from the lead over the chamber, that is, showers of the type measured in §§ 3–6 and illustrated in fig. 4 (Plate 22); they are therefore not of direct interest to this experiment. The remaining 80 showers originate in the lead plate across the centre of the chamber. Of these, 60 were obviously associated with an incoming mesotron (fig. 5, Plate 22), and from our previous analysis can all be assumed to be knock-on showers. The remaining 20 showed no incident ionizing particle, but on reprojection were found to originate from the edge of the illuminated part of the chamber plate, and are thus probably cases of oblique knock-on showers, in which the mesotron track was not photographed. From the geometrical arrangement and the known angular distribution of incoming mesotrons, it can easily be shown that an "edge" effect of this order of magnitude is to be expected. No difference exists in the phenomena under 10, 20 or 30 cm. of lead, apart from a slight decrease in the absolute shower frequency.

Thus the experiment gives no direct evidence that any non-ionizing particles (other than photons) which may exist produce showers with an appreciable probability. The experiment is not conclusive, however, since the complication of the shower phenomena does not facilitate accurate reprojection to the shower origin, and the showers emerge from the bottom of the brass box, 2 cm. from the bottom of the lead plate. Thus there can be no precise comparison between the calculated number of showers which are so oblique that the incoming mesotron is not photographed and the observed number. We estimate that if such non-cascade processes occur, they contribute less than 1 % to the totality of showers observed in the tail of the transition curve for lead.

(c) *The search for single secondary particles*

A similar experiment, using a counter in the chamber, has been made to search for single particles originating in the lead across the chamber, produced by non-ionizing particles. In this case the shower set below the chamber was replaced by two counters one above the other, so that triple vertical coincidences were recorded (fig. 1*c*). The experiment was carried out with 10 cm. of lead over the chamber, to prevent the formation of pairs in the plate, by photons incident from the air. As seen from the data of Table I we have observed 500 traversals of the lead plate by single mesotrons, but there is no indication of the creation of single particles.

The yield of tracks per photograph with such an arrangement, employing a counter in the chamber, was 85 % compared with 23 % when all three counters were placed vertically beneath the chamber.

For such transformations involving the production of single charged secondaries, the mean-free-path of a neutretto in lead should be of the order of 5 cm. (Arley and Heitler 1938). If this estimate is correct, then it is clear that the number of neutrettos in cosmic radiation at sea level must be very much smaller than the number of mesotrons, for we have photographed the traversal of 2 cm. of lead by 500 particles, which is equivalent to 10 m. of lead, and the process has not been observed.

(d) *Discussion*

The above experiments give no evidence that multiple processes occur with an appreciable probability, or that any non-ionizing particles, more penetrating than photons, are present in cosmic radiation at sea level.

A considerable number of existing experiments have been interpreted as showing the presence of penetrating particles in showers; and as evidence for the neutretto. The majority of these experiments are capable of alternative interpretation however. For example, Jánossy (1938) has shown that the results of Schmeiser and Bothe (1938) may be interpreted in terms of energetic-electron cascade showers; and recent counter experiments by Rossi and Jánossy* do not indicate the presence of an appreciable number of non-ionizing particles. This is in contradiction to the results of Maass (1936), Hsiung (1934) and Shonka (1939). The showers obtained in a deep mine by Barnóthy and Forró (1937), originally attributed to non-ionizing particles, can be alternatively explained as knock-on showers; while the majority of the remaining evidence for the existence of a neutral penetrating particle has been withdrawn (e.g. Wilson, V. C. 1938, 1939).

---

* Private communication.

Thus it seems clear that the contribution of multiple processes to the showers observed in the tail of the transition curve at sea level is insignificant.

10. CONCLUSIONS

From the analysis of §§ 4–5, it appears that the showers observed in these experiments, under 10 cm. or more of lead, may be regarded as showers produced by an electron which has been knocked-on in a direct collision by a mesotron. The experiment gives no direct information about the occurrence of cascade showers associated with the mesotron through other processes, but it is unnecessary to assume other processes of appreciable cross-section in order to account for the observations.

There is no evidence for the occurrence of groups of penetrating particles in the showers, although if only two or three penetrating particles were associated in a large electronic shower, they would be unlikely to be detected, owing to the density of tracks on the photograph.

The author is indebted to Professor P. M. S. Blackett for providing facilities for the work, and to Dr Hu Chien Shan who originally constructed the cloud chamber in 1937 at Birkbeck College, London.

SUMMARY

A counter controlled cloud chamber has been used to investigate cosmic ray showers under thick layers of lead. 5000 photographs, containing 463 electronic showers of not less than 5 particles, have been taken in a magnetic field of 750 G.

An analysis of the evidence and probabilities for various possible processes of shower production is carried out, and it is shown that the showers observed can be accounted for as cascade showers, produced by an electron which has been knocked-on in a direct collision with a mesotron. It is unnecessary to assume the occurrence of other processes of appreciable cross-section.

Due to the influence of the incident energy spectrum of mesotrons, the majority of large showers are produced as fluctuations, and in general, the lowest mesotron energy which is able to produce a shower of N particles

is only slightly lower than the most probable energy for the production of such a shower.

A search has been made to find showers, or single secondary particles, produced by neutral particles in cosmic radiation, with negative results.

REFERENCES

Arley, N. and Heitler, W. 1938 *Nature, Lond.*, **142**, 158.
Auger, P. 1935 *J. Phys. Radium*, **6**, 226–8.
Barnóthy, J. and Forró, M. 1937 *Z. Phys.* **104**, 744–61.
Bhabha, H. J. 1938 *Proc. Roy. Soc.* A, **164**, 257–94.
Bhabha, H. J. and Heitler, W. 1937 *Proc. Roy. Soc.* A, **159**, 432–58.
Blackett, P. M. S. 1937 *Proc. Roy. Soc.* A, **159**, 1–31.
— 1938 *Proc. Roy. Soc.* A, **165**, 11–31.
Blackett, P. M. S. and Occhialini, G. P. S. 1933 *Proc. Roy. Soc.* A, **139**, 699–726.
Blau, M. and Wambacher, H. 1937 *S.B. preuss. Akad. Wiss.* **146**, 623–41.
Brode, R. B. and Starr, M. A. 1938 *Phys. Rev.* **53**, 3–5.
Ehmert, A. 1937 *Z. Phys.* **106**, 751–73.
Euler, H. 1938 *Z. Phys.* **110**, 692–716.
Follett, D. H. and Crawshaw, J. D. 1936 *Proc. Roy. Soc.* A, **155**, 546–58.
Fussell, L. 1937 *Phys. Rev.* **51**, 1005.
Heisenberg, W. 1937 *Naturwissenschaften*, **25**, 749.
Heitler, W. 1938 *Proc. Roy. Soc.* A, **166**, 529–43.
Hopkins, J. I., Nielsen, W. M. and Nordheim, L. W. 1939 *Phys. Rev.* **55**, 233.
Hsiung, D. S. 1934 *Phys. Rev.* **46**, 653–8.
Jánossy, L. 1938 *Proc. Camb. Phil. Soc.* **34**, 614–19.
Jdanoff, A. 1939 *Nature, Lond.*, **143**, 682.
Kemmer, N. 1938 *Proc. Camb. Phil. Soc.* **34**, 354–64.
Maass, H. 1936 *Ann. Phys., Lpz.*, **27**, 507–31.
Massey, H. S. W. and Corben, H. C. 1939 *Proc. Camb. Phil. Soc.* **35**, 84–94.
Montgomery, C. G. and Montgomery, D. D. 1938 *Phys. Rev.* **53**, 955–9.
Schmeiser, K. and Bothe, W. 1938 *Ann. Phys., Lpz.*, **32**, 161–77.
Shonka, F. R. 1939 *Phys. Rev.* **55**, 24–7.
Street, J. C. and Woodward, R. H. 1934 *Phys. Rev.* **46**, 1029–34.
Trumpy, B. 1938 *Z. Phys.* **111**, 338–44.
Wambacher, H. 1938 *Phys. Z.* **39**, 883–92.
Williams, E. J. 1938 *Nature, Lond.*, **142**, 431.
Wilson, J. G. 1938 *Nature, Lond.*, **142**, 73.
Wilson, V. C. 1938 *Phys. Rev.* **53**, 337–43.
— 1939 *Phys. Rev.* **55**, 6–10.

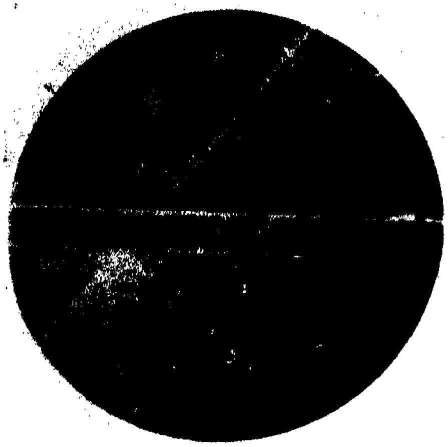

Fig. 4. Arrangement of fig. 1*a*. 2 cm. of lead across the centre of the chamber and 10 cm. of lead over the top. A shower of about 20 particles produced by an electron, knocked-on by a mesotron in the lead over the chamber. Magnetic field 750 G.

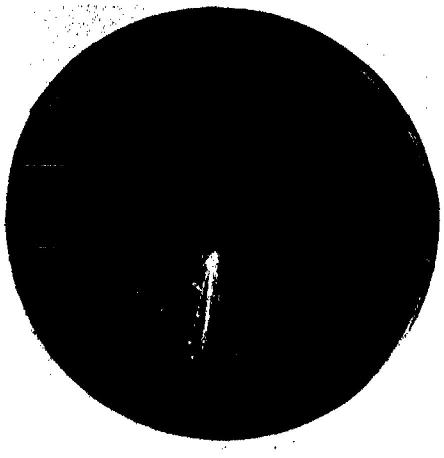

Fig. 5. Arrangement of fig. 1*b*. Brass box containing a counter, across the centre of the chamber, with 2 cm. of lead resting on top of it. The single particle in the top of the chamber is a mesotron which has penetrated 20 cm. of lead over the chamber, and produced a knock-on shower in the chamber plate. No magnetic field; the curvature of the incoming track near the plate is due to distortion.

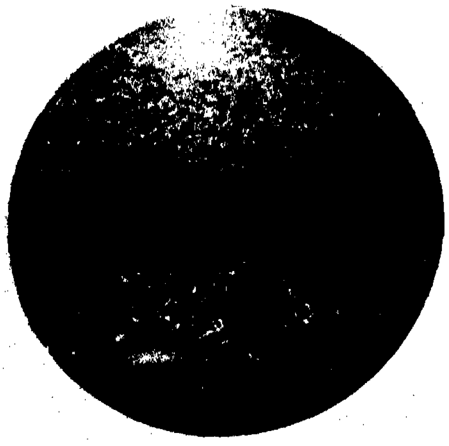

Fig. 6. Arrangement of fig. 1*b* (as in fig. 5 above). Cross-section of a large shower travelling almost horizontally, originating from the base of the chamber. Magnetic field 750 G.

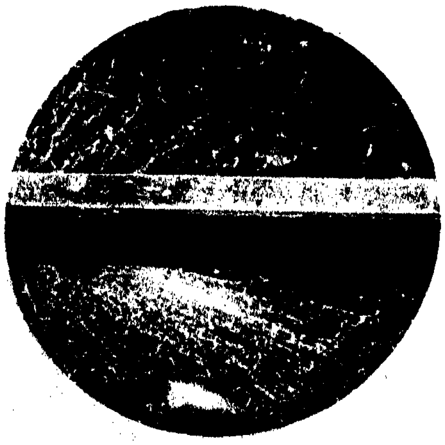

Fig. 7. Arrangement of fig. 1*b*, with 30 cm. of lead over the top of the chamber. A large oblique shower, probably a knock-on shower from the chamber wall, undergoing further cascade multiplication in the chamber plate. A short proton track is visible on the left of the photograph just under the plate. Magnetic field 750 G.

INDEX TO VOLUME CLXXII (A)

Aerofoils, moving, hydrodynamical theory (Morris), 213.

Allen, J. F. and Misener, A. D. The properties of flow of liquid helium II, 467.

Alpha particles, resonance phenomena in scattering (Devons), 127.

Alpha particles, scattering in helium (Devons), 559.

Appleyard, E. T. S. and Bristow, J. R. The electrical conductivity of thin films of mercury, 530.

Appleyard, E. T. S., Bristow, J. R., London, H. and Misener, A. D. Superconductivity of thin films: I, mercury, 540.

Arnot, F. L. *See* M'Ewen and Arnot.

Atkins, B. E., Bastick, R. E. and Ibbs, T. L. Thermal diffusion in mixtures of the inert gases, 142.

Baly, E. C. C. The photosynthesis of carbohydrates from hydrated carbon dioxide, 445.

Barium and strontium azides, action of ultra-violet radiation (Garner and Maggs), 299.

Barium azide, thermal decomposition (Wischin), 314.

Bastick, R. E. *See* Atkins, Bastick and Ibbs.

Bhabha, H. J. Classical theory of mesons, 384.

Born, M. and Fuchs, K. On fluctuations in electromagnetic radiation, 465.

Bowden, F. P. and Hughes, T. P. The friction of clean metals and the influence of adsorbed gases; the temperature coefficient of friction, 263.

—— —— The mechanism of sliding on ice and snow, 280.

Bristow, J. R. *See* Appleyard and Bristow *and* Appleyard and others.

Buckler, E. J. and Norrish, R. G. W. A study of sensitized explosions, IV, 1.

Carbon tetrachloride, fine structure of Raman lines (Menzies), 89.

Conn, G. K. T. and Sutherland, G. B. B. M. The infra-red absorption spectrum of tetra-deuteroethylene, 172.

Convection in liquids (Saunders), 55.

Corkill, A. J. and Rosenhead, L. Distribution of charge and potential in an electrolyte bounded by two plane infinite parallel plates, 410.

Cosmic ray particles, absorption in gold (Wilson), 517.

Cosmic rays, cloud chamber observations (Williams), 194.

Cosmic rays, shower production (Lovell), 568.

Crystallite size and internal strains in cold-worked metals (Wood), 231.

Curran, S. C. and Strothers, J. E. The excitation of γ-radiation in processes of electron capture, 72.

Devons, S. Resonance phenomena in the scattering of α-particles by some light nuclei, 127.

—— The scattering of α-particles in helium, 559.

Dielectric loss due to polar molecules in paraffin (Pelmore), 502.

Diffraction of X-rays by crystals at elevated temperatures (Preston), 116.

Electric polarization, theory (Piekara), 360.
Electrolyte, distribution of charge and potential (Corkill and Rosenhead), 410.
Electromagnetic radiation, fluctuations (Born and Fuchs), 465.
Explosions, sensitized (Buckler and Norrish), 1.

Friction of clean metals and temperature coefficient (Bowden and Hughes), 263.
Fröhlich, H. Theory of electrical breakdown in ionic crystals, II, 94.
Fuchs, K. *See* Born and Fuchs.

Gamma radiation, excitation in electron capture (Curran and Strothers), 72.
Garner, W. E. and Maggs, J. The action of ultra-violet radiation on barium and strontium azides, 299.
Glacier structure and flow (Perutz and Seligman), 335.
Goodeve, C. F. and Katz, S. The absorption spectrum of nitrosyl chloride, 432.

Helium hydride molecules, formation (M'Ewen and Arnot), 107.
Helium, liquid, properties of flow (Allen and Misener), 467.
Hoselitz, K. *See* Munson and Hoselitz.
Hughes, T. P. *See* Bowden and Hughes.

Ibbs, T. L. *See* Atkins, Bastick and Ibbs.
Inert gases, thermal diffusion in mixtures (Atkins, Bastick and Ibbs), 142.
Ionic crystals, electrical breakdown (Fröhlich), 94.
Iron spectrum, vacuum wave-length measurements (Williams and Middleton), 159.

Katz, S. *See* Goodeve and Katz.

London, H. *See* Appleyard and others.
Lovell, A. C. B. Shower production by penetrating cosmic rays, 568.
Luyckx, A. Luminescence of mercury vapour along an α-ray pencil, and transfer of nitrogen excitation to mercury, 492.

M'Ewen, M. B. and Arnot, F. L. The formation of HeH^+ molecules, 107.
Maggs, J. *See* Garner and Maggs.
Mesons, classical theory (Bhabha), 384.
Menzies, A. C. Fine structure of the Raman lines of carbon tetrachloride, 89.
Mercury vapour luminescence (Luyckx), 492.
Metallic azides, decomposition (Mott), 325.
Middleton, A. *See* Williams and Middleton.
Misener, A. D. *See* Allen and Misener *and* Appleyard and others.
Mobility of alkali ions in gases (Munson, Tyndall and Hoselitz), 28, 43, 51.
Morris, R. M. The two-dimensional hydrodynamical theory of moving aerofoils, III, 213.
Mott, N. F. On the decomposition of metallic azides, 325.
Munson, R. J., Tyndall, A. M. and Hoselitz, K. The mobility of alkali ions in gases, 28, 43, 51.

Nitrosyl chloride, absorption spectrum (Goodeve and Katz), 432.
Norrish, R. G. W. *See* Buckler and Norrish.

Pelmore, D. R. Dielectric loss due to polar molecules in solid paraffin wax, 502.
Perutz, M. F. and Seligman, G. A crystallographic investigation of glacier structure and the mechanism of glacier flow, 335.
Photosynthesis of carbohydrates (Baly), 445.
Piekara, A. A theory of electric polarization, electro-optical Kerr effect and electric saturation in liquids and solutions, 360.
Potassium X-ray terms, wave functions and energy values (Thatcher), 242.
Preston, G. D. Diffraction of X-rays by crystals at elevated temperatures, 116.

Rosenhead, L. *See* Corkill and Rosenhead.

Saunders, O. A. Natural convection in liquids, 55.
Seligman, G. *See* Perutz and Seligman.
Sliding on ice and snow (Bowden and Hughes), 280.
Strothers, J. E. *See* Curran and Strothers.
Sutherland, G. B. B. M. *See* Conn and Sutherland.

Tetra-deuteroethylene, infra-red spectrum (Conn and Sutherland), 172.
Thatcher, W. A. Calculated wave functions and energy values for X-ray terms of potassium, 242.
Thin films of mercury, electrical conductivity (Appleyard and Bristow), 530.
Thin films of mercury, superconductivity (Appleyard, Bristow, London and Misener), 540.
Tyndall, A. M. *See* Munson and Tyndall.

Williams, E. J. Some observations on cosmic rays using a large randomly operated cloud chamber, 194.
Williams, W. E. and Middleton, A. Vacuum wave-length measurements in the iron spectrum by means of the reflexion echelon grating, 159.
Wilson, J. G. Absorption of penetrating cosmic ray particles in gold, 517.
Wischin, A. The thermal decomposition of crystals of barium azide, 314.
Wood, W. A. The lower limiting crystallite size and internal strains in some cold-worked metals, 231.

END OF THE ONE HUNDRED AND SEVENTY-SECOND VOLUME (SERIES A)